中国科学院上海应用物理研究所

年 报

2005–2006

（第 22 卷）

《中国科学院上海应用物理研究所年报》
编辑委员会

内 容 简 介

本刊为 2005–2006 年度中国科学院上海应用物理研究所年报。本年报介绍全所各科研机构两年的主要科研工作进展，内容为中英文，顺序为上海光源、核物理、核分析技术与交叉学科研究、电子束辐照装置与高分子材料辐射改性、放射性药物、核电子学、环境治理技术。附录记载了 2005–2006 年度本所的学术活动、国际交流、人才培养等情况。

本年报供本所上级主管中国科学院和上海市各有关部门的领导与各类管理人员阅读，供各科研院所相关领域的科研人员、高等院校师生，以及本所科研人员和研究生阅读参考。

前　言

建设上海光源工程，布局研究所新发展

2005-2006 年，我所在院的领导下，学习和贯彻全国科技大会精神，按照“两个一盘棋”的要求，以上海光源工程建设为全所工作的“重中之重”，全力确保工程建设任务的完成；围绕上海光源调整组织结构，凝练学科方向，促进所内工作与工程的有机结合。认真执行在研项目，整合所内资源，积极争取科研任务，推进实验室与科研条件建设，持续开展卓有成效的国内外合作，加强人才队伍建设和研究生教育管理，不断完善研究所运行机制，深入开展创新文化建设，适时推动科技企业改制重组，在实现我所创新三期及中长期发展目标的征途中取得了良好的开端。

一、编制三期方案和中长期规划，绘就发展蓝图

2005 年，在完成我所《创新试点二期自评估报告》的基础上，全面分析国家战略需求、世界科技前沿发展趋势和我所核心竞争力，制订了我所《中长期发展战略规划》，目标是用 15 年左右时间，将我所建设成以“应用”为特色、国际先进、有中国特点的基于核技术(加速器)科学的多学科综合性科学研究基地；建设世界级的先进光子科学研究中心和国家级的应用物理研究中心，到 2020 年前后，进入国际知名的大中型综合性研究机构行列。并据此编报了我所《知识创新工程三期工作方案》，在创新三期的 2006-2010 年，我所将全力完成上海光源国家重大科学工程任务，建成一台居国际先进水平的中能(3.5 GeV)第三代同步辐射装置；围绕这一大装置，发挥张江和嘉定两个园区的互补优势，发展基础研究、核技术应用研究及其产业化三个层次的工作，下好全所“一盘棋”，为我所的长期发展奠定坚实的基础。

二、全力确保上海光源国家重大科学工程建设

上海光源(SSRF)国家重大科学工程建设任务是我所工作的重中之重。自 2004 年底开工建设以来，工程经理部认真制订了各级 CPM 计划；建立了一套以岗位责任制和质量保障体系为核心的工程管理体制；制订了工程档案管理办法和立卷归档程序，完成了前期管理性文件、工程设计与评审资料的完整收集；制定了物流工作规定，制订与落实各分总体的物流计划。为了保证工程的质量和进度，最大限度地节约经费，使工程顺利按期完成，成立了工程招标工作小组，制订并严格执行了招标工作程序及实施细则。

经过工程建设队伍和项目参建各方两年的努力，上海光源工程基本完成建筑安装任务，转入设备安装调试阶段，工程建设取得了又好又快的进展。建安工程攻克了地基基础减振与微变形控制、异型钢屋盖结构体系及节点研究、消防性能化设计、屋面铝板幕墙系统等技术难关，辅助建筑已建设完成，主体建筑已进入土建和安装收尾阶段；公用设施工程设备安装基本完成，开始调试和试运行。加速器工程启动批量生产，进入设备安装调试阶段，其中，直线加速器完成设备加工、验收，开始隧道内设备安装；增强器和储存环的主要设备采购合同都已经启动或已经完成，在完成部分关键设备的样机或首件加工以及标准单元的试安装后启动批量加工制造。光束线站工程完成首批线站的调整，全面进入工程设计阶段，部分关键设备启动样机制造和采购。随着建筑安装工程的完成，我所作为项目法人单位即将全面接收张江园区。此外，工程经理部成立了上海

光源用户委员会筹备工作组，制订了用户委员会工作框架，初步拟定了用户委员会名单和章程，并于 2006 年组织召开“上海光源应用研究研讨会”。

三、整合资源，立足特色，基础研究发展形势喜人

2005-2006 年，我所科研工作的重点在整合现有资源，力争融入国家总体科技布局并在某些领域形成特色和优势，逐渐确立我所在相关领域的地位。为此，启动了上海激光电子伽玛源和 X 射线干涉光刻 2 条光束线站的建设，部署和推进 FEL 和 T-ray 关键技术研究、先进光源和束线相关关键设备的研制项目。精心组织项目申请，采取措施提高科研骨干争取项目的能力，集成我所在相关研究方向的特点，合力争取重大科研项目。2005-2006 年度，共争取到各类科研任务 65 项、总经费 4645 万元；其中 2006 年争取到 4 项中科院创新三期重要方向性项目支持，申请到国家自然科学基金项目及经费比 2005 年增加 1 倍以上。在国内外学术期刊上共发表论文 400 余篇；申请专利 39 项、授权专利 15 项；出版专著 2 部，参与编写专著 2 部；结题科研项目 11 项，研究结果达到预期的目标。

两年来，我所研究工作取得一批重要的成果和进展。100MeV 高性能电子直线加速器顺利通过专家鉴定测试；完成深紫外自由电子激光装置的波荡器真空系统设计并签订了加工合同；与中科院高能所、清华大学合作，完成中国 X 射线 FEL 试验装置(CTF)概念设计报告。核物理领域 RHIC-STAR 国际合作相关项目争取到基金委、中科院等多项支持，国内外合作研究和交流进一步加强，成果丰硕；由我所主持的 973 项目“放射性核束物理和核天体物理”通过科技部委托的专家组验收，其中我所承担的子课题得到好评，顺利通过科技部组织的结题评审。基于 N&NBIU 的交叉学科研究就纳米水通道研究、生物传感器、纳米粒子 PCR、多肽一维外延生长模式调控、离子液体等方面发表多篇高水平论文，发展形势喜人；中科院创新方向性项目“微束在团簇中的运输机制及相关效应的研究”和“先进核分析技术在环境科学中的应用研究”于 2006 年顺利通过验收。核技术应用研究在调整中不断强化特色，由我所和复旦大学现代物理所共同研制的国内第一台高电荷离子实验装置上海 EBIT(电子束离子阱)装置于 2005 年 5 月首次出束，2006 年底通过阶段性验收；研制出基于离子迁移率谱仪(IMS)的毒品检测原理性样机，达到 10^{-10}g 毒品检测灵敏度；高分辨小动物 SPECT 成像系统研究、生物特征识别系统及检测技术研究、SBS 辐射接枝与道路沥青改性研究等也都取得重大进展。

四、发挥仪器研制特色，推进实验室与科研条件建设

仪器与设备的研制和改造、实验方法学的研究是我所的特色。截至 2006 年底，研制并建成我国第一台飞秒电子束装置，综合性能指标达到国际同类装置的先进水平，顺利通过中科院的验收；上海市低温超导高频腔技术重点实验室建设也取得阶段性进展；与上海世龙科技有限公司联合建立的电池隔膜研究联合实验室正式运行；分子标记及核素分子显像实验技术平台已初步建成。已建成的 THz-TDS 实验室、细胞与分子生物学实验室、PC-FARM 集群计算系统等运行良好，有力支撑了所内多项前沿学科领域的研究工作。2006 年成立非法人独立机构“辐射安全检测中心”，并获得了计量认证证书。

五、持续开展卓有成效的国际国内合作

巩固原有合作关系，积极拓展新的合作，与新加坡光源、英国 DIAMOND 光源、澳大利亚同

步辐射光源、俄罗斯西伯利亚核物理研究所(BINP)签订了所级合作协议，与美国伯克利国家实验室草拟了合作协议，并与韩国浦项加速器实验室(PAL)就原有的合作备忘录签署补充合作协议。积极开拓核技术应用领域的国际合作，以俄罗斯 BINP 为突破口，打开了对俄合作的通道。国际间人员交流继续向多元化、深层次发展， 2005 和 2006 年出访人员分别达 150 和 231 人次，来访人员分别达 170 和 263 人次（不含参加我所主办国际会议的国外代表）。成功举办“第十九届极端相对论性核-核碰撞国际会议” (Quark Matter2006)等 6 次大中型国际学术会议 ；上海光源在国内外组织召开多次工程总体、系统以及专项、专题技术的国际评审会和研讨会。顺利执行 2 项国家政府间科技合作项目；申报并获得基金委、中科院国际合作项目各 1 项。编制了上海光源工程引智规划，获得 2006 年度国家外国专家局引进国外技术管理人才重点项目计划资助，并顺利执行完成。与国外科学家合作发表论文 32 篇。

为推动我所科研活动融入国家科技布局，2006 年与中国科技大学签订了全面合作协议，与中科院理化所、长春光机所、沈阳科学仪器公司等单位建立了合作关系。目前，我所主要学科均与高校、科研机构建立了一定的合作伙伴关系。

六、调整核技术产业化工作，加强科技成果转化

为促进我所乃至我国民用非动力核技术产业化的发展，我所调整了产业化工作管理职能，明确由科技产业化处专业管理全所科技产业化工作，并相应调整研究部门成果转化类工作的管理模式，制定了《科技成果转化暂行管理办法》。认真组织参加工博会及其它成果推介活动，积极推动我所科技成果的转化，成功实现了“一种 DNA 电化学传感器及其制备方法”专利申请权的转让并达成科研合作协议。继续完善企业内部管理机制，印发了《关于所属企业职工薪酬管理的意见》，指导企业实施有效的薪酬管理。进一步加大与社会资源的结合力度，对日环仪器厂实施股权社会化改革，经过公开竞价投标，于 2006 年底签订了《产权转让协议》。努力推进国家发展改革委产业化示范工程项目，落实了辐射技术产业化基地项目一期工程用地，编制了基地修建性详细规划，完成了初步设计并上报中科院审批。

七、探索用人模式，多渠道引进人才，加快人才队伍建设

上海光源工程队伍建设是我所近两年人才队伍建设的重点。为此我所成立了工程人事协调小组，多渠道引进工程建设急需的科研与工程技术人员，吸收国内与同步辐射光源相关的科研院所和大学的专业人员，从国外引进或短期聘请工程建设特别需要的专家，队伍建设收效明显。另外，线站工程、公用设施、低温工程部分采用联合设计的方式，建安工程采用从上海市相关部门借调技术和管理人员的方式，解决了工程技术人员短缺的问题。借助社会资源，探索劳动关系与聘用岗位完全脱离的用人模式，并依此模式组建了张江园区公用设施运行维护人员队伍。充分挖掘我所人力资源，建立了先到岗试用、再确定人事隶属关系的用人模式，所属企业多名技术人员先后被上海光源工程试用考核合格后聘用。

以队伍规划为抓手，充分发挥科研骨干的人才引荐作用，落实重要岗位人员的引进，两年共引进与招收 171 人，其中博士学位的 42 名、高级岗位的 17 名；以借调等形式聘用高级技术人员 11 人；2006 年进站博士后 6 人，是我所进站博士后数量最多的一年。注重青年人才的培养，继续完善公开、竞争、择优为导向的岗位聘任制，建立“绿色通道”激励青年科技人员勇于挑重担、负责任。抓好研究生教育中生源、培养、思想政治工作等各个环节，以点带面提高研究生培养质量，

2005-2006 年共招收研究生 236 名(其中博士研究生 100 名)，全所在读研究生增长到 319 名(其中博士生 160 名)。

八、规范管理，推进研究所体制与机制改革

根据我所创新三期学科布局和工作任务，进行组织机构调整，将核分析室和纳米生物医药室重组为核分析科学与技术研究室，将应用加速器中心和辐照中心重组为加速器与辐射技术研究中心；调整管理部门，强化并形成科学研究处、工程办公室、科技产业化处三个科技业务管理部门的管理格局，在此基础上明确并公布了《管理部门职责》。建立了管理例会制度；针对我所管理工作已经面临的“一所两园区”课题，进行专题讨论并部署实施。为适应两个园区的工作条件，特别加强了管理活动的制度化、规范化工作，制(修)订了 46 项规章制度，同时废止了 21 项规章。为使我所的核技术应用研究和产业化工作适应所创新三期的要求，以加速器辐照中心的改革为试点，启动了研究中心的调整和改革工作。

认真组织实施中国科学院资源规划(ARP)项目，通过了中科院组织的上线实施检查和系统验收，并正式开始运行；着重开展网页信息平台建设，完成了 SINAP、SSRF 网页中英文版等的建设或改版。持续强化内部预算管理，在预算执行过程中坚持资金归口管理部门的责任，以提高预算的透明度和预算执行的严肃性；修订了《所投资企业内部审计的规定》，进一步规范和加强对我所投资企业的管理。加强安全管理，落实实验室安全责任制，实施对上海光源工程建设现场重点部位的安全保卫方案；2006 年，我所通过了上海市科教党委和上海分院组织的上海市“平安单位”验收。以张江园区后勤服务体系建设和现场保障为重点，积极探索后勤工作的社会化。

九、深入开展创新文化建设

持续加强奉献精神和使命感的培育，及时总结、提炼上海光源工程建设中形成的精神内涵，向全所发出学习“上海光源精神”的号召。开展 2005－2006 年度“文明部门”评选活动；组织开展建党八十五周年系列活动，评选表彰先进党支部和优秀党员；建设足球场、开放相关文体活动场所，整合工青妇等各方面的资源，组织各项体育比赛、文艺晚会等活动，丰富职工和研究生的所内生活。围绕上海光源工程建设和科研工作进展，加大信息和科技宣传力度，加强上海光源对外科普宣传工作，先后主办了三期东方科技论坛，参加第八届中国国际高新技术成果交易会和 2006 年中国国际工业博览会，组织并接待 350 余名大、中、小学生到我所参观科学试验装置，出版《分子手术与纳米诊疗：纳米生物学及其应用》科普著作。

园区建设成效明显，2005 年，我所创新一期、二期开展的九项园区建设项目顺利通过中科院基建局组织的竣工专业验收；此外，自筹资金完成嘉定园区部分建筑的维修改造工程，积极争取创新三期嘉定园区和张江园区的建设项目，已获得院部初步肯定。

2005-2006 年，我所在上海光源工程建设、科技创新与科研项目争取、人才队伍建设、体制机制改革、管理创新与文化建设等各方面都取得了可喜的成绩。今后的几年是关乎我所发展的重要时期，上海光源工程须经受设备安装调试的实质性考验，科研工作须在国家十一·五科技布局中争取到相当数量和规模的科研项目，核技术应用研究与产业化须突破“瓶颈”闯出“新天地”，“一所两园区”的运行对管理工作提出了现实而严峻的挑战，工作任务将更加艰巨与繁重。全所同志务必再接再厉，全力以赴，学习和发扬“上海光源精神”，按时、优质地完成上海光源工程的建设，促进所内各项工作协调持续发展，为实现我所创新三期的发展目标而拼搏。

目次

上海光源 Shanghai Synchrotron Radiation Facility

核物理 Nuclear Physics

核分析技术 Nuclear Analysis Techniques

应用加速器和辐射研究中心 EB Accelerators and Radiation Applications

放射性药物 Radiopharmaceuticals

先进探测仪器 Advanced Detectors and Instruments

新技术中心 Membrane Technology

上海光源

Shanghai Synchrotron Radiation Facility

上海光源储存环横向反馈系统模拟计算

姜伯承　刘桂民　赵振堂

关键词　上海光源，反馈，模拟，AT

同步辐射光源的阻抗壁不稳定性是一个很严重的不稳定性。要确保储存环在高流强下正常运行，须有横向反馈系统(TFS)抑制横向不稳定性。为了解在横向反馈作用下束流的动力学性质，我们建立了一套横向反馈模拟计算程序。用该程序模拟计算了上海光源(SSRF)储存环横向反馈系统在闭轨误差(COD)、束流位置探测器(BPM)读数误差以及梳状滤波(FIR filter)等条件改变下的反馈效果。通过较为全面的模拟分析，上海光源储存环须有一套横向反馈系统。模拟结果和理论结果基本吻合，有横向反馈系统的储存环的最大可储存流强为 1800 mA，2-tap FIR 滤波器能阻尼 BPM 读数噪声约 13 dB。

Simulation of a transverse feedback system for the SSRF storage ring

JIANG Bocheng　LIU Guimin　ZHAO Zhentang

Key words:　SSRF, Feedback, Simulation AT

Resistive wall instability is a serious problem in many light sources. An active transverse feedback system (TFS) is required to operate the facility in a good condition at high beam currents. A TFS simulation program was developed at Shanghai Synchrotron Radiation Facility (SSRF) for investigation of beam dynamics with a TFS. The feedback effectiveness for the SSRF storage ring was simulated against various affecting factors, such as closed orbit distortion (COD), reading errors from the beam position monitor (BPM), and different strategies for the finite-duration impulse-response (FIR) filter. The analysis, with comprehensive simulations of the resistive wall instability and transverse feed back system, shows that a transverse feedback system is needed for SSRF. The simulation results agree well with theoretical prediction and give a confirmation of the SSRF TFS design. With the TFS, the current threshold reaches 1800 mA when vertical resistive wall instability is added. TFS with 2-tap FIR filter could give just a ~13 dB damping to the BPM reading errors, a better FIR filter is desired for the SSRF TFS.

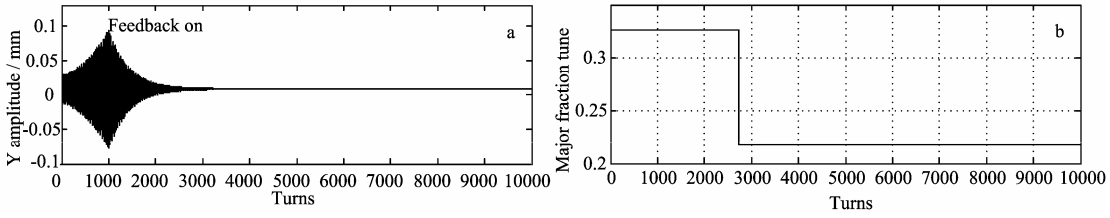

Fig.1　Lateral amplitude and major frequency of the electron beam bunches

SSRF 增强器二极铁安装排序优化

后接 刘桂民 李浩虎 张满洲

关键词 上海光源，二极铁，安装排序，一致性，测量精度

上海光源增强器将直线加速器引出的 150 MeV 电子束加速至 3.5 GeV，并全能量注入到储存环中，要求在引出能量下得到较高的引出效率并减少加速过程中的束流损失。对二极铁安装位置进行排序优化，能有效抑制由磁场一致性误差导致的束流闭轨畸变，改善机器性能。本文依据二极铁磁场一致性的实测数据进行二极铁安装排序优化，并比较了其与理想情况下排序优化的结果，给出了最终的二极铁安装顺序。

Bending magnet sorting optimization for SSRF booster

HOU Jie LIU Guimin LI Haohu ZHANG Manzhou

Key words: SSRF, Bending magnet, Sorting, Uniformity, Resolution

The Shanghai Synchrotron Radiation Facility (SSRF) booster, as a full energy injector for the storage ring, is deigned to accelerate electron beam from 150 MeV to 3.5 GeV. This demands high extraction efficiency at the extraction energy with low beam loss rate of the ramping electrons. Closed orbit distortion (COD) caused by field uniformity of the bending magnets affects the machine performance, but it could be effectively reduced by location-sorting of the bending magnets. Realistic sorting was performed based on field uniformity errors measured on the bending magnets and by comparing the results with ideal sorting. The final installation sequence of bending magnets is given in this paper.

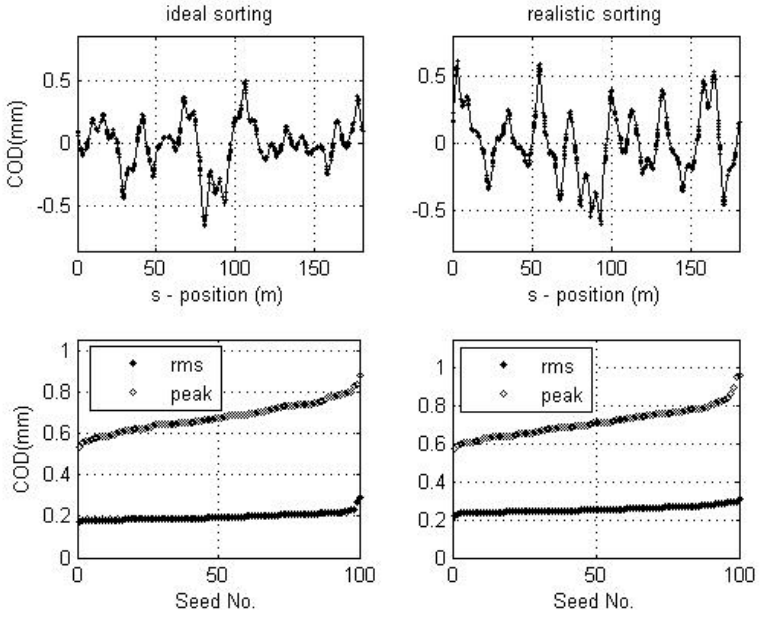

Fig.1 COD after the magnet location sorting

LLRF 中的一种基于 non-IQ 的控制算法

尹成科 戴志敏

关键词 SSRF，低电平，IQ

在上海光源(SSRF)中数字低电平控制的研制中，我们建立了基于高速 AD、DA 和 FPGA 的控制系统。该控制系统基于 IQ 调制解调和 PI 控制算法，实现了控制高频腔的相位正负 1°、幅度正负 1%的设计目标。我们发现，现有的基于 IQ 的控制技术对 AD、DA 的采样时钟和中频频率有一些特定的要求。在理论分析和仿真实验的基础上，提出了一种基于 non-IQ 的控制算法，以避免对时钟的特殊要求。此法的好处为：1)AD、DA 的采样点可较为分散，这在很大程度上抵消了由于器件的非线性带来的影响；2)不必考虑时钟关系的限制，环路可工作在较高的采样频率，从而减小环路延时，提高带宽响应；3)无须 DDS 完成中频信号的恢复工作，节省芯片，增加灵活性。

A non-IQ PI controller in LLRF

YIN Chengke DAI Zhimin

Key words: SSRF, LLRF, IQ

This paper describes a non-IQ algorithm for digital LLRF feedback control. Based on the non-IQ algorithm, arbitrary frequency relations between the ADCs/DACs sampling clock and IF signals can be employed in conditions that all the clocks are phase locked. Most nonlinearity of digital conversion can be averaged out. The linearization performance of non-IQ method is analyzed and is compared with common IQ method. The linearization reduces errors caused by frequency alias in under-sampling IQ demodulation. The non-IQ approach also improves band-limited performance and the dispensability of the DDS (Direct Digital Synthesis) for IF output regeneration. Disadvantages are also discussed. This algorithm has been simulated and testified both in software and FPGA hardware.

上海光源储存环高次谐波腔的设计

马广明 赵振堂 刘建飞

关键词 上海光源，高次谐波腔，超导射频，高次模抑制器

高次模谐波腔可提高第三代同步辐射光源储存环的托歇克寿命。上海同步辐射装置(SSRF)的高次谐波腔是一个 1.5 GHz 的无源超导腔，将安装于低温槽外的铁氧体高次模抑制吸收。基于腔压的考虑，该高次谐波腔为多 cell 腔。本文介绍谐波腔的束流动力学、无源腔的工作原理和单 cell 腔设计方案。目前，单 cell 腔正在加工制造，多 cell 腔正在研究设计中。

已加工了一个模型腔，铌材腔和铜材腔将于 2007 年开始加工。单腔优化后具有较高的分路阻抗(R/Q=82.97 Ω)和较低的功率损耗，高次模可通过较大的波导口径消除掉。

一个单腔可提供 0.5 MV 电压。为得到 1.5 MV 标称电压，须有 3 个单腔或一个 3-cell 腔，单腔结构需 3 套制冷设备，功率消耗大，投资大，因此选择 3-cell 腔。

A higher harmonic cavity for SSRF storage ring

MA Guangming ZHAO Zhentang LIU Jianfei

Key words: SSRF, Higher harmonic cavity, Superconducting RF, HOM damper

Higher harmonic cavity used in a third generation synchrotron light source increases the Touschek lifetime. The higher harmonic cavity of SSRF is a 1.5 GHz passive superconducting cavity. Its higher order modes (HOM) are extracted by a ferrite HOM damper outside the cryostat. Multi-cell cavity was chosen based on voltage considerations. The harmonic cavity dynamics, beam dynamics with passive harmonic cavity and the design of single cell cavity are included in this paper.

A higher harmonic cavity is designed for the SSRF storage ring. As a first step, two single cell cavities will be manufactured in 2007, with niobium and copper. The single cell, a low loss cavity, is optimized in its shape to have a large shunt impedance of R/Q=82.97 Ω and low dissipated power in the same voltage and surface treatment conditions. The higher order modes will be eliminated by adding enlarged beam pipes.

A single cell cavity is designed to provide 0.5 MV of voltage, hence the need of three single cell cavities or one 3-cell cavity to achieve the nominal voltage 1.5 MV, but the single-cell approach, which requests cryogenic systems, is more expensive, with more power consumption. Therefore the multi-cell cavity is chosen for the SSRF storage ring.

Fig.1 The single-cell approach

上海光源储存环闭合轨道对磁铁振动响应研究

陈建辉 赵振堂

关键词 闭轨畸变(COD)，磁铁振动，响应函数，局部补偿效应，横向振动波长

通过解析和模拟分别计算了上海光源储存环闭合轨道对随机和平面波型磁铁振动的响应，模拟计算证实了支架的局部补偿效应可有效减小该响应。还比较了组合型与分离型磁聚焦结构对磁铁振动的响应。基于响应的计算和支架的传递函数，给出了粗略计算由于地基振动引起的闭轨畸变的方法。对上海光源地基振动引起的储存环闭轨畸变作了估算。

Response of beam orbit to magnet vibrations

CHEN Jianhui ZHAO Zhentang

Key words: Closed orbit distortion (COD), Magnet vibrations, Response function, Local compensation effect, Betatron wavelength

Response functions of closed orbit distortion (COD) of the SSRF storage ring were analyzed and simulated against random and plane wave-like magnet vibrations, respectively. The results show that the use of girder is very beneficial to suppress the COD response. Comparison between the response functions of combined and separated function lattice is given. COD caused by ground motion can be roughly estimated taking into account the closed orbit response and girder transfer function. Results of the COD of SSRF are given as an example.

SSRF 次谐波聚束腔中二次电子倍增效应的模拟

张 猛 赵明华

关键词 次谐波聚束器 二次电子倍增 计数函数 模拟

上海光源直线加速器采用一个次谐波聚束腔组成预注入器，其性能的稳定性和可靠性直接关系到电子束流的品质。二次电子倍增效应是其不稳定性的原因之一，为考察其二次电子倍增效应，将上海光源次谐波聚束腔与最普通的重入式谐振腔进行对比，结果表明在实际使用的工作范围内，优化次谐波腔形状可有效抑制二次电子倍增效应。进一步的考察表明，腔体结构的圆滑设计是抑制二次电子倍增的原因。

Simulation of multipacting effect in SSRF SHB cavity

ZHANG Meng ZHAO Minghua

Key words: Sub-harmonic buncher, Multipacting, Counter function, Simulation

To guarantee reliability of the SHB cavity of the SSRF Linac, Program MultiPac was used to simulate secondary electron effect, an important factor of worsening the injection stability and optimization. Compared with the simple reentrant cavity, the simulation results show that the SHB cavity can avoid the multipacting effect successfully. It was also found that the smooth corner and nose could be of help to reduce the multipacting effect.

基于 AT & MCA 的 SSRF 低能输运线上层应用软件设计

陈光玲　刘桂民

关键词　Matlab, AT, MCA, 上层应用软件, SSRF, 输运线

AT 和 MCA 都是基于 Matlab 的介于上层应用软件和下层加速器控制系统之间的加速器物理软件工具包。本文详细介绍了基于这两个软件包的 SSRF 低能输运线上层应用软件设计。离线及在线仿真测试结果表明，SSRF 低能输运线上层应用软件所有功能基本运行正常，MCA 与 EPICS 模拟数据库之间数据读写准确，计算结果与 SSRF 低能输运线各参数相符，Simulator 模式下的计算也能达到 SSRF 设计要求。

Design of high-level application of SSRF low-energy transport based on AT & MCA

CHEN Guangling　LIU Guimin

Key words:　Matlab, AT, MCA, High-level application, SSRF, Transport

AT and MCA are accelerator physics Matlab toolboxes that resides between the high-level application and the low-level accelerator control system. In this paper we describe the design of high-level application of SSRF low-energy transport based on the two toolboxes. From the results of offline and online simulation, we can see that the high-level application of SSRF low-energy transport works well. The result agrees well with parameters of SSRF low-energy transport, and the calculation in simulation mode can satisfy the request of SSRF R&D.

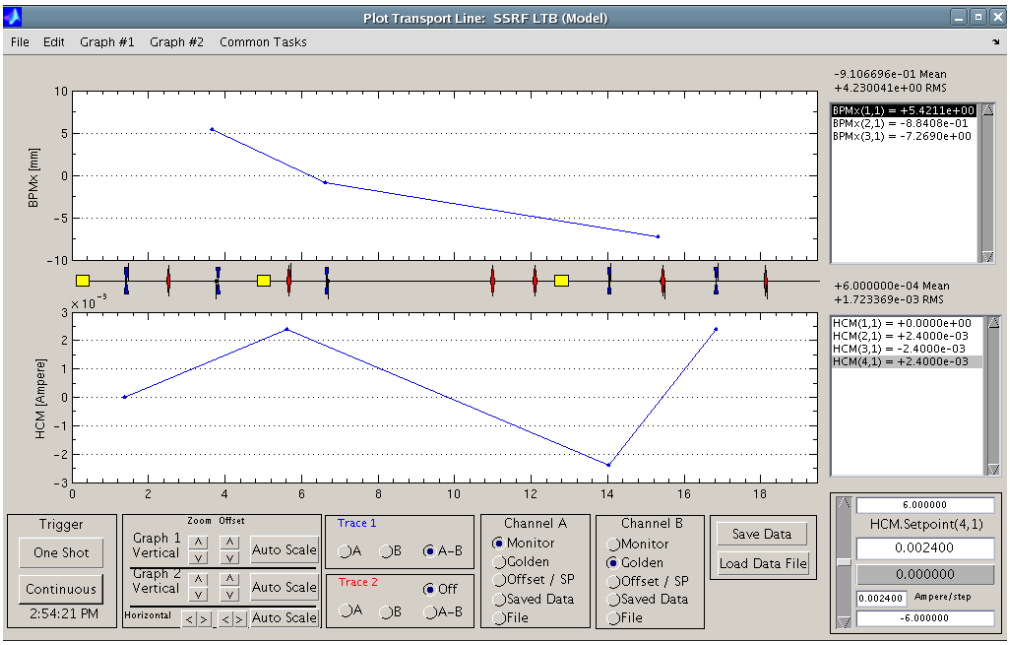

Fig.1　High-level application of SSRF low-energy transport

基于碳纳米管场致发射的电子枪的初步研究

孙启龙　林国强　戴志敏

关键词　场致发射，电子枪，碳纳米管，THz 辐射

高功率的 THz 辐射源研究是现今 THz 辐射研究的重点，而利用高亮度的飞秒电子束通过波荡器或者弯转磁铁可产生高功率的 THz 辐射。为此我们开展了基于碳纳米管场致发射的研究。本文介绍碳纳米管的场致发射能力的实验结果和基于碳纳米管场致发射电子枪的初步研究结果。实验表明，碳纳米管是很好的场致发射材料，在极间场强 2.7 MV/m 下，电流发射密度为 0.5mA/cm^2。电子枪的初步实验结果表明，碳纳米管具有较长的寿命，电子枪可稳定运行两周以上。

Preliminary study of electron gun based on field emission of carbon nanotubes

SUN Qilong　LIN Guoqiang　DAI Zhimin

Key words:　Field emission, Electron gun, Carbon nanotubes, THz radiation

The research of the high-power THz radiation source is the focus of the recent research of the THz radiation. The high-power THz radiation can be generated using the high brightness electron beam passing through the undulator of the bend magnet. The study of the electron gun based on the field emission of carbon nanotubes is started based on the requirement of the THz radiation. The paper reports the preliminary study of an electron gun based on the field emission of carbon nanotubes. The result of the field emission experiment shows that the carbon nanotubes are excellent field emitters, yielding current densities higher than 0.5mA/cm^2 with operating field about 2.7 MV/m.

碳纳米管光场致发射新型电子枪的初步方案设计

孙启龙　王兴涛　林国强　戴志敏

关键词　光场致发射，电子枪，碳纳米管，量子效率

高功率的 THz 辐射源研究是现今 THz 辐射研究的重点，而利用高亮度的飞秒电子束通过波荡器或者弯转磁铁可以产生高功率的 THz 辐射，本文正是在此基础上开展了基于碳纳米管场致发射和光场致发射的电子枪的研究。本文给出了一种基于碳纳米管光场致发射机制的新型电子枪的设计方案。该电子枪的枪体采用 Pierce 枪结构，加 200 kV 直流高压，阴极材料为碳纳米管，驱动激光波长 800~850 nm，脉冲峰值电流为 6 A, 平均电流为 12 mA。与传统的光阴极电子枪相比，这种基于碳纳米管光场致发射机制的新型电子枪具有结构简单，量子效率高等优点。此外，本文还介绍了正在搭建的该电子枪实验平台。电子枪的性能，特别是阴极寿命和量子效率将在实验中进行深入研究。

Design of a novel electron gun based on photoemission of carbon nanotubes

SUN Qilong WANG Xingtao LIN Guoqiang DAI Zhimin

Key words: Photoemission, Electron gun, Carbon nanotubes, Quantum efficiency

The research of the high-power THz radiation source is the focus of the recent research of the THz radiation. The high-power THz radiation can be generated using the high brightness electron beam passing through the undulator of the bend magnet. The study of the electron gun based on the photo-field emission of carbon nanotubes is started based on the requirement of the THz radiation. The paper reports the design of a novel electron gun based on photoemission of carbon nanotubes. The electron gun, using the traditional Pierce structure, can generate 6 A peak pulse beam current and average beam current of 12 mA when the applied DC voltage is 200 kV and the driven laser's wavelength is 800~850 nm. This novel electron gun has a simple structure and high quantum efficiency relative to traditional photocathode electron gun. Additionally the electron gun test platform undergoing was introduced in the paper. The electron performance especially the lifetime and the quantum efficiency of the cathode will be studied thoroughly.

基于上海深紫外自由电子激光的两级级联 HGHG 装置设计

邓海啸 戴志敏

关键词 时间抖动，自由电子激光，高增益高次谐波发生器

级联 HGHG 自由电子激光是通向短波长辐射的可行之路。在解析理论的指导下，基于上海深紫外自由电子激光，给出了产生 131 nm 自由电子激光辐射的两级级联 HGHG 装置设计。详细阐述了由三维软件 Genesis 计算得到的自由电子激光性能、辐射功率对参量变化的稳定性和灵敏性以及整个两级装置 Lattice 结构的设计。证明了基于上海深紫外自由电子激光的两级级联 FEL 的可行性。

Design of cascading two stages of high gain harmonic generation scheme based on Shanghai deep UV FEL

DENG Haixiao DAI Zhimin

Key words: Time jitter, Free electron laser (FEL), High gain harmonic generation (HGHG)

Cascading stages of high gain harmonic generation free electron laser (FEL) seems to be a feasible way to generate short wavelength radiation. With the help of analytical estimates, we design a two-stage cascading scheme to achieve 131 nm deep UV radiation on the Shanghai deep ultraviolet FEL test facility. The FEL performance, stability and sensitivity of the parameters variation under different output powers were calculated by GENESIS1.3. Design of the lattice structure is presented.

上海深紫外自由电子激光的非线性谐波辐射研究

邓海啸　王兴涛　李冬国　戴志敏

关键词　非线性谐波，自放大自发辐射，自由电子激光，高增益高次谐波发生器

自由电子激光中的非线性谐波辐射能达到较高的谐波功率，可用以得到短波长辐射或降低第四代先进光源对电子束团品质严酷的要求。用三维自由电子激光软件研究了上海深紫外自由电子激光装置的非线性谐波辐射，提出了谐波辐射实验和测量的建议。研究表明上海深紫外自由电子激光装置 3 次非线性谐波辐射的功率可达到基波功率的 2%水平。

Nonlinear harmonics in Shanghai deep UV FEL source

DENG Haixiao　WANG Xingtao　LI Dongguo　DAI Zhimin

Key words:　Nonlinear harmonics, Spontaneous amplification spontaneous emission (SASE), Free electron laser (FEL), High gain harmonic generation (HGHG)

Significant powers of the harmonics achieved through nonlinear harmonic generation in high gain FEL may be used for shorter wavelengths generation or to relax some stringent requirement on the electron beam quality for a 4^{th} generation light source. In this paper, nonlinear harmonic generation in Shanghai deep ultraviolet free electron laser source is described. The results show that the power of the 3^{rd} nonlinear harmonics may be as high as 2% of the fundamental power level. Experiment and measurement of the harmonic radiation are proposed.

上海深紫外自由电子激光的谐波运行研究

邓海啸　戴志敏

关键词　谐波运行，自由电子激光

研究了上海深紫外自由电子激光的谐波运行模式。通过合理选择调制段波荡器及种子激光参数，将电子束空间密度调制在辐射段波荡器辐射的高次谐波上，使辐射段波荡器工作在高次谐波下。利用通用的自由电子激光理论和数值模拟分析研究了上海深紫外自由电子激光的三次谐波运行。结果表明，谐波功率大大提高，达到基波水平的 14%左右。这一特点使谐波运行在紫外和软 X 射线范围内非常有用。

Harmonic operation in Shanghai deep UV FEL source

DENG Haixiao　DAI Zhimin

Key words:　Harmonic operation, FEL

In this paper, we investigate the possibility of harmonic operation of Shanghai deep ultraviolet (SDUV) free electron laser (FEL) source, in which the radiator undulator is operated at high harmonic mode. With the right choice of parameters in modulator and seed laser, spatial bunching of the electron beam density can be in a distribution corresponding to the 3rd harmonic of the radiator radiation, instead of the fundamental of the radiator radiation in HGHG. Theoretical analyses with conventional method were derived and numerical simulations were given. The results show that the power of the 3rd harmonic radiation in the harmonic operation of SDUV FEL can be as high as 14% of the fundamental level. This attractive character may make harmonic operation very useful in UV and soft X-ray region.

射频束流位置监测器的实验测量

储建华　童德春　赵振堂

关键词　射频 BPM，二极模，S 参数，位置灵敏度，波导

根据上海深紫外自由电子实验装置对高精度束流位置监测器的要求,设计并加工出一射频束流位置监测器,已完成冷测实验。本文给出测试结果，并对一些特性进行了分析。所获得的主要测试参数与理论分析吻合，并验证了共模抑制的有效性。选择用做束流偏移测量的模式在束孔中心 ±2 mm 范围内分辨率达 11.42 dB/mm，并且具有很好的线性度。

Test measurements of an RF beam position monitor

CHU Jianhua　TONG Dechun　ZHAO Zhentang

Key words:　RF-BPM, Dipole mode, S-parameter, Position sensitivity, Waveguide

RF cold tests of a copper prototype RF-BPM to be used in the Shanghai deep UV FEL test facility are described. The test results are given and some characteristics are discussed. Main parameters obtained are in reasonable agreement with analytical estimations. Effective suppression of the common mode id demonstrated. The position sensitivity over a ±2 mm region is about 11.42 dB/mm for the mode, and is linear in the central region of the BPM cavity.

Fig.1　RF-BPM cavity

飞秒加速器波荡器 THz 波段辐射研究

卑 华 戴志敏

关键词 超辐射，滑移，群速度，振荡器，边带效应

飞秒加速器波荡器采用 EPU 磁铁，设计波段在 THz 范围。为优化辐射功率，先用 Bonifacio 的一维理论计算 EPU 作为噪声起振放大器的功率，虽周期较少而功率很低，但可看出 EPU 工作在超辐射状态。因此将波荡器做成振荡器类型，用 Gover 超辐射振荡模型计算辐射功率、抽取效率、增益、饱和时通过次数、优化的腔镜的透射率。此计算考虑腔体损失为零，因此还须考虑腔体因素。为抑制 THz 长波段辐射的较大衍射损失，分别采用波纹波导、槽波导来限制波，同时计算色散特性，导出波的群速度以及与之相关的波的滑移。

THz rays in undulator of a femtosecond accelerator

BEI Hua DAI Zhimin

Key words: Superradiance, Slippage, Group velocity, Oscillator, Sideband effect

We have adopted EPU-type magnets in a femtosecond linac for generating THz radiations. In order to optimize the radiation power, we used Bonifacio's 1D theory to calculate the power of EPU radiation oscillating from the noise. The power was low because of the short length undulator, which was found to work in the superradiant state. Therefore, the undulator should be designed as an oscillator. By using the Gover's modal, we calculated the power, extraction efficiency, gain and the pass number at saturation, and optimized the out-coupling mirror power transmission factor. On the other hand, the diffraction loss in the long wavelengths should be reduced, hence the consideration of corrugated waveguide and groove guide. And the dispersive characteristics can be deduced which ultimately determine the group velocity and the slippage of wave.

LINAC 单边耦合器中场的不对称研究

李 烜 赵明华

关键词 耦合器，束流发射度，相位，振幅，二极场项

先进光源对束流横向品质要求越来越高，单边耦合器中场的不对称越来越成为束流横向品质提高的一个瓶颈。耦合腔内的多极场会产生对束团的横向 kick，导致束流的横向发射度的变坏，其最主要的影响来自二极场。我们用电磁仿真软件 HFSS 模拟了单边耦合器中场的相位和振幅的不对称，找到了与理论相对应的场的不对称的存在。

Field asymmetry of single-feed coupler in an RF LINAC

LI Xuan ZHAO Minghua

Key words: Coupler, Emittance, Phase, Amplitude, Dipole field

An advanced light source imposes increasingly stringent requirements on electron beam quality. Single-feed coupler became an important factor of hindering beam quality. The time dependent multi-pole field in the coupler induces a transverse kick along the bunch and causes emittance degradation, which is dominated by the phase related dipole term. HFSS was used to simulate amplitude and phase asymmetry of single-feed coupler. The simulation results show that evidence corresponding to the the-ory.

高效率隔离型准谐振 24V 1A 开关电源的实现

李 瑞　卢宋林　胡志敏　李德明

关键词　效率，准谐振，电磁干扰

分析了单端反激准谐振式开关电源的工作原理及实现方法，给出了关键电路的通用设计原则，剖析了开关损耗产生的机理及减小的措施，最后结合 IR 公司芯片 IRIS4015 在一台高效率隔离型准谐振 24V 1A 开关电源上实现，给出了完整图纸和测试波形。

Realization of the 24V1A isolating power supply of high efficiency quasi-resonant　switching mode

LI Rui　LU Songlin　HU Zhimin　LI Deming

Key words:　Efficiency, Quasi-resonance, Electro-magnetic interference (EMI)

The principle and realization of fly back quasi-resonant switching mode power supply are de-scribed in this paper. The general design consideration for some key circuits is presented, the cause of power consumption on MOSFET on-off is anatomized and the means of reducing it are put forward. Then a 24V 1A high efficiency isolating quasi-resonant power supply with the SMPS chip IRIS4015 produced by IR Company is realized, and relevant circuit diagrams and operating waveforms are given.

新型 PID 校正技术在 2Hz 动态开关电源中的运用

李 瑞　卢宋林　陈焕光　李德明

关键词　磁铁电源，跟踪误差，PID 校正

上海光源(SSRF)中的增强器磁铁电源要求输出 2 Hz 的偏置正弦波，对参考曲线的跟踪误差小于 0.1%。通常情况下，该电源的补偿回路会采用双闭环调节电路。本文结合仿真分析和理论计算，采用了独创的 PID 校正技术，并在一台 100A/100V 的电源上实现，电路简单，效果明显。

Novel PID technique for a 2 Hz dynamic switching power supply

LI Rui LU Songlin CHEN Huanguang LI Deming

Key words: Magnet power supply, Control error, PID compensation

The power supply output current of the booster magnet in Shanghai Synchrotron Radiation Facility (SSRF) is a 2Hz offset sine waveform which has the 0.1% control error between output current and reference. Usually, this kind of power supply needs two control loops, namely, one voltage and the other current. According to simulation and theory analysis, a novel PID technology was accomplished in a 100A/100V 2 Hz dynamic switching power supply. It has simple circuit but wonderful effect.

大功率增强器磁铁电源输入功率控制方案

卢家林* 罗来明* 石 涛* 白小青* 李 瑞 李德明

关键词 增强器 磁铁电源 功率控制

提出了一种新型的增强器磁铁电源输入功率控制方案，新方案在输入整流器与输出斩波器之间加入升压斩波器，通过实时地控制升压斩波器输入滤波电感的电流波形，有效地抑制了增强器磁铁电源输入功率的低频波动，降低了电源对电网的电流冲击。新方案的有效性已经在 2 Hz 600A/600V 增强器磁铁电源样机上得到证实。

A novel input power control strategy for high-power booster synchrotron magnet power supply

LU Jialin* LUO Laiming* SHI Tao* BAI Xiaoqing* LI Rui LI Deming

Key words: Booster synchrotron, Magnet power supply, Power control

This paper presents a novel input power control strategy for high-power booster synchrotron magnet power supply. A booster DC-DC chopper is staged in series between the input rectifier and the output chopper in the novel strategy and the input inductance current of the booster DC-DC chopper is controlled instantaneously. Thanks to this scheme, the low frequency pulsation of the mains power and current is restrained effectively. The validity of the proposed control scheme has been verified on a 2 Hz 600A/600V experimental prototype.

*西安爱科电子有限责任公司

基于 PLC 的 110 MW 脉冲调制器控制器设计

袁启兵 谷鸣 陈志豪 闫山川 傅禄新 范学荣

关键词 脉冲调制器，PLC 可编程控制器，安全联锁，高压恒流充电电源

本文论述了中国科学院上海应用物理研究所所建的 110 MW 脉冲调制器控制器的设计。控制器核心采用 PLC 可编程控制器。控制器实现了对调制器联锁信号、电路状态信号的实时监测，闸流管预热系统、速调管预热系统等流程的控制，高压恒流充电电源的控制以及与加速器控制室的数据通信。

Design of 110 MW PLC-based pulse modulator's controller

YUAN Qibing GU Ming CHEN Zhihao YAN Shanchuan

FU Luxin FAN Xuerong

Key words: Pulse modulator, PLC, Security interlock, H.V.CCPS

In this paper, we describe the design of 110 MW pulse modulator's controller constructed at Shanghai Institute of Applied Physics, CAS. The controller core adopts PLC (Programmable Logical Controller) to accomplish the following tasks: real-time monitoring of modulaor interlock signal and circuit status signal, procedure controlling of thyratron preheat system and klystron preheat system, controlling of H.V.CCPS, and communications of the accelerator control room.

SSRF 增强器引出凸轨磁铁研制

谷 鸣 刘 波 欧阳联华 陈 嵘

关键词 上海光源，注入引出，凸轨磁铁

上海光源(SSRF)增强器注入系统由一块切割磁铁和一块冲击磁铁组成；引出系统由一块薄切割磁铁、两块厚切割磁铁、三块凸轨磁铁和一块冲击磁铁组成。3 块凸轨磁铁结构相同，最大强度为 2.91 mrad，由此推得最大积分场为 3.3973 T·cm。重复频率 2 Hz，孔径为 50 mm×26 mm。磁场波形为半正弦，脉冲底宽 200 ms。铁芯为 C 型，由 0.5 mm 矽钢片叠成。磁铁最大电流 60 A，线包采用自然冷却，外表环氧浇注，外表环氧层厚 1.5 mm。选用聚酰亚胺漆包铜线(5.6×3.0 mm)，48 匝。磁铁铁芯长 300 mm，磁铁总长 400 mm。

委托上海克林技术开发有限公司加工，2006 年 11 月 15 日完成生产工艺制定，2007 年 4 月 10 日完成全部磁铁的加工、组装、检测。测量结果表明，磁场中心线±25 mm 范围内的积分场均匀性好于±4‰，积分场强度满足物理需求，磁铁尺寸符合设计要求。这四块磁铁完全满足工程需求，将在验收后直接应用于上海光源增强器的引出系统。

Development of SSRF booster bump magnets

GU Ming LIU Bo OUYANG Lianhua CHEN Rong

Key words: SSRF, Injection and extraction, Bump magnet

SSRF booster injection system consists of one septum and one kicker system, while the extraction

system consists of one thin septum, two thick septum magnets, three bump magnets and one kicker magnet. According to the booster extraction system, three bump magnets are designed identically. The maximum deflection angle required is 2.91 mrad, then the maximum integral field should be 3.3973 T·cm. The repetition rate is 2 Hz, and aperture is 50 mm × 26 mm. Waveform is half sine with pulse width 200 ms.

Simulations were done with POISSON, OPERA 2D and OPERA 3D. The magnet is C-type, and the core consists of 0.5 mm thick SI steel sheets. The maximum current allowed is 60 A. The coil has no special cooling, glued with epoxy coating of 1.5 mm. The coil is made of 5.6 mm×3.0 mm polyimide lacquered copper wire. In order to satisfy the requirements of field, power supply and cooling, one magnet has total 48 turn windings separated into two parts. Length of magnetic core is 300 mm, and the total mechanical length is 400 mm.

A contract was made with a local company to finish the fabrication, including 4 bump magnets. The production process started in Nov. 2006, and finished in Apr. 2007. After machining, assembling and testing, all magnets are transported to SINAP. Magnetic field measurements were done in SINAP. The results show that the homogeneity of integral field is better than ±4‰ in center ±25 mm region, and the strength satisfies physical requirement. Measurement of the dimensions also shows good consistency with design value. These bump magnets satisfy the engineering requirements, and will be installed into the tunnel and used for SSRF booster extraction after being formally checked and accepted.

SSRF 注入引出切割磁铁样机研制

谷 鸣 欧阳联华 刘 波 陈 嵘

关键词 上海光源，注入引出，切割磁铁，磁场测量

上海光源(SSRF)增强器注入、引出和储存环注入均需切割磁铁，它们的结构与工作原理基本相同，增强器引出厚切割磁铁和储存环注入切割磁铁的磁长度、磁场强度、电感、脉冲电压、脉冲电流等参数也相近。为此，特选该厚切割磁铁作为样机进行研制。

委托中科院沈阳科学仪器研制中心有限公司制造该厚切割磁铁与磁铁真空室。切割磁铁为涡流型，磁芯采用 JFE 的无取向矽钢片 10JNFH，矽钢片厚 0.10 mm，双面涂层，硅含量 6.5%；励磁线圈 1 匝；涡流切割板为无氧铜。真空箱为不锈钢质圆筒形，内径 400 mm；设计真空度为 5×10^{-6} Pa，用两台 400 L/s 离子泵。

该公司于 2006 年 6 月 14 日完成生产工艺的制定，12 月 7 日完成磁铁和真空箱加工、组装和检测，运抵上海。对该设备磁铁进行了磁场测量，点测和积分线圈测量表明，主场均匀性好于 1‰，离切割板 4 mm 处漏场小于 3‰，满足工程需要。另外，用 Faro 测量臂进行了尺寸和位置测量调整。在此基础上通过了工程验收。

Development of eddy current septum magnets for injection and extraction at SSRF

GU Ming OUYANG Lianhua LIU Bo CHEN Rong

Key words: SSRF, Injection and extraction, Septum magnets, Magnetic field measurement

Septum magnets are used at SSRF for injection and extraction of the booster, and for injection of the storage ring. They are of the eddy current type in the same structure. The thick septum magnets for booster extraction and storage ring injection have similar parameters, and a prototype magnet was developed. This, including the vacuum chamber, was done in collaboration with the Shenyang KeYi Technology Development Co., Ltd. (SKY). The magnetic core is laminated with about 5700 steel sheets (10JNEX900), which are non-oriented and double coated 0.1mm thick iron with 6.5% Si content, to ensure a low core loss and high permeability at high frequencies. The vacuum chamber is ID 400 mm cylinder, made of 304L SS. Its UHV of 5×10^{-6} Pa is achieved by two 400 L/s SIPs.

SKY finished manufacturing all the magnets and vacuum chamber in December 2006, when they were assembled, tested and shipped to SINAP. Magnetic measurements were made using both point coil and integral coil. The results showed that the main field transverse homogeneity was better than 1‰, and the field leakage at 4 mm from the septum wall was less than 3‰. Considering that a magnetic shielding material will be added later, the leakage is low enough to satisfy the requirement for storage beam. Faroarm was used to measure the dimensions and positions of the magnets and vacuum chamber. After that, a check and examination were done by SSRF relevant department and finally the magnets and vacuum system were accepted by SSRF.

SSRF 增强器注入引出冲击磁铁样机研制

谷 鸣 刘 波 欧阳联华 陈 嵘

关键词 上海光源，注入引出，冲击磁铁

上海光源(SSRF)增强器注入系统冲击磁铁于 2006 年初启动样机研制。两块冲击磁铁都采用集中参数型铁氧体铁芯结构，整体放置于真空箱内部，基本结构保持一致。物理设计要求注入冲击磁铁偏转束流 9.26 mrad，引出冲击磁铁偏转束流 1.64 mrad，对应的场强分别为 0.0116 和 0.0240 T；有效孔径为 50mm×26mm。注入冲击磁铁铁芯长 390 mm，真空箱总长 762 mm；引出冲击磁铁铁芯长 800 mm，真空箱总长 1143 mm。

委托中科院沈阳科学仪器研制中心有限公司加工冲击磁铁样机与配套真空箱。真空箱为不锈钢质圆筒形，内径 350 mm；设计真空度为 5×10^{-6} Pa，注入和引出冲击磁铁分别使用一台和 2 台 400 L/s 离子泵。2006 年 12 月 7 日完成磁铁和真空箱加工、组装、机械和真空检测、抽真空后，运抵上海。对设备进行了磁场测量，点测和积分线圈测量表明，场均匀性好于 1%，积分场强度满足物理需求。另外，使用 Faro 测量臂对磁铁的尺寸和位置进行了测量和调整。注入和引出冲击磁铁真空箱的真空度分别达到了 6.8×10^{-7} Pa 和 1.4×10^{-6} Pa。两块磁铁样机完全满足工程需求，将直接应用于上海光源增强器的注入引出系统。

Prototype of SSRF booster kicker magnets

GU Ming LIU Bo OUYANG Lianhua CHEN Rong

Key words: SSRF, Injection and extraction, Kicker magnet

Development of the kicker magnets of SSRF booster injection system started in March 2006. They are lumped ferrite inductance magnets with window-frame, constructed with nickel-zinc ferrite in an ID 350 mm vacuum chamber, where the magnet is fixed with four adjustable supports. The deflection angle for injection kicker and extraction kicker is 9.26 and 1.64 mrad, corresponding to magnetic field of 0.0116 and 0.0240 T, respectively. Magnet aperture is 50mm×26mm. Magnetic field analysis was simulated with POISSON, OPERA 2D and OPERA 3D. In a total length of 762 mm, core length of the injection kicker is 390, while the respective sizes of the extraction kicker are 800 and 1143 mm.

The prototype kickers and relevant parts were manufactured by the Shenyang KeYi Technology Development Co., Ltd. (SKY). The kicker chambers use three 400 L/s ion pumps, one for the injection kicker and two for the extraction kicker, to achieve 5×10^{-6} Pa vacuum. In December 2006, after finishing the machining, assembling, vacuum processing and mechanical tests, the magnets with vacuum chambers and supports were shipped to SINAP. Magnetic field measurements were done in our laboratory. The results of point coils and integral coils measurement show that the homogeneity is better than 1% and the integral field strength can meet the physical requirement. The dimensions and position of magnets inside chamber are also measured and adjusted with Faro arm. Vacuum of chambers for injection kicker and extraction kicker is 6.8×10^{-7} Pa and 1.4×10^{-6} Pa, respectively. The prototype magnets were checked and accepted based on the measurement results. These two kicker magnets satisfy the engineering requirements, and will be installed into the tunnel and used for SSRF booster injection and extraction.

上海光源场地地基振动测量与分析

欧阳联华 卜令山 陈建辉

关键词 束流稳定性，地基振动，功率谱密度，积分位移

上海光源（SSRF）是一台正在建造中的第三代同步辐射光源。为了达到其设计指标，该光源需在非常稳定的条件下运行；即使非常微弱的振动都会导致光束的不稳定。

上海地区是冲积平原，软土层厚达 300 m 以上；该土层对地脉动有放大作用；另外，因为稠密人口引起的人类活动如交通、工厂、建筑等也形成较强的“文化噪音”；在这样的条件下建造如此高性能的光源是一项巨大的挑战。

在光源建造过程中对场地进行了多次微振动测量；其中有 SSRF 单独进行的，也有和 DESY 合作的。本文给出了双方的测量设备、数据处理方法和结果（功率谱密度，积分位移）。另外，本文对振动对 LATTICE 的影响也进行了计算。

Ground vibration measurement at SSRF site and their effect evaluation

OUYANG Lianhua BU Lingshan CHEN Jianhui

Key words: Beam stability, Ground vibrations, Power spectral density, Integrated displacement

SSRF is a 3rd generation light source which is now under construction. In order to give full scope of its ability, it has to be operated in very stable conditions. Even slight movements of magnetic elements of the accelerator may lead to problems with beam stability.

It is a very challenging task to build an advanced 3rd generation light source on soft soil at urban Shanghai area where over 300 meters deep alluvion has an amplified effect on microseism, and the activities caused by the dense population give rise to high level cultural noises.

Vibration measurements have been carried out at SSRF site as a collaboration between SSRF and DESY. Both sides used their own measurement systems and data processing programs, and the results (power spectral density, integrated displacement) match well by comparison.

The predicted effect of the vibration on the SSRF lattice is also calculated.

模拟有源积分器在脉冲磁场测量中的分析和应用

彭程程 谷 鸣 刘 波 欧阳联华 范学荣

关键词 积分器，注入，引出，脉冲磁场

本文介绍了应用于脉冲磁场测量系统中的模拟有源积分器的研制。针对测量系统的需求和精度要求，设计了积分电路，并对实际有源积分电路的设计参数和器件参数做了误差分析，论证了电路的可行性和合理性，并给出了合理电路设计的有关参数和误差控制范围。电路实验和测试表明，脉冲磁场测量模拟有源积分器电路达到了设计要求，满足磁测系统需求。

Analysis and application of analog active integrator in pulse magnetic field measurement

PENG Chengcheng GU Ming LIU Bo OUYANG Lianhua FAN Xuerong

Key words: Integrator, Injection, Extraction, Pulse magnetic field

An analog active integrator was developed for measuring pulsed magnetic field. To meet the measurement system and precision requirement, the integral circuit has been designed and the errors of real active integral circuit parameters have been analyzed. The rationality of the proposition has been proved and some relative parameters required for rational design so that errors can be kept within the permissible range have been given. By the circuit experiment and test, it is verified that this analog active integrator can meet the design requirement in the pulse magnetic field measurement system.

SSRF 储存环注入脉冲电源的设计

范学荣 陈志豪 傅禄欣 袁启兵 谷 鸣

关键词 固态开关，脉冲电源，高稳定性

本文介绍了采用固态半导体放电开关实现的 1.7 kV、10 kA 的 septum 电源和 7.8 kV、3.7 kA 的 kicker 电源，详细分析了两台脉冲电源的电容器充电电源、脉冲放电开关、放电回路结构、热漂移校正等问题。原型样机的结果表明，其电流幅度稳定性都优于±0.1％，其他主要指标均可达到设计要求。

Development of the pulsed power supply for injection of the SSRF storage ring

FAN Xuerong CHEN Zhihao FU Luxin YUAN Qibing GU Ming

Key words: Solid-state switch, Pulsed power supply, High reproducibility

Based on solid-state switches, two pulsed power supplies for injection of the SSRF storage ring were developed, i.e. a 1.7 kV 10 kA pulser for the septum magnet and a 7.8 kV 3.7 kA pulser for the kicker magnet. The charging power supply, the discharging switch, the structure of the discharging circuit, and feed-back of current are discussed in this paper. The prototypes and the simulation show that reproducibility of the current waveform is <0.1%, which meets requirement of the design.

电子直线加速器调节器防护效力的分析和测量

李长兴 谷 鸣 陈志豪 袁启兵 范学荣

关键词 电子直线加速器，脉冲调制器，屏蔽效能，电磁干扰

高功率脉冲调制器是电子直线加速器(LINAC)的功率源。脉冲调制器在运行中会产生很强的电磁干扰。为了满足上海光源 LINAC 的高精度要求,脉冲调制器必须尽量抑制这些电磁干扰。本文介绍对上海光源 150MeV 高性能 LINAC 调制器的电磁辐射抑制的分析研究和测试。分析了电磁辐射的泄漏途径,对调制器机柜的屏蔽效能进行了定性、定量分析,并进行了测试。验证了调制器机柜的 EMC 设计制作对电磁干扰抑制的有效性。

Analysis and measurement of shielding effectiveness of LINAC modulator cabinet

LI Changxing GU Ming CHEN Zhihao YUAN Qibing FAN Xuerong

Key words: Linac, Pulse modulators, Shielding effectiveness, Electromagnetic interference (EMI)

The high-power pulse modulator of the SSRF linac, when it is in operation, will produce strong electromagnetic interference. To meet the EMC requirements for high performance linac operation, the pulse modulator should be shielded. The electromagnetic radiation interference produced by the linac modulators was studied. Possible leak paths, shielding efficiency and measurement of the modulator's EMI were analyzed. The results show that the EMC design of the modulator cabinet can restrain the electromagnetic interference.

上海光源存档数据分析系统的 Web 服务接口

李 林 沈立人 祝 晴 万天敏

关键词 XML，Web Service，接口，数据库，.NET，EPICS，AO

加速器数据库主要保存加速器各类静态参数和运行时的实时数据。上海光源使用关系数据库保存各类数据。我们开发了基于 XML Web 服务的数据分析服务系统以提供对历史数据和实时数据的分析访问接口，包括底层数据获取和适用于加速器物理分析的接口，对调用每种接口的各种客户端给出样例，提供给用户对存档数据的浏览、检索、绘图等功能，并对 Web 服务的功能、负载和性能进行了测试。

Web Services interface of SSRF archive data analysis system

LI Lin SHEN Liren ZHU Qing WAN Tianmin

Key words: XML, Web Service, Interface, Database, .NET, EPICS, AO

Accelerator database stores various static parameters and real-time data of accelerator. SSRF (Shanghai Synchrotron Radiation Facility) will adopt relational database to save these data. We develop a data retrieval system based on XML Web Services for the access of archive data, including bottom layer interface and interface applicable for accelerator physics as well as client samples exemplifying how to consume the interface. Users can browse, retrieve and plot data by the client samples. Also, we give a method to test its stability. The test result and performance is described.

基于网络串行设备转换器的嵌入式 EPICS 控制器

蒋舸扬　沈立人

关键词　嵌入式 EPICS 控制器，Ethernet/Serial 转换器，Monta Vista Linux

上海光源(SSRF)控制系统采用 Ethernet 作为系统主干网络。所有的串行设备都由 Moxa 公司网络串行设备转换器连接到 Linux IOC 上。在 SSRF 的预研阶段，该转换器仅由固件中的程序提供网络数据到串行数据的转换功能，而控制逻辑都在其它 Linux IOC 上实现。为此，我们针对光源使用的多种串口设备开发了相应的基于 Netdev 的运行在 Linux IOC 上的 EPICS 异步通讯程序。

最近，Moxa 公司升级了他们的产品，新型号采用更强劲的 Intel Xscale CPU 替代老的 arm9 CPU，同时采用 Monta Vista Linux 作为嵌入式操作系统。随机所带的 Monta Vista Linux 交叉编译器提供给用户二次开发可能，从而诞生了我们将原本运行在 Linux IOC 上的 EPICS 控制程序移植到该嵌入式设备的想法。因为最终我们决定采用新的串口服务器型号而且 EPICS 控制程序必须运行在 EPICS 核心程序上，所以必须设法移植 EPICS IOC 核心程序到新的 Monta Vista Linux 平台，从而使每台串口设备转换器成为 Linux IOC。该种方式最大的优点就是不必修改已有的各种 EPICS 设备驱动，同时使整个控制系统架构变得更简练和为将来的多层次扩展提供便利。本文描述所需整合工作的技术细节和完成后的设备运行情况。

An embedded EPICS controller based on ethernet/serial box

JIANG Geyang　SHEN Liren

Key words:　Embedded EPICS controller, Ethernet/Serial Box, Monta Vista Linux

The control system of SSRF takes the Ethernet as backbone. All kinds of serial devices such as vacuum pumps are connected to Linux IOCs via a kind of Ethernet/serial box made by Moxa Inc.. In the pre-research stage of SSRF, the old model of this Ethernet/serial box was only a simple Ethernet/serial protocol converter which was functioned by firmware. Aim to this, we have developed several kinds of EPICS device drivers based on NetDev for our serial devices.

Recently, Moxa Inc. has upgraded the converter by replacing old arm9 CPU with a more powerful Intel Xscale CPU. It supports Monta Vista Linux as its embedded OS, also cross-compiler is provided to make further development available. Since we have decided to use the new model of converter in our facility finally, we manage to port EPICS IOC core on Monta Vista Linux and implement the same function on the new converter as old one's to avoid modifying existent EPICS device driver. By these, the dedicated Linux IOC can be omitted and the whole system can be more efficient and expandable. Details of the necessary integration work and initial operation experience will be discussed in this paper.

上海光源数据存档引擎的设计与实现

祝 晴 蒋舸扬 李 林 沈立人

关键词 实验物理和工业控制系统，Channel Archiver，XML，数据存档

EPICS 是大型加速器装置普遍采用的分布式控制系统软件平台。Channel Archiver 为 EPICS 自带数据存档工具集，主要用于实现对试验数据的快速存取和检索，作为其核心的 Archive Engine，专门负责数据的存档工作。通过对 Archive Engine 的分析，提出其应用于上海光源的不足之处。针对这些不足我们结合最新的 XML 技术对存档引擎进行了修改，并测试了修改后的引擎。

Design and implementation of archiver engine based on XML technology for SSRF

ZHU Qing JIANG Geyang LI Lin SHEN Liren

Key words: EPICS, Channel Archiver, XML, Data archive

EPICS is the most popular platform to build control system in modern physics experiment facilities. As an archiving toolset for EPICS, Channel Archiver is used to store and retrieve data. Archive Engine is the core of Channel Archiver in data storage. In this paper, Archive Engine was analyzed, and some defects were proposed when applied in SSRF. Aiming at these defects, improvement was made and XML technology was combined with. The improved engine was tested.

加速器束团长度测量

黄国庆 叶恺容

关键词 束团长度测量，条纹相机，迈克尔逊干涉仪，频域

随着技术的不断发展，近年来出现了多种加速器束团长度的测量方法，主要有条纹相机测量、迈克尔逊干涉仪测量、电光晶体测量、耦合束流频谱测量等。本文综合介绍了这些方法，并指出各种方法都有自己的优缺点及适用范围。目前国际上各大型加速器实验室普遍采用的是条纹相机测量方法，对于自由电子激光等超短束团一般都是采用光学技术、频域方法测量，有些测量法的分辨率可达到飞秒级，提供了具有更高空间分辨率、更高时间分辨率的强有力研究手段。

Bunch length measurements for accelerators

HUANG Guoqing YE Kairong

Key words: Bunch length measurements, Streak camera, Martin-Puplett interferometer, Frequency domain

With the improvement of accelerator technology, many new methods for bunch length measurement were invented, such as streak camera, Martin-Puplett interferometer, electro-optic detection, frequency domain method. Each method has its respective advantages, disadvantages and applied domains. A review on various bunch-length measurement methods is given in this paper. At present many large accelerators in the world universally use streak camera to measure bunch length. For beam bunches of ultrashort duration, optic technology and frequency domain method are adopted, and the resolution of some methods can reach to the order of femtosecond.

加速器束团长度频谱法测量系统设计

黄国庆　周伟民　叶恺容

关键词　束团长度测量，软件无线电，数字下变频，数字信号处理，VME 总线

本文采用的是耦合束流频谱测量方法来测量束团长度，即将拾取电极（如条形电极、纽扣电极）安装在真空室壁内，拾取束流产生的电磁场，分析其频谱，从而得到束团长度信息。其具体方法是测量出束团频谱的两个频率成分的幅度比来得到束团的长度。

Design of bunch length measurement using beam spectrum

HUANG Guoqing　ZHOU Weimin　YE Kairong

Key words: Bunch length measurement, Soft defined radio, Digital down converter, Digital signal processing, VME

For measuring the bunch length, the amplitude ratio of two frequency components in the beam spectrum is picked up from the stripline. This gives the bunch length. Being similar to digital beam position monitor, the system uses the soft-defined radio, adopts a high speed and high resolution ADC straight sampling the middle frequency band signal. It saves some analog devices, which cause errors. Another advantage of the system is real-time measurement of the bunch length. The work is of help for development of accelerator technology.

数字 BPM 处理器的 EPICS 接口研发

阎映炳　冷用斌　刘德康　陈永忠　殷重先

关键词　EPICS, Libera, BPM, FPGA

上海同步辐射装置(SSRF)的束流诊断系统将采用新一代的电子束流位置监测设备 --- Libera 来进行束流轨道的信号处理和数据采集。为了最终数据的共享和整机的控制，我们在供应商提供的控制系统编程接口(CSPI)基础上为该设备开发了 EPICS 接口。这样，用户可以通过 EPICS 通道来实时监测电子束流的性能。在该接口中，我们专门开发了一个新的 EPICS 记录和相关的设备支持模块。

EPICS interface to Libera electron beam position monitor

YAN Yingbing LENG Yongbin LIU Dekang CHEN Yongzhong YIN Chongxian

Key words: EPICS, Libera, BPM, FPGA

SSRF diagnostics system will adopt a new generation digital electron beam position processor --- Libera, as the signal condition, signal processing and data acquisition device for beam position monitor. In order to provide a uniform data & control interface for users, we developed an EPICS interface based on Control System Programming Interface (CSPI) layer, allowing the performance of the electron beam to be monitored through EPICS channels. In this interface a new record type for BPM was defined and its associated support routines were implemented.

上海光源储存环直流流强监测系统设计

冷用斌 周伟民 陈永忠 赵国璧 余 俊 刘德康

关键词 上海光源，直流流强变压器，EPICS，束流寿命

上海光源储存环调试运行需要一个分辨率达到微安量级的直流流强监测系统。为此设计完成的硬件系统包含一个 Bergoz 公司 NPCT 型探头、一个 NI 公司 PXI 总线数字电压表模块以及一个 PXI 总线的输入输出控制器。数据采集处理软件在 LabVIEW 平台上开发，与控制系统的接口通过 EPICS Shared Memory IOCcore 技术实现。实验室测试及仿真结果表明该系统直流流强测量分辨率可达 2 μA，束流寿命相对测量精度可望达到 0.5%。

DCCT system design for SSRF storage ring

LENG Yongbin ZHOU Weimin CHEN Yongzhong

ZHAO Guobi YU Jun LIU Dekang

Key words: SSRF, DCCT, EPICS, Beam lifetime

A precise DC current transformer (DCCT) system is a must for commissioning and operation of the storage ring of Shanghai Synchrotron Radiation Facility (SSRF). Hardware of the system to be completed consists of a Bergoz NPCT sensor, an NI PXI digital voltage meter and a PXI controller. The software was developed on LabVIEW platform to communicate with accelerator control system via EPICS Shared Memory IOCcore interface. Bench test and simulation results of the DCCT showed that 2 μA resolution for DC current measurement and 0.5% relative accuracy for beam lifetime measurement could be achieved.

100MeV 直线加速器束流位置探测器系统设计

殷重先　叶恺容　周伟民

关键词　BPM 前端电子学，BPM 系统，100 MeV 直线加速器

100 MeV 直线加速器束流位置探测器系统包括 BPM(beam position monitor)、BPM 前端电子学、基于束流的准直模块(beam based calibration, BBC)、高频信号切换模块和 AD 模块。本文详细介绍了 BPM 前端电子学和数据采集系统设计。最后给出了在 100 MeV 直线加速器中测试的 BPM 系统性能。

Beam position monitor system design in 100MeV linac

YIN Chongxian　YE Kairong　ZHOU Weimin

Key words:　BPM electronics, BPM system, 100 MeV linac

The BPM system in 100 MeV linac includes BPM (Beam position monitor), BPM front-end electronics, BBC module, RF switch module and AD module. The BPM front-end electronics and the detailed design of the data acquisition system are presented in this paper. Then, the testing results for BPM system's performance in linac operation are introduced.

AWE 中的 Commands 对象在热分析中的应用

徐中民　王纳秀

关键词　AWE，APDL，Commands，热流密度

Ansys WorkBench Environment (简称 AWE) 具有友好的用户界面，提供了良好的有限元前后处理以及优化设计等功能，对于熟悉经典 Ansys 的工作人员提供更为便捷的分析手段。但是由于在 AWE 的 DesignSimulation 模块仅能对几何元素进行载荷和边界条件的加载，对于非线性载荷的分析通常是将模型导入经典 Ansys 中才能进行。而分析完成的数据也不能再返回 AWE 中，这样一来就不能很好利用 AWE 的后处理和优化功能。 通过在 AWE 的 Commands 对象中直接添加 APDL 语句，实现了在简化反射镜模型上非均匀热流密度载荷的加载，分析结果与导入到经典 Ansys 中的分析结果是完全一致的。该方法避免了 AWE 对于非均匀载荷通常需要导入经典 Ansys 所带来的不便，进而可以很好利用 AWE 的后处理及优化等功能，提高热分析的效率。

Application of Commands Object in AWE for thermal analysis

XU Zhongmin WANG Naxiu

Key words: AWE, APDL, Commands, Heat flux

Ansys Workbench Environment (AWE) provides user-friendly GUIs and excellent pre-/post- processing function, so it is convenient for engineers who are familiar with Ansys Classic. But Design-Simulation model integrated with AWE only can apply loads and boundary condition to geometry body. If a non-uniform load is needed to apply, this analysis must be export to Ansys Classic. Unfortunately, the post-processing data cannot be import to AWE and other functions such as post-processing and optimization function cannot be used, either.

By means of adding APDL commands directly to a Commands Objects in AWE (Ansys Workbench Environment), a non-uniform heat flux load is applied to a simplified model of mirror. The analysis results are absolutely same as those from Ansys Classic after the model is transferred to Ansys and is applied to the non-uniform heat flux load. Furthermore, this method can make use of the functions such as post processing and optimization in AWE, avoiding applying a non-uniform load in Ansys as usual. And this will help improve further the efficiency of thermal analysis.

基于 Tcl/Tk 语言的经典 Ansys 软件用户界面的二次开发

徐中民 王纳秀

关键词 Tcl/Tk，Ansys，用户界面，二次开发

利用 Ansys 软件进行有限元分析的过程中，有时需要许多参数和文件的输入和输出，借助于图形用户界面(GUI)可以方便用户的分析和操作，提高工作效率。Ansys 提供了用户界面设计语言(User Interface Design Language，简称 UIDL)，它是目前编写用户界面大多采用的开发工具。但是与 Visual C++、Visual Basic 等软件相比，利用 UIDL 编写出的界面功能有限，有时不能很好满足用户的要求。

针对 UIDL 语言在 Ansys 用户界面开发中的不足，我们选用 Tcl/Tk 脚本语言进行二次开发。重点介绍了窗口创建、组件添加、消息绑定以及和 Ansys 的通讯等。最后以光束线中计算功率密度的界面开发来举例说明。利用 Tcl/Tk 可以编写出更加紧凑的界面，能更好满足用户的需要。

Secondary development of user interface in Ansys Classic based on Tcl/Tk

XU Zhongmin WANG Naxiu

Key words: Tcl/Tk, Ansys, User interface, Secondary development

During the finite element analysis using Ansys Classic, input and output operations for parameters

and data files are often involved. By means of graphic user interface (GUI), it is helpful for engineers to improve working efficiency. Ansys provides a user interface design language (UIDL), which is mostly used by users. But its function of designing interface is limited, compared with others advanced languages such Visual C++ and Visual Basic. Sometimes, user's ideas can be finished using UIDL.

Tcl/Tk script language is used to develop user interface in Ansys Classic, because UIDL has some shortcomings in designing user interface. The methods such as creating a window, adding a widget, binding a message and communicating with Ansys are introduced especially. Finally, an example of designing dialog box used to calculate power density in beamline is given. Using Tcl/Tk, a compact user interface will be designed, which can meet the need of users.

内衬弹簧冷却槽晶体的热缓释研究

王纳秀　徐中民　刘 学

关键词　同步辐射，热缓释，晶体单色仪

研究了同步辐射光束线核心部件晶体单色仪的热缓释技术，重点在直接冷却晶体冷却槽内衬弹簧改善换热能力的实验研究，通过比较光滑和内衬弹簧冷却槽冷却结构晶体换热能力的差异，根据冷却槽内衬弹簧增大固液间换热系数的程度，确定晶体的热应变减小和晶体的热承受能力改善程度，给出晶体最佳吸收功率范围的实验依据。在不同的冷却水流量的条件下，有内衬弹簧的冷却槽和光滑冷却槽垂直晶面变形的测量结果表明，内衬弹簧冷却槽可降低垂直晶面变形的矢高，即内衬弹簧实现了增强固液间对流换热系数、达到降低晶体表面变形和改善晶体冷却效果的目的。

Study of cooling experimentation of the DCM crystal with spring in the circular cooling channel

WANG Naxiu　XU Zhongmin　LIU Xue

Key words:　Synchrotron radiation, Cooling, Double crystal monochromator (DCM)

We report a method of improving the solid-liquid surface heat transfer coefficient to enhance the heat transfer ability of the synchrotron radiation beamline crystal monochromator. Spring has been inserted the circular cooling channel. The experimental results of vertical distortion on crystal surface at different cooling condition show that the distortion of crystal with spring inserted is lower than the ones with smooth channel. We conclude that the heat transfer ability of channel with spring is better than that of the smooth channel, in the same thermal load or cooling conditions.

同步辐射 X 射线成像光束线劳厄双晶单色器设计

胡 雯　谢红兰　杜国浩　肖体乔

关键词　X 射线成像，同步辐射，劳厄晶体, 单色器设计

上海光源 X 射线成像及生物医学应用光束线，采用多极 wiggler 以获得大光斑尺寸、高通量密度和宽能区单色 X 射线，其高热负载是光束线设计的关键。此光束线由双晶单色器保证束线的单色光($\Delta E/E$~10^{-3})输出, 主要热负载在单色器上，故须降低其热负载。我们采用透射式劳厄双弯晶的单色器，选取两块不对称切割的 Si(111)晶体，采用柱状弯曲的劳厄几何无色散排列结构。本文讨论劳厄弯晶的聚焦特性，单色器的光学设计；计算了组合滤片及单色器上的热负载及输出光通量；讨论了单色器的冷却方案。结果表明，其可获得固定出口的平行单色光束，能量调谐范围 19~120 keV，33 keV 的光子通量及通量密度分别为 1.9×10^{13} phs·s^{-1} 和 3.8×10^{10} phs·s^{-1}·mm^{-2}。与传统双平晶方案相比，本设计在获得高通量和解决热负载等方面的优越性明显，能有效控制热形变。

Double Laue-crystal monochromator for an X-ray imaging beamline of SSRF

HU Wen　XIE Honglan　DU Guohao　XIAO Tiqiao

Key words: X-ray imaging, Synchrotron radiation, Laue-crystal, Monochromator design

An X-ray imaging beamline for biomedical applications requests high flux, large beam size and wide photon energy range, hence the need of a multi-pole wiggler. Monochromatic beam is recommended, as it is very difficult to get high flux and large beam size simultaneously while maintaining high performance of a double crystal monochromator (DCM). A new optical configuration of monochromator for X-ray imaging beamline, which allows one to obtain a parallel monochromatic beam with fixed exit by using two asymmetrically cut bent-crystals in Laue geometry, has been proposed. Based on the W14 multi-pole wiggler at SSRF, a preliminary design for the monochromator is described in this paper. The X-rays are tunable from 19 to 120 keV, with a flux density of 3.8×10^{10} phs·s^{-1}·mm^{-2} at 33 keV. The flux and energy resolution of the monochromator is estimated, and the heat-load can well meet the X-ray imaging experiments. The new configuration of monochromator, compared with traditional design in double flat-crystal, is more powerful in dealing with the high flux and high heat-load.

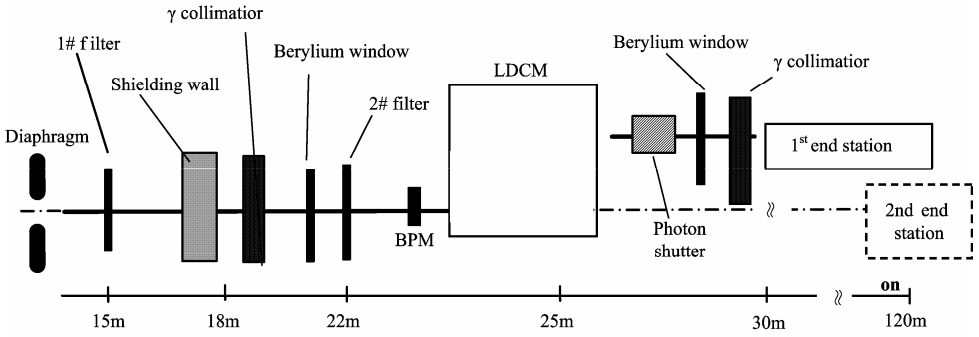

Fig.1 Beamline layout

上海光源 XAFS 光束线 QXAFS 数据采集系统的设计

邹 杨　姜 政　余笑寒　黄宇营　徐洪杰

关键词 SSRF，XAFS，QXAFS

上海光源采用快扫模式(QXAFS)进行时间分辨 XAFS 实验。XAFS 的普通模式和快扫模式的

积分时间分别为 1s 和 1ms，而透射模式信噪比 S/N=0.736×($\Delta u_A/u_A$)×(u_A/u_t)×$I_0^{0.5}$，则普通模式 S/N=23274，快扫模式 S/N=736，可见 QXAFS 模式仍有较好信噪比。QXAFS 采用有电流灵敏放大器(直接比较型 ADC)或电流灵敏放大器+V/F 转换器(间接型 ADC)。直接比较型 ADC 速度快，但数据信噪比低，不宜于低浓度样品；V/F 转换器的抗干扰能力强，可由增加积分时间提高数据精度，但转换速度慢，转换精度受计数器容量限制。此光束线的光子能量 3.5~53 keV，通量 10^{12}~10^{13} photons·s^{-1}· $(0.1\%bw)^{-1}$，其数据采集系统第一电离室的电流约为 1~40 μA，故增益在 10^7 量级的电流灵敏放大器已足够，我们拟采用 FEMTO 公司的 DHPVA-200 作为电流灵敏放大器。16 位精度(分辨率 2^{-16})的 ADC 可符合普通模式和快扫模式的上述信噪比条件，我们拟采用 hytec 公司的 ADC8401，其已用于瑞士光源的 XAFS 光束线。IK220 卡则作为普通 PCI 板卡用于读取双晶单色仪的马达的编码器中的角度数据。由于 RS232 接口的传输速度较慢，故拟采用 IEEE 488 标准的 GPIB 接口。

QXAFS data collecting system for XAFS beamline of SSRF

ZOU Yang JIANG Zheng YU Xiaohan HUANG Yuying XU Hongjie

Key words: XAFS, QXAFS

The quick X–ray absorption fine structure (QXAFS) will be used at SSRF for time- resolved XAFS experiments. Unlike conventional XAFS, QXAFS measures on-the-fly spectrum in a few seconds. The beamline will have a good flux of photon to measure dilute sample in QXAFS mode, but this demands better performance of the beamline instruments, because the S/N ratio is lower than conventional XAFS. In a transmission mode, the integration time is 1s for XAFS and 1ms for QXAFS, the S/N ratios are respectively 23274 and 736 according to S/N=0.736×($\triangle u_A/u_A$)×(u_A/u_t)×$I_0^{0.5}$. A QXAFS collects data in two ways, i.e. current amplifier + ADC, or current amplifier + V/F converter. The former converts fast, but its S/N ratio is too low to measure diluted sample, whereas the latter has better accuracy, but it converts slowly with the precision limited by capability of the counter.

The flux of 3.5~53 keV X-rays will be 10^{12} ~10^{13} photons·s^{-1}·$(0.1\%bw)^{-1}$, and at the first chambers of the collection system the current is 1~40 μA. Therefore, a FEMTO current amplifier of DHPVA-200 with 10^7 gain is good enough. An ADC of 16-bit precision (2^{-16} resolution) will satisfy the S/N ratio request mentioned above, hence the choice of the HYTEC ADC8401, which is in service on the XAFS beamline at SLS. The IK220 PCI board is used to record angle data from the rotary encoder, which is commonly used in several beamlines. As an RS232 interface is slower in data transfer, we chose GPIB interface which extends from IEEE 488 protoco.

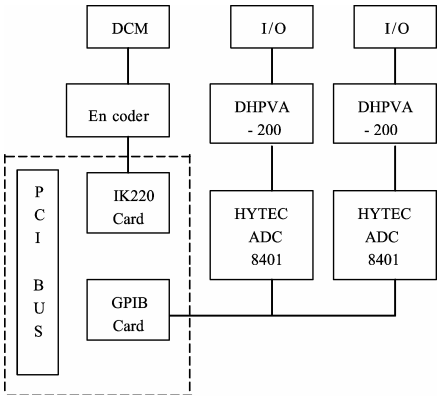

Fig.1 Scheme of the collecting system for SSRF XAFS beamline

梯形镜的优化研究

毛成文　余笑寒　肖体乔

关键词　梯形镜，椭圆，优化，斜率误差，有效长度

同步辐射光束线大多采用压弯镜系统来准直或聚焦。压弯镜是把具有一定形状的镜子用机械力压弯成圆柱面、椭圆柱面、抛物柱面和超环面等所需形状。初始形状对压弯镜面形能在多大程度上满足实际需要有很大影响。若精度要求不高，可采用类似长方体的镜块；若精度要求高，则采用变宽度或变厚度的镜体。如压弯成椭柱面，采用较易加工制作的梯形镜，能在一定尺度上满足较小的倾斜误差。但若倾斜误差须足够小，梯形镜能满足条件的有效镜面长度较为有限。我们分析了梯形镜压弯为椭柱面的倾斜误差分布，对镜面宽度变化作优化，亦即调整镜面的惯性距，使其在较长的尺度范围内保持足够小的倾斜误差。优化后的梯形镜(图 1)在适当位置改变其宽度变化系数(p = 5 m, q = 0.2 m, θ = 4 mrad)，犹如由三段梯形镜拼接而成。计算表明，对<1.0×10^{-7} 的倾斜误差，优化前后的有效镜面长度分别为 7.12 cm (x =–3.99 到 3.13)和 18.74 cm (x =–11.47 到 7.27)。

Optimization of tapered mirrors

MAO Chengwen　YU Xiaohan　XIAO Tiqiao

Key words:　Tapered mirror, Ellipse, Optimization, Slope error, Effective length

Synchrotron radiation beamlines are collimated and focused mostly by mirrors that are bended mechanically from mirrors in a given shape (*e.g.* taper) into cylindrical, elliptical, parabolic and super-annular shapes, *etc*. The original mirror shape, which decides the bending effect to a great extent, should be considered seriously. Block materials can be used as the original mirror if one requests no high surface precision. For surface of a small slope error, original mirrors with nonequivalent width or nonequivalent thickness are frequently of choice. In most cases, tapered mirrors are desirable to obtain elliptical surface. For even smaller slope errors, however, the effective length of the bending tapered mirror cannot be guaranteed. By analyzing the slope error distribution of the elliptical surface, we could solve the problem by optimizing the mirror's width distribution, hence the improved inertia moment of the tapered mirror. The shape-optimized mirror, with varying width coefficient at different locations, looks like a combination of three tapered mirrors. For a slope error of <1.0×10^{-7}, effective length of the optimized mirror (p = 5 m, q = 0.2 m, θ = 4 mrad) increased to 18.74 cm (x = –11.47 to 7.27) from 7.12 cm (x = –3.99 to 3.13) before the optimization.

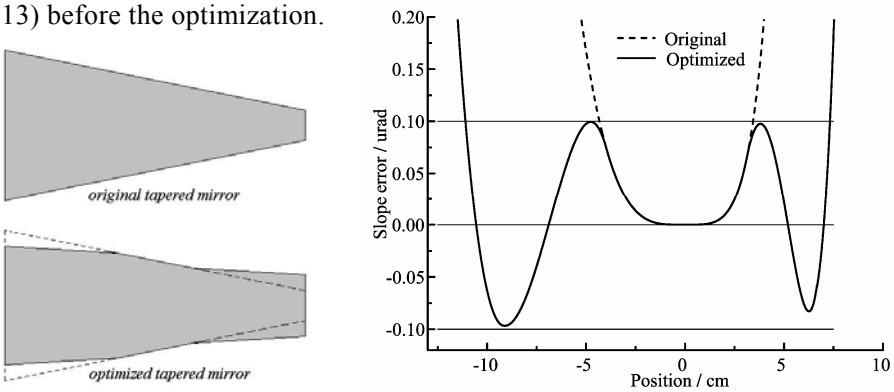

Fig.1　The optimized tapered mirror with improved slope error

混合物的太赫兹谱成分分析方法研究

张增艳　余笑寒　肖体乔　徐洪杰

关键词　THz 谱学，混合物成分分析，异构体混合物

太赫兹时域光谱(THz-TDS)技术可非常灵敏地探测物质分子结构的微小差异和变化, 具有反映物质分子结构的指纹特性。简单有效的 THz-TDS 分析方法在化学、材料、安全检查、质量监控等领域有潜在应用。本文将整个波段的 THz 吸收谱作为物质的指纹特征，给出其混合物成分定量分析方法。对同分异构体混合物分析结果表明，数据处理中考虑样品表面透射系数可提高分析精度(表 1)。分析结果 a 考虑 b THz 波在样品表面的透射系数，分析结果 b 则未作此考虑。此法对于同分异构体也同样适用。样品未含成分则可被完全排除。此法可应用于违禁品检测、安全检查等。

A method for quantitative analysis of chemical mixtures with THz time domain spectroscopy

ZHANG Zengyan　YU Xiaohan　XIAO Tiqiao　XU Hongjie

Key words:　Terahertz spectroscopy, Component analysis of mixtures, Isomer mixture

THz-TDS technique, which is sensitive to trivial differences and variations in molecular structure of compounds, possesses the ability of fingerprint identification of the molecular structures. It is of importance to find a simple and efficient method for component analyzing in THz range, for potential applications in chemistry, quality control and detection of dangerous subjects. A method for analyzing chemical mixtures quantitatively with terahertz time domain spectroscopy was proposed. The experimental results demonstrated the feasibility of this technique. Transmission coefficient of THz wave at the sample surface was taken into account to improve the analytic precision. Isomer mixtures are chosen as the experimental samples.

In Table 1, analytic content a and b were obtained, respectively, with or without considering the transmission coefficient of THz wave at sample surface. According to the analysis, we can conclude that the proposed method by taking the integrated absorption spectra as fingerprints of pure compounds is able to identify the components and their relative percentage in a chemical mixture, even for isomers. Components not included in the mixture could be excluded exactly by this method. The method has potential applications in detecting illegal drugs, poisons and dangerous articles in a mixture.

Table 1　Actual content and analyzed results for the Mixture No.1 and No.2

Acids	Benzoic acid		O-toluic acid		M-toluic acid		P-toluic acid	
	No.1	No.2	No.1	No.2	No.1	No.2	No.1	No.2
Actual content/ %	50.0	80.0	30.0	20.0	0	0	20.0	0
Analytic content a/ %	51.4	81.1	29.8	18.9	0	0	18.8	0
Analytic content b/ %	47.6	82.2	29.1	17.8	0	0	23.3	0

THz 时域光谱的新型测量方法

吉 特 余笑寒 徐洪杰

关键词 THz 时域光谱，新型扫描方法，重复性

THz 时域光谱(THz-TDS)测量中，由延迟装置改变探测光与泵浦光间的光程差，使探测光在不同时刻对 THz 脉冲的电场强度进行取样，获得 THz 脉冲电场强度的时间波形。测量参比和测样品间隔 4-6min，此期间的 THz 信号不稳定会导致测量误差。为此，我们在 THz-TDS 装置上采用新的采集数据方式，在每个时域测量点依次记录参比及样品的数据，并得到参比及样品的 THz 时域光谱及傅立叶变换频谱图。将平动样品架改为可放置多个样品的转动盘，用步进电机控制对样品精确定位。此法几乎同步比较待测样品与参比的 THz 信号，不仅消除常规扫描方式中参比与样品的探测时间不同所引起的差别，还可有效控制 THz 信号长期不稳定带给测量结果的影响。用此法测量了四个样品的 THz 光谱，共约 7min。图 1 为相邻两个 THz 信号的差值，并与常规扫描方式结果的比较。原扫描方式的测量重复性差，在 THz 脉冲峰值处尤为明显；而本方法的相邻 THz 信号的差值在整个扫描范围内的微小波动，乃 THz 信号随机涨落所致。此法对同一样品 THz 信号的重复性好，可控制 THz 信号不稳定对实验结果的影响，利于薄膜或弱吸收样品研究。

A new method for THz-TDS measurements

JI Te YU Xiaohan XU Hongjie

Key words: THz-TDS, New scan method, Data reproducibility

A THz-TDS system measures the pulses by scanning the time delay between the laser pump pulse and the laser detection pulse. A reference signal is detected without the sample, before the sample is detected. Each THz waveform is measured in a separate scan of the pump beam delay, and an interval of 4~6 minutes between two scans may cause measurement errors because of long-term instability of the THz signals. In order to solve the problem, we propose a new method for THz-TDS measurements of multiple samples. The idea and the results are as follows.

The electric field amplitude of THz wave is recorded one by one from the samples and the reference at each time delay. THz-TDS of the samples are obtained in just one time-delay scanning. A rotational sample holder is used for fast exchange and accurate positioning of the samples. Measurements of four samples were done in about 7min to record THz-TDS signal from the samples. Fig.1 shows the current difference between two waveforms by the new scan method and conventional method. The data reproducibility has been improved. The result demonstrates that the data reproducibility of a sample was greatly improved, and the influence of THz signal long-term instability on the experimental results can be reduced to almost nothing but the random fluctuation. This new method is of help for characterization of thin film and weak absorption samples.

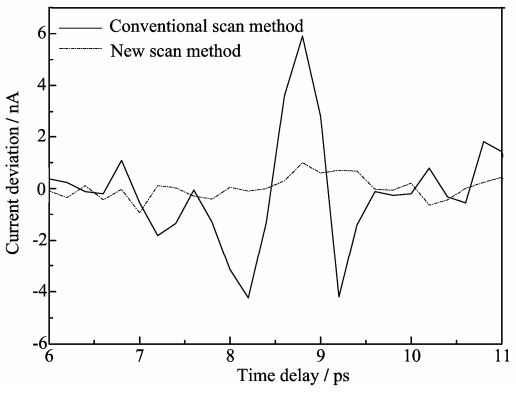

Fig.1 Comparison of data reproducibility by a conventional and new scan method

基于同步辐射 X 射线 CT 组合的非破坏性分析

邓 彪 余笑寒 李爱国 徐洪杰

关键词 组合 X 射线 CT，同时测量，图像重构，同步辐射

作为一种非破坏性分析手段，X 射线 CT 可分析样品内部结构和元素分布。常规的透射 X 射线 CT 可得到样品吸收系数三维分布，X 射线荧光 CT 可高空间分辨和高灵敏地探测元素分布，散射 CT 可得到样品内部电子密度。基于同步辐射 X 射线 CT 的组合技术，可同时得到样品结构和元素分布信息，是上海光源(SSRF)硬 X 射线微聚焦及应用光束线站的实验方法之一。我们在日本 PF-AR 的 BLNE-5A 光束线站进行了同时得到荧光 CT、透射 CT 和康普顿散射 CT 等投影数据的实验，并用图像重构程序得到探测平面的图像。图 1 是采用卷积反投影算法重构的实验样品(标准样品和大白鼠甲状腺组织)的图像。

Nondestructive analysis by combined X-ray tomography based on synchrotron radiation

DENG Biao YU Xiaohan LI Aiguo XU Hongjie

Key words: Combined X-ray tomography, Simultaneous measurement, Image reconstruction, Synchrotron radiation

X-ray tomography is a nondestructive technique to analyze sample structure and to do elemental mapping of the sample. Conventional X-ray transmission tomography reveals spatial distribution of the absorption coefficient. X-ray fluorescence tomography does the elemental mapping. Scatter tomography is used for reconstructing the spatial distribution of electron density, which is closely related to mass-density distribution. Based on synchrotron radiation, however, the X-ray tomography techniques can be combined, and these will be performed on the hard X-ray micro-focus station of SSRF (Shanghai Synchrotron Radiation Facility). An experiment was done on the bending magnet beamline BLNE-5A at PF-AR, KEK, Japan, using known test objects. Projections of transmission tomography, fluorescence tomography, and Compton tomography were obtained simultaneously, and the images (Fig.1) were reconstructed from the data by CBP algorithm without attenuation-correction.

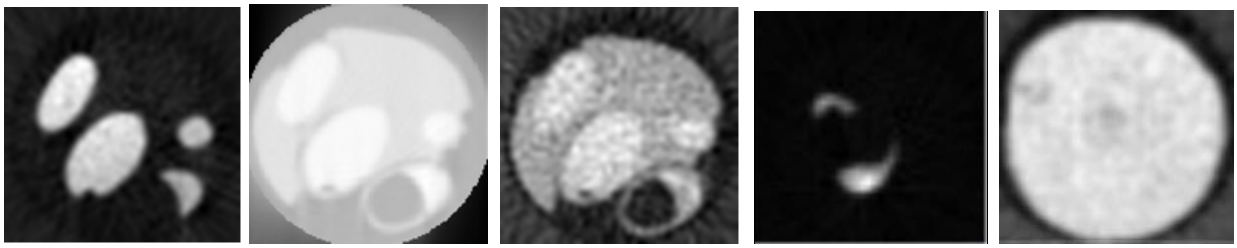

a) Fluorescence CT b) Transmission CT c) Scatter CT d) Fluorescence CT e) Scatter CT

Fig.1 Reconstruction images of standard sample (a, b, c) and hypothyroid tissue of mouse (d, e)

同步辐射微束 X 射线荧光 CT 的计算机模拟

邓 彪 余笑寒 徐洪杰

关键词 微束 X 射线荧光 CT，计算机模拟，同步辐射，图像重构

同步辐射微束 X 射线荧光 CT 是上海光源(SSRF)硬 X 射线微聚焦及应用光束线站的实验方法之一。本文用卷积反投影算法(CBP)、代数重构算法(ART)和加吸收修正的 Hogan 算法重构模拟样品的图像，并分析和比较所得图像的质量。此模拟计算射线在样品中的路径，根据 X 射线荧光发射规律，把路径长度乘以某元素的浓度和激发因子，并考虑入射 X 射线到达激发点的衰减、荧光 X 射线到达探测器时的衰减和探测器的探测效率，对整个路径求和，即可获得当前位置的荧光 CT 投影数据。 此荧光 CT 模拟法无须追踪每个粒子和物质的相互作用，只是宏观计算射线束路径上不同几何体内射线激发的荧光强度，因而速度较快；同时使用了合理的物理规律，也能反映实际情况。荧光 CT 模拟实验以微小生物样品为模拟对象，用三种算法重构的模拟样品图像，其中 CBP 算法和 ART 算法的重构图像的质量令人满意。因为模拟样品的元素浓度在边界变化剧烈，处理这样的数据 ART 算法好于比 CBP 算法。但 CBP 算法的重构速度快，且重构质量可与耗时多的 ART 算法相媲美。对比修正和未修正的重构图像，在样品对 X 射线吸收较强的情况下，Hogan 算法修正和 ART 算法修正对提高重构图像的质量有所帮助，然而，吸收较弱的样品可忽略吸收的影响。鉴此，采用何种重构算法重构图像，是否加入吸收修正，要视具体情况而定。

Computer simulation for SR XRF microtomography

DENG Biao YU Xiaohan XU Hongjie

Key words: X-ray fluorescent microtomography, Computer simulation, Synchrotron radiation, Image reconstruction

Synchrotron radiation-based fluorescent microtomography (SR-XFMT) is a nondestructive technique to do elemental mapping of a specimen with high spatial resolution and sensitivity. In this paper, computer simulation of SR-XFMT is performed. Images of a simulative sample are reconstructed using filtered back projection (CBP), algebraic reconstruction techniques (ART) and modified FBP with absorption correction (Hogan). Quality of the image reconstructions is compared and validity of the reconstruction techniques is discussed. Images reconstructed by CBP and ART are in the same quality, but the reconstruction speed of CBP is faster. The reconstruction algorithm with absorption correction improves the image quality of sample with intense self- absorption. So a selection of the algorithms depends on real experiment condition.

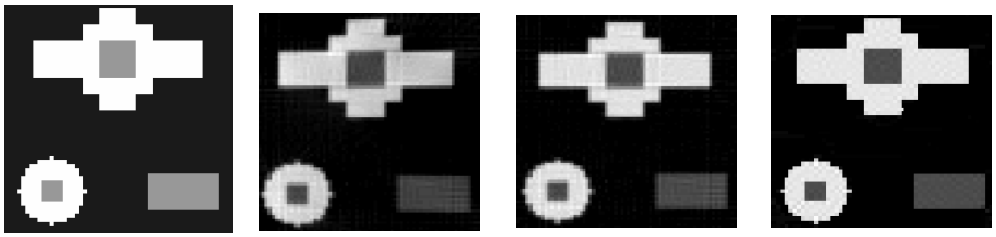

a) The simulation sample b) CBP c) Hogan d) ART

Fig.1 Shape and element distribution of the sample and elemental mapping reconstructed by different algorithms

人源 μ 晶状体蛋白与 NADPH 复合物的晶体结构

孙丽华 程中军* 何建华 龚为民*

关键词 μ 晶状体蛋白，晶体结构，脯氨酸顺/反异构，T3 结合位点，非综合性耳聋

μ 晶状体蛋白(CRYM)是人类胞质内由 NADPH 调控的 3,5,39－三碘甲状腺原氨酸结合蛋白，在向细胞核内传输 3,5,39－三碘甲状腺原氨酸(T3)和调控甲状腺激素相关基因表达中起着重要作用。有研究发现 CRYM 蛋白 C 端的两个突变 K314T 和 X315Y 与人类的非综合性耳聋有关，突变 K314T 使蛋白失去与 T3 结合的能力。人源 μ 晶状体蛋白与两个结构已解析的蛋白——假单胞菌(Pseudomonas putida)的鸟氨酸环化脱氨酶及真菌(Archaeoglobus fulgidus)的丙氨酸环化脱氢酶——在序列上有很高同源性，但 CRYM 的结构尚无报道。

我们由晶体学法得到 CRYM 与 NADPH 复合物的 2.6Å 分辨率结构。数据处理表明，晶胞中每个不对称单位含有两个蛋白分子，每个蛋白分子含有两个结构域即与 NADPH 结合的 Rossmann 卷曲结构域和一个二聚体结构域，同时还发现这两个蛋白分子在 Arg83–His92 处的弯曲结构具有不同的构象，Val89–Pro90 处的肽段在一条链上是反式构象而在另一条链上是顺式构象。将人类的 CRYM 晶状体蛋白与其同源蛋白的结构进行总体比对和活性位点叠合比对，对 T3 在人类晶状体蛋白上的结合位点做了推断。

Crystal structure of human μ-crystallin complexed with NADPH

SUN Lihua CHENG Zhongjun* HE Jianhua GONG Weimin*

Key words: μ-crystallin, Crystal structure, Cis/trans isomerization of praline, T3-binding site, Non-syndromic deafness

Human NADPH-dependent p38 cytosolic 3,5,39-triiodo-L-thyronine-binding protein, also called μ-crystallin or CRYM, plays important physiological roles in transporting 3,5,39-triiodo- L-thyronine (T3) into nuclei and regulating thyroid-hormone-related gene expression. It has been reported that two mutations, K314T and X315Y (an extension at the C terminus), at the C terminus of CRYM are associated with nonsyndromic deafness in human, and the mutation K314T even loses T3-binding ability. The crystal structure of human CRYM's bacterial homolog Pseudomonas putida ornithine cyclodeaminase and Archaeoglobus fulgidus alanine dehydrogenase have been available, but no CRYM structure has been reported.

In this study, we found that the crystal structure of human CRYM bound with NADPH refined to 2.6 Å, and there is one dimer in the asymmetric unit. The structure contains two domains: a Rossmann fold–like NADPH-binding domain and a dimerization domain. Different conformations of the loop Arg83–His92 have been observed in two monomers of human CRYM in the same asymmetric unit. The peptide bond of Val89–Pro90 is a trans-configuration in one monomer but a cis-configuration in the other. A detailed comparison of the human μ-crystallin structure with its structurally characterized homologs including the overall comparison and super-position of active sites was conducted. Finally, a putative T3-binding site in human CRYM is proposed based on comparison with structural homologs.

* 中国科学院生物物理研究所

限制性内切酶 *Sau*3AI C 末端结晶及初步 X 射线晶体学分析

郁 峰 宋佳平* 徐春艳 丁 溦* 胡小健* 张志鸿* 何建华

关键词 限制性内切酶 *Sau*3AI，结晶，X 射线晶体学分析

细菌限制-修复系统中有专一性的 DNA 甲基化酶(*Sau*3AI 甲基化酶)能甲基化胞嘧啶从而保护宿主 DNA 不被切割。*Sau*3AI N 末端与大肠杆菌(*E. coli*)错配修复内切酶 MutH 有较高的序列相似性。除相同的 GATC 识别序列外，还有许多 II 型限制性内切酶中都存在的 D(X)6-30(E/D)XK 催化结构域。*Sau*3AI 的 C 末端在 DNA 结合和切割中的活性尚不清楚。*Sau*3AI 的 C 末端(232－419)被构建在载体 pET15b 中并被克隆入 *E. coli* Rossetta pLyS，包含 his-tag 和 thrombin 酶切位点。在 25℃ 0.2 mmol/L IPTG 的条件下诱导 8h 表达，并通过金属螯合柱和强阴离子交换柱纯化。使用悬滴法结晶，在 1μL 蛋白(8 mg/mL)+1 μL 沉淀剂(10% ~12% tert-butanol / 0.1mol/L MES，pH 5.7~6.7)、4℃的条件下经过 12 h 可生长出片状晶体。使用 Rigaku R-AXIS IV^{++} 衍射仪确定晶体分辨率为 2.8Å，空间群为 $P2_12_12_1$，a = 34.75 Å, b = 76.82Å, c = 123.59 Å，每个不对称单位包含一个分子。*Sau*3AI 的 C 末端和 N 末端有一定的序列相似性，这暗示 *Sau*3AI 可能是假二聚体。若是，则 *Sau*3AI 的 C 端可能包含 DNA 结合和内切酶活力。解析 *Sau*3AI C 端的结构有助于理解该蛋白的功能与特性。

Crystallization and preliminary X-ray analysis of *Sau*3AI C-terminal fragment

YU Feng SONG Jiaping* XU Chunyan DING Yu* HU Xiaojian*

ZHANG Zhihong * HE Jianhua

Key words: *Sau*3AI endonuclease, Crystallization, X-ray analysis

In a bacterial restriction-modification system, one specific DNA methyltransferase (*Sau*3AI methyltransferase) can methylate the ‘C’ residue to protect host DNA from *Sau*3AI cleavage. The N-terminal domain of *Sau*3AI displays high sequence similarity with *Escherichia coli* mismatch repair endonuclease MutH. Besides the GATC recognition sequence, they have the same catalytic sequence motif D(X)6-30(E/D)XK as in other types of II restriction enzymes. Unlike *Sau*3AI, MutH can only cleave unmethylated daughter strand in hemimethylated DNA. Endonuclease activity of MutH depends on MutL and MutS protein. The role of C-terminal fragment of *Sau*3AI in DNA binding and cleavage specificity is still unclear. We expressed the C-terminal *Sau*3AI fragment in *E.coli* to investigate its structure and function. C terminal 232-419aa fragment of Sau3AI was constructed in pET15b, with his-tag and a thrombin digestion site. Protein was expressed in *E. coli* Rossetta pLyS cells at 25°C after 8 h with 0.2 mmol/L IPTG induction and purified by Amersham HiTrap Chelating HP column and Hi-Trap Q HP column. Crystallization was done by hanging drop vapor diffusion method in 4°C. 1μL of 8 mg/mL protein was mixed with 1 μL of 10%~12% tert-butanol/0.1 mol/L MES(pH 5.7~6.7). Plate-like crystals appeared 12 h later. XRD data were collected. The space group is $P2_12_12_1$ and a = 34.75 Å,

b=76.82Å, *c*=123.59 Å. There is one molecular per asymmetric unit. However, the C-terminal of *Sau*3AI shows some sequence similarity with the N-terminal half and it has been suggested that Sau3AI is in fact a pseudodimer. Then, C-terminal *Sau*3AI may contain a DNA binding site and enzyme activity. Solving the structure of the C-terminal half of *Sau*3AI will illustrate its role in protein function and character.

*复旦大学生理学和生物物理系

*Sau*3AI/E64A 突变体蛋白结晶及初步 X 射线晶体学分析

徐春艳 宋佳平* 丁 颁* 郁 峰 孙丽华 唐 琳 胡小健* 张志鸿* 何建华

关键词 *Sau*3AI 突变体 结晶 X 射线晶体学分析

*Sau*3AI 的结构尚不清楚，为研究其三维结构并更好了解其功能特点，我们将 64 位的谷氨酸(E)突变为丙氨酸(A)的突变体蛋白的基因克隆并在 *E.coli* 中表达。由亲和层析及阴离子交换层析纯化，得到的蛋白有单体及二聚体两个组分，并在 4°C 用悬滴法进行结晶实验。单体可以在 16% PEG 8K/ 0.1 mol/L 醋酸钠 pH 4.6/ 0.2 mol/L $CaCl_2$ 及 15% PEG 3350/ 0.1 mol/L 柠檬酸三钠 pH 5.0/ 0.2 mol/L 柠檬酸氢二铵两个条件下获得片状的晶体。二体也可以在 6%~8% PEG8K/0.1M HEPES pH7.5/2mol/L 硫酸铵/0.1 mol/L 柠檬酸三钠 pH5.6/0.2 mol/L 酒石酸钠钾获得块状的晶体。晶体在防冻液中经液氮冷冻后在带有转靶 X 射线发生装置的 MAR345dtb 像板探测器上进行 X 射线衍射分析。二聚体及单体晶体最多只能衍射到 3.0 Å，而本文的单体晶体可衍射到 2.8 Å 以上并收集了一整套数据(曝光 20 min)，用 Automar 软件进行数据的处理表明，该蛋白单体的晶体属正交晶系，空间群为 $C222_1$，晶胞参数为 a=69.44, b=197.60, c=191.46, 且一个不对称单位中含两个分子。

Crystallization and preliminary X-ray analysis of *Sau*3AI/E64A mutant protein

XU Chunyan SONG Jiaping* DING Yu* YU Feng SUN Lihua TANG Lin
HU Xiaojian* ZHANG Zhihong* HE Jianhua

Key words: *Sau*3AI mutant, Crystallization, X-ray analysis

The structure and character of *Sau*3AI endonuclease is still unknown. To investigate its 3D-structure and function, we expressed the *Sau*3AI E64A mutant in *E. coli.* After purification through affinity chromatography and anion exchange chromatography, the purified protein has monermer and dimer fraction and was crystallized was crystallized by the hanging-drop vapor-diffusion technique at 4°C. Plate-like crystals of the monomer can be grown in the conditions of 16% PEG8K/ 0.1 mol/L sodium acetate pH 4.6/ 0.2 mol/L $CaCl_2$ and 15% PEG 3350/ 0.1 mol/L sodium citrate tribasic dihydrate pH 5.0/ 0.2 mol/L di-Ammonium hydrogen citrate. Crystals of the dimer can be obtained in 6%~8% PEG8K/0.1 mol/L HEPES pH7.5 and 2 mol/L $(NH_4)_2SO4$/0.1 mol/L sodium citrate tribasic dihydrate pH5.6/0.2 mol/L K/Na Tartrate after 12 h and finally grew to about 0.4 mm×0.2 mm×0.2 mm).

Crystals were frozen in cryo-solution by nitrogen and then X-ray diffraction experiment was carried out at 100 K on a MAR345dtb image plate detector (MarResearch, Germany) with a rotating-anode X-ray generator (copper anode; RAMicro007, Rigaku, Japan). The dimer protein crystals and the monomer crystals can only diffract to 3.0 Å resolution and the monomer protein crystals can diffract to better than 2.8 Å resolution. One completed dataset (exposed 20 min for each image) has been collected and was processed by Automar. The preliminary crystallography results have shown that the monomer orthorhombic *Sau*3AI/E64A crystal is in space group $C222_1$ with unit cell parameters (69.44, 197.60, 191.46, 90, 90, 90) and contains two molecules in one asymmetric unit.

*复旦大学生理学和生物物理系

弛豫铁电体中纳米极化区域的同步光实验研究

郭 智　邰仁忠　徐洪杰　严 睿　高 琛[1]　罗豪甦[2]

关键词　小角散射；弛豫铁电体；纳米极化区域

弛豫铁电体具有优异的压电、电致伸缩特性，广泛应用于超声设备、传感器等，并可能用于人工智能、神经网络等领域。其优异特性源于其内的大量纳米极化区域(PNRs)。但对 PNRs 的实验观测，现多采用基于对晶格振动(声子)研究的非弹性中子散射和拉曼散射、或基于晶格位移的 X 射线漫散射等间接实验手段。寻找能直接反映 PNRs 结构信息的实验方法对了解 PNRs 的功能有重要意义。我们首次采用准相干 X 射线透射小角散射法研究了 $0.72Pb(Mg_{1/3}Nb_{2/3})O_3$-$0.28PbTiO_3$ 弛豫铁电体中 PNRs 的空间构造，得到在 T_m(401 K)附近明显存在、在高温 (600K 左右)时消失的中心对称衍射斑点(附加外电场)或弥散状散射斑。这些衍射斑点来源于 PNRs 的准周期性空间分布。分析表明：在 T_m 附近的自发状态下， PNRs 的形状为椭圆形，沿<001>方向的长轴为 17 nm，沿<100>方向的短轴为 10 nm；分布呈随机性，相邻 PNRs 的平均距离沿<001>和<100>方向分别为 46 nm 和 36 nm；PNRs 准周期性关联在高于 T_m 约 200K 时完全消失。在沿<100>方向加强电场(2.3 kV/cm)，PNRs 在 T_m 附近呈现沿<1±11>方向的准周期(36 nm)分布；PNRs 占主导地位的极化和关联方向随温度升高在<111>和<1-11>间变化；沿<1±11>方向的 PNRs 准周期性关联在高于 T_m 约 40 K 时完全消失。

Experimental study on polar-nano-regions among relaxor ferroelectrics with synchrotron radiation

GUO Zhi　TAI Renzhong　XU Hongjie　YAN Rui　GAO Chen[1]　LUO Haosu[2]

Key words:　Small-angle scattering, Relaxor-based ferroelectrics, Polar-nano-regions

Due to high performances of piezoelectricity and electrostriction, relaxor ferroelectrics are used as ultrasonic device and transducer, and potentially in artificial intelligence and neural networks. The high performance is related to polar-nano-regions (PNRs) inside the material. Explorations of the PNR structure, however, have been dominated by measuring lattice vibration (phonons) through inelastic neutron scattering and Raman scattering experiments, or measuring lattice structural variation through

X-ray diffuse scattering. A straight-forward structural characterization for PNRs would help to have an insight into the nature of how microscopic PNRs contribute to the high performance. Small angle scattering of quasi-coherent SR X-rays was used for the first time to study PNR spatial distribution among $0.72Pb(Mg_{1/3}Nb_{2/3})O_3$-$0.28PbTiO_3$ relaxor-based ferroelectrics. Center symmetric diffraction spots (under external electric fields) or dispersive scattering patterns were observed clearly near T_m (401K), and disappeared at high temperatures (about 600 K). The diffraction spots were originated from scattering of PNR quasi-periodic spatial distribution. In a spontaneous state near T_m, PNRs exhibited elliptical shapes and randomly distributed, estimated at 17 nm for major axis along <001> and 10 nm for minor axis along <100>. Average distances for PNRs were 36 nm along <100> and 46nm along <001>. PNRs quasi-periodic distribution disappeared completely at 643K. Clear quasi-periodic structure with a period of 36 nm were observed along <1±11> under DC field of 2.3 kV/cm near T_m. The dominating PNR orientation and their interaction directions varied between <111> and <1-11> as temperature changed. PNR quasi-periodic distribution along <1±11> disappeared at T_m + 40 K.

[1]中科大国家同步辐射实验室; [2]中科院上海硅酸盐研究所

D-、L-和 DL-青霉胺的太赫兹时域光谱

吉 特　赵红卫　余笑寒　徐洪杰

关键词　太赫兹时域光谱，青霉胺，对映异构体

青霉胺(penicillamine)是治疗风湿性关节炎的常用药，但仅 D-型有效，同时 D-型对映体也能治疗代谢性疾病和铅、汞等金属中毒，而 L-型对映体则会导致骨髓损伤、嗅觉和视觉衰退以及过敏反应等。因此，它们的鉴别十分重要。我们用太赫兹时域光谱技术测量了 D-、L-和 DL-青霉胺在 0.2~1.8 THz 波段的吸收系数随频率的变化。三个样品的吸收光谱有明显差异，DL-青霉胺有两个强吸收峰(1.36 和 1.66 THz)，在 1.53 THz 处有较弱的吸收峰；L-和 D-青霉胺的强吸收峰分别位于 1.52 THz 和 1.58 THz，这与 D-青霉胺的拉曼光谱结果基本一致。D-青霉胺在 1.0 和 1.3 THz 处还有弱吸收峰。青霉胺对映异构体及其外消旋化合物的分子晶体结构有一定差异。D-、L-青霉胺的晶体结构属正交型，单位晶胞中含四个单分子，空间群为 $P222_1$；DL-青霉胺的晶体结构属单斜晶系，单位晶胞中也含四个单分子，空间群为 $P2_1/c$。D-和 L-青霉胺是对映异构体，分子构造相同而构型互为镜像关系，这种构型的不同导致分子内及分子间相互作用的差异，引起两者吸收光谱的差异。实验表明，THz 吸收光谱能有效鉴别青霉胺对映异构体，可用于青霉胺药物的检测。

THz-TDS of L-, D- and DL-penicillamine

JI Te　ZHAO Hongwei　YU Xiaohan　XU Hongjie

Key words:　THz-TDS, Penicillamine, Enantiomers

Penicillamine is a thiol drug for rheumatoid arthritis treatment. Only pure D-penicillamine can be used since the L- form and the DL racemate are toxic, with severe adverse reactions, such as neuritis in patients treated with DL-penicillamine. Absorption coefficients of L-, D- and DL-penicillamine meas-

ured by THz-TDS in 0.2~1.8 THz are shown in Fig.1. Absorptions of the enantiomers (L- and D-penicillamine) and their racemate (DL-penicillamine) differ greatly. And the L- and D-penicillamine differ, too, in the absorption. The strong absorption peak is located respectively at 1.52 THz and 1.58 THz for L- and D-penicillamine. This is in good agreement with the Raman spectrum of D-penicillamine. In addition, the THz-TDS spectrum of D-penicillamine has two weak absorption peaks at 1.00 THz and 1.32 THz, but the L-penicillamine has none. The crystal structures of enantiomers are orthorhombic with space group $P222_1$, and DL-penicillamine is monoclinic with the space group $P2_1/c$. It suggests that THz-TDS is sensitive to changes in crystal structure. The study provides a new method to detect and analyze chiral drugs.

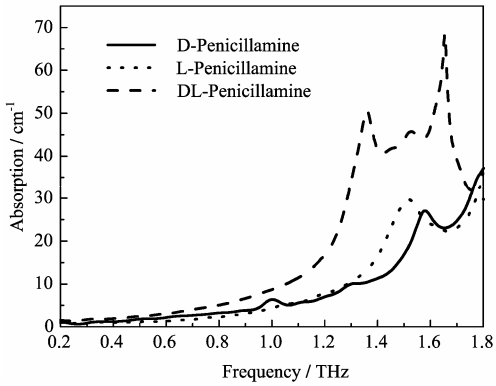

Fig.1 Absorption coefficients of L-, D- and DL-penicillamine

核 物 理

Nuclear Physics

$\sqrt{S_{\mathrm{NN}}}$ = 200GeV 的 pp 和 Au+Au 碰撞中与高横动量粒子关联的带电强子的分布

STAR 合作组

关键词 带电强子，横动量

在 $\sqrt{S_{\mathrm{NN}}}=200\mathrm{GeV}$ pp 和 Au+Au 碰撞中对与 $p_{\perp}^{\mathrm{trig}}>4\mathrm{GeV}/c$ 的粒子关联的横动量在 $0.15\mathrm{GeV}/c<p_{\perp}<4\mathrm{GeV}/c$ 范围内的带电强子进行重建，发现 Au+Au 对心碰撞中关联多重性以及 $p_{\perp}$ 值的总和相对于 pp 碰撞中有所增加。与 pp 碰撞相比，Au+Au 对心碰撞中关联 $p_{\perp}$ 分布在远离侧与靠近侧形状类似有明显的软化，这与内部强子的情况（有明显的硬化）是不同的。与喷注淬灭现象一致，这一结果表明在远离侧的碎片逐渐与横向媒介物达到平衡。

Distributions of charged hadrons associated with high transverse momentum particles in pp and Au plus Au collisions at $\sqrt{S_{\mathrm{NN}}}$ = 200GeV

STAR Collaboration

Key words: Charged hadrons, Transverse momentum

Charged hadrons in $0.15\mathrm{GeV}/c<p_{\perp}<4\mathrm{GeV}/c$ associated with particles of $p_{\perp}^{\mathrm{trig}}>4\mathrm{GeV}/c$ are reconstructed in pp and Au+Au collisions at $\sqrt{S_{\mathrm{NN}}}$=200GeV. The associated multiplicity and $p_{\perp}$ magnitude sum are found to increase from pp to central Au+Au collisions. The associated $p_{\perp}$ distributions, while similar in shape on the nearside, are significantly softened on the awayside in central Au+Au relative to pp and not much harder than that of inclusive hadrons. The results, consistent with jet quenching, suggest that the awayside fragments approach equilibration with the medium traversed.

$\sqrt{S_{\mathrm{NN}}}$ = 200GeV Au +Au 碰撞中的多重奇异性重子椭圆流

STAR 合作组

关键词 多重奇异性重子，椭圆流

报告了重离子碰撞中对多重奇异性重子 $\Xi^{-}+\Xi^{+}$ 和 $\Omega^{-}+\Omega^{+}$ 的椭圆流 $v_2\left(p_{\mathrm{T}}\right)$ 的首次测量。在 $\sqrt{S_{\mathrm{NN}}}=200\mathrm{GeV}$ 最小偏离 Au+Au 碰撞中观测到多重奇异性重子的椭圆流，与其它非奇异重子相比非常显著。这种多重奇异性重子被认为对重离子碰撞的部分子阶段的动力学有很大依赖性。多重奇异性重子 v_2 的 $p_{\perp}$ 依赖性确认了早先观测到的较轻强子的组份夸克标度数。这些结果为以下观点提供了支持，即在 RHIC 上观测到的大部分集体运动是在超相对论核碰撞早期的部分子阶段中形成的。

Multistrange baryon elliptic flow in Au+Au collisions at $\sqrt{S_{\mathrm{NN}}}$ = 200GeV

STAR Collaboration

Key words: Multistrange baryon, Elliptic flow

We report on the first measurement of elliptic flow $v_2(p_{\mathrm{T}})$ of multistrange baryons $\Xi^- + \Xi^+$ and $\Omega^- + \Omega^+$ in heavy-ion collisions. In minimum-bias Au +Au collisions at $\sqrt{S_{\mathrm{NN}}} = 200\mathrm{GeV}$, a significant amount of elliptic flow, comparable to other nonstrange baryons, is observed for multistrange baryons which are expected to be particularly sensitive to the dynamics of the partonic stage of heavy-ion collisions. The $p_{\perp}$ dependence of v_2 of the multistrange baryons confirms the number of constituent quark scaling previously observed for lighter hadrons. These results support the idea that a substantial fraction of the observed collective motion is developed at the early partonic stage in ultrarelativistic nuclear collisions at the Relativistic Heavy Ion Collider.

$\sqrt{S_{\mathrm{NN}}}$ = 62.4GeV Au+Au 碰撞中光子的多重性和赝快度分布

STAR 合作组

关键词 多重性，赝快度，光子

报告了 $\sqrt{S_{\mathrm{NN}}} = 62.4\mathrm{GeV}$ Au+Au 碰撞中对不同中心度下 $2.3 \le \eta \le 3.7$ 区间光子的赝快度分布的第一次测量。发现光子产生标度在所有研究过的碰撞中心度下都与参加核子的数目有关。光子的赝快度分布，主要是 π^0 衰变，与不同能量下的重离子碰撞、核子-核子碰撞中产生的带电 π 介子，光子以及内禀荷电粒子的赝快度进行了比较。结果显示，光子产额符合能量和中心度独立限制的碎裂机制。

Multiplicity and pseudorapidity distributions of photons in Au+Au collisions at $\sqrt{S_{\mathrm{NN}}}$ = 64.2 GeV

STAR Collaboration

Key words: Multiplicity, Pseudorapidity, Photons

We present the first measurement of pseudorapidity distribution of photons in the region $2.3 \le \eta \le 3.7$ for different centralities in Au +Au collisions at $\sqrt{S_{\mathrm{NN}}} = 62.4\mathrm{GeV}$. We find that the photon yield scales with the number of participating nucleons at all collision centralities studied. The pseudorapidity distribution of photons, dominated by π^0 decays, has been compared with those of charged pions, photons, and inclusive charged particles from heavy-ion and nucleon-nucleon collisions at various energies. The photon production has been shown to be consistent with the energy and centrality independent limiting fragmentation scenario.

$\sqrt{S_{\mathrm{NN}}}$ = 200GeV d+Au 碰撞中的开粲夸克产额

STAR 合作组

关键词 开粲夸克，产额

报告了 d+Au 碰撞中根据 $\mathrm{D}^0\left(\overline{\mathrm{D}}^0\right)\to \mathrm{K}^{\mp}\pi^{\mp}$ 直接重建得到的中心快度区域的开粲夸克谱，以及 $\sqrt{S_{\mathrm{NN}}}=200\mathrm{GeV}$ pp 和 d+Au 碰撞中通过粲夸克半轻子衰变进行的电子-正电子间接测量。$\mathrm{D}^0\left(\overline{\mathrm{D}}^0\right)$ 谱在横动量为 $0.1\mathrm{GeV}/c<p_{\mathrm{T}}<3\mathrm{GeV}/c$ 的范围内，而电子谱是 $0.1\mathrm{GeV}/c<p_{\mathrm{T}}<3\mathrm{GeV}/c$。电子谱显示出 pp 和 d+Au 碰撞具有近似的二元碰撞标度。从这两项独立的分析得知，BNL RHIC d+Au 碰撞中产生的开粲夸克在中心快度区域每核子-核子二元相互作用的微分截面是 $\mathrm{d}\sigma_{\mathrm{c\bar{c}}}^{\mathrm{N\bar{N}}}/\mathrm{d}y=0.30\pm0.04(\mathrm{stat})\pm0.09(\mathrm{syst})\ \mathrm{mb}$。将结果与理论计算进行了比较，并讨论了 A+A 碰撞的粲素结果的含意。

Open charm yields in d+Au collisions at $\sqrt{S_{\mathrm{NN}}}$ = 200GeV

STAR Collaboration

Key words: Open charm quark, Yield

Midrapidity open charm spectra from direct reconstruction of $\mathrm{D}^0\left(\overline{\mathrm{D}}^0\right)\to \mathrm{K}^{\mp}\pi^{\mp}$ in d+Au collisions and indirect electron-positron measurements via charm semileptonic decays in p+p and d+Au collisions at $\sqrt{S_{\mathrm{NN}}}=200\mathrm{GeV}$ are reported. The $\mathrm{D}^0\left(\overline{\mathrm{D}}^0\right)$ spectrum covers a transverse momentum (p_{T}) range of $0.1\mathrm{GeV}/c<p_{\mathrm{T}}<3\mathrm{GeV}/c$, whereas the electron spectra cover a range of $0.1\mathrm{GeV}/c<p_{\mathrm{T}}<4\mathrm{GeV}/c$. The electron spectra show approximate binary collision scaling between p p and d + Au collisions. From these two independent analyses, the differential cross section per nucleon-nucleon binary interaction at midrapidity for open charm production from d +Au collisions at BNL RHIC is $\mathrm{d}\sigma_{\mathrm{c\bar{c}}}^{\mathrm{N\bar{N}}}/\mathrm{d}y=0.30\pm0.04(\mathrm{stat})\pm0.09(\mathrm{syst})$ mb. The results are compared to theoretical calculations. Implications for charmonium results in A+A collisions are discussed.

寻找夸克-胶子等离子体在实验和理论上的挑战：STAR 合作组对 RHIC 碰撞实验现象的评估

STAR 合作组

关键词 夸克-胶子等离子体，RHIC核-核碰撞

回顾了 RHIC 核-核碰撞研究最初三年里最重要的实验结果，尤其是 STAR 的实验结果，并对其理论解释、与理论的比较作了评定。理论-实验的比较结果表明，RHIC 上进行的 Au+Au 对心碰撞产生致密的、迅速热化的物质，其特征为：(1)初始能量密度高于格点 QCD 所预言的能够形成夸克-胶子等离子体的临界值；(2)近似于理想流体流，由平均自由程很短的组份相互作用产生，很可能形成于强子形成阶段；(3)对喷注的不透明性。多数观测量与模型所表述的碰撞早期形成 QGP 相一致，但在强子框架内尚未有现成的解释。然而，测量本身也没有找到能够证明向这种新

的物质相转变的明确的证据。碰撞演化的理论处理不论如何成功，它调用了一套独特的模型、自由度和至今没有量化结论的假设。我们提出了一些重要的开放性问题，并建议更多的测量，其中至少有一些观测量是要强调的，其目的是奠定一个坚实的基础以断言在 RHIC 上已经产生热化的、退禁闭的夸克-胶子物质。

Experimental and theoretical challenges in the search for the quark–gluon plasma: The STAR Collaboration's critical assessment of the evidence from RHIC collisions

STAR Collaboration

Key words: Quark-gluon plasma, RHIC nucleus-nucleus collision

We review the most important experimental results from the first three years of nucleus–nucleus collision studies at RHIC, with emphasis on results from the STAR experiment, and we assess their interpretation and comparison to theory. The theory-experiment comparison suggests that central Au+Au collisions at RHIC produce dense, rapidly thermalizing matter characterized by: (1) initial energy densities above the critical values predicted by lattice QCD for establishment of a quark–gluon plasma (QGP); (2) nearly ideal fluid flow, marked by constituent interactions of very short mean free path, established most probably at a stage preceding hadron formation; and (3) opacity to jets. Many of the observations are consistent with models incorporating QGP formation in the early collision stages, and have not found ready explanation in a hadronic framework. However, the measurements themselves do not yet establish unequivocal evidence for a transition to this new form of matter. The theoretical treatment of the collision evolution, despite impressive successes, invokes a suite of distinct models, degrees of freedom and assumptions of as yet unknown quantitative consequence. We pose a set of important open questions, and suggest additional measurements, at least some of which should be addressed in order to establish a compelling basis to conclude definitively that thermalized, deconfined quark–gluon matter has been produced at RHIC.

$\sqrt{S_{\mathrm{NN}}}$ = 200GeV 的 p+p 和 d+Au 碰撞中 π，K，质子和反质子的横动量分布

STAR 合作组

关键词 p+p 碰撞，d+Au 碰撞，横动量分布

报告了 200GeV p+p 和 d+Au 碰撞产生的 $\pi^{\pm}$，$K^{\pm}$及 p($\bar{p}$)中间快度谱的鉴别。基于多气隙电阻板室技术的飞行时间探测器被用于粒子鉴别。观测到粒子种类对克罗宁效应的依赖性比低能情况下明显降低。横动量在 $1.2\mathrm{GeV}/c < p_{\mathrm{T}} < 3.0\mathrm{GeV}/c$ 范围内的质子(p+$\bar{p}$)和带电强子(h)的核修正参数的比值(R_{dAu})在最小偏离碰撞中测得值为 1.19±0.05（stat）±0.03(syst)，并且显示了很小的中心度依赖性。发现最小偏离 d+Au 碰撞中(p+$\bar{p}$)/h 的产率比 Au+Au 碰撞低一半，这表明仅有克罗宁效应是不足以导致 RHIC 重离子碰撞中观测到的重子相对增强的。

Pion, kaon, proton and anti-proton transverse momentum distributions from p +p and d+Au collisions at $\sqrt{S_{NN}}$ = 200GeV

STAR Collaboration

Key words: p+p collision, d+Au collision, Transverse momentum

Identified mid-rapidity particle spectra of $\pi^{\pm}$, $K^{\pm}$, and p($\bar{p}$) from 200GeV p + p and d + Au collisions are reported. A time-of-flight detector based on multi-gap resistive plate chamber technology is used for particle identification. The particle species dependence of the Cronin effect is observed to be significantly smaller than that at lower energies. The ratio of the nuclear modification factor (R_{dAu}) between protons (p+ $\bar{p}$) and charged hadrons (h) in the transverse momentum range $1.2\mathrm{GeV}/c < p_T < 3.0\mathrm{GeV}/c$ is measured to be 1.19 ± 0.05(stat) ± 0.03(syst) in minimum-bias collisions and shows little centrality dependence. The yield ratio of (p + $\bar{p}$)/h in minimum-bias d + Au collisions is found to be a factor of 2 lower than that in Au + Au collisions, indicating that the Cronin effect alone is not enough to account for the relative baryon enhancement observed in heavy ion collisions at RHIC.

$\sqrt{S_{NN}}$ = 200GeV 的 Au+Au 和 p+p 碰撞中的 φ 介子产生

STAR 合作组

关键词 Au+Au 碰撞，p+p 碰撞，φ 介子

报告 STAR 合作组对 $\sqrt{S_{NN}} = 200\mathrm{GeV}$ 的 Au+Au 和 p+p 碰撞中 φ 介子产生的测量。使用事件混合方法，求得了 Au+Au 碰撞在中间快度的五个中心度区间和非单衍射的 p+p 碰撞的 φ 谱和产额。发现 Au+Au 碰撞产生的 φ 的横动量分布更符合一次指数形式，而 p+p 的谱用二次指数分布描述更好。测得的核修正因子表明在 Au+Au 对心碰撞中 φ 产额在用二元碰撞数（$<N_{bin}>$)标度时相对于边缘碰撞有被抑制的现象。关于$< p_T >$与中心度的关系以及恒定的 ϕ/K^-比值与粒子束种类、中心度、碰撞能的关系的系统研究排除了 K 熔合是 φ 产生的主要机制的可能性。

φ meson production in Au +Au and p+p collisions at $\sqrt{S_{NN}}$ = 200GeV

STAR Collaboration

Key words: Au+Au collisions, p +p collisions, φ meson

We report the STAR measurement of φ meson production in Au+Au and p+p collisions at $\sqrt{S_{NN}} = 200\mathrm{GeV}$. Using the event mixing technique, the φ spectra and yields are obtained at mid-rapidity for five centrality bins in Au + Au collisions and for non-singly-diffractive p+p collisions. It is found that the φ transverse momentum distributions from Au + Au collisions are better fitted with a

single-exponential while the p + p spectrum is better described by a double-exponential distribution. The measured nuclear modification factors indicate that φ production in central Au + Au collisions is suppressed relative to peripheral collisions when scaled by the number of binary collisions (<N_{bin}>). The systematics of < p_T > versus centrality and the constant φ/K^- ratio versus beam species, centrality, and collision energy rule out kaon coalescence as the dominant mechanism for φ production.

Au+Au 和 p+p $\sqrt{S_{NN}}$ = 200GeV 碰撞中 K(892)*共振态的产生

STAR 合作组

关键词 K(892)* 共振态，相对论重离子碰撞

短寿命的 K(892)* 共振态为探测在相对论重离子碰撞过程中产生热致密物质的性质提供了一种有效的方法。这里报道在中心碰撞能量为 200GeV 的 Au+Au 和 p+p 碰撞中产生的 K(892)*，这些 K(892)*是通过它的强子衰变道 $K(892)^{*0} \rightarrow K\pi$ 和 $K(892)^{*\pm} \rightarrow K^0_S\pi^{\pm}$来重构的，是在布鲁克海文国家实验室的相对论重离子对撞机上的 STAR 探测器上实现的。K^{*0} 的质量作为横向动量 p_T 的函数已经在偏离最小的 p+p 碰撞和中心的 Au+Au 碰撞中研究过。展示了偏离最小的 p+p 碰撞和不同中心度的 Au+Au 碰撞的 K*的 p_T 谱。发现 Au+Au 的所有中心度下的 K*/K 产额比要明显低于偏离最小的 p+p 碰撞，显示了在化学和动力学的冷却过程中强子相互作用的重要性。还在 Au+Au 碰撞中观察到明显的非零的 K^{*0} 椭圆流(v_2)，并且与 K^0_s 和 Λ 的 v_2 做了比较。中间 p_T 的 K*的核修正因子和 K^0s 的相似，但是与 Λ 的不同，这就在中间 p_T (2 GeV/c≤ p_T ≤4 GeV/c)的粒子产生过程中建立了一种超越质量效应的重子-介子效应。

K(892)* resonance production in Au+Au and p+p collisions at $\sqrt{S_{NN}}$ = 200GeV

STAR Collaboration

Key words: K(892)* resonance, Relativistic heavy-ion collisions

The short-lived K(892)* resonance provides an efficient tool to probe properties of the hot and dense medium produced in relativistic heavy-ion collisions. We report measurements of K* in $\sqrt{S_{NN}} = 200GeV$ Au+Au and p+p collisions reconstructed via its hadronic decay channels $K(892)^{*0} \rightarrow K\pi$ and $K(892)^{*\pm} \rightarrow K^0_S\pi^{\pm}$ using the STAR detector at the Relativistic Heavy Ion Collider at Brookhaven National Laboratory. The K^{*0} mass has been studied as a function of p_T in minimum bias p+p and central Au+Au collisions. The K* p_T spectra for minimum bias p + p interactions and for Au+Au collisions in different centralities are presented. The K*/K yield ratios for all centralities in Au+Au collisions are found to be significantly lower than the ratio in minimum bias p+p collisions, indicating the importance of hadronic interactions between chemical and kinetic freeze-outs. A significant nonzero K^{*0} elliptic flow (v_2) is observed in Au+Au collisions and is compared to the v_2 of K^0_S and Λ. The nuclear modification factor of K* at intermediate p_T is similar to that of K^0_S but different from Λ. This establishes a baryon-meson effect over a mass effect in the particle production at intermediate p_T (2 GeV/c ≤ p_T ≤4 GeV/c).

相对论能量下入射能的 p_T 关联依赖性

STAR 合作组

关键词 横向动量，相对论能量粒子

展示了在布鲁克海文的相对论重离子对撞机上的中心能量 $\sqrt{S_{NN}}$ 为 20、62、130、220 GeV 的 Au+Au 碰撞中两粒子横向动量关联 $<p_{T,i}\ p_{T,j}>$与事件中心度的关系。发现在所有的四种入射能量下这种关联会随着中心度减小而减小。这种由多重数密度增加产生的关联会随着入射能量的增加而增加，并且它对中心度的依赖性可能提供诸如热化、喷注产生、或者横流饱和等过程存在的一些证据。这种关联除以每个事件的平均横向动量的方根与入射能量几乎没有关系，这也和先前在欧洲核子中心的大型质子同步加速器上的测量结果基本一致。

Incident energy dependence of p_T correlations at relativistic energies

STAR Collaboration

Key words: Transverse momentum, Relativistic energy particles

We present results for two-particle transverse momentum correlations, $< p_{T,i}\ \ p_{T,j} >$, as a function of event centrality for Au+Au collisions at $\sqrt{S_{NN}}$ = 20, 62, 130, and 200 GeV at the BNL Relativistic Heavy Ion Collider. We observe correlations decreasing with centrality that are similar at all four incident energies. The correlations multiplied by the multiplicity density increase with incident energy, and the centrality dependence may show evidence of processes such as thermalization, jet production, or the saturation of transverse flow. The square root of the correlations divided by the event-wise average transverse momentum per event shows little or no beam energy dependence and generally agrees with previous measurements made at the CERN Super Proton Synchrotron.

在 Au+Au $\sqrt{S_{NN}}$ = 200GeV 碰撞中方位角的各向异性

STAR 合作组

关键词 Au+Au 碰撞，方位角分布

总结了 STAR 合作组关于 Au+Au $\sqrt{S_{NN}}$ = 200GeV 碰撞中粒子各向异性方位角分布的直通流(v_1)、椭圆流(v_2)、以及四阶谐流(v_4)的结果，并且和其他实验组和一些理论模型的结果做了比较。展示了已经鉴别的粒子的结果，并且用冲击波模型进行了拟合。还对不同的各向异性流分析方法进行了比较，并且从数据中提取了非流效应。讨论了 v_2 的组分夸克数标度和部分子结合，以及 v_4 的 v_2^2 标度和夸克结合。

Azimuthal anisotropy in Au+Au collisions at $\sqrt{S_{\mathrm{NN}}} = 200\mathrm{GeV}$

STAR Collaboration

Key words: Au+Au collision, Azimuthal distribution

The results from the STAR Collaboration on directed flow (v_1), elliptic flow (v_2), and the fourth harmonic flow (v_4) in the anisotropic azimuthal distribution of particles from Au+Au collisions at $\sqrt{S_{\mathrm{NN}}} = 200\mathrm{GeV}$ are summarized and compared with results from other experiments and theoretical models. Results for identified particles are presented and fit with a blast-wave model. Different anisotropic flow analysis methods are compared and nonflow effects are extracted from the data. For v_2, scaling with the number of constituent quarks and parton coalescence are discussed. For v_4, scaling with v_2^2 and quark coalescence are discussed.

Au+Au $\sqrt{S_{\mathrm{NN}}} = 130\mathrm{GeV}$ 碰撞中平均横向动量〈 p_{T} 〉的涨落

STAR 合作组

关键词 Au+Au 碰撞，平均横向动量

展示了核子-核子动量中心碰撞能量 $\sqrt{S_{\mathrm{NN}}} = 130\mathrm{GeV}$ 的 Au+Au 碰撞中事件平均横向动量〈 p_{T} 〉涨落的首次大接受度测量。发现非统计的〈 p_{T} 〉涨落明显超过在一次典型碰撞中产生的有限数量粒子所预期的涨落。对于带电强子的赝快度范围在$|\eta|<1$、方位角为 2π、平均动量范围 $0.15\mathrm{GeV}/c \leqslant$〈 p_{T} 〉$\leqslant 2\mathrm{GeV}/c$ 的 15%的最中心碰撞，相对于统计的参考值，事件的平均动量分布的均方根分数宽度超额为 13.7±0.1(统计)±1.3(系统)% ，这种宽度超额随着碰撞中心度作缓慢而非单调的变化，而不显示能够预示临界涨落出现的快速变化。所报道的〈 p_{T} 〉涨落超额定性地大于在低能量观测到的值，并且和理论上的预期有很大的区别。还讨论了初态的半硬部分子散射与大量的色介质消散对〈 p_{T} 〉涨落的贡献。

Event-wise〈 p_{T} 〉fluctuations in Au+Au collisions at $\sqrt{S_{\mathrm{NN}}} = 130\mathrm{GeV}$

STAR Collaboration

Key words: Au+Au collisions, Mean transverse momentum

We present the first large-acceptance measurement of event-wise mean transverse momentum〈 p_{T} 〉fluctuations for Au+Au collisions at nucleon-nucleon center-of-momentum collision energy $\sqrt{S_{\mathrm{NN}}} = 130\mathrm{GeV}$. The observed nonstatistical〈 p_{T} 〉fluctuations substantially exceed in magnitude fluctuations expected from the finite number of particles produced in a typical collision. The r.m.s. fractional width excess of the event-wise〈 p_{T} 〉distribution is 13.7 ± 0.1(stat) ±1.3(syst)% relative to a statistical reference, for the 15% most-central collisions and for charged hadrons within pseudorapidity range $|\eta| < 1$, 2π azimuth, and $0.15\mathrm{GeV}/c \leqslant$〈 p_{T} 〉$\leqslant 2\mathrm{GeV}/c$. The width excess varies smoothly but

nonmonotonically with collision centrality and does not display rapid changes with centrality which might indicate the presence of critical fluctuations. The reported 〈 p_T 〉 fluctuation excess is qualitatively larger than those observed at lower energies and differs markedly from theoretical expectations. Contributions to 〈 p_T 〉 fluctuations from semihard parton scattering in the initial state and dissipation in the bulk colored medium are discussed.

在 Au+Au $\sqrt{S_{NN}}$ = 200GeV 碰撞中 π 的干涉测量

STAR 合作组

关键词 Au+Au 碰撞，π 介子，干涉测量

利用相对论重离子对撞机上的 STAR 探测器对 Au+Au $\sqrt{S_{NN}}$ = 200GeV 碰撞中的两个 π 介子的干涉测量进行了系统分析。提取了 HBT 半径并且研究了它们的多重性、横向动量、以及方位角依赖性，还研究了关联函数的高斯结构。通过对冲击波参数化的拟合估算了冷却过程中源的几何和动力学结构。最后还对源的扩散以及它和最初能量密度分布的关系进行了研究。

Pion interferometry in Au+Au collisions at $\sqrt{S_{NN}}$ = 200GeV

STAR Collaboration

Key words: Au+Au collisions, Pion, Interferometry

We present a systematic analysis of two-pion interferometry in Au+Au collisions at $\sqrt{S_{NN}}$ = 200GeV using the STAR detector at Relativistic Heavy Ion Collider. We extract the Hanbury-Brown and Twiss radii and study their multiplicity, transverse momentum, and azimuthal angle dependence. The Gaussianness of the correlation function is studied. Estimates of the geometrical and dynamical structure of the freeze-out source are extracted by fits with blast-wave parametrizations. The expansion of the source and its relation with the initial energy density distribution are studied.

Au+Au $\sqrt{S_{NN}}$ = 200GeV 中心碰撞中的横向动量依赖动力学结构修正

STAR 合作组

关键词 Au+Au 碰撞，强子分布，横向动量

在赝快度| η |≤1、方位角满 2π、横向动量区间为 0.14GeV/c≤ p_T ≤2.1GeV/c 的空间中，用离散小波扩散的方法研究了相对论 Au+Au 碰撞中产生的强子分布关联。在周边 Au+Au 碰撞中，观测到了由于微小喷注碎裂而产生的关联结构，这种结构随着碰撞中心度以及 p_T 以一种以前未见过的方式演化，这种演化暗示微小喷注在物质的纵向扩展过程中会出现很强的消散。

Transverse-momentum dependent modification of dynamic texture in central Au+Au collisions at $\sqrt{S_{NN}}$ = 200GeV

STAR Collaboration

Key words: Au+Au collision，Hadron distribution, Transverse momentum

Correlations in the hadron distributions produced in relativistic Au+Au collisions are studied using the discrete wavelet expansion method. The analysis is performed in the space of pseudorapidity ($|\eta|\leq 1$) and azimuth (full 2π) in bins of transverse momentum (p_T) from 0.14GeV/$c\leqslant\langle p_T\rangle\leqslant$2.1GeV/$c$. In peripheral Au+Au collisions a correlation structure ascribed to minijet fragmentation is observed. It evolves with collision centrality and p_T in a way not seen before, which suggests strong dissipation of minijet fragmentation in the longitudinally expanding medium.

在能量为 200GeV 内含喷注产生的极化质子碰撞反应中纵向双自旋的不对称性和反应截面

STAR 合作组

关键词 极化质子碰撞，纵向双自旋不对称性，截面

测量了在内含中心快度喷注产生的极化质子碰撞中的纵向双自旋不对称性 A_{LL} 和微分反应截面，碰撞能量 $\sqrt{S_{NN}}=200$GeV 。测量的反应截面数据的横向动量范围是 5 GeV/c < p_T < 50 GeV/c，并且与接近主要项的摄动 QCD 计算一致。A_{LL} 数据的横向动量范围是 5 GeV/c < p_T < 17 GeV/c，并且在 98% C.L.与极化核子的的最大正胶子极化不一致。

Longitudinal double-spin asymmetry and cross section for inclusive jet production in polarized proton collisions at $\sqrt{S_{NN}}$ = 200GeV

STAR Collaboration

Key words: Polarized proton collisions, Longitudinal double-spin asymmetry, Cross section

We report a measurement of the longitudinal double-spin asymmetry A_{LL} and the differential cross section for inclusive midrapidity jet production in polarized proton collisions at $\sqrt{S_{NN}}=200$GeV . The cross section data cover transverse momenta 5 GeV/c < p_T < 50 GeV/c and agree with next-to-leading order perturbative QCD evaluations. The A_{LL} data cover 5 GeV/c < p_T < 17 GeV/c and disfavor at 98% C.L. maximal positive gluon polarization in the polarized nucleon.

在 200GeV Au+Au 中心碰撞中双喷注的直接测量

STAR 合作组

关键词 带电强子，方位角关联，双喷注

STAR 合作组在相对论重离子碰撞机上测量了在比以前更高的横动量下的带电强子在 Au+Au 碰撞中的方位角关联。随着横动量的增加，一个背对背的窄峰出现在相对减少的背景之上，在所有所研究的碰撞中心度上都出现清晰的双喷注信号。在核碰撞反应中，通过这种角关联，完成了关于双喷注的产生和压制的系统研究，从而为密集物质中部分子的能量损失机制提供一个新的约束条件。

Direct observation of dijets in central Au+Au collisions at $\sqrt{S_{\mathrm{NN}}}$ = 200GeV

STAR Collaboration

Key words: Charged hadron, Azimuthal correlation, Dijet

The STAR Collaboration at the Relativistic Heavy Ion Collider reports measurements of azimuthal correlations of high transverse momentum (p_{T}) charged hadrons in Au+Au collisions at higher p_{T} than reported previously. As p_{T} is increased, a narrow, back-to-back peak emerges above the decreasing background, providing a clear dijet signal for all collision centralities studied. Using these correlations, we perform a systematic study of dijet production and suppression in nuclear collisions, providing new constraints on the mechanisms underlying partonic energy loss in dense matter.

200GeV 能量的 p+p 和 d+Au 对心碰撞中前向中性π介子的产生

STAR 合作组

关键词 p+p 碰撞，d+Au 碰撞，中性π^0介子

研究测量了在能量为 200 GeV 的 p+p 和 d+Au 对心碰撞中前向中性π^0介子的产生。在 p+p 碰撞中的产额与接近主要项的摄动 QCD 理论计算基本一致。在 d+Au 碰撞中的每二体碰撞的产额则随着赝快度 η 的增加而减少。在平均赝快度$\langle\eta\rangle = 4.00$ 时，减少到 p + p 碰撞产额的约 30%，比预期值要低。探测和测量了前向中性π^0介子与带电强子在赝快度 $\eta\approx 0$ 范围内的方位角关联，结果显示在 p+p 碰撞中有一个反冲峰，此峰在 d+Au 碰撞中在π介子能量低时是看不到的。这些现象与重核的低 x 胶子结构饱和图像在性质上是一致的。

Forward neutral pion production in p+p and d+Au collisions at $\sqrt{S_{NN}} = 200GeV$

STAR Collaboration

Key words: p+p collision, d+Au collision, π^0 mesons

Measurements of the production of forward π^0 mesons from p+p and d+Au collisions at $\sqrt{S_{NN}} = 200GeV$ are reported. The p+p yield generally agrees with next-to-leading order perturbative QCD calculations. The d + Au yield per binary collision is suppressed as η increases, decreasing to ~30% of the p + p yield at $<\eta> = 4.00$, well below shadowing expectations. Exploratory measurements of azimuthal correlations of the forward π^0 with charged hadrons at $\eta \approx 0$ show a recoil peak in p + p that is suppressed in d + Au at low pion energy. These observations are qualitatively consistent with a saturation picture of the low-x gluon structure of heavy nuclei.

在 200GeV 能量的 Au+Au 碰撞中高横动量下的重子和介子的测量

STAR 合作组

关键词 横动量谱，重子，介子

在能量为200 GeV 的 Au+Au 中心碰撞中，在中心快度区间 $\pi^{\pm}$, p 和 $\bar{p}$ 的横动量谱可以测量到 12 GeV/c。在 Au+Au 中心碰撞中，$\pi^{\pm}$ 介子和 p($\bar{p}$)重子在二体碰撞的归一化中，在横动量 $p_T \geq 4$ GeV/c 时都显示出严重的产额压低现象。在横动量范围 1.5 GeV/$c \leqslant p_T \leqslant 6$ GeV/c 内，质子和反质子的压低要小于 $\pi^{\pm}$ 介子的压低。π^-/π^+ 和 $\bar{p}/p$ 的比率至多显示出很弱的横动量相关性而未见明显的碰撞中心度相关性。在 $p_T \geqslant$ 5GeV/c 时，p/π比率在 Au + Au 中心碰撞中接近在 p + p 和 d + Au 碰撞中的数值。结果指出在高横动量范围内，当 $\pi^{\pm}$、p 和 $\bar{p}$ 的部分子源与核物质相互作用时，有相似的能量损失。

Identified baryon and meson distributions at large transverse momenta from Au+Au collisions at $\sqrt{S_{NN}} = 200GeV$

STAR Collaboration

Key words: Transverse momentum spectra, Baryons, Mesons

Transverse momentum spectra of $\pi^{\pm}$, p and $\bar{p}$ up to 12GeV/c at midrapidity in centrality selected Au + Au collisions at $\sqrt{S_{NN}} = 200GeV$ are presented. In central Au + Au collisions, both $\pi^{\pm}$ and p($\bar{p}$) show significant suppression with respect to binary scaling at $p_T \geqslant 4$ GeV/c. Protons and antiprotons are less suppressed than $\pi^{\pm}$, in the range 1.5 GeV/$c \leqslant p_T \leqslant 6$ GeV/c. The π^-/π^+ and $\bar{p}/p$ ratios show at

most weak p_T dependence and no significant centrality dependence. The p/π ratios in central Au + Au collisions approach the values in p+p and d+Au collisions at $p_T \geqslant 5$ GeV/c. The results at high p_T indicate that the partonic sources of $\pi^{\pm}$, p and $\bar{p}$ have similar energy loss when traversing the nuclear medium.

能量为 200GeV 的 p+p 和 Au+Au 碰撞中奇异重子共振态的产生

STAR 合作组

关键词 奇异重子，p+p 碰撞，Au+Au 碰撞

测量了在能量为 200GeV 的 p+p 和 Au+Au 碰撞中产生的Σ(1385) 和 Λ(1520)。研究讨论了在化学平衡和热平衡下的产额和横动量谱，并且与一些模型进行了比较。热力学和显微模型不能充分地描述在 Au+Au 中心碰撞中所有共振态的产额。结果显示在化学平衡和热力学平衡之间也许存在一个时间跨度，在此期间发生了强子的弹性相互作用。

Strange baryon resonance production in $\sqrt{S_{NN}} = 200$GeV p+p and Au+Au collisions

STAR Collaboration

Key words: Strange baryons, p+p collision, Au+Au collision

We report the measurements of Σ(1385) and Λ(1520) production in p + p and Au+Au collisions at $\sqrt{S_{NN}} = 200$GeV from the STAR Collaboration. The yields and the p_T spectra are presented and discussed in terms of chemical and thermal freeze-out conditions and compared to model predictions. Thermal and microscopic models do not adequately describe the yields of all the resonances produced in central Au+Au collisions. Our results indicate that there may be a time span between chemical and thermal freeze-out during which elastic hadronic interactions occur.

能量为 200GeV 的 p+p 和 d+Au 碰撞中高横动量下的强子谱的测量

STAR 合作组

关键词 粒子产生，摄动量子色动力学，碎裂模型，克宁效应，x_T 归一

研究测量了能量为 200 GeV 的 p + p 和 d + Au 碰撞中的带电 π 介子、p 和 $\bar{p}$ 的横向动量谱。所研究的横向动量谱在中心快度区域$|y|<0.5$、横向动量范围 0.3 GeV/c< p_T <10 GeV/c。粒子鉴别通过在时间投影室的电离能量损失及其相对论性上升以及在 STAR 中的飞行时间来进行。在 p+p 和

d+Au 碰撞中，带电 π 介子、p 和 $\bar{p}$ 的高横动量的产额谱与 EPOS 模型和带有碎裂机制与因数分解归一的 NLO 摄动量子色动力学计算结果相一致。发现在 p+p 碰撞中，所有的带电 π 介子、p 和 $\bar{p}$ 谱在强相互作用为其主要作用的动量范围内($p_T \geqslant 2$ GeV/c)都遵循 x_T 归一的规律。在中心快度区域带电 π 介子的核修正因子大于1，而对于质子来说更大。

Identified hadron spectra at large transverse momentum in p+p and d+Au collisions at $\sqrt{S_{NN}}$ = 200GeV

STAR Collaboration

Keywords: Particle production, Perturbative quantum chromodynamics, Fragmentation function, Cronin effect, x_T-scaling

We present the transverse momentum (p_T) spectra for identified charged pions, protons and anti-protons from p+p and d+Au collisions at $\sqrt{S_{NN}} = 200\text{GeV}$. The spectra are measured around midrapidity ($|y| < 0.5$) over the range of 0.3 GeV/c < p_T <10GeV/c with particle identification from the ionization energy loss and its relativistic rise in the time projection chamber and time-of-flight in STAR. The charged pion and proton + anti-proton spectra at high p_T in p+p and d+Au collisions are in good agreement with a phenomenological model (EPOS) and with next-to-leading order perturbative quantum chromodynamic (NLO PQCD) calculations with a specific fragmentation scheme and factorization scale. We found that all proton, anti-proton and charged pion spectra in p+p collisions follow x_T-scaling for the momentum range where particle production is dominated by hard processes ($p_T \geqslant 2$ GeV/c). The nuclear modification factor around midrapidity is found to be greater than unity for charged pions and to be even larger for protons.

能量为 130GeV 的 Au+Au 碰撞中通过动量子空间(η,φ)的净电荷角关联研究强子化几何学

STAR 合作组

关键词 净电荷角关联，净电荷涨落，强子化，重离子碰撞

首次研究了角关联在不同的赝快度和方位角范围内的电荷相关性。测量的是 Au+Au 能量为 130GeV 的碰撞，带电强子的横动量范围是 0.15 GeV/c≤ p_T ≤2 GeV/c，赝快度范围是$|\eta|$≤1.3。我们观察到的关联结构与理论预言不相符，但是却与强子发射几何的演化相一致。这种演化是从一维空间的色弦沿着束流方向的碎裂到至少二维强子化几何沿着束流和强子不透明的大块物质的方位角方向、并且中心度逐渐增大的情况下实现的。

Hadronization geometry from net-charge angular correlations on momentum subspace *(η,φ)* in Au + Au collisions at $\sqrt{S_{\mathrm{NN}}}$ = 130GeV

STAR Collaboration

Key words: Net-charge correlations, Net-charge fluctuations, Hadronization, Heavy ion collisions

We present the first measurements of charge-dependent correlations on angular difference variables $\eta_1-\eta_2$ (pseudorapidity) and $\varphi_1-\varphi_2$ (azimuth) for primary charged hadrons with transverse momentum 0.15 GeV/$c\leqslant p_{\mathrm{T}}\leqslant$2 GeV/$c$ and $|\eta|\leq 1.3$ from Au+Au collisions at $\sqrt{S_{\mathrm{NN}}}=130\mathrm{GeV}$. We observe correlation structures not predicted by theory but consistent with evolution of hadron emission geometry with increasing centrality from one-dimensional fragmentation of color strings along the beam direction to an at least two-dimensional hadronization geometry along the beam and azimuth directions of a hadron-opaque bulk medium.

质心系能量为 200GeV 的质子对碰撞中产生的多重数与横向动量谱的关联

STAR 合作组

关键词 质子对碰撞，多重数，横向动量谱

报道了质心系能量为 200 GeV 并且具有 10 类事件多重数的质子对碰撞时横向动量谱 p_{T} 的测量。通过分析谱的多重数依赖后发现，谱形可以分解为两部分，其一是振幅正比于多重数，且可用横向质量 m_{T} 的 Levy 分布进行描述；其二是振幅正比于多重数的平方，且可用横向快度 y_{T} 的高斯(Gauss)分布进行描述。这两部分的函数表达式几乎都与事件多重数无关。这两部分可以被看成是质子对碰撞的两组分模型中的软组分和硬组分。这一分析首次将横向动量 p_{T} 谱的硬组分看成是简单形式的横向快度 y_{T} 分布 。

Multiplicity dependence of inclusive p_{T} spectra from p+p collisions at $\sqrt{S_{\mathrm{NN}}}$ = 200GeV

STAR Collaboration

Key words：p+p collisions, Multiplicity, Transverse momentum spectrum

We report measurements of transverse momentum p_{T} spectra for ten event multiplicity classes of p-p collisions at $\sqrt{S_{\mathrm{NN}}}=200\mathrm{GeV}$. By analyzing the multiplicity dependence we find that the spectrum shape can be decomposed into a part with amplitude proportional to multiplicity and described by a

Levy distribution on transverse mass m_T, and a part with amplitude proportional to multiplicity squared and described by a Gaussian distribution on transverse rapidity y_T. The functional forms of the two parts are nearly independent of event multiplicity. The two parts can be identified with the soft and hard components of a two-component model of p+p collisions. This analysis then provides the first isolation of the hard component of the p_T spectrum as a distribution of simple form on y_T.

质心系能量为 62.4GeV 的 Au+Au 碰撞产生的带电粒子和光子向前赝快度的多重数和赝快度分布

STAR 合作组

关键词 Au+Au 碰撞，多重数, 赝快度，光子，带电粒子

我们报导了质心系能量为 62.4 GeV 的 Au+Au 碰撞中，产生的带电粒子和光子的多重数以及赝快度分布与中心度相关的测量。在赝快度的以下区间：2.9≤η≤3.9 和 2.3≤η≤3.7，我们对带电粒子和光子分别进行了研究，用参与核子数和两体碰撞数对粒子产物进行标度，发现在以上赝快度范围，碰撞表现出与能量无关的部分碎裂行为。光子遵从与中心度无关的部分碎裂模式，但是带电粒子却是与能量有关。因而我们采取对比式的研究方法，对核-核碰撞中的正电荷强子、负电荷强子、光子、π 介子以及净质子的赝快度分布与质子-质子碰撞中的这些粒子的赝快度分布进行对比分析，发现在这些带电粒子分布中，重子对与中心度有关的部分碎裂行为有着很大的贡献。介子虽遵从与能量无关的部分碎裂，但重子却与能量有关。

Multiplicity and pseudorapidity distributions of charged particles and photons at forward pseudorapidity in Au+Au collisions at $\sqrt{S_{NN}}$ = 62.4GeV

STAR Collaboration

Key words: Au+Au collision, Multiplicity, Pseudorapidity, Photons, Charged particles

We present the centrality-dependent measurement of multiplicity and pseudorapidity distributions of charged particles and photons in Au+Au collisions at $\sqrt{S_{NN}}$ = 62.4 GeV. The charged particles and photons are measured in the pseudorapidity regions 2.9≤η≤3.9 和 2.3≤η≤3.7, respectively. We have studied the scaling of particle production with the number of participating nucleons and the number of binary collisions. The photon and charged particle production in the measured pseudorapidity range has been shown to be consistent with energy-independent limiting fragmentation behavior. Photons are observed to follow a centrality-independent limiting fragmentation behavior, while for charged particles it is centrality dependent. We have carried out a comparative study of the pseudorapidity distributions of positively charged hadrons, negatively charged hadrons, photons, pions, and net protons in nucleus-nucleus collisions and pseudorapidity distributions from p+p collisions. From these comparisons, we conclude that baryons in the inclusive charged particle distribution are responsible for the observed

centrality dependence of limiting fragmentation. The mesons are found to follow an energy-independent behavior of limiting fragmentation, whereas the behavior of baryons is energy dependent.

在质心系能量为 62.4GeV 的 Au+Au 碰撞中产生的定向流

STAR 合作组

关键词 Au+Au 碰撞，定向流

本文报导质心系能量为 62.4 GeV 的 Au+Au 碰撞在中间赝快度区域$|\eta|<1.3$和向前赝快度区域$2.5<|\eta|<4.0$ 定向流v_1的测量。此结果可由三粒子累积量法、混合谐波的事件平面法以及首次在相对论重离子对撞机上应用的利用旁观中子重构事件平面的标准方法获得。上述三种方法所得结论很好相符。在所研究的赝快度范围内，我们发现带电粒子的定向流方向与碎裂中子恰好相反。

Directed flow in Au+Au collisions at $\sqrt{S_{\mathrm{NN}}}=62.4\mathrm{GeV}$

STAR Collaboration

Key words: Au+Au collision, Directed flow

We present the directed flow(v_1)measured in Au+Au collisions at $\sqrt{S_{\mathrm{NN}}}=62.4\mathrm{GeV}$ in the midpseudorapidity region $|\eta|<1.3$ and in the forward pseudorapidity region $2.5<|\eta|<4.0$. The results are obtained using the three-particle cumulant method, the event plane method with mixed harmonics, and for the first time at RHIC, the standard method with the event plane reconstructed from spectator neutrons. Results from all three methods are in good agreement. Over the pseudorapidity range studied, charged particle directed flow is in the direction opposite to that of fragmentation neutrons.

质心系能量为 130 GeV 的 Au+Au 碰撞在动量子空间(η, φ)中的微型喷注变形以及和电荷无关的角关联

STAR 合作组

关键词 Au+Au 碰撞， 动量子空间，角关联，微型喷注变形

在质心系能量为 130 GeV 的 Au+Au 碰撞中，研究了横向动量为 0.15 GeV/$c\leqslant p_{\mathrm{T}}\leqslant$2 GeV/$c$和赝快度在$|\eta|<$ 1.3 范围内所有主要带电强子的$\eta_1-\eta_2$(赝快度)和$\varphi_1-\varphi_2$(方位角)，藉以测量两粒子关联。在较宽的相对角范围内，可看到大振幅的关联，同侧和反侧（即相对角小于 $\pi/2$ 和大于 $\pi/2$）则出现区分明显的结构。主要关联结构包括与椭圆流相关的部分加一个强同侧峰。若假设后者起因于关联强子，其与重离子碰撞早期阶段准硬部分子的散射过程有关，此过程在较小的相对角内产生一个类喷注的关联峰。从周边碰撞到中心碰撞，在 $\eta_1-\eta_2$ 上峰的宽度增大 2.3 倍，预示着被散射的准硬部分子与沿纵向不断膨胀的介质间存在强耦合。这种喷注分析新方法可对横向动量远低于的部分子散射进行很好的研究。只有微扰量子色动力学和标准碎裂模型才适用的动力学范围。

Minijet deformation and charge-independent angular correlations on momentum subspace (η, φ) in Au+Au collisions at $\sqrt{S_{\mathrm{NN}}}$ = 130GeV

STAR Collaboration

Key words: Au+Au collision, Momentum subspace, Augular correlation, Minijet deformation

Measurements of two-particle correlations on angular difference variables $\eta_1 - \eta_2$ (pseudorapidity) and $\varphi_1 - \varphi_2$ (azimuth) are presented for all primary charged hadrons with transverse momentum 0.15 GeV/$c \leqslant p_T \leqslant$2 GeV/$c$ and $|\eta| \leqslant 1.3$ from Au+Au collisions at $\sqrt{S_{\mathrm{NN}}}$ = 130GeV. Large-amplitude correlations are observed over a broad range in relative angles where distinct structures appear on the same-side and away-side (i.e., relative azimuth less than $\pi/2$ or greater than $\pi/2$). The principal correlation structures include that associated with elliptic flow plus a strong, same-side peak. It is hypothesized that the latter results from correlated hadrons associated with semi-hard parton scattering in the early stage of the heavy-ion collision which produces a jet-like correlation peak at small relative angles. The width of the jet-like peak on $\eta_1 - \eta_2$ increases by a factor 2.3 from peripheral to central collisions, suggesting strong coupling of semi-hard scattered partons to a longitudinally-expanding medium. The new methods of jet analysis introduced here provide access to scattered partons at low transverse momentum well below the kinematic range where perturbative quantum chromodynamics and standard fragmentation models are applicable.

在质心系能量为 200GeV 的 Au+Au 碰撞中产生的中性 K 介子的干涉测量

STAR 合作组

关键词 中心 K 介子，干涉测量，Au+Au 碰撞

展示了质心系能量为 200GeV 的重离子碰撞从 K^0_S 两体干涉测量中得到的首批很有意义的统计结果。利用一种考虑了强相互作用的模型来拟合测量到的关联函数，并且研究单道和双道的影响。在平均横向质量 $\langle m_T \rangle$=1.07GeV 时，我们分别得到不变半径为 R=4.09±0.46（stat,统计误差）±0.31(sys,系统误差)fm, 混沌度参数 λ=0.92±0.23(stat)±0.13(sys), 这些结论与可用强集合流模式描述的用 π 介子建立的 m_T 分类是定性一致的。

Neutral kaon interferometry in Au+Au collisions at $\sqrt{S_{NN}}$ = 200GeV

STAR Collaboration

Key words Neutral kaon, Interferometry, Au+Au collision

We present the first statistically meaningful results from two-K^0_S interferometry in heavy-ion collisions at $\sqrt{S_{NN}}$ = 200GeV. A model that takes the effect of the strong interaction into account has been used to fit the measured correlation function. The effects of single and coupled channels were explored. At the mean transverse mass $\langle m_T \rangle$ = 1.07 GeV, we obtain the values R=4.09±0.46(stat)± 0.31(sys) fm and λ =0.92±0.23(stat)±0.13(sys), where R and λ are the invariant radius and chaoticity parameter, respectively. The results are qualitatively consistent with m_T systematics established with pions in a scenario characterized by a strong collective flow.

在质心系能量为 200GeV 的 Au+Au 中心碰撞中产生的质子 p 与 Λ 的关联

STAR 合作组

关键词 Au+Au 碰撞，质子，Λ 粒子，关联函数

我们根据在相对论重离子对撞机(RHIC)上的 STAR 实验中进行的质心系能量为 200GeV 的 Au+Au 中心对撞，构造了 p-Λ、p-$\bar{\Lambda}$、$\bar{p}$-Λ、$\bar{p}$-$\bar{\Lambda}$的关联函数。通过分析 p-Λ，$\bar{p}$-$\bar{\Lambda}$的关联函数，可以推断出质子 p 和Λ的源尺寸。结果显示这些源尺寸比也是在同样的 STAR 实验上测得，但具有较小的横向质量的π介子的源尺寸要小，这表明有着很强的普适集合流。至于我们首次测得的 p-$\bar{\Lambda}$和$\bar{p}$-Λ关联函数，结果显示很大程度上没有关联。为了重构测得的关联函数，必须在末态的相互作用计算中加入湮没道和/或自旋平均散射长度的负实数项。

Proton-Λ correlations in central Au+Au collisions at $\sqrt{S_{NN}}$ = 200GeV

STAR Collaboration

Key words: Au+Au collisions, Protons, Λ particles, Correlation function

We report on p-Λ, p-$\bar{\Lambda}$, $\bar{p}$-Λ, and $\bar{p}$-$\bar{\Lambda}$ correlation functions constructed in central Au+Au collisions at $\sqrt{S_{NN}}$ = 200GeV by the STAR experiment at RHIC. The proton and lambda source size is inferred from the p-Λ and $\bar{p}$-$\bar{\Lambda}$ correlation functions. It is found to be smaller than the pion source size also measured by the STAR experiment at smaller transverse masses, in agreement with a scenario of a strong universal collective flow. The p-$\bar{\Lambda}$ and $\bar{p}$-Λ correlation functions, which are measured for the

first time, exhibit a large anticorrelation. Annihilation channels and/or a negative real part of the spin-averaged scattering length must be included in the final-state interactions calculation to reproduce the measured correlation function.

在质心系能量为 200GeV 的 Au+Au 碰撞中由于平均横向动量 p_T 涨落引起的(η, φ) 方向上横向动量的关联

STAR 合作组

关键词 赝快度，空间方位角，平均横向动量

对于质心系能量为 200GeV 的 Au+Au 碰撞，我们首次测量了赝快度以及空间方位角（η,φ）与对事件求平均的横向动量〈 p_T 〉涨落之间的关联。通过转化这种关联，可以获得横向动量在差值$(\eta_\Delta,\varphi_\Delta)$内的 p_T 自相关，而这种自相关表述了在(η,φ)上的速度/温度分布。自相关的一般表达式说明了基本的关联机制在于部分子碎裂。同时自相关的值随着碰撞中心度的改变而迅速改变，这也就意味着在中心 Au+Au 碰撞中，相对于周边和质子+质子碰撞，碎裂过程更强烈地被耗散媒介所改变。

Transverse-momentum p_T correlations on (η, φ) from mean-p_T fluctuations in Au+Au collisions at $\sqrt{S_{NN}}$ = 200GeV

STAR Collaboration

Key words: Pseudorapidity, Azimuth, Mean transverse-momentum

We present the first measurements of pseudorapidity and azimuth *(η, φ)* binsize dependence of event-wise mean transverse-momentum 〈 p_T 〉 fluctuations for Au+Au collisions at $\sqrt{S_{NN}} = 200\text{GeV}$. We invert that dependence to obtain p_T autocorrelations on differences $(\eta_\Delta,\phi_\Delta)$ interpreted to represent velocity/temperature distributions on *(η, φ)*. The general form of the autocorrelations suggests that the basic correlation mechanism is parton fragmentation. The autocorrelations vary rapidly with collision centrality, which suggests that fragmentation is strongly modified by a dissipative medium in the more central Au–Au collisions relative to peripheral or p–p collisions.

RHIC 实验中喷注附近和相对方向上的奇异粒子的产额关系

左嘉旭（For the STAR Collaboration）

关键词：RHIC-STAR，双强子关联，马赫角，近角，远角融合

在 RHIC 物理中，喷注在重离子碰撞中被作为研究极端密度下的核物质形态的探针。双强子

关联是一个研究喷注和喷注与介质相互作用的有效方法。双强子关联可以提供以下信息：喷注淬火，重子与介子的比率增加，粒子与反粒子的产生机制，和马赫角的产生等。我们将报告奇异粒子（Λ，K^0_S）在对心能量 $\sqrt{S_{NN}}=200GeV$ 的 $^{197}Au+^{197}Au$ 对心碰撞中的双强子关联研究。在研究中应用带电强子作为触发粒子(3.0 GeV/c< p_T <6.0 GeV/c)，奇异粒子作为相关联的粒子(1.0 GeV/c < p_T < 4.0 GeV/c)。我们的研究集中于重子与介子的比率和粒子与反粒子的比率与$\Delta\phi$的函数关系。在远角方向研究并且观察了上述比率的曲线。结果显示，远角方向上的重子与介子的比率曲线似乎与在激波中高密度范围内的融合模型结果一致。在远角方向观察到的反粒子与粒子的比率也许对我们理解马赫角的产生大有帮助。我们同时也将提出关联粒子在近角方向和远角方向的比率，结果似乎显示，比起近角喷注，远角喷注更影响重子与介子的比率和粒子与反粒子的比率。

Particle ratios on the near- and away-side of jets at RHIC

ZUO Jiaxu (For the STAR Collaboration)

Key words: RHIC-STAR, Di-hadron correlation, Mach-cone, Near-side, Away-side, Recombination

At RHIC, jets serve as a penetrating probe of the extremely dense nuclear matter formed in heavy ion collisions. Di-hadron correlations are an effective way to study jets and their interactions with the medium in these high multiplicity collisions. Identified di-hadron correlations can provide additional information on: jet quenching, the baryon to meson ratio enhancement, the particle and anti-particle production mechanisms, and the possible production of Mach-cones. We will report di-hadron correlations of neutral strange baryons (Λ) and mesons (K^0_S) in ^{197}Au + ^{197}Au collisions at $\sqrt{S_{NN}}=200GeV$ measured by the STAR experiment. Our study is performed with unidentified hadrons triggers (3.0 GeV/c< p_T <6.0 GeV/c) and strange associated particles (1.0 GeV/c < p_T < 4.0 GeV/c). We focus on extracting the baryon to meson and the particle to antiparticle ratios as a function of $\Delta\phi$. The shape of these ratios on the away-side ratio is studied. Our results for the shape of the baryon to meson ratio on the away-side seem to be consistent with recombination in a high density region of a shock-wave. The observation of a shape in the anti-baryon to baryon ratio on the away-side maybe is useful to better understand the source of the Mach-cone like structures on the away-side. We also present the associated particles near-side to away-side ratios. The results seem to indicate that the baryon to meson ratios and particle to anti-particle ratios are both modified on the away-side of jets compared to the near-side of jets.

在部分子喷注中Ω重子的各向异性流的产生

左嘉旭　蔡翔舟　马余刚　陈金辉　马国亮

关键词： 定向流，椭圆流，四阶各向异性流，夸克数归一

在部分子层叠框架(AMPT 模型)下研究了Ω, p, K 和 π 的定向流 v_1、椭圆流 v_2 和四阶各向异性流 v_4。我们研究的是 $^{197}Au+^{197}Au$ 对心碰撞(能量为 $\sqrt{S_{NN}}=200GeV$)的各向异性流。我们研究了 v_2 和 v_4 与不变横动量之间的关系和 v_1 与快度之间的关系。结果显示，对于不同的重子和介子的 v_2 遵守夸克数归一的规律。我们看到 v_4 与 v_2^2 可以很好地被系数 1.2 归一， 且这个系数的归

一程度优于系数 0.5。我们还比较了椭圆流 v_2 在缺省的 AMPT 模型、融合的 AMPT 模型和 RQMD 模型中的不同。结果显示部分子散射对椭圆流 v_2 的产生有很大的作用，并且弦融合的 AMPT 模型更适合重建椭圆流 v_2。

Anisotropic flows of omega baryon due to parton cascades

ZUO Jiaxu CAI Xiangzhou MA Yugang CHEN Jinhui MA Guoliang

Key words: Directed flow, Elliptic flow, The fourth order anisotropic flow, Quark number scaling

The directed flow v_1, elliptic flow v_2 and the fourth order anisotropic flow v_4 of Ω, p, K and π have been studied in the framework of a parton cascade model, namely A Multi-Phase Transport (AMPT) model for ^{197}Au + ^{197}Au collisions at $\sqrt{S_{\rm NN}} = 200$GeV . Transverse momentum ($p_{\rm T}$) dependence of v_2 and v_4 and rapidity dependence of v_1 are presented. The results show that the v_2 obeys the constituent quark number scaling which has been observed for other mesons and baryons. It is seen that v_4/v_2^2 is scaled better by 1.2 than 0.5. The comparisons of elliptic flow v_2 among the default version of AMPT, the melting version of AMPT and RQMD model calculation, show that parton scattering process is important to reproduce the sizeable v_2, and the string melting AMPT model preferably reproduces elliptic flow v_2.

具有有限重子密度的化学非平衡夸克-胶子等离子体中的光子产生

贺泽君 龙家丽 马余刚

关键词 光子 化学非平衡夸克–胶子等离子体 有限重子数密度

为了揭示有限重子数密度对于 RHIC 能量下 Au+Au 对心碰撞所产生的化学非平衡夸克-胶子等离子体夸克-胶子等离子体中的光子产生的影响，我们首次把 Compton 过程(gq→qγ 和 g¯q → ¯qγ)、夸克湮没 q¯q→gγ、轫致辐射和 IPA 过程的光子产生表达式推广到了化学非平衡的具有有限重子数密度的夸克-胶子等离子体系统中。我们发现系统演化以及来自于轫致辐射和 Compton 过程 qg→γq 的巨大贡献使光子总产额成为初始夸克化学势的增函数。

Photons from a chemically equilibrating quark–gluon plasma at finite baryon density

HE Zejun LONG Jiali MA Yugang

Keywords: Photon, Chemically equilibrating quark–gluon plasma, Finite baryon density

In order to reveal the effect of finite baryon density on the photon production in a chemically equilibrating QGP system which is produced from Au +Au central collisions at the RHIC energies, we have first extended those expressions of the photon production for the Compton (gq → qγ and g ¯q

→ $\bar{q}\gamma$), annihilation $q\bar{q} \to g\gamma$, bremsstrahlung and IPA processes to the chemically equilibrating system at finite baryon density. We find that the effect of the system evolution on the photon production and large contribution of the bremsstrahlung and Compton qg→γq processes make the total photon yield as a strongly increasing function of the initial quark chemical potential.

3+1 维具有有限重子密度的非化学平衡夸克-胶子等离子体的演化方程

龙家丽　贺泽君　马余刚

关键词　3+1 维化学平衡的夸克-胶子等离子体，弛豫方程

假定弹性部分子散射足够快，能维持局域热平衡，则部分子密度的演化可用主方程描述。导致化学平衡的反应被假定为 $gg \Leftrightarrow ggg$ 和 $gg \Leftrightarrow q\bar{q}$ 。结合这些主方程和系统的能量-动量守恒方程,熵增和重子数守恒方程，可得到一组弛豫方程来描述具有有限重子密度的非化学平衡夸克-胶子等离子体在 3+1 维时空中的演化。

3+1D evolution equation of chemically equilibrating quark-gluon plasma at finite baryon density

LONG Jiali　HE Zejun　MA Yugang

Key words:　3+1D chemically equilibrating quark-gluon plasma, Relaxation equation

Assuming that elastic parton scatterings are sufficiently rapid to maintain local thermal equilibrium, the evolution of the parton densities can be given by the master equations. The dominant reactions leading to chemical equilibrium are assumed to be $gg \Leftrightarrow ggg$ and $gg \Leftrightarrow q\bar{q}$. Combining the master equations together with equation of energy-momentum conservation, entropy increase and equation of baryon number conservation, one can get a set of coupled relaxation equations describing evolutions of chemical equilibrating quark-gluon plasma at finite baryon density in a 3+1 dimensional space-time.

在 RHIC 能区的φ介子产生与部分子集体性

马余刚

关键词：φ介子，集体性，部分子

给出了实验上(RHIC-STAR)对于 Au+Au 碰撞中φ介子产额和椭圆流新的测量结果并且讨论了这些结果带来的物理信息：φ介子横向动量谱随着碰撞中心度的演化，从中心碰撞的指数分布到周边碰撞的幂级数分布，反映了随着碰撞的减弱，硬过程和其他可能的非平衡过程的贡献逐渐减弱。φ介子的核修正因子更像介子 K_s 的而偏离重子(Λ粒子)。φ介子显著的椭圆流表明了系统中已有部分子层次的集体流。在 Au+Au 中心碰撞中，由于φ介子是通过看起来已经热平衡的奇异夸克融合而成，故测量结果表明了部分子层次的集体流在高温高密物质(RHIC)中已经形成。

ϕ meson production and partonic collectivity at RHIC

MA Yugang

Key words: ϕ-meson, Collectivity, Parton

New results on ϕ-meson production and elliptic flow v_2 measurements from RHIC 2004 run (Run IV) have been reviewed. In addition, the di-hadron correlation function between the triggered ϕ and Ω and the associated soft particles was simulated. Knowledge about these results is discussed.

RHIC 能区的ϕ介子椭圆流核奇异夸克集体性

陈金辉　马余刚　马国亮　蔡翔舟　贺泽君　黄焕中*

龙家丽　沈文庆　钟 晨　左嘉旭

关键词：ϕ介子，多相输运模型，椭圆流

基于多相输运模型(AMPT)，通过 K^+K^-衰变道研究ϕ介子在极端相对论下的椭圆流。得到了ϕ介子椭圆流对于横向动量和碰撞中心度的依赖关系。研究表明ϕ介子能够携带系统早期的信息并且它遵循组分夸克标度规律。这些研究结果表明ϕ介子椭圆流表征了系统部分子层次的集体流，并且奇异夸克和轻夸克具有相同强度的椭圆流。

Elliptic flow of ϕ meson and strange quark collectivity at RHIC

CHEN Jinhui　MA Yugang　MA Guoliang　CAI Xiangzhou　HE Zejun

HUAN Huanzhong*　LONG Jiali　SHEN Wenqing　ZHONG Chen　ZUO Jiaxu

Keywords: ϕ-meson, A Multi-Phase Transport model, Elliptic flow

Based on A Multi-Phase Transport (AMPT) model, we have studied the elliptic flow v_2 of ϕ mesons from reconstructed K^+K^- decay channel at the top Relativistic Heavy Ion Collider energy at Brookhaven National Laboratory. The dependences of v_2 on transverse momentum p_T and collision centrality are presented and the rescattering effect of ϕ mesons in the hadronic phase is also investigated. The results show that experimental measurement of v_2 for ϕ mesons can retain the early collision information before ϕ decays and that the v_2 value of ϕ obeys the constituent quark number scaling which has been observed for other mesons and baryons. Our study indicates that the v_2 of ϕ mostly reflects partonic level collectivity developed during the early stage of the nucleus-nucleus collision and the strange and light up/down quarks have developed similar angular anisotropy properties at the hadronization.

---

*黄焕中(HUANG Huanzhong)：University of California, Los Angeles, CA 90095, USA

部分子/强子输运模型中的二粒子方位角关联和类马赫角结构

马国亮 张 松 马余刚 黄焕中* 蔡翔舟 陈金辉 贺泽君
龙家丽 沈文庆 施兴华 左嘉旭

关键词 二粒子方位角关联，马赫角，部分子级联，强子再散射，多相粒子输运模型

基于一个包含部分子和强子相互作用的多相粒子输运模型，通过混合事件的方法研究了触发粒子和伴随粒子之间的方位角关联。选择 200 GeV Au+Au 对撞产生的粒子进行研究，其中两种动量选择范围分别是 3 GeV/c< $p_{\mathrm{T}}^{\mathrm{trig}}$ <6 GeV/c 和 0.15 GeV/c< $p_{\mathrm{T}}^{\mathrm{assoc}}$ <3 GeV/c (软), 或 2.5 GeV/c < $p_{\mathrm{T}}^{\mathrm{trig}}$ <4 GeV/c 和 1 GeV/c < $p_{\mathrm{T}}^{\mathrm{assoc}}$ <2.5 GeV/c (硬)。我们在 200 GeV Au+Au 中心碰撞中发现了“类马赫”结构。通过比较有/无“部分子级联”和“强子再散射”的情况，发现部分子级联和强子再散射对类马赫结构的形成都有贡献。其中强子再散射对软粒子的类马赫结构形成的贡献是不可以忽略的。然而，仅仅强子再散射不能够产生实验上可观察到的类马赫结构的劈裂幅度，所以部分子级联过程对于描述实验上观察到的类马赫结构的劈裂幅度是非常必要的。另外，在包括部分子级联和强子再散射的物理图像下，观察到伴随粒子多重数和总的横向动量随着碰撞参数的增加而减少，平均的伴随粒子横向动量< p_{T} >随着碰撞参数的增加而增加。

Di-hadron azimuthal correlation and Mach-like cone structure in a parton/hadron transport model

MA Guoliang ZHANG Song MA Yugang HUANG Huanzhong* CAI Xiangzhou
CHEN Jinhui HE Zejun LONG Jiali SHEN Wenqing SHI Xinghua ZUO Jiaxu

Key words: Di-hadron azimuthal correlation, Mach cone, Parton cascade, Hadronic rescattering, AMPT

In the framework of a multi-phase transport model (AMPT) with both partonic and hadronic interactions, azimuthal correlations between trigger particles and associated scattering particles have been studied by the mixing-event technique. The momentum ranges of these particles are 3GeV/c< $p_{\mathrm{T}}^{\mathrm{trig}}$ <6GeV/c and 0.15GeV/c< $p_{\mathrm{T}}^{\mathrm{assoc}}$ <3GeV/c (soft), or 2.5GeV/c < $p_{\mathrm{T}}^{\mathrm{trig}}$ <4GeV/c and 1GeV/c < $p_{\mathrm{T}}^{\mathrm{assoc}}$ <2.5GeV/c (hard)in Au+Au collisions at $\sqrt{S_{\mathrm{NN}}} = 200\mathrm{GeV}$. A Mach-like structure has been observed in correlation functions for central collisions. By comparing scenarios with and without parton cascade and hadronic rescattering, we show that both partonic and hadronic dynamical mechanisms contribute to the Mach-like structure of the associated particle azimuthal correlations. The contribution of hadronic dynamical process cannot be ignored in the emergence of Mach-like correlations of the soft scattered associated hadrons. However, hadronic rescattering alone cannot reproduce experimental amplitude of Mach-like cone on away-side, and the parton cascade process is essential to describe experimental amplitude of Mach-like cone on away-side. In addition, both the associated multiplicity and the sum of p_{T} decrease, while the < p_{T} > increases, with the impact parameter in the AMPT model including partonic dynamics from string melting scenario.

---

*黄焕中(HUANG Huanzhong)：University of California, Los Angeles, CA 90095, USA

Au+Au 碰撞中部分子级联产生的三粒子关联

马国亮 马余刚 张 松 蔡翔舟 陈金辉 贺泽君 黄焕中*
龙家丽 沈文庆 施兴华 钟 晨 左嘉旭

关键词 三粒子关联，马赫角，部分子级联，强子再散射，多相粒子输运模型

基于一个包含部分子和强子相互作用的多相粒子输运模型，我们研究了 200 GeV Au+Au 碰撞中的一个触发粒子与两个伴随粒子之间的三粒子关联。研究发现相对于触发粒子不同方位角度的三粒子关联密度随着参加核子数的增加而增加。“扭转区域”和“马赫角区域”的三粒子关联密度比值随着参加核子数的增加而接近 1，这表明在 Au+Au 中心碰撞中强烈的部分子级联相互作用产生了部分子型的“类马赫冲击波”。

Three-particle correlations from parton cascades in Au+Au collisions

MA Guoliang MA Yugang ZHANG Song CAI Xiangzhou CHEN Jinhui
HE Zejun HUANG Huanzhong* LONG Jiali SHEN Wenqing
SHI Xinghua ZHONG Chen ZUO Jiaxu

Key words: Three-particle correlation, Mach cone, Parton cascade, Hadronic rescattering, AMPT

We present a study of three-particle correlations among a trigger particle and two associated particles in Au+Au collisions at $\sqrt{S_{\mathrm{NN}}} = 200\mathrm{GeV}$ using a multi-phase transport model (AMPT) with both partonic and hadronic interactions. We found that three-particle correlation densities in different angular directions with respect to the triggered particle (‘center’, ‘cone’, ‘deflected’, ‘near’ and ‘near-away’) increase with the number of participants. The ratio of ‘deflected’ to ‘cone’ density approaches to 1.0 with the increasing of number of participants, which indicates that partonic Mach-like shock waves can be produced by strong parton cascades in central Au+ Au collisions.

*黄焕中(HUANG Huanzhong)：University of California, Los Angeles, CA 90095, USA

强子再散射对流体力学中的椭圆流的影响

马国亮 马余刚 萨本豪[1] 蔡翔舟 贺泽君 黄焕中[2] 龙家丽 沈文庆 钟 晨
陈金辉 左嘉旭 张 松 施兴华

关键词 椭圆流，流体力学模型，强子再散射，LUCIAE 模型

使用流体力学+强子再散射模型模拟 200 GeV 的 Au+Au 碰撞，并使用 Cooper-Frye 的方法进行强子化。在中心度为 20%~40%的 200 GeV 的 Au+Au 碰撞中研究了强子再散射对于椭圆流的影

响。发现强子再散射可以压抑粒子的椭圆流使各向异性的动量空间趋向于各向同性。这种压抑效应随着横向动量的增加而减弱。另外，也研究了强子再散射对于横向动量谱和坐标空间各向异性的作用。

Effect of hadronic rescattering on the elliptic flow after the hydrodynamics model

MA Guoliang MA Yugang SA Benhao[1] CAI Xiangzhou HE Zejun
HUANG Huanzhong[2] LONG Jiali SHEN Wenqing ZHONG Chen
CHEN Jinhui ZUO Jiaxu ZHANG Song SHI Xinghua

Key words: Elliptic flow, Hydrodynamic model, Hadronic rescattering, LUCIAE model

A hydrodynamics + hadronic rescattering model is used to simulate Au+Au collisions at 200 GeV and a Cooper-Frye method is adopted for hadronization. The effect of hadronic rescattering on elliptic flow v_2 in 20%~40% Au+Au collisions at 200 GeV has been investigated. It is found that the hadronic rescattering can suppress elliptic flow v_2 and makes an asymmetric system in momentum space tend to be less anisotropic. The suppression effect becomes weak with increasing transverse momentum. In addition, the effect of hadronic rescattering on transverse momentum spectra and anisotropy of hadronic coordinate space is presented.

[2]萨本豪(SA Benhao)：中国原子能科学研究院;
[1]黄焕中(HUANG Huanzhong)：University of California, Los Angeles, CA 90095, USA

相对论离子碰撞中的 Δ-标度和热容

马余刚 马国亮 蔡翔舟 陈金根 陈金辉 方德清 郭 威 贺泽君 黄焕中[1]
龙家丽 马春旺 萨本豪[2] 沈文庆 王 鲲 魏义斌 颜廷志 钟 晨 左嘉旭

关键词 Δ−标度，热容，强子再散射，LUCIAE 模型

Δ-标度的方法被应用到相对论的 p+p、C+C 和 Pb+Pb 碰撞中总的粒子多重数的分布中。使用 LUCIAE 3.0 蒙特卡洛软件包模拟这些碰撞。我们发现 Δ-标度的参数随着碰撞系统的尺寸的增加而减小。另一方面，不同介子和重子的热容从低横向质量区域的逐事件的温度涨落中提取出来，发现热容随着碰撞参数的增加而减少。

Δ-scaling and heat capacity in relativistic ion collisions

MA Yugang MA Guoliang CAI Xiangzhou CHEN Jingen CHEN Jinhui
FANG Deqing GUO Wei HE Zejun HUANG Huanzhong[1] LONG Jiali

MA Chunwang SA Benhao[2] SHEN Wenqing WANG Kun
WEI Yibin YAN Tingzhi ZHONG Chen ZUO Jiaxu

Key words: Δ-scaling, Heat capacity, Hadronic rescattering, LUCIAE model

The Δ-scaling method has been applied to the total multiplicity distribution of the relativistic ion collisions of p+p, C+C and Pb+Pb which were simulated by a Monte Carlo package, LUCIAE 3.0. It is found that the Δ-scaling parameter decreases with increasing system size. Moreover, the heat capacities of different mesons and baryons have been extracted from the event-by-event temperature fluctuation in the region of low transverse mass and they show the dropping trend with increasing impact parameter.

---

[1]黄焕中(HUANG Huanzhong)：University of California, Los Angeles, CA 90095, USA;
[2]萨本豪(SA Benhao)：中国原子能科学研究院

相对论平均场对 Ne 和 Mg 同位素链的形变研究

陈金根 蔡翔舟 王庭太 马余刚 任中洲 方德清 钟 晨 魏义彬 郭威
周星飞 王鲲 马国亮 田文栋 陈金辉 颜廷志 左嘉旭 马春旺 沈文庆

关键词 相对论平均场，Ne 和 Mg 同位素链，四极形变，结合能，形状共存

我们用轴对称形变的相对论平均场模型借用 NL075 势对 Ne 和 Me 两个轻的同位素链进行了形变研究。计算得到的四极形变和结合能分别与其它模型得到的结果以及实验结果做了比较。比较显示用 NL075 势得到的 Ne 和 Mg 链的形变要比 NL-SH 势算得的结果好。另外计算结果显示 ^{12,29,32}Ne 和 ^{20,31}Mg 可能存在三轴形变，而 $^{25\text{-}28}$Ne 和 $^{27\text{-}30}$Mg 可能存在形状共存。此外结果还显示 ^{20}Mg 的 N=8 的中子数幻数效应非常弱。

Investigation on the deformation of Ne and Mg isotope chains within relativistic mean-field model

CHEN Jingen CAI Xiangzhou WANG Tingtai MA Yugang REN Zhongzhou
FANG Deqing ZHONG Chen WEI Yibin GUO Wei ZHOU Xingfei WANG Kun
MA Guoliang TIAN Wendong CHEN Jinhui YAN Tingzhi ZUO Jiaxu
MA Chunwang SHEN Wenqing

Key words: RMF model, Ne and Mg isotope chains, Quadrupole deformation, Binding energy, Shape coexistence

The Ne and Mg isotope chains are investigated based on the constrained calculations in the framework of deformed relativistic mean-field (RMF) model with the NL075 parameter set. The calculated quadrupole deformation and binding energy are compared with other theoretical results as well as

the available experimental data. It shows that the calculated deformations of Ne and Mg with NL075 are more accurate than those obtained with NL-SH. It is predicted that ^{19,29,32}Ne and ^{20,31}Mg maybe have triaxial deformation and $^{25\text{-}28}$Ne and $^{27\text{-}30}$Mg likely exhibit shape coexistence. The closure effect of neutron number N=8 for ^{20}Mg is predicted to be very weak.

一些轻的镜像核激发态的晕或皮

陈金根　蔡翔舟　沈文庆　马余刚　任中洲　张虎勇　蒋维洲

钟 晨　魏义彬　郭 威　周星飞　王 鲲　马国亮

关键词　球形相对论平均场，镜像核，激发态，奇异结构

用球形相对论平均场研究了三对镜像核：^{13}N-^{13}C，^{15}N-^{15}O 和 ^{21}Na-^{21}Ne。结果发现，除具有大形变的核外，用两套不同参数算得的基态和激发态结合能都非常接近实验值。结果还显示 ^{15}N 和 ^{21}Na 的 $2s_{1/2}$ 激发态均系弱束缚，且各存在一个质子晕和质子皮；而 ^{13}C 和 ^{15}O 的 $1d_{5/2}$ 和 $2s_{1/2}$ 也弱束缚，且分别存在一个中子皮。我们推算出了价核子与核物质的半径比，发现此比值可以作为判断奇异结构的一个附加判据。最后我们对 ^{13}N 的非束缚的 $1d_{5/2}$ 和 $2s_{1/2}$ 的情况也进行了讨论。

Halo or skin in the excited states of some light mirror nuclei

CHEN Jingen　CAI Xiangzhou　SHEN Wenqing　MA Yugang　REN Zhongzhou

ZHANG Huyong　JIANG Weizhou　ZHONG Chen　WEI Yibin

GUO Wei　ZHOU Xingfei　WANG Kun　MA Guoliang

Key words:　Spherical RMF model, Mirror nuclei, Excited state, Exotic structure

The properties of three pairs of mirror nuclei ^{13}N-^{13}C, ^{15}N-^{15}O and ^{21}Na-^{21}Ne (these mirror nuclei are all made of a good inert core plus an unpaired valence nucleon) are investigated by using the nonlinear relativistic mean-field (RMF) theory. It is found that the calculated binding energies with two different parameter sets are very close to the experimental ones for both the ground states and the excited states except for the large deformed nuclei. The calculations show that the $2s_{1/2}$ excited states of ^{15}N and of ^{21}Na are both weakly bound with a proton halo and a proton skin (or a pigmy proton skin), respectively. In addition, the $1d_{5/2}$ excited state of ^{13}C and the $2s_{1/2}$ excited state of ^{15}O are also weakly bound with a neutron skin, respectively. The ratio of the valence nucleon radius to matter radius is deduced and it can be regarded as an additional criterion for the existence of exotic structure. The unbound $2s_{1/2}$ and $1d_{5/2}$ excited states of ^{13}N are also discussed.

非对称核物质状态方程相对论平均场研究

蒋维洲

关键词 核物质，状态方程，对称能，超核

非对称核物质状态方程对研究奇特原子核性质、重离子碰撞反应动力学以及核天体物理性质起着至关重要的作用。非对称核物质状态方程包含对称物质的饱和性质和非对称物质的对称能。经过去三十多年的发展，人们对对称核物质的饱和性质知之甚多；但到目前为止，对非对称核物质的对称能和它的密度依赖性还知之甚少。鉴于相对论模型的优点，它们已被用于研究各种影响对称能的同位旋依赖相互作用的内在联系，给出对称能的密度依赖性的限制。过去两年里，我们在利用同位旋矢量介子的张量耦合能够增加奇特核中中子皮和电荷分布对对称能的敏感性以及利用标量超子在保持系统同位旋不变的情况下增加密度而研究对称能的密度依赖性等方面已取得了很好的理论结果。

Equation of state of asymmetric nuclear matter in relativistic models

JIANG Weizhou

Key words: Nuclear matter, Equation of state, Symmetry energy, Hypernuclei

The Equation of State (EOS) of asymmetric nuclear matter plays a crucial role in determining the structure of exotic nuclei, the reaction dynamics of heavy-ion collisions, and important astrophysical properties in celestial matter. The EOS of asymmetric nuclear matter consists of the saturation properties of symmetric matter and the symmetry energy of asymmetric matter. In past three decades, the saturation properties of nuclear matter have been almost settled down. However, the symmetry energy and its density dependence are still poorly known up to now. Based on the advantages of the relativistic models, they have been used to study the interplay of different isospin dependent interactions that influence the symmetry energy, and to give the constraints on the symmetry energy and its density dependence. In the past two years, we had made use of the tensor coupling of the isovector meson to increase the sensitivity of the neutron skin and the charge distribution in exotic nuclei to the symmetry energy and made use of the isoscalar hyperon to exploit the density dependence of the symmetry energy by increasing the density without changing the isospin of nuclei, working out very interesting theoretical results.

^{23}Al 及其邻近丰质子核奇异结构的研究

马春旺 方德清 郭 威 王 鲲 颜廷志 马余刚 蔡翔舟 沈文庆 孙志宇[1]
任中洲[2] 陈金根 田文栋 王宏伟 马二俊 刘桂华 石 钰 苏前敏 钟 晨
M. Hosoi[3] T. Izumikawa[5] R. Kannungo[6] S. Nakajima[3] T. Ohnishi[7] T. Ohtsubo[5]
T. Suda[7] K. Sugawara[3] T. Suzuki[3] A. Ozawa[4] A. Takisawa[5] K. Tanaka[7]
T. Yamaguchi[3] I. Tanihata[6]

关键词 丰质子核，奇异结构，平行动量分布，核反应总截面

我们在 RIKEN-RIPS 上测量了 ^{23}Al 等丰质子核素的核反应总截面和平行动量分布。实验用 135 MeV/A 的 ^{28}Si 轰击 ^{9}B 产生靶产生能量约为 70 MeV/A 的次级束流。次级束流在 1 mm 厚(377 g/cm^2)的 ^{12}C 反应靶上反应,通过测量在 C 靶前面和后面的粒子进行实验，靶前和靶后分别采用 $B\rho$-ToF-ΔE 和 ToF-ΔE-E 的方法联合鉴别离子。

实验测得 ^{23}Al 的反应总截面与邻近核相比有反常的增大，这与以前的结论相同，但平行动量分布的测量结果显示，^{23}Al 并不像 ^{11}Li 那样具有非常窄的动量分布而与 Goldhaber 模型一致。我们用少体 Glauber 模型分析了实验结果。少体 Glauber 模型(FBGM)采用”核心+价核子”方法，可以同时计算反应总截面和平行动量分布。动量分布计算结果显示 ^{23}Al 处于 d 态,这与测量 g 因子结果一致。为了解释反应截面增大而动量分布与 Goldhaber 模型一致的结果,我们尝试修正核心 ^{22}Mg,当核心大小比自然 ^{22}Mg 大(20±7)%时，计算结果与实验值一致。

Study of the exotic structure of ^{23}Al and its neighboring nuclei

MA Chunwang FANG Deqing GUO Wei WANG Kun YAN Tingzhi MA Yugang
CAI Xiangzhou SHEN Wenqing SUN Zhiyu[1] REN Zhongzhou[2] CHEN Jingen
TIAN Wendong WANG Hongwei Ma Erjun LIU Guihua SHI Yu SU Qianmin
ZHONG Chen M. Hosoi[3] T. Izumikawa[5] R. Kannungo[6] S. Nakajima[3]
T. Ohnishi[7] T. Ohtsubo[5] T.Suda[7] K. Sugawara[3] T.Suzuki[3] A. Ozawa[4]
A. Takisawa[5] K. Tanaka[7] T. Yamaguchi[3] I. Tanihata[6]

Key words: Proton-rich nucleus, Exotic structure, Parallel momentum distribution, Total reaction cross section

We measured the total reaction cross sections and parallel momentum distributions of ^{23}Al and its neighbors on RIKEN-RIPS. Using 135 MeV/A ^{28}Si to bombard ^{9}B, ~75 MeV/A secondary beam was produced. By measuring the ions before/after the 1mm ^{12}C (377 g/cm^2) reaction target, we obtain the total reaction cross section and parallel momentum distribution of ^{23}Al and its neighboring nuclei.

Our experiment results shows the reaction cross section of ^{23}Al has an exotic enhancement compared to its neighbors, which shares the same result of previous one’s. But its parallel momentum distribution shows no narrow distribution and consists with the Goldhaber Model. We performed theory analysis in framework of Few-Body Glauber Model (FBGM) which describes a nucleus like ‘core’+

'valence'. FBGM shows ^{23}Al should have a d-wave valence proton, which consists with the *g*-factor measurements. To explain the measured results of ^{23}Al, we tried to use an enlarged core of ^{22}Mg to reproduce the total reaction cross section. Calculation shows when the core is enlarged to (20±7)% compared to the normal ^{22}Mg, the calculated total reaction cross section can reproduce the experimental result.

[1]中国科学院院近代物理研究所;
[2]南京大学;
[3]Saitama University, Japan;
[4]Tsukuba University，Japan;
[5]Niigata University, Japan;
[6]TRIUMF, Vancouver, Canada;
[7]RIKEN, Japan

中能核反应中类弹碎片的同位旋标度的实验研究

田文栋　马余刚　王宏伟　颜廷志　苏前敏　刘桂花　马春旺　石　钰

关键词　同位旋，非对称，类弹碎片，同位旋标度

同位旋标度规律是研究具有同位旋非对称性的反应和对称能的有效手段，通过两个相似的仅在同位旋自由度上不同的反应系统的同位素的产额比，可以提取核物质状态方程中同位旋相关项的信息。最近在兰州的加速器(HIRFL)和放射性束流线(RIBLL)上，分别用 50 MeV/A 的 ^{36}Ar 和 ^{40}Ar 入射到靶 ^{64}Ni 上，测量了反应的类弹碎片的同位素分布，分析得到两个不同入射道同位旋的反应系统的同位素的产额比，以及在不同磁刚度选择下的同位素产额，数据分析及相关的理论研究正在进行中。

Isoscaling of the projectile-like fragment in intermediate heavy ion collisions

TIAN Wendong　MA Yugang　WANG Hongwei　YAN Tingzhi　SU Qianmin
LIU Guihua　MA Chunwang　SHI Yu

Key words:　Isospin, Asymmetry, Projectile-like fragment, Isoscaling

Isoscaling can be used to study the properties of reaction and symmetry energy in two isospin asymmetry system, from the isotope yield ratio produced in two similar reactions with different isospin freedom degrees, and information of the isospin dependent term in the Equation of State in nuclear matter can be extracted. Recently the isotope yield distributions of the projectile-like fragments in intermediate energy reaction ^{36}Ar and ^{40}Ar were measured on target ^{64}Ni with incident energy 50 MeV/A on HIRFL and RIBLL in Lanzhou. Isotope yield ratios from two isospin asymmetry system and isotope yields selected by different magnetic fields were analyzed, data analysis and theoretical study are in progress.

用两体级联衰变模型研究同位旋标度规律

田文栋 马余刚 王宏伟 方德清 蔡翔舟 王 鲲 陈金根 陆广成 颜廷志
苏前敏 刘桂花 马春旺 石 钰 曹喜光 傅 瑶 马二俊

关键词 同位旋，非对称性，同位旋标度，GEMINI

用两体级联衰变模型模拟计算了热力学平衡的不同初始状态的复合核衰变产物的同位旋标度规律。我们研究了对于具有不同同位旋非对称度的系统 Z=75，A=150，168，186 和 204，并且选择了在不同激发能时两体级联衰变的产物的同位素的产额比，模拟计算的结果可以用 $R_{21}(N,Z)=Y_2(N,Z)/Y_1(N,Z)=C\exp(\alpha N+\beta Z)$表示出来。同位旋标度系数$\alpha$和$\beta$依赖于平衡复合系统的同位旋自由度和激发能，但是与复合系统的大小没有关系。$|\alpha|$和$|\beta|$随着激发能的增加而减小，并且与温度 T 成反比关系，与系统的同位旋非对称度$\Delta(Z/A)^2$ 或 $\Delta(N/A)^2$ 具有线性关系，从该线性关系可以确定核物质状态方程中的同位旋相关的对称能项的系数 $C_{\rm sym}$。

Isoscaling study in sequential binary decay model GEMINI

TIAN Wendong MA Yugang WANG Hongwei FANG Deqing CAI Xiangzhou
WANG Kun CHEN Jingen LU Guangcheng YAN Tingzhi SU Qianmin
LIU Guihua MA Chunwang SHI Yu CAO Xiguang FU Yao MA Erjun

Key words: Isospin, Asymmetry, Isoscaling, GEMINI

Sequential decay model has been used to study isoscaling, i.e., the factorization of the isotope ratios from sources of different isospins and sizes over a broad range of excitation energies, into fugacity terms of proton and neutron number, $R_{21}(N,Z)=Y_2(N,Z)/Y_1(N,Z)=C\exp(\alpha N+\beta Z)$. It was found that the isoscaling parameters α and β have a strong dependence on the isospin difference of equilibrated source and excitation energy, no significant influence of the source size on α and β has been observed. α and β were found to decrease with the excitation energy, and was linear function of $1/T$ and $\Delta(Z/A)^2$ or $\Delta(N/A)^2$ of the sources. Symmetry energy coefficient $C_{\rm sym}$ was constrained from the relationship of α and source $\Delta(Z/A)^2$, β and source $\Delta(N/A)^2$.

用量子分子动力学模型和级联衰变模型研究同位旋标度规律

田文栋 马余刚 王宏伟 方德清 蔡翔舟 王 鲲 陈金根 陆广成 颜廷志
苏前敏 刘桂花 马春旺 石 钰 曹喜光 傅 瑶 马二俊

关键词 同位旋，非对称性，同位旋标度规律

用同位旋相关的量子分子动力学模型(IQMD)和级联衰变模型(GEMINI)模拟计算了 35 MeV/A 的 ^{40}Ca＋^{40}Ca，^{48}Ca+^{48}Ca 的初级产物和次级产物的同位旋标度规律。对于轻的反应产物，

同位旋标度参数α没有什么变化；对于中等质量和重的产物，α却随产物的 Z 的增加而增加。动力学效应表现在 IQMD 中，α随反应时间的延长而有所减小，重的产物则刚好相反。而次级衰变后产物的α比初级产物α要大。从初级产物和次级产物中我们都研究了密度与对称能系数的关系，初级产物的结果和输入参数比较符合，但是从次级产物提取的对称能系数与输入参数有比较大的偏离。同时我们认为对称能系数与密度的关系可以分别用“软”的和“硬”的两部分的叠加来表示 $C_{\mathrm{sym}}(\rho)\approx C_1(\rho/\rho_0)^{\gamma\mathrm{soft}}+ C_2(\rho/\rho_0)^{\gamma\mathrm{stiff}}$。

Isoscaling study in isospin dependent QMD and sequential binary decay model GEMINI

TIAN Wendong MA Yugang WANG Hongwei FANG Deqing CAI Xiangzhou
WANG Kun CHEN Jingen LU Guangcheng YAN Tingzhi SU Qianmin
LIU Guihua MA Chunwang SHI Yu CAO Xiguang FU Yao MA Erjun

Key words: Isospin, Asymmetry, Isoscaling

Isoscaling properties of the primary and final products are studied via isospin dependent quantum molecular dynamics (IQMD) model and the followed sequential decay model GEMINI, respectively. Both primary and final products' isoscaling parameter α keeps no significant change for light fragments, but increases with the mass for intermediate and heavy products. The dynamical effect on isoscaling is reflected on the α decreasing a little with the evolution time of the system, and opposite trend for the heavy products. The secondary decay effect on isoscaling is reflected on the increasing of the α value for the final products which experienced secondary decay process. Furthermore the density dependence of the symmetry energy has also been explored for the primary and secondary products, the symmetry energy coefficient can be expressed by the form of $C_{\mathrm{sym}}(\rho)\sim C_0(\rho/\rho_0)^{\gamma}$, C_0 and γ extracted from the primary products are consistent with the input parameters, but C_0 and γ extracted from the final products deviate the input values. In the paper we also suggest that it might be more reasonable to describe the density dependence of the symmetry energy coefficient by the $C_{\mathrm{sym}}(\rho)\approx C_1(\rho/\rho_0)^{\gamma\mathrm{soft}}+ C_2(\rho/\rho_0)^{\gamma\mathrm{stiff}}$ with $\gamma_{\mathrm{soft}}\leq 1$, $\gamma_{\mathrm{stiff}}\geq 1$ and C_1,C_2 constant parameters.

中能重离子碰撞中的各向异性流标度

颜廷志 马余刚 蔡翔舟 陈金根 方德清 郭 威
马春旺 马二俊 沈文庆 田文栋 王鲲

关键词 各向异性流，核子数标度，量子分子动力学模型，组合机制

用同位旋相关的量子分子动力学(IDQMD)模型, 研究了 25 MeV/A 的 ^{86}Kr+^{124}Sn 碰撞系统在较大碰撞参数(7–10 fm)下的轻碎片的各向异性流(v_2 和 v_4)的性质。发现横动量(p_t)依赖的椭圆流(v_2)和四阶流(v_4)在该能区下是正值，且随着 p_t 的增加而增加。这说明轻碎片的发射倾向于在平面发

射，且横动量越大的碎片越是倾向于在平面发射。发现在每核子的椭圆流对于每核子的横动量分布中，不同轻碎片的曲线在 $p_t < 0.25$ GeV/c 下趋于重合，这表明椭圆流存在着对碎片核子数的标度率现象。这与 RHIC 中发现的横动量相关的椭圆流对强子的组分夸克数目标度律现象是相似的。另外发现横动量依赖的 v_4/v_2^2 比值对不同轻碎片都近似等于一个常数 0.5,这一常数与极端相对论能区中理想流体力学模型预言的强子的 v_4/v_2^2 比值是一致的。这些标度律现象可以用核子层次的碎片形成的组合机制来解释。

Scaling of anisotropic flow in intermediate energy heavy ion collisions

YAN Tingzhi MA Yugang CAI Xiangzhou CHEN Jingen FANG Deqing
GUO Wei MA Chunwang MA Erjun SHEN Wenqing TIAN Wendong WANG Kun

Key words: Anisotropic flow, Number-of-nucleon scaling, IDQMD, Coalescence mechanism

Anisotropic flows (v_2 and v_4) of light nuclear clusters are studied by Isospin-Dependent Quantum Molecular Dynamics (IDQMD) model for the collision system ^{86}Kr+^{124}Sn at 25 MeV/A and large impact parameters. It shows that the transverse momentum (p_t) dependent elliptic flow (v_2) and fourth order flow (v_4) are positive in this energy range, and increase with the increasing p_t. It reflects that the light clusters are preferentially emitted within the reaction plane, and the fragments with higher transverse momentum tend to be strongly emitted within in-plane. It demonstrates in the distribution of elliptic flow per nucleon as a function of transverse momentum per nucleon that: the curves of different light clusters tend to superpose with each others when p_t<0.25 GeV/c, which means that there exists the scaling of number of nucleons of clusters for elliptic flow. This behavior is similar to the number of constituent quarks scaling of elliptic flow versus transverse momentum per constituent quark for hadrons which was observed at RHIC. In addition, the ratios of v_4/v_2^2 versus transverse momentum for different light clusters show a constant value of 0.5, which is consistent with the predicted conclusion by ideal fluid dynamics model in ultra-relativistic energy region. These scaling behaviors can be understood by the coalescence mechanism in nucleonic degree of freedom for the cluster formation.

N=10 附近丰质子核的反应截面和碎片动量分布的测量

郭 威 方德清 马余刚 马春旺 王 鲲 颜廷志 蔡翔舟 沈文庆 孙志宇[1]
任中洲[2] 陈金根 陈金辉 刘桂华 马二俊 马国亮 石 钰 苏前敏 田文栋
王宏伟 钟 晨 左嘉旭 M. Hosoi[3] T.Izumikawa[5] R.Kannungo[6] S.Nakajima[3]
T.Ohnishi[7] T.Ohtsubo[5] T.Suda[7] K.Sugawara[3] T.Suzuki[3] A.Ozawa[4]
A.Takisawa[5] K.Tanaka[7] T.Yamaguchi[3] I.Tanihata[6]

关键词 反应截面, 平行动量分布, 丰质子核, 少体 Glauber 模型

我们在日本理化所(RIKEN)的 RIken 炮弹碎片分离器(RIPS)放射性次级束装置上同时测量了

约 70 MeV/A 能量下数个 N=10 的丰质子核的反应总截面(σ_R)和单质子剥离碎片平行动量($p_{//}$)分布。其中，$p_{//}$采用直接飞行时间法测量，σ_R 采用束流透射法测量。实验所用主束为 135 MeV/A 的 ^{28}Si，反应靶为 1 mm 厚 (377 g/cm^2) 的 ^{12}C；反应靶前后分别采用 $B\rho$-ToF-ΔE 和 ToF-ΔE-E 关联来鉴别粒子。实验测得 ^{23}Al 的反应总截面与邻近核相比有反常的增大,这与以前的结论相同。实验首次获得了 ^{23}Al 单质子剥离反应碎片 ^{22}Mg 的 $p_{//}$ 分布。我们在少体 Glauber 模型框架下讨论了实验结果，少体 Glauber 模型采用“核芯+价核子”图象，可以很好地描述奇异核的弱束缚结构。对 $p_{//}$ 的分析表明 ^{23}Al 基态价质子应主要处于 d 轨道，这与另外两个近期实验结果相一致。我们尝试修正核心 ^{22}Mg，当核芯大小比自然的 ^{22}Mg 核大(20±7)%时，少体 Glauber 模型计算结果与 σ_R 的实验值一致。

Measurements of reaction cross section and fragment momentum distribution for *N*=10 proton-rich isotones

GUO Wei Fang Deqing MA Yugang MA Chunwang WANG Kun YAN Tingzhi CAI Xiangzhou SHEN Wenqing SUN Zhiyu[1], REN Zhongzhou[2] CHEN Jingen CHEN Jinhui LIU Guihua MA Erjun MA Guoliang SHI Yu SU Qianmin TIAN Wendong WANG Hongwei ZHONG Chen ZUO Jiaxu M. Hosoi[3] T.Izumikawa[5] R.Kannungo[6] S.Nakajima[3] T.Ohnishi[7] T.Ohtsubo[5] T.Suda[7] K.Sugawara[3] T.Suzuki[3] A.Ozawa[4] A.Takisawa[5] K.Tanaka[7] T.Yamaguchi[3] I.Tanihata[6]

Key words: Reaction cross section, Longitudinal momentum distribution, Proton-rich nuclei, Few body Glauber model

The longitudinal momentum ($p_{//}$) distributions of fragments after one-proton removal and reaction cross sections (σ_R) for several N = 10 isotones at intermediate energy (~70 MeV/A) have been measured simultaneously at the RIken Projectile Separator (RIPS). $p_{//}$ was measured using a direct time-of-flight (TOF) technique, while σ_R was determined using a transmission method. The primary beam is ^{28}Si at 135 MeV/A, the reaction target is ^{12}C (1 mm, 377 g/cm^2), The particles were identified by $B\rho$−Tof −ΔE correlation before reaction target, and by Tof−ΔE−E correlation after reaction target, respectively. An enhanced σ_R is observed for ^{23}Al comparing with its neighbors, which consists with our previous experiment. The $p_{//}$ distribution for ^{22}Mg fragments from ^{23}Al one-proton removal reaction has been obtained for the first time. The experimental data are discussed within a Few Body Glauber (FBG) framework. The FBG model has a “core plus nucleon” picture and is suitable to describe the weak bound structure of exotic nuclei. Analysis of $p_{//}$ indicates a dominant d-wave component in the ground state of ^{23}Al. This agrees with two other recent experimental results. We also suggest the possibility of an enlarged ^{22}Mg core for proton-rich nucleus ^{23}Al. If the ^{22}Mg core is enlarged (20±7)% , the FBG calculation can reproduce the experimental value of σ_R well.

[1]中国科学院近代物理研究所; [2]南京大学；[3]Saitama University, Japan; [4]Tsukuba University，Japan; [5]Niigata University, Japan; [6]TRIUMF, Vancouver, Canada; [7]RIKEN, Japan

轻核系统临界行为的实验研究

马余刚 J. B. Natowitz[2] R. Wada[2] K. Hagel[2] J. Wang[1,2] T. Keutgen[3]
Z. Majka[4] M. Murray[5] L. Qin[2] P. Smith[2] R. Alfaro[6] J. Cibor[7]
M. Cinausero[8] Y. El Masri[3] D. Fabris[9] E. Fioretto[8] A. Keksis[2] M. Lunardon[9]
A. Makeev[2] N. Marie[10] E. Martin[2] A. Martinez-Davalos[6] A. Menchaca-Rocha[6]
G. Nebbia[9] G. Prete[8] V. Rizzi[9] A. Ruangma[2] D. V. Shetty[2] G. Souliotis[2]
P. Staszel[4] M. Veselsky[2] G. Viest[9] E. M. Winchester[2] S. J. Yennello[2]

关键词 临界现象，准弹核碎裂反应，涨落，核的 Zipf 定律

对实验中 47 MeV/n ^{40}Ar＋^{27}Al、^{48}Ti 和 ^{58}Ni 反应所产生的小的类弹系统(氩)的碎裂性质作了深入的讨论。发展了一种新的重建类弹源的方法，并用来研究激发能在每核子 1–9 MeV 范围内的类弹系统的碎裂反应。在激发能约为每核子 5.6 MeV 时，很多的可观测量表明在退激发过程中存在最大涨落。这些量包括 Campi 图的归一化的第二级矩，归一化的序参数分布(如最大碎片的原子序数 Z_{max} 和总动能)的方差。在相同的激发能(~5.6MeV)下，最大碎片与次大碎片的原子序数关联的演化，以及双峰结构(bimodality)的特征，与相变现象一致。在相同激发能下，相关的相分离参数 S_p 的斜率有明显的改变。同时，最大碎片的 Δ 标度律分析表明此时系统的 Δ 标度律向 Δ＝1 标度的跃迁，这是无序相的特征。碎片的拓扑结构也表明在最大涨落点碎片的等级分布遵从核的 Zipf 定律，这又提供了液气相变的另一个证据。进一步，在相同激发能区的电荷分布提取的 Fisher 液滴模型的临界指数 τ 大约为 2.3，这个值接近液气相变临界指数的普适参数。该系统的量热曲线的测量显示了温度随着激发能单调增加，且没有明显的平台。在最大涨落点时的温度为 8.3±0.5 MeV。以该温度为临界温度，借助于量热曲线，我们从实验数据中提取了临界指数 β，γ 和 σ。它们的值也与液气相变的普适参数相一致。综合以上多个实验观测量的分析，这些证据强有力地揭示了平衡的介观系统（氩）在激发能大约为每核子 5.6 MeV 时，系统的相变在接近临界点时发生。

Critical behavior in light nuclear systems: Experimental aspects

MA Yugang J. B. Natowitz[2] R. Wada[2] K. Hagel[2] J. Wang[1,2] T. Keutgen[3]
Z. Majka[4] M. Murray[5] L. Qin[2] P. Smith[2] R. Alfaro[6] J. Cibor[7]
M. Cinausero[8] Y. El Masri[3] D. Fabris[9] E. Fioretto[8] A. Keksis[2] M. Lunardon[9]
A. Makeev[2] N. Marie[10] E. Martin[2] A. Martinez-Davalos[6] A. Menchaca-Rocha[6]
G. Nebbia[9] G. Prete[8] V. Rizzi[9] A. Ruangma[2] D. V. Shetty[2] G. Souliotis[2]
P. Staszel[4] M. Veselsky[2] G. Viest[9] E. M. Winchester[2] S. J. Yennello[2]

Key words: Critical behavior, Quasiprojectile fragmentation, Fluctuation, Nuclear Zipf law

An extensive experimental survey of the features of the disassembly of a small quasiprojectile system with A~36, produced in the reactions of 47 MeV/nucleon ^{40}Ar+^{27}Al, ^{48}Ti, and ^{58}Ni, has been carried out. Nuclei in the excitation energy range of 1–9 MeV/nucleon have been investigated employing a new method to reconstruct the quasiprojectile source. At an excitation energy ~5.6 MeV/nucleon

many observables indicate the presence of maximal fluctuations in the de-excitation processes. These include the normalized second moments of the Campi plot and normalized variances of the distributions of order parameters such as the atomic number of the heaviest fragment Z_{max} and the total kinetic energy. The evolution of the correlation of the atomic number of the heaviest fragment with that of the second heaviest fragment and a bimodality test are also consistent with a transition in the same excitation energy region. The related phase separation parameter, S_p, shows a significant change of slope at the same excitation energy. In the same region a Δ-scaling analysis for the heaviest fragments exhibits a transition to Δ=1 scaling, which is predicted to characterize a disordered phase. The fragment topological structure shows that the rank-sorted fragments obey Zipf's law at the point of largest fluctuations, providing another indication of a liquid gas phase transition. The Fisher droplet model critical exponent τ ~2.3 obtained from the charge distribution at the same excitation energy is close to the critical exponent of the liquid gas phase transition universality class. The caloric curve for this system shows a monotonic increase of temperature with excitation energy and no apparent plateau. The temperature at the point of maximal fluctuations is 8.3±0.5 MeV. Taking this temperature as the critical temperature and employing the caloric curve information we have extracted the critical exponents of β, γ, and σ from the data. Their values are also consistent with the values of the universality class of the liquid gas phase transition. Taken together, this body of evidence strongly suggests a phase change in an equilibrated mesoscopic system at, or extremely close to, the critical point.

[1]Institute of Modern Physics, Chinese Academy of Sciences, Lanzhou 730000, China；
[2]Cyclotron Institute, Texas A&M University, College Station, Texas 77843, USA；
[3]UCL, Louvain-la-Neuve, Belgium；
[4]Jagiellonian University, Krakow, Poland；
[5]University of Kansas, Lawrence, Kansas 66045, USA；
[6]Instituto de Fisica, UNAM, Mexico City, Mexico；
[7]Institute of Nuclear Physics, Krakow, Poland；
[8]INFN Laboratori Nazionali di Legnaro, Legnaro, Italy；
[9]INFN and Dipartimento di Fisica, Padova, Italy；
[10]LPC, Universit´e de Caen, Caen, France

^{29}P 的碎裂碎片 ^{28}Si 的平行动量分布研究

魏义斌 马余刚 蔡翔舟 钟 晨 陈金根 张虎勇 方德清 王 鲲 马国亮
郭威 田文栋 沈文庆 詹文龙* 肖国青* 徐瑚珊* 孙志宇* 李加兴*
郭忠言* 王 猛* 陈志强* 胡正国* 陈立新* 李 琛* 毛瑞士* 白 洁*

关键词 ^{29}P，动量分布，质子皮

测量了每核子 30.7MeV 的 ^{29}P 轰击 C 靶所产生碎片 ^{28}Si 的平行动量分布。该分布的半高全宽为：110.5±23.5MeV/c，这与假设 ^{29}P 存在一个价质子的 Galuber 计算结果一致。另外用 Skyrme-Hartree-Fock 理论计算了密度分布，结果表明 ^{29}P 可能存在质子皮结构。

Parallel momentum distribution of ^{28}Si fragments from ^{29}P

WEI Yibin MA Yugang CAI Xiangzhou ZHONG Chen CHEN Jingen
ZHANG Huyong FANG Deqing WANG Kun MA Guoliang GUO Wei
TIAN Wendong SHEN Wenqing ZHAN Wenlong* XIAO Guoqing* XU Hushan*
SUN Zhiyu* Li Jiaxing* GUO Zhongyan* WANG Meng* CHEN Zhiqiang*
HU Zhengguo* CHEN Lixin* LI Chen* MAO Ruishi* BAI Jie*

Key words: ^{29}P, Momentum distribution, Proton skin

Distribution of the parallel momentum of ^{28}Si fragments from the breakup of 30.7MeV/nucleon ^{29}P has been measured on C targets. The distribution has the FWHM with the value of 110.5±23.5 MeV/*c* which is consistent quantitatively with Galuber model calculation assuming a valence proton in ^{29}P. The density distribution is also predicted by Skyrme-Hartree-Fock calculation. Results show that there might exist the proton-skin structure in ^{29}P.

* Institute of Modern Physics, Chinese Academy of Sciences, Lanzhou 730000, China

核 Zipf 定律的矩分析方法

马余刚

关键词 矩分析方法，核 Zipf 定律

用矩分析方法和核碎片大小分布的 Zipf 定律研究了核物质的碎裂性质，总结了目前理论和实验上对矩分析和 Zipf 定律的研究状况。讨论了这两种方法与核物质碎裂时可能存在的临界行为或相变之间的关系。另外，还讨论了核碎裂反应中的标度分形矩和间歇。

Moment analysis and nuclear Zipf law

MA Yugang

Key words: Moment analysis, Nuclear Zipf law

The moment analysis method and nuclear Zipf's law of fragment size distributions are reviewed to study nuclear disassembly. We present a compilation of both theoretical and experimental studies on moment analysis and Zipf law performed so far. The relationship of both methods to a possible critical behavior or phase transition of nuclear disassembly is discussed. In addition, scaled factorial moments and intermittency are reviewed.

用量子分子动力学模型研究核子－核子动量关联函数

马余刚　魏义斌　沈文庆　蔡翔舟　陈金根　陈金辉　方德清　郭 威　马春旺
马国亮　苏前敏　田文栋　王 鲲　颜廷志　钟 晨　左嘉旭

关键词　同位旋相关的量子分子动力学模型，动量关联函数

用同位旋相关的量子分子动力学模型研究了 C 同位素轰击 ^{12}C 靶反应的核子－核子对动量关联函数。探究了动量关联函数对结合能的依赖关系。另外，也研究了其它对动量关联函数有影响的因素，包括与动量有关的核状态方程、介质中的核子－核子散射截面、碰撞参数、核子对的总动量和束流能量等。应特别指出的是：在较低的相对动量下，动量关联函数随着束流能量的增加表现出先上升后下降的走势。

Surveying the nucleon-nucleon momentum correlation function in the framework of quantum molecular dynamics model

MA Yugang　WEI Yibin　SHEN Wenqing　CAI Xiangzhou　CHEN Jingen
CHEN Jinhui　FANG Deqing　GUO Wei　MA Chunwang　MA Guoliang　SU Qianmin
TIAN Wendong　WANG Kun　YAN Tingzhi　ZHONG Chen　ZUO Jiaxu

Key words: Isospin-dependent quantum molecular dynamics model, Momentum correlation function

Momentum correlation functions of nucleon-nucleon pairs are presented for reactions with C isotopes bombarding a ^{12}C target within the framework of the isospin-dependent quantum molecular dynamics model. The binding-energy dependence of the momentum correlation functions is explored, and other factors influencing momentum correlation functions are also investigated. These factors include momentum-dependent nuclear equations of state, in-medium nucleon-nucleon cross sections, impact parameters, total pair momenta, and beam energy. In particular, the rise and fall of the strength of momentum correlation functions at lower relative momentum show an increase in beam energy.

裂变动力学中的同位旋标度行为

马余刚　王 鲲　蔡翔舟 陈金根 陈金辉 方德清 郭 威　马春旺　马国亮　沈文庆
苏前敏　田文栋　魏义彬　颜廷志　钟 晨　周星飞

关键词　同位旋标度，裂变动力学

用结合统计分支的朗之万方程模型模拟了 ^{112}Sn+^{112}Sn 和 ^{116}Sn+^{116}Sn 的裂变过程。两部分碎片质量的对称裂变或不对称裂变，由蒙特卡洛按高斯分布采样假定。分析了两系统产生的同中子或质子数的裂变碎片比率，发现了同位旋标度行为并分析了其产生原因。在不同的高斯采样宽度下，分别提取同位旋标度系数 α 和 β，它们分别是电荷数和中子数的函数。发现 α 对裂变的质量不对称系数的几率分布很敏感，而 β 不敏感。α 和 β 的绝对值都随能量及折合粘滞系数的升高而降低。

Isoscaling behavior in fission dynamics

MA Yugang WANG Kun CAI Xiangzhou CHEN Jingen CHEN Jinhui
FANG Deqing GUO Wei MA Chunwang MA Guoliang SHEN Wenqing
SU Qianmin TIAN Wendong WEI Yibin YAN Tingzhi ZHONG Chen
ZHOU Xingfei

Key words: Isoscaling, Fission dynamics

The fission processes of $^{112}Sn+^{112}Sn$ and $^{116}Sn+^{116}Sn$ are simulated with the combination of the Langevin equation and the statistical decay model. The mass of two fission fragments is given by assuming the process of symmetric fission or asymmetric fission by Monte Carlo sampling with the Gaussian probability distribution. From the analysis of isotopic/isotonic ratios of fission fragments from both reactions, the isoscaling behavior has been observed and investigated in detail. Isoscaling parameters α and β are extracted as a function of charge number and neutron number, respectively, in different widths of the sampling Gaussian probability distribution. It seems that α is sensitive to the width of fission probability distribution of the mass asymmetrical parameter, but β is not. Both α and $|\beta|$ drop with increasing beam energy and reduced friction parameter.

弹核碎裂反应的同位旋标度率及核的对称能系数研究

方德清 马余刚 钟 晨 蔡翔舟 陈金根 郭 威 马春旺 苏前敏 田文栋
王 鲲 颜廷志 沈文庆

关键词 统计擦碎模型，弹核碎裂反应，同位旋效应

用统计擦碎模型研究了中能区弹核碎裂反应中的同位旋标度率。发现在弹核碎裂反应中存在同位旋标度率现象，但同位旋标度率参数随每核子的激发能的增加迅速下降。而影响同位旋标度率参数变化的最主要因素是激发能及蒸发效应。用费米气体模型中激发能与核温度的关系，从同位旋标度率参数提取出核的对称能系数，其值大小及其随激发能的变化趋势跟实验数据基本一致。

Study of isoscaling in projectile fragmentation and the nuclear symmetry energy coefficient

FANG Deqing MA Yugang ZHONG Chen CAI Xiangzhou CHEN Jingen
GUO Wei MA Chunwang SU Qianmin TIAN Wendong WANG Kun
YAN Tingzhi SHEN Wenqing

Key words: Statistical abrasion-ablation model, Fragmentation reaction, Isospin effect

The isoscaling behavior in projectile fragmentation has been systematically investigated by a modified statistical abrasion-ablation (SAA) model. The reduced isoscaling parameters are found to

decrease with the excitation energy per nucleon and have no significant dependence on the size of reaction systems. Assuming a Fermi-gas behavior, the excitation energy dependence of the symmetry energy coefficients are tentatively extracted from α and β which looks consistent with the experimental data.

类弹碎片的同位旋标度律

钟 晨 马余刚 方德清 蔡翔舟 陈金根 沈文庆 田文栋 王 鲲 魏义彬
陈金辉 郭 威 马春旺 马国亮 苏前敏 颜廷志 左嘉旭

关键词 重离子碰撞，炮弹碎裂反应，同位旋标度律

修改后的统计擦碎模型(SAA)可以很好地描述炮弹碎裂反应的类弹碎片同位素和同中子素产额分布，同时我们也用这个模型研究了该反应的同位旋标度律。提取了蒸发前热核以及蒸发后冷核的同位旋标度律参数α和β。发现蒸发效应对α和β有非常大的影响；对冷核，α和$|\beta|$随着 Z 和 N 的增加单调增加。我们也讨论了同位旋标度律参数和同位旋含量变化的关系。

Isoscaling of projectile-like fragments

ZHONG Chen MA Yugang FANG Deqing CAI Xiangzhou CHEN Jingen
SHEN Wenqing TIAN Wendong WANG Kun WEI Yibin CHEN Jinhui
GUO Wei MA Chunwang MA Guoliang SU Qianmin YAN Tingzhi ZUO Jiaxu

Key words: Heavy ion reaction, Projectile fragmentation, Isoscaling

The isotopic and isotonic distributions of projectile fragmentation products have been simulated by a modified statistical abrasion-ablation model and the isoscaling behavior of projectile-like fragments has been discussed. The isoscaling parameters α and β have been extracted respectively, for hot fragments before evaporation and cold fragments after evaporation. It looks that the evaporation has a stronger effect on α and β. For cold fragments, a monotonic increase of α and $|\beta|$ with the increase of $\boldsymbol{Z}$ and $\boldsymbol{N}$ is observed. The relation between isoscaling parameter and the change of isospin content is also discussed.

中等质量核激发态奇异结构的研究

石 钰 马余刚 陈金根 方德清 王 鲲 颜廷志 马春旺 刘桂华 田文栋
王宏伟 郭 威 马二俊 苏前敏 蔡翔舟

关键词 中等质量核，单核子激发态，晕或皮结构

在球形非线形相对论平均场(RMF)的理论框架下，研究了稳定线附近中等质量(Z=20–50)的奇 A 核在激发态下存在的晕或皮结构，提取了价核子与核芯均方根半径的比值($R_{\rm vc}$)，并结合单中子

或质子的分离能($S_n(p)$)，讨论了具有晕或皮结构的激发态所呈现出的带状分布，说明了壳结构与离心势垒对激发态晕或皮结构形成有重要影响。

Exotic structure of the single nucleon excited states in the medium nuclei near the stability line

SHI Yu MA Yugang CHEN Jingen FANG Deqing WANG Kun YAN Tingzhi
MA Chunwang LIU Guihua TIAN Wendong WANG Hongwei GUO Wei
MA Erjun SU Qianmin CAI Xiangzhou

Key words Medium mass nuclei, Single particle excited states, Halo or skin structure

The halo or skin structure of excited states in odd nuclei near the stability line is studied in terms of the spherical nonlinear relativity mean field theory calculation, considering nucleus as a spherical core plus a valence nucleon outside it. The tail of density distributions of excited states with exotic structure is presented for medium-heavy nuclei. The ratio (R_{vc}) of rms radi us of valence nucleon to that of nuclear core is deduced. Together with the separation energy ($S_n(p)$), the ratio (R_{vc}) constitutes a correlation, in which the exotic nuclei excited states distribution presents a strap structure, indicating the effects of centrifugal barrier and shell structure.

电子和正电子与奇异丰质子核弹性散射的截面

马二俊 马余刚 陈金根 蔡翔舟 方德清 郭 威 刘桂华 马春旺 沈文庆
石 钰 苏前敏 田文栋 王宏伟 王 鲲 颜廷志

关键词 电子, 正电子, 奇异丰质子核, 微分截面, 电荷形状因子, 分波展开, 相对论平均场

自应用放射性核束发现晕核 ^{11}Li 以来，对晕核的研究一直是核物理的重要课题。德国 GSI 计划建造新一代电子-重离子碰撞装置，日本 RIKEN 也有类似的计划。这些计划的主要目的是研究远离稳定线的核的结构。由于将来在实验上会得到电子与不稳定核散射的数据，理论上对电子与丰质子核的弹性散射进行探索性的研究是很有意义的。我们利用相对论分波展开法研究了电子和正电子与 ^{208}Pb、^{12}C、^{12,16}O 和 ^{28,32}S 弹性散射的微分截面，核的基态电荷密度分布由自洽相对论平均场模型计算，同时也计算了 ^{12,16}O 和 ^{28,32}S 的电荷形状因子。数值计算的结果与现有的实验数据进行了比较，计算表明我们所采用的模型是可靠的。由于核对正电子和电子有不同的库仑效应，在相同的动量转移下，正电子和电子与同一靶核散射截面的大小是不同的，而且散射截面的极小值位置也发生了移动。与稳定的核 ^{16}O 和 ^{32}S 比较，正电子或电子与丰质子核 ^{12}O 和 ^{28}S 散射截面的大小以及电荷形状因子也不同，而且散射截面和电荷形状因子的极小值位置也发生了移动。这些差别归因于丰质子核 ^{12}O 和 ^{28}S 具有扩展的基态电荷分布。由于稳定核和对应的质子滴线同位素核的截面以及电荷形状因子的差别在实验上已经可以观察，电子或正电子与核的弹性散射将是研究丰质子核的质子晕现象的有效工具。

Cross sections of elastic electron and positron scattering from proton-rich nuclei

MA Erjun MA Yugang CHEN Jingen CAI Xiangzhou FANG Deqing
GUO Wei LIU Guihua MA Chunwang SHEN Wenqing SHI Yu SU Qianmin
TIAN Wendong WANG Hongwei WANG Kun YAN Tingzhi

Key words: Electron, Positron, Exotic proton-rich nuclei, Differential cross section, Charge form factor, Partial-wave expansion, Relativistic mean field

Since the halo nucleus ^{11}Li was found by using the radioactive nuclear beams (RNB), there is much interest in studying halo nuclei. Technical proposals for an electron-heavy-ion collider have been incorporated in the GSI/Germany physics program as well as the RIKEN/Japan facility. In both cases the main purpose is to study the structure of nuclei far from the stability line. Since the experimental data for the electron scattering off unstable nuclei will be available soon, it is of interest to make an exploratory investigation of elastic electron scattering from proton-rich nuclei. We investigate the cross sections of the elastic electron or positron scattering from ^{208}Pb, ^{12}C, ^{12,16}O and $^{28, 32}$S by the relativistic partial-wave expansion method using the static charge density distribution from the self-consistent relativistic mean field model and also calculate the charge form factors for $^{12, 16}$O and $^{28, 32}$S. Calculations indicate that the present theory is reliable for the elastic electron- or positron-nucleus scattering. Compared with electron, positron scattering from a nucleus displays the minimum shift and the amplitude deviation of the cross section (in the same momentum transfer), which is attributed to the different Coulomb effects of a nucleus on positron and electron. As compared to the stable nuclei ^{16}O and ^{32}S, both the shifts of the minimum and the amplitude deviations of the cross section or the form factors of ^{12}O and ^{28}S result from the existence of the long tail of the charge distribution. Since the difference of the cross sections and form factors between a stable nucleus and its proton drip-line isotopes is large enough to be experimentally observable, the elastic electron- or positron-nucleus scattering is an effective tool to investigate proton-halo phenomena of proton-rich nuclei.

基于微观相互作用的固液界面气体存在状态的理论研究

李朝霞 张雪花[1] 张立娟 曾晓成[2] 胡 钧[1] 方海平

关键词 固液界面，气体存在状态，纳米气泡，气层

如果固液界面上有纳米尺度的气体存在，体系的界面特征和动力学行为就会发生重大的改变。例如，如果固液界面上有气体存在，浸在水中的疏水界面间会出现长程引力，流体动力学中的滑移长度会大大增加，而微流体输运中的摩擦力、胶体体系稳定性以及膜的破裂均会减少等等。人们相信疏水界面间出现的长程引力会促进我们对生物过程中相互作用的理解，因此有助于对许多重要的生物过程，像蛋白质的快速折叠和自组装过程等的理解。因此，气体在固液界面上的成核行为已经在过去十几年引起了人们极大的关注。

两个疏水固体表面间存在纳米气泡的概念最早是根据实验观察到的浸没在水中的两个疏水固体表面间的相互作用力提出的。1997 年，Parker 等人用表面力测量仪测量浸没在水中的两个疏水固体表面间的疏水长程引力，发现这个力呈台阶分布，它们认为这是由于疏水固体表面间的亚微米级气泡的存在所致。近年来，一系列的实验和理论证据表明纳米尺度的气体在固液界面上成核。而最近人们争论的焦点是固液界面上成核的气体到底是纳米气泡还是纳米气层。一些实验小组在固液界面发现了纳米气泡，但是另外一些小组认为可能是气层。造成这些争议的原因可能主要是实验材料的多样化以及实验条件的不同。我们实验组报道了纳米气泡和气层都能够通过醇水交换法产生。

10 年前，De Gennes 等提出了一个统一理论来解决当时备受争议的问题——非挥发性液体在固气界面的存在状态问题。他们的理论预测了固体表面的液体可以以三种状态存在：纳米厚度的液体层(liquid pancake)，液滴以及液滴在液层上。在这个重要理论的启示下，我们认为气泡和气层可能都是固液界面上气体成核的存在状态。而且，还可能存在其他实验上没观测到的状态。因此，迫切需要一个统一的理论来描述固液界面上气体的各种存在状态。

我们应该意识到由于气体的特殊性，这个分析应该比液体的情况更加复杂。例如，固液界面上气体的密度通常随着气体的压强和气体分子与固体、液体分子的相互作用而改变，因此它有可能与界面的距离有关。在考虑到气体的特殊性的基础上，我们得到结论：纳米气泡和纳米气层都是气体在固液界面的可能的存在状态。另外还预测了一种新的气体的存在状态：纳米气泡在纳米气层上。我们希望我们的理论结果有助于气体在固液界面上成核的统一理论的发展。

Analysis of the gas states at liquid/solid interface based on interactions at the microscopic level

LI Zhaoxia ZHANG Xuehua[1] ZHANG Lijuan ZENG Xiaocheng[2]
HU Jun[1] FANG Haiping

Key words: Liquid/solid interface, Gas state, Nanobubbles, Gas pancake, The sate of nanobubble on the gas pancake

When gas on the nanoscale nucleates at the liquid/solid interface, the interfacial properties and dynamics of the system can be significantly changed, for example, by the occurrence of a long-range interaction between hydrophobic interfaces immersed in water, a long slip length in hydrodynamics and the reduction of friction in microfluidic transportation, stability of colloidal systems and rupture of film. Nanobubbles were also suggested to be associated with a wide range of applications such as fast folding of proteins and assembly.

A range of experimental evidence has been presented in support of the existence of nanoscale gas nucleated at the water/hydrophobe interface. Recently, the debate has been focused on whether the state of gas at the liquid/solid interface is a gas bubble or a gas layer. Some reported that nanobubbles were found but others suggested a gas layer. Maybe this is due to the effect of different experimental conditions and materials. Our experimental group has reported that the gas nanobubbles and gas pancakes can be formed with high reproducibility by the solvent exchange method. Therefore, it is necessary to study theoretically the gas sates at the liquid/solid interface.

Ten years ago, De Gennes and coworkers have put forward a unified picture of liquid nucleation with a continuum theory to resolve the problem of the nonvolatile liquid states at the gas/solid interface. That theory predicts three states of liquid on the solid surface: liquid pancake (film), liquid droplet surrounded by a dry solid surface, and liquid droplet coexisting with a liquid film. We expect that the seminal theory of liquid wetting developed by de Gennes and coworkers can be extended to the study of gas nucleation at the liquid/solid interface. It should be noted that the analysis should be even more complex due to the particularity of gas. By carefully taking into account the particularity of gas, we will show that gas layers and gas bubbles are both possible states of gas nucleated at the liquid/solid interface. Moreover, a new state, a gas bubble(s) coexisting with a gas film with a finite thickness, is predicted by the theory. Typical thickness of the gas pancakes is at the nanoscale within the force range of the long-range interaction, whereas the radius of the gas bubbles can be large. Our theoretical results can contribute to the development of a unified picture of gas nucleation at the liquid/solid interface.

[1]上海交通大学；
[2]University of Nebraska-Lincoln, Lincoln, USA

纳米水通道的电学开关

李敬源[1] 弓晓晶 陆杭军 李 鼎 周儒宏[2] 方海平

关键词 纳米碳管，分子开关，纳米门控

研究细胞膜蛋白水通道如何让水分子进出的具体工作机制具有重要的意义。但由于生物膜蛋白水通道结构十分复杂，对其性质进行系统研究往往难度比较大，因此，具有合适半径的纳米碳管常被用作生物膜蛋白水通道的简化模型。本文即以具有合适半径的纳米碳管作为水通道的简化模型，用全原子动力学的模拟方法研究外加电荷对水分子传输行为的影响。

我们的研究表明：改变电荷与碳管壁之间的距离，虽然通道内的电场环境会有一定程度的变化，但碳纳米管仍能在这种情况下保持一个稳定的流量，同时在碳纳米管和电荷的距离达到一个临界值的时候，流量迅速减小，从而实现真正的在噪音环境下通道迅速开关的门控。结果表明纳米尺度下水通道的这个特性对于水通道蛋白实现它的生物学功能非常关键。

Electrostatic gating of a nanometer water channel

LI Jingyuan[1] GONG Xiaojing LU Hangjun LI Ding
ZHOU Ruhong[2] FANG Haiping

Key words: Carbon nanotube, Molecular switch, Nanogate

The transportation of water molecules across nanometer water channels in membranes plays a key role in biological activities. However, the complex structure of biological channels often makes further investigations of the mechanism of biological water channels very complicated. On the other hand, primary characteristics can usually be exploited by studying a similar but structurally less complicated

problem. It has been proven that the single-walled carbon nanotube (SWNT) can be used as the simple model for the biological water channel. In this paper, we set the imposed charge at different distances from the wall of the SWNT to study the influence of external charge on water flow and net flux. Molecular dynamics is adopted.

The results show that a SWNT with an external positive charge is used as a prototype to study the response to the indispensable charges as well as the possible charge noise near water channels. Water flux of the nanochannel changes sharply when the electric field reaches a critical value, hence a distinctive gating property of the nanochannel in a thermal noisy environment, being sensitive to mechanical or charge signals and effectively resistant to noises. The observation is of help for developing SWNT-based nanoscale devices. We believe that this excellent property is important for biological systems to achieve accurate information transfer in an environment full of thermal fluctuations.

[1]浙江大学物理系；[2]IBM Thomas J. Watson Research Center, Yorktown Heights and Department of Chemistry, Columbia University, New York, USA

纳米结构表面的超大滑移长度

李 鼎 狄勤丰[1] 李敬源[2] 钱跃宏[1] 方海平

关键词 纳米结构表面，滑移长度，去浸润

在液固界面，疏水作用扮演着重要的角色。近来，人们发现，纳米尺度下，疏水界面附近会发生一种将水排开的类似于一级相变的过程，这一过程被称作去浸润过程。我们使用热力学方法分析了在纳米结构表面附近发生去浸润过程的必要条件，指出存在一个纳米结构在表面上的临界覆盖率，只有当覆盖率大于该临界值时去浸润过程才会发生。

在亚微米尺度下，流体力学的无滑边界条件往往是不适用的，取而代之的是由滑移长度描述的滑移边界条件。大的滑移长度在实际中有着广泛的应用，例如在污水处理和海水淡化等方面。在文中我们分析了处于去浸润状态的纳米结构表面的滑移长度，并且发现在一定条件下，其值可以达到微米量级，这一结果与最近发表的实验结果吻合。通常认为要减小表面对流体的阻力需要使表面平整，而我们的结果说明在发生去浸润过程的条件下，粗糙的表面可以比平整表面对流体流动有更小的阻力。

Large slip length over a nanopatterned surface

LI Ding DI Qinfeng[1] LI Jingyuan[2] QIAN Yuehong[1] FANG Haiping

Key words: Nanopatterned surface, Slip length, Dewetting

Hydrophobicity plays a key role in the liquid/solid interface systems. It is now recognized that a first-order phase transition like process named “dewetting process” occurs in nano-scale hydrophobic systems. We use a thermodynamic method to analyze the necessary conditions for causing a dewetting process at nanopatterned surface and indicate that there exists a critical value of coverage ratio of nanopatterns. The dewetting process may occur when the coverage ratio of nanopatterns is larger than

the critical value.

At sub-micro-scales, the non-slip boundary condition is usually invalid and a slip boundary condition described by a physical quantity slip length will be suitable to use. In fact, larger slip lengths are required in many practical fields, such as membrane polluted water treatment and desalination. Using wetting theory, we obtain an analytical expression about the slip length of nanopatterned surfaces and show that the nanopatterned surface at dewetting state may have an incredible large slip length about tens of micro-meters which is comparable to the experimental results reported very recently. Our results show that a rough surface may have extremely low flow resistance in fact, and it may change the traditional strategy to reduce surface friction which is based on the common knowledge that a smoother surface should have lower friction than a rough one.

[1]上海大学力学所；
[2]浙江大学物理系

哑铃在泊肃叶流中运动的晶格 Boltzmann 方法模拟

伊厚会　陈艳燕　李华兵*

关键词　晶格 Boltzmann 方法，哑铃

哑铃这一简单的力学模型在聚合物溶液动力学、DNA 的分子模型、蛋白质的结晶过程等研究领域有着广泛的应用，且基于哑铃模型从理论上能解释众多有意义的现象与实验结果。而哑铃在流体中的运动行为是进行此类研究的基础。我们利用晶格玻尔兹曼法研究了哑铃在流体中的运动行为。

我们研究了哑铃在平面泊肃叶流中的运动行为。研究发现，如同单个颗粒一样，哑铃在泊肃叶流中也具有 Segré-Silberberg 效应。我们具体分析了哑铃的运动轨迹、方向、垂直方向速度和角速度随时间的变化情况，还进一步讨论了影响哑铃稳定位置的因素：流体雷诺数、哑铃的直径和管道直径的关系及哑铃的弹性系数。我们的工作对聚合物的溶解、合成以及反应等研究具有一定的指导意义。

Lattice Boltzmann simulations of a dumbbell moving in a Poiseuille flow

YI Houhui　CHEN Yanyan　LI Huabing*

Key words:　**L**attice Boltzmann method, Dumbbell

As a simple mechanical model, the dumbbell has been applied to study various domains, including dynamics of polymer solutions, DNA molecules，protein crystallization, etc. Many significant phenomena and experiments can be well explained by dumbbell model. The property of the dumbbell moving in the fluid flow is the basis to understand the mechanism of polymers, DNA and proteins. In this paper, we concentrate on the study of behavior of dumbbell in fluid flows.

The lattice Boltzmann method is applied to simulate a dumbbell moving in a pressure-driven flow

in a planar channel with the stress-integration method for the evaluation of hydrodynamic force on the cylinders. The simulation results show that the dumbbell also has the important feature of the Segré-Silberberg effect like a particle in a Poiseuille flow. The dumbbell trajectories, orientations, and the cylinders' vertical velocities and angular velocities as functions of time have been studied. It is also found that the dumbbell equilibrium positions depend on the flow Reynolds number, blockage ratio and elastic coefficient. Our study is expected to be helpful to understand the dynamics of polymer solutions, polymer synthesis and reaction, etc.

*桂林电子科技大学材料信息学院

氢气纳米气泡的电化学可控产生和生长

张立娟 张 益 张雪花* 李朝霞 沈广霞

叶 鸣 樊春海 方海平 胡 钧*

关键词 原子力显微镜，电化学方法，纳米气泡，高序热解石墨

电化学反应中产生的气体的影响很长时间以来一直是一个很有挑战性的课题，已经引起了广泛的科学兴趣。由于电化学反应通常在溶液中进行，气体（如氢气和氧气）通常在电极表面产生，因此，电化学产生的气体可能会形成气泡并且粘在电极表面上，对电化学反应体系造成极大的影响。例如，Tsai 等人发现由于氢气气泡在电沉积膜上的吸附造成了气泡状的微小的缺陷。最近，Wang 等人利用电化学方法在阴极上生成了特殊形貌的方解石管状晶体，并认为这是由纳米气泡的生长所导致。

尽管在研究电化学产生的气体对电化学方法的影响方面有一定进展，但受观测仪器所限，以前的观测仅仅被限制在微米尺度，而在纳米尺度气体对电化学反应的影响目前还一无所知。近来，扫描探针显微镜的发明为人们探索微观世界提供了可能。在电化学方面，如腐蚀、刻蚀、电化学纳米芯片等重要方面也得到了很大的进展。

扫描探针显微镜家族中的重要一员——原子力显微镜(AFM)的发明为人们探索纳米尺度下气体在界面上的富集提供了有力的工具。自 1994 年 Parker 等提出纳米气泡可能引起界面上的长程引力以来，纳米气泡的存在不断得到证实，它们的直接证据就是原子力显微镜的检测结果。另外其它技术如快速冷冻法和中子反射法也预示了纳米气泡的存在。研究发现，纳米气泡在固液界面上的存在对表面和界面科学、流体学、纳米科学和生物科学都有着重要的影响。如它们可以造成界面的长程引力，影响胶体系统的稳定，使在微流系统中的摩擦力和阻力降低。生物学方面，研究发现气体的吸附可以导致蛋白质的组装和快速折叠，影响到生物芯片和生物传感器的效率。当然，纳米气泡的存在也可以为人们所利用，如利用脱气的水可以制成新一代的环保洗衣机，气泡可用于超声诊断和药物输送，可作为微流通道的开关和用于纳米器件的设计等。

所以，本文设计实验的主要目的，一方面是研究电化学产生的气体是否能够在电极表面稳定吸附，是否对电化学反应产生一定的影响；另一方面是尝试采用一种新的、可控的、能产生大量单一气体成分的纳米气泡的方法。这样，可克服气体来源不明、系统不可控造成的实验假象，进一步研究纳米气泡的形成规律和基本性质及它们的稳定机制。利用原子力显微镜的轻敲模式，我们观察到了电化学产生的氢气导致纳米气泡在高序热解石墨上形成。我们观察到纳米气泡只有在高于某一个电压阈值时才能出现，它的形成和生长可以通过控制电压的大小和反应时间来调节。

另外，我们还原位监控了纳米气泡的整个演化过程，即纳米气泡的形成、生长、聚结以及最后聚合的微米气泡从石墨表面逃逸的过程。

Electrochemically controlled formation and growth of hydrogen nanobubbles

ZHANG Lijuan ZHANG Yi ZHANG Xuehua* LI Zhaoxia SHEN Guangxia
YE Ming FAN Chunhai FANG Haiping HU Jun*

Key words: Atomic force microscopy, Electrochemical approach, Nanobubbles, Highly oriented pyrolytic graphite

The influence of electrogenerated gases on electrochemical reactions has historically attracted significant research interest and still remains a challenging topic. Since electrochemical reactions occur primarily in aqueous solutions, gases (e.g. hydrogen and oxygen) are usually generated at electrode surfaces. As a result, electrogenerated gases may form bubbles and stick to the electrode surface and significantly affect the electrochemical reaction system. For example, Tsai et al. elegantly demonstrated that adsorbed hydrogen bubbles were responsible for bubble-shaped microscale defects, which were often encountered in electrodeposited coatings. More recently, Wang and co-workers observed that water-electrolysis-induced mineralization led to the formation of submicrometer vaterite tubes at the cathode surface, which indirectly suggested the existence of nanoscale bubbles at electrode surfaces. In this work, we present direct evidence that electrochemical generation of hydrogen does induce the formation of hydrogen nanobubbles at the electrode surface.

Nanoscale bubbles at the solid-water interface were first predicted from force measurements in 1994, and their stable existence was recently reported by using atomic force microscopy (AFM). Other techniques, including rapid cryofixation-freeze fracture and neutron reflectometry, also suggested the existence of nanobubbles. The existence of nanobubbles has many important implications. In particular, their existence at the hydrophobic solid-liquid interface may significantly change the dynamics of a variety of systems, such as long-ranged interfacial interactions, stability of colloidal systems, and reduction of friction and drag in microfluidic transportation. Nanobubbles were also suggested to be associated with a wide range of applications such as fast folding of proteins and assembly, design of biosensors/biochips, detergent-free cleaning, ultrasound diagnostics and local drug delivery in medicine, and design of fluidic microchannels and nanodevices. However, the origin of nanobubbles still remains ambiguous and under debate. Of note, most previous experimental results on nanobubbles available in the literature were of conflict as well, which might arise from the influence of many factors such as complicated behavior of hydrophobic self-assembled monolayer surfaces, possible experimental artifacts, and dissolved gases.

To better understand electrochemical interfaces and settle the above-mentioned nanobubble debate, we focus on the study of formation and existence of hydrogen nanobubbles at highly oriented pyrolytic graphite (HOPG) electrode surfaces under electrochemical control. In fact, de Gennes suggested that high concentration of gases is crucial for their adsorption and probably for the nanobubble forma-

tion at the solid-water interface, while electrochemistry is well suited to rapidly generate a large amount of gas molecules, leading to a high local gas concentration proximal to the electrode surface. We also note that the origin of electrochemically generated gases is well defined. For example, in a diluted sulfuric acid solution, only hydrogen gas is generated at sufficiently negative potentials.

In this work, we established a well-defined system that could produce a large amount of single component gas, hydrogen by electrolysis of diluted sulfuric acid at the HOPG electrode. In our experiments, the existence of hydrogen nanobubbles was demonstrated by both phase image and perturbation of the AFM tip and was further confirmed by the ex-situ degassing method. We observed that there was a voltage threshold for the appearance of nanobubbles and that the formation and growth of nanobubbles could be well controlled by tuning the applied voltage and the reaction time. We also in situ monitored the whole evolution process of nanobubbles, that is, formation, growth, and coalescence of nanobubbles as well as eventual release of merged microbubbles from the surface.

*上海交通大学

C_{50}钝化的密度泛函研究

许子健 张 伟* 朱志远 韩家广

关键词 密度泛函理论，富勒烯，钝化，异构体，能量和电子性质

本工作使用密度泛函理论(DFT)计算方法考察了 C_{50} 的加氢加氯钝化。D_{5h} C_{50} 钝化前后的结构变化、能量学特征和电子结构性质表明类土星光环形状的 $C_{50}H_{10}$ 和 $C_{50}Cl_{10}$ 相对于 C_{50} 有显著改善的稳定性。$C_{50}H_1$、$C_{50}Cl_1$ 和 $C_{50}H_{11}$ 的异构体被优化，以考察单个碳位反应活性的变化。局域的钝化反应被证明具有全局性或扩展性效应，它不仅释放了加成位附近区域的应变，而且显著降低了远离加成位区域的应变和反应活性。有一个或两个 H 原子加成到非赤道位的 144 个 $C_{50}H_{10}$ 的异构体被完全优化，其结果与单原子加成的结合能一起，证实了 C4 位(赤道碳位)加成的优先性以及类土星光环形状的 C_{50} 加成物的独特的稳定性。根据对 $C_{50}H_{10}$ 144 个异构体的计算，本工作总结得出了确定有利加成位的三条经验规律，这将有助于减少搜索 C_nX_m 最佳异构体所需的计算量，并对预测新的富勒烯衍生物的结构具有重要意义。

A density functional study of C_{50} passivation

XU Zijian ZHANG Wei* ZHU Zhiyuan HAN Jiaguang

Key words: Density functional theory, Fullerene, Passivation, Isomer, Energetic and electronic properties

The structural, energetic and electronic properties of D_{5h} C_{50} before and after passivation by H and Cl are investigated using the density functional theory method with GGA and LDA exchange-correlation functional. The results show that H or Cl addition can lead to structural changes and energetic stabilization. Addition reactions also increase the HOMO－LUMO gaps of C_{50} derivatives which will make them chemically more stable. The passivation effect of local addition has globality character which not only partly releases the strain of the region near the addition locations of C4 site but

also remarkably reduces the strain of other areas away from addition sites. The preferment of C4 site addition is confirmed by single atom additions and by computations on 144 isomers of $C_{50}H_{10}$ with one or two H atoms added to non-equatorial sites. Three pieces of experience for choosing the favorable addition sites of fullerenes are summarized according to the computations on the 144 isomers of $C_{50}H_{10}$, which will help to reduce the computer effort in search of the best isomers of C_nX_m, and have predictive significance for the structures of new fullerene derivatives.

*北京师范大学低能核物理研究所

D_{5h} C_{50} 富勒烯的化合价

许子健　韩家广　朱志远　张 伟*

关键词　C_{50} 富勒烯，化合价，异构体，能量和电子性质，密度泛函理论

我们用基于 DFT 的第一性原理计算方法，对 640 余个 $C_{50}H_{2m}$ 异构体及少量 $C_{50}Cl_{2m}$ 异构体进行了结构优化、能量和电子结构计算。主要结果如下：(1)这些异构体的结合能及 HOMO-LUMO 能隙充分证明，10 是 D_{5h} C_{50} 赝原子的“赝化合价”或有效化合价，以及类土星光环形状的 $C_{50}H_{10}$ 和 $C_{50}Cl_{10}$ 在 $C_{50}X_{2m}$ 分子系列中，均具有最优的幻数稳定性的赝价结构。(2)构建了一条从 C_{50} 到 $C_{50}H_{14}$ 的最低能量反应路径。(3)通过对 40 个 $C_{50}H_2$ 和 139 个 $C_{50}H_8$ 附加异构体的优化计算，进一步验证了 C_{50} 赤道位加成的优先性及以前所得的选取有利加成位的三条经验。(4)提出了一个简单的空间位方法来预测(或确定)经典富勒烯的有效化合价，并用该方法推断了一些富勒烯的化合价。

Valence of D_{5h} C_{50} fullerene

XU Zijian　HAN Jiaguang　ZHU Zhiyuan　ZHANG Wei*

Key words: C_{50} fullerene, Valence, Isomer, Energetic and electronic properties, Density functional theory

In this study, structural optimizations, as well as energetic and electronic structure calculations have been performed for over 640 $C_{50}H_{2m}$ isomers and a few of $C_{50}Cl_{2m}$ isomers by first-principle computational method based on the density functional theory. The prime results obtained in this work are: (i) The binding energies and HOMO-LUMO gaps of the most stable isomers clearly prove that Saturn-shaped $C_{50}H_{10}$ as well as $C_{50}Cl_{10}$ is a pseudo-valence structure of D_{5h} C_{50} and 2m =10 is the effective valence of C_{50} fullerene “pseudoatom”. Thus, Saturn-shaped $C_{50}H_{10}$ as well as $C_{50}X_{10}$ may have the magic-number stability among molecules of $C_{50}X_{2m}$ series. (ii) A minimal energy reaction pathway is constructed from C_{50} to $C_{50}H_{14}$. (iii) The preferment of C4-site addition and the experience for determining the favorable addition sites are further confirmed by computations on additional isomers of $C_{50}H_2$ and $C_{50}H_8$ with one or two H atoms added to non-equatorial sites. (iv) A simple steric method related to C-site types (PPP, PPH, PHH, and HHH) is developed to determine the effective valences of classical fullerenes, and the valences of some fullerenes are inferred using this method.

*北京师范大学低能核物理研究所

双壁碳纳米管机械振动的模拟研究

许子健　朱志远　潘瑞芹

关键词　双壁碳纳米管，振动频率，分子动力学，初始伸出长度，能量耗散，原子约束

本工作通过系统的分子动力学模拟详细考察了初始伸出长度、能量耗散和原子约束对双壁碳纳米管振子振动频率的影响。结果显示，当内管初始伸出长度大于内管长度的 92%时，1ns 内的平均振动频率将随着初始伸出长度的增加而上升，这与解析理论的预测恰恰相反。一条关于纳米振子的普遍规律是，初始伸出长度越长，振动越不稳定。因此，在大的初始伸出情况下，频率变化的反常行为应该是由于剧烈的能量耗散导致振幅的快速衰减，而振幅的快速衰减又相应地导致频率随时间快速上升所造成的。因此在 1 ns 的多数时间内，振子都运行在远高于初始振动、也远高于理论预测的恒定振幅振动的频率上。我们算得的系统的有效摩擦力与 Cumings 和 Zettl 所预测的在同一数量级。研究还发现，在纳米振子上施加合适的约束，尤其是冻结外管两端的原子，可以有效地减少振动能量耗散，延长稳定振动的时间。该发现表明外管端口在能量耗散机制中扮演着重要角色。实际上根据我们的模拟，除了内管的摇摆运动(rocking motion)外，外管两端的横向摆动(lateral swing)也是耗散振动能量的一个重要方式；而冻结外管两端的原子将彻底消除这种横向摆动。这些研究结果为制备动力学上稳定的纳米管振子提供了具有指导意义的知识，并揭示了初步的规律。

Molecular dynamics study on the oscillation of double-walled carbon nanotube oscillators

XU Zijian　ZHU Zhiyuan　PAN Ruiqin

Key words: Double-walled carbon nanotube, Oscillation frequency, Molecular dynamics, Initial extrusion length, Energy dissipation, Atomic constraints

A series of molecular dynamics (MD) simulations have been performed to investigate the effects of initial extrusions, energy dissipation and atomic constraints on the oscillation frequency of double-walled carbon nanotube (DWNT) oscillators. The results show that when the initial extrusion length of the innertube is larger than 92% of the innertube length, the mean oscillation frequency within 1ns increases with the initial extrusion length, which is opposite to the theoretical prediction by Zheng's formula. This abnormal frequency behavior is actually due to the great energy dissipation at large initial extrusions. The calculated effective friction is on the same order as predicted by Cumings and Zettl. We also found that proper constraints could be effective ways to reduce oscillation energy dissipation and prolong the steady oscillation, especially freezing the atoms at both ends of the outershell is most effective in reducing dissipation, which indicates that the outertube ends play an important role in the energy dissipation mechanism. The study presented here may provide helpful knowledge for fabricating stable nanotube oscillators.

高能粒子与 X-射线在碳纳米管(绳)内的传输

郑里平　李 勇　许子健　王呈斌　朱志远

关键词　碳纳米管(绳)，毛细管，沟道效应，粒子与 X-射线传输

碳纳米管既可被看作为巨大的碳分子鏈又可被看作为把石墨的六边网状晶格面(层)卷成一个中空的圆柱体。碳纳米管分为单層壁碳纳米管和多層壁碳纳米管两类。碳纳米管绳由许多根碳纳米管组成。在大型加速器里，即使输出几乎平行也就是说张角接近零的高能粒子的初态束流，随着初态与末态之间的传输距离增大，末态束流的(横向)尺寸将比初态束流的(横向)尺寸增大。大功率电磁铁产生的(横向)势场能约束粒子束流的尺寸变大。通常碳纳米管绳的(横向)势场梯度=100 eV/nm，与大功率电磁铁的势场梯度相当；因此对于约束粒子束流的尺寸变大，用碳纳米管绳(超晶格结构的大单晶体) 更有效、更经济。

X-射线微束领域包括 X-射线源、传输、聚焦、成像探测等方向。为了形成足够强度的 μm 级甚至 nm 级 X-射线微束，就必须进行微聚焦。X-射线微聚焦是一个挑战性问题：X-射线是不带电的电磁波，它不能利用电磁场来偏转和聚焦；同时由于在 X-射线范围内物质的折射率近似为 1，它也不能像可见光一样利用玻璃等材料制成透镜进行折射聚焦。近年来，新毛细管光学聚焦元件由许多根弯曲的多層壁碳纳米管组成，这种新元件能被用来产生高强度的 nm 级 X-射线微束。本文介绍了这些应用研究的进展。

Propagation of high energy particle and X-ray in the nanotube-rope

ZHENG Liping　LI Yong　XU Zijian　WANG Chengbin　ZHU Zhiyuan

Key words:　Carbon nanotubes, Capillaries, Channeling, Particle and X-ray transmission

The nanotubes-rope is a large single crystal with the super-lattice structure, and it has been recently produced. In particle-beam physics field, the most intriguing applications of the nanotube-rope channeling are connected with the possibility of particle acceleration in high gradient accelerating field, and with the possibility of construction of TeV colliders.

Also recently, a new capillary optics focus element, which is composed of many bent-multi-walled nanotubes, can be used to produce the high strength nanometer-X-ray beams. This paper introduces the progress of these applied studies.

表面修饰导致的碳纳米管场发射性质的增强

勇振中　朱志远　王震遐

关键词　碳纳米管，开启电场，扫描电子显微镜

近几年来，碳纳米管薄膜作为场发射器件由于其潜在的应用价值而受到了人们的广泛关注。但是碳纳米管场发射器件的应用仍存在一些问题，如何降低开启电场、增加电流密度以及提高发

射电流的稳定性和可靠性对发射器件的应用至关重要。研究工作者通过各种实验方法来改善碳纳米管薄膜的场发射性质。我们以碳纳米管薄膜为基底，通过室温下等离子体溅射方法在碳纳米管表面镀铁催化剂颗粒。在 1000 K 的条件下，用甲烷和氢气等离子体化学气相沉积的方法在碳纳米管表面生长碳纳米棒。表面修饰过的碳纳米管薄膜的电子场发射测试表明，表面修饰前后碳纳米管薄膜的场发射开启电场(电流密度 10 μA/cm^2 时)从 2.4 V/μm 降低到 0.79 V/μm。碳纳米棒导致的场发射因子的增强以及场发射密度的增加是使碳纳米管薄膜开启电场降低的主要原因。这种方法对于开发碳纳米管薄膜场发射器件的应用可能是重要的。

Field emission enhancement of carbon nanotubes by surface modification

YONG Zhenzhong　ZHU Zhiyuan　WANG Zhenxia

Key words: Carbon nanotubes, Turn-on field, Scanning electron microscopy

Recently, a great deal of attention has been focused on the field emission property of carbon nanotube films for their promising potential practical applications. However, there are some obstacles in making electron field emission devices, such as how to lower turn-on electron field, to increase current density, to improve current stability and reliability, etc. All kinds of methods have been used to enhance the field emission property. We have produced Fe tipped carbon nanorods or carbon nanoparticles grown on the outer walls of multiwalled carbon nanotubes by combining sputtering deposition of Fe films and RF plasma enhanced chemical vapor deposition at 1000 K. The electron field emission tests indicate that the turn-on field (at 10 μA/cm^2) of the treated MWCNT films decreases from 2.4 V/μm to 0.79 V/μm and the field emission current is relatively stable. We believe that the appearance of the nanorods and particles on the surface of CNTs increase the field enhancement factor. The main reason why the turn-on field decreased is the increase of the field enhancement factor and the emission sites. It may be important for the application of carbon nanotube-based field emitters.

$^{40}Ar^+$ 诱导无定形碳到金刚石纳米晶相变的研究

勇振中　王震遐　胡建刚　朱志远

关键词　离子束，金刚石纳米晶，相变，透射电子显微镜

由于在技术应用上的重要性，金刚石的合成受到了广泛的重视。我们工作中通过 60 keV 的 $^{40}Ar^+$辐照无定形碳靶合成了大量尺寸不同的金刚石纳米颗粒。高分辨透射电子显微镜配合能量色散 X 射线谱和电子衍射以及 Raman 谱分析的结果表明，这些嵌于具有扰动式膜结构薄膜中的纳米金刚石颗粒，其成核率很高(约为 10^{13}/cm^2),而且可以生长到较大尺寸，有的甚至可以达到微米数量级。我们对其相变过程也进行了初步探讨，所得的实验结果与 Yao 等的研究结果相类似，但是所使用的辐照粒子以及起始材料等实验条件是不同的。这再次表明，在缺少氢的条件下荷能离子辐照无定形碳材料形成金刚石是一种一般现象。不过荷能离子、碳靶材料等实验条件的不同所导致的形成机制的差别也是很重要的。这方面的工作还需要作进一步系统的研究。

Phase transition from amorphous carbon to diamond nanocrystalline induced by $^{40}Ar^{+}$

YONG Zhenzhong WANG Zhenxia HU Jiangang ZHU Zhiyuan

Key words: Ion beam, Diamond nanocrystalline, Phase transition, Transmission electron microscopy

The synthesis of diamond has attracted great interests due to its important technical applications. In our work, large-scale diamond nanocrystals of different sizes were synthesized by 60 keV $^{40}Ar^{+}$ irradiation on amorphous carbon. Investigations by high-resolution transmission electron microscopy, electron diffraction and Raman spectroscopy show that the diamond crystallites embedded in graphitic film have a high nucleation density (about $10^{13}/cm^2$) and can grow to large sizes even of the micrometer order. The mechanism of phase transition is discussed preliminarily. The result is similar to that of Yao group except the experimental conditions, such as incident ions and original amorphous carbon target. It indicates that the diamond formation by irradiating carbon target with energetic ions in the absence of hydrogen is a general phenomenon. To well understand the formation mechanism, some more systematic work should be done in future.

碳纳米管芯/SiO_2壳纳米线

王震遐 勇振中 胡建刚 朱志远

关键词 碳纳米管，透射电子显微镜，电子能损谱，微结构

各种各样不同材料组成的芯/壳线状结构及其合成的研究一直都是纳米材料和纳米结构研究工作中的一个重要组成部分，化学气相沉积技术是其中一种有效的合成手段。碳纳米管已经被证明是制作纳米电子器件的理想材料，但是如何把碳纳米管作为芯材料封装到另外一种壳介质材料当中却很少被报道。封装碳纳米管的介质材料需要满足两个条件：防止碳纳米管空气敏感表面引起的退化以及降低管子之间的耦合。我们用氢等离子体刻蚀和热氧化方法处理多壁碳纳米管，合成了多壁碳纳米管芯/SiO_2壳纳米线状结构。产物的形成和微结构经过了扫描电子显微镜、透射电子显微镜和电子能量损失谱的分析。这种纳米线状结构对于在排除环境扰动的条件下研究碳纳米管电学、热学、光学以及离子传输性质具有重要的应用价值。

Nanowires with a carbon nanotube core and silicon oxide sheath

WANG Zhenxia YONG Zhenzhong HU Jiangang ZHU Zhiyuan

Key words: Carbon nanotubes, Transmission electron microscopy, Electron energy-loss spectroscopy, Microstructure

Various kinds of core/sheath wire-like structures with different compositions have been studied, using various synthesis methods including the chemical vapor deposition (CVD). However, to our knowledge, there are still few reports on how to encapsulate carbon nanotubes into another sheath

structures, although it has been known that carbon nanotube is ideal for fundamental studies of their physical properties and for the fabrication of electronic nanodevices. In addition, the encapsulation of carbon nanotubes within a stable medium should play the dual role of protecting air-sensitive surface of nanotube against degradation and reducing the coupling between individual tubes. Here, we report a simple and effective new method, using silicon wafers as a source material and by hydrogen etching and thermal oxidation reaction, to directly deposit silicon oxide on the outer surface of the CVD-multiwalled carbon nanotubes (CVD-MWCNTs), thereby forming nanowires with a nanotube core and silicon oxide sheath. The morphology and structure of the products were studied by scanning electron microscopy (SEM), transmission electron microscopy (TEM), and electron energy-loss spectroscopy (EELS).These nanocables could be an ideal system for a systematic experimental and theoretical understanding in the electronic, thermal, optical, and ionic transport processes in MWCNTs in the absence of disturbances from environmental factors.

多壁碳纳米管在循环相变过程中的结构变化初探

王震遐　勇振中　朱志远

关键词　无定形碳纳米线，高温退火，相变，透射电子显微镜

碳一维纳米结构，例如碳纳米管和碳纳米线由于其不寻常的机械、电学、和光学特性以及在纳米技术中广泛的应用前景，而受到众多科学家的重视和大力研究。最近，在本组所进行的相关实验工作当中，涉及到碳一维材料的相变问题，例如离子束辐照多壁碳纳米管使其转变成无定形碳纳米线。在当前正进行的在高温条件下无定形碳纳米线向多壁碳纳米管的转变研究中，已发现一些十分有趣的现象。我们对离子束辐照多壁碳纳米管产生的无定形碳纳米线进行了高温(2400℃)退火处理，通过透射电子显微镜观察发现，无定形碳纳米线体部转变成了与原来多壁碳纳米管相似的管状结构，而其封端区域的石墨晶体结构形态却与原来的多壁碳纳米管不同，且变化多端。基于实验结果，对其相变过程机理提出了一个概念性的模型。

Preliminary structural study of multi-wall carbon nanotubes in a returning phase transition process

WANG Zhenxia　YONG Zhenzhong　ZHU Zhiyuan

Key words: Amorphous carbon nanowire, High temperature annealing, Phase transition, Transmission electron microscopy

One dimensional carbon nanostructures, such as nanotubes and nanowires, have attracted intensive interests and extensive researches due to their novel mechanical, electronic and optical properties and potential applications in nanotechnology. In the recent work of our group, which concerns the phase transformation of one dimensional carbon nanostructures, the multi-walled carbon nanotubes (MWNTs) have been transformed into amorphous carbon nanowires (ACNWs) by ion beam irradiation. Presently, we are investigating the transformation from ACNWs to MWNTs under high temperature annealing.

The amorphous carbon nanowires, formed during the ion irradiation of multi-wall carbon nanotubes, were annealed at a high temperature of 2400°C. Transmission electron microscopy observations revealed that the body of ACNWs had transformed to a tube-like structure similar to that of the original MWCNTs, but the tip structure had various forms and was quite different from the original MWCNTs. Based on the results, we proposed a conceptual model of phase transition mechanism.

单壁碳纳米管热导率的温度、直径依赖关系

潘瑞芹　许子健　张 伟*　朱志远　韩家广

关键词　热导率，分子动力学，单壁碳纳米管

应用非平衡态的方法，首先计算了单壁碳纳米管的热导率与温度和直径的关系。在研究中选用四个不同直径的扶手椅型单壁碳纳米管(5,5)，(7,7)，(9,9)和(10,10)作为研究对象，它们的直径依次增大，分别为 0.3390，0.4746，0.6102，0.6780 nm。计算热导率所采用的管子截面积取厚度是 0.142 nm 的圆环面积，采用周期性边界条件，碳管的长度大约为 29.5 nm，时间步长取为 0.5 fs，每一个模拟运行 1.25×10^6 步。计算了在温度为 100~600 K 的范围内的热导率。研究结果显示扶手椅型单壁碳纳米管的热导率随着温度的升高而减小，随着碳纳米管直径的增大而增大。我们知道热阻主要是由声子散射中的倒逆散射造成的。对于直径较小的碳纳米管，由于布里渊区较小，更容易发生倒逆散射，所以随着直径的减小，碳纳米管的热导率有所减小。同时随着温度的升高，声子间的散射将增强，也就增加了倒逆散射过程，所以随着温度升高，碳纳米管的热导率会减小。

Temperature and diameter dependences of the thermal conductivity of single-walled carbon nanotubes

PAN Ruiqin　XU Zijian　ZHANG Wei*　ZHU Zhiyuan　HAN Jiaguang

Key words:　Thermal conductivity, Molecular dynamics, Single-walled carbon nanotubes (SWNTs)

Temperature and diameter dependences of thermal conductivity for armchair SWNTs were studied by the nonequilibrium molecular dynamics (MD) method with Brenner II potential. Four armchair-type SWNTs of (5, 5), (7, 7), (9, 9) and (10, 10) were simulated, and their diameters were 0.339，0.4746，0.6102 and 0.6780 nm, respectively. The cross-sectional area of the SWNT was taken as an annular ring of 0.142 nm thick. The periodic boundary condition was applied along the tube axis, with a length of the periodic box of about 29.5 nm. A total simulation time of 625ps (1.25×10^6 MD steps for a 0.5-fs MD step) was chosen. Thermal conductivities were calculated at 100 K to 600 K. It was found that thermal conductivity decreases with increasing temperature, but increases with the SWNT diameter. Thermal resistance is caused by the phonon–phonon interaction of Umklapp processes, which happens easily in small diameter CNTs, so the thermal conductivity increase with the diameter. At higher temperatures, the phonon-phonon Umklapp scattering increases, and this in turn increases the thermal resistance, and suppress the energy transfer, therefore the thermal conductivity decreases.

*北京师范大学低能核物理研究所

功能化碳纳米管的热导率

潘瑞芹　朱志远　许子健　王震遐

关键词　热导率，分子动力学，单壁碳纳米管，功能化

应用非平衡分子动力学方法，在 Brenner II 势下，计算了 300 K 时加氢功能化的（10，0）碳纳米管的热导率。计算结果显示，功能化碳纳米管相对于纯净的碳纳米管，热导率有明显的减小。纯净的(10，0)碳纳米管的热导率大约是 237 $W\cdot m^{-1}\cdot K^{-1}$，而有一列碳原子被氢化的碳纳米管的热导率大约为 150$W\cdot m^{-1}\cdot K^{-1}$，减小了大约 1/3。继续增强功能化程度，碳纳米管的热导率会继续减小，但是随着功能化程度的增加，热导率减小的幅度有所减缓。有 720 个碳原子被氢化的碳纳米管的热导率与有 540 个碳原子被氢化的碳纳米管的热导率相比，只有很小的变化。为了进一步解释这种功能化对碳纳米管热导率的影响，我们计算了 300 K 下 5 种不同功能化程度的碳纳米管的声子谱。纯净碳纳米管声子谱在大约 50 THz 附近有一个主峰，在 20 THz 附近有个次主峰。功能化碳纳米管的声子谱也都有同样的结果，它们在 50 THz 附近有一个声子谱的主峰，但是高度明显减小。并且随着功能化程度的加强，出现了一个大约为 86 THz 的较高频的声子谱峰，我们认为这个谱峰可能对应于 C-H 键的声子振动模式。分析认为，功能化碳纳米管热导率的减小是由声子平均自由程的减小和一些振动模式被抑制造成的。

Thermal conductivity of functionalized single-wall carbon nanotubes

PAN Ruiqin　ZHU Zhiyuan　XU Zijian　WANG Zhenxia

Key words:　Thermal conductivity, Molecular dynamics, Single-walled carbon nanotubes, Functionalization

The thermal conductivity at 300 K of (10,0) single-wall carbon nanotubes (SWNTs) that have been functionalized by chemical attachment of hydrogen atoms is studied by a nonequilibrium molecular dynamics (MD) method with Brenner II potential. The system exhibits a drop in thermal conductivity with functionalization. The thermal conductivity of pristine (10,0) CNT is about 237$W\cdot m^{-1}\cdot K^{-1}$, while functionalizing one row of 180 surface atoms (5% nanotube carbon atoms) reduces thermal conductivity by about a factor of 1.5. Additional functionalization further reduces the thermal conductivity, but with a much less amplitude compared to the drop from the pristine case to the case of 180 surface carbon atoms hydrogenated. For the case of 720 hydrogen atoms attached, there is little additional influence on the thermal conductivity relative to the case of 540 hydrogen atoms attached. To clarify this effect the phonon spectra of the nanotubes are investigated. In the spectrum of pristine nanotube a primary peak exists at around 50THz, with a minor peak at about 20THz. Similar results are obtained for the functionalized CNTs. However, the heights of the two peaks are much smaller than that of the pristine nanotube. Also as the degree of functionalization is enhanced, a high frequency peak (about 86 THz) appears, which may correspond to C-H stretch. We conclude that the degradation of thermal conductivity with functionalization arises from a reduction in the phonon scattering length and the suppression of some vibration modes.

单壁碳纳米管的长度依赖

潘瑞芹　许子健　朱志远

关键词　热导率，分子动力学，单壁碳纳米管

我们应用非平衡态方法，在 Brenner II 势作用下，模拟计算了长度从 22 nm 到 155 nm 的(5,5)和(7,7)单壁碳纳米管的热导率与长度的关系。结果显示碳纳米管的热导率对长度有很强的依赖关系，随着长度的增加，碳纳米管的热导率明显增大，同时随着长度的增长，热导率增加的幅度有所减缓。随着所模拟的碳纳米管的长度的增加，所模拟部分就越接近声子平均自由程的大小，热导率受碳纳米管长度的影响就越小。同时我们发现碳纳米管的热导率与长度满足 $\lambda \sim L^{\beta}$ 关系，对于(5,5)管 β=0.34，(7,7)管 β=0.29。也就是说指数 β 随着碳纳米管半径的增大而减小。还发现(5,5)管的热导率随着长度的增加是发散的，也许随着碳纳米管的长度的增加，当碳纳米管的长度大于碳纳米管声子平均自由程的长度的时候，热导率可能是收敛的，但是目前计算的碳纳米管的长度为 155 nm 时，热导率仍然随着长度的增加而增加。

Length dependence of the thermal conductivity of single-walled carbon nanotubes

PAN Ruiqin　XU Zijian　ZHU Zhiyuan

Key words:　Thermal conductivity, Molecular dynamics, Single-walled carbon nanotubes

Dependence of the thermal conductivity on the length of two armchair single-walled carbon nanotubes (SWNTs) is studied by the nonequilibrium molecular dynamics (MD) method with Brenner II potential. The thermal conductivities are calculated for (5, 5) and (7, 7) SWNTs with lengths ranging from 22 to 155nm. The simulation results show that the thermal conductivities of the two armchair-types SWNTs ((5, 5) and (7, 7)) have a strong dependence on the tube length. The thermal conductivity is less affected by the tube size as the periodic box gets longer and the box length becomes a larger fraction of the phonon mean free path. In other words, the thermal conductivity becomes less sensitive to the length when the length is large enough. We found the relation $\lambda \sim L^{\beta}$ with β=0.34 for (5, 5) tube and β=0.29 for (7, 7) tube. The present study shows that the value of β decreases with the radius of the tube. The results in this work for the (5, 5) tube are relatively more divergent. The thermal conductivity may converge when the tube length is much longer than the phonon mean free path. However, the thermal conductivity for the tube about 155 nm is still increasing with the tube length, which means not longer enough.

基于 Compton 背散射的高亮度伽玛射线光束线

郭 威 徐 望 陈金根 马余刚 蔡翔舟 王宏伟 徐 毅 王呈斌
陆广成 田文栋 袁仁勇 徐加强 魏中原 阎 喆 沈文庆

关键词 上海光源，同步辐射，光束线，康普顿背散射，γ射线源

本文介绍上海光源的一台高亮度的γ射线光束线：上海激光电子γ源(Shanghai Laser Electron Gamma Source, SLEGS)。SLEGS 通过 CO_2 激光束与上海光源(Shanghai Synchrotron Radiation Facility, SSRF)储存环内的 3.5 GeV 电子束之间的 Compton 背散射(Compton Backscattering, CBS)来产生最大能量为 22 MeV 的γ射线束。对激光束与电子束团之间的 CBS 过程建立了物理模型，并基于蒙特卡罗方法用 C++语言开发出了用于模拟γ射线束产生和传输的模拟程序。如果采用数百瓦功率的连续 CO_2 激光器，SLEGS 所产生的γ射线束的光子通量(未准直)可达 10^9~10^{10} s^{-1} 数量级。

A high intensity beam line of γ-rays based on Compton backscattering

GUO Wei XU Wang CHEN Jingen MA Yugang CAI Xiangzhou
WANG Hongwei XU Yi WANG Chengbin LU Guangcheng TIAN Wendong
YUAN Renyong XU Jiaqiang WEI Zhongyuan YAN Zhe SHEN Wenqing

Key words: Shanghai Synchrotron Radiation Facility, Synchrotron radiation, Beam line, Compton backscattering, Gamma ray source

Shanghai Laser Electron Gamma Source (SLEGS), a high intensity beam line of γ-ray, has been proposed recently. The beam line is expected to generate γ-rays up to the maximum energy of 22 MeV by Compton backscattering (CBS) between a CO_2 laser beam and electrons in the 3.5 GeV storage ring of the Shanghai Synchrotron Radiation Facility. The CBS process between laser beam and electron bunch is modelized, a C++ program using the Monte-Carlo method has been developed to simulate the production and the transmission of γ-ray. The flux of non-collimated γ-rays of SLEGS is estimated to be 10^9~10^{10} s^{-1} when a continuous CO_2 laser of several hundred watt power is employed.

基于 CO_2 激光和 100 MeV 电子康普顿背散射的 X 射线源

陈金根 徐 望 郭 威 马余刚 蔡翔舟 王宏伟 陆广成 徐 毅 王呈斌
潘强岩 袁仁勇 徐加强 卫中原 阎 喆 沈文庆

关键词 上海光源，同步辐射，光束线，康普顿背散射，X 射线，CO_2 激光，100 MeV 电子

本工作介绍了基于 CO_2 激光和 100 MeV 电子康普顿背散射的 X 射线源的设计。此 X 射线源可产生 8~18 keV 的 X 射线，并将作为上海光源的一条光束线——上海激光电子γ源的样机于 2007 年底之前安装完毕。给出了与此装置相关的细节描述并给出和讨论了一些模拟结果。还估算了从 100 MeV 直线加速器弯铁以及 100 MeV 电子分别产生的同步辐射和韧致辐射背景。由于所用的 CO_2 激光器的功率比较高，算得 X 射线的通量将达到 10^6 s^{-1} 量级，而相应的信噪比约为 10^6。

An X-ray source based on Compton backscattering of CO_2 laser and 100 MeV electrons

CHEN Jingen XU Wang GUO Wei MA Yugang CAI Xiangzhou
WANG Hongwei LU Guangcheng XU Yi WANG Chengbin PAN Qiangyan
YUAN Renyong XU Jiaqiang WEI Zhongyuan YAN Zhe SHEN Wenqing

Key words: Shanghai Synchrotron Radiation Facility, Synchrotron radiation, Beam line, Compton backscattering X-ray, CO_2 laser, 100 MeV electrons

The design for an X-ray source based on Compton backscattering of CO_2 laser and 100 MeV electron beam is introduced. This instrument can produce 8~18 keV X-ray and will be installed as a prototype of the Shanghai Laser Electron Gamma Source (SLEGS) at the end of 2007. Some detailed descriptions for the related instruments are presented. The related simulation results are provided and discussed. The backgrounds from the dipole magnet of the 100 MeV linac and bremsstrahlung of the 100 MeV electrons are also estimated. Due to the large power of the employed CO_2 laser, the expected flux of X-ray will achieve the order of 10^6 s^{-1}, and the corresponding signal-to-noise ratio is about 10^6.

核分析中心

Nuclear Analysis Techniques

Au(Si)探测器能量刻度与探测系统分辨率测量

刘江峰 包良满 李晓林 张桂林 李 燕

关键词 金硅面垒探测器，能量刻度，加速器

本实验室的离子束透射成像(STIM)实验系统更换了 Au(Si)探测器，我们用 3 MeV 质子对其进行了能量刻度和分辨率测量。

能量刻度：探测器置于束流入射方向的 0°角，测量入射质子和由铝箔透射的质子能量，铝箔为一层 (25.5 μm)和两层(51 μm)。这三种测量条件下的质子能峰分别在 762、619 和 420 道，已知入射束流能量为 3 MeV，由 TRIM 程序计算出束流通过 25.5 μm 和 51 μm 铝的剩余能量分别为 2380 keV 和 1617 keV。线性拟合得 E_p (keV) = –96.3+ 4.04ch，ch 为道数。

能量分辨率：探测系统的能量分辨率为基本呈高斯分布的质子能峰的半高宽。据误差分析理论，测量的标准偏差为 $\sigma_e^2 = \sigma_d^2+\sigma_s^2+ I^2/12$，式中，$\sigma_e = [\sum (x_i-\bar{x})^2/N]^{1/2}$ 为测量的平均值标准偏差，x_i 为单个事件测量结果，N 为测量的总事件数，I 为 ADC 的每道能量宽度，在本系统中的值为 4.04 keV；σ_d 和 σ_s 分别为探测系统和入射离子的能量离散造成的标准偏差。分别进行 8 次测量，每次获取 2000 个事件，计算出每次测量的平均值标准偏差。结果显示 $I^2/12+\sigma_d^2+\sigma_s^2 = 220.3 \pm 10.6$，由于 $\sigma_s \approx 2$ keV，则探测系统的能量分辨率 $\sigma_d \approx 15$ keV。

Energy calibration and resolution measurement of a Au(Si) detector

LIU Jiangfeng BAO Liangman LI Xiaolin ZHANG Guilin LI Yan

Key words: Au(Si) detector, Energy calibration, Accelerator

A new Au(Si) detector was installed for the scanning transmission ions microscope (STIM) system, and its energy calibration and resolution measurement were done with 3 MeV protons.

Energy calibration: The detector was placed at 0° of the beam incidence to detect the 3MeV protons, or protons passing one layer of aluminum foil (25.5 μm) and two layers of aluminum foil (51μm), in which the protons lose 620 and 1383 keV, respectively, as calculated by TRIM codes. Proton peaks corresponding to 3000, 2380 and 1617 keV were at 762, 619 and 420 channels, respectively. By a linear fitting of the data we found E_p(keV) = –96.3+ 4.04 ch, where ch is the channel number.

Energy resolution: The detector resolution can be obtained by measuring FWHM of the proton peak, which is in an approximate Gaussian distribution. According to theory of error analysis, the detector resolution can be derived by a data fitting with $\sigma_e^2=\sigma_d^2+\sigma_s^2+I^2/12$, where $\sigma_e = [\sum(x_i-\bar{x})^2/N]^{1/2}$ is the total standard deviation from the averaged energy of N protons, I=4.04 keV is channel width of the ADC, σ_d is the standard deviation of proton energy caused by the detector system, and σ_s, by energy straggling of the 3 MeV protons. By measuring 8 spectra with a total events of 2000 protons per spectrum, we had $\sigma_d^2 + \sigma_s^2 + I^2/12 = 220.3 \pm 10.6$, hence an approximate 15 keV of the σ_d, as the proton energy straggling is $\sigma_s \approx 2$ keV.

基于质子微探针单颗粒分析的大气颗粒物中 Fe 和 S 的来源与相关性研究

包良满　岳伟生　刘江峰　李晓林　张桂林　李 燕

关键词　大气颗粒物，PM_{10}，Fe，S，　质子微探针，源解析

对上海市的交通密集区(人民广场)和重工业区(钢研所)的大气颗粒物 PM_{10} 进行采样。用空间分辨率为 1 μm 的扫描质子微探针获得了颗粒物的 micro-PIXE 谱。根据 micro-PIXE 指纹谱，结合模式识别技术，对颗粒物中 Fe 和 S 的来源进行了识别，获得了各种排放源的贡献率。计算了颗粒物中 Fe 和 S 的相对含量比值，使用数理统计方法分析了其相关性，并对两个地区的结果进行了对比。结果表明，人民广场 PM_{10} 中含 Fe 颗粒主要来源于土壤尘和汽车尾气，二者贡献率分别为 26%和 25%；含 S 颗粒来源主要是汽车尾气和燃煤烟尘，贡献率分别为 36%和 18%。钢研所 PM_{10} 中 Fe 和 S 的污染源主要是冶金工业尘和燃煤烟尘。冶金工业尘对 Fe 和 S 的贡献率分别为 33%和 36%，燃煤尘对 Fe 和 S 的贡献率分别为 19%和 21%。人民广场 PM_{10} 中 S 和 Fe 不存在相关性，其相对含量比平均值在 0.001，钢研所 PM_{10} 中 S 和 Fe 存在弱相关性，相关系数 r=0.3，S 和 Fe 的平均相对含量比值为 0.1。

Source apportionment and correlation between iron and sulfur in PM_{10} in Shanghai by analyzing individual particles using proton microprobe

BAO Liangman　YUE Weisheng　LIU Jiangfeng　LI Xiaolin

ZHANG Guilin　LI Yan

Key words:　Atmospheric particulate matter, PM_{10}, Fe, S, Proton microprobe, Source apportionment

Atmospheric PM_{10} samples were collected simultaneously at the city center and heavy industrial areas of Shanghai in winter, 2004. Micro-PIXE spectra in 1 μm spatial resolution of the single atmospheric particle were obtained. The source identification and apportionment of Fe and S were done based on micro-PIXE spectra combining with pattern recognition technique. The relationship between relative concentration of Fe and S was studied by mathematical statistics based on PIXE calculation. The results show that the major contributions of Fe pollution in atmosphere particles at the city center are soil dust, vehicle exhaust particles and coal combustion. The sources of S pollution in the city center are vehicle exhaust and coal combustion, with a contribution about 36% and 18%, respectively. While in the heavy industrial areas, Fe and S were derived from metallurgic industry particles, contributing 33% to Fe and 36% to S. The mean value of the relative concentration ratio of S to Fe is 0.1. The S concentration is weakly correlated with Fe, the correlation coefficient is 0.3 and the confidence coefficient is 95%. But there was no correlation between S and Fe in the city center and the mean value of the relative concentration ratio of S to Fe is 0.001. This work provides the basic information for the study of the origin of the urban atmosphere particles pollution and the pollution control.

用同步 XANES 谱研究交通来源颗粒物中铅的化学种态

金 婵 李玉兰 张桂林 谈明光 李 燕

关键词 交通来源颗粒物，XANES，化学种态

大气中的铅通常依附于颗粒物中，铅对人类健康的影响与其在颗粒物中的含量有关，且与其化学形态更有密切关系。不同化学形态的铅，它的溶解性、移动性和生物效应都有很大的差异。本文用 ICP-MS 测定了隧道内外 PM_{10} 颗粒物中的 Pb 和 Cr、Mn、Zn、As 等元素含量。发现 2005 年 PM_{10} 颗粒物中铅的浓度(308.1±1.8 $\mu g \cdot g^{-1}$)，比 2000 年高 60 $\mu g \cdot g^{-1}$ 左右。可见，1997 年上海市停用含铅汽油后，交通来源颗粒物中铅的含量明显降低，汽车尾气产生的含铅颗粒物对上海市含铅颗粒物的贡献减少。但隧道外颗粒物中的铅浓度比隧道内高 600 $\mu g \cdot g^{-1}$ 左右，这可能是受上海市燃煤和冶金业排放烟尘的影响。

上海市大气颗粒物中铅主要形态为 $PbCl_2$、$PbSO_4$ 和 PbO。考虑到汽车尾气中含氮氧化物可能在一定条件下形成含氮的铅化合物，因此选择 PbO、PbO_2、$PbSO_4$、 $Pb_3(PO_4)_2$、$PbCO_3$、$PbCl_2$、$Pb(NO_3)_2$、PbS 作为参考样品。比较参考样品与隧道颗粒物中 Pb 的 XANES 谱，表明交通来源颗粒物中不含有 PbO_2, 但参考样品的 Pb XANES 谱无一与颗粒物样品的 XANES 谱相近，故颗粒物中铅并非单一化合物，而是由几种化合物组成。基于 LC-XANES，对交通来源 PM_{10} 颗粒物进行拟合，结果显示：交通来源颗粒物中铅主要以 $PbSO_4$、$Pb_3(PO_4)_2$、$PbCO_3$ 形式存在。隧道内外颗粒物中各种铅组分的拟合结果见表 1。

Speciation of lead in PM_{10} from traffic sources by XANES

JIN Chan LI Yulan ZHANG Guilin TAN Mingguang LI Yan

Key words: Particulate matter, XANES, Speciation

PM_{10} samples were collected at three different sites of a tunnel in Shanghai, and the concentration and speciation of lead in PM_{10} samples were studied. The results of ICP-MS show that the lead concentration in PM_{10} particles collected outside the tunnel was 939.4±20.6 $\mu g \cdot g^{-1}$, in comparison to 308.1±1.8 $\mu g \cdot g^{-1}$ in PM_{10} particles collected at the middle of the tunnel. Combining the LC-XANES fitting, the results of XAFS spectroscopy show that the main species of lead in PM_{10} were $PbSO_4$, $Pb_3(PO_4)_2$ and $PbCO_3$. Percentages of the lead compounds are listed in Table 1.

Table 1 Percentage of lead species in PM_{10} particles collected from different parts of Dapulu tunnel in Shanghai. The results were obtained by LC-XANES fitting in 13.0~13.1 keV

Compounds	Middle	Entrance	Outside
$PbSO_4$	24.2±2.0	28.0±2.9	28.9±2.9
$Pb_3(PO_4)_2$	52.4±2.1	57.4±2.9	52.1±3.0
$PbCO_3$	23.3±2.9	14.5±4.1	19.0±4.2

用 XAFS 研究铅中毒后血红蛋白的结构

金 婵 李玉兰 李 燕

关键词 铅中毒，血红蛋白，近邻原子，EXAFS

铅中毒现今是一个全球性健康问题。低浓度的铅损伤神经系统的许多功能，但主要是影响儿童智力发育、损伤认知功能、神经行为和学习记忆功能。高浓度的铅中毒则引起贫血、食欲不振、腹绞痛，甚至导致死亡。

血液中的血红蛋白是输送氧和二氧化碳的载体。而铅中毒后，影响血红蛋白输氧的能力，并产生一系列并发症。血红蛋白的血红素分子中，铁原子周围有 6 个配位键。4 个与吡咯环中的氮相连，第 5 个与珠蛋白的组氨酸残基中的氮连接，第 6 个与氧连接。血红蛋白有载氧(HbO_2)和脱氧(Hb)的两种形式。血红蛋白与氧结合后变得更为紧密，空腔变小。

本文主要研究铅中毒后，对血红蛋白中铁近邻原子结构是否有一定的影响。从而可以在微观角度为铅中毒对血液系统的影响的机理研究提供新的信息，开辟新的途径。

实验结果显示：对照组和铅中毒大鼠的血红蛋白中同时存在载氧血红蛋白(HbO_2)和脱氧血红蛋白(Hb)两种形式，但主要以载氧血红蛋白为主。同时，血红蛋白中铁原子的配位数没有发生变化。铅染毒以后，血红蛋白中 Fe-O 之间的距离变大，铁和 4 个吡咯环中的氮之间的距离也变大，但是同珠蛋白的组氨酸残基中氮的距离基本没有发生变化。这一系列的改变导致铁输送氧的能力降低，从而引起贫血。

Structure function of iron in haemoglobin of lead-exposed rats

JIN Chan LI Yulan LI Yan

Key words: Lead toxicity, Hemoglobin, Local atomic structures, EXAFS

Hemoglobin was the carrier of the oxygen in the blood circulation. With lead toxicity, it will cause the decrease of the oxygen transmission function. In this work, the local atomic structures of iron in hemoglobin were determined by EXAFS techniques. The relationship between lead toxicity and hemoglobin structures was observed.

Table 1 Local atomic structure around Fe in hemoglobin in rats of lead exposure. The coordination number (*N*) of Fe-O, Fe-N_p and Fe-N_ε was 1.0, 4.0 and 1.0, respectively

Sample	Bonds	*N*	Distance /Å	Debye-Waller factor δ^2 /Å	E_o
Blank	Fe-O	1.0	1.87±0.02	0.0101	7119.5
	Fe-N_p	4.0	1.96±0.01	0.0012	
	Fe-N_ε	1.0	2.05±0.01	0.0021	
0.1% $Pb(AC)_2$	Fe-O	1.0	1.93±0.01	0.0061	7119.2
	Fe-N_p	4.0	1.98±0.02	0.0012	
	Fe-N_ε	1.0	2.06±0.01	0.0012	
0.5%$Pb(AC)_2$	Fe-O	1.0	1.93±0.02	0.0011	7119.4
	Fe-N_p	4.0	2.01±0.02	0.0003	
	Fe-N_ε	1.0	2.04±0.02	0.0001	

用单颗粒分析法查证上海市市中心区大气含铅颗粒的来源

李晓林　岳伟生　万天敏　李 燕　张桂林

关键词　单颗粒分析，铅，上海市

铅污染是人类活动产生的一种重金属污染。医学研究发现铅即使在痕量水平也会影响儿童的发育和智力。上海是我国最大的工业和商业城市之一，大气中高水平的铅浓度成为上海市的一个严重的环境问题。在本次研究中，采用扫描质子微探针分析了上海市大气单颗粒物。将大气单颗粒物的 Micro-PIXE 能谱作为指纹谱，结合模式识别技术，查证含铅颗粒物的来源。研究表明，机动车尾气、燃煤烟尘和土壤尘是上海市大气含铅颗粒物的主要来源。

Analyzing individual aerosol particles for source identification of lead-containing particles collected from center of Shanghai

LI Xiaolin　YUE Weisheng　WAN Tianmin　LI Yan　ZHANG Guilin

Key words:　Analysis of individual aerosol particles, Lead, Shanghai City

Lead pollution is a heavy metal contamination produced by mankind. Medical researches showed that lead, even in trace levels, can affect children growth and intelligence. Shanghai is one of the biggest industrial and commercial cities in China. High levels of lead concentration in the local ambient air turned to be a crucial environmental problem. In this work, single aerosol particles in the ambient air of the center of Shanghai were analyzed by scanning proton microprobe to obtain characteristic X-ray spectra (micro-PIXE) of these particles. The micro-PIXE spectra were considered to be the fingerprints of these aerosol particles. The origin of the lead-containing particles was identified by the combination of the micro-PIXE spectra with pattern recognition technique. The results of this investigation show that the most of lead-containing particles in the ambient air of the center of Shanghai were derived from vehicle exhaust, coal combustion and soil dust.

铅染毒大鼠骨中元素微区分布及相关性研究

李晓林　岳伟生　刘江峰　万天敏　李 燕　张桂林
颜崇淮[1]　张忠德[1]　黄宇营[2]　何 伟[2]

关键词　钙，铅，同步辐射 X 射线探针

铅对人体健康产生多方面不利影响。铅通过肠道和呼吸道被吸收入人体后，随血液分布到全身各器官和组织。骨骼为铅在体内的储存池，容纳体内总铅量的 95%以上。骨铅又是内源性铅的污染源，铅对机体长期毒性作用在体内的蓄积，并会导致体内多种微量元素的重新分布。因此，研究铅染毒骨中元素分布及相关性，对于铅的毒理有重要意义。我们应用北京同步辐射装置上的同步辐射 X 射线探针测定铅染毒大鼠骨中铅和其它元素的微区分布，结果发现：铅主要分布在密质骨内、外边缘，而锌主要分布在密质骨和密质骨边缘。同时也获知了钙、磷、锶和铁的分布。

Micro-XRF analysis on element distribution and correlation in bone of lead-exposed rats

LI Xiaolin YUE Weisheng LIU Jiangfeng WAN Tianmin LI Yan
ZHANG Guilin YAN Chonghuai[1] ZHANG Zhongde[1]
HUANG Yuying[2] HE Wei[2]

Key words: Ca, Pb, Synchrotron radiation-induced micro X-ray fluorescence analysis

Lead is a toxic heavy-metal element, which is harmful for human health. In this study, synchrotron radiation-induced micro X-ray fluorescence analysis (μ-XRF) at Beijing Synchrotron Radiation Facility was used to determine the distribution of Pb and other elements in slices of bone of rat exposed to Pb. It was found that Pb was mostly located at the border of the compact bone and that Zn was mostly located at compact bone and the border of the compact bone. Additionally, Ca, P, Sr and Fe distributions were simultaneously recorded.

[1]上海第二医科大学附属新华医院; [2]中国科学院高能物理研究所

同步辐射微束 X 射线荧光法研究单个大气 $PM_{2.5}$ 颗粒物的源特征

李晓林 岳伟生 刘江峰 万天敏 张桂林 李 燕 黄宇营* 何 伟* 华 魏*

关键词 同步辐射微分析，模式识别，$PM_{2.5}$

$PM_{2.5}$ 是指空气动力学直径小于或等于 2.5 μm 的大气颗粒物，其表面吸附大量的有毒有害物质。由于 $PM_{2.5}$ 可深入到人体的支气管和肺泡，甚至通过循环系统到达其它器官，因此 $PM_{2.5}$ 可造成人体呼吸系统、免疫系统和心血管系统的广泛损伤。上海市 $PM_{2.5}$ 的调查表明，上海市年均 $PM_{2.5}$ 浓度值为 65.2 $\mu g \cdot m^{-3}$，与美国的标准值 15 $\mu g \cdot m^{-3}$ 相比，超标是相当严重的。因此，为了治理上海市大气 $PM_{2.5}$ 的污染，需要研究上海市大气 $PM_{2.5}$ 的污染源特征。将高灵敏度的同步辐射微束 X 射线荧光光谱分析方法与计算机模式识别技术相结合，用于上海市大气 $PM_{2.5}$ 单颗粒物的源识别。分析了污染排放源的 $PM_{2.5}$ 单颗粒物，结果表明，来自不同污染排放源的颗粒物具有不同的能谱特征。同时分析了环境空气监测样品 $PM_{2.5}$ 单颗粒物，结果表明，在上海市中心区大气 $PM_{2.5}$ 的污染源主要以机动车尾气为主，而吴淞工业区大气 $PM_{2.5}$ 的污染源主要为钢铁工业尘和燃煤烟尘。

Micro-XRF analysis of individual $PM_{2.5}$ airborne particles for their source identification

LI Xiaolin YUE Weisheng LIU Jiangfeng WAN Tianmin ZHANG Guilin
LI Yan HUANG Yuying* HE Wei* HUA Wei*

Key words: Synchrotron radiation X-ray emission, Pattern recognition, $PM_{2.5}$

$PM_{2.5}$ is particulate matter with aerodynamic diameter equal to or less than 2.5 μm. The recent investigation has shown that the annual average of $PM_{2.5}$ was 65.2 $\mu g \cdot m^{-3}$ in Shanghai, which was about

4.3 times higher than the annual US air quality standard (15 μg·m^{-3}). For cutting down $PM_{2.5}$ air pollution in Shanghai air, investigation of the origin of $PM_{2.5}$ is very important. In this work, synchrotron radiation micro-beam X-ray fluorescence (micro-SXRF) combining with pattern recognition technique was applied to identify sources of individual $PM_{2.5}$ airborne particles in ambient air of Shanghai. The $PM_{2.5}$ airborne particles of different emission sources in Shanghai were determined. The results show that each emission source has its characteristic micro-SXRF spectrum. Meanwhile, the $PM_{2.5}$ airborne particles of environmental monitor samples were determined. It was found that the major emission sources of the $PM_{2.5}$ airborne particles were vehicle exhaust in the center of Shanghai, and metallurgic industry and coal combustion in Wusong Industry District.

* 中国科学院高能物理研究所

HPLC-ICP-MS 联用测定 DNA 分子中四种脱氧核苷酸

梁 峰 李玉兰 陆文伟 谈明光 张桂林 李 燕

关键词 脱氧核苷酸 碰撞 / 反应池 液质联用 磷检测

磷在生命体细胞的信号传导、蛋白磷酸化、能量代谢等生命过程中起着重要的作用，磷构成 DNA 和 RNA 的基本磷酸骨架，DNA 的基本单位脱氧核苷酸就由磷酸和核苷组成，包括脱氧腺苷酸(dAMP)、脱氧鸟苷酸(dGMP)、脱氧胞苷酸(dCMP)和脱氧胸苷酸(dTMP)。为检测 DNA 样品中四种脱氧核苷酸的含量，我们用 HPLC 分离四种脱氧核苷酸后用 ICP-MS 结合 CCT 技术加入 O_2 形成 $^{31}P^{16}O^{+}$检测分离得到的脱氧核苷酸，测定质粒 DNA 经酶解后的产物。20 μg DNA 加热 94°C, 30min 后保持在 37°C，以 20 U/μg 的比例加入 Nuclease S1，将该反应体系置于 37°C 下 14 h。4°C 10000 r/min 超速离心 25 min，滤去 Nuclease S1，取滤液 20 μL 进样测定。

用反相离子对色谱和 ICP-MS 联用同时测定 DNA 分子中四种脱氧核苷酸的含量。液相流动相最佳条件是：pH4.8，2.5%甲醇，10 mmol/L NH_4Ac。为避免测定 ^{31}P 时 $^{14}N\,^{16}O^{1}H^{+}$、$^{15}N\,^{16}O^{+}$等复合离子的干扰，利用碰撞/反应池技术(CCT)加入 O_2 和 ^{31}P 生成 $^{31}P^{16}O$ 复合离子后测定，以提高磷测定的信噪比。四种脱氧核苷酸的检测限和经核酸酶酶解的质粒 DNA 后生成的四种脱氧核苷酸的含量的测定结果列于表 1。

Analysis deoxynucleotide of plasmid DNA by high performance liquid chromatography online with inductively coupled plasma collision cell mass spectrometry

LIANG Feng LI Yulan LU Wenwei TAN Mingguang ZHANG Guilin LI Yan

Key words: Deoxynucleotides, Hexapole collision cell, HPLC-ICP-MS, Phosphorus detection

An ion pair RP-HPLC coupled with hexapole ICP-MS method has been developed for determining deoxynucleotides in plasmid DNA. Optimum separations of four deoxynucleotides (dCMP, dTMP, dGMP and dAMP) are achieved by appropriately adjusting methanol (2.5%) and ammonium acetate (10 mmol/L, pH4.8). The hexapole collision cell technique (CCT) added with O_2 is used for eliminating

polyatomic interferences and allowing P detection as $^{31}P^{16}O^{+}$. The method reduces the effect of polyatomic isobaric interferences at m/z=31 by directly detecting $^{31}P^{+}$. Using HPLC-MS, the detection limits of the four deoxynucleotides and their analysis results in plasmid DNA are listed in Table 1.

Table 1 Detection limits of deoxynucleotides and their contents detected in plasmid DNA

Species of deoxynucleotide	Detection limits / nmol·L^{-1}	Deoxynucleotide contents detected/ μmol·L^{-1}
dCMP	211.1	152.9±2.4
dTMP	204.1	228.2±4.0
dGMP	172.7	125.3±3.0
dAMP	225.1	222.9±3.3

气管灌注 ^{59}Fe 标记的超细颗粒物在大鼠体内的分布

梁 峰 谈明光 李 超 赵金镯 林 俊 刘卫 金 婵
宋伟民 范 我 张桂林 李燕

关键词 高血压，纳米颗粒物，放射性同位素示踪

本文用放射性同位素 ^{59}Fe 合成纳米级 Fe_3O_4 颗粒，并用葡聚糖包被，以研究不可溶大气颗粒物中超细颗粒分析对高血压动物模型的毒理作用。

实验使用 24 只雄性自发性高血压模型 SHR 大鼠(180±20 g)，24 只 SHR 大鼠的同系鼠 雄性 Wistar 大鼠作为对照组(180±20 g)，均购于上海斯莱克实验动物有限责任公司。将实验组和对照组大鼠各随机分成 6 组，每组 4 只，气管灌注磁性氧化铁悬液，其中一组在灌注后 6 h、12 h、24 h、32 h、48 h 收集代谢物（粪便和尿液），最后处死。Wistar 大鼠同 SHR 大鼠分类进行实验，气管灌注 200μL 8mg/mL 的 Fe_3O_4 悬液，各组实验大鼠在灌注后 10 min、30 min、1 h、12 h、24 h 和 48 h 处死取血、心、肝、脾、肺、肾、脑等主要脏器，立即称重并进行放射性测量。

研究超细颗粒物 Fe_3O_4 模拟不溶性大气超细颗粒物对高血压模型大鼠的作用，是测定不同时间点血液及其他器官的放射性分布，以了解超细颗粒物在肺部的清除规律和进入体内的代谢途径。实验发现，无论是高血压动物还是正常动物，超细颗粒物能通过肺部进入血液,然后进入肝脏参与体内代谢,最后由肠道排出体外。高血压实验组超细颗粒物通过肺部进入血液明显快于对照组,但高血压组对超细颗粒物的排泄明显要慢于对照组。上述结果表明：由于不溶性超细颗粒物更易通过肺部进入体内又比较难于排除出体外的原因，超细颗粒物对患有心血管疾病(如高血压)的病人比正常人群有着更大的危害，患有心血管疾病的人群可能是大气颗粒物污染的易感人群。

Distribution of ultrafine particles labeled ^{59}Fe in rats

LIANG Feng TAN Mingguang LI Chao ZHAO Jinzhou LIN Jun LIU Wei
JIN Chan SONG Weimin FAN Wo ZHANG Guilin LI Yan

Key words: Hypertension, Nanometer-particles, Radioisotope tracer techniques

In order to investigate the adverse impact of hypertension SHR rats caused by simulated particle matter (nano ferric oxide), radioisotope tracer techniques were employed. By measuring the radioactivity in different tissues at different time points, we got the regular pattern of scavenging particles from

lung and the metabolism of the particles in rats. The ultrafine particles can transport from lung to blood, then participated in metabolism and excreted through feces in both hypertension rats and normal ones. The speed of unltrafine particles transporting to blood is faster than the normal ones and the excretion through feces in hypertension animals is slower than normal ones. In conclusion, the ultrafine particles are more harmful to hypertension patients because the particles can easily transport from lung to blood and be hardly scavenged from body through feces, so the hypertension patients may be the sensitive group by ultrafine particle in the atmosphere.

煤燃烧过程中硫的富集情况及铁的种态变化研究

林 俊 包良满 刘 卫 张桂林 李 燕

关键词 PIXE，穆斯堡尔谱学，硫含量，铁含量，煤

生活燃煤是影响城市大气二氧化硫浓度的重要因素，而大气中铁的种态对硫的形态变化有非常重要的作用，故研究煤燃过程中这两种元素的迁移与种态变化。用 PIXE 和穆斯堡尔谱测量了一个生活区锅炉所使用的原料煤、煤底灰和煤飞灰中硫和铁的含量和化学种态。三个样品的 PIXE 分析表明，原料煤、底灰和飞灰中硫含量分别为 0.4%，0.1%和 1.5%，硫含量在飞灰中有富集的趋势。这与 Esenlik 等对土耳其一个电厂用煤的研究结果相似，在他们的研究中发现煤飞灰比底灰有更高的富集效率。PIXE 分析未发现它们的铁含量有明显变化，但由穆斯堡尔谱可发现飞灰中的含铁量比底灰高得多。原料煤、底灰和飞灰中铁的种态有很大差别。原料煤中的含铁矿物主要是黄铁矿、伊利石和白云石。底灰和飞灰虽然都经过高温氧化过程，但铁的种态却表现出较大差异。在底灰中只有少量氧化铁和硫酸铁，而铁在飞灰中主要是氧化铁和其它一些三价铁化合物。

Enrichment of sulfur and species variation of iron in the process of coal combustion

LIN Jun BAO Liangman LIU Wei ZHANG Guilin LI Yan

Key words: PIXE, Mössbauer spectroscopy, Sulphur, Iron, Coal

Coal combustion is an important factor of SO_2 release, and iron in the air influences the sulphur species variation greatly. It is crucial to know the transference and species variation of sulfur and iron in different stages of the coal combustion. PIXE and Mössbauer spectroscopy were used to study the S and Fe species in FC (feed coal), BA (bottom ash) and FA (fly ash), which were sampled from a stove in the residential area. The PIXE spectra indicate that sulfur is enriched in the FA more than BA, with the concentration of 0.4%, 0.1% and 1.5% for FC, BA and FA, respectively. The result is well in agreement with the study of coal combustion of a power plant in Turkey. Though it is difficult to compare the concentrations of iron by PIXE spectra, distinct changes can be found from Mössbauer spectra. The iron in FA has more concentration and more abundant species than that in BA. The primary iron-bearing minerals in FC are pyrite, illite and dolomite. Both BA and FA are produced through high temperature process; however, there are many differences between them. In the BA, only ferric sulfate and little iron oxide are found. But in the FC, the main component is iron oxide with other trivalent iron compositions.

下庄地区仙人嶂铀矿围岩蚀变的穆斯堡尔谱和 XRD 研究

林 俊 杨亚新[1] 夏元复[2]

关键词 穆斯堡尔谱，XRD，沥青铀矿

UO_{2+x} 是微晶/隐晶沥青铀矿主要的 U^{4+}矿种，也是热液成因铀矿的主要矿物。研究表明，从矿脉中心向外根据蚀变强度可分为多个矿物区域。当主要以 U^{6+}形式存在的成矿流体发生迁移时，硫、硫化氢和亚铁矿物等还原矿物和气体在沥青铀矿的沉积过程中是重要的还原剂。因此含 U^{6+}的热液和富含亚铁的基性岩石发生氧化－还原的地带往往易出现沥青铀矿沉积。

六个样品取自位于广东省下庄铀矿仙人嶂铀矿田 338 矿床的硅化破碎带的不同区域。样品由矿脉向外依次编号为 1 至 6，经粉碎、研磨后用于穆斯堡尔谱和 XRD 测量。用等加速穆斯堡尔谱仪测量透射穆斯堡尔谱，放射源为 0.93 GBq 的 ^{57}Co/Pd，分析软件为 MossWinn 3.0i，同质异能移相对于室温 α-Fe 的谱中心。XRD 在 D/Max-Ra X 射线衍射仪上进行(Cu K_α)。实验结果表明，从矿脉至外围基性岩可明显分为沥青铀矿矿脉、绿泥石化蚀变带和弱蚀变基岩；随着与矿脉中心距离的增加蚀变程度逐渐减弱，经历了黄铁矿化向绿泥石化以及弱蚀变的变化过程。

Mössbauer and XRD studies on wall rock alteration at a uranium deposit in southern China

LIN Jun YANG Yaxin[1] XIA Yuanfu[2]

Key words: Mössbauer spectroscopy, XRD, Pitchblende

In pitchblende, a micro/cryptocrystalline uraninite, UO_{2+x} is a common U^{4+} mineral species, and is the main ore mineral in the hydrothermal U deposits. Studies show that the mineral stages and changes outwards from the center of the lode, and that sulfur/H_2S and the ferrous minerals may play an important role as a reducer in the deposition of pitchblende from uraniferous solution where the uranium migrates mainly in the form of various U^{6+} compounds. And the pitchblende deposition is considered to be a reduction – oxidation process between U^{6+}-bearing solution and the rock as diabase is enriched in ferrous minerals.

Six samples were collected from different zones at Xianrenzhang uranium deposit No. 338 that occurs at the intersection of silicified fracture zone with diabase dyke within Xiazhuang granitic massif, Guangdong Province, China. The samples, i.e. No.1 to No.6 from center of the lode to the diabase, were crushed and milled for Mössbauer and X-ray diffraction (XRD) measurement.

Mossbauer spectra were measured with a 0.93 GBq ^{57}Co/Pd source driven by a constantly accelerated driver in transmission geometry. The isomer shift was relative to the α-Fe at room temperature. The Mössbauer spectra were fitted by MossWinn3.0i. XRD patterns were recorded on D/Max-Ra X-ray diffractometer using Cu K_α. From the analyses, three zones could be identified from the lode to the diabase: the pitchblende lode, the altered zone and the weakly altered diabase. The experimental results indicate that the alteration decreases according to the increase of distance to the center of the lode, from pyritization to chloritization gradually.

[1] 东华理工学院探测与信息技术系; [2] 南京大学物理系

生物标准参考物质的定值分析

谈明光　李玉兰　陈建敏

关键词　标准参考物质，微量元素，ICP-MS

标准物质是一种计量器具，它能复现、保存和传递量值，在各领域的分析工作中起着重要作用。标准物质的定值分析是对标准物质特性参量的赋值过程，因此应严格要求使用可靠准确的分析方法、选择有可靠的质量保证体系的实验室、参加定值的工作人员对测量方法和样品处理等应有仔细的研究和一定的经验。

近年来，我们 ICP-MS 实验室连续参加了大米粉、小麦粉、圆白菜、人参、茶叶、奶粉、鸡肉、柑橘叶、花粉、螺旋藻、扇贝和蒜粉等 22 种生物标准物质的定值分析，使用 ICP-MS 分析技术为每个侯选标样提供了 36-42 种元素的定值结果，其中包括了 K、Na、Ca、Mg 和 Fe 等高含量的元素，也有大量的如 U、Th、Hg、Sc、Cd 和稀土元素等微量和痕量元素，定值的精度和准确性在各实验室和各种分析方法间属于优良。参加这些定值工作也促进了 ICP-MS 实验室建立分析质量保障体系，有利于今后的科研工作。

Certification analysis of biological reference materials by using ICP-MS

TAN Mingguang　LI Yulan　CHEN Jianmin

Key words:　Standard reference material, Trace elements, ICP-MS

In recent years, certification analysis on 22 candidate biological reference materials, including rice, wheat, cabbage, ginseng, tea leaves, powdered milk, chicken meat, orange leaves, pollen, alga, scallop, garlic powder, etc., has been carried out by using the ICP-MS technique. Concentrations of 36-42 elements were obtained for those materials. All the data we reported were accepted and put into the final statistic calculation processes. The elemental concentration results with good precision and accuracies demonstrated the virtual value of an analytical assurance system developed in the ICP-MS laboratory.

上海市大气颗粒物中铅污染的特征

谈明光　李玉兰　陈建敏　陆文忠　张桂林　李 燕

关键词　大气颗粒物，Pb 同位素比，Pb

汽油中曾因添加四乙基铅而造成环境铅污染和健康问题。我们已用单颗粒分析、铅同位素比、PIXE 和 ICP-MS 等技术，研究了上海市的铅污染特征，发现 1997 年停用加铅汽油后大气中仍存在较高浓度的铅污染，主要来源是燃煤、冶金和扬尘等。本工作继续这一研究，选择四个典型地区采集 2004 年 4 月至 2005 年 4 月的 PM_{10} 和 $PM_{2.5}$ 样品，用 ICP-MS 分析其 Pb 与其他元素的含量和 Pb 同位素比值，得到如下结果：

1) PM_{10} 和 $PM_{2.5}$ 含量的平均值分别为 86 ± 36 μg/m^3 和 61 ±30 μg/m^3。PM_{10} 的年均值与上海市年度环境状况数据(2004 年：99 μg/m^3；2005 年：88 μg/m^3)非常接近，说明采样点有良好代表性。目前全市的空气质量基本达到国家二级标准。PM_{10} 月均最高值(119± 41 μg/m^3，2005 年 4 月)与最低值(46 ±26 μg/m^3，2004 年 11 月)相差 2.6 倍。$PM_{2.5}$ 月均最高值(111±36 μg/m^3， 2005 年 4 月) 与最低值(32±12 μg/m^3，2004 年 11 月)相差 3.5 倍。近年来上海市空气的污染水平正在缓慢下降，但与国际水平还有较大差距，且全年仍有 5 个月的平均浓度超过了 PM_{10} 国家标准。我国尚未制定 $PM_{2.5}$ 的国家标准，但各采样点 $PM_{2.5}$ 的年平均值超过美国环保署的年均值 15 μg/m^3 标准的 2.7–5.6 倍，因此应加强对细颗粒物的排放控制和治理污染。

2) PM_{10} 中 Pb 的年平均值为 167±104 ng/m^3，冬季的 Pb 的平均浓度达到 205±78 ng/m^3，略低于 2003 年冬季的 237 ng/m^3，故 Pb 污染下降变化并不大。$PM_{2.5}$ 中 Pb 的年平均值为 108±100ng/m^3。与国内外大城市相比，上海市 PM_{10} 和 $PM_{2.5}$ 中的 Pb 仍处在较高水平。富集因子在 PM_{10} 中为 166，在 $PM_{2.5}$ 中为 180，都处于较高的污染状态，且 Pb 在细颗粒中呈明显富集。

3) $PM_{2.5}/PM_{10}$ 值为 0.73(0.60–0.89)，高于 2002 年的 0.60，也高于北京市同时期的 0.52–0.63，特别在位于吴淞工业区的采样点达 0.81，在交通密集的普陀区达 0.89，说明上海市的大气中细颗粒物的比重在继续增大，而且明显提示它是工业排放和汽车尾气污染所致。

4) $PM_{2.5}$ 中 $^{208}Pb/^{206}Pb$ 的平均值为 2.113±0.009，$^{207}Pb/^{206}Pb$ 为 0.863±0.003，数据非常集中，说明其污染来源较为一致。该数据与上海市所用燃煤的数据较接近(2.121±0.018 和 0.860± 0.010)，而与无铅汽油尾气及铁矿石相差稍大。上海市的燃煤年耗量巨大，应是大气中铅污染的最大来源。但设在吴淞工业区的采样点有 4 个数据较低，明显受到了当地排放的冶金尘的影响。

Characteristics of air lead pollution in Shanghai

TAN Mingguang LI Yulan CHEN Jianmin LU Wenzhong

ZHANG Guilin LI Yan

Key words: Air particulate matters, Lead isotope ratio, Pb

The object of this study was to keep on characterizing the variation trends of mass concentration and chemical composition of air particulates in Shanghai. PM_{10} and $PM_{2.5}$ samples were collected at four typical sites, representing industrial area, heavy traffic road, commercial center and rural area respectively. The sampling was performed concurrently for about 24 h once a month from April 2004 to April 2005. Concentrations of lead and other toxic elements were analyzed by ICP-MS. The annual average concentrations of PM_{10} and $PM_{2.5}$ during this sampling period were 86±36 and 61±30 μg·m^{-3}, respectively. The ratio of $PM_{2.5}/PM_{10}$ increased from 0.60 of 2002 to 0.73 of 2005, suggesting the increasing load proportion of fine particulates in Shanghai. The annual average concentrations of Pb in PM_{10} and $PM_{2.5}$ were 167±104 ng·m^{-3} and 108±100 ng·m^{-3}, respectively. The values were much higher than the data of other cities in the world, indicating the stringent air lead pollution load in Shanghai. The analysis on stable lead isotope ratios revealed that the coal composition and metallurgy dust might be the major air pollution sources of Pb in Shanghai.

植入贫铀后的大鼠体内铀的分布

谈明光 李玉兰 陈建敏 朱国英*

关键词 贫铀，靶器官，ICP-MS

固体贫铀既有辐射毒性，又有化学毒性，摄入体内会造成严重的内损伤。本工作研究经贫铀弹片损伤后铀在体内组织器官中的迁延、蓄积及所产生的潜在的健康危害。建立了经大鼠绯肠肌植入不同剂量贫铀片以导致长期体内 U 污染的动物模型，进行了高、中、低剂量组和钽对照组的植入实验，植入后 1，7，30，90，180 和 360 天采集各组的尿和血清样品，和胫骨、颅骨、肾、心、肌肉、肝、脾和脑等组织样品，用 ICP-MS 测定样品中的铀含量和铀同位素比值。结果表明，贫铀片植入 1d 后尿中铀浓度就增加。$^{235}U/^{238}U$ 的测定证实贫铀很快到达远离植入部位的各组织中。在植入初期，组织中铀浓度随植入时间而增加，90d 时达最大值，尔后缓慢下降。各时间点的不同剂量植铀组的组织中铀浓度与对照组相比都有非常明显的差异，而肾、肝和骨是贫铀在体内的主要蓄积器官。本工作对进一步研究贫铀的内污染所致损伤效应的生物学特性和病理机制、对预防贫铀所引起的远期危害有一定意义。

Bioaccumulation behaviours of embedded depleted uranium pellets in rats

TAN Mingguang LI Yulan CHEN Jianmin ZHU Guoying*

Key words: Depleted uranium, Target organ, ICP-MS

Internalised depleted uranium (DU) has been claimed to contribute to health problems due to its both chemo- and radio-toxic properties. In this study，the distribution and bioaccumulation behaviours were evaluated in adult SD rats implanted with 0, 1, 2 or 3 DU pellets of 2mm×2mm per rat, a group of SD rats with implantation of Ta pellets were used as the controls. The implanted animals were housed under standard laboratory conditions. At 1, 7, 30, 90, 180 and 360 days post implantation, tissue samples of kidney, heart, liver, tibia, skull bone, spleen, brain, serum and urine were collected. The tissue samples were mineralized and analyzed for uranium and other element contents by ICP-MS. The results showed that even at one day after implantation, significant increase of U concentrations could be observed in the samples. Moreover, significant decreasing of $^{235}U/^{238}U$ demonstrated a rapid distribution of DU in rat's bodies. For the DU groups, the U concentrations increased with the time, reached the maximum levels at 90d after the implantation, and then slowly decreased down. Results showed that at all time points, uranium concentrations in each group of implanted rats were significantly higher than those of control group. The highest uranium levels were found in liver, kidney and bone samples, indicating that the liver, kidney and bone were the main target organs of the embedded DU.

*复旦大学放射医学研究所

ACCU 采样 PM_{10} 和解析法定位吴淞地区的污染源

杨传俊 张元勋 谈明光 李玉兰 陆文忠 张桂林 李 燕

关键词 PM_{10}，ACCU，PIXE，化学质量平衡模式(CMB)，主成分法分析(PCA)，上海

用美国 RP 公司的自动多通道采样系统(ACCU)在吴淞地区的三个检测点进行方向性 PM_{10} 采样，用 PIXE 分析、化学质量平衡模式(CMB)和主成分法(PCA)进行污染源解析以确定该地区的污染源贡献。

结果表明，3 点 8 个风向的 PM_{10} 质量浓度分布与采样点周围的排放状况密切相关。企业多、车流大的该地区北部和中部的 PM_{10} 颗粒物浓度较高，东(长江口)西方向(农村)较低。PM_{10} 中的 S、Cr、Mn、Fe、Ni、Cu、Zn、As 和 Pb 的分布相似，在集中有老钢铁企业的该地区中部最高，其中，Cr 和 Ni 分布非常接近，显然与该处的不锈钢冶炼有关；Cl、K、Ca、Ti、Se、Sr 分布较接近，主要来自北部和中部，为化工和交通排放所致；在靠近道路的方向，Ca、Ti 、V 的浓度较高；Br 主要来自中西部，系仓储、化工厂影响。东北方向 Cl、K、Ca 偏高，是海洋源影响。

CMB 源解析表明，土壤、堆场、道路扬尘、汽车尾气、燃煤、炉灰和建筑水泥分别贡献约 20%、10%、20%、20%、15%、10%和 5%。未解析者约 10%，主要在东方向，因未收集足够的自然源。由 PCA 法，15 个元素质量浓度分析得到 3 个主成分。第一主成分贡献率 55.5%，K、Ca、Cr、Mn、Fe、Cu、Zn、As、Se、Rb、Sr、Pb 的载荷均较高，Ti、V 的载荷次之，系钢铁业排放；第二主成分贡献 18.8%， Ca、Ti、V、Sr 的载荷较高，为交通源的贡献；第三主成分贡献率 9.9%，Ca、Ti、V、Cr、Fe、Ni、Zn 的载荷较高，与特种钢冶炼相关。主成分的分析结果和 CMB 的源解析结果较一致。源解析结果还表明，该地区的主要污染源已扩散，须结合元素分布特征和更为细致的污染源成份库才能精确确定其方位。

通过结合 ACCU 的方向性采样，根据元素的方位分布特征，可以明确一些颗粒物的来源：五钢、一钢的高炉灰；不锈钢厂，钢丝厂有较大贡献的 Ni、Cr；仓储和化工 Br、Cl；还有靠近交通干道的机动车尾气和道路扬尘。

Source identification of PM_{10} by ACCU directional sampler

YANG Chuanjun ZHANG Yuanxun TAN Mingguang LI Yulan

LU Wenzhong ZHANG Guilin LI Yan

Key words: PM_{10}, ACCU, PIXE, CMB, PCA, Shanghai

There are many chemical and metallurgical industries in Wusong industrial zone of Shanghai. Three sets of ACCU systems were used to collect directional PM_{10} in the area. The samples were analyzed by proton induced X-ray emission (PIXE) to determine average concentration of 18 elements. Major pollution sources were identified by chemical mass balance (CMB) and principal component analysis (PCA). The results showed that the mass distribution of particulate matter in different directions depends on the environmental air quality. Spatial variation of elemental concentrations was closely related with residential density, traffic and industrial exhausts. It was demonstrated that the excellent combination of ACCU sampler, PIXE, CMB and PCA technique provide a fast and accurate means for environmental source detection.

用扩展 X 射线吸收精细结构谱研究大气颗粒物中铁的种态

王荫淞 李爱国 张元勋 谢亚宁* 李德禄 李 燕 张桂林

关键词 大气颗粒物，种态，铁，EXAFS，回归分析

通常把空气动力学粒径小于 10 μm 和 2.5 μm 的颗粒物分别表示为 PM_{10} 和 $PM_{2.5}$。这些颗粒物对人体的危害，不仅与元素的浓度有关，还与其化学种态，即元素的化学状态、化合物组成等密切相关。研究大气颗粒物中元素的种态，对其毒性评价、污染的形成和来源等能提供重要信息，是环境科学中的一个热点。

本工作采用基于同步辐射的扩展 X 射线吸收精细结构(EXAFS)谱研究大气颗粒物中铁的种态。对 EXAFS 谱进行回归分析，可计算混合物的化学组成，这是一种不破坏样品的定量方法。配制了一系列混合参考样品，用以观察化学组成对 EXAFS 谱的影响，并验证方法的精确性。采集了上海市不同地区不同粒径的大气颗粒物样品，将它们的 EXAFS 谱进行回归分析，得到了样品中铁的化学组成。结果表明，样品中铁主要由一定比例的三氧化二铁、四氧化三铁和硫酸铁组成, 初步观察到不同样品的化学组成的差别。用质子激发 X 射线分析法测定了样品的铁浓度。观察到钢铁工业区的大气颗粒物样品比其它地区的样品不仅铁浓度高得多，而且化学组成也有一定差别。

Speciation of iron in atmospheric particulate matter by EXAFS

WANG Yinsong LI Aiguo ZHANG Yuanxun XIE Yaning*

LI Delu LI Yan ZHANG Guilin

Key words: Atmospheric particulate matter, Speciation, Iron, EXAFS, Regression analysis

Study on the chemical speciation in atmospheric particulate matter (PM) is important for understanding the origin of pollution and evaluating their toxicity. In this paper we present the study of the speciation of iron in atmospheric PM. The study was taken up by extended X-ray absorption fine structure (EXAFS) spectra based on synchrotron radiation. As a non-destructive method, the chemical components of PM can be determined by EXAFS spectra without any influence from measurement. In order to observe the influence of chemical components on EXAFS spectra and check the method, we prepared a series of mixed reference samples. The PM samples with different particle sizes were collected from different sampling sites of Shanghai, China. The EXAFS spectra of iron for the samples were measured and the chemical components were calculated by regression analysis of EXAFS spectra. The results show that the iron in all PM samples mainly consists of Fe_2O_3, Fe_3O_4 and $Fe_2(SO_4)_3$, but their proportions are different for different samples. The differences of components in the samples were observed. The concentrations of iron in the samples were determined by proton induced X-ray emission (PIXE) technique. It is observed that the concentrations of iron in the samples from the iron and steel industrial district are much higher than those from other districts, and chemical components are also different from those of other districts.

*中国科学院高能物理研究所

用同步辐射成像研究大气颗粒 $PM_{2.5}$ 引起的小鼠肺急性损伤

张桂林 童永彭 谈明光 李 燕 陈建敏 胡宇光[1] 蔡文立[1] 许培诚[1] 吉钧洪[2]
Giorgio Margaritondo[3] 宋伟民[4] 蒋蓉芳[4] 蒋之海[4]

关键词 同步辐射成像，肺损伤，$FeSO_4$, $ZnSO_4$, $PM_{2.5}$

本文研究上海大气颗粒 $PM_{2.5}$ 的两个重要成份 $FeSO_4$ 与 $ZnSO_4$ 对肺的急性损伤。配制六种溶液，即 $PM_{2.5}$ 大气颗粒物、$FeSO_4$ 与 $ZnSO_4$ 溶液及它们的混合溶液，用气管灌注法注入小鼠肺中。灌注二天后，对活鼠进行同步辐射 X 射线界面折射增强成像。再解剖取出右肺，用福尔马林固定，作上述成像，其中一部分用石腊包埋作病理切片观察。同步辐射 X 射线活体鼠成像表明，不同溶液染毒造成肺组织的织构发生不同变化，含 $FeSO_4$ 的溶液可引起较多的出血点，$PM_{2.5}$+$FeSO_4$+$ZnSO_4$ 溶液造成的肺损伤最为严重。实验结果显示，在 $PM_{2.5}$ 中 $FeSO_4$ 主要引起肺出血，$ZnSO_4$ 主要引起肺炎和气管上皮细胞增生。

Acute lung injury of mouse caused by $PM_{2.5}$ aerosols studied by synchrotron radiation microradiography

ZHANG Guilin TONG Yongpeng TAN Mingguang LI Yan CHEN Jianmin
HWU Yeu-Kuang[1] TSAI Wen-Li[1] HSU Pei-Cheng[1] JE Jung Ho[2]
Giorgio Margaritondo[3] SONG Weimin[4] JIANG Rongfang[4] JIANG Zhihai[4]

Key words: Synchrotron radiation microradiography, Lung injury, $FeSO_4$, $ZnSO_4$, $PM_{2.5}$

Solutions of $PM_{2.5}$ aerosol particles, $FeSO_4$, $ZnSO_4$ or their mixtures were instilled into mouse lungs. Two days later, the mice were checked in vivo by synchrotron radiation refractive- index microradiography at Pohang Light Source. The right lobe of lungs were isolated and fixed by formalin for synchrotron radiation microradiography again. Corresponding parts of the lung tissues were embedded in paraffin for histopathologic study. The in vivo X-ray microradiographs showed different structured lungs of mice instilled differently. Hemorrhage points and texture changes in lung were observed for the mice instilled by toxin solutions. The synchrotron radiation X-ray microradiographs and the histopathological study of fixed tissues showed consistent results. Compared with the conventional X-ray radiography of mouse lung, the synchrotron radiation X-ray microradiography showed much high resolution. It was found that the acute lung injury of mice caused by solution of $PM_{2.5}$+$FeSO_4$+$ZnSO_4$ was more serious than other toxin solutions, and the composition of bio-available metals played a major role in the toxicity of aerosol particles. The synchrotron radiation refractive-index microradiography may be further developed to observe the pneumonia, lung cancer and other diseases at early stage in future.

[1]中国台北中央研究院物理研究所；[2]Pohang University of Science and Technology, Pohang Korea; [3]Ecole Polytechnique Fédérale de Lausanne (EPFL), CH-1015 Lausanne, Switzerland ; [4]复旦大学

人肝癌组织的同步辐射成像

童永彭 张桂林 李 燕 胡宇光[1] 蔡文立[1] 许培诚[1]
吉钧洪[2] 陈绍亮[3] Giorgio Margaritondo[4]

关键词 同步辐射，辐射成像，肝癌组织

用福马林固定从肝癌患者中取出的二块肝组织(5mm×40mm×20mm)，分别作同步辐射成像研究。从成像图可明显地在微米尺度上看到正常组织和癌组织的差别，可区分血管的精细结构、癌原发区和浸润区、以及纤维组织等。同步辐射成像的结果和病理切片的结果一致。另外，实验还观察了不同角度样品的成像。结果表明，同步辐射界面折射增强成像可能为将来肺癌的早期疹断提供一个好的手段。

Synchrotron radiography of human liver cancer tissue

TONG Yongpeng ZHANG Guilin LI Yan HWU Yeu-Kuang[1] TSAI Wen-Li[1]
HSU Pei-Cheng[1] JE Jung Ho[2] CHEN Shaoliang[3] Giorgio MARGARITONDO[4]

Key words: Synchrotron, X-ray microradiography, Liver cancer tissue

Two human liver tissue samples (5mm×40mm×20mm) fixed in formalin have been analyzed by synchrotron radiation X-ray microradiography. From the images, the cancer part and normal part of tissues can be identified in micrometer size, and the fine structure of blood vessel, cancer nest, cancer soaking area, and fiber tissues can also be clearly affirmed. The observation of tissue structures by synchrotron radiation X-ray microradiography is consistent with the corresponding histopathological observation by normal microscopy. Furthermore, the images of caner tissues at different angles were obtained by synchrotron radiation X-ray microradiography. The results suggest that synchrotron radiation X-ray microradiography could be a good method in the study of early diagnosis of cancer.

[1]中国台北中央研究院物理研究所；[2] Pohang University of Science and Technology, Pohang Korea; [3]复旦大学附属上海中山医院; [4]Ecole Polytechnique Fédérale de Lausanne (EPFL), CH-1015 Lausanne, Switzerland

裸鼠肺癌和肺炎的同步辐射相衬成像观察

张桂林 岳伟生 李 燕 刘 苹[1] 孙建奇[1] 徐学敏[1] 胡宇光[2] 吉钧洪[3]

关键词 同步辐射相衬成像，裸鼠，肺炎，肺癌

用大气颗粒物气管灌注造成裸鼠肺炎，用癌细胞注入造成肺癌。然后在韩国浦项和台湾新竹同步辐射装置上对裸鼠进行成像观察。成像采用了界面折射增强方式。研究了肺组织和活体裸鼠经不同剂量染毒和不同天数后的成像。研究发现，对未经染毒的正常组织，可以清晰地看到单个肺泡和气管，对炎症的组织可见出血点和肺泡壁增厚的现象。另外，不同地区采集的大气颗粒物造成炎症的程度有较大的差别，它们和颗粒物中的元素成份和化合物的组成有关。对癌肿瘤组织，成像显示肺泡破坏，呈无结构的图像。实验还能成功地显示在活体裸鼠中炎症和癌症组织的差别。

Pulmonary inflammation and lung cancer in mice studied by synchrotron radiation microradiography

ZHANG Guilin YUE Weisheng LI Yan LIU Ping[1] SUN Jianqi[1] XU Xuemin[1]
HWU Yeu-Kuang[2] JE Jung Ho[3]

Key words: Synchrotron radiation refractive-index microradiography, Nudes, Pulmonary inflammation, Lung cancer

The tissue of live nudes with lung cancer and pulmonary inflammation were investigated by the synchrotron radiation refractive-index microradiography in Pohang and Xinzhu, respectively. The images show individual alveolar cell and bronchi in the normal tissue, and hemorrhages and alveolus wall thickening in inflammatory tissue caused by atmospheric aerosol particle solution. In addition，it was found that the inflammation is much related to the compounds and elements in the aerosol particles. The lung cancer tumor contained in tissue shows the destroyed alveoli with no air. The pulmonary inflammation and lung cancer in nudes can be distinguished in vivo by the synchrotron radiation refractive-index microradiography.

[1]上海交通大学;[2]中国台北中央研究院物理研究所;[3] Pohang University of Science and Technology, Pohang Korea

上海市大气气溶胶中铅污染的综合研究

张桂林 谈明光 李晓林 张元勋 岳伟生 陈建敏
王荫淞 李爱国 李 燕 张元茂* 山祖慈*

关键词 铅污染，质子微探针, 扩展 X-射线吸收精细结构谱, 电感耦合等离子质谱

用质子激发 X 荧光分析(PIXE)、质子微探针、电感耦合等离子质谱(ICP-MS)和扩展 X-射线吸收精细结构谱(EXAFS)等分析手段研究了上海市大气气溶胶 PM_{10} 中铅的浓度、化学种态和铅的源解析。研究发现 2002 年冬天和 2003 年上海地区大气气溶胶 PM_{10} 中铅的平均浓度分别为 369ng/m^3 和 224ng/m^3，铅的化学种态主要是 $PbCl_2$、$PbSO_4$ 和 PbO，燃煤烟尘、钢铁烟尘和汽车尾气是主要排放源，它们对气溶胶中铅的贡献率分别为 50%、35%和 15%。这是首次提供了大城市铅污染排放源的定量贡献。同时由该研究结果，拟建议发电厂燃煤烟气脱铅后再排放。另外，我们发现在使用无铅汽油四、五年后大气中的有铅汽油颗粒才消失。

A comprehensive study of lead pollution in atmospheric aerosol of Shanghai

ZHANG Guilin TAN Mingguang LI Xiaolin ZHANG Yuanxun
YUE Weisheng CHEN Jianmin WANG Yinsong LI Aiguo LI Yan
ZHANG Yuanmao* SHAN Zuci*

Key words: Lead pollution, Proton microprobe (μ-PIXE), EXAFS, ICP-MS

The lead contamination, lead species and source apportionment were studied by a combination of several analytical techniques such as proton-induced X-ray emission analysis (PIXE), proton microprobe (μ-PIXE), inductively coupled plasma-mass spectrometry (ICP-MS) and extended X-ray absorption fine structure (EXAFS) techniques. The results indicate that the lead concentration in the air of Shanghai gradually decreased over the last years. The atmospheric lead concentration of PM_{10} in the winter of 2002 was 369ng·m^{-3}, which had declined by 28% as compared with in 2001, and in the winter of 2003 it decreased further to 237ng·m^{-3}. The main lead species in the samples collected in the winter of 2003 were probably $PbCl_2$, $PbSO_4$ and PbO. The source apportionment was calculated in terms of the combination of lead isotope ratios and lead mass balance method, assisted by single particle analysis with μ-PIXE and pattern recognition. The results suggested that the major contributors of atmospheric lead pollution in Shanghai were coal combustion dust, metallurgic dust and vehicle exhaust particles, with a contribution around 50%, 35% and 15%, respectively. It probably is the first time to give a city a quantitative estimation of lead pollution contribution from emission sources. We also observed that the influence of leaded gasoline was still present in the atmosphere by four or five years after the phasing out leaded gasoline.

*上海市环境监测中心

PIXE 技术研究上海冬季大气可吸入颗粒物特征

张元勋 王荫淞 杨传俊 陆文忠 李 燕 张桂林 张元茂* 山祖慈*

关键词 气溶胶，大气颗粒物，质子激发 X 荧光，富集因子, 污染特征

在 2001~2005 年的 12 月，采集了上海市 19 个代表性采样点的 $PM_{2.5}$ 和 PM_{10} 样品，用质子激发 X 荧光发射法(PIXE)进行多元素分析。结果发现，除了 Ti 和 P 等元素外，绝大多数元素的平均浓度是市区高于郊区。市区大气可吸入尘中 Cr、Mn、Fe、Cu、Zn、As 和 Pb 等金属元素的平均浓度是郊区的 1.3–1.8 倍，表明市区大气污染比郊区严重。不同采样点的 $PM_{2.5}/PM_{10}$ 范围为 0.32–0.85，平均值为 0.6。富集因子分析表明，上海大气可吸入颗粒物中的元素来源可分为地壳元素和人为污染元素两大类，污染元素在 $PM_{2.5}$ 和 PM_{10} 中有明显富集，大部分元素在 $PM_{2.5}$ 中的富集因子大于 PM_{10}，S、As、Pb、Ni、Mn、Se 等污染元素更趋于富集在直径小于 2.5μm 的细颗粒物中，对人体健康的危害更大。而近年来的环境整治努力见效，大气颗粒物浓度和元素污染物呈逐年下降趋势，市区下降的速度快于郊区。

Characteristics of atmospheric inhaled particulate matter in winter of Shanghai by PIXE

ZHANG Yuanxun WANG Yinsong YANG Chuanjun LU Wenzhong LI Yan
ZHANG Guilin ZHANG Yuanmao* SHAN Zuci*

Key words: Aerosol, Air particulate matter, PIXE, Enrichment factor, Pollution character

$PM_{2.5}$ and PM_{10} samples were collected in December of 2001~2005 at 19 representative sites in Shanghai to investigate chemical characteristics of aerosol particulate matter in winter. Multi- element analysis was performed with the sample using proton induced X-ray emission (PIXE). It was found that average concentrations of most elements (except for Ti and P) in the samples collected in the urban area were higher than those in the suburb area. The mean values of Cr, Mn, Fe, Cu, Zn, As and Pb in the urban samples were 1.3-1.8 times higher than in the suburb samples, indicating more serious air pollution in the urban than the suburb. The results of particulate mass concentration revealed that the $PM_{2.5}/PM_{10}$ ratio at different sampling sites ranged from 0.32 to 0.85 and averaged at 0.6. The result of enrichment factor analysis showed that sources of inhaled particulate matter might be divided into two categories, i.e. elements from earth crust and artificial pollution. The pollution elements had been enriched in $PM_{2.5}$ and PM_{10} obviously and for most elements the enrichment factors in $PM_{2.5}$ were higher than in PM_{10}. It is noticeable that the pollution elements of S, As, Pb, Ni, Mn and Se tended to enrich in fine particulate matter (< Φ2.5 μm), which is more harmful to the human health. However, rewarding effects of the city's environmental control efforts can be seen from the analytical results that the particulate mass concentrations and pollution element contents decreased annually, and the urban had faster paces of decreasing than the suburb.

*上海市环境监测中心

上海市吴淞工业区 PM_{10} 中 18 种元素的污染状况

张元勋　陆文忠　王荫淞　张桂林　李 燕　张元茂*　郑叶飞*　山祖慈*

关键词　吴淞工业区，气溶胶，大气颗粒物，元素浓度

选择吴淞工业区中心的钢铁研究所作为监测点，使用自动通道颗粒物采集仪进行为期 3 个月、8 个不同风向的 PM_{10} 采样。对样品进行了 PM_{10} 质量浓度分析，并使用质子激发 X 荧光法分析了 18 种元素浓度。结果表明，PM_{10} 和绝大部分无机元素有着一个低浓度和高浓度风向区域，低浓度变化趋势基本相同，高浓度变化范围差异较大，有 1 至 3 个风向对该测点 PM_{10} 和绝大部分无机元素浓度水平有着明显影响。8 个风向的质量浓度变化范围较大，它的分布取决于不同方位的大气质量状况。PM_{10} 的最高和最低质量浓度分别出现在西北－北和东－东南风向，最高浓度是最低浓度的 3.9 倍。将大气颗粒物中的元素浓度作为环境污染指纹，18 个元素最高与最低浓度之比的范围从 2.6 到 35.3，并且大部分无机元素的最高浓度出现在南－西南或西南－西风向，最低浓度出现在东北－东风向。各风向的无机元素浓度分布与采样点周围的居民住宅、道路交通和工矿企业的排放密切相关。

Status of 18 elements in PM_{10} of Wusong industrial area in Shanghai

ZHANG Yuanxun　LU Wenzhong　WANG Yinsong　ZHANG Guilin　LI Yan
ZHANG Yuanmao*　ZHENG Yefei*　SHAN Zuci*

Key words:　Wusong industrial district, Aerosol, Air particulate matter, Elemental concentration

PM_{10} samples from eight wind directions were collected with ACCU (Automatic Cartridge Collection Unit) method for 3 months on one monitoring site in Wusong industrial area of Shanghai. PM_{10} mass concentrations were measured and concentrations of 18 elements in the samples were determined by PIXE. The results indicated that two wind direction areas of both high and low concentrations were presented for PM_{10} and most inorganic elements. The tendency of low concentration variation was the same basically, and the change of high concentration was different greatly. There were 1 to 3 wind directions having an obvious effect on the PM_{10} and most inorganic elements. PM_{10} and the 18 elements showed a similar tendency of concentrations in relation to wind directions. The highest of PM_{10} mass concentration appeared in the NW-N wind, whereas the lowest was in E-SE wind, and the highest concentration is 3.9 times of the lowest. As the elemental fingerprint study of environmental pollution, the ratios of the highest to the lowest concentration for the 18 elements ranged from 2.6 to 35.3. Furthermore, the highest concentrations of most elements appeared in the S-SW or SW-W wind, and the lowest was in the NE-E wind. The spatial distribution of particulate matter in different directions depended on the residential denseness, the vehicle traffic, and the exhausts of refineries, chemicals and steel mills around the sampling site.

*上海市环境监测中心

上海大气纳米颗粒物粒径分布的研究

杨传俊　张元勋　陆文忠　杨永兴　张桂林　李 燕

关键词　大气纳米颗粒物，粒径分布，气溶胶

为了更深入地研究上海大气气溶胶微小颗粒物的物理和化学特性，本项工作采用 MSP 公司生产的 WPS^{TM} Model 1000XP 宽范围粒径谱仪，测量粒径介于 10~10000 nm 的气溶胶纳米颗粒物，探讨粒径在 10~500 nm 间的气溶胶纳米颗粒物随时间、高度和地区变化的时空分布特征。结果发现，大气纳米颗粒物的粒子数浓度和质量浓度的粒径分布符合对数正态分布，呈现单峰、双峰或者多峰分布模式。从时间分布上看，白天纳米颗粒物浓度高，到夜晚逐渐降低，再从第二天早晨逐渐上升，总质量浓度随时间的变化比总粒子数浓度的变化滞后。从高度分布上看，纳米颗粒物总粒子数浓度和质量浓度随高度增加呈指数衰减。纳米颗粒物总粒子数浓度和质量浓度在工业区和商业区较高，而在生活区和郊区较低，不同地区的粒子数浓度和质量浓度的平均粒径分布呈现正相关(r=0.865)。结果表明，超细颗粒对粒子数浓度贡献较大，而细颗粒对粒子质量浓度贡献较大。

Size distribution of aerosol nanoparticulate in Shanghai

YANG Chuanjun　ZHANG Yuanxun　LU Wenzhong　YANG Yongxing
ZHANG Guilin　LI Yan

Key words:　**N**anoparticulate, Size distribution, Aerosol

In order to research the physical and chemical characterization of aerosol nanoparticulate in Shanghai city, a wide range particle spectrometer (Model 1000XP WPS) produced by MSP Corporation

was used to measure the aerosol particulate size ranging from 10 to 10,000 nm in December of 2005. The results showed that the distribution of particulates in a size range of 10 to 500 nm was variable with time, height and district. The particulate sizes of both number concentration and mass concentration presented the logarithm normal distributions and unimodal, bimodal or multi peaks appeared. As to the distributions change with time, the concentration of nanoparticle was high in the daytime, and it reduced gradually until the night, then rose gradually since the next morning. It is also discovered that the change of mass concentration with time is later than that of number concentration. Both concentrations of particulate matter presented the exponential decay with the altitude increasing. Furthermore, they were higher in industrial area and shopping center but lower in living district and suburb. The average size distributions of particulate concentrations in different areas exhibited a positive correlation (r=0.865). The results indicated that the superfine matter (<100 nm) was mainly contributed to number concentration, while the fine matter (>100 nm) was mainly contributed to mass concentration.

室内气溶胶纳米颗粒物的粒径分布特征研究

张元勋　杨传俊　陆文忠　杨永兴　张桂林　李 燕

关键词　气溶胶，纳米颗粒物, 粒径分布，室内，空气质量

研究室内气溶胶纳米粒径颗粒物的环境行为和污染特征对于了解室内空气质量具有重要意义。采用 MSP 公司的 WPS^{TM} Model 1000XP 宽范围粒径谱仪测量粒径介于 10~10000 nm 的气溶胶纳米颗粒物，主要探讨粒径在 10~500 nm 间的气溶胶纳米颗粒物在不同室内条件下的粒径分布特征。结果发现，超细颗粒物（纳米粒径 10~500 nm）对总粒子数浓度贡献较大，而细颗粒物(500 nm~10 um)对总粒子质量浓度贡献较大，导致室内颗粒物粒子质量浓度通常比室外低，表现出室内污染以纳米粒径超细颗粒物为主的特点。抽烟明显增大纳米颗粒物粒子数浓度和粒子质量浓度。研究表明，室内空气质量对人体健康的影响可能超过室外，应当引起足够的重视和关注。

Size characterization of indoor nanoparticle distribution

ZHANG Yuanxun　YANG Chuanjun　LU Wenzhong　YANG Yongxin

ZHANG Guilin　LI Yan

Key words:　**A**erosol, Nanoparticle, Size distribution, Indoor, Air quality

It has a remarkable significance to study the environment behavior and the pollution characterization of aerosol nanoparticle size for the indoor air quality. The number and mass concentrations of aerosol particulates in indoor and outdoor air with size ranging from 10 to 10,000nm were measured using wide range particle spectrometer (Model 1000XP WPS) produced by MSP Corporation, and the nanoparticle size (10~500 nm) in various room conditions was highlighted. It was found that the ultrafine particles (10~500 nm) contributed more to the total number concentration, and the fine particles (500 nm~10 μm) contributed more to the total mass concentration. The results showed that the mass concentration of indoor fine particulates was lower than that of outdoor and the nanoparticles are

dominant in indoor atmosphere. The number or mass concentrations of nanoparticle increased greatly when smoking happens. The further research indicated that the effect of indoor air quality on the human health maybe surpass that of outdoor, to which more attentions should be paid.

同步辐射 X 荧光微探针用于苔藓植物监视大气污染的研究

张元勋 曹 同[1] A.Iida[2] 杨传俊 王 敏[1] 张桂林 李 燕

关键词 苔藓，生物监视器，同步辐射，X 荧光微探针，大气污染

为了探讨苔藓植物监视大气污染的机理，本项研究将苔藓活体样本同时置于受工业污染的上海钢铁研究所和作为对照的上海应用物理所暴露一个月，然后使用日本光子工厂 KEK 实验室的同步辐射 X 荧光微探针对不同大气环境暴露下的苔藓植株和叶片、茎横切面微区进行元素分布扫描测定，获取苔藓植物叶面和茎断面 Pb、Cu、Fe、Ni、Mn、Zn、Ca、K 等金属元素的精细分布。结果表明，苔藓植物的叶片和茎干吸附金属离子后不是均匀分布的，尤其是叶尖和中肋部位富集了 K、Ni、Fe、Pb 等元素。在遭受污染的状况下，叶表吸附和富集了过量的 Pb 等金属离子，污染环境导致植物超微结构和生长发育受到严重损伤，同时抑制了植物对 K、Ca 等微量营养元素的正常吸收。

Study of moss as air pollution monitor by SRXRF microprobe technique

ZHANG Yuanxun CAO Tong[1] A. Iida[2] YANG Chuanjun WANG Min[1]
ZHANG Guilin LI Yan

Key words: Moss, Biological monitor, Synchrotron radiation, X-ray fluorescence microprobe, Air pollution

In order to explore the mechanism of moss as air pollution biomonitor, the moss samples were exposed to a pollution site at Shanghai Institute of Steel Research and a control site at Shanghai Institute of Applied Physics simultaneously for one month. The elemental distributions in the micro areas of leaf and stem, as well as in the whole moss tissue, were determined using synchrotron radiation X ray fluorescence (SRXRF) method. The contents of some metal elements such as Pb, Cu, Fe, Ni, Mn, Zn, Ca, and K in the leaf surface and the stem slice were obtained. The results showed that the metallic ions did not present an even distribution after adsorption. In particular, some elements of K, Ni, Fe, Pb etc were concentrated in the leaf apex and the intermediate rib. Under pollution condition, excessive Pb was adsorbed and deposited in the leaf and caused serious damage to the plant growth and the ultrastructure, also suppressed moss's normal absorption of the nutritive elements of K, Ca, etc.

[1]上海师范大学生命与环境科学学院;[2]Photon Factory, National Laboratory for High Energy Physics, Tsukuba, Ibaraki 305, Japan

民用锅炉煤燃烧微量元素的迁移以及砷的形态变迁

包良满 张元勋 金 蝉 林 俊 刘 卫 刘江峰 张桂林 陆文忠 李 燕
Nomura Masaharu* Inada Yasuhiro* Atsuo Iida*

关键词 同步辐射，煤炭燃烧，形态，砷

为了研究民用生活锅炉燃煤释放的微量元素对环境的影响，应用同步辐射 X 射线荧光分析对锅炉原煤、底灰、飞灰以及烟囱排放的 $PM_{2.5}$ 中 V、Cr、Mn、Co、Ni、Cu、Zn、As、Pb 等痕量元素进行了测定，研究了微量元素在煤炭燃烧过程中的迁移特性以及富集规律。利用同步辐射 XAFS 测量了煤炭燃烧排放 As 的 XAFS 谱，研究了 As 在煤炭燃烧排放过程中的形态变化的特征。结果表明，V 在飞灰中亏损，在底灰富集。Mn 和 Co 在底灰中亏损，在飞灰中富集(表 1)。As、Cu、Pb、Zn 等半挥发微量元素，在飞灰和底灰中呈地球化学富集状态，在 $PM_{2.5}$ 超细颗粒中明显富集。在煤中，砷大部分以 As^{5+}存在，少部分以 As^{3+}存在。 煤经过高温燃烧，砷富集在飞灰和超细颗粒中。在飞灰和 $PM_{2.5}$ 中，五价砷约占 90%，三价砷约占 10%。

Characterization of trace element emissions and arsenic speciation from a coal-fired boiler

BAO Liangman ZHANG Yuanxun JIN Chan LIN Jun LIU Wei LIU Jiangfeng
ZHANG Guilin LU Wenzhong LI Yan
Nomura Masaharu* Inada Yasuhiro* Atsuo Iida*

Key words: Synchrotron radiation, Coal combustion, Species, Arsenic

To study the release of trace elements from civilian coal-fired boiler and its impact on the environment, the concentration of trace elements such as V, Cr, Mn, Co, Ni, Cu, Zn, As and Pb in raw coal, fly ash, bottom ash and $PM_{2.5}$ from chimney emission of boiler was determined by synchrotron radiation X-ray fluorescence analysis and the species of arsenic was measured by X-ray absorption fine spectroscopy. The characteristics of trace elements' migration and accumulation in the combustion process were studied based on the trace elements concentration in raw coal, fly ash, bottom ash and $PM_{2.5}$. The results showed that V was lost in fly ash and enriched in bottom ash, but Mn and Co were lost in bottom ash and enriched in fly ash (Table 1). Semi-volatile trace elements As, Cu, Pb and Zn in the bottom ash and fly ash were in geochemical enrichment state, while As and Pb were significantly enriched in $PM_{2.5}$. Most of the species of arsenic in coal was As^{5+} and a few was As^{3+}. After high temperature combustion of coal, As was enriched in $PM_{2.5}$ and fly ash. The XAFS results showed that As^{5+} was about 90% and As^{3+} was about 10% in fly ash and $PM_{2.5}$, respectively.

Table 1 Enrichment factors of trace elements in fly ash, bottom ash and $PM_{2.5}$

Materials	V	Cr	Mn	Co	Ni	Cu	Zn	As	Pb
Fly ash	0.9	5.0	1.3	1.1	1.5	2.4	7.2	10.0	1.9
Bottom ash	3.5	8.8	0.8	0.8	3.5	4.3	4.8	1.7	2.2
$PM_{2.5}$	1.9	5.6	1.1	1.7	1.8	26.0	77.2	113.2	90.9

*Photon Factory, Institute of Materials Structure Science, High Energy Accelerator Research Organization, Oho 1-1,Tsukuba, Ibaraki, Japan

用同步辐射荧光分析研究大气细颗粒 $PM_{2.5}$ 的昼夜变化特征

包良满 张元勋 金 蝉 林 俊 刘 卫 刘江峰 张桂林 陆文忠 李 燕

Nomura Masaharu* Inada Yasuhiro* Atsuo Iida*

关键字 同步辐射荧光分析，$PM_{2.5}$，昼夜变化，无组织排放

为研究上海郊区秋季 $PM_{2.5}$ 的昼夜变化特征，2006 年 10~11 月对本所环境监测点进行 $PM_{2.5}$ 昼夜采样和同步辐射荧光分析。结果表明 $PM_{2.5}$ 质量浓度具有明显的昼夜变化特征，白天质量浓度较低，晚间较高。白天和夜间的 $PM_{2.5}$ 平均浓度分别为 66 和 130 μg/m^3，分别超过美国环境保护署 EPA 2006 年颁布的细颗粒 $PM_{2.5}$ 24 小时标准值 35 μg/m^3 的 1.9 倍和 3.7 倍，夜间空气污染比白天严重。 白天 $PM_{2.5}$ 的 Al、Si、Ca、Ti、Fe 等元素浓度值高于夜间; 夜间 $PM_{2.5}$ 的 P、 S、Cl、 K、 Mn、Ni、Cu、Zn、As、Br、 Pb 等元素的浓度值高于白天。一般认为大气颗粒物中 Al、Si、Ca、Ti 等元素来自土壤，道路交通扬尘和建筑作业扬尘对白天的 $PM_{2.5}$ 贡献大，而 S、Cl、K、Zn、As、Br、Pb 等元素通常来自石化燃料燃烧排放、垃圾燃烧以及工厂气体排放，这些排放导致夜间污染增加。夜间温度低，空气湿度大，大气扩散能力减弱，污染物难以扩散稀释，使夜间颗粒物浓度增加。更因为采样点周围有很多工厂夜间开工，很多燃煤锅炉排放增加了空气污染。 周围居民傍晚使用民用生活锅炉烧水以及焚烧作物秸秆和垃圾，这些无组织排放是导致夜间污染的一个重要因素。

SR-XRF study on day-night changes of $PM_{2.5}$

BAO Liangman ZHANG Yuanxun JIN Chan LIN Jun LIU Wei

LIU Jiangfeng ZHANG Guilin LU Wenzhong LI Yan

Nomura Masaharu* Inada Yasuhiro* Atsuo Iida*

Key words: SR-XRF, $PM_{2.5}$, Day-night change, Unorganized release

The day-night change of $PM_{2.5}$ at Shanghai suburb was monitored at the campus of SINAP in October and November 2006. Synchrotron radiation X-ray fluorescence analysis (SR-XRF) was used for multi-element analysis. It was found that the mass concentration of daytime and night $PM_{2.5}$ was 66 and 130 μg/m^3, being 1.9 and 3.7 times, respectively, larger than 35 μg/m^3, the 24-hour $PM_{2.5}$ standard level issued in 2006 by U.S. EPA. The mass concentrations of Al, Si, Ca, Ti and Fe of daytime $PM_{2.5}$ were higher than those of nighttime $PM_{2.5}$, while the mass concentrations of P, S, Cl, K, Mn, Ni, Cu, Zn, As, Br and Pb of nighttime $PM_{2.5}$ was higher than those of daytime $PM_{2.5}$. It was observed that at day time, road and construction dusts were the major contributor of $PM_{2.5}$. Release from fossil fuel combustion, coal-fired boilers, and waste combustion led to increase pollution at night. The higher night pollution is also due to low temperature and high air humidity, which decreases atmosphere diffusion rate and pollutants dilution. Moreover, factors such as unorganized release from factories and water heating boilers, burning of crop residues and garbage around the sampling site account for substantial contributions to the increased pollution.

*Photon Factory, Institute of Materials Structure Science, High Energy Accelerator Research Organization, Oho 1-1, Tsukuba, Ibaraki, Japan

扫描质子微探针样品台的改进

刘江峰 包良满 李晓林 张桂林 李 燕

关键词 扫描质子微探针，样品台，显微镜

我们对扫描质子微探针(SPM)样品台和显微观测系统做了如下改进。

样品台: 原系安装于靶室底部的(x,y,z)三维平移台，由波纹管柔性连接的手动调节机构移动样品，调节精度 10 μm。为提高样品操控精度，并具有 STIM-CT 实验所需的 360°旋转功能，采用英国 Vacuum Generators 公司的 HPT 系列六轴高精度样品台，垂直倒扣于靶室上。(x,y,z)平移轴调节精度 1 μm，倾斜度和旋转调节精度为 0.01°。倾斜度调节为手动，其余为步进电机驱动，通过密封机构和波纹管柔性连接而传动高真空(1.33×10^{-9} Pa)室内的样品。

显微观测系统: 原显微物镜在真空室内，光线经棱镜折射后由靶室盖上目镜观测。安装六轴样品台后，显微镜光路被遮挡；且实验时须移动物镜避开束流，观测时再回原位，难以对样品精确定位。为此，设计了长焦距观测系统。显微镜工作距离 131 mm，通过靶室侧面的玻璃窗实现对靶室中心样品的观测。长焦显微镜的放大倍数仅 6 倍，但结合 CCD 摄像头与高清晰显示屏可实现 200 倍放大和 3 μm 的图像解析度。

Improvement of the SPM manipulation system

LIU Jiangfeng BAO Liangman LI Xiaolin ZHANG Guilin Li Yan

Key words: SPM, Manipulation system, Microscope

The sample manipulation and observation system of the scanning proton microscopy (SPM) have been upgraded at Laboratory of Nuclear Analysis Techniques.

The 6-axis manipulation: Originally the SPM had a 3-axis sample manipulation system installed in the chamber bottom, and the sample position was adjusted manually through the bellows connection with an accuracy of 10 μm. For improving the manipulation precision and performing STIM-CT experiment, which requires 360° rotations, it was replaced by an HPT high-precision six-axis manipulator from Vacuum Generators, installed vertically downward on the target chamber. Accuracy of three translational axes can be 1 μm, while the tilting and rotating axes can be operated with an accuracy of 0.01°. The tilting axis is adjusted manually, while the others are manipulated by stepper motor operated in atmosphere to transmit the sample in high vacuum through sealed bellows.

The long working distance microscopic observation system: A microscope provides position reference of the sample. Originally, the observation was done on top of the target chamber through an object lens receiving the lights refracted by the prisms. But installation of the 6-axis manipulator blocked the optical paths. Also, the object lens should be moved to different positions during the SPM experiment, hence uncertainties of the exact sample position. Therefore, we designed a microscopic system of 131 mm in working distance. The sample is viewed through a side window of the target chamber. Magnification of the microscope is only six, but with a CCD camera and high-definition display the system can achieve 200 times magnification and 3 μm image resolution.

离心法制备高均一性纳米金及其在 DNA 分子自组装中的应用

王丽华 宋世平 樊春海

关键词 纳米金(AuNPs)，离心浓缩，稳定性，DNA，自组装

在纳米金上组装 DNA 制备纳米探针可实现对 DNA、蛋白质及其他靶物质的快速检测。DNA 在高浓度纳米金中的组装更快更稳定，但化学还原法制备的高浓度纳米金粒径不均匀，市售纳米金浓度较低，难以满足实验要求。我们制备出 3.5 nmol/L、13 nm 的纳米金颗粒，并用高速离心法对其进行浓缩。得到纳米金离心浓缩的最佳条件为：用 Axygen 圆底离心管，离心温度 4℃，转速 12000 r/min，离心 20 min，此时的回收率最高，无团聚，且能去除小颗粒。浓缩金的耐盐度为 44 mmol/L，而直接制备组仅为 9 mmol/L。DNA 组装结果，组装后的 Au-DNA 表明，浓缩组最高可耐受终浓度为 2.6 mol/L 的 NaCl，而制备组最高仅可耐受 1.5 mol/L，证明浓缩组的表面 DNA 组装密度更高。在 0.1 mol/L PBS 4℃储存试验中，浓缩组 30 d 仍稳定, 而制备组储存 7 d 即有黑色点状沉淀，浓缩组的稳定性远优于制备组。这些结果均有利于纳米金 DNA 探针的推广应用，也为其在其他领域中的应用奠定基础。

Preparing well-dispersed gold nanoparticles by centrifuge for self-assembly of DNA molecules

WANG Lihua SONG Shiping FAN Chunhai

Key words: Gold nanoparticle (AuNPs), Centrifuge condensation, Stability, DNA, Self-assemble

Gold nanoparticles (AuNPs) were widely used in biological studies because of their excellent optical, electrical properties, chemical reactivity and biocompatibility. Since the properties were highly related with particle size, the kinetic and thermal properties of the interaction between DNA and AuNPs were dissimilar corresponding to size and concentration of AuNPs. AuNPs-DNA probe, which came from AuNPs modified DNA, formed a platform to detect gene, protein, metal ion and other targets in different fields. We found that the self assembly of DNA on surface of high concentration AuNPs was quicker and easier. But it is difficult to get uniformly sized particles of high concentration AuNPs prepared directly or products commercially available. We proposed to prepare 3.5 nmol/L 13 nm AuNPs and concentrate them with high speed centrifuge. The optimal concentration conditions are 12000 r/min at 4°C for 20 min, with the highest recovery ratio to clean off the finer nanoparticles. The concentrated AuNPs could tolerate 44mmol/L NaCl, compared with 9 mmol/L of the directly prepared AuNPs. After being self assembled with thiolated DNA, the product of concentrated Au-DNA could tolerate 2.6 mol/L NaCl, rather than 1.5 mol/L of the directly prepared AuNPs. This implies higher DNA surface density of the concentrated Au-DNA and higher stability in buffer at 4°C. In summary, a simple method of preparing high concentration AuNPs was established. Well-dispersed AuNPs with excellent salt-tolerance ability and high stability were obtained for DNA self-assembly. This method shall be of help, too, for AuNPs applications in biological, environmental and other fields of studies.

纳米金粒子放大和纳米尺度调控的计时电量 DNA 传感器

张 炯 宋世平 樊春海

关键词 电化学 DNA 传感器，计时电量，金纳米粒子，纳米调控

对基因相关疾病特异靶序列的检测在分子诊断学中具有重要地位。电化学 DNA 传感器选择性好、灵敏度高、测试费用低并适于联机化；它不破坏测试体系，不受颜色影响，操作简便；又大都使用固体电极表面固定探针，尤宜于基于表面控制杂交反应的基因诊断学研究，在分子诊断、食品检验、环境监测以及安全反恐等领域将有广泛应用。我们将金纳米粒子作为信号放大的载体引入电化学杂交检测中，采用计时电量法对超低含量的靶序列进行灵敏的检测。其原理是通过“夹心式”的杂交方式，将负载了大量信号探针的金纳米粒子拉近到电极表面。以钌离子作为电化学活性指示剂，通过杂交前后钌离子电量的变化指示杂交反应的发生。通过对组装条件的严格控制，对电极表面组装的 DNA 探针密度实现纳米级调控，并通过巯基己醇的竞争组装，取代非巯基连接的 DNA 并封闭空余位点，有效提高检测灵敏度。纳米粒子的表面负载能力大，DNA 杂交传感器可有效放大低浓度靶序列的杂交反应信号，结合电极表面探针组装密度调节，检测限可达 10^{-14} mol/L，灵敏度比常规荧光检测法提高 2~3 个量级，并对单碱基错配序列具有较强的区分能力。

Chronocoulometric DNA sensors based on nanogold amplification and nanoscale control of DNA assembly

ZHANG Jiong SONG Shiping FAN Chunhai

Key words: Electrochemical DNA sensor, Chronocoulometry, Gold nanoparticles, Nanoscale control

Sequence-specific detection of DNA targets associated with genetic or pathogenic diseases is important to molecular diagnostics. Electrochemical DNA biosensors, which are simple, portable and inexpensive, are widely recognized as a promising solution for point-of-care diagnostics and antiterrorism and environmental monitoring applications. For these reasons, nucleic acid-based electrochemical transducers have received great attention in developing sequence-specific DNA hybridization biosensors. We report a novel nanoparticle-based electrochemical DNA detection approach. The DNA sensor is based on a “sandwich” detection strategy, which involves capture probe DNA immobilized on gold electrodes and reporter probe DNA labeled with gold nanoparticles that flank the target DNA sequence. An electroactive complex, $[Ru(NH_3)_6]^{3+}$, serves as the signaling molecule and binds to anionic phosphate of DNA strands in a stoichiometric approach. Electrochemical signals are generated by chronocoulometric interrogation of $[Ru(NH_3)_6]^{3+}$ that quantitatively binds to surface-confined capture probe DNA. The treatment of mercaptohexanol could effectively erect single-strand probe and remove nonspecific adsorption. Since a single gold nanoparticle is loaded with hundreds of reporter DNA strands, it offers a significant amplification for detecting the target DNA. This significantly enhances the sensitivity and the selectivity. Nanoscale control of the self-assembly process of DNA probes at gold electrodes increases the sensor performance. The DNA sensor is reproducible, stable, and reusable. It can detect femtomolar target DNA with excellent differentiation ability for single-nucleotide polymorphisms.

基于共轭高分子构象效应的高灵敏度 Hg^{2+}生物传感器

刘兴奋　宋世平　樊春海

关键词　生物传感器，共轭高分子，Hg^{2+}，比色法，荧光法，无标记

聚噻吩(PMNT)是具有构象效应的共轭高分子，以其为传感元件的生物传感器广受关注。Hg^{2+}与碱基胸腺嘧啶(thymine, T)的特异结合，可研制无标记 Hg^{2+}传感器。我们以聚噻吩的构象效应和 T-Hg^{2+}-T 结构为基础，设计了以无标记的富含 T 的 DNA 为探针(MSO)的比色和荧光生物传感策略，用于 Hg^{2+}的快速、高灵敏检测。聚噻吩水溶液呈黄色，对应的共轭骨架呈低共轭的、柔性的自由卷曲状态，有很强的荧光。无 Hg^{2+}时，MSO 探针为柔性的自由卷曲状态，与 PMNT 结合后形成近似直线的刚性结构，对应的共轭程度和共面性都较高，紫外－可见吸收峰发生红移，溶液为红色，但 PMNT/MSO 为电中性，易发生聚集而导致荧光猝灭。但当 Hg^{2+}与 T 特异性结合，使富含 T 的 MSO 探针折叠成以 T-Hg^{2+}-T 为连接纽带的茎环结构，形成的 Hg^{2+}/PMSO/PMNT 也呈类似的茎环结构，其共轭程度较低，共面性也较差，紫外－可见吸收峰发生蓝移，溶液为黄色，而复合物间的排斥力较强，不易聚集，荧光得以恢复。而相同条件下的 Zn^{2+}不能与 MSO 探针特异结合，溶液颜色仍为红色，荧光被猝灭。根据不同的颜色和荧光，可特异性地检测 Hg^{2+}。该传感器兼具如下特点：1)可在水相中工作，为生物体内的检测提供了可能；2)选择性和灵敏度高，Pb^{2+}、Cu^{2+}等 7 种二价金属离子对其影响很小，比色法最低可检测 2.5 μmol/L Hg^{2+}，荧光法最低可检测 42 nmol/L Hg^{2+}，3)无需任何标记，4)可实现“turn-on”模式的荧光检测。

High sensitive mercury (II) biosensor based on configuration effect of water-soluble conjugated polymer

LIU Xingfen　SONG Shiping　FAN Chunhai

Key words:　Biosensor, Conjugated polymer, Hg^{2+}, Colorimetry, Fluorometry, Label-free

Hg^{2+} can specifically link T-T pairs and form T-Hg^{2+}-T complexes. We used a 28-base T-rich oligonucleotide (MSO) to probe Hg^{2+}. Conjugated polythiophene (PMNT) has large delocalized molecular structures and exhibits yellow color and intense fluorescence. Without Hg^{2+}, the probe lacks secondary structure. Cationic PMNT and the random coil-like MSO probe form an electrostatic MSO/PMNT complex in aqueous solution, which rigidified PMNT and led to a planar conformation characteristic of red color and quenched fluorescence. With Hg^{2+}, the MSO probe readily formed a stem-loop structure through the specific T-Hg^{2+}-T binding. We observed a color change from red to yellow and high fluorescence upon the addition of Hg^{2+} to the MSO/PMNT complex, with λ_{max} shifted to shorter wavelengths. This optical change possibly arises due to the wrapping of PMNT on the stem-loop structure and the resulting twisting of the conjugated backbone. Noticeably, other metal ions such as Zn^{2+} did not lead to similar color changes, implying high specificity of T-Hg^{2+}-T recognition. The sensor is featured by 1) PMNT offers a convenient “mix-and-detect” approach for rapid Hg^{2+} detection in aqueous solution, 2) extraordinarily high selectivity and sensitivity (μmol/L Hg^{2+} with naked-eyes), 3) no requirement of fluorescent labels on the oligonucleotide probe, and 4) capability of working in “turn-on” mode.

基于磁性颗粒和共轭高分子的蛋白质生物传感器

刘兴奋　宋世平　樊春海

关键词　生物传感器，共轭高分子，凝血酶，核酸适体，磁性颗粒

蛋白质检测在疾病诊断、治疗和新药研制等方面具有重要意义。最近发展起来的核酸适体(aptamer)，具有类似抗体的高度特异性，且可筛选，可由直接固相化学法合成，又较稳定，已用于很多传感检测领域。凝血酶是在凝血系统中有重要调节作用的丝氨酸蛋白酶，已有很多基于aptamer 的凝血酶检测方法，但各有其优缺点。我们以磁性颗粒为固相载体，结合共轭高分子的信号倍增功能，设计了可高灵敏度检测凝血酶的固相蛋白质生物传感策略。以亲和素修饰的微米级磁性颗粒为固相载体，biotin-aptamer 为捕获探针，荧光素修饰的 DNA 为信号探针，通过 aptamer-凝血酶的特异结合，将靶连接在固相表面，从而实现对凝血酶的快速分离和富集。为避免反应体系中磁珠等对荧光检测的影响，反应完毕后用将 FAM 标记的信号 DNA 探针变性分离，然后加入共轭导电高分子，通过导电高分子与 FAM-DNA 之间的 FRET 效应将荧光信号进行放大。研究发现，此法最低可检测 500 pmol/L 凝血酶。整个过程中无需标记、无需扩增等复杂程序，因此是一种简便、成本低廉、高特异性和高灵敏度的快速检测方法。

A high sensitive protein biosensor of thrombin based on the conjugated polymer and magnetic particles

LIU Xingfen　SONG Shiping　FAN Chunhai

Key words:　Biosensor, Conjugated polymer, Thrombin, Aptamer, Magnetic particles

Protein detection is very important in disease diagnosis and drug-screening. The newly developed aptamer has specificity similar to antigen and outstanding stability. Thrombin is an important modulating protease in the blood coagulation system. There are many technologies for the detection of thrombin such as optical methods, electrochemical methods, QCM and SPR. In this work, a highly sensitive protein biosensor for thrombin based on conjugated polymer and magnetic particles was introduced. The biotin modified aptamer acting as capture probe combined the streptavidin coated magnetic beads and target through specific aptamer-ligand bindings so that thrombin was immobilized on the solid substrate, and a fluorescein labeled DNA acting as the signal probe was used as energy acceptor to amplify the signal through the FRET between conjugated polymer and the fluorescein. It has been found that 500 pmol/L of thrombin can be detected by this method. In summary, this magnetic particles-based fast separation and conjugated polymer-based optical biosensor is simple, low costly, sensitive and selective, which is greatly needed in many fields.

$C_{60}(OH)_{24}$ 吸收自由基的 ESR 研究

蔡小青　龙建刚*　李雪森*　刘健康*　李文新

关键词　自由基，ESR，$C_{60}(OH)_{24}$,超氧自由基，羟基自由基，脂质自由基

近年来许多研究表明氧化损伤是人体衰老和一些衰老相关疾病的一个关键因素。现在我们主要采用 ESR 技术研究 C_{60} 的多羟基衍生物($C_{60}(OH)_{24}$)吸收自由基的效应。超氧自由基主要采用次

黄嘌呤-次黄嘌呤氧化酶反应产生；羟基自由基主要采用 Fenton 反应；脂质自由基主要采用 SDS-$CuSO_4$ 系统产生。超氧自由基和羟基自由基用 DMPO 进行捕获；而脂质自由基用 POBN 进行捕获。ESR 实验表明：$C_{60}(OH)_{24}$ 对三种常见的自由基均有较好的清除作用。其中，吸收超氧自由基的 IC_{50} 为 0.036 mmol/L；吸收羟基自由基的 IC_{50} 为 0.135 mmol/L,而吸收羟基自由基的“明星分子”甘露醇为 36.3 mmol/L,$C_{60}(OH)_{24}$ 吸收羟基自由基的效应比甘露醇强 268 倍；同样地，$C_{60}(OH)_{24}$ 吸收脂质自由基的 IC_{50} 为 0.495 mmol/L，较 VitE 吸收脂质自由基的 IC_{50} 强 37 倍。本文较系统地研究了 $C_{60}(OH)_{24}$ 吸收自由基的效应，为研究 $C_{60}(OH)_{24}$ 抗氧化效应提供了基础。

ESR study on free radical scavenging activity of $C_{60}(OH)_{24}$

CAI Xiaoqing LONG Jiangang* LI Xuesen* LIU Jiankang* LI Wenxin

Key words: Free radicals, ESR,$C_{60}(OH)_{24}$, Superoxide radical, Hydroxyl radical, Lipid radical

Oxidative damage is known to be a key contributor to aging and degenerative diseases. In the present study, we examined the free radical scavenging effect of $C_{60}(OH)_{24}$ with an Electron Spin Resonance spectrometer (Brucker EMX, Bruker Spectrospin Ltd., Germany). The free radicals examined included superoxide radicals generated by hypoxanthine-xanthine oxidase system, hydroxyl radicals generated by Fenton reagents, and lipid radicals generated by SDS-$CuSO_4$ system using DMPO or 2-(4-pyridyl-1-oxide)-N-t-butylnitrone(POBN) as spin trap. $C_{60}(OH)_{24}$ exhibited powerful scavenging effects on superoxide radicals and hydroxyl radicals. In addition, $C_{60}(OH)_{24}$ showed a dose-dependent scavenging effect on lipid radicals. The 50% radical signal inhibiting concentration (IC_{50}) of $C_{60}(OH)_{24}$ was 268 fold lower than mannitol for hydroxyl radicals (36.3 mmol/L over 0.135 mmol/L), and 37 fold lower than alpha-tocopherol for lipid radicals (18.4 mmol/L over 0.495 mmol/L).

*中国科学院上海生命科学研究院营养科学研究所

C_{60}-地塞米松的激光光解研究

刘瑞丽 赵红卫 张兆霞 姚思德 李文新

关键词 C_{60}-地塞米松, 激光光解, 激发三重态, 淬灭速率常数, 三重态寿命

利用激光光解装置检测了 C_{60}-地塞米松(C_{60}-DE)的苯溶液在 355 nm 激光照射下产生的激发三重态，$^3C_{60}$-DE*出现四个吸收峰，分别位于 700、 440、350 和 310 nm。在 330 nm 处观察到了它的漂白吸收最大值，这与其基态吸收最大值相对应。$^3C_{60}$-DE*能够将能量转移给 O_2 分子而淬灭。与 $^3C_{60}$*相比，$^3C_{60}$-DE*的三重态-三重态(T-T)淬灭速率常数减小($^3C_{60}$*为 $5.03\pm1.31\times10^9$ $L\cdot mol^{-1}\cdot s^{-1}$，$^3C_{60}$-DE*为 $3.53\pm0.87\times10^9$ $L\cdot mol^{-1}\cdot s^{-1}$)，而寿命增加($^3C_{60}$*为 12±2.6 μs，$^3C_{60}$-DE*为 18±3.3 μs)，这可能是 C_{60} 分子上连接了地塞米松(DE)分子后减小了 C_{60} 球之间的碰撞几率所致。

Laser flash photolysis of C_{60}-dexamethasone

LIU Ruili ZHAO Hongwei ZHANG Zhaoxia YAO Side LI Wenxin

Key words: C_{60}-dexamethasone, Laser flash photolysis, Excited triplet state, Annihilation rate constant, Triplet lifetime

Laser flash photolysis technique has been employed to characterize the triplet excited state behavior of C_{60}-dexamethasone in benzene. The time-resolved triplet-triplet (T-T) difference absorption spectrum of $^3C_{60}$-dexamethasone* with optical excitation (355nm laser pulse) was recorded. $^3C_{60}$-dexamethasone* has maxima at 700, 440, 350 and 310 nm. The bleaching maximum observed at 330 nm coincides well with the ground-state maximum in this region. $^3C_{60}$-dexamethasone* can be quenched by oxygen. Compared with $^3C_{60}$*, the T-T annihilation rate constant of $^3C_{60}$-dexamethasone* reduced ($5.03\pm1.31\times10^9$ L·mol^{-1}·s^{-1} for $^3C_{60}$* and $3.53\pm0.87\times10^9$ L·mol^{-1}·s^{-1} for $^3C_{60}$-dexamethasone*), and the life time of $^3C_{60}$-dexamethasone* increased (12±2.6 μs for $^3C_{60}$* and 18 ±3.3 μs for $^3C_{60}$-dexamethasone*). The reason is that the connection of dexamethasone may reduce the colliding probability of the C_{60} ball.

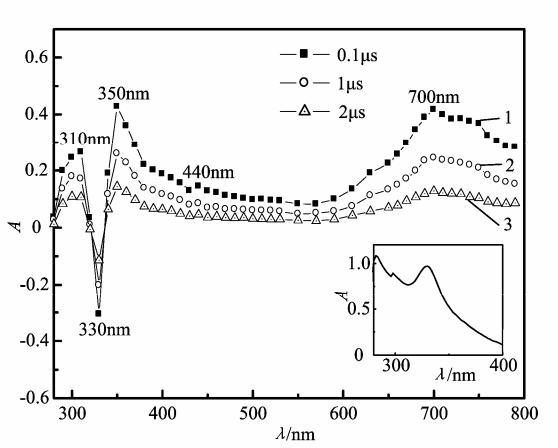

Fig.1 Laser photolysis of C_{60}-dexamethasone in benzene (0.5×10^{-4}mol/L). The insert is its UV absorption spectrum

C_{60}-糖皮质激素荧光特性的研究

刘瑞丽 尹娟娟 马继飞 李文新

关键词 C_{60}-糖皮质激素，荧光，浓度自淬灭

在室温下用 350 nm 波长的光激发 C_{60}-糖皮质激素类衍生物氯仿溶液，发现于 447 nm 处有荧光发射。C_{60} 分子中 60 个碳原子等价，属 Ih 群，呈高度对称性，故同样条件下难以观测到荧光。而 C_{60}-糖皮质激素类衍生物在形成过程中 C_{60} 分子骨架结构的对称性发生了改变，使其可在一定波长光的激发下发射荧光。浓度为 10~130 μmol/L 的 C_{60}-糖皮质激素氯仿溶液在 λ_{ex}=350 nm、λ_{em}=447 nm 处的荧光测定表明，此类化合物存在荧光浓度自淬灭现象，在 64 μmol/L 以下的浓度范围内，荧光强度随浓度的增大而增强，尔后随浓度增大而逐渐降低。

Fluorescence properties of C_{60}-glucocorticoids

LIU Ruili YIN Juanjuan MA Jifei LI Wenxin

Key words: C_{60}-glucocorticoids, Fluorescence, Concentration self-quenching

When excited with the wavelength of 350 nm at room temperature, C_{60}-glucocorticoids displayed the fluorescence emission in chloroform at 447 nm. Usually the sixty carbon atoms of a C_{60} molecule are

equivalence, belonging to the Ih group, in high symmetry. It is difficult to observe the fluorescence of C_{60} under the same condition of C_{60} molecule. The fluorescence emission of C_{60}-glucocorticoids is probably due to the decreased symmetry of C_{60} molecule. The fluorescence at 447 nm was investigated with 10~130 μmol/L of C_{60}-glucocorticoids chloroform solutions excited at 350 nm. It indicated that the C_{60}-glucocorticoids in chloroform could quench the fluorescence. The fluorescence intensity increased with the concentration from 10 to 64 μmol/L, but decreased from 64 to 130 μmol/L.

X-射线相衬成像技术在 MWCNTs 肺组织毒性检测中的应用

李俊纲　薛艳玲　韩 博*　李晴暖　刘丽想　肖体乔　李文新

关键词　X-射线相衬成像，多壁碳纳米管，肺损伤，肉芽肿

生物软组织的 X-射线相衬成像的衬度分辨率和空间分辨率均好。我们用该技术检测了多壁碳纳米管(MWCNTs)诱发的大鼠肺组织损伤。0.1 mg MWCNTs 经气管滴注到大鼠肺部，140 d 后取出肺组织和气管作 X-射线相衬成像，并切片进行常规病理学观察(图 1)。结果表明，滴注到大鼠肺部的 MWCNTs 会诱发明显的肺部肉芽肿，而 X-射线相衬成像技术可有效地检测出该病理损伤。此项技术优于常规 X 射线吸收成像，还能弥补病理切片技术本身的不足。该研究工作可能会在纳米毒理学研究和纳米材料职业安全性评估方面具有应用潜力。

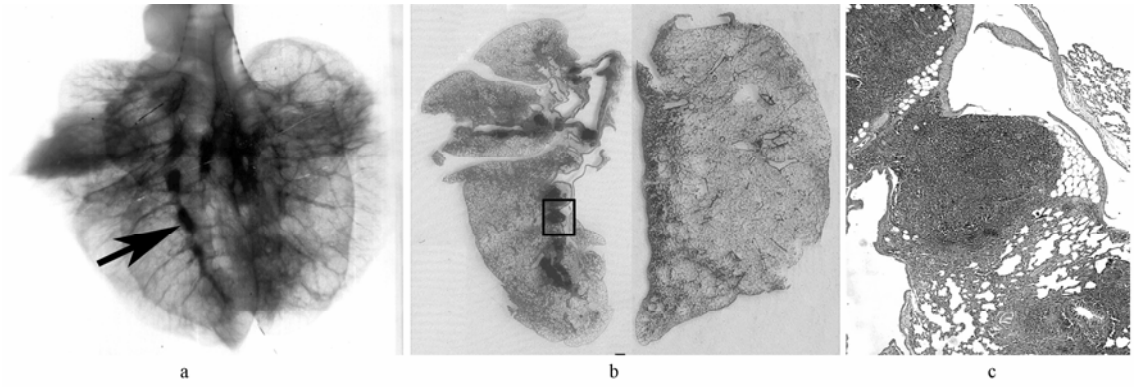

Fig.1　X-ray phase contrast image (a) and pathological slice images (b), (c) in the experimental group. Imaging conditions: voltage 70 kV, current 250 μA, source-lung distance 20.8 cm, lung-detector distance 33.7 cm, exposure time 800 s; magnification: × 2.7. The pathological slice image (b) corresponds to the phase contrast image, magnification: ×1, and (c) is the magnifying image of the marked area in (b), magnification: × 50

Application of X-ray phase contrast imaging in detecting pulmonary lesions induced by MWCNTs

LI Jungang　XUE Yanling　HAN Bo*　LI Qingnuan
LIU Lixiang　XIAO Tiqiao　LI Wenxin

Key words:　X-ray phase contrast imaging, MWCNTs, Pulmonary lesion, Granulomas

X-ray phase contrast imaging technique has potential application in medicine and biology. The technique makes the soft tissue morphology visible without complex sample treatment procedures such

as dehydrateion, fixture, embedment, section and staining. Compared with conventional X-ray radiography, the technique shows high contrast resolution and high spatial resolution in imaging soft tissue samples.

Pulmonary lesions induced in rats by multi-wall carbon nanotubes (MWCNTs) were studied with the technique. The rats were instilled intratracheally with 0.1mg MWCNTs into the lung. After 140 days, their lungs and tracheas were isolated for X-ray phase contrast imaging. Pathological slices of the lungs were prepared for microscopic examination. As shown in Fig.1, the MWCNTs particles induced obvious granulomas therein, and the pathologic lesion could be efficiently detected out via the X-ray phase contrast imaging technique, which not only gains preference over conventional X-ray adsorption contrast imaging technique but also can supplement the deficits in routine pathological slice technique. It is hoped that this work can be an impetus for further application of the X-ray phase contrast imaging technique to the nanotoxicology study and to the evaluation of occupational safety of nanomaterials.

*新疆石河子大学药学院

C_{60}-地塞米松的药理活性和副作用

刘瑞丽 蔡小青 李俊纲 李静 徐晶莹 诸颖 李永军 李晴暖 李文新

关键词 C_{60}-地塞米松，抗炎作用，学习和记忆功能

研究了口服 C_{60}-地塞米松的抗炎和免疫抑制作用及其对小鼠学习和记忆功能的影响。抗炎和免疫抑制作用由药物对二甲苯所致小鼠耳壳炎症水肿的抑制和对脾指数的影响来评估。对学习和记忆功能的影响由 Y-迷宫实验测定。结果表明地塞米松与 C_{60} 连接后，通过提高脂溶性增强了抗炎活性，并通过 C_{60} 基团的清除自由基作用降低了免疫抑制作用和副作用，减轻了对小鼠学习和记忆功能的损伤。总之，地塞米松分子上的 C_{60} 基团的连接提高了抗炎作用，而降低了副作用。

Pharmacological activities and side effects of C_{60}-dexamethasone

LIU Ruili CAI Xiaoqing LI Jungang LI Jing XU Jingying ZHU Ying
LI Yongjun LI Qingnuan LI Wenxin

Key words: C_{60}-dexamethasone, Anti-inflammatory activity, Learning and memory functions

The anti-inflammatory the immunosuppression activities as well as the influence of C_{60}-dexamethasone (C_{60}DE) on the learning and memory functions in of mice were evaluated and compared with dexamethasone (DE). C_{60}DE and DE were administered orally. Anti-inflammatory and immunosuppression activities were evaluated by the inhibition action on the edema induced by xylene on the mouse ear and the spleen indexes respectively. The influence on the learning and memory functions was given by Y-maze test. The experiments showed that the connection of DE with C_{60} enhanced the anti-inflammatory activity by the increase of the lipophilic property or by the assembling of C_{60}DE in body, decreased the influence on the learning and memory functions and the immunosuppression activity by the free radicals scavenging activity of the C_{60} group, and reduced the side effects with the mechanism waiting for further research.

含 C_{60} 的糖皮质激素类抗炎药物的制备

刘瑞丽　李文新　于伯章

关键词　富勒烯，糖皮质激素，合成

在 DCC 和 DMAP 催化条件下，C_{60} 单羧酸与五种糖皮质激素（可的松、氢化可的松、泼尼松、泼尼松龙和地塞米松）发生了酯化反应，从而在 C_{60} 分子上连接上了具有生物活性的糖皮质激素分子。对所得产物分子进行了 UV-vis、^{1}HNMR、^{13}CNMR、^{19}FNMR 以及 FT-IR 检测, UV-Vis 谱在 427nm 处有 C_{60}[6，6]环加成衍生物的特征吸收峰。^{1}HNMR 谱表明，糖皮质激素分子 21 位碳上的氢原子由 4.5×10^{-6} 位移到了 5.3×10^{-6}，向低场位移了 0.8×10^{-6}，FT-IR 谱在 1735cm^{-1} 处有酯羰基的吸收峰。^{13}CNMR 谱在 165.232×10^{-6} 处有酯羰基的共振吸收峰。^{19}FNMR 谱中， C_{60}-地塞米松分子中的氟原子在 δ -165.550×10^{-6} 处出现谱峰。由此可确定，C_{60} 单羧酸与糖皮质激素分子 21-位上的羟基发生酯化反应，生成了 C_{60}-糖皮质激素偶联物。

Synthesis of anti-inflammatory glucocorticoids containing C_{60}

LIU Ruili　LI Wenxin　YU Bozhang

Key words:　Fullerene, Glucocorticoid, Synthesis

As a kind of steroids, glucocorticoid has both anti-inflammation and immunosuppression activity. There has been increasing interest in synthesis of steroid-C_{60} hybrids in recent years. In this paper, we report for the first time the synthesis of five glucocorticoid-C_{60} hybrids (C_{60}- cortisone, C_{60}-hydrocortisone, C_{60}-prednisone, C_{60}-prednisolone, C_{60}-dexamethasone) by esterification. The hybrids were also characterized by their ^{1}HNMR, ^{13}CNMR, FT-IR, UV-vis and MALDITOF-MS spectra. The ^{1}HNMR spectra of the five hybrids showed that the 21-H of the glucocorticoids shifted from 4.5×10^{-6} to 5.3×10^{-6} because of the production of ester bonds, and the coupling constants increased from –20 Hz to –17.5 Hz. At the same time the proton on the methylene of [60]fullerenoacetic acid shifted from 5.1×10^{-6} to 4.9×10^{-6} for the same reason. The ^{13}CNMR spectra of the five hybrids showed the carbon resonances of the ester ketone bonds at 165×10^{-6}. The FT-IR spectra showed ester ketone absorption bands at 1721~1728cm^{-1} and framework absorption bands of C_{60} at 1427, 1183, 575, 525cm^{-1}. The UV absorption spectra of the five hybrids in this study showed sharp absorption at 430~435nm, which had been proposed to be characteristic of closed [6,6]-bridged fullerenes. The MALDITOF-MS spectra all showed peaks at *m*/*z* 720 for C_{60}^{+}, *m*/*z* 733 for $[C_{60}CH]^{+}$, and some showed peaks at *m*/*z* 778 for $[C_{60}CHCOOH]^{+}$. Additionally, C_{60}-dexamethasone hybrid was also characterized by the ^{19}FNMR spectrum, which showed the chemical shift of the F atom at the 165.56×10^{-6}. All the spectra revealed that the 21-OH reacted with [60]fullerenoacetic acid affording the hybrids containing newly-created ester bonds. In conclusion, we successfully linked five glucocorticoids to fullerene[60] in a simple method. Because these five glucocorticoids have excellent pharmaceutical effects, thus produced hybrids might show new useful activities. In due course their pharmaceutical effects will be tested in our laboratory.

小鼠呼吸多壁碳纳米管气溶胶后的肺部毒性

李俊纲 李晴暖 徐晶莹 蔡小青 刘瑞丽 李永军 马继飞 李文新

关键词 多壁碳纳米管(MWCNTs)，气溶胶，呼吸暴露，肺部毒性

用自然呼吸法研究了 MWCNTs 对小鼠的慢性呼吸毒性。MWCNTs 气溶胶的平均浓度为 32.61 mg/m^3，实验小鼠隔天暴露，时间为 6 h/d，在第 30 d 和 60 d 检测小鼠肺灌洗液的生化指标和肺组织的病理学变化。暴露 30d 小鼠的肺灌洗液中的总蛋白、碱性磷酸酶、酸性磷酸酶和乳酸脱氢酶无明显升高，但 60 d 时显著升高(表 1)。病理切片的结果显示，30 d 时，MWCNTs 颗粒沉积在支气管内壁并进入肺泡壁，致使肺泡壁轻度增生。60 d 时，沉积在支气管和肺泡壁的 MWCNTs 颗粒尺寸较 30 d 时明显增大;此外,沉积在肺泡壁的 MWCNTs 颗粒远小于沉积在支气管的 MWCNTs 颗粒的尺寸，并致使肺泡壁明显增生。这些结果表明， MWCNTs 气溶胶暴露 30 d 未在小鼠肺部诱发明显的炎症反应，而在 60 d 时诱发了明显的炎症反应。不同的炎症反应可能缘自 MWCNTs 特殊的理化性质，如不具有水溶性、不易生物降解和有很大的表面积。

Pulmonary toxicity in mice exposed to MWCNTs inhalation

LI Jungang LI Qingnuan XU Jingying CAI Xiaoqing LIU Ruili
LI Yongjun MA Jifei LI Wenxin

Key words: Multi-walled carbon nanotubes, Aerosol, Inhalation exposure, Pulmonary toxicity

The chronic pulmonary toxicity induced by multi-walled carbon nanotubes (MWCNTs) in mice was studied using inhalation exposure technique. The mice were exposed to MWCNTs aerosol of 32.61 mg/m^3, once every two days for 6h exposure. On Day 30 and Day 60, the pulmonary toxicity of MWCNTs was assessed using biochemical indices in bronchoalveolar lavage fluid (BALF) and pathological slice. The total protein, alkaline phosphatase, acid phosphatase and lactate dehydrogenase in BALF increased significantly in the 60-d-group, but not in the 30-d group (Table 1). The pathological examination indicated that, in the 30-d-group the aggregations of MWCNTs adhered to bronchial wall and entered into alveolar wall, respectively, and they could render alveolar wall slightly thickening, while in the 60-d-group, the aggregations that deposited in the bronchi became more obvious as their size was larger than that in the 30-d-group. On the other hand, while in the 60-d group the aggregations in alveolar wall were far smaller than those adhered to bronchial wall, and they rendered alveolar wall obviously thickening. The results indicated that aerosolized MWCNTs did not induce obvious pulmonary toxicity in the 30-d exposure group, but induced severe pulmonary toxicity in the 60-d exposure group. Perhaps the different toxic effect was attributed to the special physicochemical characteristics of MWCNTs, such as unsolvable in water, non-biodegradble, and with large surface area.

Table 1 The changes of biochemical indices in BALF in 30-day and 60-day groups

Groups	Total protein /g·L^{-1}	ALP /U·L^{-1}	ACP /U·L^{-1}	LDH /U·L^{-1}
Control	0.14 ± 0.04	1.36 ± 0.44	2.13 ± 0.43	582.04 ± 82.49
30-day	0.16 ± 0.04	1.56 ± 0.19	2.36 ± 0.84	667.09 ± 40.59
60-day	0.24 ± 0.06*	2.91 ± 0.92 *	4.96 ± 0.36**	1248.74 ± 28.05**

* $p < 0.05$ significant difference; ** $p < 0.01$ significant difference

多壁碳纳米管细胞毒性和培养液介质的依赖关系

诸 颖 冉铁成 李宇国 郭金学 李文新

关键词 依赖关系，多壁碳纳米管(MWNTs)，梨形四膜虫，细胞毒性,培养液介质

本工作研究了多壁碳纳米管(MWNTs)对单细胞原生动物四膜虫生长的影响，发现 MWNTs 在蛋白胨酵母粉(PPY)培养液中能促进四膜虫细胞的生长，这显著有别于大多数的现有研究结果。原子力显微成像和热重分析表明它们通过非共价结合形成了蛋白胨—MWNTs 复合物。荧光显微镜成像显示，细胞在含有荧光标记的蛋白胨和 MWNTs 的溶液中温育后的荧光强度远高于其在仅含有荧光标记的蛋白胨溶液中温育后的荧光强度，证明四膜虫摄取了大量的蛋白胨—MWNTs 复合物而导致细胞迅速增殖。用池塘水取代 PPY 介质，MWNTs 又显示出对细胞生长的抑制作用。丙二醛(MDA)和超氧化物歧化酶(SOD)活性检测进一步证明，由于四膜虫培养介质的不同，MWNTs 可对细胞显示出有毒性或无毒性。本工作提示，研究 MWNTs 和培养液中介质成分相互作用的生物效应，将有助于正确理解碳纳米管与生命体系相互作用的毒性机理。

Dependence of multi-walled carbon nanotubes cytotoxicity on culture medium

ZHU Ying RAN Tiecheng LI Yuguo GUO Jinxue LI Wenxin

Key words: Dependence, Multi-walled carbon nanotubes, *Tetrahymena pyriformi* , Cytotoxicity, Culture medium

This study has examined effects of multi-walled carbon nanotubes (MWNTs) on the growth of unicellular protozoan, *Tetrahymena pyriformis*. Contrary to findings by most investigations, our results indicated that MWNTs stimulated growth of the cells cultured in Proteose Peptone Yeast (PPY) extract medium. AFM images and thermogravimetric analysis (TGA) showed spontaneous formation of peptone-MWNTs conjugates in the medium by noncovalent binding. Images of fluorescent microscope showed that the fluorescence intensity detected for cells incubated in the solution containing fluorescently labeled peptone together with MWNTs was much higher than that for cells incubated in solution containing just fluorescently labeled peptone. Therefore, large amount uptake of the conjugates by *Tetrahymena pyriformis* was responsible for the growth stimulation. By replacing the PPY medium with a filtrated pond water (FPW) medium, however, growth inhibition of the cells exposed to MWNTs occurred. Measurements of malondialdehyde (MDA) level and superoxide dismutase (SOD) activity demonstrated further that MWNTs might be either toxic or nontoxic, depending on the culture medium for *Tetrahymena pyriformis*. The study on biological effects of interaction between MWNTs and some composites in culture medium would be helpful to understand the mechanisms on toxicity of carbon nanotubes to living systems.

激光诱导摄取多壁碳纳米管的四膜虫内部的气泡爆炸

诸 颖 陈 昆* 李文新

关键词 激光, 多壁碳纳米管(MWNTs), 纳米碳黑(CB), 纳米炸弹, 气泡爆炸, 梨形四膜虫

单壁碳纳米管(SWNTs)用作有效的纳米炸弹杀死癌细胞已受到很多关注，当波长为 800 nm 强度 200 mW/cm^2 的近红外光照射到细胞上，SWNTs 的光热传导效应使管束间孔隙中的水分子被加热而引发剧烈爆炸。

我们以单细胞原生动物梨形四膜虫作为试验模型，分别在多壁碳纳米管(MWNTs)和纳米碳黑(CB)溶液中温育，用波长 782 nm、强度 11.5 mW、光斑直径 1 μm 的激光研究其对细胞的作用，发现未用 MWNTs 处理的对照组细胞对光无任何反应，而 MWNTs 或 CB 溶液温育的细胞在激光照射时都被炸成碎片。激光作用于摄取有 CB 的细胞的过程相似于文献[1]：光能转化为 CB 内部热能，水的沸腾效应导致了细胞内部的爆炸。但激光照射到摄取有 MWNTs 的细胞时，引发了一系列缓慢而温和的爆炸，此现象和过程很委屈像气泡中的气体膨胀随后引起爆炸的过程。MWNTs 是良好的储气材料，细胞爆炸可归结于 MWNTs 上的热能使管腔内的气体膨胀。这种纳米炸弹在较低的温度下被引发，可对杀死癌细胞具有潜在应用。

Laser-induced gaseous bubble explosion inside *Tetrahymena pyriformis* ingesting multi-walled carbon nanotubes

ZHU Ying CHEN Kun* LI Wenxin

Keywords Laser, Multi-walled carbon nanotubes, Nanocarbon black, Nanobomb, Gaseous bubble explosion, *Tetrahymena pyriformis*

Single-walled carbon nanotubes (SWNTs) as potent nanobomb agents to kill cancer cells have received increasing attention. By irradiating the cells with near infrared light of about 800 nm and 200 mW/cm^2, dramatic explosion happens due to optothermal transition that heats the water molecule in nanopores of the SWNTs bundles.

Unicellular protozoan *Tetrahymena pyriformis* were incubated respectively in multi-walled carbon nanotubes (MWNTs) and nanocarbon black(CB) solutions. A Φ1μm laser beam of 782 nm and 11.5 mW was employed to study its interaction with the cells. While the cells untreated with MWNTs showed no response to the light, the cells treated with either MWNTs or CB were exploded into fragments by the laser. The phenomena and processes of the laser interaction with the CB-ingested cells were similar to those described in Ref.[1]. The photon energy deposited in the CB boiled water at over 100^{o}C and caused explosion inside the cells. However, we found a series of slow and gentle explosion in the MWNTs-ingested cells by the laser light, just like the phenomenon and processes of gaseous inflation and explosion of a bubble. As MWNTs are good gas storehouses, we propose that explosion occurring in the cells might be attributed to the absorbed air heated by the photon energy deposited in MWNTs. The nanobombs can be formed at relatively low temperatures, and may have potential application to kill cancer cells.

*中国科学院上海光学精密机械研究所;

Ref.[1] Balaji Panchapakesan, Shaoxin Lu, Kousik Sivakumar, *et al*. Nanobiotechnology, 2005,**1:**133-140

纳米药物 C_{60}-苯甲醛氮芥的体内分布及药效

冉铁成 刘瑞丽 诸 颖 徐晶莹 李文新 李晴暖

关键词 C_{60}-苯甲醛氮芥(C_{60}NM)，体内分布，药效

使用放射性 ^{125}I 标记的方法研究了 C_{60}-苯甲醛氮芥(C_{60}NM)的体内分布情况，并研究了 C_{60}-苯甲醛氮芥对肿瘤细胞及原位胃癌模型的疗效，结果发现 C_{60}-苯甲醛氮芥能很快直接进入血液或通过淋巴道进入血液，其中胃的摄取最高，经 1h 即高达 70%以上；药效研究结果表明与苯甲醛氮芥(NM)相比，C_{60} 的引入并没有提高氮芥对细胞的抑制率，甚至降低了对细胞的杀伤能力，而在体内，C_{60} 的引入提高了氮芥对机体肿瘤组织的杀伤作用。表 1 的数据表明，与其他几组相比，C_{60}-苯甲醛氮芥的抑瘤效果最好，可到 69.7%，并且 C_{60}-苯甲醛氮芥能有效抑制肿瘤细胞的腹膜转移和淋巴结转移。本工作得到的数据指出 C_{60}NM 是一个有效的淋巴靶向药物以及有效的胃癌靶向治疗药物。

Biodistribution and efficiency of nanopharmaceutical C_{60}-benzoyl nitrogen mustard

RAN Tiecheng LIU Ruili ZHU Ying XU Jingying LI Wenxin LI Qingnuan

Key words: C_{60}-benzoyl nitrogen mustard (C_{60}NM), In vivo distribution, Efficiency

In this work, biodistribution of C_{60}-benzoyl nitrogen mustard (C_{60}NM) was studied by labeling the compound with ^{125}I, and the efficiency of C_{60}NM on cancer cells and in situ gastric cancer model was studied, too. The results showed that C_{60}NM could enter blood system directly or through lymph system, and the uptake in stomach was the highest with uptake of more than 70% at one hour after injection. Incorporating with C_{60} did not increase but decrease the inhibition of cells in vitro. However, as shown in Table 1, incorporating with C_{60} did enhance the cancer killing ability. Compared with results of other groups, the cancer killing ability of C_{60}NM is much stronger with inhibition rate of 69.7%, at the same time C_{60}NM could inhibit cancer cells transfer to lymph nodes and peritoneum. The results indicate that C_{60}NM was an effective lymph-targeting and stomach cancer-targeting drug.

Table 1 The efficiency of C_{60}NM on cancer cells and in situ gastric cancer model

Group	Cases	Volume of in situ cancer /cm^2	Cancer inhibition rate	Peritoneum metastasis		Lymphadem metastasis	
				Cases	%	Cases	%
Saline	15	1.52±0.59	0	11/15	73.3	14/15	93.3
C_{60}	10	1.20±0.38	21.1	6/10	60.0	8/10	80.0
NM	10	1.01±0.41	33.6	4/10	40.0	5/10	50.0
Active carbon-NM	10	0.82±0.39	46.1	1/10	10.0	4/10	40.0
C_{60}NM	10	0.46±0.25	69.7	0/10	0	2/10	20.0

富勒烯苯甲醛氮芥对梨形四膜虫的毒性

冉铁成　诸 颖　李文新　李晴暖

关键词　梨形四膜虫，富勒烯(C_{60})，富勒烯苯甲醛氮芥(C_{60}NM)，氮芥(NM)，存活率，大核

本工作研究了富勒烯苯甲醛氮芥(C_{60}NM), 富勒烯(C_{60})和氮芥(NM)对活体单细胞原生动物梨形四膜虫的毒性。结果表明 C_{60}NM 和 C_{60} 能被四膜虫大量摄取。四膜虫的存活率和 C_{60}NM，C_{60}，NM 的浓度依赖关系被测定。荧光显微观察结果表明 C_{60}NM 和 NM 损伤了细胞的大核，而 C_{60} 对细胞则没有损伤。电子显微镜对细胞超微结构分析也表明 C_{60}NM 和 NM 损伤了细胞的大核。这些结果表明 C_{60}NM 和 NM 有相同的抗癌机制。对 IC_{50} 值进行比较，毒性大小顺序为 NM>C_{60}NM>C_{60}。我们的发现为 C_{60}NM 在淋巴靶向药物输运系统中的潜在应用提供了有用信息。

Toxicity of fullerene pyrrolidine benzoyl nitrogen mustard with *Tetrahymena pyriformis*

RAN Tiecheng　ZHU Ying　LI Wenxin　LI Qingnuan

Key words:　*Tetrahymena pyriformis*, Fullerene, Fullerene pyrrolidine benzoyl nitrogen mustard, Nitrogen mustard, Viability, Macronuclei

The toxicity of Fullerene Pyrrolidine Benzoyl Nitrogen Mustard (C_{60}NM), fullerene (C_{60}) and Nitrogen Mustard (NM) on living unicellular protozoan *Tetrahymena pyriformis* was studied. The results indicated that C_{60}NM and C_{60} were ingested largely by *Tetrahymena pyriformis*. The dose-effect dependence of viability of *Tetrahymena pyriformis* was determined on concentration of C_{60}NM, C_{60} and NM. The damages, detected by fluorescence microscopy, occurred on the macronuclei of the cells by C_{60}NM and NM, but no damage induced by C_{60} was detected. The ultra structural change found by electron microscopy revealed that the C_{60}NM and NM damaged the macronuclei of the cells. These facts indicate that C_{60}NM and NM have the same anti-cancer mechanism. With respect to the IC_{50} values, the sequence of toxicity was NM>C_{60}NM>C_{60}. Our findings also provide important information on the potential use of C_{60}NM in lymph target drug delivery systems.

功能化多壁碳纳米管在小鼠体内的分布

郭金学　李晴暖　李文新

关键词　碳纳米管，^{99m}Tc-CNTs-葡萄糖胺，体内分布

本工作首次合成了 ^{99m}Tc 标记的水溶性功能化碳纳米管 ^{99m}Tc-CNTs-葡萄糖胺，并研究了其在小鼠体内的生物分布和代谢情况。实验结果发现，^{99m}Tc-CNTs-葡萄糖胺在小鼠体内的分布特点是在胃、粪便和尿液中的分布高，而在肝脏和肾中不高,表明 ^{99m}Tc-CNTs-葡萄糖胺主要通过粪便和尿液进行排泄。功能化多壁碳纳米管体内分布的这些结果为其在生物医药领域的应用提供了有用的数据。

Biodistribution of functionalized multi-walled carbon nanotubes in mice

GUO Jinxue LI Qingnuan LI Wenxin

Key words: CNTs, ^{99m}Tc-CNTs-glucosamine, Biodistribution

In this work, water soluble ^{99m}Tc-CNTs-glucosamine was synthesized for the first time, and its biodistribution in mice was measured. The high level of radioactivity was found in stomach, dejection and urine, while very low level of radioactivity was found in liver and kidney. It is indicated that the ^{99m}Tc-CNTs-glucosamine was mainly excreted through feces and urine. All of these results on the biodistribution of functionalized multi-walled carbon nanotubes in mice provide useful data for its use in biomedical field.

功能化多壁碳纳米管对梨形四膜虫的不同的生物效应

郭金学 诸 颖 冉铁成 吴胜伟 李文新

关键词 多壁碳纳米管(p-MWNTs)，梨形四膜虫，γ 辐照，功能基团

经过纯化和 ^{60}Co γ 射线辐照后，多壁碳纳米管(p-MWNTs)用亚硫酰氯和葡萄糖胺进行化学修饰。对用葡萄糖胺修饰过的 p-MWNTs (g-MWNTs)进行元素分析和热重分析，结果表明 γ 辐照增加了 MWNTs 上连接的功能基团的浓度而导致其水溶性提高。分别检测嫁接了癸胺和葡萄糖胺的多壁碳纳米管(d-MWNTs 和 g-MWNTs)，对梨形四膜虫的生物活性。d-MWNTs 由于纳米管上嫁接的毒性基团癸胺浓度的增加而对细胞生长有抑制作用，而这种抑制作用与 γ 射线剂量有关。葡萄糖胺和 p-MWNTs 单独对细胞的生物学活性影响都较小，但 g-MWNTs 却对细胞有显著的生长促进作用。我们认为 g-MWNTs 亲水性的增加和纳米管与细胞培养液中主要营养物质—水溶性蛋白胨的非共价结合是导致四膜虫迅速生长的主要原因。因此在研究纳米管与活的生命体系的相互作用时，有必要考虑纳米管壁上所发生的物理和化学过程。

Different bio-response of functionalized multi-walled carbon nanotubes to *Tetrahymena pyriformis*

GUO Jinxue ZHU Ying RAN Tiecheng WU Shengwei LI Wenxin

Key words: Multi-walled carbon nanotubes (p-MWNTs), *Tetrahymena pyriformis,* γ-irradiation, Functional groups

After purification and irradiation with ^{60}Co γ-rays, the multi-walled carbon nanotubes (p-MWNTs) were subjected to chemical modification with thionyl chloride and glucosamine. Element analysis and thermogravimetric analysis for g-MWNTs, the p-MWNTs modified with glucosamine, indicated that γ-irradiation increased the concentration of functional groups bound to MWNTs, leading to enhance-

ment of the solubility in water. The multi-walled carbon nanotubes grafted in glucosamine as well as decylamine, g-MWNTs, and d-MWNTs were used to examine their biological response to *Tetrahymena pyriformis*, respectively. It was found that d-MWNTs showed a γ-ray dose-dependence of growth inhibition to the cells due to the increase of toxic decylamine concentration on the nanotubes. Although both glucosamine and p-MWNTs alone showed little biological activity, the g-MWNTs exhibited an apparent dose-dependence of growth stimulation. We proposed that rising hydrophilicity of the nanotubes and noncovalent binding between g-MWNTs and soluble peptone, a food of the cells in culture medium, were responsible for the growth stimulation to *Tetrahymena pyriformis*. Therefore in study of bio-effects of nanotubes on living system, it is necessary to take the physical and chemical processes on side-wall of the nanotubes into account.

粒径 3 nm 的 TiO_2 对小鼠的肺部损伤

李俊纲　李晴暖　徐晶莹　蔡小青　刘瑞丽　李永军　李文新

关键词　纳米颗粒，TiO_2，气管滴注，肺灌洗液，病理损伤，生化指标

微米级 TiO_2 是一种生物惰性物质，广泛应用于涂料、医药和化妆品工业。近几年纳米级 TiO_2 在人们日常生活中的应用越来越广泛。相关的研究表明尺寸是影响纳米材料毒性的一个重要因素，纳米级 TiO_2 在生产和应用过程中的安全性受到人们极大关注。

本实验对小鼠进行粒径 3 nm 的 TiO_2 的滴注，剂量分别为 0.01、0.1 和 1 mg/只。三天后，观察其肺部造成的损伤。实验组小鼠肺灌洗液中总蛋白和乳酸脱氢酶浓度比对照组略有增高。但是灌洗液中白蛋白浓度有明显增高，特别是滴注剂量为 1 mg/只的实验组的白蛋白浓度有极显著增高。各试验组中酸性磷酸酶和碱性磷酸酶的浓度均比正常组高，其中滴注剂量为 0.1 mg/只的实验组内酸性磷酸酶和碱性磷酸酶浓度比正常组有显著增高, 滴注剂量为 1 mg/只的实验组内酸性磷酸酶和碱性磷酸酶浓度比正常组有极显著增高。结合肺组织病理切片的结果，粒径 3 nm 的 TiO_2 对肺部造成的损伤表现为：肺泡巨噬细胞的过度激活和肺泡上皮 II 型细胞的过度增生造成肺泡壁增生变厚和结构的严重破坏，并伴有明显的肺气肿。

Pulmonary lesions induced by 3 nm TiO_2 particles in mice

LI Jungang　LI Qingnuan　XU Jingying　CAI Xiaoqing

LIU Ruili　LI Yongjun　LI Wenxin

Key words:　**N**anoparticles, TiO_2, Intratracheal instillation, Bronchoalveolar lavage fluid, Pathological lesions, Biochemical indices

TiO_2, being biologically inert, is a popular material in paint, pharmaceutical and cosmetics industries. Nanoscale TiO_2 is widely used nowadays. Studies demonstrated that the size of nanomaterial is an important factor for their toxicity, and nanoscale TiO_2 toxicity raised public concerns.

In this study, the pulmonary lesions induced by 3 nm TiO_2 primary particles with dosage of 0.01, 0.1 and 1 mg per mouse were investigated after the particles were intratracheally instilled into lung of

mice. Three days later, the concentrations of the total protein and lactate dehydrogenase in bronchoalveolar lavage fluid of all experimental groups was slightly higher than that in control group. However, the concentration of albumin were obviously higher than those of control group, especially for the 1-mg group, which increased significantly with $p<0.01$. The concentration of acid phosphatase and alkaline phosphatase were also higher, which increased significantly with $p<0.05$ in the 0.1-mg group and $p<0.01$ in the 1-mg group. Together with the pathological examination, the pathological lesions induced by 3 nm TiO_2 primary particles were mainly characterized by thickening of alveolar septa and destruction of general alveolar structure due to excessive activation of alveolar macrophages and proliferation of alveolar epithelium type Ⅱ cells, and emphysema around focal lesions.

多羟基富勒烯衍生物 $C_{60}(OH)_{24}$ 预防帕金森病的初步研究

蔡小青 刘中博* 贾海群* 李文新 刘健康*

关键词 富勒烯，$C_{60}(OH)_{24}$，MPP^+，氧化损伤，帕金森病

帕金森病是常见的老年疾病，其致病机制不明，但大多数认为与 MPTP 损伤基因缺陷、氧自由基损伤和线粒体损伤相关。富勒烯及其衍生物在生物医药方面的应用有广阔的前景，尤其是因其强的抗氧化性。我们采用 MPP^+诱导的帕金森急性细胞模型。细胞采用 SK-N-MC 人神经上皮瘤细胞。当给予的 $C_{60}(OH)_{24}$ 浓度大于 20 μmol/L 时，$C_{60}(OH)_{24}$ 对该帕金森细胞模型有较好的预防作用。MPP^+能引起线粒体膜电位下降，引起蛋白质氧化、DNA 损伤、体内一些抗氧化剂(GSH)活性下降等，50 μmol/L 的 $C_{60}(OH)_{24}$ 对上述指标均有较好的恢复作用。该项研究预示 C_{60} 的多羟基衍生物 $C_{60}(OH)_{24}$ 可能对帕金森病等老年性疾病有积极的预防作用。

Polyhydroxylated fullerene derivative $C_{60}(OH)_{24}$ prevents mitochondrial dysfunction and oxidative damage in MPP^+-induced cellular model of Parkinson's disease

CAI Xiaoqing LIU Zhongbo* JIA Haiqun* LI Wenxin LIU Jiankang*

Key words: Fullerene, $C_{60}(OH)_{24}$, MPP^+, Oxidative damage, Parkinson's disease

Parkinson's disease (PD), caused by the toxin 1-methyl-4-phenyl-1,2,3,6-tetrahydropyridine (MPTP) or by genetic defects, is associated with oxidative damage and mitochondrial dysfunction. Fullerene and its derivatives are promising candidates for biomedical applications, especially owing to their antioxidant activity. In the present study, we examined the protective effects of polyhydroxylated fullerene derivative $C_{60}(OH)_{24}$ in MPP^+–induced (500μmol/L, 24h) acute cellular PD model in SK-N-MC human neuroblastoma cells. Pretreatment with $C_{60}(OH)_{24}$ at the concentrations greater than 20μmol/L showed significant protective effects on MPP^+-induced decrease in mitochondrial membrane potential, increase in protein oxidation and oxidative DNA damage, and decrease in the level of antioxidant glutathione. These results provide a new promising direction for preventing PD and a new biomedical application of fullerene derivatives.

*中国科学院上海生命科学研究院营养科学研究所

用气管滴注法和呼吸法研究 MWCNT 对小鼠肺部的病理损伤

李俊纲 李晴暖 徐晶莹 蔡小青 刘瑞丽 李永军 李文新

关键词 多壁碳纳米管，气溶胶，气管滴注，呼吸，病理损伤，毒性

碳纳米管(CNTs)已可进行规模化生产，未经处理的 CNTs 浮尘可能对生产者有潜在的呼吸毒性。一些科研组用气管滴注法研究了其呼吸毒性，表明 CNTs 会对肺部造成严重的损伤。然而 CNTs 的气管滴注中，实验动物在短时间内局部大剂量被动染毒，这与实际生产中工人长时间低剂量染毒的情况有较大差异。我们用气管滴注和自然呼吸研究了多壁碳纳米管(MWCNTs)对小鼠支气管和肺泡造成的病理损伤。气管滴注试验中，每只小鼠滴注 0.05 mg MWCNTs，分布在支气管和肺泡内 MWCNTs 团聚物的尺寸相似。这些团聚物导致支气管内壁出现严重的炎症反应和肺泡的网状结构的严重破坏。自然呼吸试验中，小鼠暴露在平均浓度为 32.61 mg/m^3 的 MWCNTs 气溶胶中，在第 8、16 和 24 d， MWCNTs 在肺部的沉积剂量分别为 0.07、0.14 和 0.21 mg。沉积在肺泡内的大多数 MWCNTs 团聚物的尺寸小于沉积在支气管内的 MWCNTs 团聚物。这些团聚物致使肺泡壁增生变厚，但肺泡的整体结构仍保持着完整。此研究表明，滴注到肺部的 MWCNTs 和自然吸入到肺部的 MWCNTs 会诱发出不同的病理损伤，这可能缘于 MWCNTs 在肺内不同的尺寸和分布。

MWCNT-induced pathological lesions in mouse lungs by inhalation or intratracheal instillation

LI Jungang LI Qingnuan XU Jingying CAI Xiaoqing

LIU Ruili LI Yongjun LI Wenxin

Key words: Multi-walled carbon nanotubes (MWCNTs), Aerosol, Intratracheal instillation, Inhalation, Pathological lesions, Toxicity

Carbon nanotubes (CNTs) have been in industrial production. Unprocessed CNTs can become airborne and potentially reach into the lung. Studies on CNT pulmonary toxicity via intratrachaeal instillation of rodents have shown that CNTs could induce severe pulmonary lesions. However, intratracheal instillation of CNTs into the rodents with a single bolus dose in shorter time differs greatly from chronically inhaled CNTs by the workers. In this study, pathological lesions induced by MWCNTs in bronchi and alveoli of mice were studied by intratracheal instillation and inhalation. In the instillation groups of 0.05 mg MWCNTs per mouse, similar size clumps of MWCNTs were distributed in bronchi and alveoli. The clumps led to inflammation to the lining wall of bronchi and severe destruction of alveolar netted structure around them. The inhalation group was exposed to aerosolized MWCNTs of 32.61 mg/m^3. The intra-lung deposition doses were roughly 0.07, 0.14 and 0.21 mg on the 8th, 16th and 24th day, respectively. Most of aggregations of MWCNTs in the alveoli were smaller than that in bronchi. The aggregations induced proliferation and thickening of alveolar walls. Except for these moderate pathological lesions, no change in the general alveolar structure could be observed. The results demonstrated a difference in lung pathological lesions induced by instilled and inhaled MWCNTs. This may be due to different sizes and distributions of aggregations of MWCNTs in the lung.

一种新的纳米放射增敏剂：超氧化碳纳米管

杨建设 于伯章 李文新

关键词 放射增敏剂，超氧化物，多壁碳纳米管(MWCNTs)

肿瘤细胞氧含量越低，就越难于治疗；而高氧含量则有利于肿瘤的放射治疗，因为机体组织中的水被射线辐解产生大量的自由基，这是直接杀死癌细胞的根源。我们制备了过硫酸铵处理的MWCNTs，在其表面引入了丰富的过氧基团，它们在低剂量照射下即可释放过氧自由基，起到辐射增敏作用。扫描电镜观察表明，以0、10、25、50、100和200 μg/mL的浓度把原始的和过硫酸铵处理的碳纳米管加入到脑胶质瘤细胞C6的培养基中，两种物质均可进入细胞内。细胞的存活率测定结果显示，两种物质的进入对未照射细胞存活无影响。但^{60}Co γ射线照射0、1、2、4或6 Gy后，原始碳管组细胞存活率的下降远低于过硫酸铵处理组，相对于前者，后者的增敏效率达到8100倍。加入原始碳纳米管后，其细胞存活率结果与我们以前的研究相一致，说明原始碳纳米管对于射线照射没有增效作用，之所以过硫酸铵处理的碳纳米管掺入细胞培养基经射线照射后表现出很强的增敏效应，是与引入碳纳米管表面的过氧基团及其在射线照射下形成强自由基密不可分的。

A new nano-scaled radiosensitizer: Superoxide functionalized carbon nanotubes

YANG Jianshe YU Bozhang LI Wenxin

Key words: Radiosensitizer, Superoxide, Carbon nanotubes

Solid tumors have areas of very low oxygenation, or hypoxia, because the cells growth faster than the blood supply can keep up with, especially when blood flow is sluggish with very tortuous vessels, and the cells become further away from blood over oxygen diffusion distance of 100~150 μm. These hypoxic cells are resistant to both radiations and anticancer drugs. They also promote malignant progression and make the tumors more likely to metastasize, or spread throughout the body. This means that the more hypoxic the tumor, the harder it is to cure. Further more, hyperoxia status will benefit radiotherapy due to the large amount of free radicals resulting from radiolysis, which was commonly regarded as the direct killer for tumor cells when the low linear energy transfer radiations, such as X and gamma rays were applied.

We prepared MWCNTs fabricated with ammonium persulfate. Pure carbon nanotubes (*p*-CNT) and functionalized carbon nanotubes (*f*-CNT) were added into cell culture medium with different concentrations ranging from 0 to 100 μg/mL, and irradiated by ^{60}Co γ rays to 0~6 Gy. We found that two types of CNTs entered into cells after 4h of incubation under confocal microscope, but no significant cell death was observed in the control. In both groups of C6 glioma cells exposed to ^{60}Co γ rays, cell survival fraction decreased linear-quadratically. This agrees with our previous studies. For the *p*-CNT groups, there was 40% cells survived at 6Gy dose point, while for *f* -CNT group at the same dosage, there was just 0.005% cell survival. Thus the radiosensitization effectiveness of *f*-CNT was estimated at about 8100.

戈那瑞林性腺释放激素修饰的 MWCNT 体外杀伤癌细胞的能力

于伯章 杨建设 李文新

关键词 多壁碳纳米管，戈那瑞林性腺释放激素(GnRH)，恶性肿瘤细胞

经氧化和抛光的多壁碳纳米管(MWCNTs)弥散在水中，得到纯净、超短、羧基功能化颗粒的稳定悬浮液。能够在多种癌细胞中高度表达的戈那瑞林性腺释放激素(GnRH)通过酰胺键与 MWCNTs 结合形成融合物(MWCNTs-GnRH)。MWCNTs-GnRH 用 UV-vis、PL 和元素分析表征。UV-vis 和 PL 光谱表明共价键修饰的 GnRH 通过 π 填充能够吸附在 MWCNTs 表面，引起 UV-vis 和 PL 光谱红移。而 MWCNTs 和 GnRH 混合物则没有这种红移特征，对共价键修饰提供了有力支撑。元素分析表明 MWCNTs 表面被 GnRH 覆盖的有效表面积约 0.7%。非毒性的 GnRH 和 MWCNTs 都能够进入 DU 145 细胞。相反 GnRH-MWCNTs 能够进入该细胞并显示毒性。结果表明通过非毒性的 GnRH 和 MWCNTs 构建的这种新的毒性材料有杀死恶性肿瘤细胞的能力。

In vitro capability of multi-walled carbon nanotubes modified with gonadotrophin releasing hormone for killing cancer cells

YU Bozhang YANG Jianshe LI Wenxin

Key words: Multi-walled carbon nanotubes, Gonadotrophin releasing hormone, Malignant cells

Oxidized and polished multi-walled carbon nanotubes (MWCNTs) were dispersed in aqueous solution, providing a highly stable suspension of purified, shortened, and functionalized carboxylic acid nanotubes. A gonadotrophin releasing hormone (GnRH), which was over- expressed in the plasma membrane of several types of cancer cells, was covalently anchored onto the surface of the oxidized MWCNTs via an amide linkage. The MWCNTs modified with GnRH (MWCNTs-GnRH) were characterized by UV-vis and emission spectra, and elemental analysis. Red-shift in the optical spectra consisting of the UV-vis absorption and emission spectra with the attraction of GnRH on the surface of the MWCNTs via π stacking were observed. However there was no property for a direct mixture of MWCNTs and GnRH, supporting the successful modification. Elemental analysis revealed that the sidewall coverage of MWCNTs by the GnRH was about 0.7% of the available surface area. The non toxic GnRH and MWCNTs can separately enter the DU 145 cells. In contrast, GnRH-MWCNTs entered the cells and showed toxicity in the malignant cells. These results showed that the newly formed toxic material had potential ability to kill the malignant cells with just a simple covalent bonding of the two.

单个纳米颗粒“蘸笔”纳米刻蚀术

汪 颖 张 益 李 宾 吕军鸿 胡 钧

关键词 蘸笔纳米刻蚀术, 纳米颗粒, 原子力显微镜

以特定方式操纵单个纳米颗粒或单分子在纳米电子学和量子光学等方面极有应用潜力。本文用原子力显微镜针尖拾取单个纳米颗粒，将它精确可控地放在特定位置上。其以一次一颗的方式转移纳米颗粒，故称为单个纳米颗粒“蘸笔”纳米刻蚀技术。图 1 为此法构建的纳米图形。

Capturing and depositing a single nano-object at a time: Single particle dip-pen nanolithography

WANG Ying ZHANG Yi LI Bin LÜ Junhong HU Jun

Key words: DPN, Nanoparticle, AFM

Handling single nano-object and single molecule in a desired manner is a great challenge. Advances in methodology for precisely addressing individual nanoparticle will greatly facilitate their applications particularly in nanoelectronics and quantum optics. A novel technique for transferring nanoparticles in a one-particle-at-a-time fashion, termed as Single Particle Dip-pen Nanolithography (SP-DPN), was developed. It employs an atomic force microscope (AFM) tip to “grab” individual gold nanoparticle on a surface. The nanoparticle attached to the AFM tips can be controllably released and re-deposited site-specifically on the surface. Patterns composed of single gold particles were fabricated.

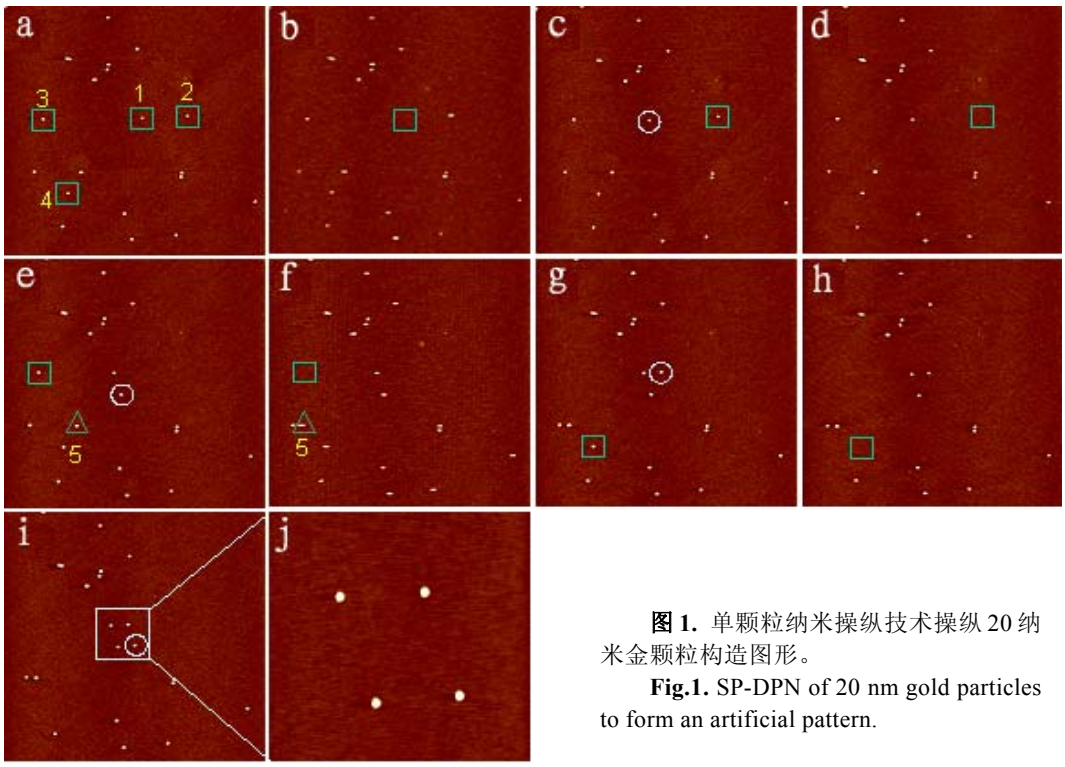

图 1. 单颗粒纳米操纵技术操纵 20 纳米金颗粒构造图形。

Fig.1. SP-DPN of 20 nm gold particles to form an artificial pattern.

一种有利于纳米操纵的 AFM 针尖物理修饰方法

王 鹏 吕军鸿 汪 颖 张 益 胡 钧

关键词 原子力显微镜，拾取，物理修饰

本文发展了一种使用 AFM 的负提升模式将针尖“压”在衬底上再进行快速磨损的物理修饰方法。此法可大幅度增加针尖的曲率半径，使其在捕获纳米粒子的过程中增加与纳米粒子间的接触面积，从而增大针尖与粒子间的吸附力，提高 AFM 针尖捕获单个纳米粒子的成功率。经扫描电镜测定和理论计算，修饰后的针尖与纳米粒子间的吸附力较修饰前提高约 1.8 倍。实验使用的纳米粒子是 Φ20 nm 左右的腺相关伴随病毒(adeno-associate virus, AAV)颗粒。

设针尖半径为 R_t，粒子半径为 R_p，则针尖与粒子间的吸附力为：$F_1 = 4\pi\gamma_{sv}R_tR_p/(R_t+R_p)$，其中，$\gamma_{sv}$ 是针尖与粒子间的界面能。因此，要提高针尖捕获纳米粒子的几率就需曲率半径较大的针尖。为了获得大半径针尖，我们对针尖进行如下的物理修饰：以裸云母为衬底，待 AFM 稳定成像后选定 300 nm×300 nm 的空白区域，使用 AFM 的负提升模式降低针尖到–100 nm~ –150 nm，改变扫描角度，同时将扫描速率设定为 100 Hz 左右，扫描时间约为 1 min，针尖与云母磨损后而得到“粗”针尖。对针尖的物理修饰，增强了针尖捕获纳米粒子的能力，从而有望建立一种用 AFM 针尖直接分离不同类型的颗粒、蛋白和病毒等纳米粒子的方法。

Physical modification of AFM tips to facilitate nano-manipulation

WANG Peng LU Junhong WANG Ying ZHANG Yi HU Jun

Key words: Atomic force microscope (AFM), Pick up, Physical modification

Individual nano-materials can be directly manipulated by using nano-scale tips of atomic force microscope (AFM). For example, nanoparticles as well as DNA molecules have been captured by the AFM tips and isolated from substrates. In this study, we report a physical method for modification of the AFM tips to improve the nanomanipulation efficiency. By rapidly rubbing the AFM tips on solid substrate, the radius of the tips can increase, which results in increasing of attractive force between the tips and nano-materials. This assumption is based on the following equation: $F_1 = 4\pi\gamma_{sv}R_tR_p/(R_t+R_p)$, where F_t is the attractive tip -particle force, R_t is the radius of tip, R_p is the radius of nano-particle, and γ_{sv} denotes the interfacial energy of solid-vapor interface.

In the current study, we modified the tips with the following procedure: first, a tip was pushed onto a mica substrate under the control of AFM software through negative lift mode; then, the tip scanned the surface for 1min with a scan angle of 90°, a scan rate of about 100 Hz, and a scan size of 300nm×300nm. The SEM photos show obvious difference between the tips with or without modification. The interactive force between modified tips and virus nano-particles with diameter of about 20nm was found 180% larger than that of tips without modification. Therefore, the probability of trapping nano-particles by AFM tip is increased. We expect that varieties of nano-particles, including proteins and virus, could be manipulated and isolated individually by AFM tips modified by using our method.

甘油对病毒在云母表面上分散的促进作用

王 鹏 吕军鸿 张 益 李 海 王化宾 张 峰 米丽娟 胡 钧

关键词 甘油，病毒，分散，原子力显微镜

原子力显微镜(AFM)已用于病毒形貌、病毒物理性质等研究。但病毒在溶液中很易团聚成较大的颗粒，且在衬底表面上也趋于积聚成团簇，从而妨碍了对病毒的后续研究。腺重组相关伴随病毒血清 2 型(rAAV2)是一种单链 DNA 病毒，直径约 20 nm，在基因治疗方面有重要应用。在大部分情况中，病毒中的遗传物质都被蛋白外壳所包被，这样病毒颗粒就可看成一个蛋白整体。甘油能够增加蛋白在溶液中的溶解程度，对生物也无毒性，还具有促进蛋白分散的功能。我们将一定量的甘油加入病毒溶液中，观察其是否可促进病毒在云母表面上的分散。本研究使用直接吸附法制备样品，未修饰的裸云母为衬底，在病毒溶液中掺入一定量的甘油，制成样品。检测发现甘油确实具有分散病毒颗粒的功效。据我们所知，这是首次报道少量甘油具有促进病毒分散的作用。

Glycerol facilitates disaggregation of adeno-associated virus on mica surface

WANG Peng LU Junhong ZHANG Yi LI Hai WANG Huabin ZHANG Feng

MI Lijuan HU Jun

Key words: Glycerol, Virus, Dispersion, Atomic force microscope

Atomic force microscope (AFM) can be used to image virus without complex process of chemical fixation, dehydration, staining or coating with heavy metals. However, viruses have tendency to agglomerate irreversibly in aqueous solutions, and to form two-dimension clusters and arrays on a surface regardless of their concentration. This hampers the AFM virus study. Recombinant adeno-associated virus serotype 2 (rAAV2) is small single-stranded DNA virus of the Dependovirus genus among the four Parvoviridae family genuses. The virion icosahedral proteinaceous shell is approximately 20nm in diameter. Recombinant adeno-associated virus serotype 2 vectors have been applied in clinical gene therapy. In view of the importance of rAAV2 in clinical application, varieties of studies about it have been conducted, including the analysis of the interaction between AAV2 and heparan sulfate by AFM.

To disperse virus, we propose to use glycerol, a cosolvent that can prevent protein aggregation. As virus genome is usually packaged in a protein shell and a whole virion can be considered as a protein particle, we speculate that glycerol can possibly facilitate virus disaggregating. Adeno-associated virus (AAV) was used as the model system. AFM and dynamic light scattering (DLS) were used to reveal the aggregation information. It was found that, by adding a proper amount of glycerol into rAAV2 solution, well-separated virus particles could be obtained on bare mica. This is vital for further single virus studies. The concentration of glycerol has an obvious influence on the dispersion of virus particles and the optimized concentrations range from 1% to 3% (v/v). In addition, the glycerol layers may help the attachment and dispersion of virus particles on mica.

纳米粒子 PCR 中纳米金与聚合酶相互作用机制探讨

米丽娟 朱红平 张晓东* 胡 钧 樊春海

关键词 PCR，纳米金，聚合酶，机制

纳米粒子 PCR 可提高 DNA 扩增特异性、扩增灵敏度与反应速度。本文以质粒 pBR322/pst I 为模板，扩增一段 309 bp 的 DNA 序列，扩增产物与 DL-2000 同时电泳，对比 DNA 的荧光强度，可计算 PCR 的产物量。对 PCR 体系 DNA 聚合酶和纳米金用量的研究表明，它们的相互作用可显著影响 PCR 过程：1) 增加聚合酶用量可消除纳米金导致的抑制；2) 纳米金可改变 DNA 聚合酶浓度-酶活性曲线的平衡点，增加 DNA 的合成量；3) 高浓度聚合酶的活性可通过添加纳米金得到恢复。由此，纳米金调控 DNA 聚合酶影响 PCR 过程的机理可简化为：

$$\text{NP-polymerase} \overset{\pm\text{NPs}}{\rightleftharpoons} \text{Polymerase} \overset{\pm\text{PTJ}}{\rightleftharpoons} \text{PTJ-polymerase} \longrightarrow \text{DNA product}$$

由此，纳米金优化 PCR 之所以有最佳浓度，是因为纳米金与聚合酶能可逆结合。聚合酶的结合位点是引物-模板形成的单双链结合区(PTJ)，纳米金通过调控游离聚合酶浓度影响 PCR 的进行性和 DNA 的扩增。此研究有利于开拓 PCR 的新方向及其在生物医学领域的应用。

Investigation of the interaction between gold nanoparticles and DNA polymerase in nanoparticle PCR

MI Lijuan ZHU Hongping ZHANG Xiaodong* HU Jun FAN Chunhai

Key words: PCR, Au(Gold) nanoparticle, polymerase, mechanism

Nanoparticle PCR optimizes DNA amplification with improved specificity, sensitivity and extending rate. Mechanisms proposed include interaction between gold nanoparticles (AuNPs) and DNA and heat transfer property of AuNPs. In this paper, we amplified a target fragment of 309 bp from pBR322 DNA/pst I markers to study the AuNPs effects. Intensity of the ethidium bromide staining and electrophoretic mobility of the PCR product were compared with corresponding band of DL-2000, and the weight of DNA synthesis was calculated. The interaction between AuNPs and DNA polymerase influenced the PCR significantly: 1) increased DNA polymerase eliminated inhibitory effects of excess AuNPs, 2) yield of the desired PCR product increased and the optimum concentration of DNA polymerase changed with the help of AuNPs, and 3) while excess polymerase might inhibit amplification efficiency, AuNPs could reverse this process to increase the PCR yield. The results suggest a mechanism that AuNPs might modulate the activity of polymerase and improve PCR amplification by:

$$\text{NP-polymerase} \overset{\pm\text{NPs}}{\rightleftharpoons} \text{Polymerase} \overset{\pm\text{PTJ}}{\rightleftharpoons} \text{PTJ-polymerase} \longrightarrow \text{DNA product}$$

This hypothesis clarifies the optimum point of AuNPs concentration. The key is reversible binding of AuNPs and free-polymerase. As the binding site of polymerase is primer-template junction (PTJ), by modulating the dynamic equilibrium of binding polymerase with PTJ, the PCR processivity and DNA synthesis can be affected. The study will help to elucidate mechanisms of nanoparticle PCR, so as to explore new ways of optimizing PCR for applying nanoparticle PCR into biomedicine.

*上海交通大学

单个黄原胶分子径向压缩特性的研究

王化斌 周星飞[1] 安红杰[2] 孙洁林[3] 张 益 胡钧

关键词 黄原胶，径向压缩特性，振动模式扫描极化力显微镜(VSPFM)

细长的生物大分子如 DNA 的弹性主要分纵向拉伸弹性、横向压缩弹性以及扭转弹性。人们已对拉伸弹性和扭转弹性作了大量研究，但对压缩弹性的研究还未有报导。在研究碳纳米管和纳米颗粒的压缩特性时，发现常用工作模式下的原子力显微镜的针尖刚接触被测物时，可使被测纳米颗粒产生约 0.5 nm 的形变，不适用研究细小柔软的生物大分子的压缩性质。

我们发展了振动模式扫描极化力显微镜，其针尖与样品的作用力从零到数纳牛连续可调，能稳定成像, 可定量测量单个生物大分子在外力作用下的径向压缩特性。与 AFM 实验中常用作生物分子衬底的镍离子修饰的云母相比，在生物大分子压缩特性测量方面，高序热解石墨(HOPG)具有明显的优势。它的同层面原子级平整特性和本身具有的疏水性可以减少衬底导致的实验误差。我们以 HOPG 为衬底，用 VSPFM 技术研究了多糖分子黄原胶的压缩特性。发现当压力小于 0.4 nN 时，黄原胶分子的弹性模量约为 20~100 MPa。此研究对深入了解生物分子的生物功能与机械特性的关系具有重要意义。

Radial compression elasticity of single xanthan molecule

WANG Huabin ZHOU Xingfei[1] AN Hongjie[2] SUN Jielin[3] ZHANG Yi HU Jun

Key words: Xanthan, Radial compression, Vibrating scanning polarization force microscopy

Elastic properties of single DNA molecules have attracted enormous attention, and direct measurements of mechanical properties of DNA will aid in controlling the final structure and mechanical properties of the constructed DNA-based structures. The stretching and twisting properties of DNA have been extensively investigated by optical tweezers, magnetic beads, atomic force microscope (AFM), etc. However, for full understanding the elastic properties and their correlation to biological functions of DNA, the radial compression properties of DNA should be included. AFM measures the forces between the tip and the sample. But an AFM in contact mode and tapping mode results in deformation of the sample at the nanometer scale, and is incapable of investigating small deformation of soft bio-macromolecules.

We developed a technique termed vibrating scanning polarization force microscopy (VSPFM). The biggest advantage of VSPFM is its stable performance in both the non-contact and tapping modes, which renders it a potential for imaging soft specimens with very small forces. In this study, xanthan molecules were aligned on highly oriented pyrolytic graphite surface and probed with vibrating scanning polarization force microscopy, which allows for pressing small and soft biomacromolecules with reliable performance. The nanomechanical response was analyzed in the terms of sequential deformation of xanthan molecules. The effective elastic moduli of xanthan molecules are estimated to be about 20~100 MPa under loads below 0.4 nN. This study would provide useful information for a better understanding of the relation between mechanical properties and functions of biomolecules.

[1]宁波大学物理系; [2]天津大学; [3]上海交通大学

纳米粒子 PCR 产物的纯化及 AFM 观察

米丽娟 李 宾 周化岚 王化斌 胡 钧

关键词 PCR，纳米金，DNA 纯化，原子力显微镜

适量浓度的纳米金粒子(AuNPs)可显著改善 PCR 扩增的特异性，提高扩增的灵敏度和反应速度。AuNPs 优化的 PCR 产物中常有微量红色沉淀，但关于纯化 PCR 产物的方法是否合适以及是否须建立针对该 PCR 产物的纯化方法，尚未见相关报道。我们制备了常规 PCR 产物并按照前期的优化比例制备了纳米粒子 PCR 产物，以比较采用不同纯化方法后纳米粒子 PCR 产物的纯化效率。结果表明，常规 PCR 产物的纯化效率为 84.52%，按常规方法纯化纳米粒子 PCR 产物，纯化效率达 92.07%，但 AuNPs 的存在降低了扩增产物的纯度，故用高速离心去除 AuNPs 再乙醇沉淀，产物纯化效率降低为 76.27%，分离的 AuNPs 中约有 4.81%的 DNA。氨丙基三乙氧基硅烷(APS)修饰的云母表面可较好地吸附 DNA，利用轻敲模式原子力显微镜 (TMAFM)观察 APS 云母上的纳米粒子 PCR 纯化产物，发现纳米粒子 PCR 中的纳米金相对于 DNA 产物仅占很小比例，未对大量扩增产物造成影响；但分离大量扩增产物，AuNPs 中的极少量 DNA 形貌会受影响，类似 AFM 操纵时卷曲状态的 DNA。高速离心后再纯化的 DNA 没有发生可辨别的显著变化。AuNPs 可优化扩增过程，对于一些非特异或产量较低的扩增体系，纯化的效率仍可保持较高的水平。

Purification of nanoparticle PCR products and their topography observed with AFM

MI Lijuan LI Bin ZHOU Hualan WANG Huabin HU Jun

Key words: PCR, Au(Gold) nanoparticle, DNA purification, AFM

Nanoparticle PCR (NP-PCR) is a new method to optimize PCR amplification. Suitable amount of Au nanoparticles (AuNPs) can improve specificity, sensitivity and extension rate of PCR. However, AuNPs are precipitated incompletely at the end of amplification. How to eliminate the effect of AuNPs on PCR products is still a question. In this paper, we compare efficiency of purifying NP-PCR products with different methods. For comparing the difference between conventional PCR and NP-PCR products, ethanol deposition method and atomic force microscope (AFM) were applied. The results showed that 84.52% DNA were purified in conventional PCR, while 92.07% DNA mixed with AuNPs in NP-PCR remained after ethanol deposition. High speed centrifugation before ethanol deposition was effective to remove AuNPs, but the purification efficiency was 76.27%, with a co-precipitation of 4.81% DNA in the centrifuged AuNPs. Topographies of the DNA products were observed with AFM. Aminopropyl triethoxysilane (APS) modified mica, which enhances DNA adsorption, is a suitable substrate to observe DNA with tapping mode AFM (TMAFM). Most of the DNA products in NP-PCR purified directly by routing method remain almost free due to less effect of nanoparticales, while topographies of a little amount of DNA subsided with AuNPs, just like a curved DNA by a manipulation step. DNA products, with AuNPs eliminated by a high speed of centrifugation were consistent with those in conventional PCR. This simple and efficient purification method is potentially useful because of wide use of NP-PCR, especially in non-specific or low yield PCR system.

衬底的亲/疏水性对单个 DNA 分子高度测量的影响

王化斌 周星飞[1] 安红杰[2] 郭云昌 孙洁林[3] 张 益 胡 钧

关键词 衬底，亲/疏水，DNA 分子，高度测量

原子力显微镜(AFM)可研究生物分子间的相互作用及形变。利用 AFM 在仿生物介面的固体表面研究生物分子的形貌，分析生物分子间的作用机理，是研究热点之一。但是，仿生物介面的固体表面对 DNA 分子形貌影响的系统研究，还未见报道。我们用轻敲模式原子力显微镜(TMAFM)与振动模式扫描极化力显微镜(VSPFM)研究了亲水性的裸云母和疏水性的高序热解石墨衬底对双链 DNA 分子高度测量的影响。对制备在裸云母和高序热解石墨(HOPG)上的 DNA 分子的高度的统计结果为：在 TMAFM 下，裸云母上 DNA 分子的高度为 0.80±0.09 nm, HOPG 上 DNA 分子的高度为 0.51±0.06 nm； 用 VSPFM 方法测量，裸云母上 DNA 分子的高度为 1.56±0.10 nm, HOPG 上 DNA 分子的高度为 1.22±0.10 nm。分析表明，衬底的亲/疏水性对 DNA 分子的测量高度有显著影响，疏水衬底上 DNA 分子测得的高度较低。本研究将有利于理解 DNA 与其它生物大分子之间的相互作用，同时，也有助于解释为什么实验中观测到的 DNA 分子高度总是低于其理论值。

Effects of substrate hydrophobicity/hydrophilicity on the height measurement of individual DNA molecules

WANG Huabin ZHOU Xingfei[1] AN Hongjie[2] GUO Yunchang

SUN Jielin[3] ZHANG Yi HU Jun

Key words: Substrate, Hydrophobicity/hydrophilicity, DNA molecule, Height measurement

Atomic force microscopy (AFM) allows direct visualization of native biological samples in various conditions with high resolution and permits direct detection of intermolecular forces at the single molecule level. AFMs are used to explore mechanism of biomolecular interactions by examining the morphological variation of target molecules adsorbed on biomimetic substrates of hydrophilic mica, hydrophobic graphite, poly-L-lysine coated mica and borosilicate glass. Effects of hydrophobicity/hydrophilicity of biomimetic substrates on the morphology of proteins were systematically investigated, indicating that the hydrophobicity/hydrophilicity can greatly influence the morphology of proteins. However, little has been addressed to investigate the influence of hydrophobicity/hydrophilicity of biomimetic substrates on the morphology of DNA molecules. Taking HOPG and mica as biomimetic substrates, we investigated effects of hydrophobicity/ hydrophilicity of substrates on the height measurement of individual ds-DNA molecules with taping mode AFM (TMAFM) and vibrating mode scanning polarization force microscopy (VSPFM). By TMAFM, the height of ds-DNA adsorbed on bare mica is 0.80±0.09 nm, while the height of ds-DNA on highly oriented pyrolytic graphite (HOPG) is 0.51±0.06 nm. By VSPFM, the heights of ds-DNA adsorbed on the two substrates are 1.56±0.10 nm and 1.22±0.10 nm, respectively. The height of ds-DNA on hydrophobic HOPG is much lower than that on hydrophilic substrate (bare mica), indicating that substrate hydrophobicity/hydrophilicity can greatly influence the height measurement of DNA molecules.

[1] 宁波大学物理系; [2]天津大学; [3]上海交通大学

DNA 纳米结构仿中国地图

钱璐璐* 汪 颖 张 钊* 赵 健* 潘 敦 张 益
刘 强* 樊春海 胡 钧 贺 林*

关键词 DNA，折纸术，纳米结构，中国地图，原子力显微镜

采用 DNA 构造了纳米尺度的中国地图形状。所构造的纳米结构由 DNA 折叠而成，尺寸约 150nm。通过原子力显微镜观测到的图形与设计图形几乎完全一致。该图形的构造方法采用了 Rothemund 于 2006 年发明的 DNA 折纸术。该研究证明了 DNA 折纸术具有构造几乎任何复杂二维纳米级图形的能力，为基于自下而上方法的纳米构造技术提供了新方法。

Analogic China map constructed by DNA

QIAN Lulu* WANG Ying ZHANG Zhao* ZHAO Jian* PAN Dun
ZHANG Yi LIU Qiang* FAN Chunhai HU Jun HE Lin*

Key words: DNA, Origami, Nanostructure, China map, AFM

In this research, a nanoscale DNA structure of analogic China map was created. The designed nanostructure of roughly 150nm in size with a spatial resolution of 6nm was constructed by just folding DNA. Its atomic force microscopic (AFM) image is almost identical to the designed shape. The DNA origami technology invented by Rothemund in 2006 was employed in constructing the shape. The results confirm the capability of DNA origami for constructing almost any complicated shape, and provide a new bottom-up method for constructing nanostructures.

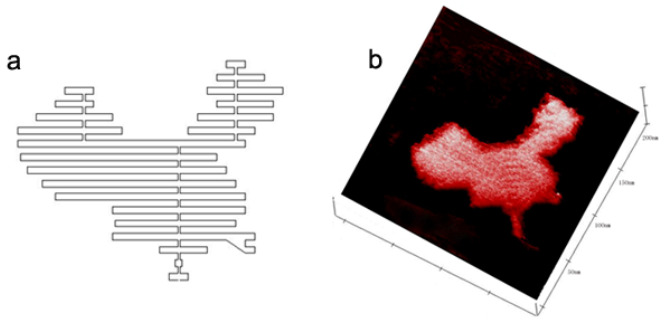

Fig.1 China map constructed by DNA origami, a) The designed scaffold of the main part of China map, b) AFM image of a well-formed DNA analogic main part of China map

*上海交通大学

纳米气泡对 TiO_2 薄膜光催化效率的影响

沈广霞 叶 鸣 张 益 胡 钧

关键词 纳米气泡，光催化，溶胶-凝胶法，纳米 TiO_2 薄膜

固液界面存在纳米气泡，这对许多领域(如界面的疏水长程力、流体边界滑移、蛋白质快速折叠与组装，胶体体系的稳定性等)产生重要的影响。本工作从实际应用的角度出发，探索纳米气泡对 TiO_2 光催化效率的影响。TiO_2 光催化性质一直是一个研究热点，其主要问题是光催化效率比较低，而效率与单位有效面积上的光电子密度、电子转移速率密切相关。在暗态条件下，轻敲模式原子力显微镜(TMAFM)扫描时未发现 TiO_2 薄膜界面上有纳米气泡吸附，激光照射样品约 1h 后界面上出现纳米气泡，随时间延长气泡数量逐渐增加; 同时，在紫外光照射下，纳米膜界面也发现吸附一定数量的气泡。我们认为界面上纳米气泡的存在可能是光催化效率较低的原因之一。

Effects of nanobubbles at the interface on TiO_2 photocatalytic efficiency

SHEN Guangxia YE Ming ZHANG Yi HU Jun

Key words: Nanobubble, Photocatalyst, TiO_2 coatings

The interface bubble hypothesis has been used to rationalize the mysterious long-range hydrophobic attractive force. Until 2001, the first series of Atom Force Microscopy (AFM) images have been reported, which strongly supported the presence of nanobubbles. Subsequently, several reproducible methods to create nanobubbles have been developed which provided opportunity for studying the properties of nanobubbles. More recently, Zhang and coworkers have created CO_2 nanobubbles at the interface of HOPG by exchanging ethanol and water, and determined the chemical identity, phase state and density of nanobubbles via infrared spectroscopy (IR) and Surface Plasmon Resonance (SPR).

Nanobubbles were also suggested to be associated with a wide range of applications such as a long-range attractive force, the slippage of simple fluids near a wall, fast folding and assembly of proteins and stability of colloidal systems. In this work, we consider a practical TiO_2 photocatalytic process. It is well known that photocatalytic property of TiO_2 has been one of hotspots and its photocatalytic efficiency strongly depends on the properties of the coating interface. By using tapping mode atomic force microscope (TMAFM), no nanobubbles were detected at TiO_2 coating interface in a dark condition. But an increasing number of nanobubbles were observed at the coating interface along with a rising temperature of the solution induced by AFM laser. On UV illumination, an amount of nanobubbles were present at the coating-water interface in our experiments. Therefore, we think the nanobubbles at the interface might be one of the reasons for the low efficiency of TiO_2 photocatalysis.

硅离子束诱导碳纳米线网络的制备

倪志春 李勤涛 朱德彰 巩金龙

关键词 碳纳米管，辐照，缺陷，碳纳米线

采用能量为 40keV 的硅离子束在室温下辐照多壁碳纳米管，利用扫描电子显微镜，透射电子显微镜和拉曼光谱对离子束辐照后的碳纳米管的形貌特征和结构变化进行了细致观察。结果表明在经过一定剂量的离子束辐照后，碳纳米管将完全转变为非晶碳纳米线，尤其重要的是碳纳米线

网络的形成。在此基础上我们对碳纳米线网络的形成过程和机制进行了探索。研究结果表明碳纳米线网络的形成要经过以下三个阶段：碳纳米管的局部非晶化、简单分子连接结的形成和碳纳米网络的形成。我们的研究结果表明利用离子束技术可以实现纳米器件的微互连，从而实现将来的更大规模、更高集成度器件的制作。此外，这些碳纳米线网络可用于在高温、耐腐蚀的环境中使用的过滤膜。

Fabrication of carbon nanowire networks by Si ion bombardment

NI Zhichun LI Qintao ZHU Dezhang GONG Jinlong

Key words: Carbon nanotubes, Irradiation, Defects, Carbon nanowires

Multiwalled carbon nanotubes were irradiated by 40keV Si ion beams to different doses. The radiation-induced structural transformation was characterized by scanning electron microscopy, transmission electron microscopy, and Raman spectroscopy. The formation of amorphous carbon nanowire and carbon nanowire networks is clearly confirmed. The processes of structural evolution and corresponding mechanism are studied. The formation of carbon nanowire networks proceeds through three periods: local amorphization of nanotubes, formation of simple junctions, and the formation of networks. The results show that the ion irradiation technique makes the fabrication of interconnection among the nanodevices possible in large-scale fabrication of nanodevices. This technique can also be used for fabricating nano-membrane, which is used in higher temperature and erosion-resistant conditions with friendlier biocompatibility, compared with traditional membranes. Further work is to precisely control the shape and dimension of networks, and to experimentally measure the electrical transport and flux in membrane.

碳纳米管的离子束焊接

倪志春 李勤涛 闫 隆 巩金龙 朱德彰

关键词 碳纳米管，焊接，离子束，辐照

IC 工业中越来越高的器件集成度要求纳电子器件和光电子器件越来越小型化，而纳米尺度范围的导线互连将促进纳电子器件和光电子器件的小型化。碳纳米管由于其优异的力学和电学性能已经被用来做纳米器件的互连导线。当前，尽管利用碳纳米管作为微互连的纳电子器件和光电子器件已经被成功制得，但是复杂的纳电子器件和光电子器件的构建依然存在许多问题。其中最主要的一个问题是多种微互连导线的制备。在纳米结构自组装方面有着广泛应用的荷能粒子束技术有可能在纳米导线微互连和碳纳米管改性方面取得很大的进展。我们用 40 keV 硅离子束在加温的条件下辐照多壁碳纳米管，用扫描电子显微镜和透射电子显微镜对经离子束轰击后的碳纳米管的形貌特征和结构变化进行了详细观察。电镜观察证实了碳纳米管的焊接已经完全被形成，这一点与芬兰一个研究小组的理论模拟结果一致。对于离子束焊接碳纳米管的机制，实验研究表明：碳纳米管焊接的实现可能与离子束轰击导致的间隙原子的插层形成和相邻碳纳米管之间的共价键形成有关。碳纳米管的离子束焊接的实现为将来纳电子器件和光电子器件的小型化提供了可能。

Welding of MWCNTs by ion beam bombardment

NI Zhichun LI Qintao YAN Long GONG Jinlong ZHU Dezhang

Key words: Carbon nanotubes, Welding, Ion beam, Irradiation

The increasing degree of device integration in integrated circuits (IC) industry requires further miniaturization of components for constructing electronic and optoelectronic devices. This can be facilitated by nanoscale interconnections among/inside building blocks of the devices. Carbon nanotubes (CNTs), due to their unique mechanical and electronic properties, have been parts of the versatile nano-scale building blocks or conducting wires incorporated into a variety of nanodevices. Even though many nanoscale electronic devices have been fabricated through simple connections of CNTs, there are large majorities of difficulties in systematically producing the nanoscale interconnection of nanodevices. One dominating difficulty is to controllably produce various multiple-way junctions for the interconnection of building blocks. Energetic ion beams, as a powerful tool for driving self-assembly of nanostructures and tuning the conductance of single-walled CNTs, may potentially be used in welding of CNTs to interconnect the building blocks. In current study, we used 40 keV Si ion beam to irradiate multi-walled carbon nanotubes (MWCNTs) to different doses at elevated substrate temperature. The welding of MWCNTs by ion beams was observed by scanning electron microscopy and transmission electron microscopy. The welding MWCNTs junctions were formed by the co-occupied graphitic sheets between the two adjacent MWCNTs. Mechanism of MWCNTs welding were discussed. The welding of MWCNTs is dependent on two factors, i.e. ion beam irradiation and high defect recombination rate. The realization of ion beam welding of MWCNTs provides a solution to nanoscale interconnections among the building blocks and inside the building blocks of devices, which promises further miniaturization of components for construction of electronic and optoelectronic devices.

低能离子束诱导碳圆锥室温生长锥角的可控性研究

李勤涛 倪志春 巩金龙 朱德彰 朱志远

关键词 碳圆锥，碳纳米纤维，离子溅射

采用能量为 1.2 keV 的 Ar^+束室温倾角溅射石墨的方法诱导了碳纳米纤维/圆锥生长。扫描电子显微镜结果表明样品表面产生的圆锥密度达 1×10^9~1×10^{10}/cm^2，沿离子束方向排列，且在每个圆锥上都有碳纳米纤维长出。随着入射倾角由 30°增大到 60°，碳圆锥的锥角从 33°降到 20°、长径比从 250nm/150nm 增大到 1200nm/400nm。Raman 光谱表明这些碳圆锥为无定型结构。有理由认为入射角增加导致的离子束诱导的表面原子有效扩散系数的减小，和溅射率增大是碳圆锥的长径比增大、碳圆锥的锥角减小及其密度增加的原因。

Controlling the apex angle of carbon cone under low energy ion beam bombardment at room temperature

LI Qintao NI Zhichun GONG Jinlong ZHU Dezhang ZHU Zhiyuan

Key words: Carbon cone, Carbon nanofiber, Ion sputtering

Carbon nanofiber-tipped-cones were fabricated by sputtering graphite at room temperature with 1.2 keV Ar^+ ions in obliquely incidence. Density of carbon cones was estimated at 1×10^9 to $1\times10^{10}/cm^2$. The cones with carbon nanofiber were directed toward the beam direction. By increasing the beam incident angle from 30° to 60°, the apex angle of cones decreased from 33° to 20°, and the aspect ratio increased from 250nm/150nm to 1200nm/400nm. Raman spectroscopy revealed that the carbon cones were amorphous. We believe that the decreased apex angle, and the increased aspect ratio and cone density were due to the decreased effective diffuse coefficient induced by the ion bombardment and the increased sputtering yield.

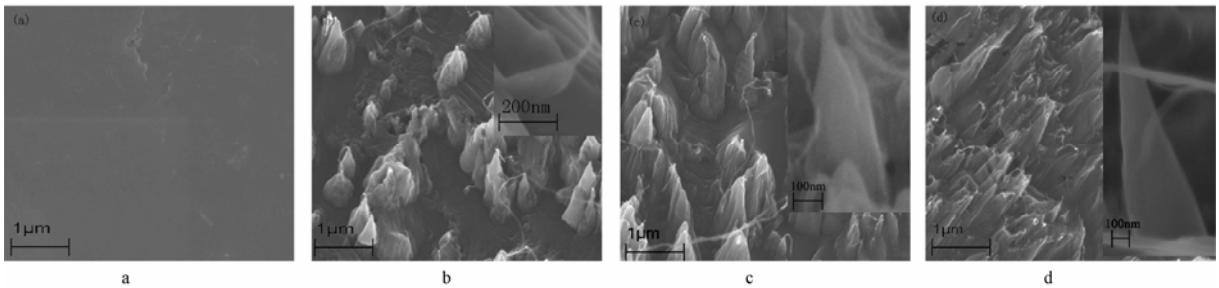

Fig.1 SEM images of (a) the initial graphite surface, and (b), (c) and (d) the graphite surface sputtered for 1 h by Ar^+ ions at 30°, 45° and 60° incidence, respectively

石墨纳米颗粒装饰的碳纳米管

李勤涛 倪志春 巩金龙 朱德彰 朱志远

关键词 石墨纳米颗粒，碳纳米管，低能碳氢离子沉积

在 700℃下采用低能碳氢离子沉积的方法制备了石墨纳米颗粒装饰的碳纳米管。扫描电子显微镜和透射电子显微镜显示石墨颗粒从纳米管表面生长出来且具有有序的结构。随着氢气百分比含量的增加，碳纳米管的直径减小。Raman 光谱显示石墨纳米颗粒的生成归因于实验中高温的使用。由于氢离子的刻蚀作用，随氢气含量的增加，这些石墨颗粒的结构有序度变得越来越低。

Carbon nanotubes decorated by graphitic nanoparticles

LI Qintao NI Zhichun GONG Jinlong ZHU Dezhang ZHU Zhiyuan

Key words: Graphitic nanoparticles, Carbon nanotubes, Low energy hydrocarbon ion deposition

Carbon nanotubes (CNTs) decorated by graphitic nanoparticles have been fabricated by low energy

hydrocarbon ion deposition at 700℃. Transmission and scanning electron microscopy show that the graphite particles extend from the nanotube surface and have well-ordered structure. The diameter of CNTs decreases with increasing percent hydrogen. Raman spectroscopy indicates that the formation of graphite nanoparticles results from the high temperature used in the experiment and their degree of crystallinity is lower with increasing hydrogen content due to the etching effect of hydrogen ions.

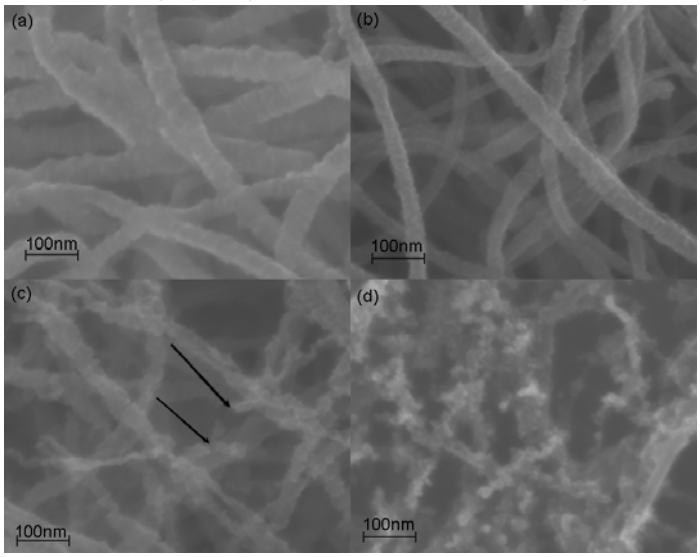

Fig. 1. Morphology of CNTs bombarded by hydrocarbon ions in H_2/CH_4 ratio of (a) 0, (b) 10/1, (c) 20/1 and (d) 30/1

缺陷辅助的高度定向的金刚石薄膜的生长

杨树敏　万冬云　巩金龙

关键词　金刚石薄膜，成核，碳化硅

利用热丝化学气相沉积技术，在手术刀刮擦过的硅衬底上生长了高度定向的金刚石薄膜。薄膜的结构分别用 X 射线衍射、扫描电子显微镜和拉曼光谱分析表明，硅衬底上的刮擦缺陷促进了金刚石颗粒的成核，长时间生长可获得高取向而致密的金刚石薄膜。用这种方法可以得到表面相当平整的(111)织构的金刚石薄膜(图 1)。研究了在硅衬底上缺陷辅助的金刚石成核的机制，对不同生长阶段的金刚石薄膜的研究表明，刮擦诱发的缺陷有助于碳化硅纳米线过渡层的形成,这对金刚石的成核非常必要。在 750℃的衬底温度下，在硅衬底上的缺陷位置得到了直径 100 nm 左右的 β-SiC 纳米线。

Defects-assisted growth of highly oriented diamond films

YANG Shumin　WAN Dongyun　GONG Jinlong

Key words:　Diamond film; Nucleation; Silicon carbide

Highly oriented diamond films were obtained by hot-filament chemical vapor deposition (HF-CVD) on scalpel-scratched silicon wafer. X-ray diffraction, scanning electron microscopy and Raman spec-

troscopy characterizations show that defects induced by the scratching conduce to the nucleation of the diamond particles, and consequently highly oriented and continuous diamond films are produced (Fig.1). Diamond films with the <111> texture can be obtained with relatively smooth surface by this method. Mechanisms of the defects-assisted diamond nucleation on silicon wafer were studied with different stages of the diamond growth. It was found that the scratching induced defects were helpful for the formation of silicon carbide nanowires, which acted as "transition" for the nucleation of diamond. β-SiC nanowires of ~Φ100 nm were grown on silicon substrate with defects by HF-CVD technique without using any catalyst at 750°C of the substrate temperature.

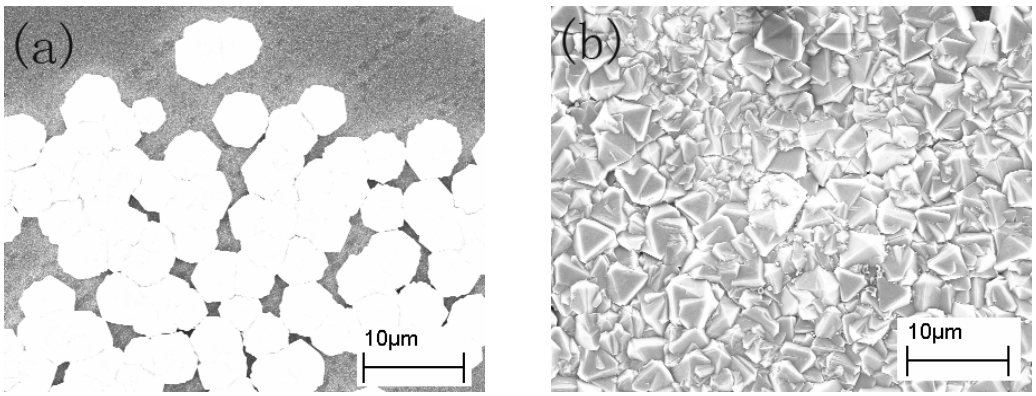

Fig.1. SEM micrographs of the films grown 8h on (a) untreated mirror polished, (b) scalpel scratched Si substrates

利用杠杆结构制备用于扫描隧道显微镜的钨针尖

汪 洋 巩金龙 朱德彰 王化斌

关键词 扫描隧道显微镜，针尖，电化学腐蚀，杠杆结构

STM 探针与样品间距离小于 1nm 便产生隧穿电流，利用这一电流可进行样品表面形貌的扫描。半径小的针尖可降低相位滞后、提高采集速率，而长径比小可降低噪声引起的随机波动。电化学腐蚀法是制备针尖的主要方法， 这一方法简便高效、容易控制。电化学方法中关键的工序是在钨丝断裂的瞬间及时切断电源并迅速提取针尖，以免继续腐蚀而变形。现有解决方案都利用钨丝断裂的电流、电压和电阻等信号经由控制电路切断电源，再由步进电机提取针尖，均需复杂的电子学线路。本工作基于杠杆原理，利用钨针尖断裂瞬间自重突变的信号，构建简单的力学结构制备钨针尖。扫描电镜观察和 STM 实验表明(图 1)，这种针尖使用效果良好。

Fabrication of tungsten tip by a leverage structure

WANG Yang GONG Jinlong ZHU Dezhang WANG Huabin

Key words: Scanning tunnel microscope, Tip, Electrochemical etching, Leverage structure

Tungsten tip is widely used as the STM tip, due to excellent rigidity and low cost. When the distance between the tip and the sample is close to 1nm, the tunnel current appears. It can be detected by STM for scanning morphology of the sample. A smaller radius of curvature is required for high resolu-

tion STM images and a lower aspect ratio is preferable for the reduction of noise induced by flexible vibration. Electrochemical etching is the main method to fabricate the STM tip because of simplicity and easily control. Its key process is the drop-off technique to separate the tip quickly from the electrolyte to avoid further etching of the fine-shaped tip. Most of methods make use of electric signals induced by the tip's drop-off to cut off the circuit and pick the tip by a step motor, with complex circuits, though. We developed a leverage structure based on gravity change of the dropping-off tip. The tip (Fig.1) is good in scanning HOPG surface and an atomic resolved image was obtained.

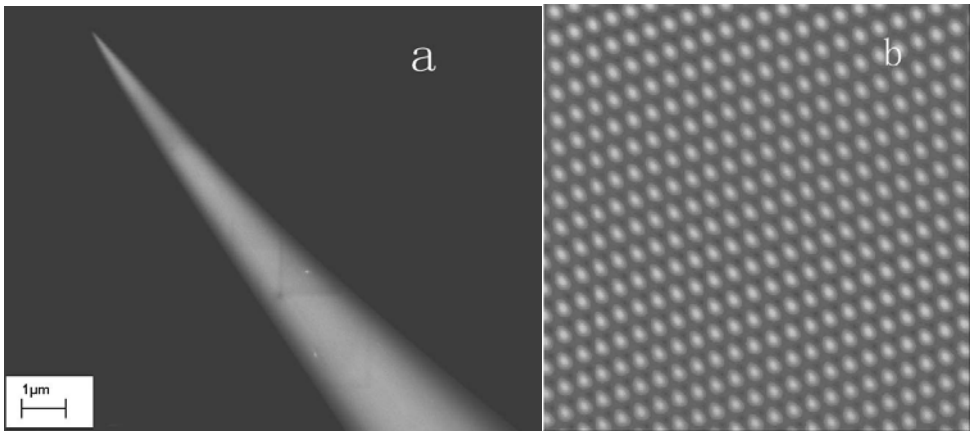

Fig.1 SEM image of the tip (a) and STM image of an HOPG surface scanned by the tip (b, 5 nm×5 nm)

碳离子注入高序热解石墨的磁性

夏汇浩　朱德彰　巩金龙　朱志远

关键词　离子束，高序石墨，铁磁性

在常温下用 70 keV ^{12}C 离子注入高序石墨，注量逐次为 3×10^{14}、8×10^{14}、2×10^{15}、5×10^{15} cm^{-2}。用超导量子干涉磁性测量仪测量各注入阶段样品的磁性，磁场垂直于 HOPG 的 *c* 轴。PIXE 测量表明 HOPG 的磁性金属杂质含量低于 1 μg/g。

C^{12} 离子注入之后，样品的磁性明显增强。在注量 $2\times10^{15}cm^{-2}$ 以下，HOPG 的饱和磁矩随着注量的增加而增加，当注量达到 5×10^{15} cm^{-2} 时，HOPG 的饱和磁矩明显降低。70 keV ^{12}C 离子在 HOPG 内的射程为 243 nm，注入 2×10^{15} cm^{-2} 的 ^{12}C 离子所产生的磁性为 9.3 emu/g。这比 H 注入 HOPG 后的磁性(1.1 emu/g)大一个量级，而与 N 注入的纳米金刚石的磁性在同一量级(0.9~11.5 emu/g) 。

为探求离子注入铁磁性的根源，用自旋极化密度泛函理论研究了离子注入产生各种缺陷的磁学性质，发现空位缺陷对磁性有主要的贡献，一种 r-缺陷(锥形缺陷)也起一定的作用。

Carbon ion-induced magnetism in HOPG

XIA Huihao　ZHU Dezhang　GONG Jinlong　ZHU Zhiyuan

Key words: Ion beam, HOPG, Ferromagnetism

HOPG (ZYA grade) samples were implanted at room temperature with 70 keV $^{12}C^{+}$ ions to 3×10^{14},

8×10^{14}, 2×10^{15} and 5×10^{15} cm^{-2}, successively. Magnetic moments of the samples were measured at 300 K at each stage of the implantation with a superconducting quantum interferometer device magnetometer (perpendicular to the *c*-axis) with a sensitivity of $\leq 10^{-7}$ emu. Proton induced X-ray emission spectra of the samples revealed that the total magnetic metal impurities (mainly Fe) were less than 1 μg/g.

The sample implanted with 3×10^{14} and 2×10^{15} cm^{-2} showed a clear ferromagnetic behavior and the saturation magnetic moment increased with the fluence, whereas that of the 5×10^{15} cm^{-2}-implanted HOPG decreased substantially. As the range of 70 keV $^{12}C^{+}$ ions in carbon is about 243 nm, the maximum magnetization induced by 2×10^{15} cm^{-2} of $^{12}C^{+}$ implantation is as high as ~ 9.3 emu/g, which is much larger than 1.1 emu/g of the proton-induced magnetization in HOPG, and is comparable to 0.9~11.5 emu/g of the $^{15}N^{+}$-implanted diamond films.

To research into the possible mechanisms, we employ the spin-polarized density functional theory (DFT) to investigate the magnetic properties of the typical defects which are usually in existence in carbon ion-bombarded graphite. The DFT calculations indicate that the magnetic moments induced by the vacancies may play a major role and the itinerant magnetism induced by the r-defects may play a minor role for the macroscopic magnetism observed.

Pd(110)基底上的 Co 超薄膜的磁性特征

闫 隆　罗锋*　卢亚锋*　M. Przybylski*　J. Barthel*

关键词　Co 膜，Pd(110)基底，磁性

Pd(110)表面有各向异性结构，生长在其上的 Co 超薄膜会有各向异性的结构和形貌。这些 Co 超薄膜远离平衡态，利用退火法通过磁光科尔(Kerr)效应可研究 Co/Pd(110)系统中形貌和结构对磁性的影响。Pd(110)基底上 2.0 ML – 4.0 ML 的 Co 膜，400 K – 600 K 退火后的实验结果表明此系统的磁性几乎未改变。此厚度的 Co 膜的结构连续，退火并不增加其结构对磁性的贡献。退火后 Co/Pd(110)的界面效应增加，但体系的磁性并不增强。

然而，在 120 K 无铁磁性的 Pd(110)基底上的 0.5 ML Co 膜，400 K 退火后呈现一个小的 Kerr 回线。提高退火温度，Kerr 信号越发明显。扫描隧道显微镜下，该 Co 膜已由 Co 纳米线转变成连续的 Co 岛。可见，Pd(110)基底上的亚单层 Co 膜的退火，能导致膜形貌变化，增加居里温度和磁性。

Magnetic characteristics of ultra-thin Co films on Pd(110) substrate

YAN Long　LUO Feng*　LU Yafeng*　M. Przybylski*　J. Barthel*

Key words:　Co films, Pd(110) substrate, Magnetism

Co/Pd system has attracted much attention as potential materials for high-density magnetic and magneto-optic recording, but its magnetic characteristics have not been fully understood so far. Using annealing and magnetic-optical Kerr effect (MOKE) method, we investigated ultra-thin Co films on a

Pd(110) substrate to clarify dominant factors which affect the magnetic characters. Because of the anisotropy structure of Pd(110), ultra-thin films grown on Pd(110) substrate have anisotropy features in structure and morphology, which are far from equilibrium and can be easily modified by annealing at different temperatures.

For Co films at 2.0 ML~4.0 ML on Pd(110) substrate annealed at 400 K ~600 K, the MOKE experiment did not show obvious changes of magnetism, because the Co film had continuous structure, which cannot enhance magnetism any more. The annealing increased interface effect of Co/Pd(110), but this cannot change the system's magnetism.

For 0.5 ML Co film on the Pd(110) substrate, which had no ferromagnetism at 120 K, a small Kerr loop was seen after annealing at 400 K. The Kerr signals became pronounced at increased annealing temperatures. Scanning tunneling microscopy images revealed that morphology of the 0.5 ML Co on the Pd(110) substrate changed from Co nanowires to continuous Co islands. It can be concluded that for submonolayer Co film on Pd(110) substrate, its annealing-induced morphology change leads to enhanced Curie temperature and magnetism.

*Max-Planck-Institut für Mikrostrukturphysik, Weinberg 2, 06120 Halle, Germany

含碳聚乙烯复合材料在太赫兹波段的光学和介电性质

陈西良　马明旺　吉 特　吴胜伟　朱智勇

关键词　THz 电磁波辐射，多壁碳纳米管，聚乙烯，吸收系数，折射率，介电性质

太赫兹辐射通常是指介于 0.1 到 10 THz 之间的电磁波辐射，在电磁波谱中太赫兹波处于红外和微波之间。这一区域蕴含有丰富的科学信息。利用 THz-TDS 技术研究了不同类型碳(多壁碳纳米管、C_{60} 和碳黑)填充的聚乙烯复合材料在 0.3~1.6 THz 的光谱学性质。研究发现碳纳米管和碳黑填充的复合体系在太赫兹波段具有很强的吸收和折射。而富勒烯填充体系的吸收系数和折射率与纯聚乙烯相近。三种材料的吸收系数和折射率随含量均呈线性增加。对于不同的材料，吸收系数和折射率随含量变化的斜率相差很大，说明虽然三者都具有类似石墨层的结构，但是由于其构型、电子结构等的不同，在太赫兹波段的色散性质存在很大的差异。将掺杂的碳颗粒等效为可以随高频电场转向的偶极子，利用 Cole-Cole 模型对实验结果作了分析，获得了各复合材料的静态和光学介电常数以及偶极子弛豫时间等参数。拟合显示，C_{60}－聚乙烯复合材料在太赫兹波段的介电性质可由单一的弛豫时间描述，而碳纳米管和碳黑与聚乙烯的复合材料则表现出宽的弛豫时间分布。

Optical and dielectric properties of carbon materials in THz region

CHEN Xiliang　MA Mingwang　JI Te　WU Shengwei　ZHU Zhiyong

Key words: THz waves, MWNT, PE, Absorption coefficient, Refractive index, Dielectric property

Terahertz (THz) lights ranging from far infrared to microwaves (0.1~10 THz) is of great impor-

tance due to the rich chemical and physical processes in this region. In this work, we characterized the optical properties of several composites, formed by filling the high density polyethylene (HDPE) with various amount of carbon black (CB), multi-wall carbon nanotubes (MWNT) and fullerene (C_{60}), respectively, in the frequence region of 0.3 to 1.6 THz by using a THz-TDS setup. It is found that the optical parameters and the details of their variation with frequency and filler concentration are significantly different for different kinds of carbon materials. At the same frequency, with the increase of filler concentration, the refractive index and absorption coefficient all increase linearly with slopes depending on the type of carbon filled. The MWNT filled composites have the biggest absorption coefficient value and slope. The HDPE/C_{60} composite shows very little changes in absorption and refractive index compared to that of the neat resin even at a filler-content of 12.3% in volume fraction. These phenomena may be related to the special properties of the fillers as well as their particulate structures, such as aspect ratio, particle size, aggregate structure, etc. The results are analyzed by using Cole-Cole theory of dipole relaxation under the assumption that carbon particles dispersed in the matrix behave like dipoles and contribute mainly to the dielectric loss in the THz frequency range.

辐射冻融结合法制备 PVA/ws-chitosan 水凝胶伤口敷料

杨小敏　刘 崎　陈西良　付海英　朱智勇

关键词　辐射冻融法，聚乙烯醇/水溶性壳聚糖水凝胶，伤口敷料

通过辐射冻融法(Irra.+FT) 结合冻融辐射法(FT+Irra.)制备聚乙烯醇(PVA)/水溶性壳聚糖(ws-chitosan)水凝胶伤口敷料，研究了增塑剂甘油和增强剂琼脂(agar)对水凝胶性能的影响。研究发现，辐射冻融法制备的水凝胶的溶胀度大于冻融辐射法；甘油可以增大水凝胶的溶胀度，而琼脂则降低其溶胀度。水凝胶的溶胀度还具有温度、pH 和离子强度敏感性：温度升高时，凝胶内氢键发生断裂，使水凝胶的溶胀度增大；ws-chitosan 在酸性条件下氨基发生质子化作用，而在碱性条件下发生去质子化作用，因此其在酸性条件下溶胀度较大；在中性盐溶液中，离子强度的增大使凝胶内外的渗透压下降，从而降低其溶胀度。

通过高级流变仪对水凝胶弹性模量的测试显示，甘油降低水凝胶的强度而琼脂可以明显增大水凝胶的强度；并且，辐射和冻融的次序同样影响水凝胶的强度，即辐射冻融法制备的水凝胶其强度大于冻融辐射法制备的水凝胶。研究发现辐照冻融法制备的水凝胶的化学交联度略大。

总之，辐射冻融法制备的水凝胶比冻融辐射法制备的水凝胶具有更优异的性能，前者既具有大的溶胀性能又具有高的强度，且前者透明度大于后者，更有利于用作伤口敷料。

PVA/ws-chitosan hydrogel dressing prepared by combind γ-ray irradiation and freeze-thawing

YANG Xiaomin　LIU Qi　CHEN Xiliang　FU Haiying　ZHU Zhiyong

Key words:　Combined irradiation and freeze-thawing, PVA/ws-chitosan hydrogel, Wound dressing

Hydrogel dressing containing poly(vinyl alcohol) (PVA) and water soluble chitosan (ws-chitosan) was prepared by combination of γ-ray irradiation and freeze-thawing (i.e. irradiation followed by

freeze-thawing or freeze-thawing followed by irradiation). The influence of glycerol and agar on the swelling behavior and rheological property of these hydrogels was investigated. It is found that hydrogels with glycerol own larger swelling capacity but smaller mechanical strength. Those with agar behave in the opposite way. The swelling capacity of these hydrogels is dependent on temperature, pH and ionic strength. Moreover, the sequence of irradiation and freeze-thawing also influences the properties of these hydrogels. It is found that hydrogels made by irradiation followed by freeze-thawing own larger swelling capacity and mechanical strength, and they are more transparent compared with those made by freeze-thawing followed by irradiation.

Influence of UV illumination on track etching process

LIU Qi ZHU Zhiyong Maekawa Yasunari* Yoshida Masaru* YAO Side

Key words: Polymer, Heavy ion, Radiation effects

Ion irradiation of polymers can induce irreversible changes in their macroscopic properties such as electrical and optical properties and the surface-related mechanical properties. Electronic excitation, ionization, chains scission, cross-links and mass losses are accepted as the fundamental events that give rise to the observed macroscopic changes. Detailed and systematic study of radiation induced effects in polymers not only enriches the knowledge of ion-material interactions but also supplies new bases for polymeric materials synthesis through ion-beam technologies. Previous work has concentrated mainly on effects induced by low-ionization particles such as γ-rays and electrons. Since 1980's the application of high energy heavy ion accelerators enables the use of high energy heavy ion as an irradiation source, and many new and exciting effects and phenomena have been revealed.

Energetic heavy ions in matter lose energy mainly through electronic excitation and ionization. Compared to low-ionization particles, high energy heavy ion possesses higher LET(linear energy transfer) values which can reach several to several tens keV/nm. As most of the primary ionizations and excitations occur close to the ion trajectory in a core of a few nanometers in diameter, a continuous damaged zone along the ion path can be induced, in which all bonds inside the zone can be destroyed due to the high rate energy deposition. Studies on this particularity of high energy heavy ion irradiation and its effects in materials will cause great influence on industry as well as on our daily life.

The previous work has revealed the great difference in the effects induced by high energy heavy ions compared to the other particles. It has been shown that under irradiation with lower LET particles gas release depends on molecular structure and material composition, whereas under irradiation with high LET particles, such as high energy heavy ions, it is not the case. Some materials that undergo degradation under γ-irradiation can be cross-linked by irradiation with high energy heavy ions. In some cases new molecular structures were induced by high energy heavy ions with sufficiently high LET values. In recent years we have irradiated polyethylterephthalate (PET), polystyrene (PS), polycarbonate (PC) and polyimide (PI) with high energy Ar, Kr, Xe and U ion beams. Chemical and physical changes of the materials induced by the high energy heavy ion beams were investigated by Fourier-transform infrared ray spectroscopy, ultraviolet and visible transmission spectroscopy and X-ray diffraction measurements, from which damage cross-sections of various functional groups were deter-

mined. An energy loss threshold for damage of phenyl ring in PET has been derived and difference in amorphization of PET under high and low LET irradiations was observed. It is found that alkyne end groups can be induced in all the materials above a certain electronic energy loss threshold, which is found to be about 0.8 keV/nm for PS and 0.4 keV/nm for PC. The production cross-section of alkyne end group increases with increasing electronic energy loss and shows saturation at high electronic energy loss values.

*Takasaki Radiation Chemistry Research Establishment, JAERI, Takasaki, Gunma 370-1292, Japan

Radiation effects in polymers induced by high energy ion beams

ZHU Zhiyong LIU Qi SUN Youmei* JIN Yunfan*

Key words Ion track, UV illumination, Chemical etching

In this study, polyethylterephthalate films (PET, 38 μm thick) were irradiated with Xe ions of 450 MeV, 3×10^5 ions/cm^2. Before etching with aqueous 0.3 mol/L NaOH solution at 40℃, the samples were illuminated with UV light (λ>310 nm) in air for different time durations. Pore growth processes during the etching were monitored by the conductometric measurement. Fig.1 shows the measurement results of radial etching rate of the pore growth in $dG^{1/2}/dt$ ($\Omega^{-1/2}$ s^{-1}) with the etching time.

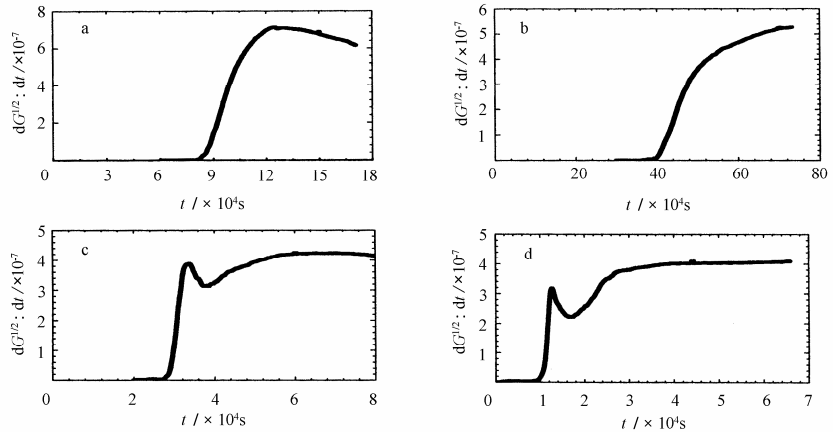

Fig.1 Radial etching rate of the pore growth with the etching time
a. Without UV illumination, b. UV illuminated for 60 min, c. UV illuminated for 180 min, d. UV illuminated for 720 min

As shown in Fig.1, the etching processes changed dramatically with UV illumination time. (1) The break through time reduced with increased sensitization time, from 8×10^4s of the control to about 1×10^4s of the 720 min UV illumination. (2) With increased UV illumination time, the shape of the pore growth rate curve changed greatly, and finally became a shape with a peak and a vale. Formation of the peak implies that pores tended to break-through on completing the UV-light illumination, whereas the vale can be related to the slower etching rate in the track halo where most molecules had been crosslinked by the heavy ion irradiation. After etching for sufficient long time, the pore grew at a con-

stant rate determined by the bulk etching rate.

To interpret the measurements, numerical analysis and fitting were carried out, from which information related to the track structures and variations with the UV illumination was obtained.

* Institute of Modern Physics, Chinese Academy of Sciences, Lanzhou 730000, China

利用太赫兹时域光谱鉴别爆炸物 2,4-DNT 和 2,6-DNT

刘桂锋 马士华 马晓菁 赵红卫 王文锋

关键词 太赫兹时域光谱，定量分析，2,4-DNT，2,6-DNT

利用太赫兹时域光谱测得了 2,4-DNT 和 2,6-DNT 在 0.3-2.0THz 频谱范围的吸收谱和折射谱。实验发现 2,4-DNT 在 0.44, 0.65THz 处有特征吸收。借助高斯 03 程序对 2,6-DNT 进行结构优化和频率计算。2,6-DNT 在 1.09, 1.36 和 1.55 THz 处有三个明显吸收并被归因于分子间的相互作用。本文使用太赫兹光谱法对 2,4-DNT 和 2,6-DNT 混合物做了定量分析。分析的结果与实际值基本一致，相对误差约为 8%。

Identification of explosives 2, 4-DNT and 2, 6-DNT using terahertz time-domain spectroscopy

LIU Guifeng MA Shihua MA Xiaojing ZHAO Hongwei WANG Wenfeng

Key words: THz-TDS, Quantitative analysis, 2,4-DNT, 2,6-DNT

The absorption spectra and refractive index of 2,4-dinitrotoluene (2,4-DNT) and 2, 6-dinitrotoluene (2,6-DNT) were measured in the region of 0.3–2.0 THz by terahertz time-domain spectroscopy (THz-TDS) at room temperature. It was found that 2,4-DNT show two new characteristic absorption peaks at 0.44 and 0.65THz. Gaussian 03 program was applied to predict geometric structure and vibration frequencies of 2, 6-DNT. Absorption peaks at 1.09, 1.36 and 1.55 THz of 2, 6-DNT were obtained and assigned to intermolecular interactions. Quantitative analysis with THz-TDS was undertaken for the mixture of 2, 4-DNT and 2, 6-DNT. The analytic weight ratio of 2, 4-DNT to 2, 6-DNT is consistent with the actual one with an analytic error about 8%.

β-胡萝卜素在乙腈体系中的激光光解研究

张兆霞 赵红卫 朱红平 郝淑梅 王文锋 Suppiah Navaratnam*

关键词 激光光解，激发三重态，2-萘乙酮，β-胡萝卜素

用纳秒级激光光解瞬态吸收光谱装置研究了以乙腈作为溶剂、以 2-萘乙酮作为敏化剂的体系在 355 nm 激光作用下敏化产生β-胡萝卜素激发三重态的机制，并研究了β-胡萝卜素激发三重态的性质。研究显示 2-萘乙酮和β-胡萝卜素的二元体系在 355 nm 激光作用下，2-萘乙酮首先被激

发为其激发三重态(420 nm)，2–萘乙酮激发三重态与β–胡萝卜素发生激发能转移，产生β–胡萝卜素激发三重态(510 nm)。通过激发能转移的方法测得了β–胡萝卜素激发三重态在最大吸收波长 510 nm 处的摩尔消光系数(23000 $L\cdot mol^{-1}\cdot cm^{-1}$)。改变β–胡萝卜素的浓度测得了其激发三重态在乙腈体系中的衰变反应速率常数($6.5\times10^{4}\ s^{-1}$)，其在乙腈体系中的三重态寿命为 15.6 μs。同时获得了激发态 2–萘乙酮与β–胡萝卜素之间激发能转移反应的速率常数($1.5\times10^{10}\ L\cdot mol^{-1}\cdot s^{-1}$)。

The triplet properties of β-carotene in acetonitrile solution

ZHANG Zhaoxia ZHAO Hongwei ZHU Hongping HAO Shumei
WANG Wenfeng Suppiah Navaratnam*

Key words: Laser flash photolysis, Triplet state, 2-acetonaphthone, β-carotene

The representative of carotenoids, β-carotene, can scavenge reactive oxygen radicals like singlet molecular oxygen, nitrogen dioxide radical and peroxyl radical due to the effective antioxidative properties. In medicine, β-carotene is used to alleviate the disease erythropoietic protoporphyria (EPP), by intercepting the triplet state of protoporphyrin (a porphyrin lacking a central metalion, a precursor to haem) therefore preventing the formation of singlet oxygen. Epidemiological evidence has suggested that dietary β-carotene may inhibit certain types of cancer. Much of work has been carried out in benzene, toluene, or chloroform as most carolenoids are sufficiently soluble in these nonpolarity solvents. In this paper, the generation and properties of triplet β-carotene in acetonitrile solution have been investigated with 355 nm laser flash photolysis. 2-acetonaphthone has been used as an excited energy donor to sensitize the production of the triplet state of β-carotene. Excitation of the solution containing 2-acetonaphthone and β-carotene upon 355 nm laser flash produced the triplet of 2-acetonaphthone (420 nm) firstly. Subsequently, the excited energy of triplet 2-acetonaphthone was transferred to β-carotene generating triplet β-carotene. Characteristic absorption spectra of triplet β-carotene (510 nm) were recorded. By means of transfer of excited energy, the triplet-triplet absorption spectrum and molar absorption coefficients of triplet β-carotene were determined to be 23000 $L\cdot mol^{-1}\cdot cm^{-1}$ at 510 nm. The triplet lifetime for β-carotene in acetonitrile solution has observed to be 15.6 μs. The rate constant for the reaction of triplet energy transfer from triplet 2-acetonaphthone to β-carotene has calculated to be $1.5\times10^{10}\ L\cdot mol^{-1}\cdot s^{-1}$. Obviously, the triplet β-carotene has very low excited energy and high molar absorption coefficients in acetonitrile solution which is the same as in nonpolarity solution. Taking the advantage of the photochemical properties of triplet β-carotene, β-Carotene has been widely used as energy acceptor to determine the excited state characteristic of other substance. This work extends the understanding of photochemical properties of β-carotene.

*The North-East Wales Institute, U.K

萘醌光敏损伤溶菌酶的激光光解和稳态研究

张兆霞 郝淑梅 朱红平 王文锋*

关键词 激光光解, 激发三重态, 萘醌, 溶菌酶

利用时间分辨的激光光解技术研究了萘醌在乙腈/水(3:1, v/v)溶液中的瞬态吸收谱。萘醌经

355 nm 的激光脉冲激发后会产生 $^3NQ^*$，其特征吸收谱在 360 nm 处。$^3NQ^*$可以很快地被氧气猝灭(k_q=1.5×10^{10} L·mol^{-1}·s^{-1})。在乙腈/水(3:1, v/v)溶液中，$^3NQ^*$可发生自猝灭反应生成 $NQ^{\cdot-}$，其特征吸收谱在 395 nm 处。同时利用脉冲辐解手段验证了 $NQ^{\cdot-}$在水溶液中的特征吸收峰在 390 nm 处。通过对萘醌和 TMPD 二元体系的研究，我们验证了萘醌在乙腈/水(3:1, v/v)溶液中的电子受体性质，并测定了 $^3NQ^*$和 TMPD 之间电子转移的速率常数 k_{t1} = 2.0×10^{10} L·mol^{-1}·s^{-1}。在本实验条件下，电子转移反应产生的 $NQ^{\cdot-}$以 $HNQ^{\cdot}$的形式存在，其特征吸收峰在 360 nm 处。萘醌可通过 $^3NQ^*$光氧化损伤溶菌酶，反应机理为氢原子转移反应，并测定了其反应速率常数 k_{t2} = 2.4×10^{10} L·mol^{-1}·s^{-1}。对萘醌、溶菌酶和 TMPD 三元体系的研究表明，TMPD 可通过自由基转移反应的方式修复受损伤的溶菌酶，这一结论得到了电泳实验结果的支持。利用稳态的 SDS-PAGE 凝胶电泳和活性测量的方法，更直接地观察到了溶菌酶损伤形成的二聚体。结合动态和稳态的实验结果，发现萘醌诱导的溶菌酶光氧化损伤是 I 型和 II 型反应协同作用的结果，其中以 II 型反应为主。

Photoreactions of 1,4-naphthoquinone with lysozyme studied by laser flash photolysis and steady-state analysis

ZHANG Zhaoxia HAO Shumei ZHU Hongping WANG Wenfeng

Key words: Laser flash photolysis, Triplet state, 1,4-naphthoquinone, Lysozyme

Photoprocesses of 1,4-naphthoquinone (NQ) and its photoreactions with lysozyme in acetonitrile/water (3:1, v/v) solution were studied using 355 nm laser flash photolysis technique, electrophoresis and turbidimetric assay. The results showed that 355 nm laser excited NQ to triplet state, which could form anion radical of NQ by self-quenching reaction. The absorption peak at 395 nm was assigned to anion radical of NQ. The electron transfer process from N,N,N′,N′-tetramethyl-p-phenylenediamine (TMPD) to the triplet state NQ ($^3NQ^*$) was investigated and the rate constant was determined to be 2.0×10^{10} L·mol^{-1}·s^{-1}. It has been found that $^3NQ^*$ can abstract hydrogen atom from lysozyme with a rate constant of 2.4×10^{10} L·mol^{-1}·s^{-1}. Furthermore, the results of steady-state analysis suggested that lysozyme can be damaged by NQ irradiated with UVA light influenced by the concentration of NQ and the different gas saturated system. The mechanisms of photosensitized damage of lysozyme induced by NQ was determined to be the same as the mechanisms induced by riboflavin, which involved both type I and type II processes in which process II was predominant.

核黄素光敏损伤溶菌酶的 SDS-聚丙烯酰胺凝胶电泳研究

张兆霞 赵红卫 朱红平 葛 敏 王文锋 姚思德

关键词 溶菌酶，核黄素，光敏损伤，凝胶电泳，抗氧化剂

在 315–375 nm 光照射下核黄素能造成溶菌酶的光敏损伤，通过十二烷基磺酸钠-聚丙烯酰胺凝胶电泳(SDS-PAGE)对稳态产物的研究分析发现，溶菌酶的光敏损伤途径和损伤产物与核黄素浓度、光照时间、体系的气氛等密切相关。在氮气气氛下为 I 型光敏损伤机制；在有氧条件下溶菌酶的损伤是 I 型和 II 型协同反应，以 II 型为主。考察了褪黑激素等抗氧化剂对溶菌酶的保护作用。

SDS-PAGE study on photosensitive damage of lysozyme by riboflavin

ZHANG Zhaoxia ZHAO Hongwei ZHU Hongping GE Min
WANG Wenfeng YAO Side

Key words: Lysozyme, Riboflavin, Photo sensitive damage, SDS-PAGE, Antioxidant

Lysozyme can be photosensitively damaged when irradiated with UVA light (315-375 nm) in the presence of riboflavin. SDS-PAGE studies show that the approaches of photosensitive damage have close relationship with the concentration of riboflavin, time of irradiation and the atmosphere of solution. The mechanism of photosensitive damage is type I in the nitrogen saturated solution. When the oxygen is present, the damage mechanism of lysozyme was mainly due to type II cooperated with type I. Antioxidants such as melatonin can reduce the damage of lysozyme effectively.

固态共结晶反应的太赫兹时域光谱研究

葛 敏 王文锋 赵红卫 张增艳 余笑寒

关键词 太赫兹时域光谱，固态反应，对苯醌， 对苯二酚

本文利用太赫兹时域光谱技术对对苯醌与对苯二酚和 2,2’-联苯酚之间的固态共结晶反应过程进行了研究。通过测量不同反应阶段的混和物在太赫兹波段的吸收，可以清晰地了解反应的进程。同时利用 X-射线粉末衍射、傅立叶变换红外光谱以及远红外光谱等常规的固态反应的研究方法同步检测这些过程，以验证太赫兹光谱测量的准确性和可靠性。实验结果表明利用太赫兹时域光谱技术可以清晰地了解固态共结晶反应的程度，同时由于 THz 技术的高灵敏度、在线无损检测以及远距离取样等特点，THz 时域光谱可能成为一种新的固态分析手段，用于化学反应动力学研究。

Characterization of crystal transformation in the solid-state byterahertz time-domain spectroscopy

GE Min WANG Wenfeng ZHAO Hongwei ZHANG Zengyan YU Xiaohan

Key words: THz-TDS, Solid-state reactions, *p*-benzoquinone, *p*-dihydroxybenzene

Terahertz time-domain spectroscopy (THz-TDS) was utilized to investigate crystal transformation between *p*-benzoquinone and *p*-dihydroxybenzene in the solid-state. This process can be clearly visualized by THz spectral patterns of the pure starting compounds and the products at different conditions. The observed results were further confirmed by characteristic X-ray powder diffraction and mid-infrared spectra. The extent of crystal-to-crystal transformation was quantified by the absorption

intensity ratio according to the Beer–Lambert law. THz-TDS was demonstrated to be a promising and complementary method in analyzing solid-state reactions.

硫辛酸的脉冲辐解和激光光解研究

宋西玉　张鹏　张兆霞　王文锋

关键词　硫辛酸，抗氧化剂，活性氧自由基，脉冲辐解

作为一种脂溶性和水溶性良好的天然抗氧化剂，硫辛酸很容易被吸收并且通过细胞膜，无论在细胞内部和细胞膜都能有效地抑制和清除活性氧和活性氮自由基。

本工作通过脉冲辐解和激光光解研究了硫辛酸与氧化性自由基和还原性自由基的反应。测定了硫辛酸与 $Br_2^{\cdot-}$在 pH7.3 的磷酸盐缓冲液中的反应速率。随着硫辛酸浓度的增加，$Br_2^{\cdot-}$的衰减速率明显加快，并与硫辛酸的浓度呈线性关系。这表明硫辛酸能够有效地清除 $Br_2^{\cdot-}$

本工作同时测量了硫辛酸与 $OH^{\cdot}$, $CO_3^{\cdot-}$, $SO_4^{\cdot-}$, e_{aq}^-的反应速率常数，表明硫辛酸能够有效地清除这些自由基。本工作能够让我们更好地认识硫辛酸的抗氧化作用。

Pulse radiolysis and laser flash photolysis studies of α-lipoic acid

SONG Xiyu　ZHANG Peng　ZHANG Zhaoxia　WANG Wenfeng

Key words:　Lipoic acid, Antioxidants, Reactive oxygen species, Pulse radiolysis

As the both water- and fat- soluble free radical antioxidants, which can be easily absorbed and transported through the cell membrane, lipoic acid (LA)　is thought to play a significant role in the inhibition of reactive oxygen and nitrogen species both inside the cell and at the membrane level.

In this study both oxidizing and reducing radicals was studied by employing pulse radiolysis and laser flash photolysis. The rate of the reaction between $Br_2^{\cdot-}$ and LA was measured directly at pH 7.3. That the addition of increasing LA concentrations led to a higher rate of $Br_2^{\cdot-}$ decay indicates that LA can effectively quench $Br_2^{\cdot-}$.

The rate constants of the reactions of LA with OH, $CO_3^{\cdot-}$, $SO_4^{\cdot-}$, $Br_2^{\cdot-}$ are also determined. The results show that LA can effectively quench $OH^{\cdot}$, $CO_3^{\cdot-}$, $SO_4^{\cdot-}$, e_{aq}^- and $Br_2^{\cdot-}$. This indicates that LA is an effective antioxidant. The work contributes to the understanding of the antioxidant actions of LA.

氟代喹诺酮类衍生物光化学性质的研究

张 鹏　宋西玉　张兆霞　王文锋

关键词　氟代喹诺酮，激光光解，激发态，光敏损伤

氟代喹诺酮类衍生物是一类在医学临床和日常生活中有着广泛应用的抗菌消炎药物。该类药物通过抑制细菌中能够控制 DNA 形状的旋转酶中的亚单位 A，从而起到药理学作用。在过去的十年中，由于发现了该类药物具有光毒性和光致癌性，众多学者对该类药物的光化学性质进行了

广泛和深入的研究。对于该类衍生物对生物分子的损伤机理，目前并不清楚，因此充分了解该类药物的光化学性质就成了探究其对生物分子损伤机理的重要前提。

本文利用 355 nm 激光光解和脉冲辐解技术对依诺沙星和诺氟沙星的光化学性质进行了研究。对 355 nm 激光激发的依诺沙星和诺氟沙星的瞬态吸收图谱进行了归属，确定了依诺沙星和诺氟沙星三线激发态的最大吸收峰位置分别为 520 nm 和 610 nm。并利用脉冲辐解技术确定了依诺沙星和诺氟沙星的阴离子自由基的吸收峰位置，其最大吸收分别在 700 nm 和 640 nm。同时，我们测定了诺氟沙星的自猝灭速率常数和被氧气猝灭的速率常数。我们下一步的工作将在继续深入了解依诺沙星和诺氟沙星光化学性质的基础上，其对生物分子损伤机理进行研究。关于该类损伤机理的研究，其他学者已取得了初步的结果：该类药物对蛋白质的光敏氧化，导致蛋白质结构的变化是造成该类药物光毒性的主要原因。在细胞中，DNA 是该类药物的主要损伤目标。

Study on photochemistry of fluoroquinolones

ZHANG Peng　SONG Xiyu　ZHANG Zhaoxia　WANG Wenfeng

Key words: Fluoroquinolones, Laser flash photolysis, Triplet, Photo sensitized damage

Fluoroquinolones (FQs) are classic drugs which are widely used as broad-spectrum antimicrobial agents. They develop their pharmacological action via specific inhibition of sub-unit A of the bacterial gyrase, an enzyme that controls DNA shape. In the past decade, these drugs have been the object of increasing interest due to the finding of their phototoxic and photocarcinogenic properties. The mechanisms underlying the phototoxic reactions are not known, and one prerequisite for a deeper understanding is the exact knowledge of the photochemistry of the drugs.

In this paper we present a study of photochemistry on two FQs, enoxacin (ENX) and norfloxacin (NFX) by 355 nm laser flash photolysis and pulse radiolysis technique. Transient spectra of ENX and NFX were observed and transient species were assigned. Pulse radiolysis experiments with ENX and NFX showed the absorption maximum of the anion radical at 700 nm and 640 nm, respectively. The absorption maxima of triplet states of ENX and NFX were located at 520 nm and 610 nm, respectively. We also determined the decay rate constant, self-quenching rate constant of NFX, and quenching rate constant by oxygen. Our next work will focus on mechanisms underlying the phototoxic reactions. There are some primary results: photosensitized protein oxidation by drugs, with the consequent modification of their structure is thought to be responsible for the occurrence of phototoxic phenomena such as photoallergy and loss of biological functions. DNA is thought to be one of the main cellular targets responsible for the drug-photoinduced disorders.

中药麻黄的有效成分的 THz 指纹频谱研究

马士华　刘桂锋　马小菁　王文锋

关键词　麻黄, 太赫兹时域光谱, 中药质量监控

在疾病治疗中，中药以其安全、有效、价格便宜而获得了世界医学和卫生组织的重视和肯定。但是另一方面，由于缺乏完善的现代化质量评价标准体系，中药的合法性也一直受质疑。因此，

发展和完善专业的、多学科交叉的中药质量监控和检测分析技术就显得尤为重要。太赫兹时域光谱技术对分子的结构、环境和分子间相互作用等因素高度敏感，因此在评价包括中药在内的药物质量方面有巨大的应用前景。在本文中，用 THz-TDS 装置测试了麻黄的两种主要有效成分：麻黄碱和伪麻黄碱的 THz 频谱，并对单一组分和双组分混合物都进行了测试，同时对不同比例的混合物进行了定量分析。实验结果证明，THz-TDS 在评价和检测中药质量方面是一个有巨大潜力的应用技术手段。

The THz fingerprint spectra of the active ingredients of a TCM—Herba Ephedrae

MA Shihua LIU Guifeng MA Xiaojing WANG Wenfeng

Key words: Herba Ephedrae, Terahertz time-domain spectroscopy, Quality control

The Traditional Chinese Medicine (TCM) has more merits such as safe, effective and low loss. Unfortunately, locating unbiased information on commonly used herbs can be difficult. TCM has to meet the modern and scientific quality control standards necessary for international recognition. Therefore, it is important that the development of many methods involving many interdisciplinary or disciplinary techniques and analytical instruments for evaluating quality control and inspection. Terahertz time-domain spectroscopy (THz-TDS) is highly sensitive to the changes of the structure, environment elements and intermolecular interaction. So terahertz spectroscopy has tremendous potential for applications in evaluating the quality of the drugs including the TCM. In this paper, THz-TDS has been used to measure the spectral properties of two active ingredients of Herba Ephedrae: ephedrine and pseudoephedrine. The THz spectra of both the sole-ingredient and two-ingredient compound are studied. We also measured the mixtures of by two active ingredients at the different ratios and the quantitative analysis is applied to determine the principal components in samples. The terahertz spectroscopy is a potential and promising technique in evaluating and inspecting the quality of the drugs in the TCM field.

羟基肉桂酸类化合物的太赫兹光谱研究

葛 敏 赵红卫 王文锋 张增艳 余笑寒

关键词 太赫兹时域光谱, 羟基肉桂酸

本文利用太赫兹时域光谱技术对几种羟基肉桂酸类化合物即咖啡酸，阿魏酸，芥子酸以及绿原酸在 0.3-2.0 THz 波段的性质进行了研究，得到了这一系列化合物在该频率范围内的吸收系数，折射指数以及介电常数等相关信息。为了进一步理解羟基肉桂酸类化合物的太赫兹响应与化合物结构和周围环境的关系，我们利用密度泛函理论对这些化合物的远红外吸收性质进行了研究。根据理论计算的结果，对实验所观察到的化合物的吸收带进行了归属。分子间氢键对该类化合物在 2.0 THz 波段的吸收有着重要的贡献。

Terahertz time-domain spectroscopy of four hydroxycinnamic acid derivatives

GE Min ZHAO Hongwei WANG Wenfeng ZHANG Zengyan YU Xiaohan

Key words: Terahertz time-domain spectroscopy, Hydroxycinnamic acid

The hydroxycinnamic acid (HCA) derivatives are produced from L-phenylalanine or L-tyrosine via the shikimate pathway, are the most widely distributed phenolic components in plant tissues. The well-resolved absorption spectra of the hydroxycinnamic acid (HCA) derivatives, namely caffeic acid, ferulic acid, sinapic acid and chlorogenic acid were measured over the frequency region from 0.3 to 2.0THz at 294K with terahertz time-domain spectroscopy (THz-TDS). Theoretical calculation was applied to assist the analysis and assignment of the individual THz absorption spectra of the HCA derivatives with density functional theory (DFT) method. The distinctive spectral features were originated from the collective motion of molecules held together by hydrogen bonds. The real and imaginary parts of dielectric function of the four HCA derivatives were also obtained.

羟基肉桂酸衍生物在防止溶菌酶氧化中的作用–保护和修复

朱红平 陈仕谋 郝淑梅 张兆霞 王文锋 姚思德

关键词 活性氧自由基,羟基肉桂酸衍生物,抗氧化剂,蛋白质

体内过多的活性氧自由基(ROS)能损伤 DNA、蛋白质和脂类等，从而改变基因表达、影响信号传导，导致疾病和衰老。Harman 于 1955 年提出了衰老的自由基理论(the free-radical theory of aging)，越来越多的实验结果证实了这个理论的正确性。研究结果显示：最大寿命与 ROS 的产生成反比，与抗氧化剂的保护作用成正比。由于生物体系中蛋白质的含量很大，并且蛋白质与 ROS 反应的速度很快，因此蛋白质是 ROS 进攻的主要对象。但是，与 DNA 和脂氧化比较而言，对蛋白质氧化的研究相对滞后。最近的研究表明：阿尔茨海默症、帕金森氏症和动脉粥样硬化等很多退行性疾病都与蛋白质的氧化有关。如何阻止蛋白质的氧化在生物和医学界引起了极大关注，对抗氧化剂的研究尤其活跃。已有的研究结果表明：经常摄入富含抗氧化剂的食物可以减少心脑血管等疾病的发生率。但是，到目前为止，抗氧化剂的抗氧化机理尚不十分明确。

本工作利用稳态光解的方法，研究了羟基肉桂酸衍生物(HCA)在核黄素光敏氧化溶菌酶中的作用。HCA 可以减少光敏氧化导致的蛋白质交联。为了弄清 HCA 的保护机理，我们采用动态光解的方法对核黄素激发三重态与溶菌酶和 HCA 间的反应进行了研究，测得溶菌酶和 HCA 猝灭核黄素激发三重态的反应速率常数分别为 $2.8\sim0.7\times10^{9}$ 和 $0.4\times10^{9}\ \mathrm{L\cdot mol^{-1}\cdot s^{-1}}$。

此外，我们研究了抗氧化剂对蛋白质辐射损伤的保护，电泳结果和荧光分析表明：HCA 可以有效防止 γ 射线引起的蛋白质损伤。

通过分析动态和稳态光解两方面的结果以及不同浓度的 HCA 的保护作用，我们发现：当 HCA 浓度较大时，在 ROS 或氧化性三重态进攻蛋白质之前，抗氧化剂可以直接清除它们从而保护蛋白质；当抗氧化剂浓度很低时，通过修复受损伤的蛋白质分子来减少蛋白质的损伤。

Double roles of hydroxycinnamic acid derivatives in protection against lysozyme oxidation

ZHU Hongping CHEN Shimou HAO Shumei ZHANG Zhaoxia
WANG Wenfeng YAO Side

Key words: Reactive oxygen species, Hydroxycinnamic acid derivatives, Antioxidant, Protein

One of the most compelling theories explaining age-related deterioration is the free radical theory of aging. It has been shown that reactive oxygen species (ROS) are involved in oxidative damage to biomolecules which is related to a number of diseases. Proteins are the most abundant components of cells by weight next to water and they are now increasingly recognized as major biological targets of oxidative damage. Convincing evidence has indicated that damage to protein has been implicated in Alzheimer's disease, Parkinson's disease, cancer, and ageing.

Antioxidant has been the subject of great attention because they are known to lower the risk of cardiovascular and other diseases. Hydroxycinnamic acid derivatives (HCA) are antioxidants abundant in tea, red wine, fruits, beverages and various medicinal plants. Results showed that they exhibit remarkable activity for scavenging oxidizing radicals and triplet states.

The protective effects of four HCA on the oxidative damage to lysozyme were investigated in our work. Protein damage was induced by two different paradigms: photosensitizer-sensitized photooxidation and hydroxyl ($^{\bullet}$OH)-mediated oxidation. The protective mechanism was proposed based on the kinetic study. HCA were found to protect protein against oxidation by scavenging oxidizing species and repairing the damaged protein.

褪黑激素的光物理和光化学性质

朱红平 张兆霞 赵红卫 王文锋 姚思德

关键词 褪黑激素，抗氧化剂，激发三重态

利用纳秒级激光光解吸收光谱装置，研究了褪黑激素(melatonin，ML)的光物理和光化学性质。在266 nm激光作用下，既产生激发三重态(^{3}ML*)，又可光电离生成水合电子和阳离子自由基(ML$^{\bullet+}$)；用$SO_4^{\bullet-}$自由基氧化褪黑激素产生自由基，求得了此反应的速率常数；在355 nm 激光下产生核黄素(riboflavin，RF)三重态 ^{3}RF*，求得了 ML 猝灭 ^{3}RF* 的速率常数；对它清除 ABTS 阳离子自由基(ABTS$^{\bullet+}$)的能力与其它抗氧化剂进行了比较。

Transient species and its properties of melatonin

ZHU Hongping ZHANG Zhaoxia ZHAO Hongwei WANG Wenfeng YAO Side

Key words: Melatonin, Antioxidant, Excitated triplet state

The photo-physical and photo-chemical properties of melatonin (ML) were studied by 266 nm la-

ser flash photolysis (LFP). ML undergoes photo-ionization to produce radical cation of ML ($ML^{\bullet+}$) and hydrated electrons (e_{aq}^-), while excited triplet state $^3ML^*$ is also formed during photolysis. The oxidation via one electron transfer from ML to $SO_4^{\bullet-}$ and the triplet state of riboflavin ($^3RF^*$) has been also investigated and the rate constants for the process have been determined to be 8.0×10^9 and 1.4×10^9 $L\cdot mol^{-1}\cdot s^{-1}$ respectively. The radical cation of 2,2'-azinobis(3-ethylbenzothiazoline-6-sulfonic acid) ($ABTS^{\bullet+}$) scavenging capacities of melatonin and other antioxidants are compared in this paper.

醌类化合物的太赫兹光谱研究

葛 敏　赵红卫　王文锋

关键词 赫兹时域光谱, 醌类化合物

本文利用太赫兹时域光谱技术对对苯醌、1,4-萘醌以及 9,10-蒽琨在 0.3-2.0 THz 波段的性质进行了研究。得到了这一系列化合物在该频率范围内的吸收系数、折射指数以及介电常数等相关信息。为了进一步理解醌类的太赫兹响应与化合物结构和周围环境的关系，我们利用 AM1, HF 和 DFT 等方法对化合物的远红外吸收性质进行了计算研究。根据理论计算的结果可以看出该类化合物在实验范围内的吸收峰主要是由于醌类化合物的集体平动和转动所引起的。

Terahertz spectroscopy and theoretical calculation of quinones

GE Min　ZHAO Hongwei　WANG Wenfeng

Key words: Terahertz time-domain spectroscopy, Quinone

Interests in quinone and its derivatives arise from the biological importance and chemical properties. The 1, 4-naphthoquinone structure is common in numerous natural products associated with antifungal, antibacterial, antiviral and antitumour activities. 9, 10-Anthraquinone is the parent compound for a large palette of anthraquinone dyes and so is the most important starting material in their production. It plays significant role in dye industry, medicinal chemistry, biological electron transport processes and other fields. The far-infrared spectra of 1,4-benzoquinone, 1, 4-naphthoquinone and 9,10-anthraquinonme have been measured with terahertz time domain spectroscopy at room temperature. The characterizations of the absorption power and index of refraction in the frequency range 0.3-2.0 THz are presented. Theoretical calculation was applied to assist the analysis and assignment of the individual THz absorption spectra of the *p*-quinones with semiempirical AM1, Hartree-Fock (HF) and density functional theory (DFT) method. Observed THz responses are assigned to the translational and torsional vibrations of *p*-quinone dimer held together by weak hydrogen bonds.

氨基酸和硫杂蒽酮衍生物三线态之间反应的激光光解研究

朱红平　王文锋　姚思德

关键词 硫杂蒽酮衍生物,抗肿瘤,三线态,氨基酸

355 nm 的激光激发硫杂蒽酮衍生物(TXs): 2,4-二乙基硫杂蒽酮 (DETX) 和 2-(2,3-环氧丙氧基)硫杂蒽酮 (ETX) 的乙腈/水(体积比 1:1)溶液产生 TXs 激发三线态(^{3}TXs*)。 ^{3}TXs*在 590 nm 处有特征吸收，^{3}DETX*和 ^{3}ETX*被 O_2 和自身基态猝灭的速率常数分别为 9.8×10^9, 7.3×10^9 和 2.6×10^8, 2.2×10^8 mol^{-1}·L·s^{-1}。^{3}TXs*氧化氨基酸的研究结果显示色氨酸(Trp)和酪氨酸(Tyr)可以通过电子传递猝灭 ^{3}TXs*,相关的猝灭反应速率常数已经测知。用凝胶电泳研究了 ^{3}TXs*引发的蛋白质损伤，在有氧和无氧条件下均观察到明显的蛋白质二聚体,讨论了光敏剂光氧化氨基酸和蛋白质的构效关系。

Studies on reaction of amino acids and triplet thioxanthone derivatives by laser flash photolysis

ZHU Hongping WANG Wenfeng YAO Side

Key words: Thioxanthone derivatives, Anti-tumor, Ttriplet state, Amino acid

Excitation of the thioxanthone derivatives (TXs), 2,4-diethylthioxanthone (DETX) and 2-(2,3- epoxypropyloxy) thioxanthone (ETX) in acetonitrile/water mixture solution (1:1, v/v) upon 355 nm laser flash produced the triplet of TXs (^{3}TXs*). Characteristic absorption spectra of ^{3}TXs* (590 nm) were recorded and rate constants of ^{3}DETX* and ^{3}ETX* quenched by O_2 and by its ground state were determined (9.8×10^9, 7.3×10^9 and 2.6×10^8, 2.2×10^8 mol^{-1}·L·s^{-1} respectively). The reactions of some amino acids oxidized by ^{3}TXs* were carried out. It has been found that tryptophan (Trp) and tyrosine (Tyr) can quench ^{3}TXs* via electron transfer process and related quenching rate constants were obtained. ^{3}TXs* induced protein damage was investigated using electrophoresis and significant levels of dimerization were observed under aerobic and anaerobic conditions. The influence of photosensitizer's structure on photo-oxidation of amino acid and protein has been discussed.

杜醌光敏损伤溶菌酶活性的研究

郝淑梅 张兆霞 朱红平 王文锋

关键词 杜醌，溶菌酶，光敏损伤

光敏剂可以诱导肿瘤细胞的凋亡，光动力疗法已经被证实可用于对肿瘤的治疗中。从上世纪九十年代至今已有不少光敏剂陆续在美国、欧洲等国家上市，显示了非常可观的市场前景。醌类化合物可以发生一系列复杂的光化学反应，其光生物学功能受到广泛关注。溶菌酶(Lyso)常被作为研究蛋白稳定性、折叠和变性的模型蛋白。

本研究采用杜醌(DQ)为光敏剂，Lyso 为模型蛋白，研究蛋白质光敏损伤所致的结构和功能改变。实验采用 500 W 的氙灯作为稳态光照光源，经透射波长为 315~375 nm 的滤光片，聚焦到石英样品池上。光辐照能量为 34.3 mW·cm^{-2}。经稳态光照处理的样品进行十二烷基磺酸钠-聚丙烯酰胺凝胶电泳实验和活性测量。结果显示：Lyso 活性变化显示与结构改变相同的规律。Lyso 的光敏损伤途径和损伤产物与 DQ 浓度、光照时间、体系的气氛等密切相关。Lyso(5×10^{-4} mol·L^{-1})溶液及 DQ(1.5×10^{-3} mol·L^{-1})和 Lyso(5×10^{-4} mol·L^{-1})的混合溶液分别在氮气、空气和氧气饱和的条件下光照 30 min 后电泳，溶液在不同气氛下光照，均在 28~29 kDa 处出现大分子量的蛋白质片段，该片段

恰好是 Lyso 分子量 14.6 kDa 的两倍，说明其为二聚产物。以空气中的二聚产物最为明显，氧气次之。相同气氛条件下，DQ 的存在使二聚产物明显增加，随 DQ 浓度增加 Lyso 的损伤加剧,说明 DQ 会敏化 Lyso 的损伤. DQ 损伤 Lyso 的光照时间效应与 DQ 浓度效应相似，光照时间的延长会产生更多的 DQ 激发态，并通过电子转移和激发能转移这两种途径加剧 Lyso 的光敏损伤。

Photooxidative effect on lysozyme activity induced by duroquinone

HAO Shumei ZHANG Zhaoxia ZHU Hongping WANG Wenfeng

Key words: Duroquinone, Lysozyme, Photooxidation

Photodynamic therapy (PDT) has been reported to be effective for treating various tumors and to induce apoptosis in many tumor cells. To apply theoretical reference for choosing appropriate photosensitizer, many approaches were employed. We studied the photooxidative reaction between duroquinone (DQ) and lysozyme (Lyso). In the study, DQ was excited by 315-375 nm UVA light at an irradiance of 34.3 $mW \cdot cm^{-2}$. The solutions of Lyso (5×10^{-4} $mol \cdot L^{-1}$) and the mixed solutions of DQ (1.5×10^{-3} $mol \cdot L^{-1}$) and Lyso (5×10^{-4} $mol \cdot L^{-1}$) were irradiated for 30 min continuously bubbled with nitrogen, air and oxygen, respectively. To analyze the irradiated solution, sodium dodecyl sulfate-polyacrylamide gel electrophoresis (SDS-PAGE) was carried out to obtain the structural changes of Lyso. The lytic activity of Lyso against Micrococcus lysodeikticus was turbidimetrically determined. The result of SDS-PAGE showed a new band at 28-29 kDa under three different ambiences, which was the dimer of Lyso (14.6 kDa). Both the results of the structural changes and the activity changes demonstrated that DQ can induce photooxidation damage of Lyso. Interestingly, the degree of Lyso damage was the greatest when the solution was bubbled with air and the damage was the smallest with nitrogen bubbling. The degree of damage increased with increasing concentration of DQ. The effect of irradiated time on Lyso damage was also investigated. It indicated that Lyso damage was strengthened at higher DQ concentration or longer irradiation.

应用加速器和
辐射技术研究中心

EB Accelerators and Radiation Applications

离子液体的固液共存现象

刘耀东 张 益 吴国忠 胡 钧

关键词 离子液体，微观结构，AFM，界面

离子液体是全部由阴阳离子构成、在室温下呈现液态的特殊熔融盐，具有良好应用前景，但离子液体在固体表面的微观结构的研究报道很少。我们用原子力显微镜观察到一种咪唑类离子液体[bmim][PF_6] 在原子级平整的云母表面上的固液共存现象。改变制样手段，可观测到该离子液体所形成的单层、多层和液滴的结构，且形成的固体层在室温下非常稳定。进一步研究表明，固体层生长是沿着云母晶界进行的取向生长，表明该离子液体与云母表面存在强烈的界面相互作用。该工作有助于了解离子液体在固体表面的微观结构以及离子液体这种特殊介质的相结构特征。

Coexistence of liquid and solid phases of [bmim][PF_6] ionic liquid on mica surface at room temperature

LIU Yaodong ZHANG Yi WU Guozhong HU Jun

Key words: Ionic liquid, Microstructure, AFM, Interface

Room temperature ionic liquids (RTIL) are a kind of melt salts, consisting solely of ions, with the melting point at or near room temperature. RTIL have received much attention in past years due to its importance in a broad range of applications, whereas little is understood about the microstructure of RTIL on a solid surface. In this paper we report the coexistence of liquid and solid phases of a prototype ionic liquid (1-butyl-3-methylimidazolium hexafluorophosphate, ([bmim][PF_6]) on mica surface, observed by tapping mode atomic force microscopy (AFM) in air. Single-layer, multi-layers and drop-on-the-layer structures of the ionic liquid were revealed. The solid layers were very stable, and their orientations had a correlation with the mica lattice, indicating the ionic liquid bearing a template-induced ordering process. The study helps understanding interfacial structures of RTILs on solid surface, the analogous structural patterns in both of its solid and liquid phases, and its heterogeneity.

离子液体在碳纳米管内部的相变研究

陈仕谋 吴国忠 沙茂林 黄师荣

关键词 离子液体，碳纳米管，填充，相变

将一种咪唑类室温离子液体[bmim][PF_6]填充到碳纳米管内部，发现该离子液体可以形成一种超高熔点的晶体，其熔点高达 200°C 以上。而在本体中[bmim][PF_6]的熔点只有 6°C。结合离子液体本身的物理化学性质，探讨了在纳米管内部空腔的限域作用下离子液体结构的变化及其稳定晶体的形成机制。我们的结果不但提供了一种制备碳纳米管复合材料的新思路，而且对理解纳米受限空间下的物理化学行为具有重要参考意义。

Transition of ionic liquid [bmim][PF_6] from liquid to high-melting-point crystal when confined in multi-walled carbon nanotubes

CHEN Shimou WU Guozhong SHA Maolin HUANG Shirong

Key words: Ionic liquid, Carbon nanotubes, Filling, Phase transition

A prototype ionic liquid [bmim][PF_6] was encapsulated in MWNTs by capillarity. It was found that [bmim][PF_6] undergoes a fully different phase transition and crystal formation when confined in MWNTs, resulting in the formation of a stable polymorphous crystal possessing a melting point of above 200°C, instead of just 6°C in its bulk system. This novel crystallization behavior is explained by the nano-sized effect of CNTs on the structure of ionic liquid. The results may provide a new way to develop novel type CNTs-based nanocomposite, and are of help for understanding the phase transitions of dimensionally confined environments and the related phenomena within the nanoscale confines.

用超临界 CO_2 发泡法制备开孔 PMMA 微球

黄师荣 吴国忠 陈仕谋

关键词 PMMA 微球，超临界二氧化碳，发泡，开孔微孔

用超临界 CO_2 经快速降压发泡法制得了具有非孔皮层和开孔核心结构的 PMMA 微球。用粒度分析仪、扫描电镜和透射电镜对所得微球进行了表征。详细研究了发泡条件如 CO_2 压力、温度和孔生长时间对所得微球的粒径、粒径分布和形貌的影响。结果表明：粒径随饱和压力和温度的升高而增大，而随孔生长时间的延长而减小。这类微球由于其冲击强度和热稳定性均很高，可用作液晶显示器的间隔球。这类微球也可用于化妆品或药物载体。

Preparation of open cellular PMMA microspheres by supercritical carbon dioxide foaming

HUANG Shirong WU Guozhong CHEN Shimou

Key words: PMMA microspheres, Supercritical carbon dioxide, Foaming, Open cellular pores

Poly(methyl methacrylate) (PMMA) microspheres with a nonporous skin and open cellular core structure were obtained by supercritical carbon dioxide foaming via a pressure quench method. The microspheres were characterized by particle size analyzer, scanning electron microscopy (SEM), and transmission electron microscopy (TEM). Effects of foaming conditions, such as CO_2 pressure, temperature, and cell growth time, on the particle size, size distribution, and morphology of the PMMA microspheres were investigated. It was found that higher foaming temperature and higher pressure re-

sulted in an increase of particle size. However, a longer cell growth time caused a decrease in size of the foamed PMMA microspheres. This type of PMMA microspheres may find use as spacer spheres for liquid crystal displays, due to their high impact strength and high thermal stability. The open cellular microspheres may also be used in cosmetics or as a drug delivery material.

用超临界 CO_2 进行非溶剂诱导相转化以制备微孔 PVDF 膜

黄师荣　吴国忠　陈仕谋

关键词　聚偏氟乙烯，聚甲基丙烯酸甲酯，微孔膜，超临界二氧化碳，相转化

用超临界二氧化碳做非溶剂诱导相转化从聚偏氟乙烯(PVDF)/N,N-二甲基乙酰胺(DMAC)溶液制得了微孔 PVDF 膜。经用 SEM 和 DSC 测试表明，所得 PVDF 膜既具有液－液分相所形成的形貌特性，又具有结晶作用所形成的形貌特性，即由互相连接的 PVDF 粒状微晶所包围的蜂窝状结构。这一结构表明在用超临界二氧化碳诱导的相转化过程中液－液分相和结晶作用两种相分离过程均已发生。研究了 CO_2 压力、温度和起始聚合物浓度对所得膜形貌和结构的影响。也研究了在铸膜液中添加与 PVDF 混溶性好的另一种聚合物 PMMA 对所得膜形貌和结构的影响。结果表明所得膜结构随铸膜液中 PVDF/PMMA 质量比的变化以及聚合物浓度的变化而发生显著的变化。CO_2 压力和温度变化对所得膜结构和形貌的影响较小。此方法可直接得到干膜，无须额外的后处理过程。所得膜可用于生物医药领域。

Preparation of microporous poly(vinylidene fluoride) membranes via phase inversion in supercritical CO_2

HUANG Shirong　WU Guozhong　CHEN Shimou

Key words: Poly(vinylidene fluoride), Poly(methyl methacrylate), Microporous membrane; Supercritical CO_2, Phase inversion

Microporous poly(vinylidene fluoride) (PVDF) membranes were prepared from PVDF/N,N-Dimethylacetamide (DMAC) solutions by using supercritical CO_2 phase inversion process. As revealed by scanning electron microscope (SEM) and differential scanning calorimeter (DSC), the PVDF membranes exhibit morphological characteristics resulting from both liquid–liquid phase separation and crystallization, i.e., cellular pores surrounded by interlinked PVDF particulate crystallites. This indicates that both types of phase-separation processes take place in the supercritical CO_2 phase inversion process. The effects of pressure, temperature, and initial polymer concentration on the final membrane structures were investigated. We also investigated the effect of addition of poly(methyl methacrylate) (PMMA) in the casting dope on the PVDF membrane structure. The membrane structure changed significantly with the variation of PVDF/PMMA mass ratio in the casting dope as well as polymer concentration. It was found that the variation of temperature and pressure has a minor influence on the membrane structure. Dry membrane was directly obtained without additional post-treatment by using this process. The obtained membrane can be used in biomedical fields.

利用两步辐照方法制备聚丙烯酸接枝的碳纳米管

陈仕谋 吴国忠 刘耀东 龙德武

关键词 碳纳米管，辐射聚合，水溶性

我们利用两步辐照的方法：先将多壁碳纳米管(MWNTs)置于乙醇中在 γ 射线下辐照，由于乙醇辐解产生大量的活性物种(如·CH_2CH_2OH, CH_3·$CHOH$)，它们可以与 MWNTs 表面的双键反应并接枝到纳米管的表面，进而达到活化 MWNTs 的目的。这样使得经过活化的 MWNTs 在丙烯酸的水溶液中更易于吸附丙烯酸单体，从而实现丙烯酸在 MWNTs 周围的原位辐射接枝聚合。FT-IR, ^{1}H NMR 和 TGA 的测试结果表明聚丙烯酸高分子链成功地接枝到碳纳米管的表面。透射电镜分析发现改性的碳纳米管表面包覆了一层高分子层，使所得到的纳米管外径增大。通过该法制备的聚丙烯酸改性碳纳米管具有良好的水溶性，而且此法可以用于其他高分子链在碳纳米管表面的接枝聚合改性。

Preparation of poly(acrylic acid) grafted multi-walled carbon nanotubes by a two-step irradiation technique

CHEN Shimou WU Guozhong LIU Yaodong LONG Dewu

Key words: Carbon nanotubes, Radiation polymerization, Water solubility

A facile strategy to prepare water soluble multi-walled carbon nanotubes (MWNTs) by two steps of gamma radiation is developed. Firstly, MWNTs are irradiated in ethanol. The radiolysis of ethanol produces many active species such as·CH_2CH_2OH, CH_3·$CHOH$ which react with C=C bonds on the surface of MWNTs. Afterwards, poly(acrylic acid) (PAA) is covalently grafted to the surface of modified MWNTs by radiation in the presence of acrylic acid. FT-IR, ^{1}H NMR and TGA results showed that PAA chains were successfully grafted onto the surface of MWNTs. The TEM images also provide direct evidence of the formation of a core-shell structure and the external diameter of resultant MWNTs is increased remarkably. The PAA-g-MWNTs have very good solubility in water and other polar solvents. This two-step grafting approach may also be employed to introduce other functional polymer chains onto MWNTs.

聚四氟乙烯(PTFE)分散液的 γ 射线辐照研究

苏杰龙 吴国忠 刘耀东 曾虹燕*

关键词 聚四氟乙烯，辐射降解

聚四氟乙烯(PTFE)具有极低的摩擦系数、非润湿性、高度的热稳定和化学稳定性，也是典型的辐射降解型聚合物。其辐照剂量率、剂量、温度、含氧量等对辐照后产品的化学结构、表面形貌和分子量影响很大。研究了 PTFE 的辐射降解机理，在室温下空气或真空中辐照，主要发生 PTFE 主链断裂。我们着重于研究 PTFE 水性分散液的辐射效应。用差示扫描量热分析，X 射线衍射，

动态光散射，扫描电子显微镜等分析手段考察了辐射剂量对分散液中 PTFE 分子量，结晶度，介质的 pH 值，聚合物颗粒尺寸和形貌等物性的影响。结果表明辐照 100 kGy 后，PTFE 颗粒粒径从原来的 250 nm 降低到 170 nm。辐照 20 kGy 后，PTFE 结晶度升高。剂量继续增大对结晶度影响不大。辐照过程中的化学产额 G(S)为 0.46 μmol/J。

Polytetrafluoroethylene aqueous dispersion irradiated by ^{60}Co gamma rays

SU Jielong　WU Guozhong　LIU Yaodong　ZENG Hongyan*

Key words: Polytetrafluoroethylene, Radiation degradation

PTFE has attracted wide attention for its excellent properties such as low friction coefficient, non-wetting property, and high thermal and chemical resistance. However, PTFE is highly sensitive to radiation and its molecular weight (M_n) decreases rapidly with radiation dose. Upon irradiation by electron beam or γ rays, the chemical structure, morphology and molecular weight of PTFE change considerably depending on the factors including dose rate, dose range, temperature, oxygen content etc. The mechanism of radiation-induced degradation of PTFE has been extensively studied. PTFE predominantly undergoes chain scission when irradiated at room temperature in air or vacuum. The motivation of this work is to investigate in detail the radiation induced degradation of PTFE in dispersion. Radiation effects on molecular weight, crystallinity, medium pH, size and morphology of PTFE particles were studied over a wide dose range. The change in property of PTFE was characterized by photon cross correlation spectroscopy (PCCS), scanning electron microscopy (SEM),X-ray diffraction (XRD), FT-IR spectroscopy and X-ray photoelectron spectroscope (XPS)，differential scanning calorimetry (DSC), etc. It was found that the mean particle size of PTFE reduces from 250 nm of the control to 170 nm at 100 kGy, as confirmed by dynamic laser scattering and SEM. The crystallinity degree of PTFE increased at 20 kGy but remained unvaried at higher doses. *G*-value of scission was 0.46 μmol/J.

*湘潭大学化工学院

辐射乳液聚合制备含氟整理剂

苏杰龙　吴国忠　曾虹燕*

关键词 辐射，乳液聚合，整理剂

采用 γ 射线辐照引发丙烯酸六氟丁酯和甲基丙烯酸十二氟庚酯进行乳液聚合，成功制备了具有拒水拒油功能的含氟织物整理剂。同时研究了甲基丙烯酸十二氟庚酯与丙烯酸丁酯的共聚。分别用傅立叶红外、动态光散射纳米粒度分析仪、透射电镜对产物的化学组分、乳胶粒子尺寸和微观形貌进行了表征。研究了辐照剂量、乳化剂和单体种类对产品制备及性能的影响。结果表明，当辐照剂量为 5 kGy 时，甲基丙烯酸十二氟庚酯的转化率达到 98%，而丙烯酸六氟丁酯的转化率为 76%；当剂量为 10 kGy 时，丙烯酸六氟丁酯单体可聚合完全。经甲基丙烯酸十二氟庚酯聚合物乳液处理的织物表面拒水性能达到六级、拒油性能达到三级。

Preparation of fluorocarbon finishing agents by gamma-ray initiated emulsion polymerization

SU Jielong WU Guozhong ZENG Hongyan*

Key words: Radiation, Emulsion polymerization, Finishing agents

Fluorocarbon finishing agents were prepared by γ-ray initiated emulsion polymerization of fluorine-containing acrylates at different doses. Copolymerization of the fluorocarbon monomer and butyl acrylate was studied. Morphology and size distribution of the emulsion particles were investigated by transmission electron microscopy and dynamic light scattering. Influence of fluorine-containing monomer on water and oil repellency property of final products was discussed. It was found that conversion of the dodecafluoroheptyl methacrylate was 98% at 5 kGy and hexafluorobutyl acrylate was fully polymerized at 10 kGy. Water repellency of the emulsion product derived from dodecafluoroheptyl methacrylate was Grade 6, and oil repellency, Grade 3.

*湘潭大学化工学院

离子液体[bmim][PF6] γ 射线辐射裂解的研究

戚明颖 吴国忠 陈仕谋 刘耀东

关键词 离子液体，γ 射线辐照

室温离子液体在核燃料循环及辐射化学中的应用有赖于对离子液体在辐射状态下稳定性和化学性质作深入研究。我们用 γ 射线辐照纯离子液体[bmim][PF_6]，当剂量增加，[bmim][PF_6]的辐射裂解导致紫外吸收增加，荧光强度下降。拉曼光谱证明伽马发射线辐照造成阳离子正丁基基团化学键的断裂和[PF_6]-阴离子的损坏。DSC 曲线表明，离子液体在低温时呈现两种晶体共存，γ 射线辐照使两种晶体遭到持续的破坏，但辐照剂量对两种晶体的影响不同。

Gamma radiolysis of ionic liquid 1-butyl-3-methylimidazolium hexafluorophosphate

QI Mingying WU Guozhong CHEN Shimou LIU Yaodong

Key words: Ionic liquid, Gamma irradiation

The applications of room-temperature ionic liquids in the nuclear fuel cycle and radiation chemistry depend on a comprehensive knowledge of their stability and chemical properties under radiation conditions. In this work, the effect of γ radiation on pure ionic liquid [bmim][PF_6] was investigated in detail. The radiolysis of [bmim][PF_6] leads to an increase of UV-vis absorbance and a decrease of fluorescence intensity with increasing radiation dose. Raman spectra proved that γ radiation induced significant chemical scission of the n-butyl group (e.g. C-H and C-C scission) and damage to the [PF_6]−

anion. When the irradiated [bmim][PF_6] samples were cooled, two crystal structures were found to co-exist, and they suffered a continuous destruction under irradiation; their dose dependence, however, was different.

SBS 辐射接枝共聚研究(II):线型 SBS 液固相辐射接枝 MAA

付海英　谢雷东　虞 鸣 李林繁　姚思德

关键词　苯乙烯-丁二烯-苯乙烯，接枝聚合物，甲基丙烯酸，辐射接枝

利用 γ 射线辐射接枝法制备苯乙烯-丁二烯-苯乙烯(Styrene-Butadiene-Styrene, SBS)粉体接枝甲基丙烯酸(MAA)聚合物，讨论了单体浓度、辐照剂量、气氛及辐照状态等因素对接枝率的影响，并采用傅立叶红外光谱(FT-IR)、差示扫描量热分析(DSC)、凝胶渗透色谱(GPC)、扫描电镜(SEM)、动态剪切流变(DSR)等分析手段对接枝聚合物进行了表征。研究结果表明，平均粒径为 0.2 mm 的线型 SBS 粉体在辐照剂量为 12 kGy、剂量率为 0.75 kGy/h、MAA/SBS 的质量比为 0.6 时，可获得最大接枝率。FT-IR 谱中 1705 cm^{-1} 处羰基的吸收峰证实了接枝聚合物的存在，分子量分布测定表明 SBS-g-MAA 聚合物的分子量分布变宽；动态剪切流变中接枝聚合物的粘度增大，表明单体在 SBS 链上有接枝链的增长；热分析曲线中聚苯乙烯嵌段的玻璃化转变温度升高以及损耗因子转折温度升高都说明单体 MAA 对 PS 嵌段的影响较大。

Styrene-butadiene-styrene graft copolymerization by γ-ray irradiation (II): Liquid-solid phase graft of MAA onto linear SBS

FU Haiying　XIE Leidong　YU Ming　LI Linfan　YAO Side

Key words:　Styrene-butadiene-styrene, Graft copolymer, Methacrylic acid, Radiation graft

Graft copolymerization of methacrylic acid (MAA) onto SBS powder was studied by ^{60}Co γ-ray irradiation. Effects of the irradiation dose, MAA concentration, and irradiation conditions on the graft yield were studied. The graft copolymer, SBS-g-MAA, was characterized by means of Fourier-transform infrared (FT-IR) spectroscopy, gel permeation chromatography (GPC), scanning electron microscopy (SEM), differential scanning calorimetry (DSC) and dynamic shear rheology (DSR). The -C=O- absorption peak at 1705 cm^{-1} of the FT-IR spectra, and the wilder molecule number distribution of SBS-g-MAA by GPC analysis indicated that the MAA monomer had been grafted onto SBS molecular chains. The DSC analysis revealed all increment of glass transition temperature with PS phase of the grafted SBS, while the DSR showed that the MAA monomer affected the PS phase of SBS more easily.

SBS 辐射接枝 α-甲基丙烯酸(MAA)及含量的测定

付海英 虞 鸣 谢雷东 李林繁 姚思德

关键词 SBS，α-甲基丙烯酸，辐射接枝，定量分析

用辐射法制备了苯乙烯-丁二烯-苯乙烯嵌段聚合物(SBS)接枝 α-甲基丙烯酸(MAA)的接枝聚合物(SBS-g-MAA)，研究了辐射接枝反应中单体转化率、接枝率的变化规律。结果表明：单体浓度为 0.10 g/mL 时，接枝率可达 10.9%。辐照前滤去含有多余单体的清液，接枝率会下降，但减少了单体均聚，滤出液可重复使用，提高了单体的利用率，降低了成本。以滴定法和红外分光光度法结合，测定 SBS-g-MAA 中 1705 cm^{-1} 羰基峰的峰面积，以 SBS 的 1493 cm^{-1} 苯乙烯的特征峰作为内标峰的峰面积，分别以两者峰面积之比与滴定分析测定结果标定 SBS-g-MAA 接枝率，通过线性拟合发现二者具有良好的相关性。该表达式可用于快捷表征 SBS-g-MAA 中 MAA 的含量。

Synthesis of SBS-g-MAA by radiation graft with quantitative express method for measuring MAA content

FU Haiying YU Ming XIE Leidong LI Linfan YAO Side

Key words: SBS, α-methacrylic acid, Radiation graft, Quantitative analysis

In this paper methacrylic acid was grafted onto SBS powder using γ-ray radiation grafting co-polymerization to produce SBS-g-MAA. The effects of monomer concentration, radiation dose and dose rate on graft yield were discussed. The result showed that when MAA was 0.10 g/mL, the graft yield was 10.9%. Although the graft yield was lower if the remaining dipped solution was filtered before radiation, the filtered solution can be reused, which may decrease the cost. The structure properties were also studied through FTIR. The MAA content in the graft product was measured by both titration and FTIR method. A work plot and equation for expressly measuring the MAA content in SBS-g-MAA was obtained by linear fitting.

真丝绸表面光接枝 2-(双甲基胺)乙基甲基丙烯酸酯改性研究

刘瑞芹* 谢雷东 姚思德 盛康龙

关键词 真丝绸，光化学接枝，染色性能，2-(双甲基胺)乙基甲基丙烯酸酯

真丝绸的染色性能差，是制约真丝绸市场竞争力的主要因素之一。在前人使用化学方法和高能辐射方法对真丝绸接枝共聚改性的研究基础上，本工作在不添加任何光引发剂或光敏剂的前提下，利用紫外光对真丝绸表面进行光化学接枝改性。详细研究了紫外光源类型、单体类型、单体浓度、光照时间、反应环境温度、表面活性剂、pH 值等诸多因素对接枝率和相应接枝共聚物的物理化学性质的影响，探索接枝条件对接枝共聚物微观结构和性能的影响规律，并着重研究接枝单体、接枝条件与真丝绸染色性能的对应关系。

为提高真丝绸常用染料——酸性染料在真丝绸上的上染率和耐皂洗色牢度，选择阳离子型单体 2-(Dimethylamino)ethyl methacrylate 作为染座增加剂，对真丝绸进行表面光接枝改性。研究表明，不同接枝体系对真丝绸的各种性能（包括热性能、表面结构、结晶度等）影响差异显著，尤其是对真丝绸染色性能的影响表现出完全相反的结果。

本工作寻找到一种合适的反应体系，在接枝率仅为 4%时，其手感和光泽度、表面微观结构几乎没有变化，但是其他性能发生显著变化，主要表现为：(1) 接枝真丝绸的热稳定性显著提高，接枝链和真丝蛋白之间的作用力较强，相容性较好；(2) 接枝真丝绸的结晶度提高 11.5%；(3) 接枝真丝绸的亲水性有所降低；(4) 改性真丝绸的干弹性也有明显提高，接枝真丝绸的急弹角提高 14.6%，缓弹角提高 12.1%；(5) 改性真丝绸的染色性能显著改善：(a) 酸性染料上染率提高 20%以上; (b)实现常温条件下染色，15℃染色的最终上染率比 90℃常规染色工艺高 16%; (c) 染色深度显著提高;(d) 染色后再进行光接枝，可显著提高染色真丝绸的耐皂洗色牢度。

与 ^{60}Co γ 射线或电子束辐射接枝相比，真丝绸 UV 光接枝法具有设备简单、操作方便、反应易控制、适用范围宽、安全性好、易于在真丝绸印染后整理工序实施等优点；与传统的化学接枝方法相比，无引发剂或光敏剂的真丝绸光接枝改性方法除设备简单等优点外，还可最大程度地降低对真丝绸的污染，而且均聚物少、接枝均匀、后处理简单。

Photo-induced graft-copolymerization of 2-(dimethylamino) ethyl methacrylate onto silk fabrics to improve dyeing properties

LIU Ruiqin* XIE Leidong YAO Side SHENG Kanglong

Key words: Silk fabrics, Photo-induced graft-copolymerization, Dyeing properties, 2-(dimethylamino) ethyl methacrylate

A new method has been established to graft vinyl monomers onto silk fabrics by ultraviolet rays without any initiator or photosensitizer, in an attempt to improve undesirable properties of the materials with increased wrinkle recovery, better dyeing ability and color-fastness, and higher resistance to photo-yellowing, etc. In this work, effectiveness of different types of UV devices and experimental conditions of the photo-induced graft-copolymerization were investigated to control the influential factors on the grafting yield and properties of the graft-copolymer. Surface characteristics and structure changes, thermal properties and wrinkle resistance of grafted silk fabrics were studied. The grafted silk fabrics showed improved properties in crease resistance, dyeing ability and color-fastness, and heat stability as well. In detail, graft-copolymerization of 2-(dimethylamino)ethyl methacrylate onto silk fabrics can make silk fabrics undergo from slight to drastic changes in their dyeing behavior, i.e., rate of dyeing and uptake of acid dyes. Different reaction systems of the same monomer can lead to reverse dyeing properties, indicating not only the function but also the structure affects the properties of grafted silk fabrics, especially the color-fastness. The UV light graft copolymerization method is of significance in silk industrial applications in terms of the facility cost, operation convenience and grafting efficiency, in comparison to ^{60}Co γ-ray and electron beam irradiation facilities.

*上海交通大学机械与动力工程学院

SBS 的辐照效应研究

李林繁　谢雷东　张 艳　付海英　张凤英　盛康龙

关键词　苯乙烯–丁二烯–苯乙烯，γ 射线，辐照效应

研究了室温下苯乙烯-丁二烯-苯乙烯(Styrene-Butadiene-Styrene，SBS)在 ^{60}Coγ 射线下的辐照效应。采用傅立叶红外光谱(FT-IR)、差示扫描分析(DSC)、热重分析(TG)、扫描电镜(SEM)、动态剪切流变(DSR)等分析方法对辐照产物进行了表征。辐照产物经红外光谱分析，未发现有氧化物生成；SBS 辐照后发生交联反应，随着吸收剂量的升高，不溶于甲苯的交联 SBS 量增加；DSC 和 TG 表明辐照后材料的柔性聚丁二烯嵌段和刚性聚苯乙烯嵌段的玻璃化温度向高温方向移动，同时有更高的玻璃化温度点形成，耐高温物质量增加；动态剪切流变分析表明辐照后出现新的网络松弛行为，吸收剂量越高，材料的损耗因子峰越明显；辐照后 SBS 剪切粘度变大，储能模量增加，损耗模量下降，材料的温度敏感性下降；扫描电镜分析表明 SBS 辐照后抗氧化性能也得到了提高。

Irradiation effects of styrene-butadiene-styrene copolymer

LI Linfan　XIE Leidong　ZHANG Yan　FU Haiying　ZHANG Fengying
SHENG Kanglong

Key words:　Styrene-Butadiene-Styrene (SBS), γ-ray, Irradiation effect

The effect of SBS irradiated with ^{60}Co γ-rays at ambient temperature was studied in this article. SBS before and after irradiation were characterized by means of Fourier-transform infrared spectroscopy(FT-IR), differential scanning calorimetry (DSC), thermal gravimetric analysis(TG), scanning electron microscopy(SEM), and dynamic shear rheology(DSR). Almost no oxidation substance product was found in FT-IR spectra of the irradiated SBS. Cross-linking reaction occurred after SBS irradiation, and with increasing doses, the mass ratio of indiscerptible content in toluene developed, increasing sharply with the dose when it exceeds 50 kGy. The DSC and TA analyses indicated that T_g of the flexible segment PB and rigid part PS shifted to a high temperature to some extent. A higher T_g of about 120 ℃ came into being and the substance of resisting high temperature increased. According to DSR analysis, a network relaxation was observed after irradiation. The higher the irradiation dose was, the more obvious the peak value of tan δ was. In addition, the shearing viscosity and the storage modulus G' became larger and the loss modulus G'' became smaller than those before irradiation. Temperature sensitivity of the irradiated SBS also reduced. The SEM analysis showed that irradiation can improve the antioxygenic performance of SBS.

SBS 液相共辐射接枝马来酸酐/苯乙烯二元单体研究

张 艳　谢雷东　李林繁　付海英　盛康龙

关键词　苯乙烯-丁二烯-苯乙烯嵌段共聚物，马来酸酐，苯乙烯，辐射接枝

本文在苯乙烯-丁二烯-苯乙烯嵌段共聚物 (Styrene-Butadiene-Styrene triblock copolymer, SBS)辐射接枝马来酸酐（Maleic anhydride, MAH）的基础上，进行 MAH/苯乙烯 (Styrene, St)二元单体辐射接枝研究，讨论了 MAH /St 比例和总浓度及吸收剂量对接枝率的影响。就 MAH 接枝产物 SBS-g-MAH 和 MAH/St 二元接枝产物 SBS-g-MAH/St 进行了傅立叶红外光谱(FT-IR)、热重(TG)分析与差示扫描量热(DSC)分析等表征与分析。结果表明：MAH/St 二元接枝可明显提高 MAH 接枝率。

Liquid phase radiation graft copolymerization of MAH/St onto SBS

ZHANG Yan　XIE Leidong　LI Linfan　FU Haiying　SHENG Kanglong

Keywords: Styrene-butadiene-styrene block copolymer, Maleic anhydride, Styrene, Radiation graft

Based on studies at SINAP on radiation-induced graft copolymerization of styrene-butadiene- styrene (SBS) copolymer with maleic anhydride (MAH), maleic anhydride/styrene (MAH/St) binary monomers system grafting onto SBS was investigated. Effects of the comonomer composition, concentration and irradiation dose were studied. The graft copolymer was characterized by Fourier-transform infrared, thermogravimetric analysis and differential scanning calorimetry. The results showed that binary graft could increase the grafting yield of MAH.

废水中 4-氯酚的辐射处理新方法

姚思德　窦大营　付海英　刘思恒* 汪世龙* 孙晓宇*

关键词 持久性有机物，4－氯酚，辐射，废水

污染的 80%源于工业，清洁水源的缺乏将严重影响环境和人类健康，故持久性有机物(POP)降解具有重大意义。POP 的绝大多数组分为含苯环衍生物，故辐射技术是 POPs 矿化的有效方法。但是，目前依然存在废水处理设备及其运行成本过高的问题。可以设想在低辐照剂量条件下(小于 20kGy)将 POP 的苯环打开，并在氧气条件下转化为有机酸和其他化学物，那么持久性有机物在辐照后可以采用生物方法来进行处理。很显然，将不同工艺结合起来可用于处理芳烃污染废水，能克服去除 TOC 所需高辐照剂量的缺点。本文以 4-氯酚作为 POP 模型，采用脉冲辐解和激光光解研究了其降解机理。实验结果表明，4-氯酚在碱性条件、饱和氧气氛围下可有效转化为有机酸。

Innovation technique of radiation for the treatment of 4-chlorphenol as a model of POP's in waste water

YAO Side　DOU Daying　FU Haiying　LIU Siheng*　WANG Shilong*
SUN Xiaoyu*

Key words: POPs, 4-chlorphenol, Radiation, Waste water

The pollution becomes more serious with the development of economy in China especially for waste water, among which 80% comes from industries. The absence of fresh water has large limitation to the development of China now. Because it will bring the most harmful results to environment and health of people, the degradation of POPs is very important. Radiation is one of the effective methods for mineralization of POPs as most of their compounds are derivatives of phenyl ring. However, the costs of equipment and operation are too high to use for irradiation.

It should be supposed that breakage of benzene ring of POPs at lower irradiated dosage (below 20kGy) in developed radiation processing turns into organic acids and other compounds, which could be removed by micro-organisms easily. It means that after irradiation organic materials can be treated by the use of biological method. It is obvious that integration of different processing could both use the advantage of breaking phenyl ring under lower dosage and overcome the disadvantage of reducing the TOC at very high dosage by use of irradiation.

In this paper, the radiolytical mechanism of 4-chlorphenol as a model of POPs has been studied by the use of pulse radiolysis and analysis of stable products irradiated in different conditions. It has been shown that 4-chlorphenol can be turned into organic acids effectively in basic aqueous solution saturated with oxygen under lower irradiated dosages.

*同济大学

蒽醌在离子液体[bmim][PF_6]与有机溶剂混合体系中的激光光解研究

朱光来　徐静静　吴国忠　朱红平　龙德武　陈仕谋　姚思德

关键词　1-丁基-3-甲基咪唑六氟磷酸盐，激光光解，蒽醌，速率常数

利用时间分辨激光光解技术对咪唑型离子液体 1-丁基-3-甲基咪唑六氟磷酸盐([bmim][PF_6])与有机溶剂(MeCN，DMF)的混合体系中的光化学反应行为进行了研究。考察了探针分子存在下[bmim][PF_6]/organic 比例对体系中化学反应动力学的影响，结果表明，离子液体自身参加了反应，且反应速率常数随着 RTIL/organic 比例的变化呈现规律性的变化，观察到一个明显的临界点。在临界点之前，表观速率常数随离子液体体积分数 V_{RTIL} 的增大而增大；在临界点后，表观速率常数随 V_{RTIL} 的增大而减小。给出了混合体系中激光诱导化学反应的速率常数，并确定其反应机理。

Laser photolysis study of anthraquinone in binary mixtures of ionic liquid [bmim][PF_6] and organic solvent

ZHU Guanglai　XU Jingjing　WU Guozhong　ZHU Hongping　LONG Dewu
CHEN Shimou　YAO Side

Key words: 1-butyl-3-methylimidazolium hexafluorophosphate, Laser photolysis, Anthraquinone, Rate constant

Photochemical properties of the ionic liquid (RTIL) 1-butyl-3-methylimidazolium hexafluorophosphate [bmim][PF_6] and its binary mixed solutions with organic solvent (DMF and MeCN) were

investigated by laser photolysis at an excitation wavelength of 355 nm, using anthraquinone (AQ) as a probe molecule. It was indicated that the triplet excited state of AQ (^{3}AQ*) can abstract hydrogen from [bmim][PF_6]. Moreover, along with the change of the ratio of RTIL to organic solvent, the reaction rate constant changes regularly. Critical points were observed at volume fraction V_{RTIL} = 0.2 for RTIL/MeCN and V_{RTIL} = 0.05 for RTIL/DMF. For both systems, before the critical point, the rate constant increases rapidly with increasing V_{RTIL}; however, it decreases obviously with V_{RTIL} after the critical point. We conclude that the concentration dependence is dominant at lower V_{RTIL}, while the viscosity and phase transformation are dominant at higher V_{RTIL} for the effect of ionic liquid on the decay of rate constant.

离子液体[bmim][PF_6]的激光光解研究

朱光来　吴国忠　龙德武　沙茂林　姚思德

关键词　[bmim][PF_6]，激光光解，三线态，光电离

利用时间分辨激光光解技术研究了咪唑型离子液体[bmim][PF_6]的光解行为，研究发现离子液体能被 266 nm 激光光激发和光电离，生成阳离子自由基、中性自由基等瞬态产物。观察到咪唑阳离子激发三线态与 β-胡萝卜素的能量转移过程，以及与 TMPD 的电子转移过程，测定了其单电子转移速率常数为 1.2×10^5 L·mol^{-1}·s^{-1}。验证了咪唑阳离子确实能够快速捕获水合电子或溶剂化电子。

Laser photolysis of ionic liquid [bmim][PF_6]

ZHU Guanglai　WU Guozhong　LONG Dewu　SHA Maolin　YAO Side

Key words:　[bmim][PF_6], Laser flash photolysis, Triplet state, Photoionization

Photoinduced chemical reactions of 1-butyl-3-methylimidazolium hexafluorophosphate ([bmim][PF_6]) were studied by laser photolysis at a wavelength of 266 nm. Excited triplet state ^{3}[bmim]$^{+*}$ was observed, radical cation [bmim]$^{2+\bullet}$ and neutral [bmim]$^{\bullet}$ radical via photoionization were also formed. Energy transfer from ^{3}[bmim]$^{+}$* to β-carotene was investigated. Oxidation via one electron transfer from TMPD to ^{3}[bmim]$^{+}$* has been also observed and the rate constant was determined to be 1.2×10^5 L·mol^{-1}·s^{-1}. The reaction of [bmim][PF_6] with hydrated electron (e_{aq}^-) was confirmed by laser photolysis in aqueous solution.

己烯雌酚活性瞬粒子的辐解与光解研究

窦大营　刘永彪　赵红卫　孔 玲　姚思德

关键词　己烯雌酚，辐解，光解

己烯雌酚是环境中普遍存在的雌激素，本文用脉冲辐解和激光光解考察了其辐解瞬态产物的动力学特性。众所周知，苯环的双键被认为是高能电子束辐照产生羟基自由基攻击的最敏感位点。激光光解研究表明，己烯雌酚在 248 nm 处光电离生成脱质子的中性自由基或被激发产生三线态；

研究表明在 UV、氧气饱和氛围下己烯雌酚能被有效降解。由于脉冲辐解和激光光解中产生的活性粒子都会引发环境生物学效应，因此对己烯雌酚降解机理的研究将有助于解决环境激素问题。

Radiolysis and photolysis studies on active transient species of diethylstilbestrol

DOU Dayin LIU Yongbiao ZHAO Hongwei KONG Ling YAO Side

Key words: Diethylstilbestrol, Radiolysis, Photolysis

Diethylstilbestrol (DES) is one of the most active estrogens in the environment. In this paper pulse radiolysis and laser flash photolysis studies were carried out to investigate mechanisms and dynamic characteristics of the transient species of DES produced by UV light and electron beam irradiations. The double bond between the benzene rings was supposed to be the most sensitive site attacked by hydroxyl radicals under high-energy electron beam irradiations. In laser flash photolysis DES was found to be either photoionized or excited by 248 nm laser to produce deprotonated radical cations and excited triplet states. It was found that DES could be degraded completely in oxygen- saturated aqueous solution under the UV lights. All the active species produced in pulse radiolysis and laser flash photolysis can cause environmental biologic effects. The work on degradation mechanisms of DES can be of help in finding ways to solve the environmental DES problems.

$[Me_3NC_2H_4OH]Zn_2Cl_5$ 水溶液的激光光解研究

付海英 吴国忠 龙德武 刘耀东 王文峰 姚思德

关键词 离子液体，胆碱，单光子电离，激光光解

用时间分辨激光光解技术研究了季铵盐型离子液体$[Me_3NC_2H_4OH]Zn_2Cl_5$(R–Zn_2Cl_5)的光解行为，研究发现离子液体能被 266 nm 激光单光子电离，生成阳离子自由基、$[Zn_2Cl_5]$,中性自由基和水合电子，观察到胆碱激发三线态的存在，并测定了离子液体光电离的量子产额为 0.04．利用 266 nm 激光对离子液体、胆碱、氯化锌、氯化钠的光解行为进行比较，发现胆碱阳离子的贡献很小，$[Zn_2Cl_5]^-$阴离子起主要作用。采用氧化性自由基 $SO_4^{\cdot -}$引发离子液体的氧化，揭示其光电离机理，测定离子液体的动力学反应速率常数，测得 $SO_4^{\cdot -}$ 在 460 nm 的衰减速率常数为 1.3×10^9 $L\cdot mol^{-1}\cdot s^{-1}$，在 320 nm 测得离子自由基瞬态产物的生成速率常数为 1.5×10^9 $L\cdot mol^{-1}\cdot s^{-1}$，两者很接近，说明 $SO_4^{\cdot -}$ 自由基的衰减与瞬态自由基的生成是同步的。

Laser photolysis of $[Me_3NC_2H_4OH]Zn_2Cl_5$ aqueous solution

FU Haiying WU Guozhong LONG Dewu LIU Yaodong

WANG Wenfeng YAO Side

Key words: Ionic liquid, Choline, Monophotonic ionization, Laser photolysis

The absorption spectra of $[Me_3NC_2H_4OH]Zn_2Cl_5$ (R-Zn_2Cl_5) in aqueous solutions were studied by time-resolved laser photolysis, and the mechanism of monophotonic ionization was suggested. The oxi-

dizing radical SO4·- was used to produce radical cation. Comparing the laser flash photolysis of R-Zn_2Cl_5 with that of NaCl, $ZnCl_2$ and choline system, it can be found that [Zn_2Cl_5]- played an important role in photo-ionization, while [$Me_3NC_2H_4OH$]·+ cation had little contribution to its photolysis. Rate constant for the oxidation reaction was determined in R-Zn_2Cl_5 ionic liquid system. The second-order decay rate constant of SO_4·- observed at 460 nm, 1.3×10^9L·mol^{-1}·s^{-1}, was almost equal to the forming rate constant of 1.5×10^9L·mol^{-1}·s^{-1} observed at 320nm with the transient species produced in laser photolysis of R-Zn_2Cl_5 aqueous solution. It was confirmed that the decay process of SO_4·- was synchronic with the forming process of (Zn_2Cl_5).

焦脱镁叶绿酸-a 作为光活化农药的光活化机理研究

吴铁一 屠铁城 赵红卫 陈志龙* 姚思德

关键词 焦脱镁叶绿酸-a，光活化农药，单线态氧，电子自旋共振

介绍了焦脱镁叶绿酸-a 作为光活化农药的可能性，利用激光光解时间分辨吸收技术和自旋捕获 EPR 技术对其光活化机制进行了研究。研究发现，焦脱镁叶绿酸-a 的光活化反应主要沿 II 型即单线态氧机制进行。另外，还就单线态氧对选定的光敏氧化损伤生物靶分子(DNA，亚油酸和 L-色氨酸)的作用进行了探索。

Mechanisms of pyrophaeophorbide-a, a photoactivated pesticide

WU Tieyi TU Tiecheng ZHAO Hongwei CHEN Zhilong* YAO Side

Key words: Pyrophaeophorbide-a, Photoactivated pesticide, Singlet oxygen, Electron paramagnetic resonance

Possibility of pyrophaeophorbide-a as a photoactivated pesticide was presented. Its photoactivated mechanism was studied by use of time-resolved laser flash photolysis and spin trapped EPR technique. It has been revealed that the photo-activation of pyrophaeophorbide-a is mechanism II of oxygen singlet. And the photo-sensitized damage of biological macromolecules, such as DNA, oleic acid and tryptophane has been explored by use of pyrophaeophorbide-a as photo-activator.

*中国人民解放军第二军医大学海军医学系

光化学制备用于链亲和素固定的胺基磁性纳米凝胶的研究

宫培军 洪 军 刘兴奋 余家会 樊春海 董 黎 姚思德

关键词 聚烯丙基胺，磁性纳米凝胶，紫外辐照，链亲和素

本工作提出制备胺基磁性纳米凝胶的一种改进方法。在含有烯丙基胺的 Fe_3O_4 水分散液中，运用紫外光辐照引发烯丙基胺原位聚合，一步法制备了聚烯丙基胺磁性纳米凝胶(PAA-MNGs)。透射电子显微镜(TEM)和光子相关光谱(PCS)表征了 PAA-MNG 的形貌和粒径分布；热重分析(TGA)确定了磁性成分的含量，振动样品磁强计(VSM)测试表明其呈现超顺磁性。利用表面的伯胺基，

PAA-MNGs 可方便地偶联蛋白等生物大分子。链亲和素(SA)经 1-乙基 3-(3-二甲氨基)碳化二亚胺盐酸盐和 N-羟基琥珀酰亚胺活化后可共价固定在 PAA-MNGs 上，得到链亲和素包覆的纳米磁球(SA-MNPs)。用探针生物素对硝基苯酯(BNPE)通过光谱检测证实了 SA-MNPs 的生物素结合能力。表明 PAA-MNGs 适合于作为载体偶联蛋白等生物大分子，并可用于生物技术领域的诸多方面

Photochemical preparation of amino-functionalized magnetic nanogels for immobilization of streptavidin

GONG Peijun HONG Jun LIU Xingfen YU Jiahui FAN Chunhai
DONG Li YAO Side

Key words: Polyallylamine, Magnetic nanogels, UV irradiation, Streptavidin

An improved approach for preparing amino-modified magnetic nanogels has been developed in this paper. Polyallylamine magnetic nanogels (PAA-MNGs) were synthesized in one step by photoinitiation and in situ photopolymerization of allylamine in Fe_3O_4 aqueous suspension under UV irradiation. Morphology, mean diameter and diameter distribution of the PAA-MNGs were measured by TEM and PCS respectively, while the magnetite content was confirmed by TG and the superparamagnetism identified by VSM. Biomolecules, such as proteins, can be coupled to the surface of PAA-MNGs in virtue of amino groups. Streptavidin-coated magnetic nanoparticles (SA-MNPs) were prepared by covalent immobilization of streptavidin (SA) activated by 1-ethyl-3-(3-dimethyl- laminopropyl) carbodiimide hydrochloride (EDC) and N-hydroxysuccinimid (NHS) on PAA-MNGs. The biotin binding capacity of SA-MNPs was proved by colorimetric measurements using the probe biotin p-nitrophenyl ester (BNPE). Therefore, PAA-MNGs may be a suitable vehicle to carry biomolecules for biotechnology applications.

聚丙烯酰胺包覆磁性纳米凝胶的光化学法制备及机理研究

孙汉文 徐冬梅 孟繁宗* 王敦青* 洪 军 宫培军 薛艳玲 董 黎 姚思德

关键词 聚丙烯酰胺，光化学合成，磁性纳米凝胶，电子自旋共振波谱

以丙烯酰胺为单体，N,N'-亚甲基双丙烯酰胺为交联剂，用光化学法在水溶液体系中制备了聚丙烯酰胺(Polyacrylamide, PAM)包覆的磁性纳米凝胶，用傅立叶变换红外光谱(FT-IR)、光子相关光谱(PCS)和电子自旋共振(ESR)波谱表征了聚丙烯酰胺磁性纳米凝胶。研究了磁性纳米凝胶粒径随反应时间、单体浓度、交联剂浓度的变化规律，并探索了聚丙烯酰胺磁性纳米凝胶的包覆机理。

Polyacrylamide-coated magnetic nanogels prepared via photochemical method and the coating mechanism

SUN Hanwen XU Dongmei MENG Fanzong* WANG Dunqing* HONG Jun
GONG Peijun XUE Yanling DONG Li YAO Side

Key words: Polyacrylamide, Photochemical synthesis, Magnetic nanogels, ESR

Polyacrylamide-coated magnetic nanogels were synthesized via photochemical polymerization under UV light irradiation. Polyacrylamide-coated magnetic nanogels were characterized by Fourier transform infrared spectroscopy and photo correlation spectroscopy. It was found that particle size of the polyacrylamide-coated magnetic nanogels increased with the reaction time and monomer concentration, but decreased with increasing concentration of the cross-linker of N, N'-methylene-bis-(acrylamide). The coating mechanisms were studied by ESR measurements of the nanogel samples.

*德州学院

粒径可控的羧基化磁性纳米凝胶的合成

洪 军　徐冬梅　宫培军　余家会　孙汉文　姚思德

关键词　光化学原位聚合，磁性纳米凝胶，可控合成

采用光化学原位聚合法制备了粒径可控的羧基化磁性纳米凝胶，研究了滴加单体的量、体系pH、光照时间和链转移剂等对羧基化磁性纳米凝胶粒径的影响。

Synthesis of particle size controllable carboxyl-functionalized magnetic nanogels

HONG Jun　XU Dongmei　GONG Peijun　YU Jiahui　SUN Hanwen　YAO Side

Key words:　Photochemical in situ polymerization, Magnetic nanogels, Controllable synthesis

In this paper, particle size-controllable carboxyl-functionalized magnetic nanogels were synthesized via photochemical in situ polymerization. Effects of system pH value, volume of monomer dropped irradiation time and chain transfer agent on the particle size of the carboxyl-functionalized magnetic nanogels were detailedly investigated.

光化学原位合成 PHEMA 磁性纳米凝胶

宫培军　孙汉文　洪军　徐冬梅　姚思德

关键词　磁性纳米凝胶，光化学聚合，甲基丙烯酸 2-羟基乙酯，超顺磁性

本文用光化学方法一步合成磁性纳米凝胶。在亲水性 Fe_3O_4 磁流体中，以甲基丙烯酸 2-羟基乙酯(HEMA)为单体，N,N-亚甲基双丙烯酰胺(MBA)为交联剂，紫外光辐照下原位聚合制备了聚(甲基丙烯酸 2-羟基乙酯)(PHEMA)磁性纳米凝胶。其磁含量达 90%，磁性测量表明凝胶呈现超顺磁性，用 SEM 和 TEM(扫描和透射电子显微镜)观测了表面形貌和粒径，用光子相关光谱(PCS)测得其平均水合粒径及粒径分布，发现外壳层凝胶溶胀能力大。单体浓度、光照时间对产物粒径的影响研究表明，磁性纳米凝胶的平均水合粒径可调控在 55.4~144.5 nm 范围内。对包敷机制也进行了探索。

One-pot synthesis of magnetic nanogels via photochemical method

GONG Peijun SUN Hanwen HONG Jun XU Dongmei YAO Side

Key words: Magnetic nanogels, Photochemical polymerization, 2-hydroxyethyl methacrylate, Superparamagnetism

One-pot synthesis of magnetic nanogels via photochemical method is reported in this paper. Poly (2-hydroxyethyl methacrylate) (PHEMA) magnetic nanogels are synthesized by in-situ polymerization of 2-hydroxyethyl methacrylate (HEMA) and N,N'-methylene-bis-(acrylamide) (MBA) in Fe_3O_4 aqueous suspension under UV irradiation. The structure and compositions of magnetic nanogels are characterized by FTIR, TGA, SEM, TEM and PCS. TGA measurement indicates that magnetic nanogels contain 90% magnetite. Both naked Fe_3O_4 and magnetic nanogels are superparamagnatic at room temperature according to magnetization curves. The swollen capability of the hydrogel shell is proved by contrasting the particles sizes obtained by SEM, TEM and PCS. Particle diameters can be manipulated by changing monomer concentration and irradiation time. A mechanism of the coating process is proposed.

羟基磁性纳米凝胶的紫外光辐照制备及其表征

宫培军 余家会 孙汉文 洪 军 赵素芳 徐冬梅 姚思德

关键词 磁性聚合物，凝胶，光化学，逐步生长聚合，溶胀性

作者发明了一种采用 UV 诱导光聚合生成带有溶胀性壳层的高分子磁性凝胶的方法。该实验以甲基丙烯酸 2-羟基乙酯(HEMA)为单体，N,N-亚甲基双丙烯酰胺(MBA)为交联剂，在无任何添加剂的条件下，紫外光辐照下原位聚合制备了聚（甲基丙烯酸 2-羟基乙酯）(PHEMA)磁性纳米凝胶。由于聚合物的一步聚合，可通过改变光照时间、滴加单体的量实现对纳米凝胶粒径的控制。通过 X-射线衍射、傅立叶红外光谱、热重分析等对 Fe_3O_4 核的晶体结构及纳米凝胶的化学组成进行了表征。采用光子相关光谱和 TEM 分别对纳米凝胶在溶涨状态及干态下粒径大小及分布进行了表征。采用 TEM 观察纳米凝胶在溶胀状态下及酸腐蚀后的形貌。通过磁滞回线的测定确认了磁性纳米凝胶的高磁性和室温下的超顺磁性。

Preparation and characterization of OH-functionalized magnetic nanogels under UV irradiation

GONG Peijun YU Jiahui SUN Hanwen HONG Jun ZHAO Sufang
XU Dongmei YAO Side

Key words: Magnetic polymers, Gels, Photochemistry, Step-growth polymerization, Swelling

A novel preparation method of net magnetic polymer nanogels with swollen shell was developed. UV-induced photopolymerization of 2-hydroxyethyl methacrylate (HEMA) was performed in magnetite aqueous suspension free of additive to obtain monodisperse magnetic nanogels with swollen shell. Ow-

ing to step-growth polymerization of the monomer, particle size of the magnetic nanogels can be conveniently manipulated by controlling the irradiation time and the monomer amount. Crystalline structure of the Fe_3O_4 core and chemical composition of the nanogels were characterized by X-ray diffraction (XRD), Fourier transform infrared spectroscopy (FTIR) and thermogravimetric analysis (TGA), respectively. Particle sizes, size distributions of magnetic nanogels in swollen state and dry state were measured by photo-correlation spectroscopy (PCS) and transmission electron microscopy (TEM). Morphology of the swollen nanogels and polymer capsules obtained from magnetic nanogels etched by hydrochloride acid were observed by TEM. The high magnetizations and superparamagnetic behaviors of naked Fe_3O_4 and magnetic nanogels at room temperature were confirmed by the measurement of hysteresis curves.

新型核壳型聚丙烯酰胺包覆的磁性纳米粒子的光化学制备

孙汉文 洪 军 孟繁宗* 宫培军 余家会 薛艳玲 赵素芳
徐冬梅 董 黎 姚思德

关键词 磁铁矿，光化学聚合，包覆，核壳结构

在磁铁矿纳米粒子的悬浊液中，采用光化学引发来制备聚合物包覆的磁性纳米粒子，并就其机理进行了讨论；分别采用 TEM、XRD、VSM 等手段对纳米粒子的形貌、晶体结构、磁学性质进行表征；采用磁滞回线来确认磁性纳米粒子的超顺磁性、强磁性和磁响应性。

Novel core-shell structure polyacrylamide-coated magnetic nanoparticles synthesized via photochemical polymerization

SUN Hanwen HONG Jun MENG Fanzong* GONG Peijun YU Jiahui
XUE Yanling ZHAO Sufang XU Dongmei DONG Li YAO Side

Key words: Magnetite, Photochemical polymerization, Coating, Core-shell structure

A novel synthesis method of polymer-coated magnetic nanoparticles was developed. UV-induced photochemical polymerization of acrylamide in magnetite aqueous suspension was used to obtain core-shell structure polyacrylamide-coated magnetic nanoparticles. Mechanism of UV-induced photochemical coating was discussed. Morphology, crystalline structure and magnetic properties of the polyacrylamide-coated magnetic nanoparticles were characterized by transmission electron microscopy (TEM), X-ray diffraction (XRD) and vibrating sample magnetometer (VSM). Superparamagnetic behaviors, high saturation magnetization and good response to external magnetic field were confirmed by measuring the magnetic hysteresis curves.

*德州学院

Alpha-胰凝乳蛋白酶在含高分子亲水性纳米层的磁性纳米粒子上的固定化

洪 军 宫培军 余家会 徐冬梅 孙汉文 姚思德

关键词 固定化酶，光化学原位聚合，Alpha-胰凝乳蛋白酶，磁性纳米凝胶

通过霍夫曼降解聚丙烯酰胺包覆的纳米粒子制备表面带有活性氨基的磁性纳米凝胶，采用 EDC 和 NHS 将 alpha-胰凝乳蛋白酶成功固定到其表面；简要讨论了光化学原位聚合机理。研究发现，磁核 Fe_3O_4 在酶固定化后依然保持其超顺磁性，但其磁饱和强度略有降低；氙灯辐照并未导致 Fe_3O_4 晶体结构的改变。用 BCA 蛋白测试和热重分析分别得出固定化酶的载酶量为 69 mg 酶/g 凝胶和 61 mg 酶/g 凝胶。固定化酶的比活力为 0.93 U/(mg min)，仅为自由酶活力的 59.3%。固定化后，酶的热稳定性提高。

Conjugation of alpha-chymotrypsin on a polymeric hydrophilic nanolayer covering magnetic nanoparticles

HONG Jun GONG Peijun YU Jiahui XU Dongmei SUN Hanwen YAO Side

Key words: Immobilized enzyme, Photochemical in situ polymerization, Alpha-chymotrypsin, Magnetic nanogel

Magnetic nanoparticles, covered by hydrophilic nanolayer containing reactive amino groups, were obtained *via* Hoffman degradation of polyacrylamide-coated Fe_3O_4 nanoparticles synthesized by photochemical *in situ* polymerization, and conjugated the model enzyme—alpha-chymotrypsin (CT) by EDC·HCl and NHS at room temperatures. Mechanism of the *in situ* polymerization was proposed. Superparamagnetic properties were retained for Fe_3O_4 after enzyme immobilization while slightly reducing the value of saturation magnetization. Crystalline structure of Fe_3O_4 after CT immobilization was consistent with freshly prepared Fe_3O_4. The binding capacity was 69 and 61 mg enzyme/g nanogel determined by standard BCA protein assay and thermogravimetric (TG) analysis respectively. Specific activity of the immobilized CT was 0.93U/(mg min), only 59.3% as that of free CT. Thermal stability of the CT bound to amine-functionalized magnetic nanogel was improved.

水溶液体系中光化学可控合成核壳结构磁性纳米凝胶

孙汉文 余家会 徐冬梅 宫培军 洪军 张春富 姚思德

关键词 磁性纳米凝胶，光化学方法，核壳结构，控制合成

用光化学法合成并经 Hoffmann 降解获得了壳层带有伯胺基核壳结构的磁性纳米凝胶，粒径分布窄且粒径可控。其壳层水凝胶具有很好的亲水性和生物相容性，且反应过程中不加入任何表面活性剂，为该磁性纳米凝胶的生物应用奠定了良好基础。光化学法合成窄粒径分布且粒径可控的磁性纳米凝胶，尚未见到文献报道，有望为磁性纳米凝胶的合成提供新方法。用傅立叶变换红外光谱、光子相关光谱、原子力显微镜和透射电子显微镜对产物进行了表征。

Core-shell magnetic nanogel synthesis in aqueous solution via surfactant-free photochemical reaction

SUN Hanwen YU Jiahui XU Dongmei GONG Peijun HONG Jun
ZHANG Chunfu YAO Side

Key words: Magnetic nanogels, Photochemical method, Core-shell structure, Controllable synthesis

Core-shell poly(acrylamide) modified magnetic nanogels with narrow particle size distribution were synthesized in surfactant-free aqueous solution via photochemical method. Size of the nanogels can be controlled by varying the reaction time, or contents of the monomer and cross-linker. After Hoffmann degradation of amido groups, the magnetic nanogels with amino groups were obtained. The magnetic nanogels were characterized by Fourier transform infrared spectroscopy (FT-IR), photo correlation spectroscopy (PCS), atomic force microscopy (AFM) and transmission electron microscopy (TEM).

光化学法合成高基因转染效率的聚乙烯亚胺

徐冬梅 余家会 刘永彪 孙汉文 宫培军 洪 军 姚思德

关键词 聚乙烯亚胺，光化学，基因转染

本文介绍在室温下用光化学方法合成聚乙烯亚胺凝胶的新方法，合成的凝胶粒径在 8－200 nm 间可控，且具有窄的粒径分布。合成的新型基因转导载体纳米凝胶的粒径和表面电位用 PCS 进行表征，其圆球型结构可用 SEM 测定，并被 AFM 的测定所证实。使用人源肺和肝癌细胞所作的体外研究，以小鼠所作的动物体内研究表明，这种基因载体纳米凝胶具有高的储存稳定性、低的细胞毒性和免疫毒性。有关合成和应用的后续研究还在继续之中。

Photochemistry synthesis of PEI for gene delivery with high transfection efficiency

XU Dongmei YU Jiahui LIU Yongbiao SUN Hanwen GONG Peijun
HONG Jun YAO Side

Key words: Polyethylenimine, Photochemistry, Gene delivery

In this paper, we report a novel method to synthesize polyethylenimine (PEI) nanogels in the range of 8~200 nm with narrow size distribution by photo-chemistry at room temperature in aqueous solution. The nanogels'size, size distributions and zeta potential were determined by photo correlation spectroscopy (PCS). Spherical morphology of the nanogels was characterized by scanning electron microscopy (SEM) and confirmed by atomic force microscopy (AFM). The nanogels are of high stability, low tox-

icity and low immunogenicity, as having been confirmed in *in vivo* tests with mice as animal model, and in vitro tests with human lung and liver cancer cells as wel1. Efforts are being made for further studies on synthesis and applications of the nanogels.

苯胺类污染物的电子束辐照降解研究

王 敏　边绍伟　杨睿媛　王文锋

关键词　电子束辐照，苯胺，对硝基苯胺，间氯苯胺，化学需氧量

本工作研究了苯胺、对硝基苯胺和间氯苯胺水溶液的电子束辐照降解过程。三种溶液初始浓度均为 0.5 mmol/L，其辐照前后稀释五倍的紫外可见吸收光谱表明，苯胺在 230 nm 的吸收峰，对硝基苯胺在 380 nm 的吸收峰，以及间氯苯胺在 236 nm 的吸收峰，均随辐照吸收剂量的增加而逐渐降低。辐照吸收剂量为 23 kGy 时，分别降低到初始吸光度的 42.8%、4.3%和 27.7%。表明电子束辐照能够较为有效地破坏苯胺、对硝基苯胺和间氯苯胺的分子结构，使其得到降解。水溶液中苯胺、对硝基苯胺和间氯苯胺的浓度随辐照吸收剂量的增加而逐渐降低。辐照吸收剂量为 23 kGy 时，苯胺、对硝基苯胺和间氯苯胺的去除率均达 95%以上。在相同辐照吸收剂量下，对硝基苯胺和间氯苯胺的去除率高于苯胺的去除率。苯胺、对硝基苯胺和间氯苯胺水溶液的化学需氧量(Chemical oxygen demand，COD)去除率，随辐照吸收剂量的增加而逐渐上升。辐照吸收剂量为 23 kGy 时，苯胺、对硝基苯胺和间氯苯胺水溶液的 COD 去除率分别为 34%、56%和 35%。溶液 COD 的去除率之所以低于苯胺、对硝基苯胺和间氯苯胺的去除率，是因为苯胺、对硝基苯胺和间氯苯胺分子被辐照降解后，生成的中间产物并没有完全被转化为 H_2O 和 CO_2 等简单的无机物，需要额外的辐照吸收剂量才能使生成的中间产物进一步降解，COD 才能够得到完全的去除。

Degradation of aniline and its derivatives in aqueous solution by electron beam irradiation

WANG Min　BIAN Shaowei　YANG Ruiyuan　WANG Wenfeng

Key words:　Electron beam irradiation, Aniline, p-nitroaniline, m-chloroaniline, COD

The degradation of aniline, p-nitroaniline and m-chloroaniline by electron beam irradiation was studied. Removal of aniline, p-nitroaniline and m-chloroaniline reached 95% at an initial concentration of 0.5 mmol/L at 23 kGy. The results showed that electron beam irradiation is an effective process for the degradation of aniline and its derivatives.

4–氯酚的 γ 射线辐照降解研究

王 敏　杨睿媛　朱志远　王文锋

关键词　γ 射线辐照，4-氯酚，降解，化学需氧量，脱氯

利用 ^{60}Co γ 射线(2.2–14.9 kGy)辐照 4-氯酚水溶液，研究了其辐照降解特性。通过对辐照前

后 4-氯酚的紫外可见光谱、有机氯脱除率、化学需氧量(Chemical oxygen demand, COD)去除率的研究，探讨了吸收剂量、H_2O_2 加入量、初始浓度、溶液 pH 值对降解效果的影响。结果表明，这一辐射技术能有效降解 4-氯酚，有机氯脱除率可达 100%，COD 去除率可达 65.8%。

γ–ray induced degradation of 4-chlorophenol in aqueous solution

WANG Min YANG Ruiyuan ZHU Zhiyuan WANG Wenfeng

Key words: γ-ray irradiation, 4-chlorophenol, Degradation, Chemical oxygen demand, Cl removal

Degradation of 4-chlorophenol in aqueous solutions has been studied by γ-ray irradiation of 2.2−14.9kGy. Absorption spectra, chemical oxygen demand (COD) and Cl removal efficiency of the sample solutions were investigated under different irradiation conditions. COD removal efficiency and the Cl removal efficiency could be 65.8% and 100%, respectively. In addition, the results show that H_2O_2 plays an important role in the radiolysis degradation of 4-chlorophenol. It is concluded that the irradiation technology is an effective method for treatment of waste effluents with chlorophenol.

活性染料的辐照降解研究

马红娟 杨睿媛 赵 君 王 敏

关键词 辐射降解，活性染料，脱色

用 ^{60}Co γ 射线辐照甲基橙和活性艳蓝 KNR 水溶液，以研究染料分子的降解特性。结果说明辐射降解反应既破坏了染料分子的发色基团，同时也破坏了染料的有机分子结构。此外，辐照后染料水溶液的脱色率和化学需氧量(Chemical oxygen demand，COD)去除率的分析表明，吸收剂量是影响脱色率和 COD 去除率的最主要因素，脱色率和 COD 去除率均随吸收剂量的增加而增加。该实验还表明，辐照处理印染废水的 pH 值适用范围很广，溶液的初始浓度越大，COD 去除和脱色效果越差。另外，不同气体饱和实验证明，氧的存在可促进染料分子的降解。

研究了多种活性染料(活性红 m-3BE、活性艳红 KE-3B、活性蓝 XBR、活性橙 K-2RL 和活性黄 X-R)的电子束辐照降解。对辐照前后溶液的紫外可见光谱、COD 去除率和脱色率、以及辐照后溶液的 pH 值随吸收剂量的变化进行了详细研究。在同样辐照条件下，染料的辐射降解效果因染料分子的结构不同而略有不同。研究发现，染料溶液受到电子束辐照后，其 pH 值呈现下降趋势。表明染料分子能被降解成有机酸等中低分子的有机物，与生化法的厌氧酸化工艺的效果相似。

还研究了过氧化氢与辐射的协同作用。辐照前，在染料溶液中加入了不同量的过氧化氢以考察其与辐射的协同作用，研究发现，在相同的吸收剂量下，脱色率和 COD 去除率均随过氧化氢的浓度增加而增加，当过氧化氢的浓度达到一定量时，脱色率和 COD 去除率趋于饱和。电子束辐照时过氧化氢的作用比 γ 射线辐照时更明显。上述研究表明，电离辐射可有效地降解染料水溶液，辐射技术和其它技术有很好的协同作用。与常规污染物处理技术相比，辐射技术在常温常压下进行，具有工艺简单、无二次污染等特点，对难降解有机污染物的处理更有其独特的长处。

Radiation degradation of reactive dyes in aqueous solution

MA Hongjuan YANG Ruiyuan ZHAO Jun WANG Min

Key words: Radiation degradation, Reactive dye, Decolorization

Electron beam and γ-rays irradiation as adopted to investigate the decolorization and decomposition of reactive dyes in aqueous solution. Decomposition and mineralization of the dyes were investigated with the changes of absorption spectra, degradation efficiency, COD removal, TOC removal and pH changes of the solutions in different irradiation systems. Complete degradation of the dyes was observed at different absorbed doses under diverse irradiation condition. The degradation efficiency was enhanced in the presence of H_2O_2. The experimental results showed that reactive dyes in aqueous solution could be removed effectively by electron beam or γ-rays irradiation.

The present status of the Shanghai electron beam ion trap

GUO Panlin HU Wei[1] GONG Peirong LU Di[1] HE Mianhong[1] WU Shimin[1]
YAO Ke[1] HUANG Min[1] ZHANG Xuemei WANG Xincheng[1]
ZHU Xikai JIANG Dikui HUTTON R[2] ZOU Yaming[1]

Key words: Electron beam ion trap, Electron collector, Ultra-high vacuum, Superconducting magnets

The Shanghai EBIT was developed at SINAP and installed at Fudan University at the end of 2004. Fairly soon it ran 50 keV electron beams with a 60 mA beam current at magnetic field of 3 T. The electrons collection efficiency is 99.97%. Argon, krypton and xenon gases were successfully injected into the EBIT, with an optimum injection condition by maximizing the photon intensity of preferred ions. X-ray spectra of injected gas elements, Kr and Xe, and of evaporated cathode elements, Ba and W, were measured by using a high purity germanium detector. A primary experiment to observe *KLL*, *KLM*, *KLN* di-electronic recombination of krypton was done to test the event-mode data acquisition system.

[1] Fudan University, Shanghai 200433, China, [2] Astronomy Institute, Lund University, Sweden

放射性药物

Radiopharmaceuticals

3-(4-氟苄基)-8-羟基-1,2,3,4-四氢苯并吡喃[3,4-c]吡啶-5-酮的合成

李谷才　尹端沚　夏姣云　汪勇先

关键词　苯并吡喃[3,4-c]吡啶-5-酮，合成，表征

以间苯二酚和 4-酮-3-甲酸甲酯哌啶盐酸盐为原料，通过两步反应，合成了 3-(4-氟苄基)-8-羟基-1,2,3,4-四氢苯并吡喃[3,4-c]吡啶-5-酮，并用元素分析、IR、^{1}H NMR、ESI-MS 等方法对其进行了表征。

Synthesis of 3-(4-fluorobenzyl)-8-hydroxy-1,2,3,4-tetrahydrochromeno[3,4-c]pyridin-5-one

LI Gucai　YIN Duanzhi　XIA Jiaoyun　WANG Yongxian

Key words:　Chromeno[3,4-c]pyridin-5-one, Synthesis, Characterization

The 3-(4-fluorobenzyl)-8-hydroxy-1,2,3,4-tetrahydrochromeno[3,4-c]pyridine-5-one was prepared from resorcinol and methyl-4-oxo-3-piperidine carboxylate hydrochloride through two-step reactions and their structures were confirmed by elemental analysis, IR, ^{1}H NMR and ESI-MS spectra.

阿尔茨海默病发病机理研究进展

李谷才　尹端沚　夏姣云　汪勇先

关键词　阿尔茨海默病，病因学，发病机理

本文综述了阿尔茨海默病(AD)的发病机理，提出了探索各种可能的发病因素之间的内在联系，有助于找到导致 AD 发生的根本原因。

The progress of studies on aetiology and pathogenesis of Alzheimer's disease

LI Gucai　YIN Duanzhi　XIA Jiaoyun　WANG Yongxian

Key words:　Alzheimer's disease, Aetiology, Pathogenesis

The review aimed at the aetiology and pathogenesis of Alzheimer's disease (AD), and discussed the internal relations between different hypotheses and nosogenetic factors, which might be useful to find the fundamental reason of AD.

微量元素与神经退行性疾病

李谷才　尹端沚　汪勇先

关键词　微量元素，神经退行性疾病

综述了铝、锰、锌、铜在神经退行性疾病发生中的作用，提出保持体内各种微量元素的动态平衡对神经退行性疾病的预防和治疗具有积极作用。

Microelements and neurodegenerative diseases

LI Gucai　YIN Duanzhi　WANG Yongxian

Key words:　Microelements, Neurodegenerative diseases

The effects of aluminum，manganese，zinc and copper on neurodegenerative disorders were reviewed and it was suggested that to keep homeostasis of microelements will be helpful to the prevention and treatment of neurodegenerative diseases.

3-(4-[^{18}F]氟苄基)-8-羟基-1,2,3,4-四氢苯并吡喃[3,4-c]吡啶-5-酮的放射化学合成

李谷才　尹端沚　程登峰　王明伟　郑明强　汪勇先

关键词　苯并吡喃[3,4-c]吡啶-5-酮，氟-18，放射化学合成，多巴胺 D_4 受体

多巴胺 D_4 受体是一种 G 蛋白偶联受体，在精神分裂症病因发展中起着重要作用。通过核医学显像仪器，利用 PET 显像剂可以确定受体在活体内的分布、含量变化等。本文用三氟甲基磺酸-4-三甲基铵苯甲醛作标记前体，采用“一锅法”制备了一种潜在的多巴胺 D_4 受体 PET 显像剂 3-(4-[^{18}F]氟苄基)-8-羟基-1,2,3,4-四氢苯并吡喃[3,4-c]吡啶-5-酮 (^{18}F-FHTP)。其总的合成时间为 105 min，放射化学产率为 19.7% (衰变校正)，比活度为 120 GBq/μmol。

Radiochemical synthesis of 3-(4-[^{18}F]fluorobenzyl)-8-hydroxy-1,2,3,4-tetrahydrochromeno[3,4-c]pyridin-5-one

LI Gucai　YIN Duanzhi　CHENG Dengfeng　WANG Mingwei

ZHENG Mingqiang　WANG Yongxian

Key words:　Chromeno[3,4-c]pyridin-5-one, Fluorine-18, Radiochemical synthesis, Dopamine D_4 receptor

A putative dopamine D_4 receptor radioligand, 3-(4-[^{18}F]fluorobenzyl)-8-hydroxy-1,2,3,4-tetrahydrochromeno[3,4-c]pyridin–5-one (^{18}F-FHTP), was prepared from 4-trimethylammoniumbenzaldehyde

trifluorate through a two-step one-pot procedure with a total radiochemical yield of 19.7% (decay-corrected). The radiochemical synthesis of ^{18}F-FHTP took about 105 min and its specific activity was 120 GBq/μmol.

锌和铜在阿尔茨海默病中的作用

李谷才　汪勇先　尹端沚

关键词　阿尔茨海默病，锌，铜，β-淀粉样蛋白，氧化应激

综述了锌和铜在阿尔茨海默病中的作用及阿尔茨海默病患者脑中氧化还原活性金属之间的相互作用与作用机理，提出阿尔茨海默病的螯合疗法前景乐观。

The roles of zinc and copper in Alzheimer's disease

LI Gucai　WANG Yongxian　YIN Duanzhi

Key words: Alzheimer's disease, Zinc, Copper, Amyloid-β, Oxidative stress

The interactions of the redox active metals in brain of Alzheimer's disease (AD) patients and their mechanisms were reviewed, and the paradoxical roles of zinc in AD were discussed. It suggests a promising future of the chelation therapy for AD.

4-[^{18}F]氟苯甲醛的放射化学合成

李谷才　尹端沚　程登峰　王明伟　郑明强　汪勇先

关键词　4-[^{18}F]氟苯甲醛，氟-18，放射化学合成，正交法

用三氟甲基磺酸-4-三甲基铵苯甲醛作标记前体制备了一种用途广泛的氟-18 标记中间体4-[^{18}F]氟苯甲醛，并用正交实验法对标记条件进行了优化。在最佳标记条件下，其合成时间为 45 min，标记率为 62.1%，放化产率为 56.5% (衰变校正)。标记物经纯化后，放射化学纯度大于 95%。

Radiochemical synthesis of 4-[^{18}F]fluorobenzaldehyde

LI Gucai　YIN Duanzhi　CHENG Dengfeng　WANG Mingwei

ZHENG Mingqiang　WANG Yongxian

Key words: 4-[^{18}F]fluorobenzaldehyde, Fluorine-18, Radiosynthesis, Orthogonal method

A useful fluorine-18 labelled intermediate 4-[^{18}F]fluorobenzaldehyde was prepared from trimethylammoniumbenzaldehyde trifluorate and [^{18}F]fluoride and the labeling procedure was optimized by orthogonal-method. Under the optimized conditions, the radiochemical yield was 56.5% (decay-corrected) and after purification, its radiochemical purity was greater than 95%.

3-(4-羟基苄基)-8,9-二甲氧基-1, 2, 3, 4-四氢苯并吡喃[3,4-c]吡啶-5-酮的合成

李谷才　尹端沘　夏姣云　汪勇先

关键词：苯并吡喃[3, 4-c]吡啶-5-酮，多巴胺

以 3, 4-二甲氧基苯酚和哌啶-4-酮-3-甲酸甲酯盐酸盐为原料，通过分子间环加成反应和 N-烷基化反应，合成了一种潜在的多巴胺 D_4 受体配基 3-(4-羟基苄基)-8, 9-二甲氧基-1, 2, 3, 4-四氢苯并吡喃[3, 4-c]吡啶-5-酮，并用 IR、^{1}H NMR、ESI –MS 等方法对其进行了表征。

Synthesis of 3-(4-hydrobenzyl)-8,9-dimethoxy-1,2,3,4-tetrahydrochromeno[3,4-c]pyridin-5-one

LI Gucai　YIN Duanzhi　XIA Jiaoyun　WANG Yongxian

Key words: Chromeno[3,4-c] pyridin-5-one, Dopamine

The 3-(4-hydrobenzyl)-8,9-dimethoxy-1,2,3,4-tetrahydrochromeno[3,4-c]pyridin-5-one was prepared as a potential dopamine D_4 receptor ligand from 3,4-dimethoxyphenol and methyl 4-oxo-3-piperidinecarboxylate hydrochloride by intermolecular reaction and N-alkylation reaction, and structures of the products were confirmed by IR, ^{1}HNMR and the ESI -MS spectra.

苯并吡喃[3,4-c]吡啶-5-酮类化合物的的合成

李谷才　尹端沘　沈玉梅　汪勇先

关键词　苯并吡喃[3,4-c]吡啶-5-酮, 多巴胺 D_4 受体, 合成, 表征

以 4-酮-3-甲酸甲酯哌啶盐酸盐为原料，通过分子间环加成反应和 N-烷基化反应，合成了一系列潜在的多巴胺 D_4 受体配基苯并吡喃[3,4-c]吡啶-5-酮类化合物，并用元素分析、IR、^{1}H NMR、ESI-MS 等方法对其进行了表征。

Synthesis of chromeno[3,4-c]pyridin-5-ones

LI Gucai　YIN Duanzhi　SHEN Yumei　WANG Yongxian

Key words: Chromeno[3,4-c]pyridin–5-ones, Dopamine D_4 receptor, Synthesis, Characterization

A series of novel chromeno[3,4-c]pyridin–5-ones as potential dopamine D_4 receptor ligands were prepared from proper phenols and methyl-4-oxo-3-piperidine carboxylate hydrochloride through intermolecular cycloaddition reaction and N-alkylation reaction. Their structures were confirmed by elemental analysis, IR, ^{1}H NMR and ESI-MS spectra.

Synthesis of two potential dopamine D_4 receptor radioligands: ^{18}F labelled chromeno[3,4-c]pyridin-5-ones

LI Gucai YIN Duanzhi WANG Mingwei CHENG Dengfeng WANG Yongxian

Key words: Fluorine-18, Chromeno[3,4-c]pyridin–5-ones, Radiochemical synthesis, PET, Dopamine D_4 receptor, Radioligand

The dopamine D_4 receptor is hypothesized to relate with the pathophysiology and pharmacotherapy of schizophrenia while its level in brain regions is much low and to date no suitable tracer is available for the study of D_4 receptor in vivo. Therefore, selective imaging agents for the D_4 subtype are badly needed. Based on the structure-activity analysis of chromeno[3,4-c]pyridin-5-ones as dopamine D_4 receptor ligands, two fluorine-18 labelled chromeno[3,4-c] pyridin-5-one derivatives, 3-(4-[^{18}F] fluorophenyl)-8-hydroxy-1,2,3,4-tetrahydrochromeno[3,4-c]pyridin-5-one and 3-(4-[^{18}F]fluorophenyl)-8,9-dimethoxy-1,2,3,4-tetrahydrochromeno[3,4-c]pyridin-5-one, were synthesized through a one-pot method. Their radiochemical yields were 19.7% (decay-corrected) and radiochemical purities were higher than 95% with specific activities of 120 GBq/μmol and 123 GBq/μmol, respectively.

Preparation and stability of rhenium [^{188}Re] sulfide suspension with different particle size distributions

YU Yanbao WANG Yongxian DONG Mo YU Junfeng HU Weiqing*
ZHOU Wei YANG Xuezhong* YIN Duanzhi

Key words: Rhenium [^{188}Re] sulfide, Suspension, Particle size distributions

Two different dispersion methods were studied in order to obtain rhenium [^{188}Re] sulfide suspension with different particle size distributions. The manufactured swirling device offers Suspension I with larger particles (55%>5 μm, 19%>10 μm). However, ultrasonication can only produce Suspension II with smaller particles (93%<5 μm, 0.3%>10 μm). Stability tests indicated that deposition appears after 6 and 15 minutes for Suspensions I and II, respectively. Radiochemical purity and particle size distribution did not change distinctively within 24 hours. So, both suspensions can be used in animal tests to find out the optimal particle size ranges for intra-articular injection.

*Amersham Kexing Pharmaceutical Co.Ltd., Shanghai 201800, China

两种方法制备不同颗粒度 ^{188}Re-硫化铼混悬液的生物分布研究

于延豹 汪勇先 于俊峰 李世强 董 墨 周 伟 程登峰 尹端泓

关键词 铼，硫化物，药代动力学，兔

为了解两种方法制备的不同粒径 ^{188}Re-硫化铼混悬液在生物体内各主要脏器的分布,以选择合

适粒径范围的混悬液进行关节腔注射，采用超声和涡旋两种分散方法制备粒径大小区分明显的 ^{188}Re-硫化铼混悬液。36 只正常兔分成两组，膝关节腔分别注射不同粒径的 ^{188}Re-硫化铼混悬液,在 10、30 min 和 5、24 h 各处死 3 或 6 只实验兔,取脏器称重并测放射性计数。结果显示，涡旋法所制混悬液注射 10 min 时在肺、肝、脾等组织中的摄取[每克组织百分注射剂量率(%ID/g)分别为 0.004%、0.003%、0.002%ID/g]明显低于超声法所得混悬液(放射性摄取分别为 0.05%、0.04%、0.10%ID/g)；其他脏器中的放射性摄取也较少，减少了对非靶组织的辐射损伤。^{188}Re-硫化铼在血中清除快，10 min 即达峰值，并很快降低；主要经肾脏排泄。研究表明，涡旋法所制 ^{188}Re-硫化铼混悬液非靶组织摄取明显低于超声法所得混悬液，且其质量可控、制备简捷,在关节滑膜切除方面可能有更大的应用前景。

Biodistribution of ^{188}Re-sulfide suspension with different particle sizes

YU Yanbao WANG Yongxian YU Junfeng LI Shiqiang DONG Mo
ZHOU Wei CHENG Dongfeng YIN Duanzhi

Key words Rhenium, Sulfides, Pharmacokinetics, Rabbits

To evaluate biodistribution of ^{188}Re-sulfide suspension prepared with different particle sizes in normal rabbits in order to select an optimal particle size for intra-articular injection, two separate groups of a total 36 normal rabbits were injected intra-articularly into the knee joint with 22.2 MBq (0.2 mL) of the suspension. The 12 rabbits of group 1 were sacrificed at 10, 30min and 5, 24h (3 rabbits each) after injection of suspension I preparated by ultrasonic dispersion. The other 24 rabbits received suspension II dispersed by swirling device, and 6 rabbits sacrificed at each time. Then samples of various organs were obtained, weighed and their radioactivity was counted. Significant differences were detected during the first 10min from the extra-articular leakages of radioactivity into lung, spleen and liver. Suspension I produced far less uptake by these organs (0.004%, 0.003%, 0.002%ID/g) than suspension I (0.05%, 0.04%, 0.10%ID/g). Negligible leakages were found in other major organs throughout the whole study, such as brain, heart, testes, etc. The above data indicated that radioactivity in the blood declined rapidly 10min after administration and most of ^{188}Re-sulfide suspension were retained in the injected site, while the remaining of injected dose was excreted via kidneys. Therefore the radiation injury of the nontargetingt issue was minimal. The present study indicates that particle size of ^{188}Re –sulfide suspension plays an important role on extra-articular leakage.^{188}Re –sulfide suspension dispersed by swirling device would be an attractive radiosynovectomy agent in terms of its lack of leakage, easy to prepare and quality controllable.

Synthesis of polyacrylamide modified magnetic nanoparticles and radiolabeling with ^{188}Re for magnetically targeted radiotherapy

ZHANG Chunfu SUN Hanwen XIA Jiaoyun YU Junfeng
YAO Side YIN Duanzhi WANG Yongxian

Key words: Nanoparticles, Rhenium-188, Radiotherapy, Radiolabeling, Polyacrylamide, Histidine

Magnetic nanoparticles were synthesized, modified with polyacrylamide, and then characterized by TEM, FTIR, VSM and PCS. Rhenium-188 (^{188}Re) was bound to the nanoparticles by imidazolyl groups of histidine immobilized on the surface. The labeling yield was about 90% with good in vitro stability. Such nanoparticles might be useful for magnetically targeted radiotherapy.

三羰基铼[^{188}Re]的放射化学合成

夏姣云 汪勇先 于俊锋 张春富 周 伟 李谷才 王明伟 程登峰 尹端泓

关键词 三羰基铼，^{188}Re，放射化学合成

合成了化合物 $[N(Et_4)Br]_2[Re(CO)_3Br_3]$，并使用 IR、ICP-MS、元素分析等方法对化合物进行了表征。分析了此化合物溶于水后，阴离子部分的三个 Br^-可定量地被三个 H_2O 分子取代，得到前体化合物 fac-$[Re(CO)_3(H_2O)_3]^+$。同时合成了放射性前体化合物 fac-$[^{188}Re(CO)_3(H_2O)_3]^+$，放射化学产率约为 80%，Sep-Pak 分离后，放射化学纯度大于 95%。通过 HPLC 分析比较了这两个前体，从而确定了放射化学前体 fac-$[^{188}Re(CO)_3(H_2O)_3]^+$的结构。

Radiosynthesis of tricarbonal rhenium[^{188}Re]

XIA Jiaoyun WANG Yongxian YU Junfeng ZHANG Chunfu ZHOU Wei
LI Gucai WANG Mingwei CHENG Dengfeng YIN Duanzhi

Key words: Tricarbonyl rhenium, ^{188}Re, Radiosynthesis

The complex of $[N(Et_4)Br]_2[Re(CO)_3Br_3]$ was prepared and characterized by IR, ICP-MS and elemental analysis. When the complex was dissolved in water, the three Br^- ligands were quantitatively exchanged by three water molecules and the precursor of fac-$[Re(CO)_3(H_2O)_3]^+$ can be obtained. The complex of fac-$[^{188}Re(CO)_3(H_2O)_3]^+$ was synthesized with an overall radiochemical yield of 80%, and with more than 95% radiochemical purity after Sep-Pak seperation. Taking the complex of fac-$[Re(CO)_3(H_2O)_3]^+$ as a standard sample, the structure of the precursor, fac-$[^{188}Re(CO)_3(H_2O)_3]^+$, was comfirmed by HPLC.

含吡啶基的乙酸衍生物的合成及表征

夏姣云 汪勇先 于俊峰 李谷才 唐 林 刘振峰 尹端沚

关键词 吡啶基，乙酸衍生物，合成，表征

分别以吡啶-2-甲醛和二吡啶甲基胺为原料，合成了两种含有吡啶环的新型乙酸衍生物——[(6-胺基-己基)-吡啶-2-甲基氨基]-乙酸和[二(2-吡啶甲基)-氨基]-乙酸。并通过 IR、MS (ESI)、^{1}HNMR 和（或）元素分析对两个化合物进行了表征。

Synthesis and characterization of two novel acetic acid derivatives containing pyridyl

XIA Jiaoyun WANG Yongxian YU Junfeng LI Gucai

TANG Lin LIU Zhenfeng YIN Duanzhi

Key words: Pyridyl, Acetic acid derivatives, Synthesis, Characterization

Two novel acetic acid derivatives containing pyridyl，[(6-amino-hexyl)-pyridyl-2-methyl-amino] acetic acid and [bis(2-pyridylmethyl)-amino]-acetic acid, were synthesized from pyridine carbaldehyde and bispicolylamine, respectively. Both were characterized by IR, ^{1}HNMR, MR(ESI) and/or elemental analysis.

铼[^{188}Re]羰基化合物标记新双功能螯合剂的研究

夏姣云 汪勇先 李世强 于俊峰 唐 林 尹端沚

关键词 铼-188，羰基化合物，双功能螯合剂

合成了三种新的三齿配体 L^1NH_2、L^2H 和 L^3NH_2，用于设计合成新的以 fac-[^{188}Re(CO)$_3$]$^+$为核心的放射性药物。标记条件实验证明，三种配体在低浓度 (10^{-5}mol/L)的条件下，反应时间为 60min 内，配体标记率可达 88%以上，放射化学纯度大于 90%。同时合成了冷羰基铼配合物 fac-[Re(CO)$_3$$L^1NH_2$]$^+$ 、 fac-[Re(CO)$_3$$L^2H$] 和 fac-[Re(CO)$_3$$L^3NH_2$]作为参照标准品。稳定性实验也说明三种标记物均具有很高的体外稳定性，标记后 24 h 内基本不发生分解；组氨酸和半胱氨酸体外竞争实验证实 fac-[^{188}Re(CO)$_3$$L^1NH_2$]$^+$ 和 fac-[^{188}Re(CO)$_3$$L^2H$] 比 fac-[^{188}Re(CO)$_3$$L^3NH_2$]稳定，不易被组氨酸和半胱氨酸取代，可能羧基上的-OH 与 fac-[^{188}Re(CO)$_3$]$^+$ 的配位能力比吡啶环上的 N 稍低，也可说明三种配体均是较理想的标记 fac-[^{188}Re (CO)$_3$$(H_2O)_3$]$^+$的双功能螯合剂。

Research of novel bifunctional chelating agents for the ^{188}Re-tricarbonyl complexes labeling

XIA Jiaoyun WANG Yongxian LI Shiqiang YU Junfeng TANG Lin YIN Duanzhi

Key words: Rhenium-188, Tricarbonyl complexes, Bifunctional chelating agents

The organometallic precursor fac-[^{188}Re $(CO)_3(H_2O)_3$]$^+$ is reacted with three novel tridentate ligands (L^1NH_2, L^2H , L^3NH_2) and the properties of their ^{188}Re complexes in vivo have been evaluated. The results of labeling condition experiments show that a radiochemical purity higher than 90% can be obtained within 60 min by the reaction of fac-[^{188}Re $(CO)_3$]$^+$ core in a condition (pH=7.4) with a very small amount (10^{-5} mol/L) of these three new ligands. At the same time, three Re-tricarbonyl complexes of three ligands were also synthesized as reference samples, which were used to confirm the structures of ^{188} Re-tricarbonyl complexes of three ligands by HPLC. The stability experiments in vitro demonstrate that fac-[^{188}Re$(CO)_3L^1NH_2$]$^+$, fac-[^{188}Re$(CO)_3L^2H$] and fac-[^{188}Re$(CO)_3L^3NH_2$] do not decompose within 24 h (37℃, new born small calf serum). Histidine and cysteine challenge experiments (37℃, PBS, pH =7.4) show that fac-[^{188}Re$(CO)_3L^1NH_2$]$^+$ and fac-[^{188}Re$(CO)_3L^2H$] have higher stabilities than fac-[^{188}Re$(CO)_3L^3NH_2$], which indicate that combination ability of –OH on –COOH with fac-[^{188}Re$(CO)_3L^2H$] core was higher than that of –N on pyridine. It is also indicated that the three novel tridentate ligands (L^1NH_2, L^2H , L^3NH_2) are better bifunctional chelating agents for the labeling by the precursor fac-[^{188}Re $(CO)_3(H_2O)_3$]$^+$.

叶酸在放射性金属标记应用中的研究进展

夏姣云 汪勇先 唐 林 于俊峰 尹端泓

关键词 叶酸，放射性标记，肿瘤

综述了基于叶酸的放射性标记化合物的研究与临床试验情况的新进展。着重介绍了放射性核素 ^{111}In、^{67}Ga 和 ^{99m}Tc(Re)标记叶酸的螯合物以及它们在肿瘤诊断方面的应用与展望。

Recent progress in application of folate in radio-metals labeling

XIA Jiaoyun WANG Yongxian TANG Lin YU Junfeng YIN Duanzhi

Key words: Folate, Radiolabeling, Tumor

Current study and clinical application of the radiolabeled folate-chelate conjugates were summarized, and the application of ^{111}In, ^{67}Ga and ^{99m}Tc (Re) labeling folate-chelate conjugates in tumor diagnostic imaging were mainly reviewed. The forecasts of developing radiolabeled folate-chelate conjugates were also made.

Characterization and application of the fac-[^{188}Re(CO)$_3$(H$_2$O)$_3$]$^+$ core

XIA Jiaoyun WANG Yongxian YU Junfeng CAO Jinquan
ZHANG Chunfu YIN Duanzhi

Key words: Rhenium-188, Tricarbonyl complex, Magnetite nanoparticles

The complex of fac-[^{188}Re(CO)$_3$ (H$_2$O)$_3$]$^+$ was synthesized with an overall radiochemical yield of (80±5)%, and more than 95% radiochemical purity after a plus QMA Sep-Pak separation. The complex of fac-[Re(CO)$_3$ (H$_2$O)$_3$]$^+$ was also synthesized as a reference sample. The structure of the precursor, fac-[^{188}Re(CO)$_3$ (H$_2$O)$_3$]$^+$, was confirmed by high performance liquid chromatogram(HPLC). Magnetite nanoparticles coated with silica and modified with an amino silane coupling agent, N-[3-(trimethyoxysilyl) propyl]-ethylenediamine (SG-Si900) and immobilized with histidine were radiolabeled with ^{188}Re with a labeling yield of (91.4±0.3)% and good stability in vitro using fac-[^{188}Re(CO)$_3$(H$_2$O)$_3$]$^+$ core.

铼羰基化合物的制备及其在小鼠体内的生物分布研究

夏姣云 汪勇先 李世强 于俊峰 郑明强 李谷才 刘振锋
程登峰 唐 林 刘秀青 尹端沚

关键词 铼-188，双功能螯合剂，标记

选择三齿配基 L^1、L^2、L^3 及 L^4 (L^1 =histidine, L^2=nitrilotriacetic, L^3 = 2-picolylamine-N,N-diacetic acid, L^4 = bis(2-pyridymethy) amine)作为双功能螯合剂以连接受体、多肽、蛋白等靶向分子，用于设计合成新的以[^{188}Re(CO)$_3$]$^+$为核心的放射性药物。标记实验证明，四个配基的浓度为 10^{-5}~10^{-4} mol/L、反应时间 30 min 时，放射化学产率大于 90%。用 HPLC 分离后，放射化学纯度大于 95%。电泳实验也表明，配合物显示不同的价态。稳定性实验证明：四种配合物在体外很稳定，24h 几乎不发生分解。组氨酸和半胱氨酸竞争实验也说明 24 h 内，四个配合物很难发生配基与组氨酸和半胱氨酸的交换反应，推测在体内也有可能有很高的稳定性。小鼠动物试验表明，四个配合物均能较快地从血液和多数组织器官中清除，主要在肝和肾中浓集，是较理想的双功能螯合剂。

Synthesis and biodistribution of ^{188}Re-tricarbonyl complexes

XIA Jiaoyun WANG Yongxian LI Shiqiang YU Junfeng ZHENG Mingqiang
LI Gucai LIU Zhenfeng CHENG Dengfeng TANG Lin LIU Xiuqing YIN Duanzhi

Key words: ^{188}Re, Bifunctional chelating agents, Labeling

Radiolabeling of biologically active molecules with the fac-[^{188}Re(CO)$_3$(H$_2$O)$_3$]$^+$ unit has been of primary interest in recent years. Therefore, we herein report ligands L^1~L^4 (L^1=histidine,

L^2=nitrilotriacetic, L^3 = 2-picolylamine-N,N-diacetic acid, L^4 = bis(2-pyridymethy) amine) that have been evaluated in radiochemical reactions with the fac-$[^{188}Re(CO)_3(H_2O)_3]^+$. These reactions yielded the radioactive building blocks fac-$[^{188}Re(CO)_3L]$ (L = L^1~L^4), which were identified by HPLC. Tricarbonyl complexes, with log (P_o/W) values ranging from –2.23 to 2.18, were obtained in (P_o/W) yields of ≥90% using ligand concentrations within the 10^{-5}~10^{-4} mol/L range. Challenge studies with cysteine and histidine revealed high stability for all of these radioactive complexes, and biodistribution studies in mice indicated a fast rate of blood clearance and high rate of total radioactivity excretion occurring primarily through the renal-urinary pathway. In summary, complexes 1~4 are potent chelators for the future functionalization of biomolecules.

常用 ^{18}F 标记中间体的合成与其应用研究

王明伟　尹端沘　汪勇先

关键词　^{18}F，亲核放射氟化，标记中间体，合成，应用

通过亲核放射氟化标记法，正电子核素[^{18}F]氟被引入到目标分子中有两种途径：直接亲核放射氟化标记和间接亲核放射氟化标记。后者的关键是选择合适的标记中间体。本文根据 $^{18}F^-$的取代位置，介绍了两大类、数十种标记中间体的合成及其在放射性药物合成领域中的应用。

Syntheses and applications of ^{18}F-labeled intermediates

WANG Mingwei　YIN Duanzhi　WANG Yongxian

Key words　Fluorine-18, Nucleophilic radiofluorination, Labeled intermediates, Synthesis, Application

The positron-emitting nuclide fluorine-18 is of great importance to modern nuclear medicine with the increasing clinic demands of positron emission tomography (PET) and R&D of PET radiopharmaceuticals worldwide. Fluorine-18 can be introduced into a target molecule to prepare the corresponding ^{18}F-labeled radiopharmaceuticals through direct and indirect radiofluorinations. However, it is not suitable for the preparation of biomacromolecular-oriented radiopharmaceuticals such as peptides and protein using the direct labeling methods because of the lack of reaction selectivity. Thus, it is necessary to choose an appropriate ^{18}F-labeled intermediate for the indirect labeling methods. According to the classification of precursors displaced by ^{18}F, this paper briefly introduces two species of ^{18}F-labeled intermediates originated from aliphatic and aromatic displacements and their syntheses and applications in PET radiopharmaceutical fields.

直接亲核放射氟化法合成 O-(2-[^{18}F]氟乙基)-L-酪氨酸

王明伟 尹端沚 程登峰 李谷才 郑明强 周 伟 汪勇先

关键词 O-(2-[^{18}F]氟乙基)-L-酪氨酸，[^{18}F]FET，亲核放射氟化，一步法

本文利用一种方便易得的前体 N-叔丁氧羰基-(O-(2-对甲苯乙氧基))-L-酪氨酸甲酯，采用“一步法”直接亲核放射氟化法合成了 O-(2-[^{18}F]氟乙基)-L-酪氨酸。采用易于自动化的固相萃取法代替比较耗时的高效液相法分离目标产物，简化了制备过程，缩短了总合成时间。放射化学产率约为 40%(未经衰变校正)，放射化学纯度大于 97%，合成时间约为 50 min。

A one-step synthesis via direct radiofluorination of O-(2-[^{18}F]fluoroethyl)-L-tyrosine

WANG Mingwei YIN Duanzhi CHENG Dengfeng LI Gucai
ZHENG Mingqiang ZHOU Wei WANG Yongxian

Key words: O-(2-[^{18}F]fluoroethyl)-L-tyrosine，[^{18}F]FET, Nucleophilic radiofluorination, One-step method

O-(2-[^{18}F]fluoroethyl)-L-tyrosine was synthesized via one-step direct nuclephilic radiofluorination from a novel precursor N-BOC-(O-2-tosyloxyethyl)-L-tyrosine methyl ester easily obtained. The separation was performed on Sep-Pak silica plus cartridge via solid phase extraction instead of HPLC, which simplified its operation process and ensured its total synthesis time less than 50 min. The radiochemical yield was about 40% (no-decay-corrected), with a radiochemical purity of over 97%.

O-(2-[^{18}F]氟乙基)-L-酪氨酸的新合成路线及其生物学评价

王明伟 尹端沚 李世强 程登峰 李谷才 郑明强 蔡汉成
梁 胜 沈 华 张 炯 汪勇先

关键词 L-酪氨酸，氟乙基，氟化，体内外稳定性，PET，脑瘤

为研究代谢型脑肿瘤 PET 显像剂 O-(2-[^{18}F]氟乙基)-L-酪氨酸([^{18}F]FET)的一步直接亲核放射氟化法合成路线，以 N-叔丁氧羰基-O-(2-对甲苯磺酰乙氧基)-L-酪氨酸甲酯为标记前体，用直接亲核放射氟化法合成了[^{18}F]FET。用体内外稳定性实验和药代动力学实验，评价其生物学性能。结果表明：[^{18}F]FET 的合成时间约为 50 min，放化产率为 40%(未经衰变校正)，放化纯度>97%；体内外稳定性好，在 PBS 缓冲溶液中放置 3 个半衰期后，放化纯度无变化；跟踪注射[^{18}F]FET 后 1h 的小鼠血样，未发现代谢产物。[^{18}F]FET 在动物体内的血药浓度-时间曲线符合二室模型，分布相较短，适合显像，消除相很长，其良好的体内行为使其有望成为一种合适的脑肿瘤 PET 显像剂。

A novel synthesis and biological evaluation of O-(2-[^{18}F]fluoroethyl)-L-tyrosine

WANG Mingwei YIN Duanzhi LI Shiqiang CHENG Dengfeng LI Gucai
ZHENG Mingqiang CAI Hancheng LIANG Sheng SHEN Hua
ZHANG Jiong WANG Yongxian

Key words: L-tyrosine, Fluoroethyl, Fluorination, *In vivo* and *in vitro* stability, PET, Brain tumor

In this paper we describe a novel synthesis and biological evaluation of O-(2-[^{18}F]fluoroethyl)-L-tyrosine as metabolic PET tracer for brain tumor imaging. [^{18}F]FET was synthesized via one-step direct nucleophilic radiofluorination from an easily obtained precursor N-BOC-(O-2-tosyloxyethyl)-L-tyrosine methyl ester. Its biological evaluation was performed by experiments *of in vivo* and *in vitro* stability and pharmacokinetics. Its *in vivo* stability was characterized by HPLC assaying the blood sample from mice injected with [^{18}F]FET. The [^{18}F]FET was prepared in 50 min with good radiochemical yield (40%, without decay correction) and radiochemical purity (> 97%). The radiochemical purity was not changed after incubation with PBS for 3 half-lives and no metabolite in mice was found within 1h, which showed that this tracer was very stable *in vivo* and *in vitro*. The pharmacokinetics was fitted to two-compartment model with short distribution phase and long clearance phase. With good biological properties, the tracer is suitable for PET imaging of brain tumor.

用微波加热法合成脑肿瘤 PET 显像剂 O-(2-[^{18}F]氟乙基)-L-酪氨酸

王明伟 尹端沚 郑明强 夏姣云 周 伟 汪勇先

关键词 ^{18}F，氟乙基，L-酪氨酸，微波加热

O-(2-[^{18}F]氟乙基)-L-酪氨酸(O-(2-[^{18}F]fluoroethyl)-L-tyrosine，[^{18}F]FET)是最近研究的氨基酸类脑肿瘤 PET 显像剂。为了缩短合成时间，简化操作过程，减少工作人员的辐射剂量，本文从反应组分、加热方法与反应模式等三个方面改进和优化了[^{18}F]FET 的“两步法”放射化学合成路线。实验选择 L-酪氨酸、氢氧化钠溶液与 DMSO 作为反应组分，加热方式更换为微波法，采用简化的“一锅式”反应方式，总合成时间缩短在 20 min 以内。

Microwave radiosynthesis of O-(2-[^{18}F]fluoroethyl)-L-tyrosine as PET imaging agent for brain tumor diagnosis

WANG Mingwei YIN Duanzhi ZHENG Mingqiang
XIA Jiaoyun ZHOU Wei WANG Yongxian

Key words: ^{18}F, Fluoroethyl, L-tyrosine, Microwave heating

O-(2-[^{18}F]fluoroethyl)-L-tyrosine, a newly developed radiolabelled amino acid, is a promising PET imaging agent for brain tumor diagnosis. For less synthesis time, simple operation process and reduced

irradiation exposure to operators, the radiosynthesis was optimized with an improved two-step method, including reaction components, heating methods and reaction models. The synthesis can be done in 20 min by microwave heating in a one-pot model, with L-Tyr, NaOH/H_2O and DMSO as reactants.

Comparative and optimized studies on radiosynthesis of O-(2-[^{18}F]fluoroethyl)-L-tyrosine

WANG Mingwei YIN Duanzhi WANG Yongxian

CHENG Dengfeng LI Gucai ZHOU Wei

Key words: ^{18}F, L-tyrosine, Comparison, Optimization, Radiosynthesis

O-(2-[^{18}F]fluoroethyl)-L-tyrosine ([^{18}F]FET), one of radiolabeled amino acids, is a very promising brain tumor PET imaging agent and holds huge clinical potential. This paper carried out a comparative and optimized study on radiosynthesis of [^{18}F]FET, according to three aspects of its two-step method of synthesis, including reaction components, heating methods and reaction models.

肿瘤 PET 显像剂 O-(2-[^{18}F]氟乙基)-L-酪氨酸的放射化学合成

王明伟 尹端沚 汪勇先 李俊玲 张 岚 周 伟

关键词 氨基酸，酪氨酸，氟烷基化，FET，PET，脑肿瘤

放射性核素标记的氨基酸近年来已成为放射性药物领域的研究热点。O-(2-[^{18}F]氟乙基)-L-酪氨酸([^{18}F]FET)从问世以来一直备受关注，是一种很有希望的脑肿瘤 PET 显像剂。本文选择“两步法”合成了[^{18}F]FET：1. 通过 1，2-二对甲苯磺酸基乙烷的[^{18}F]氟化制备标记中间体，即烷基化试剂 2-[^{18}F]氟乙基对甲苯磺酸酯；2. L-酪氨酸的[^{18}F]氟乙基化合成了目标化合物[^{18}F]FET。总合成时间约为 50 min，放射化学产率为 20%~30% (未经衰变校正)，放射化学纯度大于 98％。

Radiochemical synthesis of O-（2-[^{18}F]fluoroethyl）-L-tyrosine as PET imaging agent for tumor diagnosis

WANG Mingwei YIN Duanzhi WANG Yongxian LI Junling ZHAN Lan ZHOU Wei

Key words: Amino acids, L-tyrosine, Fluoroalkylation, FET, PET, Brain tumor

Radiolabelled amino acids have been the interesting field of radiopharmaceuticals for several years, of which O-(2-[^{18}F]fluoroethyl)-L-tyrosine is very promising as PET imaging agent for tumor diagnosis. [^{18}F]FET was synthesized via a two-step reaction consisting of [^{18}F]fluorination of 1,2-bis (tosyloxy) ethane for preparing the alkylating agent 2-[^{18}F]fluoroethyltosylate and [^{18}F]fluoroethylation of L-tyrosine for obtaining [^{18}F]FET. Typically, the synthesis can be done in less than 50 min with overall radiochemical yields of 20%~30% (without decay correction) and radiochemical purity of > 98%.

^{188}Re 标记免疫靶向磁性纳米微粒及其生物学分布

李贵平* 汪勇先 张春富 张 辉*

关键词 磁性纳米微粒，同位素标记，铼，药代动力学，小鼠

为研究 ^{188}Re 标记具有 HER-2/neu 癌基因靶向特异性的 Herceptin 免疫磁性纳米微粒及其在小鼠体内的生物学分布，利用戊二醛作为交联剂，将人源性单克隆抗体 Herceptin 与化学修饰的磁性纳米微粒进行连接，构建免疫磁性纳米微粒。采用直接标记法将 ^{188}Re 标记到免疫磁性纳米微粒上。采用羰基铼标记法，以 fac-[^{188}Re(CO)$_3$(H$_2$O)$_3$]$^+$作为放射性标记前体，对表面固载组氨酸的磁性纳米微粒进行标记。分别测定所制备 ^{188}Re 标记物的标记率和体外稳定性及免疫磁性纳米微粒的单克隆抗体免疫活性,并观察 ^{188}Re 标记的磁性纳米微粒及免疫磁性纳米微粒的小鼠体内生物分布。结果显示，经扫描电镜证实免疫磁性纳米微粒的单个粒径大小平均为 60 nm，而表面固载组氨酸的磁性纳米微粒的粒径平均为 30 nm。^{188}Re 对 Herceptin、免疫磁性纳米微粒及固载组氨酸的磁性纳米微粒的标记率均＞90%，在小牛血清中具有良好的体外稳定性,并且磁性纳米微粒上连接的单克隆抗体仍保持较高的免疫活性。小鼠体内分布实验显示 ^{188}Re 标记的磁性纳米微粒及免疫磁性纳米微粒在血液中有较高的放射性分布且血循环时间较长，同时两者在肝内均有较多的摄取。总之，^{188}Re 标记的磁性纳米微粒及免疫磁性纳米微粒在体外及动物体内较稳定,无明显的 ^{188}Re 脱落，可用于下一步荷瘤裸鼠体内分布的研究。

^{188}Re labeling and biodistribution of magnetic nanoparticles for the tumor targeting

LI Guiping* WANG Yongxian ZHANG Chunfu ZHANG Hui*

Key words: Magnetic nanoparticles, Isotope labeling, Rhenium, Pharmacokinetics, Mice

To prepare ^{188}Re labeled monoclonal antibody (Herceptin)-coated magnetic nanoparticles for tumor targeting and to study its biodistribution in mice, Herceptin and histidine were covalently linked to the amine group upon silica-coated magnetic nanoparticles modified by N-[3-(trimethyoxysilyl) propyl]-ethylenediamine using glutaraldehyde method. The Heceptin-coated magnetic nanoparticles and Herceptin were radiolabeled with ^{188}Re by a direct labeling method, whereas the histidine-coaled magnetic nanoparticles were radiolabeled with ^{188}Re using fac-[^{188}Re(CO)$_3$,(H$_2$O)$_3$]$^+$ as a precursor. The labelling efficiency and immunoreactivity as well as labelling stability were determined. Also, the biodistributions of ^{188}Re-magnetic and ^{188}Re-Herceptin-magnetic nanoparticles in mice were observed. Results showed that Herceptin-coated magnetic nanoparticles were characterized by transmission electron microscope (TEM) with diameter about 60nm, while histidine-coated magnetic nanoparticles about 30nm. The labeling efficiencies for ^{188}Re-Herceptin, ^{188}Re-magnetic nanoparticles and ^{188}Re-Herceptin-magnetic nanoparticles were all >90% and had a better stability *in vitro*. The immunoreactivity of Herceptin linked to magnetic nanoparticles was still high. The biodistributionin in mice showed that ^{188}Re-magnetic nanoparticles and ^{188}Re-Herceptin-magnetic nanoparticles had high radioactivity levels in blood. Magnetic nanoparticles with diameter of 30 or 60nm had a long half-life in blood stream and were accumulated in liver. It is concluded that the ^{188}Re-Herceptin-coated magnetic nanoparticles and ^{188}Re-labeling magnetic nanoparticles are suitable for *in vivo* study of tumor-bearing nude mice models.

*第一军医大学附属南方医院核医学科，广州 510515

Radioimmunotherapy of nasopharyngeal carcinoma overexpressing HER2/neu in nude mice model with intratumoral injection of ^{188}Re-herceptin

LI Guiping* WANG Yongxian HUANG Kai* ZHANG Hui*
PENG Wuhe* ZHANG Chunfu

Key words: Rhenium-188, Nasopharyngeal carcinoma, Herceptin, Radioimmunotherapy

The therapeutic efficacy of radioimmunotherapy (RIT) of ^{188}Re-labeled herceptin, which is a humanized anti-p185-HER2/neu monoclonal antibody (mAb), was studied. The nude mice bearing nasopharyngeal carcinoma (NPC) expressing HER2/neu protooncogene were injected with ^{188}Re-herceptin intratumorally and intravenously. The biodistribution was observed on day 2 (n=3). The tumor growth inhibition rate (IR) was determined by measurement of tumor volume. In the intratumorally treated mice, tumor uptake of ^{188}Re-herceptin was significantly greater than in the intravenously treated mice [11.53% injected dose (ID)/g vs. 2.79% ID/g at 48h], and lower normal organ uptake was also seen. The intratumoral administration of ^{188}Re-herceptin caused greater inhibition of tumor growth at the fourth week as compared to the intravenous administration. The intratumoral administration of ^{188}Re-herceptin makes high level of radioactivity retained in tumor with significantly low radioactivity retained in normal tissues, and provides a more effective regional therapy for NPC overexpressing HER2/neu.

*Department of Nuclear Medicine, Nanfang Hospital, First Military Medical University, Guangzhou 510515

Avidin chase reduces side effects of radioimmunotherapy in nude mice bearing human colon carcinoma

LI Guiping* WANG Yongxian HUANG Kai* ZHANG Hui* ZHANG Chunfu

Key words Avidin chase, Radioimmunotherapy, Side effects, Colon cancer, Nude mice

To evaluate the influence of avidin chase on the side effects of radioimmunotherapy (RIT) in nude mice bearing human colon carcinoma and therapeutic outcome, purified anti-CEA monoclonal antibody (McAb)was biotinylated with NHS-biotin, and then radiolabeled with ^{188}Re by the direct method. The ^{188}Re-labeled biotinylated anti-CEA McAb (^{188}Re-CEA McAb-Bt) was intravenously injected followed by intravenous injection of avidin after 24h. SPECT imaging and biodistribution study were performed at 28~48 h after the injection of ^{188}Re-CEA McAb-Bt. Three groups of nude mice subcutaneously grafted with human colon carcinoma were treated 7 d after the graft. Mice in the avidin chase group received intravenous injection of ^{188}Re-CEA McAb-Bt (11.1 MBq/20 μg) followed by intravenous injection of cold avidin (80μg) after 24 h. Mice in the control group (treated group without avidin chase) only received the injection of ^{188}Re-CEA McAb-Bt (11.1MBq/20μg), while the other control group (non- treated group) only received 0.1mL normal saline solution. Toxicity was evaluated on the basis of change of body weight and peripheral WBC counts, and therapy effects were determined by variation in

tumor volume. Histological analysis of tumors was also performed. The results show that avidin chase markedly accelerated the clearance of ^{188}Re-CEA McAb-Bt from the blood and normal tissues. The tumor uptakes of ^{188}Re-CEA Mc Ab-Bt at 28 h were 5.90% and 6.42% ID/g, respectively, in chase group and in non-chase group, while the tumor-to-background (T/NT) ratios were 3.19 and 0.56, respectively. The tumor uptake was slightly decreased by avidin chase, but the T/NT ratios were increased. In treated groups the growth rate of body weight and the number of WBC decreased after injection of ^{188}Re-CEA McAb-Bt, and the WBC counts recovered earlier in the group with avidin chase than in the group without avidin chase. Compared to the nontreated group, treated groups with and without avidin chase showed significant anti-tumor effects. It is concluded that avidin chase can effectively reduce the side effects of RIT, and improve therapeutic efficacy.

[1]Department of Nuclear Medicine, Nanfang Hospital, First Military Medical University, Guangzhou 510515

Dopamine D_4 receptor antagonist 3-(4-[^{18}F]fluorobenzyl)-8-methoxy-1,2,3,4-tetrahydrochrome [3,4-c]pyridin-5-one([^{18}F]FMTP): Radiosynthesis and *in vivo* characterization in rats

TIAN Haibin YIN Duanzhi ZHANG Lan WANG Lihua ZHANG Chunfu WANG Mingwei WU Chunying* LI Gucai WANG Yongxian

Key words: Fluorine-18, Chroomeno[3,4-c]pyridine, Dopamine D_4 receptor, PET, Tissue distribution, Metabolism

We synthesized a novel ^{18}F-labeled dopamine D_4 receptor antagonist (K_i=4.3nmol/L), 3-(4-[^{18}F]fluorobenzyl)-8-methoxy-1,2,3,4-tetrahydrochromeno[3,4-c]pyridin-5-one ([^{18}F]FMTP), which has exhibited high affinity and selectivity. Radiosyntheses were accomplished by the reaction of fluorine-18-labeled intermediate with 8-methoxy-1,2,3,4-tetrahydrochromeno[3,4-c]pyridin-5-one (1) followed by HPLC purification. The overall radiochemical yield of the radiosynthesis was 19.5% (decay corrected), the specific radioactivity was about 110 GBq/μmol and the radiochemical purity was greater than 99%. The time of synthesis and purification was approximately 110 min. Tissue distribution studies of the [^{18}F]FMTP in rats showed that the radioactivity in the brain was concentrated in frontal cortex and medulla, the region that has a high density of D_4 receptors. Pre-treatment with nonradioactive FMTP (1.0mg/kg) produced a significant reduction of radioactivity in all the regions. About 40% of total radioactivity in plasma and 100% in rat brain extract represented unchanged radioligand at 60min after injection as determined by HPLC. The results indicate that [^{18}F]FMTP has some specific binding to the D_4 receptor.

*Department of Nuclear Medicine, Huashan Hospital, Fuadn University, Shanghai 200040

Radiolabelling of poly(histidine) derivatized biodegradable microspheres with the ^{188}Re tricarbonyl complex $[^{188}Re(CO)_3(H_2O)_3]^+$

YU Junfeng Häfeli Urs O * XIAO Jiaoyun LI Shiqiang
DONG Mo YIN Duanzhi WANG Yongxian

Key words: Microsphere, Radiolabelling, ^{188}Re, Tricarbonyl, Histidine, Radiation synovectomy

Many radiopharmaceuticals have been studied as radiation synovectomy agents. In this study, we developed a new potential agent for radiation synovectomy: poly(lactic acid)-histidine (PLA-his) microspheres radiolabelled with $[^{188}Re(CO)_3(H_2O)_3]^+$. The reaction conditions for the chelation of $[^{188}Re(CO)_3(H_2O)_3]^+$ and the radiolabelling of PLA microspheres were optimized and the stabilities for both steps tested *in vitro*. The chelation efficiency of $[^{188}Re(CO)_3(H_2O)_3]^+$ reached (93.12±1.82)% with >95% radiochemical purity once the colloidal and free ^{188}Re were removed by a small Sep-Pak column (Plus QMA). More than 90% of radioactivity stayed in the $[^{188}Re(CO)_3(H_2O)_3]^+$ form over 5h. The radiolabelling efficiency of PLA-his microspheres with $[^{188}Re(CO)_3(H_2O)_3]^+$ was above 92%. After 3 days incubation at 37℃ in calf serum, more than 80% of the radioactivity was still bound to the microspheres. So such microspheres are potentially useful as a radiation synovectomy agent for the treatment of chronically inflamed arthritic joints. Furthermore, they might be valuable in cancer brachytherapy.

*The University of British Columbia, Faculty of Pharmaceutical Sciences, Vancouver, Canada

小动物 PET

周 伟 尹端沚 汪勇先

关键词 小动物 PET，动物模型，动物显像

小动物 PET 正成为动物模型研究的强有力工具。本文综述了小动物 PET 扫描仪的发展及其在脑和心肌葡萄糖代谢、神经受体、肿瘤学、报告基因显像和反义 PET 显像等方面的应用，同时对小动物 PET 的发展趋势进行了讨论。

Small animal PET

ZHOU Wei YIN Duanzhi WANG Yongxian

Key words: Small animal PET, Animal model, Animal imaging

Small animal PET appears to be developed as a powerful tool for the animal model research. This paper provides a review of the development of small animal PET and the applications in glucose metabolism study in brain and heart, neuroreceptor imaging, oncology, reporter gene expression imaging and antisense imaging. In addition the future of small animal PET is also discussed.

手性在放射性药物中的作用

沈玉梅

关键词 手性，靶向性，放射性药物

本文简要介绍了手性、靶向性的基本概念以及手性与靶向性的关系。在放射性药物研发中如果放射性核素标记的药物分子中含有不对称因素，必须将两个对映异构体分开，否则它的靶向性不会好。手性是研究受体放射性药物构效关系时必须考虑的因素之一。

Chirality plays important roles in radiopharmaceuticals

SHEN Yumei

Key words Chirality, Target specific selectivity, Radiopharmaceuticals

The paper introduces the basic concept of chirality, target specific selectivity and their relationship in radiopharmaceuticals. If the ligands labeled by radionuclides have chiral centers, the enantiomers must be separated, or the target specific selectivity will not be good. Chirality is one of the most important factors which must be considered in the study of the structure-activity relationship of radiopharmaceuticals.

^{99m}Tc 放射性药物中的配位化学

冯翠兰 王谋华 成康民 沈玉梅

关键词 ^{99m}Tc 放射性药物，配位化学，双功能螯合剂

^{99m}Tc 作为一种优良的诊断用放射性核素，在核医学领域中有着广泛的应用。作为一种过渡金属，锝易与 N、O、S、P 等原子配位且具有多种配位方式，这就决定了 ^{99m}Tc 放射性药物结构的多样性。本文以配位方式的不同分类，分别就 $N_xS_{(4-x)}$型配体、“3+1”混合配体、含膦配体以及以 $[^{99m}Tc(CO)_3]^+$为配位中心的 ^{99m}Tc 放射性药物逐一进行介绍。

The role of coordination chemistry in the development of ^{99m}Tc radiopharmaceuticals

FENG Cuilan WANG Mouhua CHENG Kangmin SHEN Yumei

Key words: ^{99m}Tc radiopharmaceuticals, Coordination chemistry, Bifunctional chelation agent

This paper reviewed the role of coordination chemistry in the development of ^{99m}Tc radiopharmaceuticals. ^{99m}Tc is an excellent radionuclide used in nuclear medicine for the diagnosis of various diseases. Many kinds of bifunctional ligands and chelating agents have been designed and tested. This review summarized the recent development of coordination chemistry for ^{99m}Tc radiopharmaceuticals with different coordinated styles, such as $N_xS_{(4-x)}$ ligands, “3+1” mixed ligands, phosphane ligands and $[^{99m}Tc(CO)_3]^+$ core.

环戊二烯三羰基铼络合物的合成及其在放射性药物应用中的研究进展

王谋华　冯翠兰　成康民　沈玉梅

关键词　环戊二烯三羰基铼络合物，合成，标记

综述了三种环戊二烯三羰基铼络合物的合成方法，分别介绍了合成机理和应用范围;评述了环戊二烯三羰基铼络合物在标记小分子、雌激素受体配基和多肽方面的研究进展。

Progress in the synthesis of cyclopentadienyltricarbonyl rhenium complexes and its application in radiopharmaceuticals

WANG Mouhua　FENG Cuilan　CHENG Kangmin　SHEN Yumei

Key words: Cyclopentadienyltricarbonyl rhenium complexes, Synthesis, Labeling

Three synthesis methods, reaction mechanism and applied range of cyclopentadienyltricarbonyl rhenium complexes are summarized. Applications of cyclopentadienyltricarbonyl rhenium complexes in labeling little molecules, estrogen receptor(ER) ligands and peptide are especially reviewed.

双功能偶联剂 5-(三正丁基锡)-3-吡啶甲酸-N-琥珀酰亚胺酯的优化合成及其碘标记

刘秀青　汪勇先　刘振锋　尹端泔

关键词　碘，间接标记，标记前体，SPC，^{125}I-SIPC

为了改善碘标记生物分子在体内的脱碘问题，在无水无氧条件下合成了碘标记前体 5-(三正丁基锡)-3-吡啶甲酸-N-琥珀酰亚胺酯(SPC)，并优化了合成条件，产率达到 45%，并用核磁共振、质谱法进行了表征。在此基础上，合成了 5-碘-3-吡啶甲酸-N-琥珀酰亚胺酯(SIPC)。对标记前体 SPC 的 ^{125}I 标记条件进行了摸索，最终标记率达到 80%以上，经高效液相色谱(HPLC)分离后，放化纯度达到 97%。标记后的 ^{125}I-SIPC 在 4℃保存 24 h，放化纯度仍在 92%以上，稳定性良好。

Synthesis of N-succinimidyl-5-(tributylstannyl)-3-pyridinecarboxylate(SPC) and its iodination

LIU Xiuqing　WANG Yongxian　LIU Zhenfeng　YIN Duanzhi

Key words: Iodine, Indirect labeling, Precursor, SPC, ^{125}I-SIPC

In order to alleviate the *in vivo* deiodination of radioiodine labeled biomolecules, a novel precursor, N-succinimidyl-5-(tributylstannyl)-3-pyridinecarboxylate(SPC), was synthesized in an oxygen- and water-free argon atmosphere. After optimization of the synthetic conditions the SPC yield reached 45%. The product was characterized by ^{1}H NMR and MS. N-succinimidyl-5-iode-3-pyridinecarboxylate (SIPC) was also synthesized as a standard reference material. The ^{125}I labeled SPC was prepared with a labeling rate better than 80% and radiochemical purity higher than 97% after HPLC purification. The radiochemical purity remained over 92% after 24 h storage at 4℃.

铼[^{188}Re]羰基化合物标记含 RGD 的环肽及其生物分布

唐 林 于俊峰 郑明强 夏姣云 尹端沘

关键词 铼-188，羰基化合物，含 RGD 的多肽，生物分布

含 RGD（精氨酸－甘氨酸－天冬氨酸）序列的小分子多肽是整合素 $\alpha_v\beta_3$ 受体拮抗剂，是一类具有潜在临床应用价值的肿瘤显像剂及治疗剂。本文以 *fac*-[^{188}Re(CO)$_2$ (H_2O)$_3$]$^+$ 为前体标记了含 RGD 的环形多肽，并对其在普通小鼠和荷 S180 肉瘤小鼠体内的生物分布作了初步研究。铼[^{188}Re]羰基化合物标记含 RGD 环肽的标记方法简单易行，75℃反应 30 min，标记率在 90%以上，不会引起红细胞的溶血和凝聚现象。普通小鼠和荷 S180 肉瘤小鼠的生物分布实验表明，标记肽主要通过泌尿系统和肝胆代谢清除，1、4、24 和 48 h 肿瘤/肌肉比分别为：4.41±0.11、5.15±0.54、4.47±0.49 和 4.88±3.16。

Radiolabeling and biodistribution of RGD peptide with ^{188}Re-tricarbonyl complex

TANG Lin YU Junfeng ZHENG Mingqiang XIA Jiaoyun YIN Duanzhi

Key words: ^{188}Re, Carbonyl complex, RGD, Biodistribution

Three amino acids residues of Arg-Gly-Asp (RGD) are often the primary site of recognition by integrins which are responsible for tumor invasion and metastasis. In this research, the peptides containing RGD were radiolabeled with ^{188}Re-tricarbonyl complex. High radiolabeling ratios (>90%) were achieved under the reaction condition of 75℃, 30min. The radiolabeled peptides had high stability in PBS at room temperature for 4h. The hemolysis of red blood cells was not observed during incubation at 37℃ for 3h. Biodistribution studies were performed in normal male mice and S180-bearing mice, respectively. The radioactivities were rapidly eliminated by the hepatobiliary and urinary system. Tumor/Muscle ratios were 4.41±0.11，5.15±0.54，4.47±0.49 and 4.88±3.16 at 1h, 4h, 24h and 48h after injection, respectively. The results showed that ^{188}Re-tricarbonyl peptide containing RGD was a potential agent for tumor treatment.

Synthesis of amino-modified magnetite nanoparticles coated with Hepama-1 and radiolabeled with ^{188}Re for bio-magnetically targeted radiotherapy

LIANG Sheng WANG Yongxian ZHANG Chunfu LIU Xiuqing
LIU Zhenfeng XU Ronghui YIN Duanzhi

Key words: ^{188}Re, Amino-modified magnetite nanoparticles, Hepama-1

Ultrafine well-dispersed magnetite nanoparticles were directly prepared in aqueous solution using the controlled coprecipitation method. This paper discusses the preparation of novel surface silica modified colloids with a core of single-domain magnetite particles. Amino-silane was covalently coupled to the colloids and activated by glutaraldehyde. The underlying idea is to tailor the silica shell thickness and surface properties such that the colloids became stable spheres with isotropic interactions,

whereas an external magnetic field produces weak dipolar attractions and consequently reversible anisotropic structures. Hepama-1, a humanized monoclonal antibody directed against liver cancer, was coated on functional magnetic nanoparticles by the cross-linker glutaraldehyde to prepare immuno-magnetic nanoparticles (IMN). A direct labeling method was adopted to radiolabel IMN with ^{188}Re. The radiolabeling efficiency was about 90% with good *in vitro* stability. Such nanoparticles might be useful for bio-magnetic radiotherapy.

3-正丁基锡-N-琥珀酰亚胺苯甲酸酯的合成及其碘(^{125}I)标记

刘振锋　汪勇先　周 伟　王丽华　夏姣云　尹端泓

关键词　化学合成, 3-正丁基锡-N-琥珀酰亚胺苯甲酸酯(ATE), N-琥珀酰亚胺-3-碘苯甲酸酯($S^{125}IB$)

合成了 3-正丁基锡-N-琥珀酰亚胺苯甲酸酯(ATE)和 N-琥珀酰亚胺 3-碘苯甲酸酯(SIB)，其产率分别为 45.4%和 71.42%。用核磁、质谱、红外等对它们进行了表征 。并对 ATE 进行了碘标记，得到 N-琥珀酰亚胺-3-碘苯甲酸酯($S^{125}IB$)， 标记率可达 93%，放化纯度>98%。本方法为放射性药物碘的间接标记提供了一个平台。

Synthesis and radioiodination of N-succinimidyl 3-（tri-n-butylstannyl）benzoate (ATE)

LIU Zhenfeng　WANG Yongxian　ZHOU Wei　WANG Lihua
XIA Jiaoyun　YIN Duanzhi

Key words: Chemical synthesis, N-succinimidyl 3-(tri-n-butylstannyl) benzoate (ATE), N-succinimidyl 3-iodobenzoate ($S^{125}IB$)

N-succinimidyl-3-(tri-n-butylstannyl) benzoate (ATE) and N-succinimidyl-3-iodobenzoate (SIB) were synthesized. The structures of ATE and N-succinimidyl-3-iodobenzoate (SIB) were confirmed with ^{1}H NMR, MS and IR spectra. The yields of ATE and SIB were 45.4% and 71.4%, respectively. ATE was labeled with iodine-125. The radiolabeling rate was 93% and radiochemical purity was over 98%. The synthesis of ATE and the labeling of SIB were a platform for indirect radioiodination of radiopharmaceuticals.

中药对肿瘤放射治疗的增敏作用

孙艳红　沈玉梅

关键词　中药，放疗增敏，放射防护

中药作为放疗辅助用药广泛应用于恶性肿瘤的防治，它具有多靶点、多效性的特点，毒副作用比较低，一方面可以增强放疗的敏感性，有助于癌症的治疗、防止转移和复发；另一方面对机体具有整体调节作用，对正常组织还有一定的放射防护作用。本文就放射增敏类中药及其增敏机制进行了总结归纳，为放射增敏中药的研究提供借鉴。

The radiotherapy sensitization effect of traditional Chinese medicine on cancer

SUN Yanhong SHEN Yumei

Key words: Traditional Chinese medicine, Radiotherapy sensitization, Radiation protection

The traditional Chinese medicine is extensively applied in cancer radiotherapy because of its radiotherapy sensitization and radioprotective effect. The traditional Chinese medicine with radiotherapy sensitization effect and the sensitization mechanism are summarized in the paper in order to provide some reference for the research of drugs on radiotherapy sensitization.

β-榄香烯三羰基铼衍生物的放射化学合成

成康民 沈玉梅

关键词 β-榄香烯衍生物，三羰基铼，放射性标记

本文报道了 β-榄香烯三羰基铼衍生物的合成及其同位素 ^{188}Re 标记。标记配体由 β-榄香烯与双功能螯合剂二（2-吡啶甲基）-胺反应制得。标记产物直接由配体与 fac-[^{188}Re(CO)$_3$(H$_2$O)$_3$]$^+$制得，并经反向 HPLC 分离纯化。结果显示，标记前体收率为 64%，标记物放化产率 40%，HPLC 检测放化纯度大于 95%。表明该法简单易行，其标记化合物有可能发展成为一种新的放射性药物。

Radioactive synthesis of β-elemene Re(CO)$_3$ derivatives

CHENG Kangmin SHEN Yumei

Keywords: β-elemene derivatives, Rhenium-tricarbonyl, Radiolabeling

This paper describes the preparation of β-elemene derivative of Re(CO)$_3$ and [^{188}Re]-labelled radioactive β-elemene derivative of Re(CO)$_3$. β-elemene derivative was synthesized by purified β-elemene with di-(2-picoyl)amine. Radioactive β-elemene derivative of Re(CO)$_3$ was synthesized by β-elemene di-(2-picoyl)amine with fac-[^{188}Re(CO)$_3$(H$_2$O)$_3$]$^+$ and purified by C_{18} reverse phase HPLC. The β-elemene derivative of Re(CO)$_3$ was synthesized with yield of 64%. Radioactive β-elemene derivative of Re(CO)$_3$ was prepared with radiochemical yield of 40%. The radiochemical purity is up to 95% after separation by HPLC. The radioactive β-elemene derivative of Re(CO)$_3$ may be a potential therapeutic radiopharmaceutical in the future.

β-榄香烯衍生物的合成

成康民　沈玉梅　冯翠兰　王谋华　孙艳红　刘贵锋　任云峰

关键词 β-榄香烯衍生物，聚乙二醇，氨基酸

β-榄香烯是我国自行从中草药温莪术中提取的抗癌有效成分，是一种新型的具有免疫活性的抗癌药物。该药不良反应小，对肝肾功能无损害，无骨髓抑制，不同于一般的细胞毒性化疗药物。但是 β-榄香烯分子极性较小，不溶于水，故不易被肌体所吸收，这大大限制了其临床应用。为此以 β-榄香烯为先导物，对其结构进行改造，寻找出水溶性好、生物利用度高的 β-榄香烯衍生物成为研究的重点。本文以中草药有效成分 β-榄香烯为起始原料，在碱性条件下与氨基化的 PEG 反应合成了一系列 β-榄香烯单取代 PEG 衍生物，在对氨基酸未进行保护的条件下合成了一系列 β-榄香烯单取代氨基酸衍生物。通过 IR、^{1}H-NMR 及 HRMS 对其结构进行了表征。结果表明我们得到了一系列 β-榄香烯衍生物。

Synthesis of β-elemene $Re(CO)_3$ derivative

CHENG Kangmin　SHEN Yumei　FENG Cuilan　WANG Mouhua

SUN Yanhong　LIU Guifeng　REN Yunfeng

Key words: β-elemene derivatives, PEG, Amino acid

β-elemene, which is isolated from the essential oil of *curcuma wenchowesis*, shows certain cytostatic activity against various human malignancies.

Clinical studies showed that β-elemene exhibits obvious and reliable antitumor potency. At the same time β-elemene has lower toxicity. But β-elemene suffers the disadvantages of bad water solubility due to its property of olefins. So searching a new kind of β-elemene derivative which has good aqueous solubility and high antitumor potency is very important.

A series of β-elemene monosubstituted PEG (polyethylene glycol) derivatives were prepared using aminated PEG as starting materials. A series of β-elemene monosubstituted amino acid derivatives were prepared without protecting groups. The derivatives were characterized by IR, ^{1}H NMR and HRMS.

β-榄香烯单取代醚衍生物的合成及其体外抗增殖活性

刘贵锋　王谋华　孙艳红　成康民　沈玉梅

关键词　β-榄香烯,衍生物,醚

β-榄香烯是一种广谱抗肿瘤试剂,目前已广泛应用于临床。我们首次合成了 β-榄香烯单取代醚的化合物，它们对肿瘤细胞 K562 和 Hela 细胞的体外抗肿瘤活性与 β-榄香烯相比都有了明显的提高。

Synthesis and *in vitro* anti-proliferative activity of β-elemene monosubstituted ether derivatives

LIU Guifeng WANG Mouhua SUN Yanhong CHENG Kangmin SHEN Yumei

Key words: β-elemene, Derivatives, Ether

β-elemene is a broad-spectrum anti-tumor agent and is commercially available in the Chinese market. β-elemene monosubstituted ether derivatives were synthesized for the first time. Their *in vitro* antitumor activities against K562 and Hela cell lines were improved compared with that of β-elemene itself.

β-榄香烯单取代胺衍生物的合成

刘贵锋 成康民 沈玉梅

关键词 β-榄香烯，衍生物，胺，合成

以中草药有效成分 β-榄香烯为起始原料，在碱性条件下与胺反应，合成了一系列 β-榄香烯单取代胺衍生物，利用 IR，^{1}H NMR 和 MS 对其结构进行了表征。

Synthesis of β-elemene monosubstituted amine derivatives

LIU Guifeng CHENG Kangmin SHEN Yumei

Key words: β-elemene, Derivatives, Amine, Synthesis

A series of β-elemene monosubstituted amine derivatives were prepared by the reaction of β-elemene and amine under basic conditions. The derivatives were characterized by IR, ^{1}H NMR and MS.

β-榄香烯金属配合物的合成及其 ^{188}Re 的标记研究

任云峰 成康民 刘贵锋 孙艳红 沈玉梅

关键词 β-榄香烯，^{188}Re，N,N,N 三齿配体，放化标记率

本文合成了两种新的 β-榄香烯 N,N,N 三齿配体化合物，并对其进行了 ^{188}Re 放射性标记。标记实验证明，两种配体在低浓度(10^{-6}~10^{-4} mol/L)条件下，反应时间为 50 min，用 HPLC 分离后，配合物的放化纯度大于 95%。同时，经过修饰的水溶性好的配体标记率显著提高。

Synthesis and labeling of rhenium-188 β-elemene complexes

REN Yunfeng CHENG Kangmin LIU Guifeng SUN Yanhong SHEN Yumei

Key words: β-elemene, Rhenium-188, N,N,N ligands, Radiochemical yield

Two β-elemene complexes containing N,N,N ligands were synthesized and labeled with ^{188}Re. The ligand concentrations in the reactions were in the range of 10^{-6}~10^{-4}mol/L and the labeling time was 50min. The ^{188}Re tricarbonyl complexes were separated by RP-HPLC and radiochemical purity of the products could be better than 95%.In addition, the results showed that the higher the water-solubility, the better the radiochemical yield.

CdS 纳米晶的稳定化处理及介质极性对荧光光谱的影响

许荣辉 汪勇先 贾广强* 徐万帮 尹端沚

关键词 CdS 纳米晶，荧光增强，稳定化处理，介质极性，波长移动

用硫脲、聚乙烯吡咯烷酮、L-半胱氨酸水溶液对水热法合成的硫化镉纳米晶进行稳定化处理，发现 L-半胱氨酸和聚乙烯吡咯烷酮(PVP)能有效稳定硫化镉纳米晶，荧光发射强度比处理前增大 50 倍以上。以氯仿、氧化三(正)辛基膦(TOPO)氯仿溶液以及 3-巯基丙酸为萃取(或处理)剂，对水热法合成的水溶性 CdS 半导体纳米晶进行处理，经荧光光谱分析发现，介质水、氯仿、TOPO 氯仿溶液和 3-巯基丙酸均会影响 CdS 纳米晶的最大荧光激发峰与发射峰位置，极性大的水分子使荧光峰蓝移，极性小的氯仿、TOPO 氯仿溶液和 3-巯基丙酸使荧光峰红移(最大位移为 31 nm)。

Stabilization of CdS nanocrystals and influence of solvent polarization on fluorescent excitation/emission wavelength

XU Ronghui WANG Yongxian JIA Guangqiang* XU Wanbang YIN Duanzhi

Key words: Cadmium sulfide nanocrystals, Photoluminescence enhancement, Stabilization, Solvent polarization, Wavelength shift

High-quality CdS semiconductor nanocrystallites of wurtzite structure synthesized via hydrothermal method were characterized by transmission electron microscopy (TEM), high resolution transmission electron microscopy (HRTEM), and X-ray powder diffraction (XRD). The fluorescence intensity emitted by the nanocrystals is surprisingly enhanced after thiourea, polyvinylpyrrolidone and L-cysteine treatments. The fluorescence intensity increases over 50 times after stabilization treatment by polyvinylpyrrolidone and L-cysteine. Fluorescence excitation and emission wavelengths changed with the water-soluble CdS nanocrystallites treated with solvents or extractants of chloroform, trioctylphosphine oxide in chloroform solution, and 3-mercaptopropionic acid, which cause a maximum shift of 31nm.

*上海大学仪器分析与研究中心，上海 200444

CdS 纳米晶的制备及其荧光研究

许荣辉　汪勇先　徐万帮　尹端沚

关键词　CdS 纳米晶，水热合成法，荧光，量子点

以醋酸镉、L-半胱氨酸为主要原料，采用水热法制备了尺寸小于 10 nm、具有强光致荧光的纤锌矿结构 CdS 半导体纳米晶。水热法可以将晶核形成与晶体生长阶段较好地分开，加上提供的高温熟化条件，可以得到粒度小而均匀、结构良好的纳米晶。用高分辨透射电镜(HRTEM)、XRD 对产品的晶体大小、结构进行了详细的表征，分析了影响纳米晶尺寸的因素，用相关性较好的荧光激发与发射光谱研究了硫化镉纳米晶的光致荧光性能。制备的硫化镉(CdS)纳米晶结构良好、粒度均匀；荧光激发专一，最大激发波长在 338 nm，其发射荧光的波长位于 419 nm，发射强度大。

Synthesis of CdS nanocrystals and study on its fluorescent property

XU Ronghui　WANG Yongxian　XU Wanbang　YIN Duanzhi

Key words:　CdS nanocrystallites, Hydrothermal method, Photoluminescence, Quantum dots

The preparation of high-quality CdS semiconductor nanocrystallites of wurtzite structure is described. Crystallites about 10nm in diameter with consistent crystal structure and a high degree of monodispersity are synthesized using cadmium acetate dehydrates and L-cysteine as precursors via hydrothermal method, which separates nucleation stage from growth stage and favors the formation of nanocrystals with perfect structure after Ostwald ripening process and sufficiently structural adjustment. High quality of the sample results in sharp fluorescence excitation at 338nm and strong photoluminescence emission at 419nm. The combination of transmission electron microscopy (TEM), high resolution transmission electron microscopy (HRTEM), and X-ray diffraction (XRD) spectroscopy provides a description of crystallite structure. Parameters influencing the nanocrystalite's sizes and photoluminescence are also discussed.

Radiolabeling and *in vitro* and *in vivo* characterization of [^{18}F]FB-[R^{8,15,21}, L^{17}]-VIP as a PET imaging agent for tumor over-expressed VIP receptors

CHENG Dengfeng　YIN Duanzhi　LI Gucai　WANG Mingwei　LI Shiqiang

ZHENG Mingqiang　CAI Hancheng　WANG Yongxian

Key words:　Vasoactive intestinal peptide, Imaging, ^{18}F, Radiolabeling, Colorectal tumor, PET

In an effort to develop a peptide-based radiopharmaceutical for detecting tumors over-expressed VIP receptors with positron emission tomography (PET), we have prepared a novel [$R^{8,15,21}$, L^{17}]-VIP peptide for ^{18}F labeling. This peptide inhibited ^{125}I-VIP binding to rat's lung membranes with high affinity (half-maximal inhibitory concentrations (IC_{50}) of 0.12 nmol/L). Additionally, [$R^{8,15,21}$, L^{17}]-VIP showed higher stability than native VIP *in vivo* of mice. With N-succinimidyl 4-[^{18}F] fluorobenzoate ([^{18}F]SFB) as labeling prosthetic group, [^{18}F]FB-[$R^{8,15,21}$, L^{17}]-VIP was obtained in greater than 99% radiochemical purity within 100 min in decay-for-corrected radiochemical yield of (33.6±3%) (n=5) and a specific radioactivity 255 GBq/μmol at the end of synthesis (EOS). Stability of [^{18}F]FB-[$R^{8,15,21}$, L^{17}]-VIP *in vitro* and *in vivo* were investigated. Biodistribution of this trace was carried out in mice with induced C26 colorectal tumor. Fast clearance of [^{18}F]FB-[$R^{8,15,21}$, L^{17}]-VIP from nontarget tissues and specific uptakes by tumors resulted in higher tumor-to-muscle ratio (3.55) and tumor-to-blood ratio (2.37) 60 min post injection (p.i.) . Clear difference was observed between the blocking and unblocking experiments in biodistribution and whole body radioautography. [^{18}F]FB-[$R^{8,15,21}$, L^{17}]-VIP has demonstrated its potential for diagnosing tumors over expressed VIP receptors both *in vitro* and *in vivo*.

N-琥珀酰亚胺 4-[^{18}F]氟苯甲酸酯的合成

程登峰　尹端沚 王明伟　李谷才　周 伟　汪勇先

关键词　^{18}F，N-琥珀酰亚胺 4-[^{18}F]氟苯甲酸酯([^{18}F]SFB)，放射性合成

合成了 ^{18}F 标记多肽和蛋白类药物中常用的中间体 N-琥珀酰亚胺-4-[^{18}F]氟苯甲酸酯([^{18}F]SFB)。由于[^{18}F]SFB 能和生物分子结合达到较高的标记率以及具有较好的体内稳定性，成为一种最适宜的氟-18 标记试剂。本工作先合成标记前体乙基-4-三甲胺苯甲酸酯-三氟磺酸盐，经三步放射合成，再经 Sep-Pak C18 柱分离可得[^{18}F]SFB，并对第一步的 ^{18}F 标记反应进行了优化。合成时间约 1 h；放化产率约 50%(衰变校正)；经放射性 TLC 和 HPLC 分析，放化纯度大于 98%。

Synthesis of N-succinimidyl-4-[^{18}F]fluorobenzoate

CHENG Dengfeng　YIN Duanzhi　WANG Mingwei　LI Gucai

ZHOU Wei　WANG Yongxian

Key words　Fluorine-18, N-succinimidyl-4-[^{18}F]fluorobenzoate, Radio-synthesis

We have synthesized ^{18}F–labeled prosthetic group, N-succinimidyl 4-[^{18}F]fluorobenzoate ([^{18}F]SFB) for fluorine-18 labeling peptides and proteins. [^{18}F]SFB seems to be the most suitable ^{18}F-labeling agents because of its higher labeling yield and better stability of the conjugates in vivo. Labeling prosthetic group, triflate salt of ethyl p-trimethylammonium benzoate, was synthesized first, then the radio-synthesis with three steps was carried out, and the reaction condition of the first step about ^{18}F –labeling was optimized. After purifying through Sep-Pak C-18 cartridge, [^{18}F]SFB was produced with the decay-corrected radiochemical yield of 50% within 1 hour. The radiochemical purity was more than 98% by using radio-TLC and HPLC.

9-[(4-氟)-3-羟基甲基丁基]鸟嘌呤(FHBG)的改进合成方法

蔡汉成　尹端沚　张 岚　汪勇先

关键词　9-[(4-氟)-3-羟基甲基丁基]鸟嘌呤，正电子发射型计算机断层扫描，报告基因

报道了 9-[(4-氟)-3-羟基甲基丁基]鸟嘌呤(FHBG，Ⅱ)的改进合成方法，对起始原料喷昔洛韦(III)的氨基和一个羟基用 4-甲氧基氯化三苯甲烷保护，对另一个羟基磺酯化，得到 N^2(p-甲氧基苯酰基二苯基甲基) [(4-甲苯磺酰)-3-p-甲氧基苯酰基二苯基-甲氧基甲基丁基]鸟嘌呤(V)，收率为 70.5% ；再用四丁基氟化铵(TBAF)对化合物 V 亲核取代 4-甲苯磺酰基团，水解脱去保护基，即得 FHBG。产品用 ^{1}H NMR 、IR 、MS 表征，并用 HPLC 分析 V 和Ⅱ，保留时间分别为 5. 89 min 和 4. 41 min，积分计算得质量分数分别为 $w_{(V)}$= 99. 5% 和 $w_{(Ⅱ)}$= 99. 3% 。

The improved synthesis of 9-[(4-fluoro)-3-hydroxymethylbutyl] guanine（FHBG）

CAI Hancheng　YIN Duanzhi　ZHANG Lan　WANG Yongxian

Key words:　9-[(4-fluoro)-3-hydroxymethylbutyl] guanine, Positron emission tomography, Reportergene

The improved synthesis of 9-[(4-fluoro)-3-hydroxymethylbutyl] guanine (FHBG, II)is reported. Penciclovir (III) was converted to ditrityl-penciclovir (IV) by treatment with methoxytrityl chloride. IV was transformed to ditrityl-4-tosyl-penciclovir (V) by tosylation with high yield (up to 70.5%). V reacted with tetrabutylammonium fluoride to afford ditrityl-4-fluoro-penciclovir (VI). Removal of the methoxytrityl groups in VI by acidic hydrolysis produced II. Structures of the products were characterized by IR, ^{1}H NMR spectra and MS. For the quality control, II and V were analyzed by HPLC on a reverse-phase C-18 column, eluting at 5.89 min and 4.41min, respectively, and $w_{(II)}$=99.5% and $w_{(V)}$= 99.3% were obtained by HPLC area normalization method.

早期诊断阿尔茨海默病的 PET 分子探针

蔡汉成　尹端沚　张 岚　李谷才　郑明强　汪勇先

关键词　阿尔茨海默氏病，PET 分子探针，β-淀粉样蛋白斑块，乙酰胆碱

阿尔茨海默氏病(Alzheimer’s disease，以下简称为 AD)是一种退行性神经功能障碍性疾病，其典型病理学特征为 β-淀粉样蛋白斑块和神经纤维缠结，以及基底前脑乙酰胆碱能损害。目前核医学正电子发射断层显像(PET)技术是最可靠的 AD 早期检测手段之一。本文就近年来关于 AD 早期检测的 PET 分子探针特别是靶向 β-淀粉样蛋白斑块和乙酰胆碱酯酶或受体显像的分子探针研究进展作一回顾。

PET molecular probes for early detection of Alzheimer's disease

CAI Hancheng YIN Duanzhi ZHANG Lan LI Gucai

ZHENG Mingqiang WANG Yongxian

Key words: Alzheimer's disease, PET molecular probe, β-amyloid plaques, Acetylcholine

Alzheimer's disease (AD) is the most common age-related neurodegenerative disorder. The characteristic pathological lesions are deposits of β-amyloid plaques and neurofibrillary tangles after post-mortem examination, and degeneration of cholinergic neurons of the basal forebrain. The molecular imaging by positron emission tomography (PET) techniques is one of the most reliable tools for AD detection. In this review, we will present the recent development of PET molecular probes targeting at β-amyloid plaques or acetylcholinesterase for AD detection.

Synthesis of a new probe for PET imaging reporter gene HSV1-tk: 2-amino-6-[^{18}F] fluoro-9-(4-hydroxy-3-hydroxymethylbutyl) purine (6-[^{18}F]fluoropenciclovir)

CAI Hancheng YIN Duanzhi ZHANG Lan WANG Yongxian

Key words: Fluorine-18, Synthesis, Penciclovir, Radiofluorination

The synthesis of 2-amino-6-[^{18}F]fluoro-9-(4-hydroxy-3-hydroxymethylbutyl) purine (6-[^{18}F] fluoropenciclovir) (VII) is reported. The 2-amino-6-chloro-9- (4-acetoxy-3-acetoxy-methylbutyl) purine was hydrolyzed to 2-amino-6-chloro-9-(4-hydroxy-3-hydroxymethylbutyl) purine by using potassium carbonate in water solution, and then was converted to the corresponding trimethylammonium chloride (IV) by treatment with trimethylamine in ethanolic solution. Compound IV was reacted with anhydrous KF in DMF to produce the reference compound 2-amino-6-fluoro-9-(4-hydroxy-3-hydroxy-methylbutyl) purine (6-fluoropenciclovir) in 87.3% yield. Radiolabeled product 6-[^{18}F]fluoropenciclovir (VII) was prepared by radiofluorination of compound IV with [^{18}F]KF and isolated by a Silica Sep-Pak cartridge. The radiochemical yield of compound VII was 45%~55% (decay corrected) with radiochemical purity >98%, and the radiosynthesis time was 35~42min from end of bombardment (EOB).

2-氨基-6-氟-9-(4-羟基-3-羟甲基丁基)嘌呤的合成

蔡汉成 尹端沚 张 岚 汪勇先

关键词 2-氨基-6-氟-9-(4-羟基-3-羟甲基丁基)嘌呤，抗病毒制剂，氟化反应，合成

本文报道了 2-氨基-6-氟-9-(4-羟基-3-羟甲基丁基) 嘌呤(I)的合成，通过对起始原料 2-氨基-6-

氯-9-(4-乙酰氧基-3-乙酰氧甲基丁基) 嘌呤(II)水解脱去乙酰基，得到 2-氨基-6-氯-9-(4-羟基-3-羟甲基丁基)嘌呤(III)。化合物 III 与三甲胺乙醇溶液在混合溶剂 ($V_{(THF)}$: $V_{(DMF)}$ =3:1)中反应得到相应的氯化铵盐(IV)，然后与 KF 在 DMF 溶剂中反应，得到产物即化合物 I。产品经 UV、IR、^{1}H NMR、^{19}F NMR、MS 表征。考察了反应温度、氟化试剂等因素对氟化反应的影响，为 6 位含氟的嘌呤核苷类化合物的合成提供了一种直接、简易的新方法。

Synthesis of 2-amino-6-fluoro-9-(4-hydroxy-3-hydroxymethylbutyl) purine

CAI Hancheng YIN Duanzhi ZHANG Lan WANG Yongxian

Key words 2-amino-6-fluoro-9-(4-hydroxy-3-hydroxymethylbutyl) purine, Antiviral agent, Fluorination reaction, Synthesis

The fluorinated nucleoside analogue 2-amino-6-fluoro-9- (4-hydroxy-3-hydroxymethylbutyl) purine (I) is a potential antiviral agent and ^{18}F-radiopharmaceutical reference compound. Its synthesis was described. The 2-amino-6-chloro-9- (4-acetoxy-3-acetoxymethylbutyl) purine (II) was hydrolyzed to 2-amino-6-chloro-9-(4-hydroxy-3-hydroxymethylbutyl) purine (III) by using potassium carbonate in a mixed solution of water and methanol at 0°C, then was converted to the corresponding trimethylammonium chloride (IV) by treatment with trimethylamine (TMA) in ethanolic solution in a mild condition. Compound IV was reacted with anhydrous KF in DMF to produce 2-amino-6-fluoro-9-(4-hydroxy-3-hydroxymethylbutyl)purine (I) in 87.3% yield. The structures of the products were characterized by IR, NMR spectra and MS. Some factors affecting the yield of fluorination reaction were investigated.

The new convenient synthesis of fluorinated Penciclovir analogues 9-(4-fluoro-3-hydroxymethylbutyl) guanine (FHBG) and 2-amino-6-fluoro-9-(4-hydroxy-3-hydroxymethylbutyl) purine (6-fluoropenciclovir)

CAI Hancheng YIN Duanzhi ZHANG Lan WANG Yongxian

Key words: Penciclovir, Anti-viral agent, PET, Fluorination reaction, Synthesis

The 9-(4-hydroxy-3-hydroxymethylbutyl) guanine (Penciclovir) is a potent and selective inhibitor of members of the herpes virus family. A new convenient synthesis of fluorinated Penciclovir analogues 9-(4-fluoro-3-hydroxymethylbutyl) guanine (FHBG) and 2-amino-6-fluoro-9-(4-hydroxy-3-hydroxymethylbutyl) purine (6-fluoropenciclovir) was described. The structures of the products were characterized by UV, IR, ^{1}H NMR, ^{19}F NMR spectra and MS.

II-VI 型量子点的制备、修饰及其生物应用

徐万帮　汪勇先　许荣辉　尹端沚

关键词　量子点，制备，修饰，生物应用

根据近 10 年的研究对 II-VI 型量子点的制备、修饰进行了介绍，分析了量子点制备过程中的优点和缺点。探讨了 II-VI 量子点在生物应用方面的最新研究成果,并对其研究前景进行了预测。

Synthesis and modification of quantum dots and the application in biology

XU Wanbang　WANG Yongxian　XU Ronghui　YIN Duanzhi

Key words:　Quantum dots, Preparation, Modification, Application in biology

A review is given on developments of synthesis and modification of II-VI QDs in the last decade. The disadvantages and advantages of these methods were analyzed. Meanwhile, new achievements of the application in medicine and biology as well as the trends of II-VI QDs research were presented.

标记平台的试运行及放射性标记化合物的制备

董 墨　包广粮　周 伟　胡伟青 韩彦江 汪勇先

关键词　标记平台，试运行，氚，碳-14，碘-125

本标记平台自 2006 年初建成并进行试运行。已建成氚标记化合物制备实验室、碳－14 化合物制备实验室、质控室、产品分装室、贮存室等。完成了从瑞士引进的氚标记真空系统的验收工作，并通过了所组织的专家组对标记平台的试运行验收。

试运行期间我们完成了包括中药有效成分栀子苷元、抗血吸虫药吡喹酮、抗肿瘤药物紫草素乙酰阿卡宁(Akj-2)、抗肿瘤药物 SMC003 等四个化合物的氚标记制备研究，并进行了碳-14 化合物 $NaHCO_3$ 的标记制备任务。完成了碘-125 对化合物 HAS、M6P-HAS 的标记研究。

Commissioning of labeling platform and preparation of radio-labeled compounds

DONG Mo　BAO Guangliang　ZHOU Wei　HU Weiqing
HAN Yanjiang　WANG Yongxian

Key words:　Labeling platform, Commissioning, Tritium, Carbon-14, Iodine-125

A new labeling platform has been in operation since its foundation in 2006. The plateform consists of the laboratories for labeling of tritium and carbon-14 , quality control, product's packing and storage. The labeling platform together with the tritium manifold system imported from Switzerland has been checked and accepted by the experts of SINAP.

The drug molecules of anti-*Schistosoma japonicum* praziquantel and anti-tumor SMC003, as well as two Chinese medicine active ingredients, genipin and acetyalkannin (Akj-2) are all labeled with tritium. The carbon-14 labeled sodium bicarbonate and iodine-125 labeled HAS and M6P-HAS were also prepared.

中药有效成分栀子苷元和乙酰阿卡宁的氚标记制备

董 墨 包广粮 韩彦江

关键词 中药有效成分，氚标记，栀子苷元，乙酰阿卡宁

化合物中药有效成分栀子苷元和乙酰阿卡宁具有共同的结构特征，都含有单个不饱和双键，当进行一般的氚气氚化反应时，该双键容易被加成，使化合物的结构被破坏。我们采用了分步制备的方法。首先，将氚气经催化剂催化后制得极微量高活性的氚水，在冷冻后使多余的氚气回吸，然后用一特殊装置将反应原料加入刚制得的氚水中，进行与氚水的交换反应。我们使用该方法分别制备了氚标记的栀子苷元和乙酰阿卡宁。氚标记化合物的比活度分别为栀子苷元 1.35 GBq/mmol，乙酰阿卡宁 0.73 GBq/mmol。放射化学纯度经放射性 TLC 扫描都大于 95%。

Preparation of tritium labeled Chinese medicine active ingredients of genipin and acetyalkannin

DONG Mo BAO Guangliang HAN Yanjiang

Key words: Chinese medicine active ingredients, Tritium labeling, Genipin, Acetyalkannin

Two active ingredients of Chinese medicine, genipin and acetyalkannin, have similar chemical structure containing single double bond. When a conventional tritiated reaction was carried out using tritium gas, the single double bond would be reduced, resulting in destruction of chemical structure. So the method of two-steps was used for the labeling of the above chemicals with tritium. As the first step, the trace tritiated water with high reaction activity was generated by catalysis and the excessive tritium gas was re-absorbed for cycle use. As the second-step, the material to be labeled was added to the tritiated water in a special device and the tritium-hydrogen exchange reaction happened between the material and the tritiated water in the presence of catalyst. Using the method, the Chinese medicine active ingredients genipin and acetyalkannin were labeled with tritium and the specific activities were 1.35 GBq/mmol and 0.73 GBq/mmol respectively. The radiochemical purity for the two products was all above 95% by radio-TLC.

SMC003 的氚标记制备研究

包广粮 董 墨 韩彦江

关键词：标记，氚，SMC003

利用 5-溴-2-氰基吡啶作前体，经过卤氚交换反应得到氚标记的 2-氰基吡啶，经硅胶柱分离纯化，氚标 2-氰基吡啶的放射化学纯度达 100%。氚标 2-氰基吡啶与等物质量的格氏试剂在无水乙醚溶剂中、搅拌状态下、氮气氛围中、冰浴环境下混合，产生黄色固体；撤掉冰浴回温，室温搅拌反应 2 h 后用饱和 NH_4Cl 水溶液淬灭反应，固体消失，溶液呈橙红色，再经萃取、干燥、抽干处理得到红棕色油状物。接着将该产物与肼在二氯甲烷溶剂中混合，室温搅拌反应 10 h，反应液

减压浓缩至干，加入无水乙醇加热溶解，然后自然冷却，析出针状晶体，结晶用冷无水乙醇洗涤一次，得终产物氚标 SMC003。终产物放射性活度为 284.9 MBq，放射性比活度为 4.26 MBq/mg(1.23 GBq/mmol)，放射化学纯度为 98%。

Preparation of tritium labeled SMC003

BAO Guangliang DONG Mo HAN Yanjiang

Key words: Labeling, Tritium, SMC003

Tritium labeled 2-cyanopyridine was obtained through an exchange reaction between bromine and tritium by using 5-bromo-2-cyanopyridine as a precursor. The radiochemical purity of the tritium labeled 2-cyanopyridine reached 100% after purification by a silica gel column. It was mixed with the Grignard reagent of the same mole quantity in the absolute aether solvent in ice bath under stirring and protected by nitrogen atmosphere. A yellow solid substance was immediately produced in the reaction system. The ice bath was removed and the temperature of the reaction system was slowly raised to room temperature. The reaction was quenched by the saturated NH_4Cl aqueous solution after 2 h at room temperature. The solid substance was dissolved and the solution showed a color of salmon pink. A red and brown oleaginous substance was obtained through a serial process in turn of extraction, desiccation and evaporation. Then, the oleaginous substance was reacted with hydrazine in dichloromethane solvent for 10 h at room temperature. The reaction solution was dried under decompression. The absolute ethanol was added to dissolve the product by elevating the temperature. After the solution was cooled naturally, acicular crystals were produced. Then the crystals were washed by cooled absolute ethanol. Finally, the product with high quality was gained. The radioactivity of the product was 284.9 MBq, the specific activity was 4.26 MBq/mg (1.23 GBq/mmol), and the radiochemical purity was 98%.

先进探测仪器

Advanced Detectors and Instruments

高效抛物面型 IMS 进样系统结构的研究

蒋大真　魏永波　朱海云

关键词　抛物面，IMS

IMS 测量中，常用的进样系统结构是用采样试纸采集被检固体样品，加热后在载气(通常为干燥空气)直吹方式下进入电离室进行软电离，这种进样系统的缺点是气化的被检样品分子被载气带入电离室的效率低。我们设计了抛物面结构的 IMS 进样系统，使载气气流方向与带有被检物质颗粒的试纸面相切，可有效提高被检测样品分子被载气带入电离室的效率，提高 IMS 的检测灵敏度。

A high efficient paraboloid sampling injection structure for IMS

JIANG Dazhen　WEI Yongbo　ZHU Haiyun

Key words:　Paraboloid, IMS

In IMS measurement, the carrier gas in normal sampling structure is brought in to penetrate the sampling paper to carry the sample molecules into the ionization zone. Its disadvantage is that only a few per cent of sample molecules can be carried into that zone. The paraboloid injection structure can carry more sample molecules into the ionization zone, hence higher efficiency and sensitivity in comparison with the traditional structure.

IMS 标准样品制备及灵敏度测试

蒋大真　王丽华　魏永波

关键词　IMS 标准样品制备 灵敏度

衡量 IMS 技术优劣的主要技术指标之一就是 IMS 检测灵敏度，用标准的 IMS 被检测样品来对 IMS 仪器进行定标实验，就能够得到仪器性能的相关参数。因此 IMS 标准物质的制备非常重要，用规范的方法配置可供 IMS 检测的标准物质，是一项非常重要的工作。用标准待检样品对仪器进行测试，就能够得到 IMS 仪器的灵敏度指标。

Preparation of standard samples for IMS detection and its sensitivity testing

JIANG Dazhen　WANG Lihua　WEI Yongbo

Key words:　IMS, Preparation of standard samples, Sensitivity

The sensitivity of an IMS instrument is one of the most important specifications. The procedure of

preparing various standard samples will be crucial. Different procedures and methods have been explored and tested.

HADAMARD 变换在 IMS 技术中的应用

蒋大真　魏永波

关键词　HADAMARD 变换，IMS

传统的 IMS 门控技术采用单次开门单次扫描技术来实现，开门时间就是 IMS 离子测量的相对时间零点，离子到达法拉第板的相对时间代表某种属性的物质，进而可以依此来将多种物质进行分离。传统的门控技术门的开启/闭合时间比非常小，因此这种方案的 IMS 门控效率很低。HADAMARD 门控技术是用一系列的有规律的离散信号来控制门的开启/闭合，这样在一个扫描周期内能够有多个相互独立的时间零点，将这种扫描信号反演以后，就可以得到比传统门控技术多得多的信息量，得到比传统 IMS 高得多的灵敏度。

Application of HADAMARD transform in IMS

JIANG Dazhen　WEI Yongbo

Key words:　HADAMARD transform, IMS

In IMS measurement, the traditional gate control is implemented by using a narrow pulse (several tens microseconds) to trigger a scanning period (usually several tens millisecond) and act as time zero, so the duty cycle is very low, a large proportion of sample ions will be neutralized during the scan period, and the efficiency of sample ion usage is very low. HADAMARD transform technology use a pseudo random pulse series to control and trigger the overlapped scans, and the resulting spectrum is extracted by de-convolution of the overlapped spectra. The duty cycle is greatly increased and hence the sensitivity.

IMS 漂移管中气体流动微细结构的 COMSOL 软件模拟及分析

魏永波　蒋大真

关键词　IMS，气体，COMSOL，模拟

研究 IMS 漂移管内部气体的流动情况，对提高 IMS 的灵敏度和分辨率有很重要的意义。采用可用于多物理量模拟的 COMSOL 软件，对 IMS 漂移管的具体结构模型进行模拟，可以分析出 IMS 漂移管局部气流的微细结构。通过对这些微细结构的分析，在新设计改进的漂移管内部气路结构中，尽可能地减少内部涡流、湍流等的影响，能够有效提高 IMS 仪器的分辨率和稳定性等性能。

Simulation and analysis of minute structure of gas flow in IMS drift tube by using COMSOL

WEI Yongbo JIANG Dazhen

Key words: IMS, Gas, COMSOL, Simulation

The behavior of gas flow in the drift tube of an ion mobility spectrometry (IMS) is critical to the sensitivity and resolving power of the IMS. By using the COMSOL code, a series of simulation for different IMS drift tube structures have been studied and analyzed. The improved sensitivity and resolving power is obtained by reducing the effect of backset and onflow.

SIMION 7.0 离子仿真及模拟分析在 IMS 技术中的应用

魏永波 蒋大真

关键词 IMS，SIMION，模拟

IMS 技术是在大气环境条件下把采集到的样品分子离子化，然后将离子在弱电场里进行分离，根据离子不同的空间构相将各种物质区分开来。漂移管的电场结构设计研究对 IMS 分离技术有很大的影响。SIMION 7 软件能够在一定条件下实现对设定离子的空间运动径迹的模拟，能够对 IMS 电场设计起到有效的辅助作用。通过 SIMION 7 软件对实际的漂移管结构进行模拟，依据模拟结果对漂移管进行改进，取得了比较好的效果。

SIMION 7.0 emulation and simulation applied to IMS

WEI Yongbo JIANG Dazhen

Key words: IMS, SIMION, Simulation

An IMS identifies different ions under atmospheric pressure chemical ionization (APCI) in weak electric field. Design of the electric structure would affect the separation capability of IMS. The SIMION 7.0 code, which simulates the trace of ions in certain conditions, can provide efficient design of the electric structure. We can get the better result by using the new structure.

IMS 漂移管中气体流量的测量方法及电路实现

魏永波 蒋大真

关键词 IMS，气体流量，IIC 总线

IMS 漂移管中的漂移气体、载气、回路抽出流量对 IMS 仪器的灵敏度、分辨率影响比较大。回路气体抽出流量过大，易造成待检测样品离子在电离区存留时间过短和离子浓度相对较低，从

而影响 IMS 测量性能。一定条件下合适流量的干燥空气能够使 IMS 达到比较好的性能。采用合适的传感器并用 IIC 技术，可以实现对 IMS 漂移管内部气体流量、气压的实时有效监控。

The method and circuit to measure gas flux in IMS

WEI Yongbo JIANG Dazhen

Key words: IMS, Gas flux, IIC BUS

The fluxes of drift gas and carrier gas in the drift tube of IMS (Ion Mobility Spectrometry) affect sensitivity and resolution of the IMS. Using a suitable flux of dry air can improve the sensitivity and resolution of IMS. Real-time monitoring of the gas flux and pressure can be realized using an appropriate sensor and the IIC technology.

指纹识别技术应用产品识读指标测试方法研究

李勇平 汪勇旭 敖新宇

关键词 生物特征识别，指纹防盗锁，产品标准，统计模式识别，操作评估，拒真率，认假率

在公安部行业标准《指纹防盗锁通用技术条件》编制过程中，编制小组针对生物特征识别性能参数和试验方法的制定所开展的研究工作，提出了一种基于数学和统计模式识别方法的配置轮换和等效标准指纹数据库变换的检测模型，实现了利用有限规模的数据库资源，科学公平地测定通用指纹识别模块的拒真率和认假率等指标的目标。初步测试结果表明，这种方案可操作性强，适用于指纹防盗锁产品的拒真率和认假率指标检测，亦适合于其它指纹识别技术应用产品的识读指标检测。

A method for performance test of fingerprint identification product

LI Yongping WANG Yongxu AO Xinyu

Key words: Biometrics, Burglary resistant fingerprint locks, Product standard, Statistical pattern recognition, Operational evaluation, False rejection rate, False acceptance rate

Research work was fulfilled on biometric performance index and experimental method for the standard of *General Specification of Burglary Resistant Fingerprint Locks* by the formulating team during the developing period for this occupation standard of Ministry of Public Security. A testing model utilizing the configuration alternating and equivalent transformation of reference standard fingerprint databases was established based on mathematics and statistical pattern recognition methodology. The false rejection rate (FRR) and the false acceptance rate (FAR) of general fingerprint recognition module could be evaluated scientifically and impartially by this solution. Test results showed strong operability of proposed solution that could be used for testing the FRR and FAR of burglary resistant fingerprint locks, and other products based on fingerprint recognition technology.

生物特征身份证照技术研究

敖新宇　李勇平　黄跃峰　鲍 强　张甦宁

关键词　国际民航组织，生物特征，机读旅行证件，公钥体系，逻辑数据结构

生物特征身份证照系统对证件持有者进行生物特征的“人证合一”认证，以排除伪造旅行证件。国际民航组织(ICAO)和国际标准化委员会为此推出 Doc9303 标准，符合该标准的生物特征身份证照系统已在许多欧美国家使用，但我国尚处在研究阶段。电子护照持有者的生物特征数据按逻辑数据结构(LDS)格式保存在 CPU 智能卡中，并有功能防止数据篡改、盗窃与通讯窃听。

机读验证系统先通过国家证书(KPr 密钥)确认机读旅行证件的合法性，再获取对应的生物特征数据，并根据护照中的协议与卡中存有的生物特征信息进行比对并确认持证人。我们设计的 PC 系统仿真测试系统分为智能卡读写、生物特征采集和认证等模块。智能卡读写模块采用 Gemplus 公司的 GCX4 Java 卡和 GemProx 读卡器，Java 卡完全符合智能卡安全标准，GemProx 读卡器遵循 ISO14443A/B 标准，其通讯速率完全符合生物证照的要求。生物特征采集模块分为人脸和指纹，人脸由网络照相机采集，指纹由指纹传感器采集。生物采集模块和智能卡读写模块以外设形式和 PC 机交互，而认证模块实现了卡的真实性识别和生物特征识别功能。

Biometric enabled personnel identity card and passport

AO Xinyu　LI Yongping　HUANG Yuefeng　BAO Qiang　ZHANG Suning

Key words: International Civil Aviation Organization (ICAO), Biometrics, Machine Readable Travel Document (MRTD), Public key infrastructure (PKI), Logical data structure (LDS)

Biometric-based passport or personnel identity (ID) card system is a personal identification system advocated by ICAO and International Standard Organization (ISO) to boost security of international travel and deterring criminal of fake ID. As specified in Standard Doc9303, the cutting-edge biometric pattern matching technology and information communication security know-how are used to verify the bearer’s ID. Over 20 countries are deploying biometric enabled e-passports that conform to Doc9303, whereas in China the technique is in early stage research and technical evaluation. The biometrics data of a card holder are kept in Smart Card with CPU. This prevents illegal copy, tamp and illegal access. It also encodes the outward-sending message to prevent eavesdropping. When the bearer passes the checking system, relevant public/private key is downloaded to the card reader machine to check legality of the passport, biometrics data are then extracted from the passport to verify the person’s live captured biometric data by biometric sensors. We have developed a system which consists of a smart card I/O module, a biometrics capture module and a verification module. The smart card I/O module uses the GCX4 card and GemProx card reader (Gemplus), which confirm with the ISO specifications. The biometrics capture process includes facial image and fingerprint image, by respectively a web-camera and fingerprint sensors. The information is checked by biometrics matching and smart card security verification.

基于分块子特征的人脸的表征和识别

杜远凤　李勇平

关键词　人脸识别，特征提取，二维主成分分析，本征图像

统计特征是人脸表示和识别的一种常用方法，它是把规范化的人脸图像作为整体来提取特征的。我们提出一种新的特征提取方法：利用人脸图像的多个子块来提取特征，将人脸分为上中下三个子块。运用两个最近提出的识别方法：二维主成分分析法(2DPCA)和本征图像(Eigenimages)法，在公用人脸数据库 YALE 和 XM2FDB 上比较了采用整体特征和分块子特征的效果，实验结果表明采用多个分块子空间特征提取法优于整体特征提取。

Facial image representation and recognition using multi-block sub-features

DU Yuanfeng　LI Yongping

Key words:　Face recognition, Feature extraction, 2DPCA, Eigenimages

Statistical features used for facial image representation and recognition are conventionally extracted from the whole detected and normalized facial image. Our new approach uses multiple sub-blocks of the facial image for feature derivation. With 2DPCA and Eigenimages, the two newly-introduced recognition recipes, the multi-block sub-feature method was tested using YALE and XM2FDB, the two face databases available. A performance comparison shows that the multi-block sub-features extraction method is better than the normal features extraction method.

一种用于人脸识别的二维 Gabor 小波窗方法

王 琳　李勇平　张鸿洲　王成波

关键词　人脸识别，Gabor 小波窗，主成分分析(PCA)，特征提取，局部特征矢量

近年来，小波分析理论在人脸识别研究领域引起了很大关注。Gabor 小波能很好模拟哺乳动物皮质细胞的感受区域剖面，具有优良的空间局部性和方向选择性，能够提取图像局部区域内多个方向的空间频率和局部结构特征。这种与生物信息相关的特性使得 Gabor 小波成为人脸识别中应用最多的一种小波函数。利用 Gabor 小波表征的人脸图像具有对光照和表情变化的鲁棒性，二维 Gabor 小波窗(GWW)方法就是用一个窗口从左到右、从上到下扫描整幅图像，提取局部特征矢量，再由降采样并连接局部特征矢量得到参数化的特征矢量。和基于整幅图像的 Gabor 小波表征法相比，GWW 算法的代价显著降低，最大可达 39%，在 ORL 和 XM2VTSDB 数据库上的实验分析表明，其性能比传统的 PCA 算法有很大提高。

A 2D Gabor wavelets window method for face recognition

WANG Lin LI Yongping ZHANG Hongzhou WANG Chengbo

Key words: Face recognition, Gabor wavelets window, Principal component analysis (PCA), Feature extraction, Local feature vectors (LFVs)

In recent years, many methods based on Gabor wavelets have been proposed. Because the Gabor kernels can model receptive fields of orientation-selective mammalian cortical simple cells, the Gabor wavelets exhibit desirable characteristics of spatial localization and orientation selectivity, and are localized in the spatial and frequency domains optimally. Gabor wavelets are being used extensively and successfully in various computer vision applications including face recognition due to their biological relevance and computational properties. And the Gabor wavelet representation of face images is robust for illumination and expressional variability. A novel algorithm, 2D Gabor Wavelets Window (GWW), is proposed that scans the facial image from top left to bottom right to extract the local feature vectors (LFVs). A parametric feature vector is derived by down-sampling and concatenating these LFVs for face representation and recognition. Compared with the Gabor Wavelets representation of the whole image, the total cost is reduced by maximum of 39% whilst the performance achieved better than the conventional PCA method when experimented on both the ORL and XM2VTSDB databases.

跨姿态人脸识别中的特征转换

张鸿洲 李勇平 王 琳 王成波

关键词 人脸识别，跨姿态，特征转换

作为一种生物特征识别手段，人脸识别技术具有广泛应用前景。其实际应用须面对和解决姿态问题，也是算法研究的难点和热点之一。传统的基于表象的人脸识别算法难以克服姿态问题，本工作发展了基于表象的人脸识别法，可满足实际应用中跨姿态人脸识别的要求。对于处于侧面视角的测试向量 V_{probe} 首先通过 $V'_{probe}=W\cdot V_{probe}$ 特征转换，生成到正面视角的测试向量，再进行识别，其中 W 为转换矩阵，描述特征空间中姿态转动的先验知识。特征表示空间和转换矩阵通过一组训练样本图像学习得到。在标准的 FERET 数据库上的实验取得了较好识别效果，表明特征转换是解决跨姿态人脸识别的一种有效手段。

Face recognition across poses using feature transformation

ZHANG Hongzhou LI Yongping WANG Lin WANG Chengbo

Key words: Face recognition, Across pose, Feature transformation

Face recognition is an advanced identification solution which can meet the crying needs in security areas. Pose effect is a big challenge for robust applications of this technology. In real application, gallery image of face recognition system is front view, and probe image is non-frontal. Appearance-based

face recognitions use statistical properties of face images to accomplish recognition task, they are successful in frontal view recognition and are suitable for applications under live conditions. Appearance-based face recognition is limited for face recognition across poses. In this work, we improved the appearance-based face recognition for across pose scenario. For a probe image feature vector, it was first transformed into front view by $V'_{probe}=W\cdot V_{probe}$, where W is transformation matrix which encapsulate prior knowledge of pose transition in feature subspace. Experiment in FERET face database show that the proposed approach is an effective solution for face recognition across pose.

一种基于主成分分析的指纹识别算法

汪勇旭　敖新宇　杜远凤　李勇平

关键词　指纹识别，主成分分析，统计特性量，特征向量，特征匹配

目前大多数指纹识别算法都基于指纹图形特性（特征点），我们提出了一种基于指纹统计特性的算法——基于主成分分析(PCA)的指纹识别算法。大量实验发现，指纹图像处于中心位置的区域很重要，迄今为止，并无两枚指纹的图像具有相同的中心区域，故可用中心区域识别来代替整个图像的识别。我们利用中心区域的统计特性来进行识别，采用了 PCA 方法。首先，对指纹图像计算 Poincare 指标，得到指纹的中心位置和方向；然后在中心位置周围，根据方向，裁剪出一块区域，并把这块区域进行对齐；再使用 PCA 进行特征提取；最后，通过测量获得的特征向量之间的欧氏距离来识别两个比对的指纹。

A fingerprint recognition algorithm based on principal component analysis

WANG Yongxu　AO Xinyu　DU Yuanfeng　LI Yongping

Key words:　Fingerprint recognition, Principal component analysis (PCA), Statistics features, Feature vector, Feature matching

Most automatic fingerprint identification systems (AFIS) use fingerprint minutiae in the matching process. In this work, we proposed a fingerprint recognition algorithm based on statistics. Experiments up to now proved that no identical area around singular points can be found in different fingerprints. Therefore, the area labeled as region of interest (ROI) near the singular points instead of whole image can be used for fingerprint identification. Statistical characters of ROI are extracted for recognition. First, the Poincare index is computed to detect the singular points with orientation of the fingerprint image. The central position and established direction of ROI are localized according to the singular points. Then we segment an $m\times n$ block at the central position along the ROI direction, and the PCA is applied to the ROIs of all training samples to get feature vector. Finally, Euclidean distance between feature vectors of two fingerprint images is used for recognition.

ARM 与 DSP 通信接口设计

黄跃峰　李勇平

关键词　主机接口，数字信号处理器，ARM 控制器

嵌入式电子护照的机读系统采用“ARM+DSP”方式以满足生物特征样本的实时采集与处理以及智能卡的操作（通讯、读写和比对）等多任务需求，其中 ARM 与 DSP 间如何进行高效的通信是实现“人证合一”的关键环节。利用 DSP 的主机接口特性，设计专门线路可建立 S3C2440 (ARM9 核) 和 TMS320DM642 (DSP 核)间的数据通信链。通过在 ARM 端和 DSP 端各自的软件编程，实现两端的实时数据交换接口。实验结果表明，该方法能满足嵌入式系统数据传输速度的要求，且连接简便、节省软硬件成本。

Design of communication interface between ARM and DSP

HUANG Yuefeng　LI Yongping

Key words:　HPI (Host-port interface), DSP (Digital Signal Processor), ARM controller

A host ARM for smart-card operations (communicate, read/write, verify) and a digital signal processor (DSP) for real-time biometric sampling and processing are needed for the reader of embedded e-passport system. Effective communication between the host ARM and DSP plays a key role to check that the passport and bearer have the same identity. Data inter-linkage between the S3C2440 (ARM 9 kernel) and TMS320DM642 (DSP kernel) is setup by designing specific hardware circuits through the host port interface (HPI). With respective software implemented on the two processors, efficient real-time data exchange was realized. Experimental results show that this mechanism, with simplified linkage and cost effective for both hardware and software, satisfies the speed requirement of data communication for the embedded system.

小动物 microSPECT 成像系统研究

漆玉金　张猛蛟　代秋声　张雪竹　朱海云　赵翠兰

关键词　MicroSPECT，针孔准直器，亚毫米成像分辨率

高分辨 microSPECT 成像系统在肿瘤、心血管和神经精神疾病等动物模型的研究中发挥着重要作用。我们研制了一台高分辨的小动物 microSPECT 成像系统，其 NaI(Tl)晶体阵列为 1.2mm ×1.2mm×5mm 像元，日本滨松 Φ5 英寸 R3292 位置灵敏光电倍增管；用针孔准直器取代常规的平行孔准直器以获高分辨成像。经 Monte Carlo 模拟，优化的针孔准直器的聚焦长度为 10 cm，张角 62°，配 Φ0.5~2.0 mm 针孔插入件，以满足不同分辨率与探测效率的成像要求。系统成像视野为 Φ102 mm，能量探测范围 20~250 keV，适用于 ^{99m}Tc、^{125}I、^{123}I、^{111}In 等核素标记的显像。系统的性能通过标准的模具及小鼠骨骼显像实验来测试与评估。标准的 Jaszczak 模具测试的结果显示，用 Φ0.5 mm 针孔，可清楚分辨 1 mm 的物体，探测效率约 1200 cps/mCi。用 ^{99m}Tc-MDP，小鼠的

每根肋骨都清晰分辨。这些结果表明：我们研制的国内第一台 microSPECT 成像系统的成像分辨率达亚毫米的国际先进水平。

Development of a microSPECT for small-animal imaging

QI Yujin ZHANG Mengjiao DAI Qiusheng ZHANG Xuezhu

ZHU Haiyun ZHAO Cuilan

Key words: MicroSPECT, Pinhole collimator, Submillimeter spatial resolution

High-resolution microSPECT for pre-clinical small-animal studies is an important tool in the small-animal models of cancer, cardiac and neural diseases. We developed a microSPECT system with a pixellated NaI(Tl) crystal array in 1.2mm ×1.2mm ×5mm pixel size and 1.4 mm pixel pitch coupled to a 5” Hamamatsu R3292 position-sensitive photomultiplier tube. Pinhole collimation was utilized to replace the standard parallel-hole collimation for high spatial resolution. Monte Carlo simulations were performed to optimize the pinhole collimator to 10-cm focal length with an acceptance angle of 62°. The pinhole collimator was equipped with a set of pinhole apertures with diameters of 0.5, 1.0, 1.5 and 2.0 mm for different requests in spatial resolution and detection efficiency. Having a field-of-view of Φ102 mm for 25~250 keV γ-rays, it is suitable for imaging isotopes of ^{99m}Tc, ^{125}I, ^{123}I and ^{111}In. The performance of the system was characterized by experiments on standard phantom and a mouse bone scan. The microSPECT system can resolve 1mm rods with a 0.5 mm pinhole aperture with detection efficiency of around 1200 cps/mCi. Using ^{99m}Tc-MDP on normal mouse, the individual ribs can be clearly distinguished in the image. In conclusion, the first microSPECT system developed in China has achieved a very good performance and sub-millimeter image resolution as compared to the similar systems existing in the world. The system has been successfully used to a variety of researches of small-animal imaging experiments.

MicroSPECT 读出电子学的研究

张猛蛟 漆玉金

关键词 MicroSPECT，位置灵敏光电倍增管，局域重心法，全通滤波器

高分辨率与高灵敏度 microSPECT 成像系统的一个重要组成部分是优化的前端读出电子学，包括位置读出电路与采集触发电路。位置读出电路采用基于局域重心算法的阻抗电桥读出，以克服传统的阻抗电荷分配法带来的图像边缘压缩等定位不确定性；数据采集触发电路采用了基于全通滤波器的双极性信号成形方法来实现对输入脉冲峰值的检测。用联机实验对比传统阻抗电荷分配法的位置读出电路板(Hamamatsu 公司提供)和局域重心算法的阻抗电桥读出，传统的位置读出电路的图像压缩效应显著，在 X 与 Y 方向上最多只能区分 64 个像素，占 PSPMT 灵敏面积(~Φ10 cm)的 89%，而基于局域重心法的阻抗电桥读出电路则能清晰区分 73 个像素，基本达到 PSPMT 的灵敏面积；采集触发电路可准确控制峰值信号采集，采集触发电路对输入信号的定时晃动<40ns，电路稳定性很好。此读出电子学完全满足 microSPECT 成像系统的要求。采用局域重心法结合阻抗电桥读出法还可以应用于高集成度的多阳极位置灵敏光电倍增管的位置读出。

Readout electronics of microSPECT

ZHANG Mengjiao QI Yujin

Key words: MicroSPECT, PSPMT, Truncated center-of-gravity, All pass filter

An important part of developing a high-resolution and high-sensitivity microSPECT is to design optimized readout electronics. This includes the front-end readout circuits and the trigger circuits for the data acquisition. The readout circuits is based on truncated center-of-gravity (COG) output analog with charge division, so as to overcome uncertainties in position determination with the conventional resistive-chain readout. The design of the trigger circuits utilizes a new method of bipolar shaping by all pass filter (APF) to strobe the peaks of input signal pulses. Comparison tests were done on the microSPECT system with the newly developed readout and the conventional resistive-chain readout provided by Hamamatsu. The conventional readout resulted in a significant compress effect on the image. In both X and Y axis, only 64 pixels were distinguishable and the area was just about 89% of the active area of the PSPMT (~Φ 10cm). However, the new readout circuit could distinguish up to 73 pixels, which accounted for almost the full active area of the PSPMT. The trigger circuits showed accurate determination of the peaks of input pulses and good stability in peak detections, even though the time jitter of the input signals could be kept within 40 ns. In conclusion, the readout electronics we designed and implemented have well met the needs of our MicroSPECT system in both performance and stability. The method of truncated COG with analog output with charge division was proved to be an effective approach to the readout electronics for microSPECT system and this readout method could extend to the readout electronics of the newly developed multi-anode PSPMT with much higher integration.

多巴胺转运体在大鼠头部的 microSPECT 显像初探

漆玉金 张猛蛟 代秋声 赵 娟* 刘兴党*

关键词 多巴胺转运体，动物模型，MicroSPECT 显像

此研究旨在演示用 microSPECT 研究多巴胺转运体(DAT)在大鼠头部显像的可行性。重约 250g 的豚鼠和约 200 g 的大鼠各一，注射 ^{99m}Tc-TRODAT-1，豚鼠为脊背注射，约 148 MBq；大鼠为静脉注射，约 130MBq。药物吸收约 2 h 后进行麻醉，对鼠头部进行成像实验。先用高分辨的平行孔准直器对鼠头部作 10 min 的平面显像，再作断层扫描。在平面与 SPECT 断层扫描中，两只鼠都呈现清晰的多巴胺转运体显像。实验结果表明，microSPECT 是多巴胺转运体在鼠头部显像的有效工具。

Dopamine transporters in rat head using high-resolution microSPECT

QI Yujin ZHANG Mengjiao DAI Qiusheng ZHAO Juan* LIU Xingdang*

Key words: Dopamine transporters, Animal model, MicroSPECT imaging

The study is to demonstrate the feasibility of using high-resolution microSPECT to observe the dopamine transporters (DAT) in rat head. ^{99m}Tc-TRODAT-1 was injected in a 250-g guinea pig from its back (148 MBq) and a 200-g normal rat via its tail vein (130MBq). Two hours later, they were anesthetized and head imaging were scanned with the microSPECT system. The planar imaging with a high-resolution parallel-hole collimator was made first and then the tomography imaging. Both the planar and tomography images show a clear DAT concentration in the heads of the guinea pig and the normal rat. The results indicate that microSPECT imaging is an effective tool to investigate the dopamine transporters in the rat head.

*复旦大学附属华山医院核医学科

高分辨 microSPECT 针孔准直器的优化设计研究

代秋声 漆玉金

关键词 针孔准直器，microSPECT，蒙特卡罗模拟

针孔成像具有图像放大功能，广泛应用于高分辨的 microSPECT。本工作旨在研制一套优化设计的针孔准直器插件。用蒙特卡罗法模拟了系统的点源响应函数，以及 γ 射线通过针孔准直器的几何、透射及散射效应。针孔材料为钨合金，针孔为刀口或钝口，γ 射线能量 140 keV，优化关键是多深的针孔可最大限度地减少 γ 射线在准直器上的透射和康普顿散射。模拟结果表明，孔深过小无法有效地减少透射和散射份额，而过大则在远离轴线的区域会减少几何响应的份额，增加透射、散射响应与几何响应的比值。对 Φ1 mm 针孔插件，最佳孔深厚度是 0.5 mm。实验测得针孔准直器的效率曲线和空间分辨率，与理论结果符合较好，达到了 microSPECT 的设计要求。该套优化设计方法可推广应用于多针孔准直器的优化设计。

Optimized design of pinhole apertures for high-resolution microSPECT

DAI Qiusheng QI Yujin

Key words: Pinhole collimator, MicroSPECT, Monte Carlo simulation

Pinhole collimation, with its unique imaging property of magnification, has been widely used in high-resolution microSPECT. The study is to optimize design of pinhole apertures for our microSPECT. Monte Carlo simulations were used to compute the point response function of the system, and the geometric, penetration and scatter effects of the incident γ-rays. The pinhole apertures were made of tung-

sten alloy, with either knife-edge or keel-edge designs. The pinhole aperture design was optimized with 140keV γ-rays. The key is how to determine the channel heights of the apertures to minimize the percentages of penetration and scattering on the pinhole apertures. The calculation results show that a too-shallow channel fails to reduce the penetration and scattering effects, while a too-long channel reduces the geometric response and increases the ratios of the penetration and scattering to the geometric response in the region away from the central axis of the pinhole collimator. Therefore, the optimized channel-height is 0.5mm for the 1mm pinhole aperture. The spatial resolution and detection efficiency of the system were measured. The results agree well with the simulations. The optimized design of pinhole apertures satisfied the requirements of our microSPECT. The method of pinhole apertures optimization can be applied in designing multi-pinhole collimator.

高分辨的 microSPECT 用于乳腺癌骨转移小鼠模型的研究

漆玉金　张猛蛟　凌立君*

关键词　乳腺癌骨转移，小鼠模型，MicroSPECT 显像

此研究旨在探讨用高分辨率 microSPECT 研究乳腺癌骨转移小鼠模型的可行性。三只重 22g 左右小鼠，带有乳腺癌及人骨细胞移植，每只静脉注射剂量约 111MBq 的 ^{99m}Tc-MDP，药物吸收 1h 后腹腔注射一些利尿剂，清除小鼠膀胱里积淀的放射性代谢物，再麻醉小鼠，进行成像实验。先是用高分辨的平行孔准直器对小鼠作 10min 全身平面显像，再作断层扫描。实验显示：在平面及 SPECT 断层扫描中，其中一只小鼠呈现清晰的骨转移显像。实验结果表明：microSPECT 对乳腺癌骨转移小鼠模型的研究是一个非常有效的研究工具。

Investigation of a mouse model of human breast cancer metastasis to human bone using high-resolution microSPECT

QI Yujin　ZHANG Mengjiao　LING Lijun*

Key words:　Breast cancer metastasis, Mouse model, MicroSPECT imaging

The study is to demonstrate the feasibility of using high-resolution microSPECT in mouse model studying human breast cancer metastasis to the bone. Three mice of 22 g, which had been implanted with breast cancer and human bone cells, were injected with ^{99m}Tc-MDP via tail vein by 111 MBq per mouse, and 1 h later hydragogue injection was done to empty its bladder. The mice were anesthetized and scanned by the microSPECT system. A planar whole body imaging was made first in a 10-min scan with a high-resolution parallel-hole collimator. This decided the necessity of performing the tomography imaging on a mouse. One of the mice was found with a significant breast cancer metastasis to the implant site of human bone in both planar and tomography images. These results indicate that microSPECT imaging is an effective tool to investigate the mouse model of human breast cancer metastasis to human bone.

*江苏省人民医院乳腺内分泌外科

针孔 SPECT 精确定量三维图像重建的研究进展

张雪竹　漆玉金

关键词　针孔 SPECT，图像重建，FDK 算法，OS-EM 算法

本研究的目的是为针孔 SPECT 成像开发精确定量的三维图像重建方法。针孔 SPECT 图像重建跟锥束 CT 图像重建非常相似。锥束 CT 图像重建常采用 Feldkamp-Davis-Kress 算法(FDK 算法)，是基于圆轨道扫描的近似解析算法。此法假定扫描断层切面可用相应的倾斜扇束切面来近似，所需重建时间较少，针孔角度较小时能得到较好的重建图像。本研究的第一步是把 FDK 算法应用于针孔 SPECT 图像重建。对针孔 SPECT 成像研究中常用的 Jaszczak 模型进行的 FDK 三维图像重建结果表明，在针孔几何的中心平面附近能够得到很好的重建结果，但在远离中心平面区域，由于投影数据的不完备，得到的重建图像出现较大的伪影和失真。针孔 SPECT 投影数据的不完备可用其它数据采集方式(如螺旋轨道或多针孔)来克服，这些也是我们的研究内容。由于 SPECT 成像获得的投影数据通常都有较严重的统计噪声，因而以统计理论为基础的统计迭代重建算法更适用于开发精确定量的 SPECT 图像重建。我们正在研究基于统计迭代的 OS-EM(有序子集期望值最大化)算法应用到针孔 SPECT 的图像重建，同时加入非均匀衰减、散射效应等校正，以获得精确定量的三维图像重建。

Progress in 3-D image reconstruction for pinhole SPECT

ZHANG Xuezhu　QI Yujin

Key words:　Pinhole SPECT, Image reconstruction, FDK algorithm, OS-EM algorithm

The study is to develop accurate and quantitative image reconstruction methods for pinhole SPECT. The image reconstruction for pinhole SPECT is very similar to cone-beam CT's. For cone-beam CT with a circular obit scan, Feldkamp-Davis-Kress (FDK) algorithm is popularly used as an approximately analytic algorithm. Based on fan-beam reconstructions, it assumes that the non-central slices can be approximately derivate from the slant fan-beam geometry. It can provide reasonable good reconstructions with less reconstructing time for the cone-beam geometry with a small cone angle. The first step of our studies is to implement the FDK algorithm for the pinhole SPECT image reconstructions. In the reconstructed images from the Jaszczak phantom in a pinhole SPECT using the FDK algorithm, the data from the central plane of the pinhole were well reconstructed, but the data from the non-central plane resulted in significant artifacts in the reconstructed images due to the incompleteness of the project data. The problem can be solved by other data acquisition strategies such as helical-orbit scan and multiple-pinhole scan, which are included in our studies. However, the iterative reconstruction methods based on statistics is more suitable for the pinhole SPECT since there is significant statistic noise in the measurements of SPECT. Efforts were made to study the OS-EM (Ordered Subset Expectation Maximization) algorithm for the pinhole SPECT. The non-uniform attenuation and scatter corrections would be incorporated in the OS-EM algorithm in order to obtain accurate and quantitative image reconstructions.

上海 EBIT 装置的控制系统

龚培荣 李纪明 郭盘林 肖龙笙 季 萍 李华萍

关键词 EBIT，电源，控制

上海电子束离子阱(EBIT)是我国研制的首台研究高电荷态物理的装置。其控制系统分为静态控制和动态控制，静态控制包括各电源输出参数的设置、回读及保存，安全联锁信号的控制，采用 Group3 模块进行系统设计；动态控制是使离子的注入、引出以及束缚电离过程协调动作，由时序发生器主导工作。上海 EBIT 电源系统共配备 36 台电源，分布在七个不同电位的电压平台上，除超导电源外的所有电源受控制系统控制。除电源参数设置、状态监测、联锁控制以保护人身和设备安全外，静态控制还需根据实验需要对 DT2B 电源输出电压进行调制以实现电子束能量的慢扫描。上海 EBIT 于 2004 年 12 月出束，2006 年 6 月，在 3T 的超导磁场下输出 110 keV/155 mA 的束流。其间，控制系统的功能也不断完善，工作可靠。电源的动态控制操作还须进一步改进，能满足各种物理实验要求的电源动态控制仪也在调试中，即将投入使用。

The control system for Shanghai EBIT

GONG Peirong LI Jiming GUO Panlin XIAO Longsheng JI Ping LI Huaping

Key words: EBIT, Power supply, Control

Shanghai Electron Beam Ion Trap (EBIT) is the first device developed in China for physics study of highly charged particles. The control system includes the static and dynamic subsystems. The static control, designed with Group3 module, decides, and reads and stores, the power output parameter, and performs the safety and interlock signal control. The dynamic system controls ion injection and extraction, working via a timing generator. The Shanghai EBIT has 36 power supplies distributed in seven level potential platforms. The system controls all the power supplies except for the superconductor power supply. Besides settings and monitoring power parameters, and interlock control for personal and the equipment protection, the static control performs slow scanning of the electron beam energy according to experiment demands, by modulating the DT2B power output voltage. The Shanghai EBIT had its first beam in December 2004. In June 2006, it had 110 keV/155 mA electron beams with 3T superconducting magnet. By continuous efforts to improve the control system in the two years, the EBIT worked reliably. However, the dynamic control of power supply needs further improvement. A power supply dynamic control meter that will satisfy most requirements of the physics experiments was at the final stage of development.

用于 EBIT 装置的可快速关断的高压电源

龚培荣 李纪明 刘 平 肖龙笙

关键词 高压电源，快速开关，干簧继电器，IGBT

在上海 EBIT 装置中，束流的快速切断通过关断电子枪阳极电压实现，以免装置被束流所损坏。由于 EBIT 的电子枪通常处在较高的负电压平台上，故阳极电压的联锁信号由光纤输入，一旦联锁信号有效，阳极电源马上驱动半导体开关动作，在 10 μs 内将阳极电压降为零输出，并保持到联锁故障解除且人工复位后。我们选择功率 IGBT 管串联输出来快速关断阳极高压电源。半导体开关的关断时间与驱动电路的脉冲频率有关，频率越高，关断时间越短，并且，一般要在约 2 个驱动脉冲周期后，半导体开关才能全导通。实际应用过程中，在半导体开关两端还并联一个高压型干簧继电器，以保持高压电源 0V 输出直到人为复位；这种只让半导体开关工作极短时间的工作方式可以极大地降低电路设计的成本，提高电源运行的可靠性。我们设计制造的可快速关断阳极电源的技术要求简述如下:

输出电压电流：0~9000 V 连续可调，最大负载电流 1 mA；

光纤联锁输入：有光信号，电源正常输出，一旦光信号灭, 电源应在 10 μs 内输出为零

输出电压的纹波和稳定性：＜9Ⅴpp 和 0.05%；

此电源应用于上海 EBIT 装置中，可靠地实现了输出束流的快速保护。

A high voltage power supply with quick shutdown for Shanghai EBIT

GONG Peirong　LI Jiming　LIU Ping　XIAO Longsheng

Key words: HV power supply, Fast switch, Reed relay, IGBT

We designed a HV power supply which can be shutdown within 10μs from output 9kV to 0V and can be interlocked via an optical fiber cable. The HV power supply is used to stop electron beam quickly after the EBIT has fault, and hold 0 volt output until getting a reset signal. The HV power supply adopts a bank of IGBT and reed relay to shutdown its output voltage, and a bank of IGBT is a fast switch which can be driven by high frequency pulse signal and reed relay holds 0 volt output following IGBT. This HV power supply has been employed at Shanghai EBIT successfully.

电子帘加速器电源控制系统的研制

龚培荣　刘　平　郭洪雷　王　君　林叶春*

关键词　电子帘加速器，电源，PLC，控制

该电子帘加速器用于橡胶乳液的辐射硫化，系 300 keV 60 mA 高压型加速器。高压电源采用工频二倍压整流电路，空载最高电压 350 kV。电子枪由多根灯丝组成，灯丝最大加热功率为 1 kW，由两级隔离变压器供电。加速器电源控制系统由计算机、控制机柜、电源调节机柜和电源钢筒组成。控制机柜包括 PLC 和信号接口电路、能量稳定调节电路等，作为整个加速器电源的控制中心，采集信号，实现加速器的联锁保护、输出控制调节等。采用西门子公司的 PLC(主控模块 CPU 313C)，共有 40 个开关量输入、16 个开关量输出、12 个模拟量输入、2 个模拟量输出，四种控制信号的冗余量约为 20%。电源调节机柜包括两个可控硅控制器，分别用于调节高压输出和灯丝电流输出，输入输出电压的调节范围不同，可实现加速器能量和束流的“本地”控制，但“本控”模式

输出控制时不具有输出稳定功能。高压电源调试表明，可实现各种逻辑保护功能和状态显示，高压电源空载输出达 350 kV，“遥控”模式控制下电压设定与实际输出间误差小于 1%，且能稳定运行。灯丝电源调节在 “本控”模式下可控硅输出电压步进幅度小于 0.5 V，可满足现场调试的要求。

The control system for power supply of a curtain accelerator

GONG Peirong LIU Ping GUO Honglei WANG Jun LIN Yechun*

Key words: Electron curtain accelerator, Power supply, PLC, Control

An electron curtain accelerator was developed for radiation vulcanization of rubber latex. It is a high voltage accelerator of 300 kV/60 mA beam power. The high voltage power supply generates 350 kV without load with a double voltage rectification of industrial frequency. The electron gun consists of tungsten filaments heated by currents from two serial isolation transformers. The power supply of the electron curtain accelerator is composed of industrial computer and console and power pot and box. The control system uses Siemens PLC (mainly CPU313C) with 40 digital input signals, 16 digital output signals, 12 analogy input signals and 2 analogy output signals. It performs local and remote control of the accelerator. Tests of the control system showed satisfactory results.

*上海海事大学

钴源辐照装置的 PLC 控制

龚培荣 刘 平 肖龙笙 何宝发 张 琴

关键词 钴源，辐照，控制，管理

为提高钴源辐照装置的运行性能，我们基于西门子 S7-300 型 PLC，配合工控机，完成了钴源辐照装置的控制改造。开发了多种管理功能，使钴源辐照装置操作简单，维护方便。除常规安保功能、钴源升降操作外，此控制装置还进行源棒的信息管理，如源棒所在位置、强度、装源日期等，管理人员可由其数据查询功能方便地检查值班情况、故障信息、链速和吊具的进出情况等。设计有两套操作界面，一套为工控机，用鼠标或键盘操作，通过专用通讯卡向 PLC 发控制指令。另一套为手动按钮控制盒，安装了各种 LED 指示灯和按钮，可直接向 PLC 发控制指令，两套方案可自动切换。

A PLC control system for ^{60}Co irradiator

GONG Peirong LIU Ping XIAO Longsheng HE Baofa ZHANG Qin

Key words: ^{60}Co, Irradiation, Control, Management

A new control system was developed for improving performance of a ^{60}Co irradiation facility. It combines PLC and industry computer, with human interface. A number of management tasks were de-

signed for easy operation and maintenance of the irradiator. It controls the safety interlock and source lifting, and provides information of the source pencils, such as the position, the radioactivity and date of replacement. Operation status of the irradiator can be checked, such as the records of chain speed, and product loading and unloading of the overhead carriers. The control system can be operated automatically or manually.

废钢中放射性物质检测装置的预研究

徐慧超　龚培荣　陈国营*　沈　毅*

关键词　废钢，放射性，能谱，塑料闪烁体

我所与宝山钢铁股份有限公司合作开展了废钢中放射性物质检测装置的可行性研究，以探测并判断废旧钢材中可能含有的放射性。我们以塑料闪烁体和光电倍增管检出 γ 射线，以 BF_3 正比计数管为中子探测器，用便携式能谱分析仪确定放射性元素。塑料闪烁体探测效率随体积增大，可实现 0.1 μSv/h 的探测灵敏度，对 ^{137}Cs、^{241}Am、^{60}Co、^{238}Pu 作了全能谱测定(NaI 晶体探测器和 CZT 半导体探测器)，1.7mm 厚 CZT 探测器对 ^{241}Am (59.5 keV)和 ^{238}Pu(44 keV)的能量分辨率分别为 5.39%和 11.27%。用 BF_3 正比计数管(Φ30mm×300mm)完成了镅铍中子源(20mm×35mm)全能峰的测量。采用适当大小尺寸的塑料闪烁体，合理的布局探测器阵列，再辅以相应的电子学仪器以及解谱软件，将能完全区分 ^{137}Cs、^{241}Am、^{60}Co、^{238}Pu、^{226}Ra、^{232}Th 和 ^{238}U 等放射性物质。

The feasibility of detecting radioactivity in scrap returns

XU Huichao　GONG Peirong　CHEN Guoying*　SHEN Yi*

Key words:　Scrap returns, Radioactivity, Energy spectrometer, Plastic scintillator

This is a feasibility study for developing an instrument to detect and identify radionuclides in scrap returns loaded in a truck, for Baoshan Iron & Steel Co., Ltd. According to practical conditions, plastic scintillator with PMT was used to detect γ-rays, BF_3 proportional counter tube was for neutron detection, and a portable energy dispersive spectrometer was used radionuclide identification. As detection efficiency increases with the volume of the plastic scintillator, a sensitivity of 0.1 μSv/h is realizable. Energy spectra of ^{137}Cs, ^{241}Am, ^{60}Co and ^{238}Pu γ-rays were obtained with either NaI(Tl) detector or CZT(cadmium zinc telluride), a new type semiconductor detector. A 1.7mm thick CZT detector has resolution at room temperature of 5.39% for^{241}Am at 59.5 keV and 11.27% for ^{238}Pu at 44 keV. With a BF_3 proportional counter tube (Φ30mm×300mm), neutron spectrum from an Am-B neutron resource (Φ20mm×35mm) was obtained. With an array of plastic scintillators in suitable volume, improved electronics system and analysis software, it is feasible to develop an instrument to detect radionuclides, e.g. ^{137}Cs, ^{241}Am, ^{60}Co, ^{238}Pu, ^{226}Ra, ^{232}Th and ^{238}U, in a scrap-return-loaded truck.

*宝钢集团宝山钢铁股份有限公司

一种新型毛细管电泳高压电源

龚培荣 李纪明 施学兰

关键词 高压电源，定时，毛细管电泳

此高压电源专为毛细管电泳实验而设计。电源输出极性可切换，且自动指示，“进样电压”时间既可人工操作，也可定时输出，电源还可接受外来电压信号遥控调节输出。电源采用 PWM 电路设计，输出频率 50 kHz 左右的脉冲信号，经高压变压器升压后，倍压整流产生 30 kV 的直流电压，由极性转换电路输出正或负高压。采用输出控制及保护电路实现电源输出电压的升或降，以及过压，过流保护功能；同时，对输出电流进行限制输出，一旦达到限定的电流值(0.5 mA)，电源输出电流将不再增加。定时电路完成进样电压的定时输出控制，定时精度小于 0.1 s。

A new type HV power supply for capillary electrophoresis

GONG Peirong LI Jiming SHI Xuelan

Key words: HV power supply, Timing, Capillary Electrophoresis

We developed a new type high voltage power supply, with which output polarity can be selected by jumping pin and maximum output is ±30kV/0.5mA. It is designed specially for capillary electrophoresis experiment. Its sample voltage output is controlled by timing circuit or manually. Output voltages can be remotely adjusted via an analogue voltage signal. The power supply designed with the PWM sends 50 kHz pulse signal to drive a high frequency transformer and a rectification filter circuit to produce 30 kV DC output. It has over voltage and over current protection, limiting its output current to 0.5mA. A timing circuit module guarantees time precision of < 0.1 s for the sample voltage output.

新技术中心

Membrane Technology

聚乙烯醇缩丁醛超滤膜的制备与亲水性

沈 飞 陆晓峰 卞晓锴 施柳青

关键词 聚乙烯醇缩丁醛(PVB)，超滤膜，制备，亲水性

用聚乙烯醇缩丁醛(PVB)作为本体高分子材料，用浸没沉淀相转化法制备 PVB 不对称超滤膜并用扫描电镜照片显示所制膜的超滤结构。研究了 PVB 本体浓度、制膜间隙、凝胶浴温度，特别是溶剂种类等因素对 PVB 不对称超滤膜性能的影响。研究了四种不同溶剂体系对 PVB 超滤膜皮层的形成机理的影响。同时还比较了 PES 和 PVB 的亲水性。结果显示，PVB 膜表面结构的形成是铸膜液平衡热力学和成膜过程扩散动力学这两种因素相互结合共同作用的结果，而 PVB 膜的断面结构则主要受溶剂-非溶剂相互扩散速度的控制。膜的渗透及分离性能可通过改变制备条件进行调节。PVB-PES 共混膜表面接触角随着 PVB 含量的增加而减小，共混膜表面接触角可由 81.0° 降至 76.6°。同时在三元相图中可看到 PVB-DMAC-Water 体系浊点位置稍接近于聚合物-溶剂轴，因此在 DMAC 中 PVB 亲水性稍高于 PES。

Preparation and hydrophilicity of poly(vinyl butyral)-based ultrafiltration membranes

SHEN Fei LU Xiaofeng BIAN Xiaokai SHI Liuqing

Key words: Poly(vinyl butyral), Ultrafiltration membrane, Preparation, Hydrophilicity

Poly(vinyl butyral) (PVB)-based ultrafiltration membranes were prepared by immersion– precipitation in water coagulation bath. The effects of different factors, such as PVB concentration, scraper clearance, water temperature and especially solvent nature on the performance of final membranes were extensively investigated. The toplayer formation mechanism of the PVB membranes prepared in four different PVB–solvent–water systems was discussed. By comparison with poly(ether sulfone) (PES), the hydrophilicity of PVB was also studied. Experimental results showed that PVB-based ultrafiltration membranes with an asymmetric structure were successfully prepared by the observations of scanning electron microscope (SEM). The formation of the toplayer of the PVB membranes above-mentioned from different solvents was the result of the combination of the equilibrium thermodynamics and membrane formation kinetics, whereas the sublayer of those membranes was dominated by the diffusion rate of solvent–nonsolvent. The permeability and separation performance of the final PVB membranes could be adjusted under different preparation conditions. PVB–PES blends were the nonmiscible systems, and the increase in mass ratio of PVB in the components decreased the surface contact angle of the resulting PVB–PES composite membranes from 81.0° to 76.6°. In phase diagram, the width of the liquid–liquid homogeneous region of the PES–DMAC–water system was very close to but slightly smaller than that of the PVB–DMAC–water system, which indicated that PVB was a little more hydrophilic than PES while in solution.

聚丙烯酸钠复合超滤膜研制(II) :UPANA-1 复合膜的性能与结构

樊文玲　陆晓峰

关键词　膜性能与结构，原子力显微镜，复合超滤膜

研究了 UPANA-1 复合超滤膜分离性能，以及压力、时间、进样浓度等操作条件对 UPANA-1 膜性能的影响。同时研究了 UPANA-1 复合膜的抗污染情况及其膜表面微观状态。结果表明：(1) UPANA-1 复合超滤膜的截留相对分子质量为 1000；(2) 操作压力的提高、运行时间的延长和溶液浓度的变化对 UPANA-1 复合超滤膜的截留率影响较小；(3) 与基膜相比，UPANA-1 复合膜的耐污染性有大幅度的提高。

Preparation of polyacrylic sodium composite ultrafiltration membrane (II): Performance and structure of UPANA-1 composite membrane

FAN Wenling　LU Xiaofeng

Key words:　Membrane performance and structure, AFM, Composite ultrafiltration membrane

Separation performance of UPANA-1 membrane and effects of such operating conditions as pressure, time, concentration of solution, etc. on the performance of membrane were studied. At the same time, the resistance ability to contamination and the fine structure of UPANA-1 membrane surface were preliminarily studied. Results showed that: (1) the MWCO of UPANA-1 membrane was 1000; (2) increase in operating pressure, extension of operation time and change in solution concentration have little effect on the rejection of membrane; (3) compared with the substrate PES membrane, UPANA -membrane's resistance to contamination was largely improved.

聚乙烯醇缩丁醛超滤膜的制备

沈　飞　陆晓峰　卞晓锴　施柳青

关键词 聚乙烯醇缩丁醛(PVB)，超滤膜，浸没沉淀相转化法，膜制备

用聚乙烯醇缩丁醛(PVB)作为本体高分子材料,用浸没沉淀相转化法制备 PVB 不对称超滤膜；扫描电镜照片显示所制膜的超滤结构。研究了 PVB 本体浓度、制膜间隙、凝胶浴温度以及乙酸添加剂等因素对 PVB 不对称超滤膜性能的影响；比较了乙酸及聚乙烯基吡咯烷酮(PVP)作为添加剂对大孔径 PVB 超滤膜皮层结构的影响。当 PVB 本体浓度为 12%时，膜的纯水通量及牛血清白蛋白(BSA)溶液通量分别为 876.4 $L\cdot m^{-2}\cdot h^{-1}$ 和 89.8 $L\cdot m^{-2}\cdot h^{-1}$，此时膜对 BSA 的截留率为 96.8%；PVB 膜纯水通量随着制膜间隙的增加及凝胶浴温度的上升而降低；乙酸及 PVP 的添加均提高了 PVB 超滤膜的纯水通量，通量增加幅度分别为 136%和 171%。

Preparation of poly(vinyl butyral) ultrafiltration membranes

SHEN Fei LU Xiaofeng BIAN Xiaokai SHI Liuqing

Key words: Poly (vinyl butyral), Ultrafiltration membrane, Immerged phase-inversion process, Membrane preparation

Poly (vinyl butyral) (PVB) ultrafiltration membranes were prepared by immerged phase– inversion process. From SEM images, it could be found that PVB membranes with macropores were successfully prepared. Effects of concentration of PVB, clearance of scraper, temperature of gelling bath and concentration of acetic acid additive on membrane performance were investigated. The influence of acetic acid and poly (vinyl pyrrolidone) (PVP) on morphology of the top layer of PVB membranes was studied. When PVB concentration was 12%, the pure water flux of PVB membrane was about 876.4 $L \cdot m^{-2} \cdot h^{-1}$, and the flux and rejection of Bovine Serum Albumin (BSA) solution was about 89.8 $L \cdot m^{-2} \cdot h^{-1}$ and 96.8%, respectively; pure water flux of PVB membrane decreased as the increase of clearance of scraper and temperature of gelling bath. The addition of acetic acid and PVP increased the pure water flux of PVB membranes by 136 % and 171%, respectively.

热致相分离法平片式聚(乙烯-乙烯醇)微孔膜的制备和表征

谢林锋 陆晓峰 李 磊 沈 飞 李文俊

关键词 热致相分离，聚(乙烯-乙烯醇) (EVOH)，平片式微孔膜

以丙三醇为稀释剂，用热致相分离方法(TIPS)制备了无纺布支撑的平片式聚(乙烯-乙烯醇)(EVOH)微孔膜。实验研究了冷却速率及 EVOH 初始浓度对膜结构及性能的影响，测定了 EVOH/丙三醇体系的相图，用扫描电子显微镜(SEM)及泡点法表征了微孔膜的微观结构及表面孔径，同时测试了膜的纯水通量。结果表明，随着冷却速率的加快，结晶曲线向低温移动。EVOH 初始浓度决定了体系的相分离方式，由液-液相分离及固-液相分离机理形成的膜分别具有花边结构与球间缝隙结构；冷却速率影响膜的孔径大小和形态。随着冷却速率及 EVOH 初始浓度的降低，膜的孔径及纯水通量均逐渐增大。

Preparation and characterization of poly(ethylene-co-vinyl alcohol) flat sheet microporous membranes via thermally induced phase separation

XIE Linfeng LU Xiaofeng LI Lei SHEN Fei LI Wenjun

Key words: Thermally induced phase separation, Poly (ethylene-co-vinyl alcohol), Flat sheet microporous membrane

Microporous membranes supported on the non-woven fabrics were prepared by the crystalline poly (ethylene-co-vinyl alcohol) (EVOH) via thermally induced phase separation, using the glycerol as diluent. In this paper the diagram of the EVOH/ glycerol system was determined. The influence of some factors as concentration and cooling rate on the performance and the morphology was investigated. The results showed that the crystallization curve shifted to low temperature with the decrease of cooling rate.

The polymer concentration determines the mode of phase separation. Liquid-liquid phase separation results in leafy structure and solid phase separation results in spherulite structure. The porosity and the diameter of pores increase when the cooling rate and the initial concentration decreased. The water permeability increase when the diameter of pores increases.

大颗粒高浓度硅溶胶的制备

许念强　顾建祥　罗 康　郑松保

关键词　水玻璃，硅粉，硅溶胶，纳米二氧化硅，大颗粒

以水玻璃为原料, 采用滴加工艺制备一定粒径大小的二氧化硅作为母核; 采用在催化剂和分散剂共同作用下水解硅粉的方法使母核二氧化硅颗粒进一步增长, 得到了高均匀分布的平均粒径在 100 nm 以上、浓度可达 50%的二氧化硅溶胶。并对新方法下 pH 值、温度以及母核 SiO_2 的浓度、粒径大小对二氧化硅平均粒径及其均匀性的影响进行了分析。研究结果对制备大颗粒、高浓度的硅溶胶具有积极意义。

Preparation of large particle size high concentration silica sol

XU Nianqiang　GU Jianxiang　LUO Kang　ZHENG Songbao

Key words:　Sodium silicate, Silica powder, Silica sol, Nano silicon dioxide, Large particle size

Silicon dioxide (mother nuclide) with a specific particle size was prepared from sodium silicate through the dropwise technique. The mother nuclide was further growing by hydrolyzing silica powder under the combined effect of catalyst and dispersant, then the silicon dioxide with highly uniform particle diameter of more than 100 nm was prepared, and the concentration of the silica sol can reach 50%. The effects of such parameters as pH, temperature, concentration and particle size of mother nuclide on the average diameter and uniformity of silicon dioxide were investigated.

MBR 与 CAS 法处理市政污水的比较

陆晓峰　梁国明　陈 洁　余江林　沈 飞

关键词　膜生物反应器，浸没式平片膜组件，传统活性污泥工艺，市政污水处理

比较了采用浸没式平片膜组件的膜生物反应器(MBR)与传统活性污泥工艺(CAS)处理市政污水时平均容积负荷率、平均污泥负荷率及各自出水 BOD_5/COD 值；考察了 MBR 中水温及水力停留时间(HRT)对 NH_3-N 去除效果的影响。MBR 对有机物去除效果好于 CAS，当 MBR 的 HRT 为 3.2 h，处理后出水 COD 去除率为 93.07%，BOD_5 为 99.08%，都好于 CAS 处理后的出水。水温由(8±4)℃升至(25±5)℃，MBR 对 NH_3-N 去除率由 7.55%升至 71.9%；提高 MBR 的 HRT 至 6 h，NH_3-N 去除率可达 97.3%。

Performance of MBR and CAS in municipal wastewater treatment

LU Xiaofeng LIANG Guoming CHEN Jie YU Jianglin SHEN Fei

Key words: Membrane bioreactor (MBR), Submerged-flat membrane module, Conventional activated sludge process (CAS), Treatment of municipal wastewater

Average volume load rate, average sludge load rate and the effluent value of BOD_5/COD of a submerged-flat membrane bioreactor (MBR) and a conventional activated sludge process (CAS) which was used in the treatment of municipal wastewater were compared. Effects of temperature and HRT on NH_3-N removal in MBR system were examined. MBR system had better organic compound removal than that in CAS system. When the HRT of MBR was 3.2 h, the average COD and BOD_5 concentrations in MBR effluent were 35.99 mg/L (93.07%) and 3.5 mg/L (99.08%), respectively, whereas in CAS the COD was 62.88 mg/L (88.55%) and BOD_5 was 21.5 mg/L (94.31%). At (8±4)℃ and (25±5)℃ of the liquid mixture, the average NH_3-N removal in MBR system was 7.55% and 71.9%, respectively. Furthermore, a 6 h HRT could increase the average NH_3-N removal to 97.3%.

膜生物反应器中的基质降解动力学

林红军 陆晓峰 施柳青

关键词 膜生物反应器，基质降解动力学，有机物，氨氮

通过动力学推导, 得到了膜生物反应器降解有机物和氨氮的的动力学模型, 并采用膜生物反应器处理人工配制的生活污水,确定了相关的动力学参数 K_S=264.04 mgCOD/L, $v$max=2.01d^{-1}, K=0.0076 L·d^{-1}·mg^{-1} COD, y=0.44 mgMLSS/mgCOD, K_d=0.021d^{-1}, K_N=0.061d^{-1}, 并得到了动力学方程, 实验表明该动力学方程能较好地预测MBR的出水水质状况, 可为膜生物反应器处理污水的工艺设计提供参考。

Substrate biodegradation kinetics of a membrane bioreactor

LIN Hongjun LU Xiaofeng SHI Liuqing

Keywords: Membrane bioreactor (MBR), Substrate degradation kinetics, Organic matter, Ammonium

Substrate degradation kinetics of a membrane bioreactor (MBR) was analyzed and discussed, and a reaction kinetics model of organic matters and ammonia degradation was developed. The kinetic parameters and equations were determined by using MBR to treat artificial domestic wastewater. Results indicated that the kinetics model is satisfactory to predict the effluent qualities of MBR, which can provide reference for process design.

缺氧/好氧膜生物反应器处理尿液污水

林红军　陆晓峰　陈 洁

关键词　缺氧/好氧膜生物反应器，尿液污水，硝化反应，膜污染

采用缺氧/好氧膜生物反应器(A/O MBR)对尿液污水进行处理。结果表明：当进水 NH_4^+-N、COD 和 BOD_5 分别为 400~980 (容积负荷为 0.42~1.01 $kg\cdot m^{-3}\cdot d^{-1}$)、390~630 和 120~280 mg/L 时，平均去除率分别为 79.5%、75.1%和 95.0%。同时系统对色度也有一定的脱除效果，经过 A/O MBR 和活性炭(PAC)处理后出水色度降为 8 倍。运行期间膜污染较严重，膜内表面微生物的滋生和膜外表面形成沉积层是造成膜污染的主要原因。

Treatment of urine wastewater with an anoxic/ aerobic membrane bioreactor

LIN Hongjun　LU Xiaofeng　CHEN Jie

Key words: Anoxic/aerobic membrane bioreactor, Urine wastewater, Nitrification, Membrane fouling

An anoxic/aerobic membrane bioreactor was used to treat urine wastewater. The results showed that 79.5% N H^+_4-N, 75.1% COD and over 95.0% BOD_5 could be removed when NH_4^+-N, COD and BOD_5 in the influent were 400~980 (volume loading of 0.42~1.01 $kg\cdot m^{-3}\cdot d^{-1}$), 390~630 mg/L and 120~280 mg/L, respectively. Meanwhile, the color decreased to 8 after further treatment by MBR and PAC filter. It was also found that membrane fouling was serious in the experiment, mainly due to bio-fouling on the inner membrane surface and sludge cake layer on the outer membrane surface.

预处理对热电池阳极材料 LiB 合金结构和性能的影响

段 伟　章四琪　刘志坚

关键词　LiB 合金，预处理，冷挤压，热处理

在 LiB 合金材料制备中加入冷挤压和热处理两步预处理工艺；采用 X 射线衍射仪、扫描电镜测试合金的物相；研究了预处理工艺对材料密度、硬度、力学性能、热稳定性和放电性能的影响。结果表明：相对直接轧制方法制备的 LiB 合金材料, 采用预处理工艺可提高合金中 Li7B6 的相对含量，使合金结构和成分更均匀、致密，提高了合金的密度、硬度、抗拉强度和断裂延伸率；预处理使材料骨架孔洞缩小且分布均匀，有助于提高材料的热稳定性；材料的放电容量由 5244 提高至 6552 C/g。与直接轧制工艺相比，冷挤压和热处理预处理减少了多孔合金锭与可反应气氛接触的时间，防止氧化，消除开裂、麻点等缺陷，材料的加工成材率由不到 50%提高至 70%以上。

Effect of pre-treatment procedures on structure and performance of thermal battery anode LiB alloy

DUAN Wei　ZHANG Siqi　LIU Zhijian

Key words: LiB alloy, Pre-treatment, Cold extrusion, Heat treatment

Two pre-treatment procedures, cold extrusion and heat treatment, were introduced in preparing LiB alloy. By means of X-ray diffraction and scanning electron microscopy, phase composition and microstructure characteristics of the LiB alloy were observed. Influence of the pre-treatment procedures on density, rigidity, mechanics performances, thermal stability and discharging performance were investigated. The results show that compared to the LiB alloy using direct-rolling method, the LiB alloys by the pre-treatments have higher Li7B6 content and more uniform and compact structure and composition. The density and rigidity of alloys are enhanced. The anti-draw intention and rupture prolongation ratio increase significantly. The treatments make the holes of framework smaller and arrangement more uniform, with increased thermal stability. The discharging capacity is enhanced from 5244 to 6552 C/g. By the treatments, the porous alloy ingot has reduced time to contact reactive atmosphere, hence prevention of oxidation and perforation and speckle in the alloy strip. The production rate of LiB alloys is greatly enhanced from below 50% to over 70 %.

市政污水处理中 MBR 和 CAS 工艺的污泥特性

林红军　陆晓峰　沈 飞　余江林

关键词　膜生物反应器，传统活性污泥工艺，污泥混合液特征

采用膜生物反应器(MBR)和传统活性污泥法(CAS)两种工艺处理相同水质的市政污水，考察了两种工艺运行状况和污泥混合液的特性。结果表明，MBR 可以达到非常好的 COD、BOD 和 NH4+-N 的去除效果，去除率高于 CAS；MBR 比 CAS 具有更高的污泥浓度，较低的污泥产率，较差的污泥沉降性能，同时两者的粘度与污泥浓度关系可以用不同的方程来表达；在运行天数为 50"50-161d 期间，MBR 系统中未发现可溶性微生物产物(SMP)明显的积累现象，在 SMP 中分子量大于 14000 的总有机碳(TOC)含量占总量的 49.6%，CAS 系统中相应值为 22.5%；两种工艺的污泥耗氧速率均随系统运行呈下降趋势，并且 MBR 中的污泥耗氧速率大于 CAS 中的相应值；另外两种工艺中微型动物在种类和数量上表现出了不同的变化规律。

Sludge characteristics of MBR and CAS processes in municipal wastewater treatment

LIN Hongjun　LU Xiaofeng　SHEN Fei　YU Jianglin

Key words:　Membrane bioreactor, Conventional activated sludge process, Sludge characteristics

A submerged-flat membrane bioreactor and a conventional activated sludge process were used for municipal wastewater treatment, and the characteristics of sludge liquor were investigated. It was found that satisfactory chemical oxygen demand (COD), biological oxygen demand (BOD) and ammonia nitrogen (NH_4^+-N) removal efficiencies were achieved in MBR, demonstrating a more stable and excellent effluent quality than CAS. Sludge concentration, sludge production and sedimentation in MBR were different from those in CAS. Meanwhile, relations between sludge viscosity and sludge concentration in the two processes can be expressed by different equations. The accumulation of soluble microbial products (SMP) was not observed in supernatant of MBR during 50-161d experimental period, and SMP with a molecular weight(MW)>140 000 in supernatant accounted for 49.6% in contrast to 22.5% in CAS. Experiments showed that oxygen uptake rate (OUR) of two systems decreased with an increases of the operation time, and OUR of MBR was higher than that of CAS. The microfauna in two systems were different from each other in their species and population.

膜生物反应器中的膜过滤特征及膜污染机理

林红军 陆晓峰 段 伟 沈 飞

关键词 膜生物反应器，膜污染机理，活性污泥，阻力分布

以膜生物反应器处理市政污水，研究活性污泥终端过滤膜的污染机理。实验表明，起初的内膜污染模型为膜孔堵塞，尔后为沉积层阻力模型，最后为膜污染的主要控制阶段。膜的相对通量随过滤时间呈指数衰减，压力越大，通量衰减越快；污泥沉积层存在压密过程，其污泥比阻随压力增大，处理市政污水的污泥压密指数为 0.8078；沉积层阻力占总阻力的 90%以上；活性污泥各组分对膜污染均有贡献，其中悬浮固体、胶体颗粒和溶质产生的阻力分别占 87.98%、6.20%和 5.82%；探讨了 MBR 处理市政污水过程中可能的膜污染机理.

Filtration characteristics and mechanism of membrane fouling in a membrane bioreactor for municipal wastewater treatment

LIN Hongjun LU Xiaofeng DUAN Wei SHEN Fei

Key words: Membrane bioreactor, Mechanism of membrane fouling, Activated sludge, Resistance distribution

Filtration characteristics and mechanism of membrane fouling were investigated. It was found that variation of filtration resistance fit to the standard blocking filtration mode1 in initia1 process and to cake filtration model in later process. The relative flux was in exponentia1 decay with filtration time, and decreased quickly at higher pressures. The sludge was compressed during filtration process, and resistance of the sludge increased with the filtration pressure. The compressibility index was 0.8078. Calculations showed that cake resistance made up over 90% of tota1 resistance. In addition, the relative contribution of each sludge fractions to membrane was respectively 87.98%, 6.20% and 5.82% for suspended solids, colloids and solutes. A possible mechanism of membrane fouling was proposed.

用水解酸化池-膜生物反应器处理活性艳红 X–3B 废水

梁国明 陆晓峰 王文浪

关键词 活性艳红 X–3B，水解酸化池，膜生物反应器，膜污染，废水处理

采用水解酸化池-膜生物反应器处理含活性艳红 X-3B 的模拟废水，研究了水力停留时间(HRT)对水解酸化池废水处理效果的影响，考察了水解酸化池-膜生物反应器对废水的处理效果及膜生物反应器中污泥沉降性能对膜污染的影响。实验结果表明：水解酸化池 HRT 为 16 h 时，废水的生物降解性最好，挥发性脂肪酸质量浓度与 COD 比值为 0.5；HRT 为 17 h 时，废水脱色率达 69%，而 COD 的去除率受 HRT 影响较小；膜生物反应器主要起去除废水中 COD 的作用；水解酸化池-膜生物反应器处理后废水的脱色率和 COD 去除率分别为 83%和 97%；膜生物反应器中活性污泥沉降性能的变化直接影响膜污染的速率。

Treatment of wastewater containing reactive brilliant red X-3B by hydrolysis acidification pool-membrane bioreactor process

LIANG Guoming LU Xiaofeng WANG Wenlang

Key words: Reactive brilliant red X–3B, Hydrolysis acidification pool, Membrane bioreactor, Membrane fouling; Wastewater treatment

The simulated wastewater containing reactive brilliant red X-3B was treated in a hydrolysis acidification pool and a membrane bioreactor. Effects of HRT on hydrolysis acidification, of the whole process on wastewater treatment, and of sludge sedimentation performance on membrane fouling rate were investigated. The experimental results show that with16 h of HRT, biodegradability of wastewater was the best with 0.5 of P(VFA)/COD, and with 17 h of HRT, the chroma removal rate was 69% whereas the COD removal rate was less affected by HRT. The main function of membrane bioreactor was to remove COD. By the hydrolysis acidification pool and membrane bioreactor, the chroma and COD removal rate of the wastewater was 83% and 97%, respectively. The sedimentation performance of activated sludge in membrane bioreactor directly affected membrane fouling rate.

不对称聚乙烯醇缩丁醛超滤膜的形成

沈 飞 陆晓峰 施柳青 卞晓锴

关键词 聚乙烯醇缩丁醛(PVB)，不对称超滤膜，膜形成机理，浸没沉淀相转化法

采用浸没沉淀相转化法在二甲基乙酰胺(DMAC)、*N*-甲基吡咯烷酮(NMP)、二甲基甲酰胺(DMF)及二甲亚砜(DMSO)等溶剂下制备聚乙烯醇缩丁醛(PVB)超滤膜，铸膜液组成为 PVB-溶剂二元体系，水为非溶剂。利用扫描电子显微镜观察了 PVB 膜的表面形貌与断面结构，并对其渗透及分离性能进行了测试，讨论了 PVB 膜表面结构的形成机理。结果表明，溶剂种类不仅决定 PVB-溶剂二元体系的热力学稳定性，同时也影响其成膜过程的动力学效应；PVB 膜断面结构受溶剂-非溶剂相互扩散速度的控制，而膜表面形貌则是铸膜液平衡热力学与成膜动力学结合的结果；不同溶剂的 PVB 超滤膜纯水通量大小依次为 DMSO>DMAC>DMF>NMP，其截留分子量则在 40~50 kD。

Formation of asymmetric poly (vinyl butyral) ultrafiltration membranes

SHEN Fei LU Xiaofeng SHI Liuqing BIAN Xiaokai

Key words: Poly (vinyl butyral), Asymmetric ultrafiltration membrane, Membrane formation mechanism, Immersion precipitation phase inversion process

Asymmetric ultrafiltration membranes were prepared from ternary PVB-solvent-water systems through the immersion precipitation process, and four different solvents were used. The toplayer morphology and cross-section structure of the PVB membranes were characterized by SEM. Infiltration and separation performance of the membranes were also evaluated. The toplayer formation mechanism of the membranes was then mainly discussed. The results showed that not only the thermodynamics stability of the binary PVB-solvent systems, but also the formation kinetics of the membranes was determined by the solvent nature. The cross-section structure of the membranes was controlled by the sol-

vent-nonsolvent diffusivity, whereas the toplayer morphology of the membranes was the result of the combination of the equilibrium thermodynamics of casting system and the membrane formation kinetics. Using the four solvents, the order of pure water flux of the membranes was: DMSO>DMAC>DMF> NMP. The rejection molecule weights of the membranes were located between 40~50 kD.

辐射接枝丙烯酸聚乙烯表面碳酸钙的结晶

张凤英　侯铮迟　盛康龙　邓 波　谢雷东

关键词　辐射接枝，丙烯酸，聚乙烯膜，碳酸钙晶体成核生长

尝试了用辐射接枝丙烯酸的聚乙烯膜作为模板控制碳酸钙晶体的成核和生长。用扫描电子显微镜观察了在过饱和碳酸氢钙溶液中形成的该晶体其形貌随时间的变化，用红外吸收光谱研究了晶体与接枝膜之间的化学相互作用。研究结果表明：接枝膜表面的羧基有利于碳酸钙晶体的异相成核，晶体的形貌特征与用原子力显微镜所揭示的接枝官能团分布相匹配。作为一种有效的聚合物表面功能化手段，辐射接枝在生物矿化研究中也将发挥重要的作用。

Crystallization of calcium carbonate on polyethylene grafted with acrylic acid

ZHANG Fengying　HOU Zhengchi　SHENG Kanglong　DENG Bo　XIE Leidong

Key words:　Radiation graft, Acrylic acid, Polyethylene film, $CaCO_3$ nucleation and crystal growth

The use of high-density polyethylene (HDPE) films grafted with acrylic acid by γ-ray irradiation as a template to control the nucleation and growth of calcium carbonate crystals was attempted. The morphology evolution of crystals formed from supersaturated calcium bicarbonate solution on the grafted HDPE films was observed by scanning electron microscopy, and the interaction between the formed crystals and the grafted HDPE films was revealed by Fourier transform infrared spectroscopy. Results of the characterizations proved that carboxylic acid functional groups on the grafted HDPE films significantly facilitated the heterogeneous nucleation of calcium carbonate crystals, and the distribution of the crystals was in congruity with that of the grafted carboxylic acid groups, as discovered by the atomic force microscopic images. It can be concluded that radiation-induced grafting, a method for functional modification of polymer surfaces, is also an effective means for studying biomineralization.

壳聚糖薄膜诱导碳酸钙晶体生长

张凤英　侯铮迟　虞 鸣　谢雷东

关键词　壳聚糖薄膜，碳酸钙，晶体异相成核和生长

以壳聚糖薄膜作为模拟生物矿化的模板，实现了在过饱和碳酸氢钙溶液中诱导碳酸钙晶体的异相成核和生长。光学显微镜、扫描电子显微镜、红外光谱和 X 射线衍射等观测表明，生成的碳

酸钙晶体呈片状，由细小晶粒聚集而成，晶型为方解石。选择合适的添加剂(M_W=2000 的聚丙烯酸)浓度、培养温度等能有效地抑制碳酸钙晶体的均相成核，促进其异相成核和生长。

Growth of calcium carbonate crystals on chitosan film

ZHANG Fengying HOU Zhengchi YU Ming XIE Leidong

Key words: Chitosan, Calcium carbonate, Heterogeneous nucleation and crystal growth

Biomimetic heterogeneous nucleation and growth of calcium carbonate crystals on the chitosan film as the template took place in supersaturated calcium bicarbonate solution. The specimens were characterized by optical microscopy, scanning electron microscopy, X-ray diffraction, and attenuated total reflectance infrared spectroscopy. The crystals proved to be calcite in sheets composed of fine crystal particles. The results indicated that proper additives (poly acrylic acid of M_W=2000 in certain concentrations) and proper temperature are capable of suppressing homogeneous nucleation of the calcium carbonate, and facilitate heterogeneous nucleation and growth of calcium carbonate crystals.

聚合物表面辐射接枝改性研究进展

侯铮迟 谢雷东 盛康龙

关键词 聚合物，辐射接枝，表面改性

本文讨论了接枝单体和基材的性质、溶剂、酸、阻聚剂以及其它添加剂对聚合物辐射接枝反应的影响，介绍了利用光学显微镜、扫描电子显微镜、原子力显微镜、凝胶色谱、X 射线光电子能谱、拉曼光谱、红外光谱等所取得的接枝条件对接枝层的形态结构及接枝链链长影响的研究结果。对近年来出现的能精确控制接枝链分子量和结构的活性聚合方法也作了简单介绍。

Recent progresses in surface modification of polymers by radiation grafting

HOU Zhengchi XIE Leidong SHENG Kanglong

Key words: Polymer, Radiation grafting, Surface modification

In this paper, we give a review on recent progresses in this field of research. Factors affecting degree of the grafting, such as the monomer and base polymer, the solvent, the initiator and other additives, are discussed. Studies on morphologies of the grafted layers and distributions of the grafted molecular chains characterized by OM (Optical microscopy), SEM (Scanning electron microscopy), AFM(Atomic force microscopy), GPC(Gel permeation chromatography), XPS(X-ray photoelectron spectroscopy), Raman and IR (Infra-red) spectroscopy are reviewed. Immerging grafting method of living polymerization induced by ionizing radiations, with which one is able to accurately control molecular weight and structure of the grafted molecular chains, is also briefly introduced.

附录 1

2005–2006 年论文统计
Papers Published in 2005–2006

上海光源 Shanghai Synchrotron Radiation Facility

1. 郑丽芳, 李纪堂, 刘松强. 用于加速器数字反馈控制研究的实验平台, 核技术, 2005, **28** (1): 13
2. 李纪堂, 郑丽芳, 陆承蒙, 等. 基于 EPICS 的磁铁电源控制系统, 核技术, 2005, **28**(10): 729
3. 丁建国, 沈国保, 刘松强. 基于数字延迟线的高分辨率 TDC 系统, 核技术, 2005, **28**(3): 173
4. 郑丽芳, 刘松强. 加速器数字反馈控制的 MATLAB 仿真平台, 核电子学与探测技术, 2005, **25**(6): 617
5. 张继东, 欧阳联华, 周巧根. 直线加速器磁元件的磁场测量, 仪器仪表学报, 2005, **26**(8): 76
6. 蒋迪奎, 姜晓丽. SSRF 储存环高频屏蔽波纹管的研制, 核技术, 2005, **28**(2): 93
7. CAO Hongping, CHEN Huanguang, LI Deming, A distributed control system for picosecond accelerator at SINAP, Nuclear Science and Techniques, 2005, **16**(4): 201
8. 曹红萍, 李德明, 陈焕光. 基于组态王 6.5 的皮秒加速器控制.doc, 云南大学学报(自然科学版), 2005, **27**(5A): 318
9. FU Luxin. Analysis and estimate of the influence of the leakage inductance of the charging transformer primary on the amplitude stability of the PFN charging voltage, Nuclear Instruments and Methods in Physics Research Section A, 2005, **547**: 313
10. 许瑞年, 张继东, 李德明. 一种实现微秒级多路时序的方法, 核技术, 2005, **28**(3): 169
11. 张建兵, 王芳, 王光伟. I/Q 技术用于加速器鉴相的实验研究, 高能物理与核物理, 2005, **29**(3): 312
12. LIU Aiqin, LIU Guimin, DAI Zhimin. Characteristics of coherent diffraction terahertz radiation at SDUV-FEL, Nuclear Science and Techniques, 2005, **16**(2): 70
13. 刘爱琴, 刘征平, 陈永忠, 等. 相干衍射辐射在超短电子束团长度测量中的应用, 高能物理与核物理, 2005, **29**(5): 517
14. DAI Zhimin. Induced ion-channel instability, Nuclear Science and Techniques, 2005, **16**(2): 65
15. ZHANG Feng, JI Lina, HE Jianhua, *et al*. Structural evidence for α-synuclein fibrils using *in situ* atomic force microscopy, Acta Biochimica et Biophysica Sinica, 2005, **37**(2): 113
16. TANG Lin, HUANG Yibo, LIU DQ. Effects of the silanized mica surface on protein crystallization, Acta Crystallographica Section D, 2005, **61**: 53
17. 柳 义, 吴志方, 柳 林, 等. 块体非晶合金 Zr55Cu30Al10Ni5 结构弛豫的研究, 物理学报, 2005, **54**(4): 1679
18. XIAO T Q, Bergamaschi A, Dreossi D. Effect of spatial coherence on application of in-line phase contrast imaging to synchrotron radiation mammography, Nuclear Instruments and Methods in Physics Research A, 2005, **23**(2): 352
19. WEI Xun, XIAO Tiqiao, LIU Lixiang. Typical microstructures of Chinese medicines with X-ray microscopy in phase contrast, Chinese Physics Letters, 2005, **22**(9): 2239
20. WEI Xun, XIAO Tiqiao, LIU Lixiang. Application of X-ray phase contrast imaging to microscopic identification of Chinese medicines, Phys Med Biol, 2005, **50**: 4277
21. 魏逊, 肖体乔, 陈敏. 中药显微结构的微聚焦管 X 射线相衬成像研究, 核技术, 2005, **28**(12): 889
22. 朱海君, 刘德康, 沈立人. 远程文件管理系统的设计及其应用, 核电子学与探测技术, 2006, **26**(4): 507
23. 朱海君, 沈立人, 刘德康. VC++ .net 中数据库报表的设计与实现, 核电子学与探测技术, 2006, **26**(5): 701
24. ZHANG Lihua, LIAO Yi, LIU Guimin. Effects of insertion device on SSRF storage ring, Nuclear Science and Techniques, 2006, **17**(1): 1
25. 姜伯承, 刘桂民, 戴志敏, 等. 上海光源储存环注入段纵向耦合阻抗的计算, 高能物理与核物理, 2006, **30**(增刊 I): 22
26. 后接, 刘桂民. 基于响应矩阵和 SVD 算法的输运线束流轨道校正, 高能物理与核物理, 2006, **30**(增刊 I): 37

27. 李浩虎, 刘桂民. 上海光源增强器动态升能过程分析, 高能物理与核物理, 2005, **30**(增刊 I): 66
28. LIU Guimin, DAI Zhimin, LI Haohu, *et al*. Lattice design for SSRF storage ring, 高能物理与核物理, 2006, **30**(增刊 I): 144
29. 孙小影,谢东, 沈立人, 等. 基于 Web 的 SDUV-FEL 工程数据库系统的设计与实现, 核电子学与探测技术, 2006, **26**(2): 164
30. WANG Naxiu, ZHENG Hongwei. Preliminary design of multi-function LIGA beamline, Nuclear Science and Techniques, 2006, **17**(1): 11
31. 王纳秀, 陈永林, 阎和平, 等. 上海电子束离子陷低温超导磁体系统的研制, 核技术, 2006, **29**(3): 169
32. 王纳秀, 朱毅, 傅远. 液氮间接冷却晶体单色器第一晶体热变形模拟计算, 高能物理与核物理, 2006, **30**(8): 802
33. 王纳秀, 朱毅, 朱卫华, 等. 同步辐射单色器晶体热应变的模拟与实验结果的比较, 核技术, 2006, **29**(5): 326
34. 胡勇, 郑丽芳, 李纪堂, 等, EPICS 下的 EtherNet/IP 协议的研究, 核技术, 2006, **29**(11): 805
35. 丁建国, 郑丽芳, 胡守明, 等. EPICS 环境下的 LINAC 控制系统, 核电子学与探测技术, 2006, **26**(1): 36
36. 陈焕光, 李德明, 曹红萍. 基于 Quartus II 4.2 的 FPGA 生成 PWM 模块设计, 计算机应用研究, 2006, **23**(增刊): 626
37. 范学荣, 陈志豪, 傅禄欣, 等. SSRF 储存环注入脉冲电源的设计, 核技术, 2006, **29**(6): 406
38. 张继东, 周巧根, 张红辉, 等. 可变椭圆极化波荡器 EPU10.0 的传动控制, 原子能科学技术, 2006, **40**(5): 602
39. 于成浩, 柯明. 基于激光跟踪仪的三维控制网测量精度分析, 测绘科学, 2006, **31**(3): 25
40. 于成浩, 柯明, 赵振堂. 论测量仪器的精密整平及对中技术, 测绘科学, 2006, **31**(6): 87
41. 于成浩, 柯明, 杜涵文, 等. 三维准直测量技术在 BEPCII 储存环控制网中的应用, 高能物理与核物理, 2006, **30**(11): 1107
42. 于成浩, 殷立新, 杜涵文, 等. 上海光源准直测量方案设计, 强激光与粒子束, 2006, **18**(7): 1167
43. 于成浩, 吴冠原, 杜涵文, 等. 皮秒和飞秒直线加速器的准直测量方案比较, 核技术, 2006, **29**(11): 801
44. YU Feng, SONG Jiaping, XU Chunyan, *et al*. Crystallization and preliminary X-ray analysis of Sau3AI C-terminal 232-419 amino acids fragment, Protein & Peptide Letters, 2006, **13**(6): 627
45. TANG Lin, LI Hongtao, DU Haining, *et al*. Study of the disassembly–assembly process of α-synuclein fibrils by in situ atomic force microscopy, Micron, 2006, **37**: 675
46. XI Zaijun, XIAO Tiqiao, ZHANG Zengyan, *et al*. Outline imaging by THz time domain spectroscopy, Chinese Physics Letters, 2006, **23**(2): 352
47. ZHANG Zengyan, JI Te, YU Xiaohan, *et al*. A method for quantitative analysis of chemical mixtures with THz time domain spectroscopy, Chinese Physics Letters, 2006, **23**(8): 2239
48. ZENG Danhua, XIAO Tiqiao, DU Guohao, *et al*. New long trace profiler based on phase plate diffraction for optical metrology of SSRF, Review of Scientific Instruments, 2006, **77**(9): 93305–1
49. 刘丽想, 杜国浩, 胡雯, 等. 利用定量相衬成像消除 X 射线同轴轮廓成像中散射的影响, 物理学报, 2006, **55**(12): 6387–6394
50. 席再军, 肖体乔, 张增艳, 等. 样品内部非平行界面的反射式 Terahertz 波层析研究, 物理学报, 2006, **55**(5): 2293
51. 吴衍青, 肖体乔, 离子振荡对低压脉冲负电性放电条件的影响, 物理学报, 2006, **55**(7): 3443
52. 曾丹华, 肖体乔, 席再军, 等. 相移干涉仪中探测器非线性误差及其补偿, 光学学报, 2006, **26**(9): 1358
53. 席再军, 肖体乔, 张增艳, 等. 二维透射式 Terahertz 波时域谱成像研究, 光子学报, 2006, **35**(8): 1171
54. 柳义. 上海光源 X 射线小角散射光束线站的概念设计, 核技术, 2006, **29**(4): 245
55. 吉特, 葛敏, 王文锋, 等. 碳家族一些成员在太赫兹波段的特性, 核技术, 2006, **29**(8): 561
56. 吉特. D-、L-和 DL-青霉胺的太赫兹时域光谱, 物理化学学报, 2006, **22**(9): 1159
57. 邓彪. 同步辐射微束荧光 CT 及应用最新进展, 物理, 2006, **35**(12) 1055

核物理 Nuclear Physics

1. STAR Collaboration. Distributions of charged hadrons associated with high transverse momentum particles in pp and Au plus Au collisions at $\sqrt{S_{\rm NN}} = 200{\rm GeV}$, Phys Rev Lett, 2005, **95**: 152301
2. STAR Collaboration. Multistrange baryon elliptic flow in Au plus Au collisions at $\sqrt{S_{\rm NN}} = 200{\rm GeV}$, Phys Rev Lett, 2005, **95**: 122301
3. STAR Collaboration. Multiplicity and pseudorapidity distributions of photons in Au plus Au collisions at $\sqrt{S_{\rm NN}} = 62.4{\rm GeV}$, Phys Rev Lett, 2005,**95**: 062301
4. STAR Collaboration. Open charm yields in d + Au collisions at $\sqrt{S_{\rm NN}} = 200{\rm GeV}$, Phys Rev Lett, 2005, **94**: 062301
5. STAR Collaboration. Experimental and theoretical challenges in the search for the quark gluon plasma: The STAR Collaboration's critical assessment of the evidence from RHIC collisions, Nucl Phys A, 2005,**757**: 102
6. STAR Collaboration. Pion, kaon, proton and anti-proton transverse momentum distributions from p+p and d+Au collisions at $\sqrt{S_{\rm NN}} = 200{\rm GeV}$, Phys Lett B, 2005, **616**: 8
7. STAR Collaboration. Φ meson production in Au+Au and p+p collisions at $\sqrt{S_{\rm NN}} = 200{\rm GeV}$, Phys Lett B, 2005, **612**: 181
8. STAR Collaboration. K(892)* resonance production in Au+Au and p+p collisions at $\sqrt{S_{\rm NN}} = 200{\rm GeV}$, Phys Rev C, 2005, **71**: 064902
9. STAR Collaboration. Incident energy dependence of pt correlations at relativistic energies, Phys Rev C, 2005, **72**: 044902
10. STAR Collaboration. Azimuthal anisotropy in Au plus Au collisions at $\sqrt{S_{\rm NN}} = 200{\rm GeV}$, Phys Rev C, 2005,**72**: 014904
11. STAR Collaboration. Event-wise $p_{\rm T}$ fluctuations in Au-Au collisions at $\sqrt{S_{\rm NN}} = 130{\rm GeV}$, Phys Rev C, 2005, **71**: 064906
12. STAR Collaboration. Pion interferometry in Au+Au collisions at $\sqrt{S_{\rm NN}} = 200{\rm GeV}$, Phys Rev C, 2005, **71**: 044906
13. STAR Collaboration. Transverse-momentum dependent modification of dynamic texture in central Au+Au collisions at $\sqrt{S_{\rm NN}} = 200{\rm GeV}$, Phys Rev C, 2005, **71**: 031901(R)
14. WEI Yibin, MA Yugang, WANG Kun, *et al.* HBT study of the nuclear reaction with exotic nuclei at intermediate energy, Journal of the Graduate School of the Chinese Academy of Sciences, 2005, **22**(5): 560
15. STAR Collaboration. Production of K0s, f, L and X from 200GeV d+Au collisions at RHIC, J Phys G, 2005, **31**(6): S1015
16. MA Y G, WANG K, CAI X Z, *et al.* Isoscaling behavior in fission dynamics, Phys Rev C, 2005, **72**: 064603
17. HE Z J, LONG J L, MA Y G, *et al.* Hard photons from a chemically equilibrating quark-gluon plasma at finite baryon density, Phys Lett B, 2005, **628**: 25
18. LONG J L, HE Z J, MA YG, *et al.* Hard photon production from a chemically equilibrating quark-gluon plasma with finite baryon density at one loop and two loop, Phys Rev C, 2005, **72**: 064907
19. 沈水法, 李燕, 顾嘉辉. ^{76}Se 的低自旋新能级及其晕带能级结构的讨论, 高能物理与核物理, 2005, **29**(2): 139
20. CHEN Jingen, CAI Xiangzhou, WANG Tingtai, *et al*, Investigation on the deformation of Ne and Mg isotope chains within relativistic mean field model , Chin Phys, 2005, **14**: 2444
21. MA Y G, Natowitz J B, Wada R, *et al.* Towards the critical behavior for the light nuclei by NIMROD detector, Nucl Phys A, 2005, **749**: 106
22. MA Y G, MA G L, CAI X Z, *et al.* Δ-scaling and heat capacity in relativistic ion collisions, J Phys G, 2005, **31**(6): S1179
23. CHEN J G, CAI X Z, SHEN W Q *et al.* Halo or skin in the excited states of some light mirror nuclei, Eur Phys J A, 2005, **23**: 11
24. TIAN Wendong, MA Yugang, CAI Xiangzhou, *et al.* Isoscaling behavior in the isospin dependent quantum molecular dynamics model, Chin Phys Lett, 2005, **22**(2): 306

25. WEI Yibin, MA Yugang, CAI Xiangzhou, *et al.* Parallel momentum distribution of ^{28}Si fragments from ^{29}P, Chin Phys Lett, 2005, **22**(1): 61
26. WANG Kun, MA Yugang, WEI Yibin, *et al.* Isoscaling of the fission fragments with Langevin equation, Chin Phys Lett, 2005, **22**(1): 53
27. HE Zejun, LONG Jiali, MA Yugang, *et al.* Photon from a chemically equilibrating quark-gluon plasma at finite baryon density, Chin Phys Lett, 2005, **22**(6): 1350
28. HE Zejun, LONG Jiali, MA Yugang. Hard Photons from a non-equilibrated quark-gluon plasma with finite baryon density at a two-loop level, Chin Phys Lett, 2005, **22**(10): 2519
29. SHEN Shuifa, LI Yan, SHI Shuanghui, *et al.* New low-spin levels in ^{72}Ge and discussion of its yrast band structure, Journal of the Physical Society of Japan, 2005, **77**(1): 299
30. LEI Xiaoling, WANG Xiaofeng, HU Jun, *et al.*, Dynamic simulation of single DNA molecule at the base level, Chin Phys Lett, 2005, **22**(6): 1540
31. WAN Rongzheng, LI Jingyuan, LU Hangjun, *et al.* Controllable water channel gating of nanometer dimensions, J Am Chem Soc, 2005, **127**: 7166
32. YI Houhui, XU Shixiong, QIAN Yuehong, *et al.* Lattice Boltzmann simulation of the blood flow in blood vessels with the rolling massage, Chin Phys Lett, 2005, **22(1**2): 3210
33. WANG Zhenxia, WU Yongqing, ZHANG Wei, *et al.* Catalytic synthesis of carbon nanotubes under ion irradiation, Carbon, 2005, **43**: 447
34. HAN Jiaguang, WANG Fan, ZHU Zhiyuan, *et al.* Shift in low-frequency vibrational spectra of transition-metal zirconium compounds, Appl Phys Lett, 2005, **87**: 172107
35. ZHANG Wei, XU Zijian, ZHU Zhiyuan, *et al.* Study of thermal stability of fullerenes by molecular dynamics, Int J Mod Phys B, 2005, **19**: 2892
36. ZHANG Wei, ZHU Zhiyuan, XU Zijian, *et al.* Molecular dynamics study of motion of low energy carbon atom in SWCNT, Nanotechnology, 2005, **16**: 2681
37. 王震遐, 王森, 胡建刚, 等. 多壁碳纳米管在循环相变过程中结构变化初探, 物理学报, 2005, **54**: 4263
38. ZHENG Liping, MA Yugang, XU Zijian, *et al.* Analysis of Ni-Al-Cr grain boundary structures with a double species mode, Chin Phys Lett, 2005, **22**(6): 1484
39. JIANG W Z, ZHAO Y L. Charge density of light exotic nuclei and ρ_{NN} tensor coupling, Phys Lett B, 2005, **617**: 33
40. JIANG Weizhou, ZHAO Yaolin, ZHU Zhiyuan, *et al.* The role of ρ_{NN} tensor coupling and $2s_{1/2}$ occupation in light exotic nuclei, Phys Rev C, 2005, **72**: 024313
41. JIANG W Z, REN Z Z, WANG T T, Relativistic mean-field study for Zn isotopes, Eur Phys J A, 2005, **25**: 29
42. ZHENG Liping, LI Douxing, ZHANG Xiurong. Simulations of bulk effects of Zr on cohesion of Ni_3Al grain boundary, 原子核物理评论, 2005, **22**(1): 106
43. 郑里平, 许子建, 朱志远, 荷能带电粒子在碳纳米管绳内的沟道效应, 核技术, 2005, **28**: 273
44. FANG Deqing, MA Yugang, MA Chunwang, *et al.* One-proton halo structure in ^{23}Al, Chin Phys Lett, 2005, **22**(3): 572
45. STAR Collaboration. Identified Baryon and meson distributions at large transverse momenta from Au+Au collisions at $\sqrt{S_{NN}} = 200\text{GeV}$, Phys Rev Lett, 2006, **97**: 152301
46. STAR Collaboration. Direct observation of dijets in central Au+Au collisions at $\sqrt{S_{NN}} = 200\text{GeV}$, Phys Rev Lett, 2006, **97**: 162301
47. STAR Collaboration. Forward neutral pion production in p+p and d+Au collisions at $\sqrt{S_{NN}} = 200\text{GeV}$, Phys Rev Lett, 2006, **97**: 152302
48. STAR Collaboration. Strange baryon resonance production in $\sqrt{S_{NN}} = 200\text{GeV}$ p+p and Au+Au collisions, Phys Rev Lett, 2006, **97**: 132301

49. STAR Collaboration. Longitudinal double-spin asymmetry and cross section for inclusive jet production in polarized proton collisions at $\sqrt{S_{\rm NN}} = 200{\rm GeV}$, Phys Rev Lett, 2006, **97**: 252001
50. STAR Collaboration. Hadronization geometry from net-charge angular correlations on momentum subspace (η, φ) in Au–Au collisions at $\sqrt{S_{\rm NN}} = 130{\rm GeV}$, Physics Letters B, 2006, **634**: 347
51. STAR Collaboration, Identified hadron spectra at large transverse momentum in p+p and d+Au collisions at $\sqrt{S_{\rm NN}} = 200{\rm GeV}$, Physics Letters B, 2006, **637**: 161
52. STAR Collaboration. Multiplicity dependence of inclusive $p_{\rm T}$ spectra from p-p collisions at $\sqrt{S_{\rm NN}} = 200{\rm GeV}$, Phys Rev D, 2006, **74**: 32006
53. STAR Collaboration. Multiplicity and pseudorapidity distributions of charged particles and photons at forward pseudorapidity in Au+Au collisons at $\sqrt{S_{\rm NN}} = 62.4{\rm GeV}$, Phys Rev C, 2006, **73**: 34906
54. STAR Collaboration. Directed flow in Au+Au collisions at $\sqrt{S_{\rm NN}} = 62.4{\rm GeV}$, Phys Rev C, 2006, **73**: 34903
55. STAR Collaboration. Minijet deformation and charge-independent angular correlations on momentum subspace (η, φ) in Au-Au collisions at $\sqrt{S_{\rm NN}} = 130{\rm GeV}$, Phys Rev C, 2006, **73**: 64907
56. STAR Collaboration. Neutral kaon interferometry in Au+Au collisions at $\sqrt{S_{\rm NN}} = 200{\rm GeV}$, Phys Rev C, 2006, **74**: 54902
57. STAR Collaboration. Proton-lambda correlations in central Au+Au collisions at $\sqrt{S_{\rm NN}} = 200{\rm GeV}$, Phys Rev C, 2006, **74**: 64906
58. STAR Collaboration. Transverse-momentum p_t correlations on (η, φ) from mean-p_t fluctuations in Au–Au collisions at $\sqrt{S_{\rm NN}} = 200{\rm GeV}$, J Phys G, 2006, **32**: 37
59. MA G L, ZHANG S, MA Y G, *et al.* Di-hadron azimuthal correlation and Mach-like cone structure in parton/hadron transport model, Physics Letters B, 2006, **641**: 362
60. YAN T Z, MA Y G, CAI X Z, *et al.* Scaling of anisotropic flow and momentum-space densities for light particles in intermediate energy heavy ion collisions, Physics Letters B, 2006, **638**: 50
61. MA Y G, WEI Y B, SHEN W Q, *et al.* Surveying the nucleon-nucleon momentum correlation function in the framework of quantum molecular dynamics model, Phys Rev C, 2006, **73**: 14604
62. CHEN J H, MA Y G, MA G L, *et al.* Elliptic flow of φ meson and strange quark collectivity at RHIC, Physical Review C, 2006, **74**: 64902
63. MA Y G. Φ meson production and partonic collectivity at RHIC, J Physics G, 2006, **32**: s373
64. LONG J L, HE Z J, MA Y G, *et al.* Photon emission from a chemically non-equilibrated parton gas at finite baryon density, Nuclear Physics A, 2006, **766**: 201
65. CAI X Z. Measurements of the nuclear modification factor and elliptic flow of mesons at RHIC, Nuclear Physics A, 2006, **774**: 485
66. MA Y G. Moment analysis and Zipf law, Eur Phys J A, 2006, **30**: 227
67. CHEN J H, MA Y G, MA G L, *et al.* Strange quark collectivity φ meson at RHIC, Eur Phys J A, 2006, **29**: 11
68. GUO W, FANG D Q, MA Y G, *et al.* Measurements of reaction cross section and fragment momentum distribution for N=10 proton-rich isotones, Int J Mod Phys E, 2006, **15**: 1523
69. SU Q M, FANG D Q, MA Y G. Study of isoscaling phenomena for projectile-like fragments, Int J Mod Phys E, 2006, **15**: 1803
70. LONG J L, HE Z J, MA Y G. Photon production in a chemically equilibrating quark-gluon plasma at finite baryon density, Chin Phys Lett, 2006, **23**: 800
71. MA E J, MA Y G, CHEN J G, *et al.* Cross sections of elastic electron and positron scattering from proton-rich nuclei, Chin Phys Lett, 2006, **23**: 2695
72. ZHONG C, MA Y G, FANG D Q, *et al.* Isoscaling of projectile-like fragments, Chinese Physics, 2006, **15**: 1481
73. MA G L, MA Y G, SA B H, *et al.* Effect of hadronic rescattering on the elliptic flow after the hydrodynamics model, Nukleonika, 2006, **51**(Suppl): 21

74. 王鲲, 马余刚, 蔡翔舟，等. 朗之万方程模拟核裂变碎片的同位旋标度, 高能物理与核物理, 2006, **30**: 277
75. 马春旺, 方德清, 郭威，等. ^{23}Al 及其邻近核的奇异结构研究, 高能物理与核物理, 2006, **30**: 186
76. 颜廷志, 马余刚, 蔡翔舟，等. 中能重离子碰撞中的各向异性流标度, 高能物理与核物理, 2006, **30**: 235
77. MA Y G, CAI X Z, FANG D Q, *et al.* Isoscaling analysis and symmetry energy, 高能物理与核物理, 2006, **30**: 219
78. FANG D Q, MA Y G, ZHONG C, *et al.* Study of isoscaling in projectile fragmentation and the nuclear symmetry energy coefficient, 高能物理与核物理, 2006, **30**: 274
79. 田文栋, 马余刚, 方德清, 等. 同位旋标度规律的动力学和统计衰变效应, 高能物理与核物理, 2006, **30**: 280
80. 徐毅, 徐望, 马余刚，等. 基于上海激光电子 γ 源的天体核合成关键反应 ^{12}C(α,γ)^{16}O 的反应率研究, 高能物理与核物理, 2006, **30**: 252
81. 石钰, 马余刚, 陈金根，等. 中等质量核激发态奇异核结构的研究, 高能物理与核物理, 2006, **30**: 180
82. JIANG W Z. Roles of isoscalar hyperons in probing the density dependence of the nuclear symmetry energy, Physics Letters B, 2006, **642**: 28
83. JIANG W Z. Exotic nuclear structures with isospin dependent interactions in relativistic mean-field models , International Journal of Modern Physics E, 2006, **15**: 1487
84. JIANG W Z. Magnetic susceptibility of collapsed stars in hardron and quark phases, International Journal of Modern Physics A, 2006, **10**: 2201
85. HU Jiangang, WANG Zhenxia, ZHANG Wei, *et al.* Nanowires with a carbon nanotube core and silicon oxide sheath, Carbon, 2006, **44**: 1581
86. 胡建刚, 王震遐, 勇振中, 等. ^{40}Ar 诱导无定形碳到金刚石纳米晶相变的研究, 物理学报, 2006, **55**: 6538
87. ZHANG Lijuan, ZHANG Yi, ZHANG Xuehua, *et al.* Electrochemically controlled formation and growth of hydrogen nanobubbles, Langmuir, 2006, **22**: 8109
88. WANG Xiaofeng, LEI Xiaoling, FANG Haiping, *et al.* What governs the unzipping process of double-stranded DNA?, Chinese Physics Letters, 2006, **23**: 1339
89. ZHANG Lijuan, WANG Huabin , Investigation of elasticity of polymer nanoparticle by vibrating scanning polarization force microscopy, Chinese Physics Letters, 2006, **23**: 2315
90. HAN Jiaguang, ZHU Zhiyuan, *et al*. Optical and dielectric properties of ZnO tetrapod structures at terahertz frequencies, Applied Physics Letters, 2006, **89**: 31107
91. HAN Jiaguang, *et al*. Far-infrared characteristic of ZnS nanoparticles measured by THz-TDS, Journal of Physical Chemistry B, 2006, **110**: 1989
92. HAN Jiaguang, JI Kai, ZHU Zhiyuan, *et al.* Spectral evolution of angle resolved photoemission due to Holstein type electron-phonon scattering within the adiabatic approximation, Physical Review B, 2006, **73**: 125111
93. XU Zijian, ZHANG Wei, ZHU Zhiyuan, *et al.* A density functional study of C_{50} passivation, Chemical Physics, 2006, **331**: 111
94. ZHENG Liping, XU Zijian, WANG Chengbin, *et al.* Low energy ion channeling in single-wall nanotubes, Chinese Physics Letters, 2006, **23**: 2169
95. WAN Fan, HAN Jiaguang, ZHU Zhiyuan, *et al.* Magneto-optical effect of $La_{0.7}Ca_{0.3}MnO_3$ at low temperature, Nuclear Science and Techniques, 2006, **17**: 24
96. 郑里平, 许子健, 王呈斌, 等. 高能粒子在碳纳米管里的沟道效应, 原子能科学技术, 2006,**40**: 74

核分析技术 Nuclear Analysis Techniques

1. CHEN S M, LIU Y D, WU G Z. Stabilized and size-tunable gold nanoparticles formed in a quaternary ammonium-based room-temperature ionic liquid under gamma-irradiation, Nanotechnology, 2005, **16**(10) 2360
2. LONG D W, WU G Z, CHEN D Y, *et al.* Spectroscopic study of the interaction between methyl viologen and core-shell-structured polymer nanoparticles, Research on Chemical Intermediates, 2005, **31**(7): 613

3. LIU Y D, WU G Z, LONG D W, *et al.* Co-60 gamma-initiated polymerization of vinyl monomers in room temperature ionic liquid/THF mixed solutions , Polymer, 2005, **46**(19): 8403
4. LIU Y D, WU G Z, LONG D W, *et al.* Co-60 gamma-irradiation initiated polymerization in ionic liquids—The effect of carbon-chain length of monomer, Nuclear Instruments & Methods in Physics Research Section B, 2005, **236**: 443
5. LIU Y D, WU G Z, QI M Y. Polymorphous crystals from chlorozincate-choline chloride ionic liquids in different molar ratios , Journal of Crystal Growth, 2005, **281**(2): 616
6. LIU Y D, WU G Z. On the mechanism of radiation-induced polymerization of vinyl monomers in ionic liquid, Radiation Physics and Chemistry, 2005, **73**(3): 159
7. CHEN S P, WU G Z, ZENG H Y. Preparation of high antimicrobial activity thiourea chitosan-Ag^{+} complex, Carbohydrate Polymers, 2005, **60**(1): 33
8. WU G Z, LONG D W, CHEN S P, *et al.* High efficient fabrication of chitosan micropowder by combination of gamma radiation and jet pulverization, Carbohydrate Polymers, 2005, **60**(1): 61
9. WU G Z, LIU Y D, LONG D W. Effects of ionic liquid $[Me_3NC_2H_4OH]^{(+)}[ZnCl_3]^{(-)}$ on gamma-radiation polymerization of methyl methacrylate in ethanol and N'N-dimethylformamide, Macromolecular Rapid Communications, 2005, **26**(1): 57
10. 龙德武, 吴国忠, 秦宗英. 辐射法降解壳聚糖及其抑菌性能研究, 高分子材料科学与工程, 2005, **21**(6): 240
11. JI Lina, GAO Yongguang, ZHANG Feng, *et al.* Studies on aggregation-propensities and secondary structural transformations of proteins, Nuclear Science and Techniques, 2005, **16**(1): 6
12. 张志祥, 李民乾. 电场驱动微悬臂生物传感器及对 DNA 的快速、高灵敏度检测, 生物化学与生物物理进展, 2005, **32**(4): 314
13. GUO Yunchang, LIU Zhongdong, AN Hongjie, *et al.* Nano-structure and properties of maize zein studied by atomic force microscope, Journal of Cereal Science, 2005, **41**: 277
14. 张志祥, 沈铮, 赵辉, 等. 蛋白质 DNA 混合微点阵和微流控芯片的整合, 化学学报, 2005, **63**(18): 1743– 1746
15. ZHOU Xingfei, XU Hui, FAN Chunhai, *et al.* Compression of single conjugated-polymer nanoparticles with AFM tips, Chemistry Letters, 2005, **34**(11): 1488
16. ZHOU Xingfei, SUN Jielin, AN Hongjie, *et al.* Radial compression elasticity of single DNA molecules studied by vibrating scanning polarization force microscopy, Physical Review E, 2005, **71**: 62901
17. LI Bin, ZHANG Yi, HU Jun, *et al.* Fabricating protein nanopatterns on a single DNA molecule with dip-pen nanolithography, Ultramicroscopy, 2005, **105**: 312
18. 李晓林, Ebihara M. 铂族元素中子活化分析的微型镍锍试金预富集方法研究, 岩矿测试, 2005, **24**(3): 167
19. LI X L, YUE W S, LI Y, *et al.* Source identification of the lead-containing particles in the ambient air of the center of Shanghai by analyzing individual aerosol particle, J Radioanal Nucl Chem, 2005, **266(**1): 141
20. 李晓林, 岳伟生, 刘江峰, 等. 铅染毒大鼠骨中元素微区分布及相关性研究, 高能物理与核物理, 2005, **29**(增刊): 65
21. 万天敏, 李晓林, 岳伟生, 等.基于 Micro-PIXE 能谱的大气单颗粒物污染源模式识别研究, 核技术, 2005, **28(**12): 904
22. TONG Yongpeng, ZHANG Guilin, LI Yan, *et al.* Synchrotron refractive-index microradiography of human liver cancer tissue, Chinese Science Bulletin, 2005, **50**(22): 2657
23. 李爱国, 张桂林, 童永彭, 等. 上海市大气气溶胶中铁的来源和化学种态研究, 环境科学学报, 2005, **25**(2): 148
24. 陈建敏, 谈明光, 李玉兰, 等, 电感耦合等离子体质谱法分析水泥样品中的铅同位素比值研究, 分析化学, **33(**1): 943
25. CHEN J M, TAN M G, LI Y L, *et al.* A lead isotope record of Shanghai atmospheric lead emissions in total suspended particles during the period of phasing out of leaded gasoline, Atmos Environ, 2005, **39**: 1245

26. 金婵, 邹杨, 张桂林, 等. 用 XAFS 谱研究隧道颗粒物中元素的种态, 高能物理与核物理, 2005, **29**(增刊): 892
27. 张元勋, 李德禄, 李爱国, 等. ACCU 采样和 PIXE 技术用于 PM10 污染溯源的研究, 环境科学学报, 2005, **25**(2): 155
28. 李德禄, 张元勋, 李爱国, 等. 冬季上海吴淞地区大气颗粒物 PM10 的元素主成分分析, 核技术, **28(**2): 109
29. ZHANG Yuanxun, CHENG Feng, LI Deyi, *et al.* Investigation of elemental content distribution in femoral head slice with osteoporosis by SRXRF microprobe, Biological Trace Element Research, 2005, **103**(2): 177
30. 张元勋, 王荫淞, 李德禄, 等. 上海冬季大气可吸入颗粒物的 PIXE 研究, 中国环境科学, 2005, **25**(增): 1
31. 张元勋, 王荫淞, 李德禄, 等. SRXRF 研究鼠脑中 Zn 和 ZnT3mRNA 的表达, 高能物理与核物理, 2005, **29**(增): 68
32. LAO Ruojun, SONG Shiping, WU Haiping, *et al.* Electrochemical interrogation of DNA monolayers on gold surfaces, Anal Chem, 2005, **77**(19): 6475
33. WU Haiping, XU Hui, FAN Chunhai, *et al.* Spectroscopic interrogation of layer-by-layer assembled films of conjugated polyelectrolytes, Chin J Chem, 2005, **23**(7): 925
34. YIN Juanjuan, JIN Limei, LIU Ruili, *et al.* Reactions of fullerenes with reactive methylene organophosphorus reagents: Efficient synthesis of organophosphorus group substituted C_{60} and C_{70} derivatives, J Org Chem, 2005, **71**(6): 2267
35. XU Hui, WU Haiping, HUANG Fei, *et al.* Magnetically assisted DNA assays: High selectivity using conjugated polymers for amplified fluorescent transduction, Nucleic Acids Research, 2005, **33(**9): e83
36. FAN Chunhai, Kevin W Plaxco, Alan J Heeger, Biosensors based on binding-modulated donor-acceptor distances, Trends in Biotechnology, 2005, **23**(4): 186
37. SONG Shiping, LI Bin, WU Haiping, *et al.* Protein microarray platform based on antibody fragments and its applications in simultaneous multianalysis, 分析试验室, 2005, **24**(Suppl): 192
38. ZHAO Q, LI Y, XU J, *et al.* Radioprotection of fullerenols for stylonychia mytilus exposed to gamma-rays, International Journal of Radiation Biology, 2005, **81**(2): 169
39. LI Yuguo, HUANG Xuan, LIU Ruili, *et al.* Preparation of $^{67}Ga–C_{60}(OH)_x$ and its biodistribution, Journal of Radioanalytical and Nuclear Chemistry, 2005, **265**(1): 127
40. YU Bozhang, LI Hulin, ZHANG Yafei. Formation and photoluminescence properties of self-assembled films of 2-naphthyl-D2-1,3,4-oxadiazoline-5-thione, Thin Solid Films, 2005, **476**: 331
41. YIN Juanjuan, LI Yuguo, LI Bin, *et al.* Facile and potent synthesis of carbon bridged fullerene dimmers ($HC_{60}–CR_2–C_{60}H$ type), Chemical Communications, 2005, 3041
42. GUO Jinxue, LI Yuguo, WU Shengwei, *et al.* The effects of gamma-irradiation chemical modification of multi-carbon nanotubes, Nanotechnology, 2005, **16**: 2385
43. 徐慧, 余笑寒, 张增艳, 等. 固态氨基酸的 THz 时域光谱研究, 中国科学院研究生院学报, 2005, **22**(1): 90
44. 郭金学, 李宇国, 吴胜伟, 等. CNTs 化学修饰的 γ 剂量效应, 辐射研究与辐射工艺学报, 2005, **23**(2): 112
45. 郭金学, 李宇国, 吴胜伟, 等. 多壁碳纳米管 γ 辐照后的化学修饰, 辐射研究与辐射工艺学报, 2005, **23**(3): 155
46. 徐慧, 韩家广, 余笑寒, 等. 固态多环芳香烃化合物的 THz 时域光谱研究, 化学通报, 2005, **68**(3): 220
47. 刘瑞丽, 姜庆军, 刘士远, 等. 三碘苯酚乙基纤维素微球的制备, 中国科学院研究生院学报, 2005, **22**(5): 575
48. 赵群芬, 诸颖, 李宇国, 等. 富勒醇对贻贝棘尾虫的辐射防护机制, 辐射研究与辐射工艺学报, 2005, **23**(5): 296
49. 尹娟娟, 李文新, 李燕, 等. 新型含磷 C_{60} 二聚体的合成, 科学通报, 2005, **50(**24): 2729
50. 包伯荣, 杨燕琴, 叶国安, 等. NNNN-四丁基-3-氧-戊二酰胺辐解产物研究—二定胺的定性和定量分析, 核化学与放射化学, 2005, **27(**1): 19
51. 张晓岚, 包伯荣, 叶国安, 等. NNNN-四丁基-3-氧-戊二酰胺辐解机理研究, 辐射研究与辐射工艺学报, 2005, **23**(5): 282

52. 张晓岚, 包伯荣, 叶国安, 等. NNNN-四丁基-3-氧-戊二酰胺辐解产物研究—液相辐解产物的定性分析, 辐射研究与辐射工艺学报, 2005, **23**(5): 292
53. SUN L T, GONG J L, WANG Z X, *et al.* Irradiation-induced phase transformations in carbon nanostructures, Nucl Instrum Meth B, 2005, **228**: 26
54. SUN L T, GONG J L, ZHU Z Y, *et al.* Synthesis and characterization of diamond nanowires from carbon nanotubes, Diamond & Related Materials, 2005, **14**: 749
55. 俞国军, 王森, 巩金龙, 等. 乙醇作为碳源的碳纳米管阵列氧化铝模板法制备, 科学通报, 2005, **51**(1): 20
56. YU Guojun, GONG Jinlong, ZHU Dezhang, *et al.* Synthesis of carbon nanotubes over rare earth zeolites at low temperature, Carbon, 2005, **43**: 3002
57. 王森, 俞国军, 巩金龙, 等, 碳纳米管的氧化铝模板法合成及其退火效应研究, 物理学报, 2005, **54**(10): 4949
58. YU Guojun, WANG Sen, GONG Jinlong, *et al.* Synthesis of carbon nanotube arrays using ethanol in porous anodic aluminum oxide template , Chinese Science Bulletin, 2005, **50**(11): 1097
59. 赵红卫, 葛敏, 王文锋, 等. 太赫兹时域光谱技术在化学和生物学中的应用, 化学通报, 2005, **68**(2): 87
60. 王文锋, 姚思德, 苗金玲, 等. 皮秒级脉冲辐解装置及其在抗氧化剂研究中的应用, 辐射研究与辐射工艺学报, 2005, **23**(2): 79
61. 张兆霞, 朱红平, 葛敏, 等. 单线态氧引起的蛋白质损伤研究, 辐射研究与辐射工艺学报, 2005, **23**(2): 77
62. 朱红平, 张兆霞, 赵红卫, 等. 蛋白质自由基损伤的保护和修复, 辐射研究与辐射工艺学报, 2005, **23**(2): 80
63. 葛敏, 赵红卫, 张兆霞, 等. 太赫兹时域光谱—气体自由基检测新方法, 辐射研究与辐射工艺学报, 2005, **23**(2): 83
64. ZHAO Hongwei, DOU Daying, WANG Wenfeng, *et al.* Theoretical calculation and experimental studies of rare tricyclic nucleoside derivative, 辐射研究与辐射工艺学报, 2005, **23**(2): 76
65. 葛敏, 赵红卫, 张增艳, 等. 两种联苯酚类化合物的太赫兹时域光谱研究 , 物理化学学报, 2005, **21**(9): 1063
66. 葛敏, 赵红卫, 吉特, 等. 常见五元糖的太赫兹时域光谱, 中国科学 B 辑, 2005, **35**(6): 441
67. YUE Weisheng, LI Xiaolin, WAN Tianmin, *et al*. Origins of PM_{10} determined by the micro-PIXE spectra of single aerosol particles, Applied Spectroscopy, 2006, **60**(6): 698
68. YUE Weisheng, LI Xiaolin, LIU Jiangfeng, *et al*. Characterization of $PM_{2.5}$ in the ambient air of Shanghai city by analyzing individual particles, Science of the Total Environment, 2006, **368**: 916
69. CHEN Jianmin, TAN Mingguang, Nemmar A, *et al*. Quantification of extrapulmonary translocation of intratracheal-instilled particles in vivo in rats: Effect of lipopolysaccharide, Toxicology, 2006, **222**(3): 195
70. 彭岚, 谈明光,李玉兰, 等. 微波辅助萃取-液质联用技术测底泥砷、硒的化学形态, 分析试验室, 2006, **25**(5): 10
71. 金婵, 张桂林,李爱国, 等. 上海地区 PM_{10} 和 $PM_{2.5}$ 中铁元素的种态研究, 核技术, 2006, **29(**6): 410
72. TAN M G, ZHANG G L, LI X L, *et al*. Comprehensive study of lead pollution in Shanghai by multiple techniques, Analytical Chemistry, 2006, **78**: 8004
73. TONG Yongpeng, ZHANG Guilin, LI Yan, *et al*. Synchrotron microradiography study on acute lung injury of mouse caused by $PM_{2.5}$ aerosols, Eur J Radiol, 2006, **58**: 266
74. WANG Yinsong, LI Aiguo, ZHANG Yuanxun, *et al*. Speciation of iron in atmospheric particulate matter by EXAFS, Chinese Science Bulletin, 2006, **51**(18): 2275
75. 李晓林, 岳伟生, 刘江峰, 等. 应用同步辐射微束 X 射线荧光光谱法研究单个大气 $PM_{2.5}$ 颗粒物的源特征, 岩矿测试, 2006, **25**(3): 206
76. 张桂林, 谈明光, 李晓林, 等. 上海市大气气溶胶中铅污染的综合研究, 环境科学, 2006, **27**(5): 831
77. 王荫淞, 李爱国, 张元勋, 等. 用扩展 X 射线吸收精细结构谱研究大气颗粒物中铁的种态, 科学通报, 2006, **51**(12): 1464
78. ZHANG Yuanxun, ZHANG Yuanmao, WANG Yinsong, *et al*. PIXE characterization of PM_{10} and $PM_{2.5}$ particulate matter collected during the winter season in Shanghai city, Journal of Radioanalytical and Nuclear Chemistry, 2006, **267**(2): 497

79. ZHANG Yuanxun, ZHANG Yongping, LI Delu, *et al.* Zinc distribution in mouse brain by SRXRF, Journal of Radioanalytical and Nuclear Chemistry, 2006, **269**(1): 235
80. 张元勋, 李德禄, 陆文忠, 等. 大气颗粒物 PM_{10} 污染监测和源解析新技术研究, 过程工程学报, 2006, **6(**增 2): 60
81. 张元勋, 李德禄, 陆文忠, 等. 上海吴淞地区气溶胶粒径分布和元素浓度研究, 过程工程学报, 2006, **6(**增 2): 95
82. 杨传俊, 张元勋, 陆文忠, 等. 上海大气纳米颗粒物粒径分布的研究, 过程工程学报, 2006, **6(**增 2): 105– 109
83. 张元勋, 龙建刚, 王荫淞, 等. 小鼠脑中 Zn 元素和 ZnT3 mRNA 表达的研究, 中国病理生理杂志, **22**(9): 17847
84. 程硕, 王伟, 谈明光, 等. 上海市吴淞工业区大气 $PM_{2.5}$ 水溶成分的元素分析及细胞毒性研究, 核技术, 2006, **29**(3): 182
85. 刘崎, 朱智勇, 杨小敏, 等. PVDF-g-N-IPAAm 温敏膜的辐射合成及性能研究, 辐射研究与辐射工艺学报, 2006, **24**(2): 97
86. 刘崎, 朱智勇, 姚思德, 等, 聚合物离子径迹化学蚀刻过程的数值分析, 核技术, 2006, **29**(5): 329
87. ZHAO Hongwei, GE Min, ZHANG Zhaoxia, *et al.*, Spectroscopic studies on the interaction between riboflavin and albumins, Spectrochimica Acta Part A, 2006, **65**(3): 811
88. 朱红平, 张兆霞, 赵红卫, 等. 褪黑激素的瞬态产物及其性质, 中国科学 B 辑化学, 2006, **36**(1): 76
89. ZHU Hongping, ZHAO Hongwei, ZHANG Zhaoxia, *et al.* Laser flash photolysis study on antioxidant properties of hydroxycinnamic acid derivatives, Radiation and Environmental Biophysics, 2006, **45**(1): 73
90. GE Min, ZHAO Hongwei, JI Te, *et al.* Terahertz time-domain spectroscopy of some pentoses, Science in China Series B, 2006, **49**(3): 204
91. 王文锋, 朱红平, 葛敏, 等. 天然抗氧化剂的光化学反应及 THz-TDS 研究, 生物物理学报, 2006, **22**(增刊): 134
92. ZHU Hongping, ZHANG Zhaoxia, ZHAO Hongwei, *et al.* Transient species and its properties of melatonin, Science in China Series B, 2006, **49**(4): 308
93. 张兆霞, 赵红卫, 朱红平, 等. 核黄素光敏损伤溶菌酶的 SDS-聚丙烯酰胺凝胶电泳研究, 中国科学 B 辑:化学, 2006, **36**(6): 501
94. ZHU Hongping, CHEN Shimou, HAO Shumei, *et al.* Double role of hydroxycinnamic acid derivatives in protection against lysozyme oxidation, Biochimica et Biophysica Acta - General Subjects, 2006, **1760**(12): 1810
95. ZHU Hongping, WANG Wenfeng, YAO Side. Studies on reaction of amino acids and triplet thioxanthone derivatives by laser flash photolysis, Investigational New Drugs, 2006, **24**(6): 465
96. ZHU Hongping, ZHAO Hongwei, ZHANG Zhaoxia, *et al.* Laser flash photolysis studies on gallic acid, Chin J Chem, 2006, **24**(10): 1332
97. 赵红卫, 王文锋, 姚思德, 苯甲酸及其甲基取代物的激光光解研究, 光谱学与光谱分析, 2006, **26**(11): 1969
98. GE Min, ZHAO Hongwei, WANG Wenfeng, *et al.* Terahertz time-domain spectroscopy of four hydroxycinnamic acid derivatives, Journal of Biological Physics, 2006, **32**: 403
99. LIU Ruili, YIN Juanjuan, LI Wenxin, *et al.* Synthesis of glucocoticoid-C_{60} hybrids, Carbon, 2006, **44**: 381
100. YIN Juanjuan, LI Qingnuan, LI Wenxin, *et al.* Synthesis of novel organophosphorus C_{60} dimers, Chinese Science Bulletin, 2006, **51**(4): 394
101. ZHAO Xingke, LI Wenxin. Morphology and hydrophobicity of a polyurethane film molded on a porous anodic alumina template, Surface & Coatings Technology, 2006, **200**: 3492
102. RAN Tiecheng, LIU Ruili, YIN Juanjuan, *et al.* , Radiolabeling of 1-[N′,N′-Bis(2-chloroethyl) -4-aminophenyl]-N-methyl-fullereno-C_{60}-[1,9-c]pyrrolidine with iodine-125, Journal of Radioanalytical and Nuclear Chemistry, 2006, **268**(3): 599
103. ZHU Ying, ZHAO Quanfen, LI Wenxin. The interaction and toxicity of multi-walled carbon nanotubes with stylonychia mytilus, J Nanoscience and Nanotechnology, 2006, **6**(5): 1357
104. ZHU Ying, RAN Tiecheng, LI Yuguo, *et al.* Dependence of multi-walled carbon nanotubes cytotoxicity on culture medium, Nanotechnology, 2006, **17**: 4668

105. 冉铁成, 刘瑞丽, 尹娟娟, 等. C_{60}吡咯烷苯氮芥的合成和放射性碘标记, 核技术, 2006, **29**(5): 349
106. 诸颖, 赵群芬, 蔡小青, 等. 碳纳米管(CNTs)与贻贝棘尾虫的相互作用及研究, 核技术, 2006, **29**(3): 202
107. ZHAO Qunfen, ZHU Ying, RAN Tiecheng, *et al.* Cytotoxicity of fullerenols on *Tetrahymena pyriformis*, Nuclear Science and Techniques, 2006, **17**(5): 280
108. GUO Jinxue, LI Wenxin. Modification of water-soluble MWNTs after γ-irradiation, 辐射研究与辐射工艺学报, 2006, **24**(4): 193
109. 李俊纲, 徐晶莹, 李晴暖, 等. 纳米气溶胶的呼吸毒性研究, 毒理学杂志, 2006, **20**(6): 411
110. LU Junhong, AN Hongjie, LI Haikuo, *et al.* Nanodissection, isolation, and PCR amplification of single DNA molecules, Surface and Interface Analysis, 2006, **38**: 1010
111. ZHANG Feng, DU Hainong, ZHANG Zhixiang, *et al.* Epitaxial growth of peptide nanofilaments on inorganic surfaces: Effects of interfacial hydrophobicity/hydrophilicity, Angew. Chem Int Ed, 2006, **45**: 3611
112. LIU Yaodong, ZHANG Yi, WU Guozhong, *et al.* Coexistence of liquid and solid phases of bmim-PF6 ionic liquid on mica surfaces at room temperature, J Am Chem Soc, 2006, **128**(23): 7456
113. LIN Weizhen, LU Changyuan, DU Fuqiang, *et al*. Reaction mechanisms of riboflavin triplet state with nucleic acid bases, Photochemical and Photobiological Sciences, 2006, **5**(4): 422
114. ZHANG Jiong, SONG Shiping, ZHANG Lanyong, *et al.* Sequence-specific detection of femtomolar DNA via a chronocoulometric DNA sensor (CDS): Effects of nanoparticle-mediated amplification and nanoscale control of DNA assembly at electrodes, J Am Chen Soc, 2006, **128**: 8575
115. WANG Lihua, LIU Xingfen, HU Xiaofang, *et al.* Unmodified gold nanoparticles as a colorimetric probe for potassium DNA aptamers, Chem Commun, 2006, 3780
116. CHEN Xi, WANG Yifei, LIU Qiang, *et al.* Construction of molecular logic gates with a DNA-cleaving deoxyribozyme, Angew Chem Int Ed, 2006, **45**: 1759
117. 樊春海, 宋世平, 王丽华. 通过调控纳米粒子与生物分子的相互作用实现高性能的生物检测, 南昌大学学报(理科版), 2006, **30**: 1202
118. 宋世平, 樊春海. 小分子抗体芯片及其在同步多元分析中的应用, 南昌大学学报(理科版), 2006, **30**: 991
119. 王森, 俞国军, 巩金龙, 等. 低能氩离子束对多孔铝阳极氧化膜表面的刻蚀效应研究, 物理学报, 2006, **55**: 1517
120. YU G J, GONG J L, ZHU D Z, *et al.* Efficient synthesis of carbon nanotubes over rare earth zeolites by thermal chemical vapor deposition at low temperatures, Diamond & Related Materials, 2006, **15**: 1261
121. YU G J, GONG J L, WANG S, *et al.* Etching effects of ethanol on multi-walled carbon nanotubes, Carbon, 2006, **44**: 1218
122. WANG S, GONG J L, YU G J, *et al.* Large area fabrication of periodic Fe nanoring with controllable aspect ratios in porous alumina template, Nanotechnology, 2006, **17**: 1594
123. NI Z C, LI Q T, ZHU D Z, *et al.* Fabrication of carbon nanowire networks by Si ion beam irradiation, Appl Phys Lett, 2006, **89**: 53107

加速器辐照中心 EB Accelerators and Radiation Applications

1. HOU Zhengchi. Ray tracing study for a detuned non-dispersed double crystal monochromator, Review of Scientific Instruments, 2005, **76**: 13305
2. 李晶, 侯铮迟, 谢雷东, 等. γ 辐射接枝甲基丙烯酸改善聚醚砜膜亲水型的研究, 辐射研究与辐射工艺学报, 2005, **23**(1): 25
3. 邓波, 侯铮迟, 张凤英, 等, γ 共辐射接枝丙烯酸改善聚醚砜粉体亲水性的研究, 辐射研究与辐射工艺学报, 2005, **23**(1): 337
4. 侯铮迟, 孙大宽, 秦宗英, 等. 高剂量辐照猪肉的挥发物、脂氧化和感官特征分析, 辐射研究与辐射工艺学报, 2005, **23**(1): 35

5. 李林繁, 谢雷东, 虞鸣, 等. SBS 辐射接枝共聚研究(I)：SBS/MMA 液相辐射接枝, 辐射研究与辐射工艺学报, 2005, **23**(3): 159
6. 付海英, 虞鸣, 李林繁, 等. SBS 辐射接枝共聚研究(III): 星型 SBS 接枝改性, 辐射研究与辐射工艺学报, 2005, **23**(4): 223
7. 付海英, 谢雷东, 虞鸣, 等. SBS 辐射接枝共聚研究(II)：线型 SBS 液固相辐射接枝 MAA, 辐射研究与辐射工艺学报, 2005, **23**(3): 179
8. 付海英, 虞鸣, 谢雷东, 等. SBS 辐射接枝甲基丙烯酸及 MAA 含量的测定, 功能高分子学报, 2005, **18**(3): 409
9. DOU Daying, LIU Yongbiao, ZHAO Hongwei, *et al*. Radiolysis and photolysis studies on active transient species of ethylstilbestrol, Journal of Photochemistry and Photobiology A-Chemistry, 2005, **171**: 209
10. SUN Hanwen, YU Jiahui, GONG Peijun, *et al*. Novel core–shell magnetic nanogels synthesized in an emulsion-free aqueous system under UV irradiation for targeted radiopharmaceutical applications, Journal of Magnetism and Magnetic Materials, 2005, **294**: 273
11. SUN Hanwen, YU Jiahui, GONG Peijun, *et al*. Photochemical synthesis and characterization of novel narrow size distribution core-shell magnetic nanogels, 辐射研究与辐射工艺学报, 2005, **23**(2): 73
12. SUN Hanwen, GONG Peijun, LIU Xiuqing, *et al*. ^{188}Re labeled MPRG-modified superparamagnetic nanogels: Preparation and preliminary application in mice, Nuclear Science and Techniques , 2005, **16**(5): 278
13. YAO Side, DOU Daying, FU Haiying, *et al.* Innovation technique of radiation for the treatment of 4-chlorphenol as a model of POPs in waste water, Nuclear Instruments & Methods B, 2005, **236**: 266
14. 徐冬梅, 余家会, 刘永彪, 等. 光化学合成高基因转染效率的聚乙烯亚胺, 辐射研究与辐射工艺学报, 2005, **23**(2): 81
15. SUN Hanwen, YU Jiahui, XU Dongmei, *et al*. Core-shell magnetic nanogel synthesis in aqueous solution via surfactant-free photochemical reaction, 辐射研究与辐射工艺学报, 2005, **23**(4): 193
16. LIU Qi, ZHU Zhiyong, Maekawa Yasunari, *et al*. Influence of UV illumination on track etching process, 辐射研究与辐射工艺学报, 2005, **23**(2): 108
17. ZHU Zhiyong, LIU Qi, SUN Youmei, *et al*. Radiation effects in polymers induced by high energy heavy ion beams, 辐射研究与辐射工艺学报, 2005, **23**(2): 75
18. ZHU Zhiyong, Maekawa Yasunari, LIU Qi, *et al*. Influence of UV light illumination on the etching process of PET, Nuclear Instruments and Methods B, 2005, **236**: 61
19. 刘瑞芹, 谢雷东, 姚思德, 等, 真丝绸表面光接枝 2-(双甲基胺)乙基甲基丙烯酸酯改性研究, 辐射研究与辐射工艺学报, 2005, **23**(2): 116
20. 王敏, 杨睿媛, 朱志远, 等. 4-氯酚的 γ 射线辐照降解研究, 辐射研究与辐射工艺学报, 2005, **23**(1): 19
21. 王敏, 朱志远, 杨睿媛, 等. 电子束辐照处理水溶液中的活性染料, 核技术, 2005, **28(**1): 40
22. 王敏, 杨睿媛, 王文锋, 等. 染料水溶液的辐射降解研究, 辐射研究与辐射工艺学报, 2005, **23**(2): 120
23. 边绍伟, 王敏, 杨睿媛, 等. 苯胺类污染物的电子束辐照降解研究, 辐射研究与辐射工艺学报, 2005, **23**(2): 119
24. 杨睿媛, 王敏, 王文锋, 等. 活性红 m-3BE 的辐照降解研究, 环境科学与技术, 2005, **28**(增刊): 1
25. 边绍伟, 王敏, 杨睿媛, 等. 对硝基苯胺的辐照降解研究, 辐射研究与辐射工艺学报, 2005, **23**(4): 211
26. GUO Panlin, HU Wei, GONG Peirong, *et al*. The present status of the Shanghai electron beam ion trap, Nuclear Science and Techniques, 2005, **16**(6): 335
27. 张聪. 辐射交联高分子材料产业化的进展, 辐射研究与辐射工艺学报, 2005, **23**(2): 114
28. CHEN Shimou, WU Guozhong, LIU Yaodong, *et al*. Preparation of poly(acrylic acid) grafted multi-walled carbon nanotubes by a two-step irradiation technique, Macromolecules, 2006, **39**: 330
29. CHEN Shimou, WU Guozhong, CHEN Daoyong. An easy approach to hydroxyethylated SWNTs and the high thermal stability of the inner grafted hydroxyethyl groups, Nanotechnology, 2006, **17**: 2368
30. CHEN Shimou, CHEN Daoyong, WU Guozhong. Grafting of poly(tBA) and PtBA-b-PMMA onto the surface of SWNTs using carbanions as the initiator, Macromol Rapid Commun, 2006, **27**: 882

31. CHEN Shuiping, WU Guozhong, LONG Dewu, *et al*. Preparation, characterization and antibacterial activity of chitosan–$Ca_3V_{10}O_{28}$ complex membrane, Carbohyd Polym, 2006, **64**: 92
32. SU Jielong, WU Guozhong, LIU Yaodong, *et al*. Study on polytetrafluoroethylene aqueous dispersion irradiated by gamma ray, J Fluor Chem, 2006, **127**: 91
33. ZHU Guanglai, XU Jingjing, WU Guozhong, *et al*. Laser photolysis study on binary mixtures of ionic liquid [bmim][PF_6] and organic solvent, Int J Mol Sci, 2006, **7**: 590
34. GONG Peijun, YU Jiahui, SUN Hanwen, *et al*. Preparation and characterization of OH-functionalized magnetic nanogels under UV irradiation, Journal of Applied Polymer Science, 2006, **101**(3): 1283
35. HONG Jun, GONG Peijun, YU Jiahui, *et al*. Conjugation of α-chymotrypsin on a polymeric hydrophilic nanolayer covering magnetic nanoparticle, Journal of Molecular Catalysis B: Enzymatic, 2006, **42**(3-4): 99
36. SUN Hanwen, HONG Jun, MENG Fanzong, *et al*. Novel core-shell structure polyacrylamide-coated magnetic nanoparticles synthesized via photochemical polymerization, Surface and Coatings Technology, 2006, **201**(1-2): 250
37. 宫培军, 孙汉文, 洪军, 等. 光化学原位合成 PHEMA 磁性纳米凝胶, 中国科学 B 辑, 2006, **36**(4): 331
38. HONG Jun, GONG Peijun, XU Dongmei, *et al*. Stablization of alpha-chymtrpsin by covalent immobilization on amine-functionalized magnetic nanogels, Journal of Biotechnology, 2006, **128**(3): 597
39. 宫培军, 洪军, 刘兴奋, 等. 光化学制备用于链亲和素固定的胺基磁性纳米凝胶的研究, 辐射研究与辐射工艺学报, 2006, **24**(6): 345
40. 孙汉文, 徐冬梅, 孟繁宗, 等. 聚丙烯酰胺包覆磁性纳米凝胶的光化学法制备及其机理研究, 辐射研究与辐射工艺学报, 2006, **24**(5): 271
41. 洪军, 徐冬梅, 宫培军, 等. 粒径可控的羧基化磁性纳米凝胶的合成, 辐射研究与辐射工艺学报, 2006, **24**(5): 279
42. 付海英, 吴国忠, 龙德武, 等. [$Me_3NC_2H_4OH$]Zn_2Cl_5 水溶液的激光光解研究, 化学学报, 2006, **64**(6): 483
43. 吴铁一, 屠铁城, 赵红卫, 等. 焦脱镁叶绿酸-a 作为光活化农药的光活化机理研究, 化学学报, 2006, **64**(1): 17
44. WANG Min, YANG Ruiyuan, WANG Wenfeng, *et al*. Radiation-induced decomposition and decoloration of reactive dyes in the presence of H_2O_2, Radiat Phys Chem, **75(**2): 286
45. 杨睿媛, 王敏, 王文锋, 等. TiO_2 对水溶液中 4, 2 氯酚电子束辐照降解和矿化的影响, 环境化学, 2006, **25**(6): 692
46. 边绍伟, 王敏, 杨睿媛, 等. 苯胺水溶液的电子束辐照降解, 环境科学学报, 2006, **26**(1): 27
47. 付海英, 谢雷东, 虞鸣, 等. 辐射接枝 SBS 的性能研究, 中国塑料, 2006, **20**(3): 56
48. FU Haiying, XIE Leidong, DOU Daying, *et al*. Storage stability and compatibility of asphalt binder modified by SBS graft copolymer, Construction and Building Materials, 2006, **21**: 1528
49. 张艳, 谢雷东, 李林繁, 等. SBS 液相共辐射接枝马来酸酐/苯乙烯二元单体研究, 辐射研究与辐射工艺学报, 2006, **24**(5): 293
50. 李林繁, 谢雷东, 张艳, 等. SBS 的辐照效应研究, 辐射研究与辐射工艺学报, 2006, **24**(2): 91
51. WANG Hengdong, YE Yin, ZHANG Xuebing, *et al.* Study of radiation-induced grafting of acrylic acid-sodium styrene sulfonate onto FEP film, Nuclear Science and Techniques, 2005, **16**(1): 25

放药中心 **Radiopharmaceuticals**

1. LI Guiping, WANG Yongxian, HUANG Kai, *et al.* The experimental study on the radioimmunotherapy of the nasopharyngeal carcinoma overexpressing HER2/neu in nude mice model with intratumoral injection of ^{188}Re-herceptin, Nuclear Medicine and Biology, 2005, **32**: 59
2. YU Junfeng, Häfeli Urs O, XIA Jiaoyun, *et al.*, Radiolabelling of poly(histidine) derivatized biodegradable microspheres with the ^{188}Re tricarbonyl complex [$^{188}Re(CO)_3(H_2O)_3]^+$, Nuclear Medicine Communications, 2005, **26**(5): 453

3. ZHANG Chunfu, SUN Hanwen, XIA Jiaoyun, *et al.* Synthesis of polyacrylamide modified magnetic nanoparticles and radiolabeling with ^{188}Re for magnetically targeted radiotherapy, Journal of Magnetism and Magnetic Materials, 2005, **293**: 193
4. YU Yanbao, WANG Yongxian, DONG Mo, *et al.* Preparation and stability of rhenium [^{188}Re] sulfide suspension with different particle size distributions, Journal of Radioanalytical and Nuclear Chemistry, 2005, **265**(3): 395
5. 夏姣云, 汪勇先, 于俊峰, 等. 三羰基铼[^{188}Re]的放射化学合成, 核化学与放射化学, 2005, **27**(2): 87
6. 王明伟, 尹端沚, 汪勇先, 等. 肿瘤 PET 显像剂 O-(2-[^{18}F]氟乙基)-L-酪氨酸的放射化学合成, 核技术, 2005, **28**(9): 654
7. 李谷才, 尹端沚, 夏姣云, 等. 3-(4-羟基苄基)-8,9-二甲氧基-1,2,3,4-四氢苯并吡喃[3,4-c]吡啶-5-酮的合成, 精细化工, 2005, **22**(9): 694
8. 刘振锋, 汪勇先, 周伟, 等. 3-正丁基锡-N-琥珀酰亚胺苯甲酸酯的合成及其 ^{125}I 标记, 同位素, 2005, **18**(3): 148
9. XIA Jiaoyun, WANG Yongxian, YU Junfeng, *et al.* Characterization and application of the fac-[^{188}Re(CO)$_3$(H$_2$O)$_3$]$^+$ core, Journal of Radioanalytical and Nuclear Chemistry, 2005, **266**(2): 313
10. WANG Mingwei, YIN Duanzhi, WANG Yongxian, *et al.* Comparative and optimized studies on radiosynthesis of O-(2-[^{18}F]fluoroethyl)-L-tyrosine, Nuclear Science and Techniques, 2005, **16**(5): 283
11. 于延豹, 汪勇先, 于俊峰, 等. 两种方法制备不同颗粒度 ^{188}Re-硫化铼混悬液的生物分布研究, 中华核医学杂志, 2005, **25**(5): 306
12. 李谷才, 尹端沚, 夏姣云, 等. 3-(4-氟苄基)-8-羟基-1,2,3,4-四氢苯并吡喃[3,4-c]吡啶-5-酮的合成, 化学试剂, 2005, **27**(10): 577
13. TIAN Haibin, YIN Duanzhi, ZHNAG Lan, *et al.*, Dopamine D$_4$ receptor antagonist 3-(4-[^{18}F]fluorobenzyl)-8-methoxy-1,2,3,4-tetrahydrochromeno[3,4-c]pyridin-5-one([^{18}F]FMTP): Radiosynthesis and *in vivo* characterization in rats, Applied Radiation and Isotopes, 2005, **63**: 333
14. 夏姣云, 汪勇先, 唐林, 等. 叶酸在放射性核素标记研究中的应用, 同位素, 2005, **18**(4): 237
15. 王明伟, 尹端沚, 郑明强, 等. 微波加热法合成 O-(2-[^{18}F]氟乙基)-L-酪氨酸, 核化学与放射化学, 2005, **27**(4): 248
16. 夏姣云, 汪勇先, 于俊峰, 等. 含吡啶基的乙酸衍生物的合成及表征, 化学试剂, 2005, **27**(12): 710
17. 周伟, 尹端沚, 汪勇先. 小动物 PET, 核技术, 2006, **29**(3): 207
18. 蔡汉成, 尹端沚, 张岚, 等. 9-[(4-氟)-3-羟基甲基丁基]鸟嘌呤(FHBG)的改进合成方法, 精细化工, 2006, **23**(8): 813
19. 王明伟，尹端沚，李世强, 等, O-(2-^{18}F-氟代乙基)-L-酪氨酸的新合成路线及其生物学评价, 中华核医学杂志, 2006, **26**(4): 238
20. 王明伟，尹端沚，汪勇先. 常用 ^{18}F 标记中间体的合成及其应用研究, 核技术, 2006, **29**(1): 63
21. 李谷才，尹端沚，程登峰, 等. 3-(4-[^{18}F]氟苄基)-8-羟基-1,2,3,4-四氢苯并吡喃[3,4-*c*]吡啶-5-酮的放射化学合成, 核技术, 2006, **29**(5): 368
22. 李谷才，尹端沚，沈玉梅, 等. 苯并吡喃[3,4-*c*]吡啶-5-酮类化合物的合成, 有机化学, 2006, **26**(6): 852
23. 李谷才，尹端沚，程登峰, 等. 4-[^{18}F]氟苯甲醛的放射化学合成, 同位素, 2006, **19(**2): 87
24. 唐林，于俊峰，郑明强, 等. 铼[^{188}Re] 羰基化合物标记含 RGD 的环肽及其生物分布, 核技术, 2006, **29**(6): 448
25. 王明伟，尹端沚，程登峰, 等. 直接亲核放射氟化法合成 O-(2-[^{18}F]氟乙基)-L-酪氨酸, 核技术, 2006, **29**(7): 522
26. LI Gucai, YIN Duanzhi, WANG Mingwei, *et al.* Syntheses of two potential dopamine D$_4$ receptor radioligands: ^{18}F labelled chromeno[3,4-*c*]pyridin-5-ones, Radiochim Acta, 2006, **94**: 119
27. CAI Hancheng, YIN Duanzhi, ZHANG Lan, *et al.* The synthesis of a new probe for PET imaging reportergene HSV1-tk: 2-amino-6-[^{18}F] fluoro-9-(4-hydroxy-3-hydroxymethylbutyl) purine (6-[^{18}F]fluoropenciclovir), Journal of Labelled Compounds and Radiopharmaceutiacls, 2006, **49**: 653
28. CAI Hancheng, YIN Duanzhi ZHANG Lan, *et al.* The new convenient synthesis of fluorinated penciclovir analogues 9-(4-fluoro-3-hydroxymethylbutyl) guanine (FHBG) and 2-amino-6-fluoro-9-(4-hydroxy-3-hydroxymethylbutyl) purine (6-fluoropenciclovir), Journal of Fluorine Chemistry, 2006, **127**(7): 837

29. 蔡汉成, 尹端沚, 张岚, 等. 2-氨基-6-氟-9-(4-羟基-3-羟甲基丁基)嘌呤的合成, 有机化学, 2006, **26**(12): 1709
30. CHENG Dengfeng, YIN Duanzhi, LI Gucai, *et al.* Radiolabeling and in vitro and in vivo characterization of [^{18}F]FB-[R8,15,21, L17]-VIP as a PET imaging agent for tumor over-expressed VIP receptors, Chemical Biology and Drug Design, 2006, **38**: 319
31. 程登峰, 尹端沚, 王明伟, 等. N-琥珀酰亚胺 4-[^{18}F]氟苯甲酸酯的合成, 核技术, 2006, **29**(12): 917
32. 许荣辉, 汪勇先, 徐万帮, 等. CdS 纳米晶的制备及其荧光研究, 人工晶体学报, 2006, **35**(5): 1007
33. 徐万帮, 汪勇先, 许荣辉, 等. II-VI 型量子点的制备、修饰及其生物应用, 无机材料学报, 2006, **21**(5): 1031
34. 夏姣云, 汪勇先, 李世强, 等. 铼羰基化合物的制备及其在小鼠体内的生物分布, 核化学与放射化学, 2006, **28**(1): 31
35. 刘秀青, 汪勇先, 刘振锋, 等, 双功能偶联剂 5-(三正丁基锡)-3-吡啶甲酸-N-琥珀酰亚胺酯的优化合成及其碘标记, 核化学与放射化学, 2006, **28**(1): 38
36. 夏姣云, 汪勇先, 李世强, 等, 铼[^{188}Re]羰基化合物标记新双功能螯合剂的研究, 核技术, 2006, **29**(12): 921
37. 许荣辉, 汪勇先, 贾广强, 等, CdS 纳米晶的稳定化处理及介质极性对荧光光谱的影响, 人工晶体学报, 2006, **35**(6): 1341
38. 李贵平, 汪勇先, 张春富, 等, ^{188}Re 标记免疫靶向磁性纳米微粒及其生物学分布, 中华核医学杂志, 2006, **26**(4): 231
39. LIANG Sheng, WANG Yongxian, ZHANG Chunfu, *et al.* Synthesis of amino-modified magnetite nanoparticles coated with Hepama-1 and radiolabeled with ^{188}Re for bio-magnetically targeted radiotherapy, Journal of Radioanalytical and Nuclear Chemistry, 2006, **269**: 3
40. 沈玉梅. 手性在放射性药物中的作用, 核技术, 2006, **29**(7): 518
41. 王谋华, 冯翠兰, 成康民, 等. 环戊二烯三羰基铼络合物的合成及其在放射性药物应用中的研究进展, 核技术, 2006, **29**(10): 765
42. 冯翠兰, 王谋华, 成康民, 等. ^{99m}Tc 放射性药物中的配位化学, 化学进展, 2006, **18**(12): 1615

先进探测仪器 Advanced Detectors and Instruments

1. 蒋大真, 魏永波, 赵国璧, 等. 离子迁移率方法在毒品、爆炸物品检测中的初步研究, 同位素, 2005, **18**(1): 51
2. 刘平, 阮裕泉, 浦世节. 基于 Windows 的多道脉冲幅度分析器的软件开发, 核技术, 2005, **28**(1): 69
3. 徐慧超, 张金洲, 沈浩元, 等. N 型碲锌镉探测器的制备和性能, 核技术, 2005, **28**(10): 791
4. 魏永波, 蒋大真. 离子迁移率探测器电场优化设计的研究, 高能物理与核物理, 2005, **29**(12): 1214
5. 杜远凤, 李勇平, 基于分块子特征的人脸的表征和识别, 计算机应用研究, 2006, **23**(增下): 793
6. QI Yujin. High-resolution SPECT for small-animal imaging , Nuclear Science and Techniques, 2006, **17**(3): 164
7. LI Yongping. Biometrics technology overview, Nuclear Science and Techniques, 2006, **17**(2): 97
8. CHENG Cheng, WEI Yongbo, XU Huichao, *et al*. Research of CdZnTe detector based portable energy dispersive spectrometer, Nuclear Science and Techniques, 2006, **17**(2): 106
9. WANG Lin, LI Yongping, ZHANG Hongzhou, *et al*. A novel 2D Gabor wavelets window method for face recognition, Lecture Notes in Computer Science, 2006, **4105**(11): 497

新技术中心 Membrane Technology

1. SHEN Fei, LU Xiaofeng, BIAN Xiaokai,*et al*. Preparation and hydrophilicity study of poly(vinyl butyral)-based ultrafiltration membranes, Journal of Membrane Science, 2005, **265**(1): 74
2. 许念强, 顾建祥, 罗康, 等. 大颗粒、高浓度硅溶胶的制备新方法, 化工进展, 2005, **24**(8): 925
3. 沈飞, 陆晓峰, 卞晓锴, 等. 聚乙烯醇缩丁醛超滤膜的制备, 膜科学与技术, 2005, **25**(6): 59
4. 梁国明, 陆晓峰, 王文浪. 用水解酸化池-膜生物反应器处理活性艳红 X-3B 废水, 化工环保, 2006, **26**(6): 488
5. 陆晓峰, 梁国明, 陈洁, 等. MBR 与 CAS 法处理市政污水的比较, 水处理技术, 2006, **32**(9): 56

6. 段伟, 章四琪, 刘志坚. 预处理对热电池阳极材料 LiB 合金结构和性能的影响, 中国有色金属学报, 2006, 16(2): 273
7. 林红军，陆晓峰，陈洁. 缺氧-好氧膜生物反应器处理尿液污水的研究, 环境污染与防治, 2006, **28**(1): 72
8. 林红军, 陆晓峰, 施柳青. 膜生物反应器中的基质降解动力学研究, 环境科学与技术, 2006, **29**(10): 10
9. 林红军, 陆晓峰, 沈飞, 等. 市政污水处理中 MBR 和 CAS 工艺的污泥特性的研究, 水处理技术, 2006, **32**(11): 45
10. 林红军，陆晓峰，段伟，等. 膜生物反应器中膜过滤特征及膜污染机理的研究, 环境科学, 2006, **27**(12): 154
11. 沈飞, 陆晓峰, 施柳青, 等. 不对称聚乙烯醇缩丁醛超滤膜的形成, 膜科学与技术, 2006, **26**(6): 33
12. ZHANG Fengying, WANG Jie, HOU Zhengchi, *et al*. Study of growth of calcium carbonate crystals on chitosan film, Materials & Design, 2006, **27**(5): 422
13. ZHANG Fengying, WANG Jie, SHENG Kanglong, *et al*. Crystallization of calcium carbonate on polyethylene γ-radiation-grafted with acrylic acid, Journal of Materials Chemistry, 2006, **16**(13): 1215
14. 侯铮迟, 谢雷东, 盛康龙, 等. 聚合物表面辐射接枝改性研究进展, 辐射研究与辐射工艺学报, 2006, **24**(1): 5

附录 2

2005–2006 举办(承办)国际会议表

International Meetings Sponsored by SINAP in 2005–2006

2005

No.	会议名称 Meetings	日期 Dates	协办方 Cosponsors	P/FS/N*
1	第 59 届东方科技论坛：高能核物理的大型国际合作与中国的机遇 59th Eastern Forum of Sci. & Tech.: Int. Cooperation in High Energy Physics and the Opportunity of China	June28-29	上海市政府 City of Shanghai	46/9/1
2	同位旋物理与原子核的相变研讨会 Int. Symp. on Iso-spin Physics and Phase Transition of Nuclei	Aug.19-21	—	50/4/ 3
3	第六届束流动力学研讨会 6th International Workshop on Beam Dynamics	Nov.1-2	日本 KEK KEK of Japan	30/14/2
4	第 69 届东方科技论坛：同步辐射在工业中的应用 69th Eastern Forum of Science and Technology: Synchrotron Radiation Application in Industries	Dec.23-24	上海市政府 City of Shanghai	40/2/2

2006

No.	会议名称 Meetings	日期 Dates	协办方 Cosponsors	P/FS/N
1	中英精英科技年同步辐射科学研讨会 China-UK N+N Workshop on Synchrotron Science	Feb. 20-22	中国科学院，英国研究理事会中央实验室委员会 Chinese Academy of Sciences, Central Laboratories Committee of Research Council, U K	50/7/2
2	第六届中日核物理研讨会 6th Sino-Japan Joint Symposium on Nuclear Physics	May 16-20	—	80/30/2
3	原子和原子核交叉物理学国际研讨会 International Seminar on Atomic and Nuclear Cross-Disciplinary Physics	June 10-13	复旦大学，上海市科协 Fudan University, Sci. and Tech. Com. of Shanghai	75/13/7
4	第四届 OCPA 加速器学校 4th OCPA Int. Accelerator School	July 10-13	海外华人物理协会(OCPA) Oversea Chinese Physicist Assoc.	109/30/4
5	第一届亚太地区辐射化学国际会议 1st Asia-Pacific Symp. on Radiation Chemistry	Sept. 17-21	—	154/61/10
6	第十九届极端相对论性核-核碰撞国际会议 19th International Conference on Ultra-relativistic Nucleus-Nucleus Collisions	Nov. 13-21	华中师范大学 Normal University of Central China	600/500/7
7	第 86 期东方科技论坛：第三代同步辐射光源束流轨道稳定性问题 86th Eastern Forum of Sci. and Tech: Orbit Stability in 3rd Generation Synchrotron Radiation Light Source	Dec. 7-8	上海市政府,中国科学院, 中国工程院 City of Shanghai, Chinese Academy of Sciences, Chinese Academy of Engineering	50/5/5

* P/FS/N : Number of participants, foreign scholars and nations 与会代表/国外学者/与会国数

附录 3

2005–2006 国际学术会议报告表

Presentations by SINAP Scientists at International Scientific Meetings in 2005–2006

No.	Meetings in 2005	Date & Place	Presentations	No.
1	Nanotech 2005	May 8-12, Anaheim, CA, USA	Poster, 李民乾(Li M Q)	1
2	1st Sino-US Chemistry Professors Conference	June 13-14, Tianjin, China	Invited, 沈玉梅(Shen Y M)	2
3	52nd Annual Meeting of the Soc. of Nucl. Medicine	June 18-22, Toronto, Canada	Poster, 漆玉金(Qi Y J)	3
4	16th Int. Symp. on Radiopharmaceutical Chemistry	June 24-28, Iowa, USA	Poster, 尹端沚(Yin D Z) Poster, 夏姣云(Xia J Y) Poster, 汪勇先(Wang Y X)	4 5 6
5	8th Int. Conf. on X-ray Microscopy	July 26-30, Himeji, Japan	Oral, 肖体乔(Xiao T Q)	7
6	18th Int. Conf. on Ultra-relativistic Nucleus-Nucleus Collisions (Quark Matter 2005)	Aug. 4-9, Budapest, Hungary	Oral, 马余刚 (Ma Y G) Oral, 蔡翔舟(Cai X Z) Poster, 马国亮(Ma G L)	8 9 10
7	Particles 2005: Surface Modifi. in Particle Tech.	Aug.13-16,San Francisco, USA	Poster, 汪勇先(Wang Y X)	11
8	14th Int. Conf. on Discrete Simulation of Fluid Dynamics in Complex System	Aug.22-26, Kyoto, Japan	Invited, 方海平(Fang H P)	12
9	27th Int. Conf. of the IEEE Engineering in Medical and Biology Society	Sept.1-4, Shanghai, China	Invited, 方海平(Fang H P)	13
10	11th Int. Conf. on Ion Sources	Sept.12-16, Caen, France	Oral, 郭盘林(Guo P L)	14
11	4th World Congress of Cellular and Molecular Biology	Oct.7-12, Poitiers, France	Poster, 李民乾(Li M Q)	15
12	Asia-Pacific Symposium on Radiochemistry	Oct.17-21, Beijing, China	Plenary, 李谷才(Li G C) Poster, 尹端沚(Yin D Z)	16 17
13	5th NAREGI Int. Nanoscience Symposium	Nov.7-9, Tsukuba, Japan	Oral, 韩家广(Han J G)	18
14	Int. Symposium on Trends in Radiopharmaceuticals	Nov.14-18, Vienna, Austria	Poster, 汪勇先(Wang Y X)	19
15	Int. Workshop on Terahertz Technology	Nov.16-18, Osaka, Japan	Oral, 王文锋(Wang W F)	20
16	Symposium on Science with Rare Isotope Beams (Part of PacifiChem 2005)	Dec.15-20, Honolulu, HI, USA	Oral, 肖体乔(Xiao T Q) Oral, 马余刚(Ma Y G)	21 22
17	69th Oriental Forum of Science and Technology : Synchrotron Radiation Application in Industries	Dec.23-24, Shanghai	Invited, 邰仁忠(Tai R Z) Poster, 漆玉金(Qi Y J)	23 24

No.	Meetings in 2006	Date & Place	Presentations	No
1	Workshop on Multiscale Modeling: Complex Fluids and Microfluidics	Jan.9-13, Hong Kong, China	Plenary, 方海平(Fang H P)	1
2	Joint Sino-German Symposium on Hardon Physics at Cosy & CSR	Jan.14-16, Lanzhou, China	Plenary, 马余刚(Ma Y G)	2
3	亚洲学术文化交流网络国际研讨会	Jan.20-23, Kanagawa, Japan	Plenary, 郜仁忠(Tai R Z)	3
4	Application of Radiotracers in Chemical, Environmental and Biological Sciences	Jan.23-27, Calcutta. India	Plenary, 张桂林(Zhang G L)	4
5	RCNP-JAEA Workshop on Nucl. Photon Science: "Hadron-nuclear physics probed by photon"	Feb.16-18, Kyoto, Japan	Plenary, 徐望(Xu W)	5
6	China-UK N+N Workshop on Synchrotron Science	Feb.20-22, Shanghai, China	Plenary, 徐洪杰(Xu H J) Plenary, 赵振堂(Zhao Z T)	6 7
7	14th Int. Meeting on Radiation Processing	Feb.26-Mar.3, Kuala Lumpur, Malaysia	Plenary, 盛康龙(Sheng K L)	8
8	STAR Collaboration Meeting-BNL	Feb.27-Mar.4, BNL, USA	Plenary, 钟晨(Zhong C)	9
9	第三届中韩光学技术研讨会	Mar. 1-4, Jeju Island, Korea	Plenary, 赵振堂(Zhao Z T)	10
10	22nd Winter Workshop on Nuclear Dynamics	Mar.11-19, San Diego, USA	Plenary, 马余刚(Ma Y G)	11
11	Strangeness in Quark Matter	Mar.26-31, Los Angeles, USA	Plenary, 马余刚(Ma Y G) Poster, 龙家丽(Long J L) Poster, 钟晨(Zhong C)	12 13 14
12	Medical/Biochemical Diagnostic, Pharmaceutical, and Drug Delivery Applications of Particle Tech.	May 13-15, Orlando, FL, USA	Oral, 汪勇先(Wang X Y)	15
13	37th ICFA Advanced Beam Dynamics Workshop on Future Light Sources	May 15-19, Hamburg, Germany	Oral, 戴志敏(Dai Z M)	16
14	Hot Quarks 2006	May 15-20, Villasimius, Sardinia, Italy	Plenary, 钟晨(Zhong C)	17
15	Pre-meeting for the Council of Sino-Japan Collaboration on Nuclear Physics	May 16, Shanghai, China	Plenary, 马余刚(Ma Y G)	18
16	6th China-Japan Joint Nucl. Phys. Symposium	May 16-20, Shanghai, China	Plenary, 马余刚(Ma Y G) Plenary, 王鲲(Wang K) Plenary, 陈金辉(Chen J H) Plenary, 徐望(Xu W) Plenary, 马国亮(Ma G Y) Plenary, 蒋维洲(Jiang W Z)	19 20 21 22 23 24
17	Int. Workshop on Mechanical Engineering Design of Synchr. Radia. Equipment and Instrumentation	May 24-26, Egret Himeji, Hyogo, Japan	Poster, 王纳秀(Wang N X) Poster, 陈永林(Chen Y L)	25 26
18	9th Int. Conf. on Synchr. Radia. Instrumentation	May 28-June 2, Daegu, Korea	Plenary, 徐洪杰(Xu H J)	27
19	超导技术在同步辐射光源中的应用研讨会	June 5-6, 台湾新竹, 中国	Plenary, 赵振堂(Zhao Z T)	28
20	2nd Int. Conf. on Hard and Electromagnetic Probes of High-Energy Nuclear Collisions	June 9-16, Pacific Grove, CA, USA	Oral, 马国亮(Ma G Y)	29
21	Int. Semi. on Atom. & Nucl. Cross-Disc. Physics	June 10-13, Shanghai, China	Oral, 胡钧(Hu J)	30
22	International Symposium on Nuclear Structure	June 12-17, Shanghai, China	Plenary, 苏前敏(Su Q M) Plenary, 郭威(Guo W) Plenary, 蒋维洲(Jiang W Z)	31 32 33
23	1st Int. Conf. on Nanobiomedical Technology and Structural Biology	June 25-28, Chengdu, China	Poster, 张益(Zhang Y)	34

No.	Meetings in 2006	Date & Place	Presentations	No
24	6th OCPA (第 6 届华人物理学家大会)	June 25 –July.4,中国 台北,	Plenary, 马余刚(Ma Y G)	35
			Oral, 徐洪杰(Xu H J)	36
25	European Particle Accelerator Conference	June 26-30, Edinburgh, UK	Plenary, 赵振堂(Zhao Z T)	37
26	1st Asian Triangle Heavy Ion Conf. (ATHIC 2006)	June 29-July 1, Seoul, Korea	Plenary, 马余刚(Ma Y G)	38
			Plenary, 陈金辉(Chen J H)	39
27	10th Int. Conf. on Nucl. Microprobe Tech. & and Appl.	July 9-14, Singapore	Plenary, 张元勋(Zhang Y X)	40
			Plenary, 李晓林(Li X L)	41
28	RIBF 相关的核物理国际研讨会	Aug. 2-6, RIKEN, Japan	Plenary, 方德清(Fang D Q)	42
29	Annual RIBF Users Meeting	Aug.3-4, RIKEN, Japan	Plenary, 田文栋(Tian W D)	43
			Plenary, 方德清(Fang D Q)	44
30	18th Int. IUPAP Conf. on Few-Body Problems in Phys.	Aug.21-26, São Paulo, Brazil	Oral, 马余刚(Ma Y G)	45
31	9th Int. Conf. on Nucleus-Nucleus Collisions	Aug.28-Sept.1, Rio de Janeiro, Brazil	Oral, 马余刚(Ma Y G)	46
32	5th Annual Meeting of the Society for Molecular Imaging	Aug.30-Sept.2, Big Island, HI, USA	Poster, 蔡汉成(Cai H C)	47
33	Int. Workshop on Strangeness Nuclear Physics	Sept.5-9, USA	Plenary, 马余刚(Ma Y G)	48
34	7th Int. Symp. on Technetium in Chemistry and Nuclear Medicine	Sept.6-9, Bressanone, Italy	Poster, 周伟(Zhou W)	49
			Poster, 于俊峰(Yu J F)	50
			Poster, 尹端沚(Yin D Z)	51
35	多媒体内容表征、安全与识别	Sept.10-14, Istanbul, Turkey	Plenary, 李勇平(Li Y P)	52
36	23rd Int. Conf. on Nuclear Tracks in Solids	Sept.11-15, Beijing, China	Poster, 朱智勇(Zhu Z Y)	53
			Poster, 朱智勇(Zhu Z Y)	54
37	1st Asia-Pacific Symposium on Radiation Chemistry	Sept.17-21, Shanghai, China	Plenary, 朱志远(Zhu Z Y)	55
			Plenary, 吴国忠(Wu G Z)	56
			Plenary, 姚思德(Yao S D)	57
			Oral, 侯铮迟(Hou Z C)	58
			Oral, 李林繁(Li L F)	59
			Oral, 赵红卫(Zhao H W)	60
			Oral, 陈仕谋(Chen S M)	61
			Oral, 朱红平(Zhu H P)	62
			Oral, 马红娟(Ma H J)	63
			Oral, 赵红卫(Zhao H W)	64
			Poster, 孙汉文(Sun H W)	65
			Poster, 张朝霞(Zhang Z X)	66
			Poster, 朱光来(Zhu G L)	67
			Poster, 郝树梅(Hao S M)	68
			Poster, 戚明颖(Qi M Y)	69
			Poster, 侯铮迟(Hou Z C)	70
			Poster, 侯铮迟(Hou Z C)	71
			Poster, 张聪(Zhang C)	72
			Poster, 张艳(Zhang Y)	73
38	Joint 31st Int. Conf. on Infrared and Millimeter Waves and 14th Int. Conf. on Terahertz Electronics	Sept.18-22, Shanghai, China	Oral. 赵红卫(Zhao H W)	74
			Oral, 赵红卫(Zhao H W)	75
			Poster, 朱智勇(Zhu Z Y)	76
39	3rd Shanghai Int.Symposium on Analytical Chemistry	Sept.19-21, Shanghai, China	Oral, 樊春海(Fan C H)	77

No.	Meetings in 2006	Date & Place	Presentations	No
40	7th Int. Symp. on Environmental Geochemistry	Sept.24-27, Beijing, China	Poster, 刘卫(Liu W)	78
41	9th International Workshop of Accelerator Alignment	Sept.25-29, SLAC, USA	Plenary, 于成浩(Yu C H)	79
42	2nd Int. Conf. on Molecular Imaging & 1st Conf. on Small Animal Molecular Imaging.	Sept., Hangzhou, China	Plenary, 张岚(Zhang L) Plenary, 漆玉金(Qi Y J) Plenary, 李谷才(Li G C) Plenary, 尹端沚(Yin D Z) Plenary, 程登峰(Cheng D F) Plenary, 李晴暖(Li Q N)	80 81 82 83 84 85
43	6th Int. Conf. on Dynamical Aspect in Fission Dynamics	Oct.2-6, Smolenice Castle, Slovakia	Plenary, 马余刚(Ma Y G) Plenary, 王鲲(Wang K)	86 87
44	2nd Asian and Oceanic Congress for Radiation Protection	Oct.9-13, Beijing, China	Poster, 刘卫(Liu W)	88
45	Sino-German Forum on Nanoscience and Biomedicine	Oct.12-14, Beijing, China	Plenary, 樊春海(Fan C H)	89
46	9th Con. of World Federation of Nucl. Medi. & Biology	Oct.22-27, Seoul, Korea	Poster, 程登峰(Cheng D F)	90
47	Asia Biometrics Forum 2006	Oct.30-31, Beijing, China	Plenary, 李勇平(Li Y P)	91
48	3rd Asian Biological Inorganic Chemistry Conference	Oct.31-Nov.3, Nanjing, China	Poster, 沈玉梅(Shen Y M)	92
49	3rd Sino-Australia Bilateral Symposium	Nov. 5-7, Sydney, Australia	Plenary, 徐洪杰(Xu H J)	93
50	国际实验合作研讨会	Nov. 5-10, RIKEN, Japan	Plenary, 方德清(Fang D Q)	94
51	International Symposium on Biological and Chemical Superfast Processes	Nov. 9-11, Beijing, China	Plenary, 吴国忠(Wu G Z)	95
52	PKU-CCAST-RIKEN Joint Conference	Nov. 10, Beijing, China	Plenary, 马余刚(Ma Y G)	96
53	19th Int. Conf. on Ultra-relativistic Nucleus-Nucleus Collisions (Quark Matter 2006)	Nov.13-21, Shanghai, China	Plenary, 陈金辉(Chen J H) Oral, 马国亮(Ma G Y) Oral, 钟晨(Zhong C) Oral, 龙家丽(Long J L) Poster, 左嘉旭(Zuo J X) Poster, 施兴华(Shi X H)	97 98 99 100 101 102
54	IEEE Region 10 Conference(TENCON 2006)	Nov.14-17, Hong Kong, China	Oral, 敖新宇(Ao X Y) Poster, 张鸿洲(Zhang H Z)	103 104
55	第 4 届高亮度电子枪会议	Nov. 20-21, Ricoti, Tokai, Japan	Plenary, 顾强(Gu Q)	105
56	Asia/Oceania Forum for Synchrotron Radiation Research	Nov.24-25, Tsukuba, Japan	Plenary, 徐洪杰(Xu H J) Plenary, 赵振堂(Zhao Z T) Poster, 郭智(Guo Z) Poster, 邹杨(Zou Y)	106 107 108 109
57	第五届海峡两岸纳米科学与技术研讨会	Dec.8-11,中国 香港	Plenary, 樊春海(Fan C H)	110

附录 4

2005–2006 所内举办的学术报告

Invited Seminars at SINAP in 2005–2006

2005

No.	报告	报告人	日期
1	核磁共振图谱解析	沈玉梅博士	Jan.13
2	核医学成像前沿研究介绍——从人体到小动物的 SPECT 成像技术研究	漆玉金博士	Jan.19
3	我国核物理及核科学研究进展	沈文庆院士	Jan.21
4	X-ray fluorescence detection with a bright beamline	Zhang Ke (美国 APS)	Jan.28
5	Prototype experiments for the future XFEL science	Prof.Kazumichi Namikawa (Tokyo Gakugei University)	Jan.31
6	How to get published in world prestigious physics journals	Dr. John Haynes (Deputy Director, Journals Institute of Physics Publishing, UK)	Feb.21
7	复杂系统和系统生物学	刘曾荣教授 (上海大学数学系)	Mar.04
8	DNA/protein interactions at the single molecule level	Prof. David Bensimon(法国巴黎高等师范学校)	Apr.07
9	State-of-the-Art X-ray tomography imaging using laboratory sources	云文斌博士 (美国 Xradia 公司)	Apr.11
10	低激发态的核结构理论和其它有限量子系统	赵玉明教授 (上海交通大学)	Apr.21
11	Web of Knowledge——整合的学术资源环境	张帆 (SCI 中国办事处助理经理)	Apr.25
12	CdZnTe 晶体材料及探测器的发展现状和应用前景	李陇遐 (美国著名半导体材料专家)	Apr.30
13	强激光与核物理	靳根明研究员 (中科院近物所)	May 24
14	重核的 alpha 衰变	任中洲教授 (南京大学)	May 24
15	物理学与化学和生命科学的交叉前沿——聚合物、胶体、膜蛋白组装研究	马余强 教授 (南京大学)	May 27
16	Shell model for heavy deformed nuclei	孙杨博士 (美国 Notre Dame 大学)	June 01
17	The one dimensional mesoporous silica nano-structure within porous anodic alumina membrane	姚宝殿博士(复旦大学化学系)	June 02
18	Surface phonons and phonon confinement in semiconducting nanowires	Prof. Peter C.Eklund (美国宾夕法尼亚州立大学)	June 15
19	Instrumental, preconcentration and radiochemical neutron activation methods for total iodine and its species	Prof. A. Chatt (Dalhousie University, Canada)	June 17
20	Constraining symmetry energy with heavy ion collisions	Prof. Betty Tsang (Michigan State University，USA)	June 30
21	Folding, misfolding and initial aggregation of a WW domain: replica exchange simulation study	Dr. Yuguang Mu (School of Biological Sciences, Nanyang Technological Univ, Singapore)	July 08
22	Equation of state of neutron-rich matter and heavy-ion collisions	Prof. Bao-An Li (Arkansas State University, USA)	July 08
23	Dewetting transition in nanoscale hydrophobic plate collapse and protein aggregates	Dr. Ruhong Zhou (Computational Biology Center, Deep Computing Institute)	July 12
24	PET imaging tracer development for amyloid plaques and its application in the diagnosis of Alzheimer's diseases	蔡利生博士 (National Institute of Mental Health(NIH), USA)	July 12
25	Controllable transport channel of carbon nanotubes	黄博达博士 (山东大学)	July 13
26	Radiation induced chemical reactions in supercritical water	林铭章博士(东京大学)	Aug.09
27	From nanoscience to X-ray microspectroscopy of soft matters—some recent applications of synchrotron radiation	Prof.T.K.Sham (University of Western Ontario, Canada)	Aug.09

2005

No	报告	报告人	日期
28	Introduction to the Taiwan Photon Source project	Wu Tsung Weng (Brookhaven National Laboratory, USA)	Aug.19
29	Simple math is enough: Inferring functional associations from genomic data	Prof. Shoudan Liang (Department of Biostatistics and Applied Mathematics, M. D. Anderson Cancer Center, University of Texas, USA)	Aug.22
30	Radiation chemistry and the anti oxidants	Dr. Jai Pal Mittal (Bhabha Atomic Research Center, India)	Aug.23
31	Heavy ion collision studies of the symmetry energy at high temperature and very low density	Prof. Natowitz Joe (Texas A&M University, USA)	Aug.24
32	Synthesis and decay properties of the HEAVIEST ELEMENTS	Prof. Oganessian Yuri (Russian Academician, DUBNA)	Aug.24
33	Isospin dependence of nucleus-nucleus collisions	Dr. M. Veselsky (Institute of Physics, Slovak Academy of Sciences)	Aug.30
34	Isospin effects in heavy ion collisions from low to relativistic energies: EOS-sensitive observables	Prof. M. Di Toro (Catania, INFN, Italy)	Sept.01
35	Turbulent drag reduction and degradation with DNA	Prof. C. K. Chan (中国台湾中央大学)	Sept.05
36	Structure genomics, drug discovery & ion channel	Ye,Sheng 博士	Sept.06
37	实验室核天体物理的最新进展	陈永寿研究员(中国原子能研究院物理所)	Sept. 14
38	物理学中的能量标度	李小源研究员(中国科学院理论物理所)	Sept. 14
39	Overview of synchrotron radiation facility and researches in Australia	Dr. Richard Garret (Australian Light Source)	Sept.27
40	Flame chemistry study with tunable synchrotron radiation photoionization technique	Prof. Terrill A. Cool, (Cornell University, UK)	Oct. 17
41	Synchrotron-based structural biology	郝权教授 (美国 Cornell 大学 MacCHESS 中心)	Oct. 17
42	哈萨克斯坦——一个核大国	杨福家院士	Oct. 20
43	Closing in on the AMPA receptor: Synthesis and evaluation of 2-acetyl-1-(p-chlorophenyl)-6-methoxy-7-[^{11}C]methoxy -1,2,3,4-tetrahydroisoquinoline as a novel PET ligand	Dr. Erik Arstad Hammersmith Hospital, London	Oct. 25
44	时序微扰理论的应用	朱伟教授 (华东师范大学物理系)	Nov.02
45	复杂液体中旋转颗粒的电荷弛豫理论	顾国庆教授 (华东师大信息学院)	Nov.02
46	电离辐射医学应用及其放射防护进展	郑钧正研究员(中国疾病控制中心)	Nov.03
47	Developing technologies for structural proteomics research	Dr. Thomas Earnest (LBNL, USA)	Nov.04
48	Study on carbon cycle in soil using radiocarbon and carbon isotopic composition of organic matter and CO_2	刘卫 博士乱（Nagoya University, Japan）	Nov.10
49	微生物群落的结构解析与功能调控	赵立平教授 (上海交通大学)	Nov.17
50	Simulations of flows with multiphase and multicomponent	Dr. Xiaowen Shan （Exa Cooperation, Boston, USA）	Nov.22
51	Shear stress in the region of a stenosis in the carotid artery: A lattice Boltzmann simulation	Prof. James M. Buick (University of New England, Australia)	Dec.01
52	Atomic force microscopy: a powerful probe of molecular details	邵志峰(Zhifeng Shao) 教授，（美国弗吉尼亚大学医学院 生物物理学教授）	Dec.27

2006

No.	报告	报告人	日期
1	Nitrogen metabolism of E. coli from the structure point of view	Dr. Xiaodan Li (Biomolecular Research, Paul Scherrer Institute, Switzerland)	Jan. 04
2	Trapping of radioactive atoms and the physics one can do with them	Prof. Gene Sprouse (Nuclear Structure Lab, State University of New York, USA)	Jan. 11
3	同步辐射单光子电离技术在燃烧及其它研究中的应用	齐飞教授 (中国科学技术大学国家同步辐射实验室)	Feb.22
4	基于虚拟仪器架构的远程核物理实验平台研究	黄文达博士 (厦门大学物理系教授)	Mar.02
5	我国辐射防护新标准	郑钧正研究员 (中国疾病预防控制中心辐射防护与核安全医学所)	Mar.07
6	新奇异粒子 X(1835)的衰变	阎沐霖教授 (中国科技大学物理系理论物理)	Mar.28
7	KEK-PF 光束线站现状	河田洋教授 (KEK, 日本)	Mar.28
8	KEK-PF 展望—ERL 光源计划进展	KEK 河田洋教授 (KEK, 日本)	Mar.30
9	Di-hadron correlation and the strongly interacting matter at RHIC energies	Prof. Peter Levai (KFKI Institute for Particle and Nuclear Physics, the Hungarian Academy of Sciences)	Apr. 06
10	Trimodality molecular imaging system PET/SPECT/CT for animal research	Dr.Zho, Dr.Koji Iwata, Dr.Joann and Dr.Zhao （美国 GAMMA MEDICA 公司）	Apr.13
11	Globally polarized QGP in non-central AA collisions	梁作堂教授 (山东大学物理系)	Apr.17
12	小角度范围内弱束缚核 ^{17}F 弹性散射微分截面的奇异行为	王琦研究员 (中国科学院近代物理研究所)	Apr.19
13	Chemical and microchemical characterization of ribologically generated filmsusing X-ray spectroscopy and spectromicroscopy (X-PEEM)	Prof. G. M Bancroft (Academician, Department of Chemistry, University of Western Ontario, London Ontario, Canada)	Apr.24
14	Introduce the installation of SpearIII	Prof. Robert Hettel (美国斯坦福大学同步辐射实验室 SSRL)	Apr.25
15	小 RNA 研究进展	陈润生研究员 (中科院生物物理研究所)	Apr. 27
16	X 射线光学显微技术前沿	Dr. Yun Wenbing (云文兵) (President, Xradia, Inc., USA)	May 09
17	A low cost massive parallel DNA tag sequencing system for functional genomics	盛司潼博士 (美国弗吉尼亚大学)	May 16
18	New scientific directions at the advanced photon source	Dr. John Murray Gibson (Associate Director of ANL, and Director of Advanced Photon Source, ANL USA)	May 26
19	亚波长金属微结构器件的光谱特性	张伟力 (美国俄克拉荷马州立大学)	June 01
20	阿尔茨海默氏病、 帕金森氏病、 肌萎缩侧索硬化模式生物研究进展——揭示神经变性的分子生物学机制	乐卫东教授 (上海交通大学)	June 02
21	放射治疗技术的发展与展望	宋世鹏 (上海伽玛星科技发展有限公司)	June 02
22	国内外纳米技术标准化工作进展	沈电洪研究员 (中科院物理所)	June 07
23	X-ray photoelectron spectroscopy study of metal and semiconductor interface	潘冀生博士 (Institute of Materials Research and Engineering, Singapore)	June .08
24	Group symmetries and solvable models in nuclear structure	Prof.V.K.B Kota (Physics Research Lab, Ahmedabad, India)	June 19

2006

No.	报告	报告人	日期
25	阿尔茨海默氏病的发病机理	周江宁教授 (中国科技大学生命科学院)	June 22
26	Comparative proteomics	Dr. Xiang Zhang (Purdue Univ, USA)	June 29
27	Life at the edge: Emergent phenomena at surfaces/interfaces of transition-metal oxides	Dr. Jiandi Zhang (Florida International University, USA)	July 03
28	腺相关病毒(AAV)研究进展	吴小兵研究员(中国疾病控制中心)	July 06
29	食品中农药抗生素残留及转基因成分检测	张大兵教授(上海交通大学)	July 06
30	Program in bioinformatics	Jie Liang (Dept. of Bioengineering, University of Illinois at Chicago, USA)	July 11
31	生物芯片研究与全基因组测序技术	陆祖宏教授(东南大学)	July 14
32	斯坦福大学分影像项目和靶向碳酸酐酶 IX 的新型肿瘤乏氧分子影像探针	张岚博士	July 18
33	技术标准制订方法讲座	张训彪教授 (全国微束分析标准化技术委员会委员)	July 21
34	纳米微粒监测评估与控制	简弘民研究员 (中国台湾工业技术研究院)	Aug.15
35	Toward quantitative biorheology: Quantitative characterization and computational modeling	Dr Xue-Feng Yua (Manchester Interdisciplinary Biocentre, The University of Manchester, UK)	Aug.11
36	New approaches to some old problems with asymptotic normalization coefficients	Prof. Robert Tribble (Cyclotron Institute / Physics Depart., Texas A&M Univ., USA)	Aug.17
37	Dynamic properties of biomolecules based on spectroscopy analysis	Prof. Salim Abdali (Quantum Protein Centre, QuP Department of Physics, Technical University of Denmark)	Aug.17
38	From clusters to nanomaterials: A few “small“ stories	杨世和教授 (香港科技大学化学系)	Aug.22
39	Bionano devices : Protein-based memory	Prof. V. Renugopalakrishnan (Harvard Medical School, Boston, MA, USA)	Aug.28
40	癌特异性放射药物研究开发中的经验及问题	苏自奋研究员 (四川大学)	Aug.29
41	Semiconductor quantum dots and their applications in life science	汪联辉教授 (复旦大学)	Sept.04
42	有机电子发光与显示	王坚教授 (华南理工大学)	Sept.11
43	Tip characterizer for atomic force microscopy	Dr. Hiroshi Itoh, (National Institute of Advanced Industrial Science and Technology, Japan)	Sept.19
44	Nanobubbles: A nanoscale gaseous state	张雪花博士 (Depart. of Chemical and Biomolecular Engineering, University of Melbourne, Australia)	Sept.27
45	激光操纵技术在生物领域中的应用	降羽强博士 (日本大阪大学)	Sept.28
46	钚的海洋地球化学行为研究	山田正俊博士 (日本国立放射线医学综合研究所)	Sept.29
47	海洋环境中放射性核素分析化学进展	郑健 (日本国立放射线医学综合研究所)	Sept.29
48	现代微束技术及其应用	Dr.Gene E Ice (Oak Ridge National Laboratory , USA)	Oct.08
49	From surface science to nano science	Dr. Peter Blanckenhagen (Karsluhe Nano Science and Technology Research Center, Germany)	Oct.10
50	Boundary slip in Newtonian fluids	Dr. Vincent Craig (Depart. of Appl. Math., School of Phys. Sci. and Eng., Australian National University)	Oct.25

2006

No.	报告	报告人	日期
51	Biomembrane: Adsorption and transport of a smallmolecule	Prof. Mahn Won Kim (Department of Physics, Korea Institute for Advanced Study)	Nov.08
52	Present results in neutrino physics	Prof. Ettore Fiorini (Department of Physics, Milano-Bicocca Univ., Milano Section, INFN, Italy)	Nov. 09
53	Double beta decays with MOON (Mo Observatory Of Neutrinos)	Prof. Hiro Ejiri, (RCNP, Osaka University, Japan)	Nov.10
54	Symmetries in atoms and nuclei	Prof. Akito Arima (有马朗人教授)	Nov.13
55	钙信号调控与细胞生理	麻建杰教授 (美国罗伯特伍德强生医学院生理与生物物理系)	Nov.14
56	Semiconducting nanomaterials research	Prof. Shuit-Tong Lee (Center of Super-Diamond and Advanced Films, Depart. of Phys. and Materials Sci., City Univ. of Hong Kong)	Nov.20
57	Nanofabrication and biodetection	Dr. Wenjiang Shen (Innovative Micro Technology, Inc., Santa Barbara, CA, USA)	Nov.22
58	Present status and future plan of structural biology beamlines at SPring-8	Dr. Masaki Yamamoto (Division of Synchrotron Radiation Instrumentation, RIKEN/SPring-8)	Nov.29
59	含能材料及相关物的计算机模拟	姬广富教授(中国工程物理研究院流体物理研究所)	Dec.04
60	原子尺寸金属纳米线的结构和物理性质	赵纪军教授 (大连理工大学高科技研究院)	Dec.04
61	Searching for signatures of relativistic Dirac dynamics via proton-induced polarization phenomena on nuclei	Prof. Greg Hillhouse (Department of Physics, University of Stellenbosch, Stellenbosch, South Africa)	Dec.15
62	Challenges and opportunities of using streak camera for ultra-fast X-ray science	邓石博士 (美国 ALS)	Dec.15
63	中子星的性质和结构	刘波研究员 (中科院高能物理研究所)	Dec.21
64	微纳米技术在细胞生物学中的应用	蒋兴宇研究员 (国家纳米中心)	Dec.22
65	DNA 分子马达	刘冬生研究员 (国家纳米中心)	Dec.23
66	Synchrotron radiation R&D at SSLS	Prof. Herbert O. Moser (Director, Singapore Synchrotron Light Source)	Dec.26
67	Linac undulator light installation	Dr. Diao Caozheng (Singapore Synchrotron Light Source)	Dec.26
68	高能辐射领域的辐射防护及高放废物的处置	夏晓彬博士 (EcoTopia Science Institute,Nagoya University, Japan)	Dec.28
69	碲锌镉(CZT)探测器研究的最新进展和应用	李陇遐教授 (美国 Yinnel Tech Inc.总裁和创建人，美国光学工程院士)	Dec.28

附录 5

2005–2006 年专利申请授权一览表

Patents in 2005–2006

2005

No.	专利名称	专利申请号	授权专利号	专利类型
1	单个生物大分子分离装置	200520039969.6		实用新型
2	硅溶胶的制造方法及制得的硅溶胶	200510024230.2		发明
3	O-(2-[^{18}F]氟乙基)-L-酪氨酸的合成方法	200510025005.0		发明
4	聚醚砜接枝改性的方法	200510025006.5		发明
5	电化学电解装置	200520040819.7		实用新型
6	电子束烟气脱硫脱硝的方法及其装置	200510025131.6		发明
7	一种修饰的云母衬底及其修饰方法和应用	200510025356.1		发明
8	弧矢聚焦双晶单色器	200520041551.9		实用新型
9	聚烯亚胺凝胶的光化学合成方法	200510026477.8		发明
10	聚烯亚胺纳米凝胶及其应用	200510026746.0		发明
11	高分子聚合反应装置	200520042466.4		实用新型
12	二吡啶甲基胺衍生物及其螯合物、以及它们的制备方法	200510026747.5		发明
13	[二(2-吡啶甲基)-氨基]-脂肪酸的制备方法及其中间体	200510027150.2		发明
14	硫化镉裸量子点及其制备方法	200510031067.2		发明
15	大孔径聚醚砜膜及其制备方法和用途	200510031066.8		发明
16	MBR 平片膜在线机械擦洗工具	200520047262.X		实用新型
17	小型 MBR 装置混合液污泥干化处理设备	200520047260.0		实用新型
18	IMS 检测仪	200520047493.0		实用新型
19	放射性支架及其放射性聚氨酯涂层材料、以及它们的制备方法	200510111475.9		发明
20	生长纳米级气泡的方法及其观察并控制装置与方法	200510111757.9		发明
21	一种产氢储氢一体化方法和装置	200510111758.3		发明
22	水产养殖用壳聚糖溶液剂及其应用	200510111756.4		发明
23	DNA 的荧光检测方法及其试剂盒	200510131792.7		发明
24	长程面形仪	02110541.3	ZL02110541.3	发明
25	C_{60}-糖皮质激素及其用途	O2137642.5	ZLO2137642.5	发明
26	电子加速器加速管保护环装置	200420090483.0	ZL200420090483	实用新型
27	工业用电子加速器引出窗	200420090481.1	ZL200420090481.1	实用新型
28	强流电子枪阴极装置	200420090482.6	ZL200420090482.6	实用新型

2006

No.	专利名称	专利申请号	授权专利号	专利类型
1	银纳米粒子的制备方法及制得的银纳米粒子	200610025544.9		发明
2	采用裸云母作为蛋白质晶体生长基底的方法	200610025545.3		发明
3	C_{60}-苯甲酸氮芥在制备抗肿瘤药物中的应用	200610025953.9		发明
4	一种[^{18}F]氟标记的嘌呤类化合物及其制备方法和应用	200610026601.5		发明
5	2-氨基-6-氟-9-(4-羟基-3 羟甲基丁基)嘌呤及其中间体的制备方法	200610026602.X		发明
6	一种 DNA 电化学传感器及其制备方法	200610026823.7		发明
7	VIP 类似物及其放射性标记物，以及它们的制备方法	200610027652.X		发明
8	低烟无卤阻燃聚烯烃材料及其制备方法和应用	200610028750.5		发明
9	研究极性接枝链在透明或半透明的高分子薄膜内层分布的方法	200610028985.4		发明
10	用于 AFM 研究的病毒样品的制备方法及制得的病毒样品	200610029275.3		发明
11	β-榄香烯衍生物及其 Re 配合物和 ^{188}Re 标记物、以及它们的合成方法	200610116542.0		发明
12	β-榄香烯聚乙二醇胺衍生物及其合成方法和用途	200610117008.1		发明
13	β-榄香烯单取代醚衍生物及其合成方法和用途	200610117229.9		发明
14	一种反应中间体 β-榄香烯醇的合成方法	200610117230.1		发明
15	微流控阵列蛋白质芯片及其使用方法	200610117234.X		发明
16	β-榄香烯氨基酸衍生物及其合成方法和用途	200610117399.7		发明
17	转动样品架	200620047378.8		实用新型
18	氨水中和法生产乙酰甲胺磷产生的废水的处理方法	200610147619.0		发明
19	β-榄香烯单取代醚衍生物及其合成方法和用途	200610167532.X		发明
20	一种储存气体的方法	PCT/CN2006/003046		发明
21	6-[^{18}F]氟-L-多巴的制备方法	02110721.1	ZL02110721.1	发明
22	光化学制备粒径分布窄的纳米凝胶的方法	02137404.X	ZL02137404.X	发明
23	^{18}F 氟标记的苯并吡喃类化合物及其制备方法和作为多巴胺 D4 受体显像剂的应用	03115164.7	ZL03115164.7	发明
24	DNA 单分子有序化测序方法	03115428.X	ZL03115428.X	发明
25	单个生物大分子的分离方法	03115943.5	ZL03115943.5	发明
26	木材和竹板用酚醛数脂胶粘剂的制造方法	03141762.0	ZL03141762.0	发明
27	人造板中甲醛含量的快速无损分析方法	200310108145.5	ZL200310108145.5	发明
28	膜——生物反应器专用滤膜的测试装置	200420022771.2	ZL200420022771.2	实用新型
29	工业用电子加速器的扫描盒	200420110679.1	ZL200420110679.1	实用新型
30	电子加速器钛箔更换装置	200420110680.4	ZL200420110680.4	实用新型
31	单个生物大分子分离装置	200520039969.6	ZL200520039969.6	实用新型
32	电化学电解装置	200520040819.7	ZL200520040819.7	实用新型
33	弧矢聚焦双晶单色器	200520041551.9	ZL200520041551.9	实用新型
34	高分子聚合反应装置	200520042466.4	ZL200520042466.4	实用新型

附录 6

上海应用物理所博士学位授予一览表(2005~2006)

PhD Programs Completed at SINAP in 2005–2006

2005

No.	学生	专业	导师	论文题目	研究方向
1	李 宾	粒子物理与原子核物理	李民乾	单分子研究和定位单分子反应	纳米科技
2	刘爱琴	核技术及应用	戴志敏	太赫兹 CTR/CDR 的产生及其在束测中的应用	同步辐射光源与束线技术及应用
3	龙家丽	粒子物理与原子核物理	贺泽君	夸克胶子等离子体中双轻子、奇异性和光子的产生	相对论重离子碰撞
4	张 伟	粒子物理与原子核物理	朱志远	碳纳米结构的热动力学及输运性质研究	粒子物理与原子核物理
5	张志祥	粒子物理与原子核物理	李民乾	纳米生物传感器的研究	纳米科技
6	周星飞	粒子物理与原子核物理	沈文庆	基于原子力显微镜技术的生物大分子与纳米颗粒的力学性质研究	纳米科技
7	付海英	无机化学	姚思德	辐射接枝 SBS 及其改性道路沥青的性能研究	辐射改性材料
8	魏 逊	核技术及应用	徐洪杰	硬 X 射线相衬成像在中药材显微鉴定中的应用研究	射线成像
9	吴胜伟	无机化学	李文新	碳纳米管的填充、切割及其若干复合材料的研制与应用	纳米材料
10	徐 慧	无机化学	李文新	分子结构的 THz-TDS 及基因识别的荧光探测研究	纳米科技
11	雷晓玲	粒子物理与原子核物理	方海平	碱基水平 DNA 离散化模型的动力学研究	DNA 的弹性力学研究
12	陈金根	粒子物理与原子核物理	沈文庆	丰质子核性质和核的激发态奇异结构	放射性核束与奇异核结构
13	张晓岚	无机化学	包伯荣	荚醚、磷类萃取剂的辐射化学研究和机理探讨	核燃料后处理
14	魏义彬	粒子物理与原子核物理	马余刚	奇异轻核的碎裂产物的动量分布和核子－核子动量关联函数	粒子物理与原子核物理
15	孙小影	核技术及应用	戴志敏	上海深紫外自由电子激光数据库系统	核信息获取及应用
16	俞路阳	核技术及应用	刘德康	自由电子激光相位控制系统研究	数据采集及控制
17	沈水法	粒子物理与原子核物理	顾嘉辉	A~80 区原子核结构的研究	原子核结构和核谱学
18	孙立涛	粒子物理与原子核物理	朱志远	粒子束诱导碳纳米管的相变研究	纳米材料与粒子物理
19	孔 玲	无机化学	姚思德	若干天然抗氧化剂光解机理及清除自由基机理的理论研究	光化学、辐射化学、量子化学
20	刘永彪	无机化学	姚思德	纳米载体及自由基的肿瘤生物学效应研究	肿瘤分子生物学 辐射生物学
21	吉丽娜	无机化学	胡 钧	α-synuclein 蛋白积聚的分子机制：GAV 基序和无规卷曲结构	纳米生物学

2006

No.	学生	专业	导师	论文题目	研究方向
1	王纳秀	核技术及应用	夏绍建	同步辐射光束线热缓释技术研究及冷却技术的应用	同步辐射光束线技术
2	冉铁成	无机化学	李文新	抗肿瘤药物富勒烯 C_{60} 吡咯烷苯氮芥研究	富勒烯药物化学
3	韩家广	粒子物理与原子核物理	朱志远	基于远红外太赫兹光谱和 X 射线光电子谱材料的性质研究	材料研究
4	马国亮	粒子物理与原子核物理	马余刚	相对论重离子碰撞中 Φ 介子性质和 QGP 相变实验观测量	相对论重离子碰撞
5	王　鲲	粒子物理与原子核物理	马余刚	中低能重离子反应截面和动量分布测量以及同位旋标度律研究	粒子物理与原子核物理
6	席再军	粒子物理与原子核物理	徐洪杰	Terahertz 波相位成像研究	Terahertz 技术
7	岳伟生	粒子物理与原子核物理	李　燕	基于单颗粒分析的上海大气颗粒物污染来源研究	核技术在环境科学中的应用
8	陈建敏	无机化学	李　燕	颗粒物的污染特征及其心血管毒性的机理研究	核技术在环境科学中的应用
9	郭金学	无机化学	李文新	碳纳米管的表面化学修饰及其生物效应研究	纳米材料和生物医药
10	李谷才	无机化学	尹端沚	多巴胺 D4 受体分子显像研究	受体显像药物
11	李林繁	无机化学	盛康龙	辐射改性 SBS 道路沥青性能及其机理研究	辐射改性材料
12	孙汉文	无机化学	姚思德	放射性同位素药物磁靶向载体制备及其动物靶向研究初探	靶向药物载体、纳米材料
13	王明伟	无机化学	尹端沚	肿瘤 PET 显像剂 O-(2-[^{18}F]氟乙基)-L-酪氨酸的研究	放射性药物
14	俞国军	无机化学	巩金龙	碳纳米管的化学气相沉积制备与纯化研究	纳米材料
15	张凤英	无机化学	盛康龙	辐射接枝聚乙烯表面生长碳酸钙晶体研究	辐射改性材料
16	曹红萍	核技术及应用	李德明	皮秒、飞秒加速器控制逻辑研究及软件系统建立	核技术及应用
17	成　诚	核技术及应用	蒋大真	便携 X 荧光能谱仪的研制	核仪器
18	韩毅昂	核技术及应用	李德明	上海光源束流输运线物理设计与技术方案优化的计算研究	加速器技术及应用
19	李冬梅	核技术及应用	叶愷容	数字 BPM 系统在束流诊断中的应用	加速器技术及应用
20	傅　远	核技术及应用	夏绍建	同步辐射光束线控制系统研究	同步辐射光束线控制系统
21	骆玉宇	粒子物理与原子核物理	徐洪杰	基于 X 射线相干特性的成像及其应用研究	X 射线光学显微成像
22	侯铮迟	无机化学	盛康龙	聚乙烯聚醚砜表面辐射接枝研究	辐射化学
23	夏姣云	无机化学	汪勇先	[^{188}Re(CO)$_3$]+核及其配合物的合成和应用研究	放射性药物
24	尹娟娟	无机化学	李文新	含磷富勒烯衍生物的合成及性质研究	纳米生物医药
25	张　峰	无机化学	何建华	α-synuclein 蛋白的纤维结构与 GAV-9 肽的自组装研究	蛋白质折叠
26	郑丽芳	核技术及应用	刘松强	数字化反馈控制实验平台的研究	同步辐射光源与束线技术及应用
27	赵群芬	无机化学	李文新	纳米碳团簇与原生动物作用的生物效应	纳米科技
28	王　森	粒子物理与原子核物理	巩金龙	基于氧化铝模板的阵列纳米结构制备研究及相关磁性表征	纳米材料
29	沈　飞	无机化学	陆晓峰	不对称 PVB 超滤膜的制备研究及其在 MBR 中的应用	高分子分离膜制备及应用